HIGH PERFORMANCE POLYMERS and ENGINEERING PLASTICS

Edited by
Vikas Mittal

WILEY

Scrivener

This page intentionally left blank

High Performance Polymers and Engineering Plastics

Scrivener Publishing
3 Winter Street, Suite 3
Salem, MA 01970

Scrivener Publishing Collections Editors

James E. R. Couper	Ken Dragoon
Richard Erdlac	Rafiq Islam
Pradip Khaladkar	Vitthal Kulkarni
Norman Lieberman	Peter Martin
W. Kent Muhlbauer	Andrew Y. C. Nee
S. A. Sherif	James G. Speight

Publishers at Scrivener
Martin Scrivener (martin@scrivenerpublishing.com)
Phillip Carmical (pcarmical@scrivenerpublishing.com)

High Performance Polymers and Engineering Plastics

Edited by
Vikas Mittal
Chemical Engineering Department,
The Petroleum Institute,
Abu Dhabi, UAE

Scrivener

WILEY

Copyright © 2011 by Scrivener Publishing LLC. All rights reserved.

Co-published by John Wiley & Sons, Inc. Hoboken, New Jersey, and Scrivener Publishing LLC, Salem, Massachusetts.
Published simultaneously in Canada.

No part of this publication may be reproduced, stored in a retrieval system, or transmitted in any form or by any means, electronic, mechanical, photocopying, recording, scanning, or otherwise, except as permitted under Section 107 or 108 of the 1976 United States Copyright Act, without either the prior written permission of the Publisher, or authorization through payment of the appropriate per-copy fee to the Copyright Clearance Center, Inc., 222 Rosewood Drive, Danvers, MA 01923, (978) 750-8400, fax (978) 750-4470, or on the web at www.copyright.com. Requests to the Publisher for permission should be addressed to the Permissions Department, John Wiley & Sons, Inc., 111 River Street, Hoboken, NJ 07030, (201) 748-6011, fax (201) 748-6008, or online at http://www.wiley.com/go/permission.

Limit of Liability/Disclaimer of Warranty: While the publisher and author have used their best efforts in preparing this book, they make no representations or warranties with respect to the accuracy or completeness of the contents of this book and specifically disclaim any implied warranties of merchantability or fitness for a particular purpose. No warranty may be created or extended by sales representatives or written sales materials. The advice and strategies contained herein may not be suitable for your situation. You should consult with a professional where appropriate. Neither the publisher nor author shall be liable for any loss of profit or any other commercial damages, including but not limited to special, incidental, consequential, or other damages.

For general information on our other products and services or for technical support, please contact our Customer Care Department within the United States at (800) 762-2974, outside the United States at (317) 572-3993 or fax (317) 572-4002.

Wiley also publishes its books in a variety of electronic formats. Some content that appears in print may not be available in electronic formats. For more information about Wiley products, visit our web site at www.wiley.com.

For more information about Scrivener products please visit www.scrivenerpublishing.com.

Cover design by Russell Richardson

Library of Congress Cataloging-in-Publication Data:

ISBN 978-1-118-01669-5

Printed in the United States of America

10 9 8 7 6 5 4 3 2 1

Contents

Preface xiii

List of Contributors xv

1 **High Performance Polymers: An Overview** 1
V. Mittal
1.1 Introduction 1
1.2 Poly(ether amide) and Poly(ether amide-imide) 3
1.3 Poly(arylene ether) 7
1.4 Benzoxazine Polymers 8
1.5 Poly(ether ether ketone) (PEEK) 11
1.6 Polytriazole 14
1.7 Hyperbranched Conjugated Polymers 15
1.8 Alternating Copolymers 19
1.9 References 20

2 **Synthesis and Properties of Polyoxadiazoles** 21
Dominique de Figueiredo Gomes
2.1 Introduction 21
2.2 Synthesis of Polyoxadiazoles in Poly(phosphoric acid) 24
2.3 Thermal and Mechanical Properties of Polyoxadiazoles 27
2.4 Application Fields 32
2.5 References 46

3 **Conjugated Polymers Based on Benzo[1,2-*b*:4,5-*b'*] dithiophene for Organic Electronics** 49
Huaxing Zhou and Wei You
3.1 Introduction 49

3.2 General Synthetic Methods for BDT Monomers and Polymers 50
3.2.1 Synthesis of BDT Monomers 51
3.2.2 Polymerization Methods of Polymers Incorporating BDT Unit 53
3.3 Application of BDT-Based Polymers in OFET and PSC 56
3.3.1 Introduction of OFET 56
3.3.2 BDT Based Polymers in OFET Application 58
3.3.3 Introduction of PSC 61
3.3.4 BDT Based Polymers for High performance PSC 65
3.4 Outlook 76
3.5 References 76

4 Polysulfone-Based Ionomers 81
Cristina Iojoiu and Rakhi Sood
4.1 Introduction 81
4.2 Polysulfone Backbone and Selection of the Ionic Function 83
4.3 Ionomer Synthesis and Characterization 85
4.3.1 Chemical Modification of Commercially Available Polysulfones 86
4.3.1.1 Acidic Ionic Function Attached Directly at Ortho-to-Ether Position of the Polymer 86
4.3.1.2 Ionic Function Attached Directly to Ortho-to-Sulfone Position of the Polymer 89
4.3.1.3 Ionic Function Attached to Main-Chain Through Side Chains 90
4.3.2 Polymerisation of Ionic Monomers by Step Growth 99
4.3.2.1 Ionomers Containing Hexafluoro-Isopropylidene or/and Polar Functions 99
4.3.2.2 Multi-block Ionomeric Polycondensates Based on Medium to Long Blocks 102

4.3.2.3 Multi-block Copolymers and Random- Ionomeric Copolymers 104
4.4 Conclusion 107
4.5 References 107

5 High-Performance Processable Aromatic Polyamides 111
S Banerjee and S Maji
5.1 Introduction 111
5.2 Monomers 113
5.2.1 Monomers Containing Flexibilizing Spacers 113
5.2.2 Monomers with Bulky Side Substituents 114
5.2.3 Monomers Containing Cardo Moieties 115
5.2.4 Monomers Containing Trifluoromethyl Groups 115
5.3 Polymerization 116
5.3.1 Low Temperature Solution Polycondensation 117
5.3.2 High Temperature Phosphorylation Polyamidation Reaction 119
5.4 Major Problem with Aromatic Polyamides 121
5.5 Approaches to Processable Polyamides 121
5.6 Processable Linear Aromatic Polyamides 122
5.6.1 Polyamides Containing Flexibilizing Spacers 122
5.6.2 Polyamides with Bulky Side Substituents 124
5.6.3 Polyamides with Cardo Moieties 131
5.6.4 Polyamides Containing Trifluoromethyl Groups 132
5.7 Processable Hyperbranched Aromatic Polyamides 134
5.8 Properties 143
5.9 Applications 149
5.9.1 Aromatic Polyamides for Membrane Application 149
5.9.1.1 Aromatic Polyamides for Pervaporation Application 149
5.9.1.2 Aromatic Polyamides for Gas Separation Application 151
5.9.1.3 Aromatic Polyamides as Reverse Osmosis and Nanofiltration Application 153

5.9.1.4 Aromatic Polyamides as Ion Exchange Membrane 154
5.9.2 Polyamides with Special Properties 155
5.9.2.1 Optically Active Polyamides (OAPs) 155
5.9.2.2 Luminescent and Electrochromic PAs 156
5.10 Conclusion 162
5.11 References 162

6 Phosphorus-Containing Polysulfones 167
Oana Petreus and Tudor Petreus
6.1 Introduction 167
6.2 Synthesis of Phosphorus Containing Polysulfones 171
6.2.1 Functionalization of Preformed Polysulfones 171
6.2.1.1 Functionalization of Sulfone Moiety 171
6.2.1.2 Functionalization of the Bisphenol A Moiety 173
6.2.2 Polycondensation of Phosphorus Containing Diols with Dihalogen Substituted Aromatic Sulfones 175
6.3 Properties of Phosphorus-Containing Polysulfones (P-PSF) 178
6.3.1 Spectral Features 178
6.3.2 Solubility 180
6.3.3 Thermal Stability 180
6.3.3.1 Thermal Gravimetric Aspects 181
6.3.3.2 Glass Transition and Mechanical Properties 185
6.3.3.3 Differences Between Thermal and Thermo-Oxidative Degradation of Phosphorus Containing Polysulfones 186
6.4 High Performance Applications of Phosphorus-Containing Polysulfones 188
6.4.1 Membrane Materials in Proton exchange Membrane Fuel Cell 188

6.4.2 Protein-Adsorption-Resistant Membranes 191
6.4.3 Flame Resistant Materials 195
6.5 References 198

7 Synthesis and Characterization of Novel Polyimides 205
Atsushi Morikawa
7.1 Introduction 205
7.2 Synthesis of Polyimides 207
7.2.1 Two-step Procedure 207
7.2.2 One-step Procedure 208
7.2.3 Three-step Procedure 210
7.3 Properties of Aromatic Polyimides 211
7.3.1 Kapton-type Polyimide 211
7.3.2 Biphenyl-type Polyimides and Polyimides with a Connecting Group (-X-) between the Phthalimides 212
7.3.3 Polyimides from Characteristic Monomers 212
7.3.3.1 Polyimides from Isomeric Biphenyltetracarboxylic Dianhydrides 212
7.3.3.2 Polyimides from Isomeric Oxydiphthalic Anhydride 217
7.3.3.3 Polyimides Containing p-Phenylene Units, $-(C_6H_4)m-$ (m = 2, 3, 4), between Phthalimides 222
7.3.3.4 Polyimides Containing Ester Linkages, $-COOC_6H_4OCO-$, between Phthalimides 235
7.3.3.5 Polyimides Containing Ether Linkages, -O-Ar-O- (Ar: Bulky Moiety) 234
7.4 Conclusions 238
7.5 References 240

8 The Effects of Structures on Properties of New Polytriazole Resins 243
Farong Huang, Liqiang Wan, Lei Du, Yanhong Hu, Yanpeng E and Yujing Li
8.1 Introduction 244

8.2 The Preparation of Polytriazole Resins 245
8.3 Reactivity of Crosslinkable Polytriazole Resins 251
8.4 Glass Transition Temperatures of Polytriazole Resins 253
8.4.1 The Effect of Molecular Rigidity and Polarity on the Glass Transition Temperature (Tg) 253
8.4.2 The Effect of Monomer Functionality on Tg 255
8.4.3 The Effect of Crosslinked Network Grid Size on Tg 256
8.5 Mechanical Properties of Polytriazole Resins 259
8.5.1 The Effect of Structures On Mechanical Properties of Polytriazole Resins 259
8.5.2 The Effect of Crosslinking on Mechanical Properties of Polytriazole Resins 259
8.6 Dielectric Properties of Polytriazole Resins 260
8.7 Thermal Stabilities of Polytriazole Resins 261
8.8 Conclusions 263
8.9 Acknowledgement 265
8.10 References 265

9 High Performance Fibers 269
Mehdi Afshari, Richard Kotek, Peng Chen
Introduction 269
9.1 PIPD or "M5" Rigid Rod 270
9.1.1 A New HM-HT Fiber 270
9.1.2 Monomer Selection and Syntheses 271
9.1.3 Polymerization 273
9.1.4 Fiber Spinning and Fiber Properties 274
9.1.5 Applications and Outlook 278
9.2 "Zylon" PBO Rigid Rod Polymer Fibers 279
9.2.1 Introduction 279
9.2.2 Monomer Synthesis 281
9.2.3 Polymerization 283
9.2.4 Solution Properties 285
9.2.5 Fiber Spinning 285
9.2.6 Structure and Morphology 287
9.2.7 Fiber Properties 290
9.2.7.1 Mechanical Properties 290

9.2.7.2 Thermal Properties 294
9.2.7.3 Ballistic Properties 295
9.2.7.4 Applications and Outlook 295
9.3 Aromatic Polyamide-Rigid Rod "Kevlar" Poly(p-Phenylene Terephthalamide) Fibers 296
9.3.1 Introduction 296
9.3.2 Polymer Synthesis 299
9.3.3 Fiber Spinning 301
9.3.4 Structure and Properties 303
9.3.5 Application and Outlook 306
9.4 Spectra, Dyneema UHMWPE Flexible Polymer Chain 307
9.4.1 Introduction 307
9.4.2 Polymerization 309
9.4.3 Spinning and Fiber Properties 312
9.4.4 Application and Outlook 318
9.5 Carbon Fibers 318
9.5.1 Introduction 318
9.5.2 PAN-Based Carbon Fibers 319
9.5.3 Pitch-Based Carbon Fibers 319
9.5.4 Vapor-Grown Carbon Fibers 321
9.5.5 Carbon Nanotubes 321
9.5.6 Applications 322
9.6 Advances in Improving Performance of Conventional Fibers 323
9.6.1 Introduction 323
9.6.2 Conventional Methods 324
9.6.3 Innovative Liquid Isothermal Bath (Lib) Method 325
9.6.3.1 Liquid Isothermal Bath (LIB) 326
9.6.3.2 Properties of LIB Fibers 327
9.6.3.3 Morphology of LIB Fibers 330
9.7 Conclusions 331
9.8 Acknowledgments 331
9.9 References 332

10 Synthesis and Characterization of Poly (aryl ether ketone) Copolymers 341
G Wang
10.1 Introduction 341

10.2 General Synthetic Methods of PAEK Copolymers 342
10.3 Synthesis and Characterization of Structural Poly (aryl ether ketone) Copolymers 342
10.4 Synthesis and Characterization of Liquid Crystalline Poly (aryl ether ketone) Copolymers 351
10.5 Synthesis and Characterization of Poly (aryl ether ketone) Copolymers with Pendent Group 367
10.6 Synthesis and Characterization of poly (aryl ether ketone) copolymers with Containing 2 ,7 -Naphthalene Moieties 377
10.7 References 383

11 Liquid Crystalline Thermoset Epoxy Resins 387
P. Kannan and P. Sudhakara
11.1 Liquid Crystals 387
11.1.1 Characterization of Liquid Crystals 390
11.1.2 Electric and Magnetic Field Effects 391
11.1.3 Liquid Crystalline Polymers (LCPs) 392
11.2 Liquid Crystalline Thermosets Based on Epoxy Resins 392
11.3 Synthesis and Physical Properties of LCERs 396
11.3.1 Synthesis of LCERs 396
11.3.2 Cure Behavior LCERs 399
11.3.3 Properties of Liquid Crystal Epoxy Thermosets Cured in a Magnetic Field 403
11.3.4 Curing of LCERs at Different Temperatures 406
11.3.5 Curing of LCERs with Deferent Curing Agents 407
11.3.6 Fracture Mechanism of LCTs 407
11.3.7 Water Absorption 412
11.3.8 Thermal Properties 414
11.4 References 420

Index 423

Preface

During the last years, several new families of high performance polymers and engineering plastics have been reported which find enhanced application potential in the more challenging areas like aerospace, defense, energy, electronics, automotives etc. as compared to the commodity or conventional polymers. Such polymers provide improved set of properties like higher service-temperatures at extreme conditions and good mechanical strength, dimensional stability, thermal degradation resistance, environmental stability, gas barrier, solvent resistance, electrical properties etc. even at elevated temperatures. Various categories of high performance polymers include poly(phenylene ether), polysulfones, poly(aryl ether ketone), poly(oxadiazole), poly(imide), poly(ether amide), poly(ether amide imide), poly(naphthalene), liquid crystalline polymers and poly(amide imide) etc. Owing to the large number of such high performance polymers with accurately designable structure property correlations developed and reported in the recent years, the book aims to focus on up-to-date synthesis details, properties and applications for such systems in order to stress the high potential of these engineering polymers.

The subject of high performance polymers and engineering plastics is introduced in Chapter 1 where a review of various categories of materials such as poly(ether amide), poly(ether amide-imide), poly(arylene ether), benzoxazine polymers, poly(ether ether ketone) (PEEK), polytriazole, hyperbranched conjugated polymers, are presented. Chapter 2 focuses on the synthesis and properties of polyxadiazoles. The applications of these polymers are also discussed. Chapter 3 describes conjugated polymers based on benzodithiophene for organic electronics. Polsulfone based iononers are discussed in Chapter 4. Various routes of ionomer synthesis are described. High performance processable aromatic polyamides are reviewed in Chapter 5. Various polymerization strategies as well as

applications of such polymer systems are presented. Properties and applications of phosphorus-Containing polysulfones are the focus of Chapter 6. Synthesis and characterization of novel polyimides are then described in Chapter 7. The effect of chemical structure of the polytriazole resins on thermal, mechanical, and dielectric properties are discussed in Chapter 8 while Chapter 9 describes various high performance fibers synthesized from high performance polymer matrices. Synthesis and characterization of poly (aryl ether ketone) copolymers is the subject of Chapter 10 whereas synthesis and properties of liquid crystalline thermoset epoxy resins are presented in Chapter 11.

It gives me immense pleasure to thank Scrivener Publishing and John Wiley for kind acceptance to publish the book. I dedicate this book to my mother for being constant source of inspiration. I express heartfelt thanks to my wife Preeti for her continuous help in co-editing the book as well as for her ideas to improve the manuscript.

Vikas Mittal
May 10, 2011

List of Contributors

Mehdi Afshari is currently Research and Development Scientist at Fiberweb Inc., and Adjunct Assistant Professor at North Carolina State University. He obtained his PhD in Polymer and Fiber Science from Amirkabir University of Technology in 2002. In 2006, he joined North Carolina State University as a Research Associate and then became a Research Assistant Professor. From 2002–2006 he was an Assistant Professor in Textile Engineering Department at Yazd University, Iran.

Susanta Banerjee is currently an Associate Professor in the Materials Science Centre, Indian Institute of Technology, Kharagpur, India. His research interests includes high performance polymers, membrane based separations and polymeric materials in general. He has published more than 100 research papers in international journals and supervised more than 25 students for their master and PhD degrees.

Peng Chen is working at Ningbo Institute of Materials Technology and Engineering in China and earned his PhD in Polymer Engineering. He was Research Associate at North Carolina State University from 2006–2008.

Lei Du is an honorable Professor at East China University of Science & Technology.

Yanpeng E is pursuing his PhD in the School of Materials Science and Engineering at ECUST. His current research interests include click chemistry, adhesives, and heat-resistant polymers and composites.

Dominique de Figueiredo received his PhD in 2002 from the Universidade Federal do Rio de Janeiro, Brazil and in 2002 she moved to Germany where she worked at GKSS on her postdoctoral activities. In 2006 she was awarded with the direction of a

Helmholtz-University Young Investigators Group on the development of functionalized polyoxadiazole nanocomposites in cooperation with the Technical University of Hamburg-Harburg. After moving to the chemical industry, she gained her six sigma green belt in 2009. She is currently working at Lehmann & Voss & Co. in Hamburg with the development of LUVOCOM® high performance engineering thermoplastic compounds.

Yanhong Hu is engaged in the research of polymer design and synthesis, especially for the resins and their carbon fibers reinforced composites with high properties, such as interface modification of fiber reinforced resin matrix composites. She is also familiar with the analyses and characterization of polymers and chemicals. She has published articles in more than 30 journals in recent years as well as authoring 4 patents.

Farong Huang is a member of the Chinese Society of Composites and Director of Key Laboratory for Specially Functional Polymeric Materials and Related Technology of the Ministry of Education at ECUST. His research interests focus on the design, synthesis and chemical modification of specialty polymers, the surface, interfaces and manufacture techniques of advanced polymeric composites, and the functional polymeric materials. He is an author or coauthor of more than 200 article as well as 4 books. He has contributed to more than 30 Chinese patents.

Cristina Iojoiu graduated as a Chemical Engineer and obtained her PhD in 2001 from the Montpelier 2 University, France and "Gh. Asachi" University, Iasi, Romania. She is a CNRS scientist at LEPMI, France and her research focuses on the development of electrolytes for electrochemical devices based on polymers and ionic liquids (PEMFC, lithium batteries and photovoltaic cells). She has published more than 40 peer-reviewed papers, 3 book chapters and is co-inventor of 8 patents.

P. Kannan obtained his PhD degree from Anna University, Chennai in 1988 and worked as a Research Associate at the Indian Institute of Science, Bangalore during 1988–1991. He joined the Department of Chemistry, Anna University in 1991 as a lecturer and has been a Professor since 2008. He worked as a Post-Doctoral Fellow at Washington University of St. Louis, during 1999–2000. Fourteen students have earned their PhD under his supervision. He has published 90 research papers in national and international journals.

His research interests are in the domains of fire retardant, photo-crosslinkable, liquid crystalline polymers, LC thermosets, polymer-metal complexes, optical data storage, and photo and electrically switchable polymers.

Richard Kotek is Associate Professor in the College of Textiles at North Carolina State University since 1999. He graduated from the Man-Made Fibers Institute at Lodz Polytechnic, Poland. Following completion of his PhD he worked at the Man-Made Fibers Institute and then as Research Associate at Duke University, and finally joined the R&D department at BASF.

Yujing Li is pursuing her PhD in the School of Materials Science and Engineering at ECUST. Her current research interests include click chemistry, novel rigid polytriazole resins and their composites.

Samarendra Maji is working as a postdoctoral researcher in the Department of Chemistry at the Philipps-Universität Marburg. He obtained his PhD from the Indian Institute of Technology, Kharagpur, India. His research interests includes high performance polymers, biodegradable and biocompatible polymers, structure property-relationship studies of polymers.

Atsushi Morikawa studied organic materials science at the Tokyo Institute of Technology. In 1992 he obtained his doctor's degree on siloxane dendrimers and polyimide-silica hybrid materials by sol-gel method. After a two-year spell as a research engineer at Asahi Chemical Company, he transferred to the Faculty of Engineering at Ibaraki University to continue his research on poly(ether ketone) dendrimers and polyimides.

Oana Petreus is a senior researcher at "Petru Poni" Institute of Macromolecular Chemistry from Iasi, Romania. She has a PhD in chemistry (1979) and has published 3 books and more than 120 articles in international journals. She is the author of 17 patents. She leads and is a coworker to many national and international scientific programs and is a specialist in synthesis of organic and macromolecular compounds with phosphorus, halogens, nitrogen and sulfur used as flame retardants.

Tudor Petreus, MD and PhD (cell and molecular biology), is an Assistant Professor and researcher at "Gr.T.Popa" University of Medicine and Pharmacy Iasi, Romania and vice president of Iasi Branch of the Romanian Society for Biomaterials. He has published

3 books (as co-author) and more than 50 journal articles. He is leading a research team on matrix metalloproteinase's inhibitors. His other main research areas are extracellular matrix proteins investigation and the biomaterials-cell interface investigation by a proteomic approach.

Racki Sood obtained in 2009 a Masters of Science diploma in the field of Functionalized & Advanced Materials - Erasmus Mundus Joint program (Grenoble-INP, France & University of Liege, Belgium). She is now working on her PhD in the field of Polymer Electrolytes for Fuel Cells collaborating with three laboratories in France: LEPMI-St. Matin D'Heres; SPrAM-CEA-Grenoble; LMPB-Claude Bernard 1- Lyon University.

P. Sudhakara obtained his PhD from Anna University, Chennai in 2010. He was awarded Senior Research Fellowship by Council of Scientific & Industrial Research (CSIR), New Delhi, India in 2009. He joined as a Post-doctoral Researcher in the Department of Mechanical Engineering, Changwon National University, Changwon, South Korea in 2011. He has published 8 papers in national and international journals in the domain of photocross-linkable, liquid crystalline polymers, fire retardant LC thermosets, and natural fiber composites.

Liqiang Wan obtained his PhD in ECUST. He is now an Associate Professor at Key Laboratory for Specially Functional Polymeric Materials and Related Technology of the Ministry of Education at ECUST. His major interests are in the high properties resins and their fiber reinforced composites. He has published more than 20 papers, submitted more than 10 Chinese patent applications of which 4 have been approved.

Guibin Wang received his BS degree in 1988 from Jilin Institute of Engineering and Technology. He went to work at Jilin University where he obtained his PhD in 2000 in polymer chemistry and physics. In 2001 he became a full Professor. Wang's research interests are in synthesis, modification and processing of high performance polymer.

Wei You obtained his BS from University of Science and Technology of China in 1999. He obtained his PhD from the University of Chicago in 2004 and completed his postdoctoral training at Stanford University in 2006. He later joined the

University of North Carolina at Chapel Hill as an Assistant Professor in Chemistry. His research interests include organic solar cells, molecular electronics and spintronics.

Huaxing Zhou is currently a PhD candidate at the University of North Carolina at Chapel Hill. He obtained his BS degree in polymer chemistry from University of Science and Technology of China in 2007. His current research interests focus on rational design of conjugated polymers for organic solar cells.

This page intentionally left blank

1

High Performance Polymers: An Overview

V. Mittal

The Petroleum Institute, Chemical Engineering Department, Abu Dhabi, UAE

Abstract

During the last years, several new families of high performance polymers and engineering plastics have been reported which find enhanced application potential in the more challenging areas like aerospace, defense, energy, electronics, automotives etc. as compared to the commodity or conventional polymers. Such polymers provide improved set of properties like higher service-temperatures at extreme conditions and good mechanical strength, dimensional stability, thermal degradation resistance, environmental stability, gas barrier, solvent resistance, electrical properties etc. even at elevated temperatures.

Keywords: Poly(ether amide) and poly(ether amide-imide), poly(arylene ether), benzoxazine polymers, poly(ether ether ketone) (PEEK), polytriazole, hyperbranched conjugated polymers, alternating copolymers

1.1 Introduction

During the last years, several new families of high performance polymers and engineering plastics have been reported which find enhanced application potential in the more challenging application areas like aerospace, defense, energy, electronics, automotives etc. as compared to the commodity or conventional polymers. Such polymers provide improved set of properties like higher

Vikas Mittal (ed.) High Performance Polymers and Engineering Plastics, (1–20)
© Scrivener Publishing LLC

service-temperatures at extreme conditions and good mechanical strength, dimensional stability, thermal degradation resistance, environmental stability, gas barrier, solvent resistance, electrical properties etc. even at elevated temperatures. For example, aromatic polyesters and polybenzamide have decomposition temperatures around 480–500°C, whereas polybenzimidazole, polypyrrole and poly(p-phenylene) decompose around 650°C. Various other categories of high performance polymers include poly(phenylene ether), polysulfones, poly(aryl ether ketone), poly(oxadiazole), poly(imide), poly(ether amide), poly(ether amide imide), poly(naphthalene), liquid crystalline polymers and poly(amide imide) etc [1]. The raw materials involved in the synthesis of poly(phenylene ether) are described in Figure 1.1, whereas Figure 1.2 shows the chemical structures of the monomers used for the synthesis of poly(oxadiazole) polymers [1]. Poly(aryl ether ketone)s have aromatic groups in the main chain and both the ether group and the keto group are in the backbone. Liquid crystal polymers partly maintain the crystal structure is in the liquid phase above the melting point and exhibit a long range orientational order. Molecular structure/processability/property relationships of many of high performance polymers and engineering plastics have been reported in the literature along with their applications, a brief overview of a few of which is provided in the following sections.

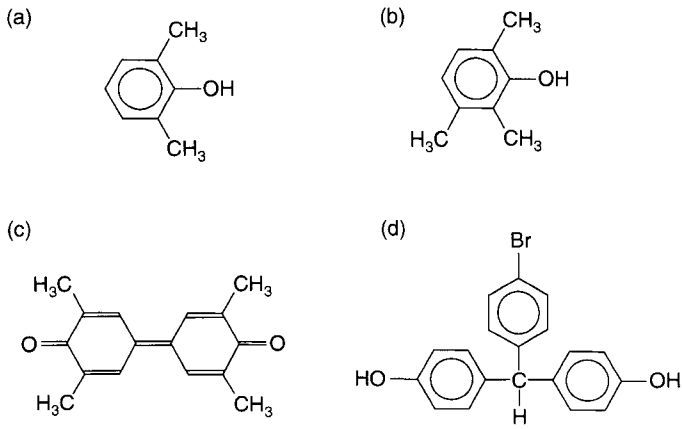

Figure 1.1 Monomers used for the synthesis of poly(phenylene ether) [1], (a) 2,6-xylenol, (b) 2,3,6-trimethylphenol, (c) tetramethyldiphenylquinone and (d) 4-bromo-4′,4″-dihydroxytriphenylmethane.

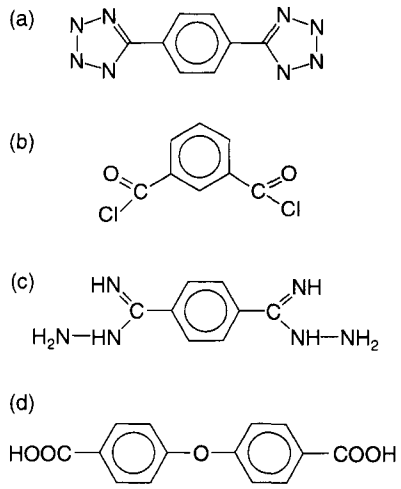

Figure 1.2 Monomers used for the synthesis of poly(oxadiazole) [1], (a) 1,4-phenylene-5,5′-tetrazole, (b) isophthaloyl chloride, (c) 1,4-benzenedicarboximidic acid dihydrazide and (d) 4,4′-diphenylether dicarboxylic acid.

1.2 Poly(ether amide) and Poly(ether amide-imide)

Vora [2] reported the synthesis and properties of high-performance thermoplastic fluoro-poly(ether amide)s (6F-PEA), fluoro-poly(ether amide-imide)s (6F-PEAI), and their co-polymers. The synthesis was based on the 6F-polyimide chemistry using using the novel state-of-the-art 2-(3,4′-carboxy anhydrophenyl-2(4-carboxyphenyl) hexafluoropropane (6F-TMA) and 2,2′-bis(4-carboxyphenyl) hexafluoropropane (6F-DAc) monomers. Various co-polymers like fluoro-copoly(ether amide-(ether imide))s (6F-co(PEA-PEI)), fluoro-copoly(ether amide-(ether amide-imide))s (6F-co(PEA-PEAI)) and fluorocopoly(ether amide-imide-(ether imide))s (6F-co(PEAI-PEI)) were also synthesized. The authors synthesized the films of the polymers and studied their their solution properties, solubility, morphology, thermal and thermo-oxidative stability, and moisture absorption. The polymers had high viscosity and high degree of polymerization with narrow polydispersity between 1.7 and 2.9. Figure 1.3 shows the synthesis schemes for these polymers and copolymers. It was ascertained by XRD spectroscopy that the

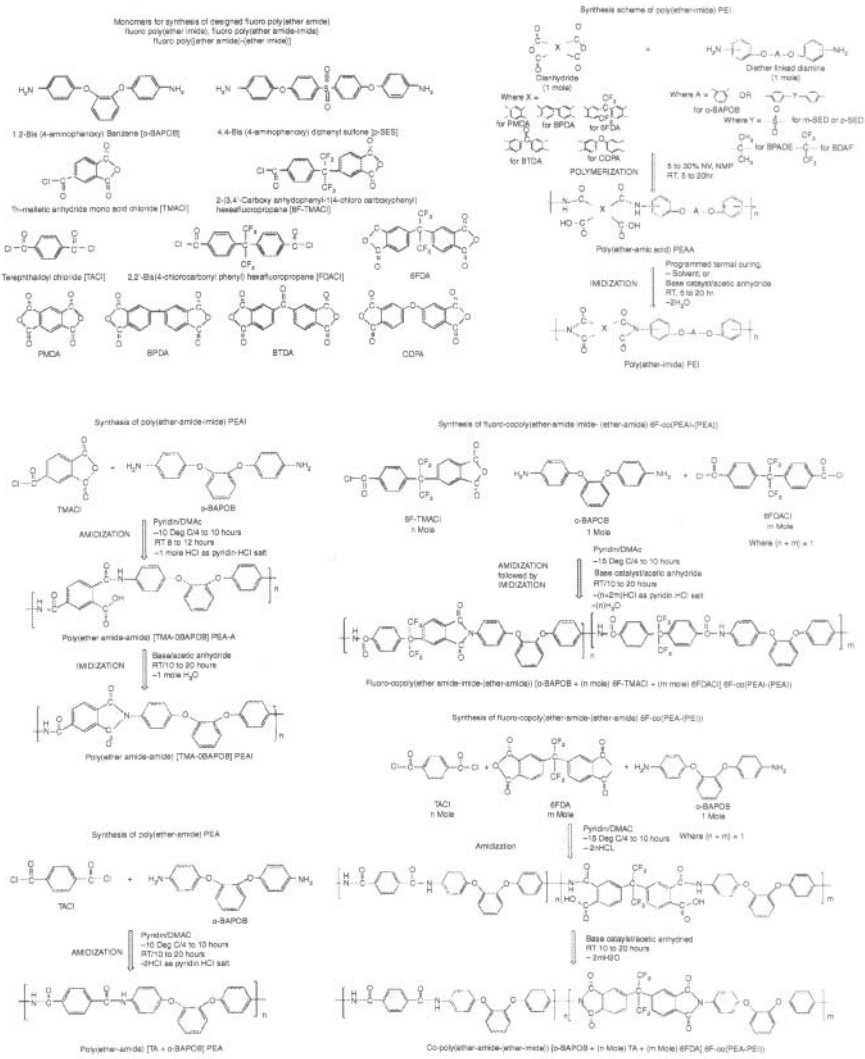

Figure 1.3 Chemical structures of the monomers, poly(ether amide) & poly(ether amide-imide) polymers and their copolymers. Reproduced from reference 2 with permission from Elsevier.

polymers were amorphous in nature as no peaks were observed in the diifractograms measured in the range of 10 to 35° 2θ. The polymers were observed to be soluble in almost all organic solvents and the films prepared by thermal curing at elevated temperature were either partially soluble or insoluble in such solvents indicating

increased solvent resistance. The polymers were observed to possess moderate to high glass transition temperatures (Tg). The TGA analysis indicated that the 5% weight losses for the polymers in air were in the range of 480–515°C. The weight loss in nitrogen was observed on an average about 15–25°C higher than in air. The polymers also had excellent thermal resistance in isothermal heating at temperature 300°C for 300 h. Most of the polymers had low moisture uptake at 100% relative humidity at 50°C over 100 h. The amorphous nature of the polymers led to their easy processability into films, sheets, molded articles, etc. Dielectric constant values of all the synthesized fluorinated polymers was observed in the range of 2.85 to 3.1 measured at 1 kHz at 25°C. These values were also lower than the values reported for the commercially available non-fluorinated polymers. The authors also commented on the enhancement of polymer properties by the addition of inorganic montmorillonite clays as filler.

Xie *et al.* [3] also reported the synthesis of polyimides with low moisture absorption and high hygrothermal stability. Four different aromatic dianhydrides, viz. 4,4′-oxydiphthalic anhydride (ODPA), 3,3′,4,4′-benzophenone tetracarboxylic dianhydride, 4,4′-(hexafluoroisopropylidene)diphthalic anhydride, and pyromellitic dianhydride were used during the synthesis and the resulting polyimides are shown respectively in Figure 1.4. The authors observed better solubility over a wider range of solvents in the case of chemically imidized films when compared to the films prepared by thermal methods owing to more compact structure due to stronger aggregation of the polyimide molecules during thermal imidization. The authors also suggested that the cemical method leads to incomplete imidization which was the cause of lower stability of the films generated by this method.

Rajagopalan *et al.* [4] reported the synthesis of sulphonated polyetherimide and subsequent synthesis of ionic polymer metal composites (IPMC) by depositing platinum on both sides of the polymer membrane by electroless plating process for use in actuators. The TGA and NMR analysis confirmed the successful incorporation of sulfonic groups in the polymer backbone. The content of sulfur in the polymer membrane was measured to be 4.68% by EDX analysis and the degree of sulfonation could also be controlled. SEM micrographs of the composite membrane also confirmed the uniform formation of small platinum particles on the surface of polymer membrane as shown in Figure 1.5. The thickness of

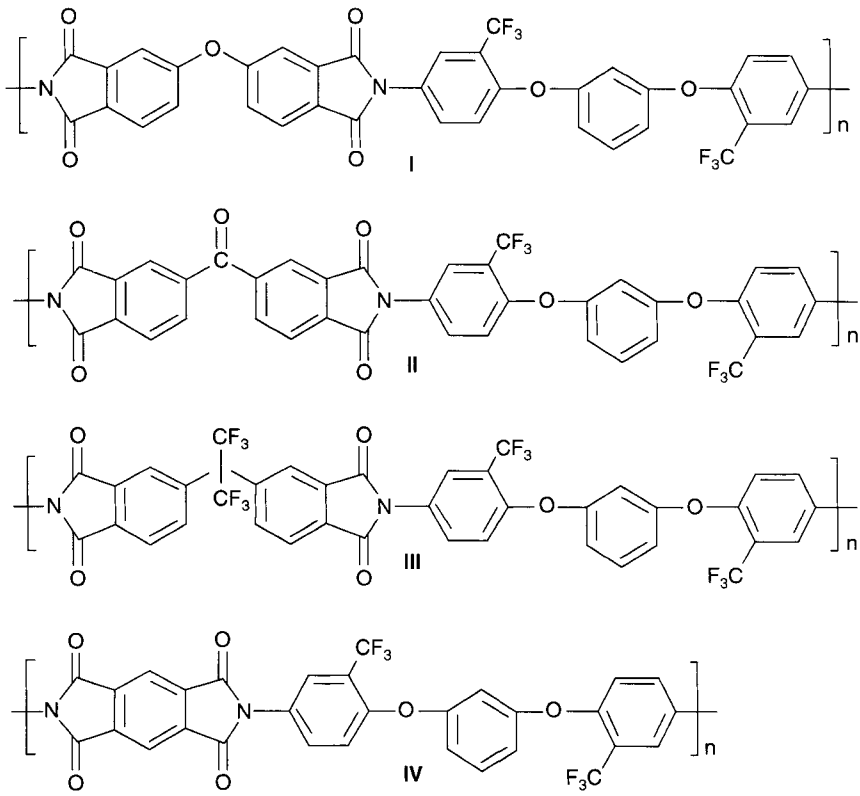

Figure 1.4 Structures of poly(ether imide) polymers synthesized from 1,3-bis (4-amino-2-trifluoromethylphenoxy)benzene and various anhydrides. Reproduced from reference 3 with permission from Elsevier.

platinum coating was observed to be 15–18 μm. The surface of the uncoated membrane was very smooth whereas platinum deposition led to the formation of rough surface morphology. The ionic polymer–metal composite actuator showed good harmonic and step responses similar to an electro-active polymer.

Guhathakurta *et al.* [5] characterized the polyelectrolytes based on sulfonated PEI and triazole. Bisphenol A based polyetherimide was sulfonated using trimethylsilylchlorosulfonate (TMSCS) as sulfonating agent. Polyelectrlayes were prepared by solution blending of sulfonated PEI and triazole in the presence of dimethylacetamide. The amount of sulfonated PEI and traizole was altered, the PEI had also different degrees of sulfonation. The effect of degree of sulfonation in the sulfonated PEI and triazole concentration in the

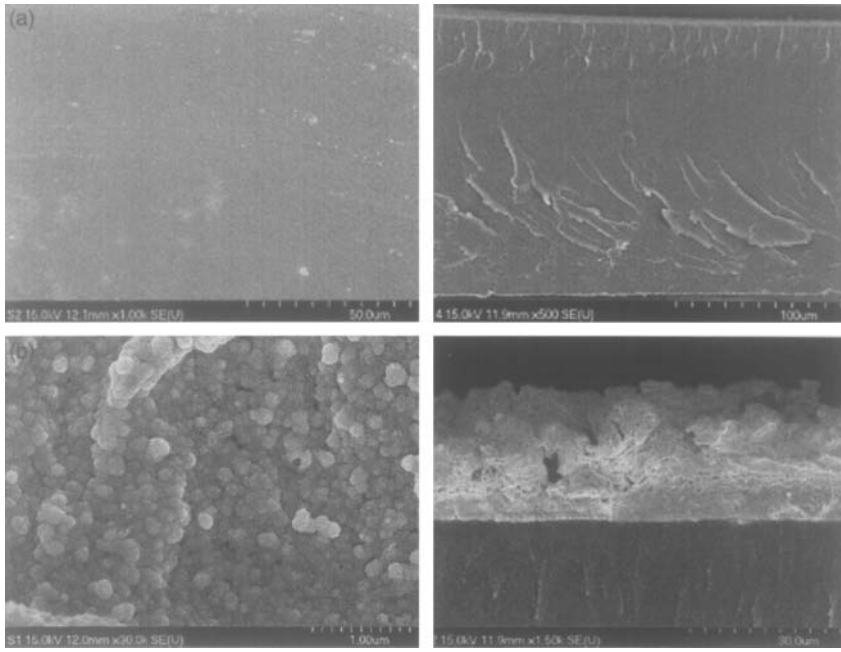

Figure 1.5 SEM micrographs of the (a) surface and cross-section of the sulfonated PEI membrane and (b) surface and cross-section of the platinum coated sulfonated PEI membrane. Reproduced from reference 4 with permission from Elsevier.

blend on size, shape and crystal morphology of triazole crystals in sulfonated polyetherimide were examined. It was observed that at a constant triazole weight percent, increased sulfonation level caused enhanced nucleation density, reduction of crystallite size and their uniform distribution throughout the polymer matrix as shown in Figure 1.6. The crystal domains were also elevated at lower sulfonation level and embedded at higher level of sulfonation.

1.3 Poly(arylene ether)

Dhara *et al.* [6] reviewed the synthesis and properties of poly(arylene ether) polymers. The role of trifluoromethyl groups on the polymerization process and polymer properties was also demonstrated. Kim *et al.* [7] also reported the synthesis of hyperbranched pol(arylene ether) polymer. The selective and sequential displacement of the

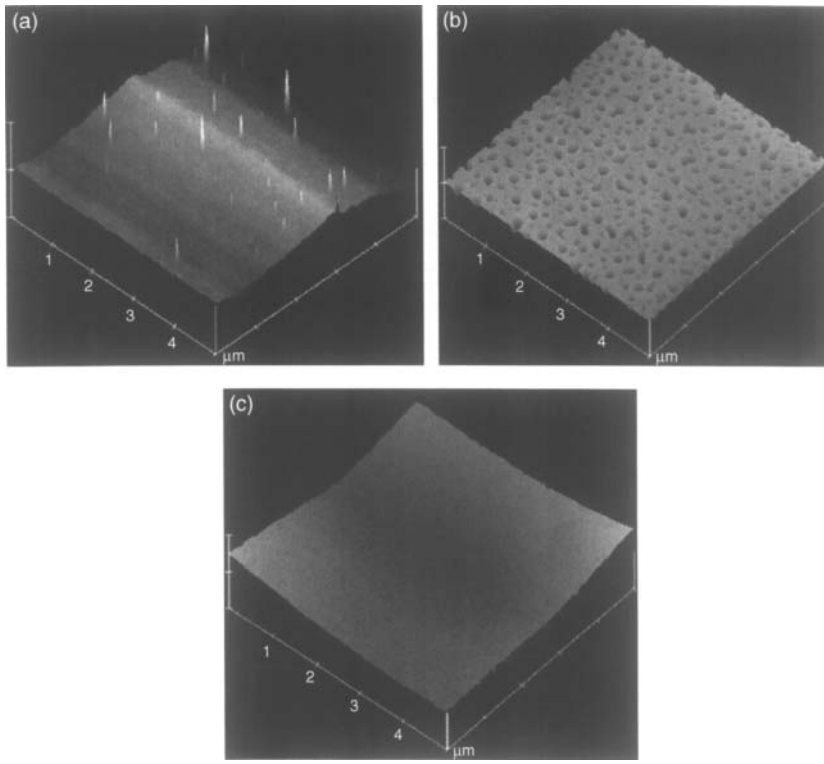

Figure 1.6 Tapping mode three dimensional topographic images of suphonated PEI and triazole (70:30) polyelectrolytes. Degree of suphonation (a) 22%, (b) 48% and (c) 62%. Reproduced from reference 5 with permission from Elsevier.

fluorine group and the nitro group of 5-fluoro-2-nitrobenzotrifluoride was used as a basis for the synthesis of the hyperbranched poly(arylene ether) containing pendent trifluoromethyl groups as shown in Figure 1.7.

1.4 Benzoxazine Polymers

Liu *et al.* [8] reported improved processability of main-chain benzoxazine polymers by synthesizing novel benzoxazine main-chain oligomers which are low in viscosity. Bisphenol-F based benzoxazine monomers were obtained from the reaction of bisphenol-F isomers, para-formaldehyde and aniline in toluene. Main chain benzoxazine oligomers were obtained by the reaction involving

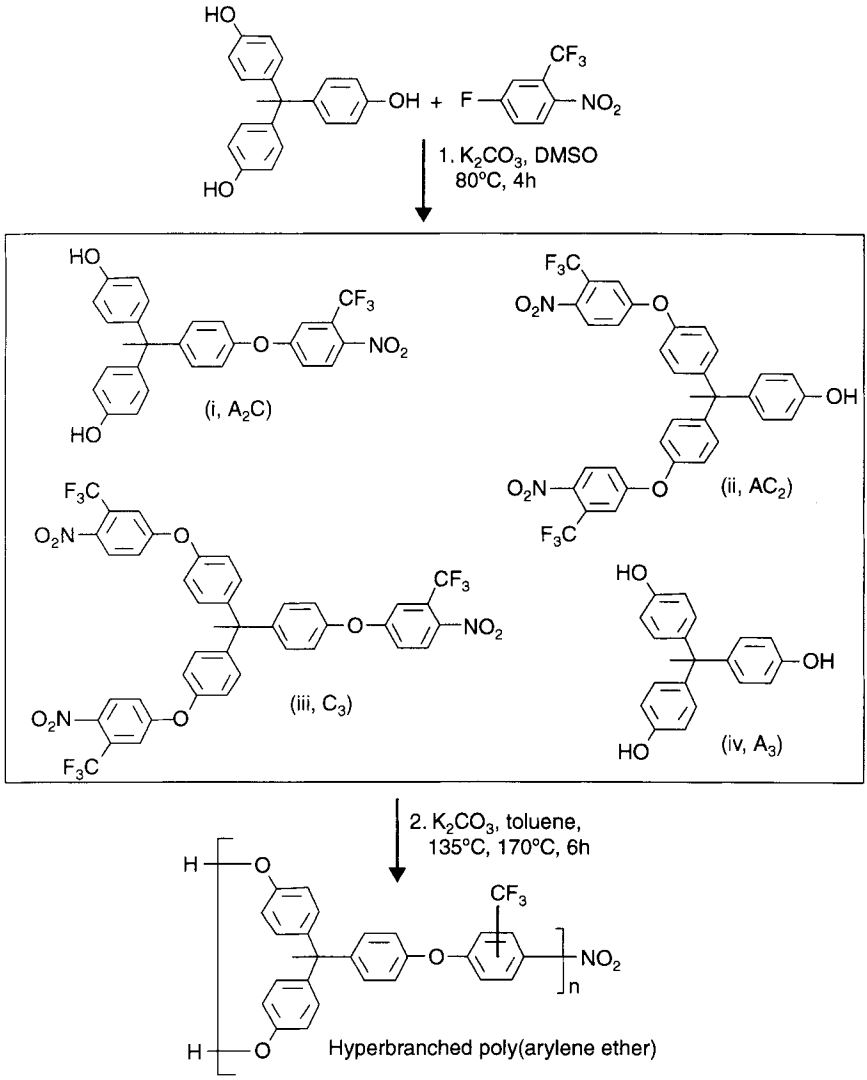

Figure 1.7 Synthesis of hyperbranched poly(arylene ether). Reproduced from reference 7 with permission from American Chemical Society.

bisphenol-F isomers, aniline, 4,4′-diamino-diphenylmethane and para-formaldehyde. The polymer films from both monomers and oligomers were obtained by casting followed by thermal curing. For the thermoset polymerized from benzoxazine monomers, the glass transition temperature (Tg) was determined to be 154°C.

On the other hand, the crosslinked polybenzoxazine derived from benzoxazine oligomers had a glass transition temperature of 213°C. The increase in glass transition temperature for the crosslinked polymers from oligomers was due to the presence of the difunctional amine linkage. The polybenzoxazines derived from the oligomers also showed an increase in 5% weight loss temperature as compared to polybenzoxazines derived from the monomers owing to reduced evaporation rate around 300°C. Figure 1.8 shows the synthesis strategy of bisphenol-F isomer-based benzoxazine monomer and oligomers.

Choi *et al.* [9] also reported the synthesis of functional benzoxazine monomers and polymers containing phenylphosphine oxide. Phosphorus-containing group was introduced into polybenzoxazine via monomer modification. Three phosphorus-containing bisphenol compounds, bis(4-hydroxyphenyl)phenylphosphine oxide (BHPPO), bis(4-hydroxyphenoxyphenyl) phenylphosphine

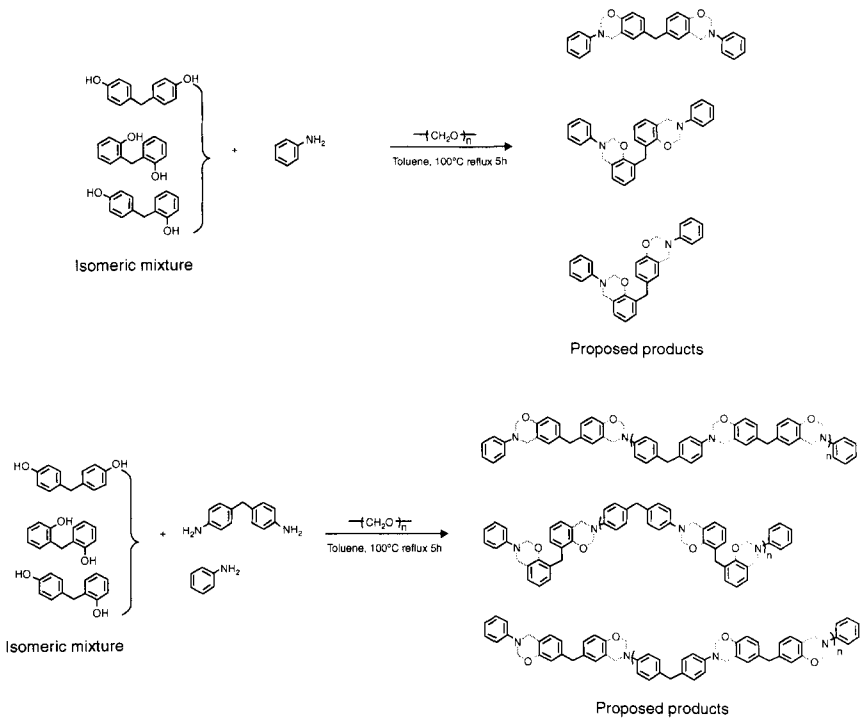

Figure 1.8 Synthesis of bisphenol-F isomer-based benzoxazine monomer and oligomers. Reproduced from reference 8 with permission from Elsevier.

oxide (BPPPO), and bis(4-hydroxyphenoxy)phenylphosphine oxide (BPHPPO) were synthesized as starting materials for the synthesis of benzoxazine monomers. Polymerization was carried out by ring opening polymerization initiated thermally. The presence of phenylphosphine oxide group in the polymer chain led to an improvement in the thermal stability of polybenzoxazines. Figure 1.9a shows the scheme of the synthesis of bis(4-benzyloxyphenoxy)phenylphosphine oxide (BBHPPO) and bis(4-hydroxyphenoxy)phenylphosphine oxide (BPHPPO). A schematic representation of the synthesis of BPHPPO-based benzoxazine monomers (R1, R2, and R3 represent methyl, phenyl, and 3-ethynylphenyl, respectively) is shown in Figure 1.9b. Thermal degradation patterns were found to be similar for all the BHPPO-based, the BPPPO-based and the BPHPPO based benzoxazine polymers. Methylamine and aniline-based polymers showed a distinct two-stage degradation pattern while the acetylene functionalized polymers showed a one-stage degradation pattern. The extent of char yield was also different in the different polymers. As an example, in BPPPO and BPHPPO, the aniline-based polymers showed a char yield of 51% (thus significant improvement of thermal stability) as compared to the methylamine-based polymers (31% char yield).

1.5 Poly(ether ether ketone) (PEEK)

Sulfonation of polymers is an important chemical modification process utilized for enhancing proton conductivity of proton conductive polymers. Inan *et al.* [10] reported the sulfonation of PEEK by reaction with concentrated sulfuric acid. The glass transition temperature was reported by the authors to be affected significantly by the degree of sulfonation of the polymer. Figure 1.10 shows the enhancement if the glass transition temperature as a function of degree of sulfonation. At 80% degree of sulfonation, the glass transition temperature increased from 167°C for pure PEEK to 238.5°C upon sulfonation owing to the incorporation of bulkier sulfonyl groups in the polymer chain.

Blends of PEEK with other high performance polymers have also been reported for applications like fuel cells. Inan *et al.* [10] reported the blend of sulfonated PEEK with poly(vinylidene fluoride) (PVDF). Effect of the type and molecular weight of the fluorinated polymer was investigated for low temperature fuel cell

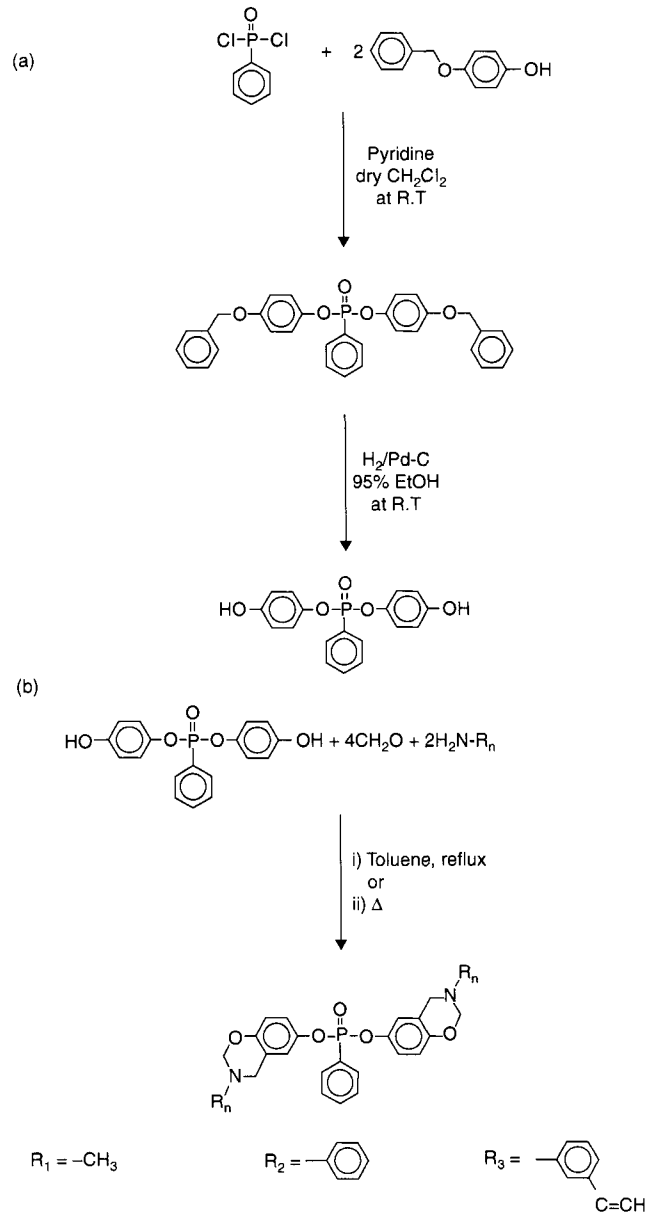

Figure 1.9 (a) Scheme showing the synthesis of bis(4-benzyloxyphenoxy) phenylphosphine oxide (BBHPPO) and bis(4-hydroxyphenoxy)phenylphosphine oxide (BPHPPO) and (b) schematic representation of the synthesis of BPHPPO-based benzoxazine monomers (R1, R2, and R3 represent methyl, phenyl, and 3-ethynylphenyl, respectively). Reproduced from reference 9 with permission from Elsevier.

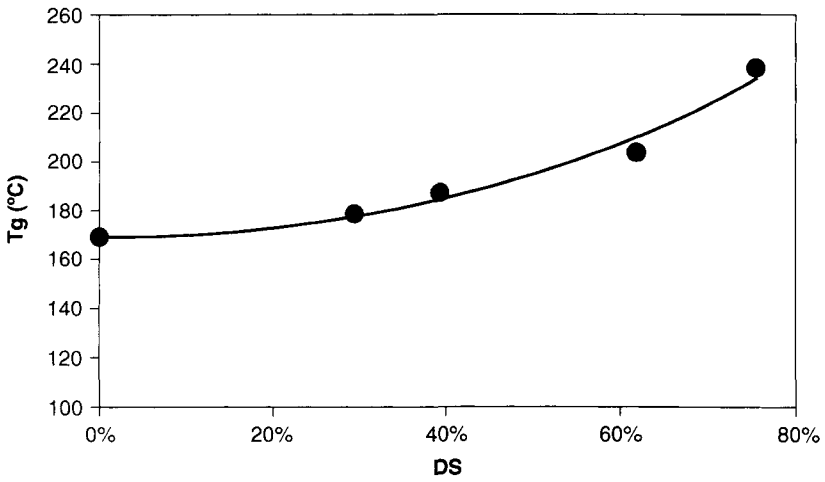

Figure 1.10 Increase in glass transition temperature as a function of degree of sulfonation. Reprinted from reference 10 with permission from International Association of Hydrogen Energy.

applications. Figure 1.11 shows the SEM micrographs of the blend membranes of sulfonated PEEK with varying amounts of PVDF of different molecular weights. The blend membranes were observed to have homogeneous structure and no phase separation was observed. Phase separated morphology was however observed for PVDF-HFP (Figure 1.11d) in all concentrations suggesting that PVDF-HFP and sulfonated PEEK are thermodynamically immiscible due to their dissimilar structures.

Fu *et al.* [11] reported the acid–base blend membranes based on 2-amino-benzimidazole (basic polymer) and sulfonated poly(ether ether ketone) (SPEEK) (acidic polymer) for direct methanol fuel cells. A novel polymer, polysulfone-2-amide-benzimidazole (PSf-ABIm), using carboxylated polysulfone and 2-amino-benzimidazole was synthesized for this purpose. The blend membrane of SPEEK/PSf-ABIm showed high performance a s represented by Figure 1.12. The blend membrane with 3 wt% PSf-ABIm was evaluated continuously for 120 h and little or no decline in performance was found after 120 h. On the other hand, the Nafion 112 membrane standard was observed to have a decline in performance due to a much higher amount of methanol crossover.

The authors opined that the membranes based on acidic and basic polymer blends can offer a promising strategy to replace

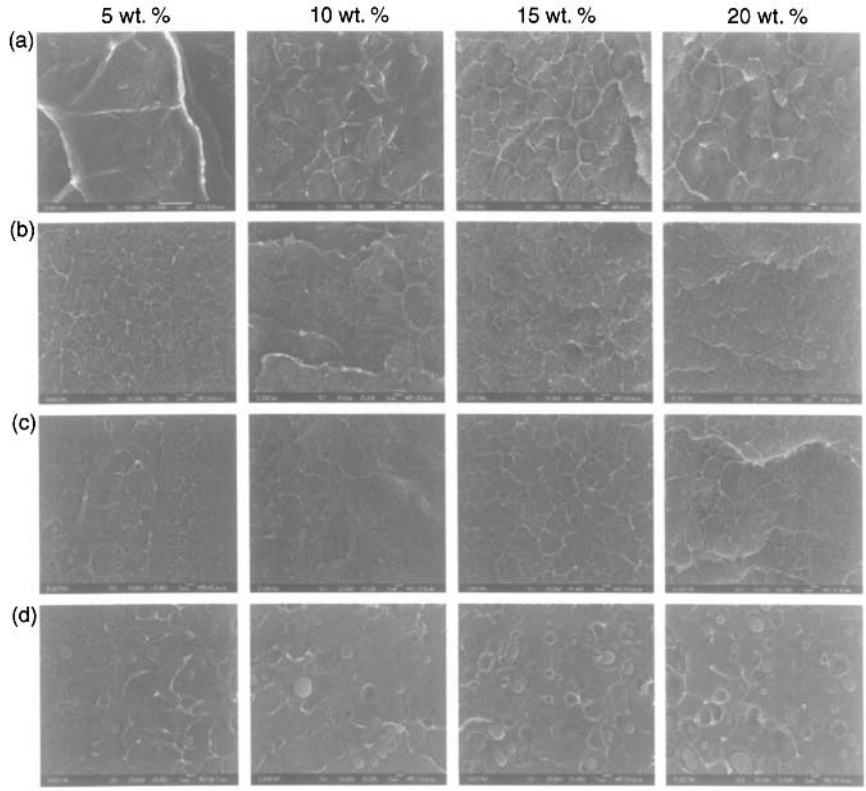

Figure 1.11 SEM micrographs of the sulfonated PEEK/PVDF blend membranes with different amounts of PVDF (a) Mw = 180,000 g/mol (b) Mw = 275,000 g/mol (c) Mw = 530,000 g/mol and (d) Mw = 130.000 g/mol PVDF-HFP (Poly(vinylidene fluoride-co-hexzafluoro propylene)). Reprinted from reference 10 with permission from International Association of Hydrogen Energy.

lithium ion batteries in portable electronic devices like laptop computers and cell phones.

1.6 Polytriazole

Boaventura *et al.* [12] reported the generation of polytriazole based proton conducting membranes. Sulfonated polytriazole membranes were doped with three different agents: 1H-benzimidazole-2-sulfonic acid, benzimidazole and phosphoric acid. Figure 1.13 also shows the storage modulus and tan δ curves for pure polymer

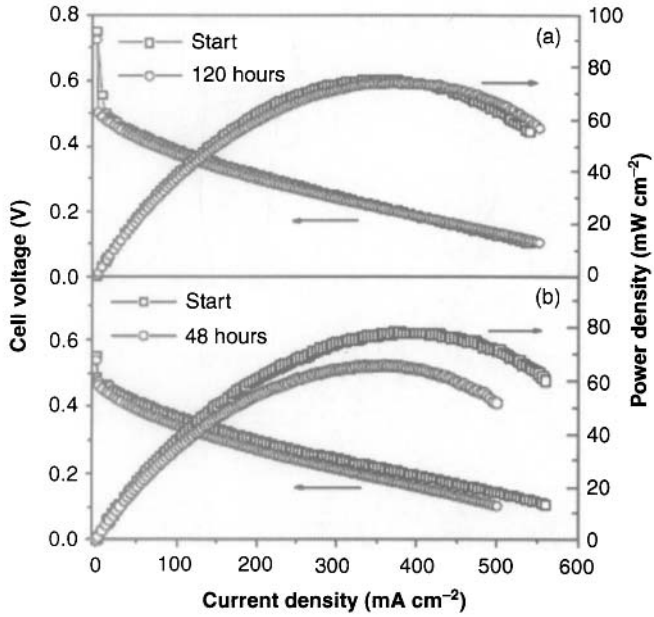

Figure 1.12 Long-term performance tests carried out with the (a) SPEEK/PSf-ABIm blend membrane and (b) Nafion 112 membrane. Reproduced from reference 11 with permission from Elsevier.

membrane and membranes after doping with different amounts of 1H-benzimidazole-2-sulfonic acid (BiSA) and benzimidazole (BI). The glass transition temperature was observed to generally decrease with increasing the doping agent concentration. This was attributed to the plasticization of the chain backbone after doping. The plasticizing effect in the case of doped membranes also led to the reduction in the storage modulus. It was further observed that adding BI and BiSA to polytriazole did not significantly improve the conductivity of the membranes, whereas doping with phosphoric acid led to the generation of membranes with conductivity of 2.10^{-3} S cm^{-1} at 120°C and 5% relative humidity.

1.7 Hyperbranched Conjugated Polymers

Hyperbranched conjugated polymers (HBPs) are specialty high performance polymers which possess advanced structure and properties as compared to conventional linear conjugated

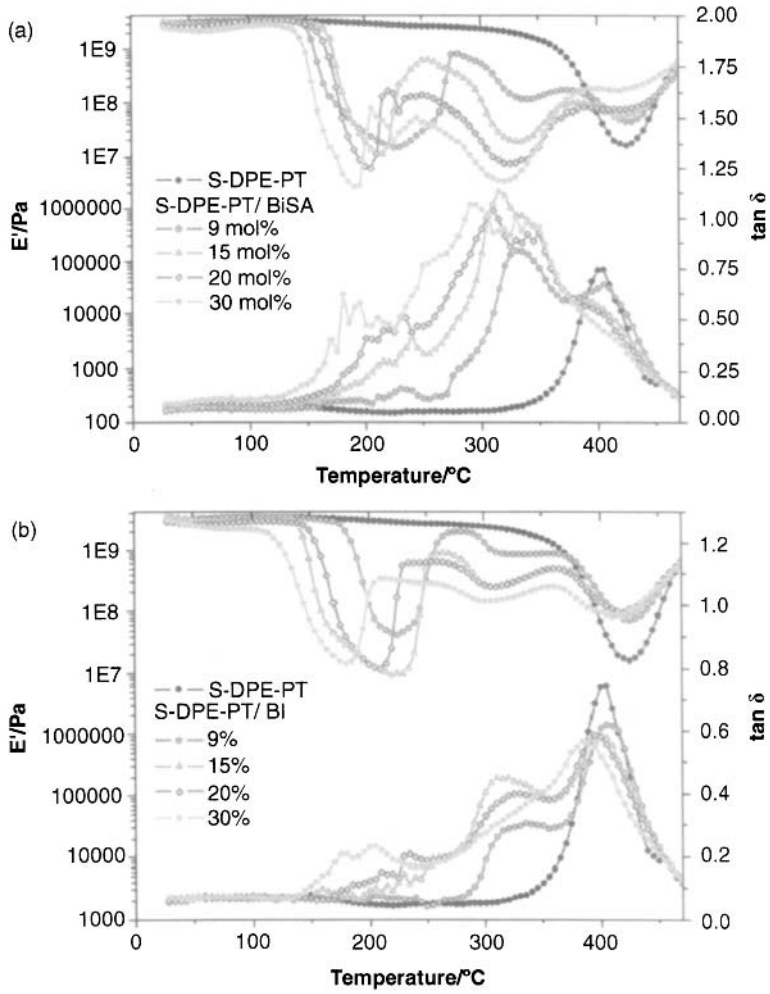

Figure 1.13 Storage modulus and tan δ curves (a) for pure polymer membrane and doped with 9, 15, 20 and 30 mol% of BiSA and (b) for pure polymer membrane and doped with 9, 15, 20 and 30 mol% of BI. Reproduced from reference 12 with permission from International Association of Hydrogen Energy.

polymers. Tang *et al.* [13] reported the synthesis and photovoltaic properties of three HBPs photosensitizers (H-tpa, H-cya, and H-pca). The chemical structures of these Hyperbranched polymers are shown in Figure 1.14. The polymer had the same conjugated core structure and different functional terminal units. The polymers were synthesized following Wittig-Horner polymerization

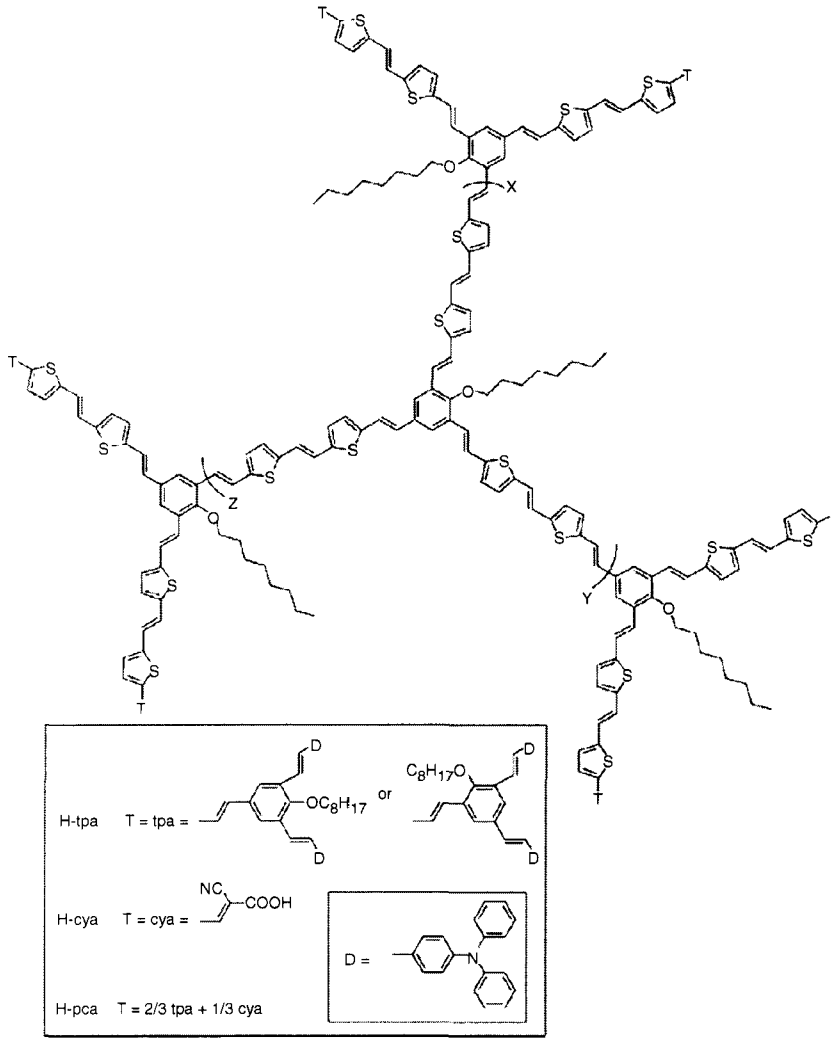

Figure 1.14 Chemical structure of the hyperbranched conjugated polymers. Reproduced from reference 13 with permission from Elsevier.

method. The polymers had broad absorption band in the range of 260–600 nm which was consistent with the hyperbranched structure of conjugation chain length. Two distinct absorption bands were exhibited by all the polymers: one absorption band is in the UV region (271–284 nm) and the other is in the visible region (413–455 nm). The authors reported that the donor-π-acceptor

architecture in hyperbranched molecule benefited intramolecular charge transfer and consequently increased the generation of photocurrent. It was observed that the three-dimensional (3D) steric configuration of generated hyperbranched polymers effectively suppressed the aggregation of dyes on TiO_2 film, which was beneficial for achieving good photovoltaic functional performance.

Qu *et al.* [14] reported the synthesis of carbazole-based hyperbranched conjugated polymers. These carbazole-based hyperbranched conjugated polymers which were linked with triphenylamine and benzene moieties were synthesized by Sonogashira coupling polycondensation of N-octadecyl- and N-octyl-3,6-diethynylcarbazoles with tris(4-iodophenyl)amine and 1,3,5-tribromobenzene. Figure 1.15 shows the synthesis strategy for these polymers. The generated polymers were solvent-soluble polymers and had number-average molecular weights in the range of 3500–21,000. The absorption spectrum of polymers was red-shifted as compared to

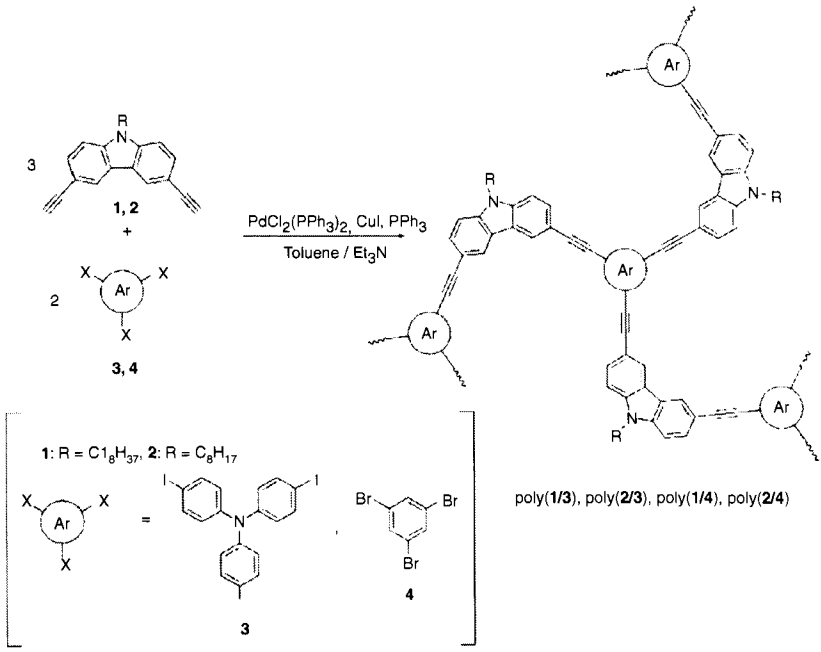

Figure 1.15 Polycondensation reaction of N-alkyl-3,6-diethynylcarbazoles **1** and **2** with tris(4-iodophenyl)amine (**3**) and 1,3,5-tribromobenzene (**4**) for the synthesis of carbazole based hyberbranched conjugated polymers. Reproduced from reference 14 with permission from Elsevier.

carbazole which confirmed the extension of conjugation length. The fluorescence quantum yields of the hyperbranched polymers reached 67% in $CHCl_3$, which were larger than those of polyacetylenes carrying carbazole moieties in the side chains. There were differences in the fluorescence quantum yields among the polymers, as the fluorescence quantum yields of poly(1/3) and poly(1/4) which had longer N-alkyl chains were larger than those of poly(2/3) and poly(2/4), respectively. The branched structure of the polymers was observed to be effective to suppress the decay of fluorescence. The polymers were observed to be electronically redox-active.

1.8 Alternating Copolymers

Lim *et al.* [15] reported the synthesis of a new thienylenevinylene–benzothiadiazole copolymer, poly{1,2-(E)-bis[2-(5-bromo-3-dodecyl-2-thienyl)-5-thienyl]ethene-2,1,3-benzothiadiazole} (PETVTBT) for potential use in solar cells. Thus generated alternating copolymer comprised of electron-rich 1,2-(E)-bis[2-(5-bromo-3-dodecyl-2-thienyl)-5-thienyl]ethane and electron-deficient 2,1,3-benzothiadiazole units. Figure 1.16 shows the synthesis scheme of the PETVTBT polymer. The copolymer was thermally stable with a decomposition temperature of 390°C (loss of less than 5% of weight). The differential scanning calorimetry analysis revealed the glass transition

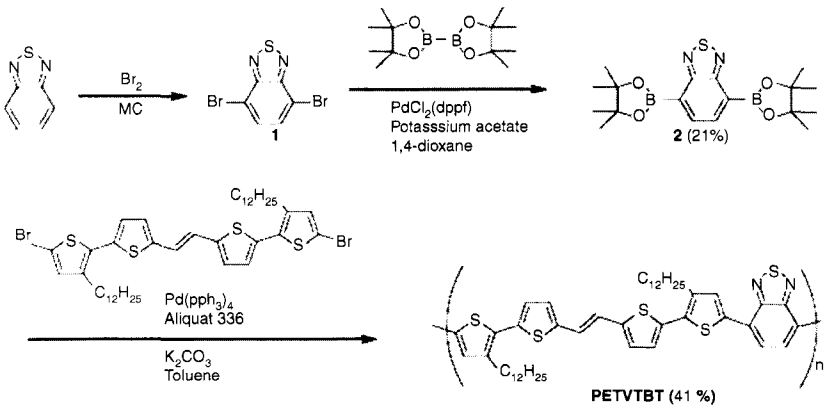

Figure 1.16 Synthesis scheme for PETVTBT polymer. Reproduced from reference 15 with permission from Elsevier.

temperature of 149°C for the polymer. The UV–vis absorption spectrum of PETVTBT covered a broad absorption range 350–700 nm. The optical band gap of PETVTBT was observed to be 1.57 eV, which lied near to the ideal band gap for a polymer solar cell. The potential of the usefulness of the generated copolymer in polymer solar cell applications was further confirmed by low HOMO level of about 5.1 eV and relatively high hole mobility of 0.025 cm^2/Vs.

1.9 References

1. J.K. Fink, *High Performance Polymers*, New York, William Andrew, 2008.
2. R.H. Vora, *Materials Science and Engineering B*, Vol. 168, p. 71, 2010.
3. K. Xie, J.G. Liu, H.W. Zhou, S.Y. Zhang, M.H. He, and S.Y. Yang, *Polymer*, Vol. 42, p. 7267, 2001.
4. M. Rajagopalan, J.-H. Jeon, and I.-K. Oh, *Sensors and Actuators B*, Vol. 151, p. 198, 2010.
5. S. Guhathakurta, and K. Min, *Polymer*, Vol. 50, p. 1034, 2009.
6. M.G. Dhara, and S. Banerjee, *Progress in Polymer Science*, Vol. 35, p. 1022, 2010.
7. Y.J. Kim, M.A. Kakimoto, and S.Y. Kim, *Macromolecules*, Vol. 39, p. 7190, 2006.
8. J. Liu, T. Agag, and H. Ishida, *Polymer*, Vol. 51, p. 5688, 2010.
9. S.-W. Choi, S. Ohba, Z. Brunovska, K. Hemvichian, and H. Ishida, *Polymer Degradation and Stability*, Vol. 91, p. 1166, 2006.
10. T.Y. Inan, H. Dogan, E.E. Unveren, and E. Eker, *International Journal of Hydrogen Energy*, Vol. 35, p. 12038, 2010.
11. Y. Fu, A. Manthiram, and M.D. Guiver, *Electrochemistry Communications*, Vol. 9, p. 905, 2007.
12. M. Boaventura, M.L. Ponce, L. Brandao, A. Mendes, and S.P. Nunes, *International Journal of Hydrogen Energy*, Vol. 35, p. 12054, 2010.
13. Y. Tang, P. Shen, T. Ding, H. Huang, B. Zhao, and S. Tan, *European Polymer Journal*, Vol. 46, p. 2033, 2010.
14. J. Qu, M. Shiotsuki, N. Kobayashi, F. Sanda, and T. Masuda, *Polymer*, Vol. 48, p. 6481, 2007.
15. B. Lim, J. Jo, D. Khim, H.-G. Jeong, B.-K. Yu, J. Kim, and D.-Y. Kim, *Organic Electronics*, Vol. 11, p. 1772, 2010.

2

Synthesis and Properties of Polyoxadiazoles

Dominique de Figueiredo Gomes

**GKSS Research Centre Geesthacht GmbH, Institute of Materials Research, Geesthacht, Germany*

Abstract

This chapter is focused on polyoxadiazoles, whose mechanical properties are high enough to enable their use as film, fibers, membranes, sheets or polymer matrices for composites. Although the synthesis of polyoxadiazoles, has been a known process for more than forty years, many aspects related to the synthesis of high molecular weight polyoxadiazoles have not been properly understood yet. Probably the observed experimental fluctuations in laboratory scale have been the major drawback for the systematic use of polyoxadazole in certain applications and for the design and scale-up of its synthesis. An understanding and proper control of its synthesis is described here as an essential prerequisite to achieve tailor-made polyoxadiazoles with great potential for engineering applications requiring thermally and chemically resistant polymers.

Keywords: Polyoxadiazole, molecular weight, mechanical properties, thermal stability, sulfonation, composites, coating, corrosion, fuel cell, PEMFC, proton conductivity, carbon nanotubes

2.1 Introduction

There have been many misunderstandings as to how the well known chemically, thermally and mechanically stable polyoxadiazoles

*Actual address: Lehmann & Voss & Co., Schimmelmannstraße 103, D-22043 Hamburg, Germany.

Vikas Mittal (ed.) High Performance Polymers and Engineering Plastics, (21–48)
© Scrivener Publishing LLC

synthesized in actual lab-scale polymerization reactors do not fulfill these properties as stated. While during the 60's the majority of the works relied on insoluble aromatic polyoxadiazole in common organic solvents [1], e.g. with a phenylene group attached to the main chain, in the 90's polyoxadiazoles with easier processability but at the same time with unexpected lower chemical and mechanical stabilities have been investigated [2–4]. Gomes *et al.* [5–7] have shown that not only poor micromixing is the major drawback for the polyoxadiazole synthesis but also the chemical group attached to the main polyoxadiazole chain. For instance, the replacement of an ether electron-donor substituent (-O-) in *para* position to the oxadizole groups in the main chain by an electron-withdrawing group (-C-$(CF_3)_2$-) in *para* position increased significantly the chemical stability of the polyoxadiazole [6]. While for polyoxadiazole containing diphenyl ether groups after treatement for 1 h in lower acid concentration, H_2SO_4: oleum (20% SO_3) (3:1), the molecular weight decreased significantly (from 358000 to 17000 g mol^{-1}) [7], for the fluorinated polyoxadiazole no changes in the molecular weight could be observed even in more drastic conditions, 19 days in H_2SO_4: oleum (30% SO_3) (2:1) [6].

Whatever the kind of the chemical group attached to the main polyoxadiazole chain as well as the synthesis route, correlations among final polyoxadiazole properties with the synthesis parameters remained unclear for a long time. Different methods for polyoxadiazole synthesis have been described in the literature [8–13]. However, two of these methods seem to be more advantages to synthesize polyoxadiazole (preparation of polymers with higher molecular weight and lower residual hydrazide content): the solid state cyclodehydration of polyhydrazides [8, 11–13], and the polymerization of a dicarboxylic acid and a salt of hydrazine in solution [2, 4, 5, 10, 13]. Both methods are presented schematically in Figure 2.1. Gomes *et al.* [5, 10, 14] have performed the first systematic studies on the influence of distinct synthesis parameters on the final properties of a polyoxadiazole containing a diphenyl ether group attached to the polymer chain by both methods. These works [10, 14] were also the firsts that relied on a statistical experimental design to analyze the simultaneous effects of various synthesis parameters. Therefore, it was not surprising to find out that these works were the firsts to report reproducibility problems during the polyoxadiazole synthesis, which is the realm of these syntheses. During the synthesis of the polyoxadiazoles an intermediate

Method 1: Cyclodehydration of polyhydrazide

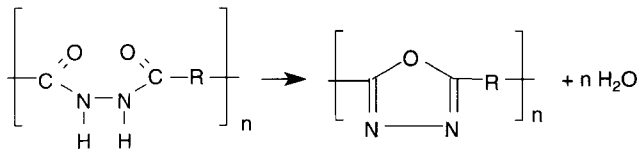

Method 2: Polymerization in solution of a dicarboxylic acid with a salt of hydrazine

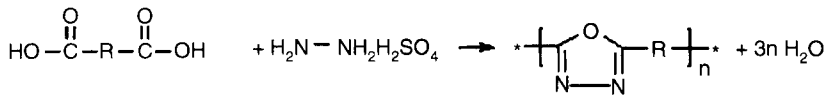

Figure 2.1 Common methods used for the polyoxadiazole synthesis.

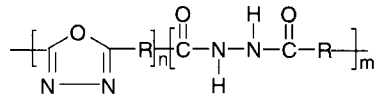

Figure 2.2 Poly(1,3,4-oxadiazole-hydrazide) copolymer.

linear polymer, polyhydrazide, is formed. Depending on the reaction conditions, residual hydrazide groups can be present in the final polymer [15], leading to the formation of a poly(oxadiazole-hydrazide) copolymer (Figure 2.2). However, the hydrazide groups present neither the thermal nor the chemical stability of the oxadiazole rings. Particularly, the outstanding thermal stability of poly(1,3,4-oxadiazole)s (stable up to 450°C) was ascribed to the fact that the oxadiazole ring is spectrally and electronically equivalent to the p-phenylene ring structure.

The polymerization in solution of a dicarboxylic acid with a salt of hydrazine follows the classical mechanism of polymerization by polycondensation [16]. In this case, the polymerization takes place by the continuous reaction between the functional groups of the multi-functional molecules. The basic characteristics of these reactions are known since the beginning of the 20's century [17] and include the continuous growth of the average molecular weight with the time, the high sensitivity to mono-functional impurities and the possibility of formation of three-dimensional crosslinked structures, when there is presence of three or more reactive groups per molecule. The main sources of fluctuation of the average molecular weight presented by the polymerization in solution of a dicarboxylic

acid in poly(phosphoric acid) are the high viscosity of the reaction medium, degradation reactions caused by the acid solvent, and the occurrence of secondary reactions (non-linear cyclodehydration reaction and crosslinking reaction) which compete with the linear cyclodehydration reaction of polyhydrazide into polyoxadiazole. The influence of each of these factors will then depend even more on the chemical group attached to the main polyoxadiazole chain, resulting in some cases in powder polyoxadiazoles with very low mechanical stability or "spaghettis" structures with very higher molecular weights and outstanding chemical stabilities (Figure 2.3).

For this reason, the polyoxadiazole synthesis may present low reproducibility and different polymer materials may be produced at similar reaction conditions at actual lab-scale polymerization reactors [10]. These observed experimental fluctuations constitute a major drawback for the systematic use of polyoxadiazole in certain applications and for the design and scale-up of its synthesis.

2.2 Synthesis of Polyoxadiazoles in Poly(phosphoric acid)

The pioneering work of Iwakura *et al.* [1] regarding a route for production of polyoxadiazole based on the reaction of hydrazine sulphate with dicarboxylic acids, was published for more than forty years ago. Nevertheless, correlations among final polyoxadiazole

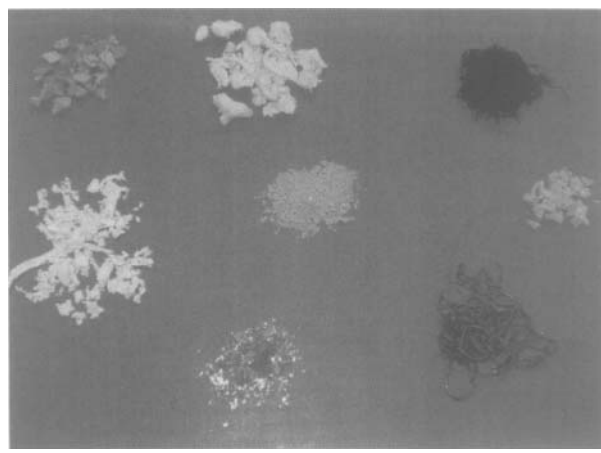

Figure 2.3 Morphologies of polyoxadiazole with different chemical groups attached to the main chain.

properties with the synthesis parameters remained unclear for a long time. So far, many aspects regarding the synthesis of high molecular weight polyoxadiazole have not been properly understood yet.

One of the factors affecting the reproducibility of the polyoxadiazole synthesis in poly(phosphoric acid), PPA, is poor micromixing, given the high viscosities of the reaction medium during the course of polymerization. The high viscosity of the reaction medium may cause significant fluctuations of local monomer compositions, leading to decrease of the polymer chain length. Gomes *et al.* [5, 10] suggested that homogenization should be improved through addition of an inert solvent into the reaction medium in order to improve the reproducibility of the polyoxadiazole properties synthesized at similar reaction conditions. Addition of small solvents amounts to PPA does not lead to improvement of mixing conditions [5]. The addition of large amounts of solvent into PPA could eventually cause the reduction of the solution viscosity. In this case, however, polymerization rates can be severely reduced, as reaction is catalyzed by PPA. Addition of small quantities of water into the reaction medium may be effective to reduce the PPA viscosity [10]. However, water may also interfere with the condensation reaction and modify the final polyoxadiazole properties.

Gomes *et al.* [5] have shown that the reproducibility of the polymerization in solution of a dicarboxylic acid with a salt of hydrazine is improved when the reactor load increases, indicating that micromixing effects may be indeed fundamental for proper understanding of the polyoxadiazole synthesis. It is also shown that removal of the residual acid solvent by tight control of the pH during polyoxadiazole purification exerts a significant impact on the final properties of the polymer material, which indicates that purification is a key process step during polyoxadiazole production.

Regarding the influence of the anhydride content (P_2O_5) in PPA, when the reactions were carried out in the presence of P_2O_5 [4], by keeping all reaction variables constant (temperature, time, monomer concentration, molar dilution) and then adding different amounts of P_2O_5 to the medium does not lead to any significant improvement of the reproducibility. Addition of P_2O_5 increased further the reaction medium viscosity, reaction mixture cannot be stirred in a reaction apparatus, decreasing homogenization.

More recently, Gomes *et al.* [18] have shown that by increasing the catalyst activity of PPA (or at least to keep it) without decreasing the homogenization of the reaction medium and avoiding micromixing

effects in the polymerization medium, polyoxadiazole with very high mechanical properties and a narrow final distribution of the molecular weight was achieved (Table 2.1). Figure 2.4 shows the stress-strain curves of the polymer film (The insert shows the SEC profile relative to polystyrene standard).

By aging treatment of PPA, free phosphoric acid content in the poly(phosphoric acid) has been increased, and in turn, its catalyst activity. The increase of phosphoric acid content in the poly(phosphoric acid) was followed by ^{31}P NMR spectroscopy analysis. Figure 2.5 shows the ^{31}P NMR the PPA spectrum after thermal treatment with the respective assignments for the phosphorus species. Table 2.2 shows the relative amounts of the three phosphorous

Table 2.1 Mechanical properties of POD by the previous method and after PPA aging.

Sample	Young Modulus (MPa)	Tensile Strength (MPa)	Elongation at Break (%)
Previous method	4016 ± 194	100 ± 5.04	14 ± 3.20
After PPA aging	3802 ± 268	190 ± 7.82	57 ± 5.03

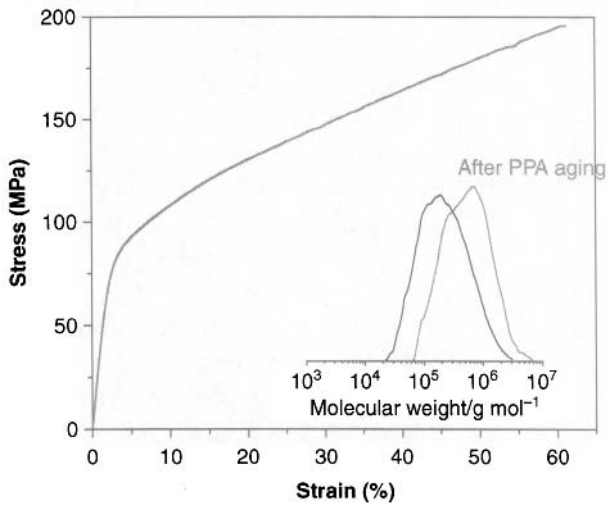

Figure 2.4 Stress-strain curves of the POD film, whose polymer was synthesized with the optimized reaction condition by thermal treatment of the poly(phosphoric acid).

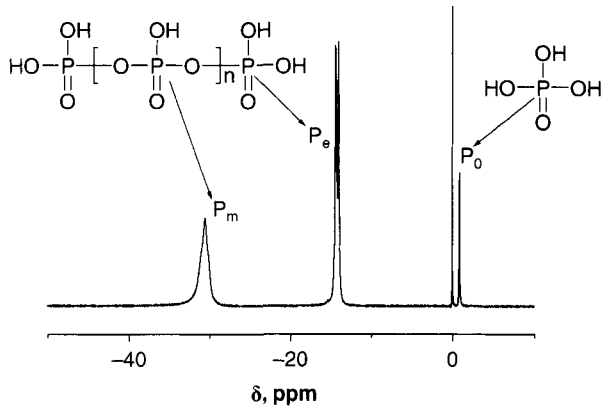

Figure 2.5 ^{31}P NMR the PPA spectrum after thermal treatment.

Table 2.2 Relative amounts of the phosphorous species before and after PPA aging.

PPA Aging Time (h)	P_0	P_e	P_m	Free Phosphoric Content ($P_0/P_0 + P_e + P_m$)
0	1.05	15.98	17.24	0.030
3	1.39	17.58	15.49	0.044

species before and after PPA aging, which were determined by integrating the individual P_0, P_e and P_m peaks. The analysis of Table 2.2 indicates that after PPA aging an increase of free phosphoric acid concentration and a decrease of the mid-chain phosphorous in the PPA are observed. The amount of free phosphoric acid is estimated to increase around 40%, which is enough to improve the catalyst activity of the PPA and therefore resulting in polyoxadiazole with very high molecular weights and mechanical properties.

2.3 Thermal and Mechanical Properties of Polyoxadiazoles

A series of polyoxadiazoles were synthesized by the single-step optimized method of synthesis at high temperature (160°C) using hydrazine sulfate in poly(phosphoric acid) during 3 to 6 h. Chemical structures of the polyoxadiazoles are shown in Figure 2.6.

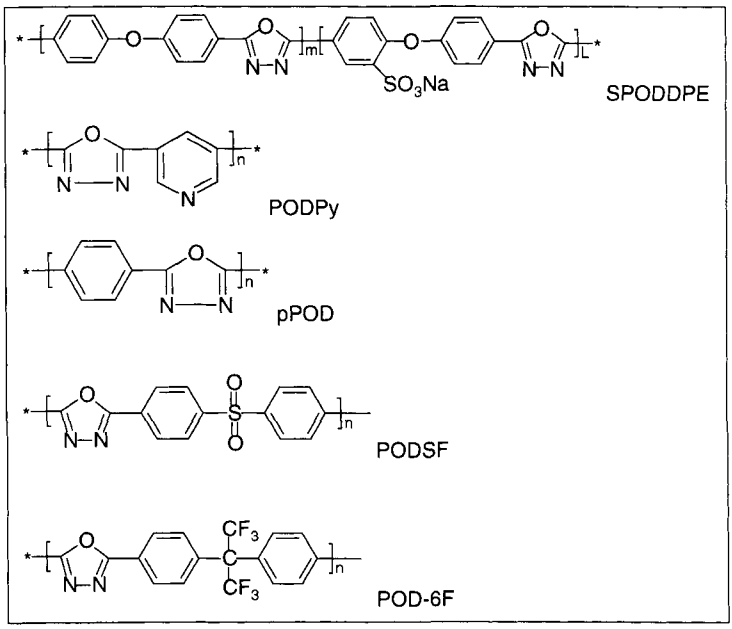

Figure 2.6 Polyoxadiazole structures with different chemical groups attached to the main chain.

The poly(phenylene-1,3,4-oxadiazole), pPOD, was synthesized in fuming sulfuric acid 20% SO_3 because the oleum has been shown to be a better solvent than poly(phosphoric acid) for this polymer [19–20]. The introduction of different groups in the main polyoxadiazole chain offers many advantages as the improve of polymer processability, thermal and chemical stability as well as allowing for design of specific properties (e.g. proton and electrical conductivity, gas selectivity and permeability, corrosion inhibition potential, outstanding chemical stability etc) relevant for different application fields. Most of time a compromise should be found when designing polymer molecular structures. For instance, the increase of polymer solubility in organic solvents normally is accompanied by a simultaneous decrease of chemical and/or hydrolytic stability. An additional factor is also that the chemical group changes monomer reactivity and solubility which further affects the polymerization design conditions. Therefore, the choice of the polymerization conditions depends on many factors such as the reactivity of the monomers, reaction time, solvent, homogeneity, polymer or monomer degradation stability, crosslinking and solubility of the polymer.

Whether the final mechanical and thermal properties of the polymers depend only on the chemical structure is not well addressed today. Iwakura *et al.* [21] have, for instance, reported poly-1,3,4-oxadiazoles where the phenylene ring has been replaced by a pyridine ring. These polymers were indeed soluble in formic acid and organic solvents; however polymers with very low inherent viscosities were obtained. Similarly, when polyoxadiazoles were synthesized under the same conditions by replacing a diphenyl ether group (SPODDPE) by a pyridine group (PODpy) a significant lower molecular weight was obtained for the PODpy (73.000 g/mol instead 358.000 g/mol) [22]. The PODpy polymer was soluble in formic acid and organic solvents but mechanical properties were very low and no film forming property was found.

pPOD and PODSF should have outstanding chemical stability but were insoluble in organic solvents and also the synthesis parameters to obtain high molecular weight polymers are not described in details in literature. Polyoxadiazoles containing sulfone linkages have already been prepared by cyclodehydation of their soluble intermediate polyhydrazide polymers [23]. Tensile strengths of these final polyoxadiazoles should be lower than 90 MPa, the maximum strength obtained for the intermediate polyhydrazides. As reported by Gomes [14], after polyhydrazide cyclodehydration significant decrease of molecular weight, and in turn, decrease of mechanical property occurs. Homopolymers or copolymers of polyoxadiazoles reported in literature so far are limited by a tensile strength of 100 MPa [23–28]. Except for SPODPE, where tensile strengths up to 250 MPa [29] have been obtained. In this section, emphasis will be given to the SPODDPE and POD-6F structures once many details regarding their synthesis to obtain high mechanical and thermal stability were pointed out [4–7, 10, 29].

The thermal stability of the poly(hexafluor propane-1,3,4-oxadiazole), POD-6F, was analyzed by thermogravimetric analysis (TGA) and dynamic mechanical thermal analysis (DMTA). No weight losses of eventually absorbed water were detected in the temperature range from 20 to 150°C. Furthermore in the range of temperatures between 275 and 375°C no loss of water which could result from conversion of hydrazide groups to oxadiazole [15] was observed. These results confirm the high hydrophobicity of the polymer, which first starts to decompose at 430°C. The mechanical property of the polymer was evaluated by means of DMTA. Good dimensional stability and high storage modulus (E′) of about 1 GPa

at 250°C were observed. With a molecular weight of 200000 g/mol, the glass transition temperature (T_g) is in the range 295–304°C (measured by DSC and DMTA) [6].

The thermal and mechanical properties of the sulfonated polyoxadiazole (SPODDPE) membranes in salt and in acid form were evaluated by means of dynamic mechanical thermal analysis. All SPODDPE show 5% weight loss in the range of 463–470°C and the residue at 500°C was in the range of 79–81%. Sulfonated polyoxadiazoles with high thermal stability with T_g ranging from 364 to 442°C in sodium salt form and from 304 to 340°C in acid form and with good mechanical properties (storage modulus about 3 GPa at 300°C) have been prepared.

Table 2.3 shows the T_g taken as the maximum in the tan δ and loss modulus (E″) curves. The increase of the sulfonation level of polymers resulted in an increase of the T_g. This result may be attributed to the introduction of bulky substituent on the aromatic rings, an increase of chain-chain interactions though hydrogen bonds and the inonic character of the substituent [30, 31]. As shown in Table 2.3, the type of counterion has a very strong effect on the dynamic mechanical properties of the membranes. When converted to the H-form, the T_g shifted to slightly lower temperatures. A higher T_g for the sodium salt form is expected [30, 31], since the dipole-dipole interaction between sodium sulfonate groups is much stronger than hydrogen-bond interaction between the SO_3H groups.

The tensile properties of polymer samples are directly affected by the molecular weight values [29]. Figure 2.7 shows the tensile strength

Table 2.3 T_g values of sulfonated poly(diphenyether-1,3,4-oxadiazole) membranes.

S/C (molar ratio) [a]	T_g (°C)			
	E″		Tan δ	
	-Na	-H	-Na	-H
0.065	364	304	396	307
0.098	415	322	429	328
0.103	416	321	430	333
0.124	430	330	442	340

[a]determined by elemental analysis.

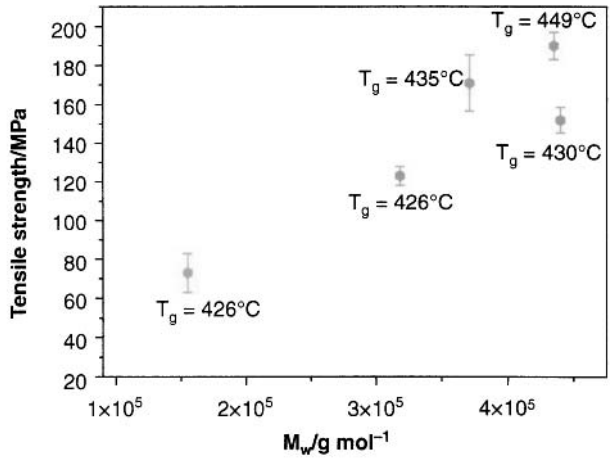

Figure 2.7 Tensile properties of polyoxadiazole samples as a function of molecular weight (M_w).

values as a function of molecular weight. For the same polydispersity, as high the molecular weight as high the tensile strength. Similar trend has been observed by a NASA group when tensile strength is plotted as a function of polyimide molecular weights [32]. Additional factor is the sulfonation level which influences the dipole-dipole interaction between the sulfonated groups and as a consequence the T_g and mechanical properties. As sulfonated samples prepared by a direct method still have very high molecular weights in contrast to the sulfonated samples prepared by a post-sulfonation route [7], T_g increases with sulfonation level. For similar molecular weights and polydispersity, the sample with higher sulfonation level shows the higher tensile strength, once the introduction of sulfonic acid groups increases the intermolecular interaction [33].

The effect of the bath time on the molecular weight, thermal stability and tensile properties of SPODDPE was for the first time analyzed. Sulfonated polyoxadiazoles with excellent and reproducible tensile properties (tensile strength up to 200 MPa, elastic modulus around 4 GPa and elongation at break in the range 40–60%) could be synthesized through a polycondensation reaction of the hydrazine sulphate salt and an aromatic dicarboxylic acid in poly(phosphoric acid) in the frame of time of 4–5 h. The tensile properties of the sulfonated polyoxadiazole films obtained in this study, confirms the classification of this polymer as high performance polymers with great potential for engineering applications.

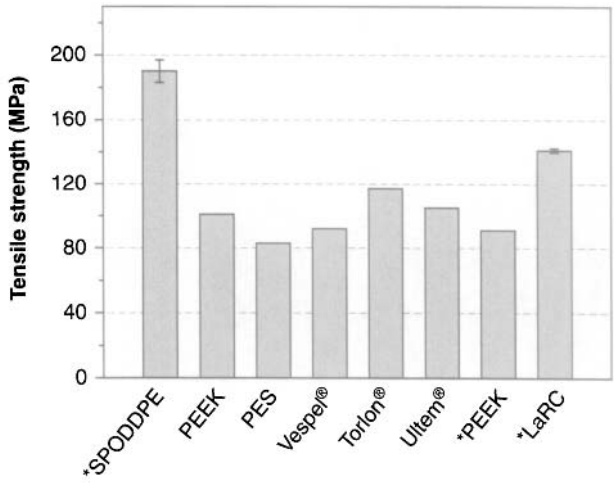

Figure 2.8 Tensile properties of high performance polymers (SPODDPE, sulfonated polyoxadiazole; PEEK, poly(ether ether ketone); PES, poly(ether sulfone); Vespel®, Poly(pyromellitimide-1,4-diphenyl ether); Torlon®, poly(amide imide); Ultem®, poly(ether imide); LaRC, aromatic poly(imide) [34, 35].

Figure 2.8 shows the maximum reproducible tensile strength (190 ± 6.9 MPa) obtained [29]. The comparison of the tensile properties of the sulfonated polyoxadiazoles (SPODDPE) according to the ASTM D 882- 00 with other high performance polymers according to the ASTM D 882- 00 (marked with * in Figure 2.8) as well as according to the ASTM D 638 clearly shows that the SPODDPE offers high strength, making it useful for high strength/ high heat applications.

2.4 Application Fields

Polyoxadiazoles, like most thermally stable polymers, are good candidates for applications that require flame-resistance, fire-resistance or self-extinguishing properties. The polyoxadiazole fibers are competitive in performance when compared to other reinforcing agents, such as glass, steel and commercial high-temperature fibers (Kevlar, X-500, Cermel, Nomex) [36–38]. They are good candidates for application as high temperature fibers [36], reinforcement materials [39], graphitized fibers [39], acid sensors and emissive layers in light-emitting diodes [40], membrane materials for gas

separation, ultrafiltration, reverse osmosis and fuel cell [6, 7, 37, 41, 42, 44] as well as inhibitor materials for the corrosion of metals [45]. In this section the application fields for the homopolymers and/or copolymers of SPODDPE and POD-6F, whose mechanical properties are high enough to enable their use as film, fibers, membranes and sheets will be discussed in more details when applied as coating materials, fuel cell membranes and polymer matrices for composites.

Coating Materials

One of the most coating effective and simple techniques for introducing a metallic coating to a substrate is by electrochemical plating. Other coating possibilities are conversion coating, anodizing, chemical vapor deposition, organic coatings and others. Organic coating systems are typically used in the final stages of a coating process and can include a variety of different processes that make use of organic polymers, such as painting, powder coating, E-coating, sol-gel process, plasma polymerization and others [46]. Polymers with electron-withdrawing units like aromatic oxadiazole rings have strong electron affinity and as a result they are capable of enhancing their electron transport properties. Conducting polymers are promising materials for corrosion protection of metals [46] because of the four possible mechanisms: (1) the coating acts as a barrier (2) it acts as sacrificial anode (3) the coating act as a reservoir for corrosion inhibiting ions that are released as the conducting polymer changes its redox state (4) the conducting polymer could stabilize a passive oxide layer.

Heterocyclic compounds containing sulphur, nitrogen and oxygen have been seen as effective inhibitors for the corrosion of metals and alloys in different corrosive environments [47–51]. The effectiveness of organic compounds containing sulphur as corrosion inhibitors for steels in sulphuric acid is well known. They suppress the anodic and/or the cathodic reactions involved in the corrosion process by adsorbing on the metal surface [52]. Different organic groups have been reported to inhibit corrosion of mild steel in acidic media, including oxadiazole groups [53]. Polyoxadiazole containing a hydrophobic group (POD-6F) in the main chain has been shown to afford an excellent corrosion protection of magnesium allloy [45]. The corrosion resistance of the polyoxadiazole coated sample was about 5 orders of magnitude higher than the

bare metal. After 36h immersion in 0.1M NaCl, polarization resistance was 1.31×10^3 ohm.cm^2 while for the coated Mg alloy with polyoxadiazole the coating resistance value was kept constant after 36h about 8.0×10^7 ohm.cm^2. Polarization curves for the bare metal and the coated samples in 0.1M NaCl are shown in Figure 2.9. The polyoxadiazole coated sample showed a significant improvement in the corrosion resistance than the bare metal. The corrosion current density of the polyoxadiazole coated sample decreased to 1.4×10^{-6} mA.cm^{-2} from 5.6×10^{-3} mA.cm^{-2} of the bare metal. Moreover, the polyoxadiazole coated sample did not show any break-down potential even up to 1000mV above corrosion potential. This shows the higher stability of the coating in the corrosive environment.

Water permeation through coatings was shown to be an important factor to be considered in the polyoxadiazole coating formulation [45, 46]. Generally, water becomes the major cause of swelling and loss of adhesion of the coating and eventually allows the electrolyte to contact the bare metal and accelerates the corrosion process [46]. Another important parameter is the polymer adhesion to the metallic surface. To improve adhesion of the aromatic polyoxadiazole coating, a copolymer containing hydrazide groups (-CO-NH-NH-CO-) groups has been shown to enhance both adhesion as well as the anti-corrosion ability of the polyoxadiazole coating, 1,2,3-benzotriazole (BET) inhibitor was added to

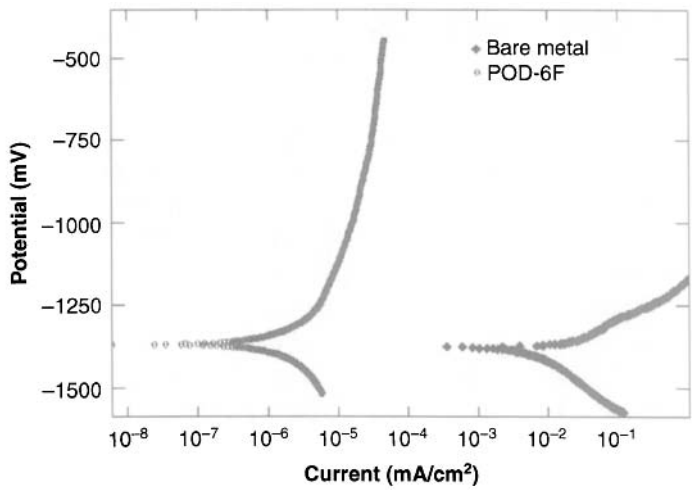

Figure 2.9 Polarization curves for polyoxadiazole coated and uncoated magnesium alloy.

the poly(hydrazide oxadiazole) copolymer [54]. A second layer composed of only a hydrophobic fluorinated polyoxadiazole was used to avoid that water penetrates through the coating. The poly(hydrazide oxadiazole) copolymer presents both sulfonated and fluorinated groups, which should improve the interaction with the BET inhibitor by "self-doping" effect (nitrogen protonation by the sulfonic acid groups) and the interaction with the top layer, respectively.

The structure of the copolymer was quantitatively determined by elemental analysis and interpretation of ^{1}H-NMR spectrum. Figure 2.10 shows the ^{1}H-NMR spectra and the structures of the fluorinated polyoxadiazole (a), of the sulfonated polyoxadiazole (b) and of the sulfonated/fluorinated poly(oxadiazole hydrazide) copolymer, DPE-HF (c). Duplets at 7.59 ppm for the H_1 protons and at 8.17 ppm for the H_2 protons are observed for the fluorinated polyoxadiazole, as expected by analyzing the structure of this polymer (Figure 2.10a). The sulfonated polyoxadiazole shows signals at 7.20 ppm, 7.36 ppm, 8.15 ppm, 8.21 ppm and 8.58 ppm relative to the H_4, $H_{4'}$, H_5, $H_{5'}$ and H_6 protons, respectively (Figure 2.10b) [44]. The DPE-HF copolymer spectrum shows additionally to all the signals for aromatic protons present in the fluorinated and polyoxadiazole samples, small signals at 10.9–10.5 ppm and in the region of aromatic protons at 8.52 ppm, 8.01 ppm, 7.59 ppm and 7.14 ppm (assigned with * in Figure 2.10c), which are relative to hydrazide groups [15]. Based on these assignments, the amount of repeating units containing hydrazide groups was equal to 39% and the amount of repeating units containing fluorinated groups was equal to 14%, with 86% constituting of ether groups.

For the polyoxadiazole coating composition containing 0.36% BET, a corrosion inhibition efficiency of 67% was obtained [54]. This result indicates that BET molecules adsorbed on the metal surface retarding the dissolution of metal atoms from the reactive sites. Heterocyclic compounds containing nitrogen have seen as effective inhibitors for the corrosion of metals because they can form complex with metals. The formation of complex is the result of the reaction between the triazole on the metal surface through the NH group and the metal cation formed during the corrosion of metal.

Further characterization on the DPE-HF coated samples was conducted by XPS analysis after immersion in NaCl solution used for electrochemical characterization confirmed this result. Two components at 399.3 (H–N–C = O) and 401.0 (N^+–R) eV in the XPS

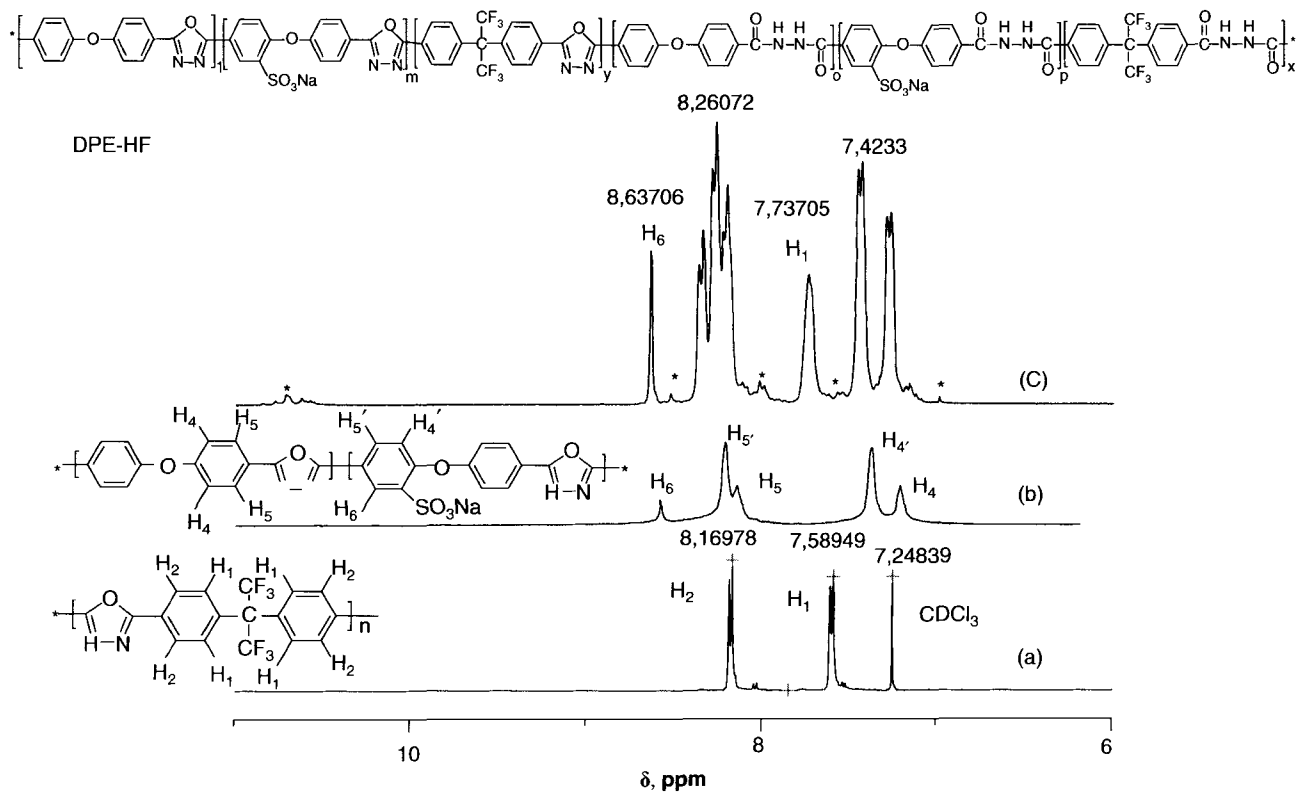

Figure 2.10 ^{1}H-NMR spectra and the structures of the fluorinated polyoxadiazole (a), of the sulfonated polyoxadiazole (b) and of the sulfonated/fluorinated poly(oxadiazole hydrazide) copolymer, DPE-HF (c).

spectra were observed in the N 1s region [54–57]. The presence of the positively charged nitrogen atoms (N^+–R) is due to the nitrogen protonation by the sulfonic acid groups ("self-doping'). With addition of BET, N 1s region experiences a dramatic change resulting in a decrease of the main component centered at 401.0 eV. The doping level, calculated by the N+ (at 401.0 eV)/N (centered at 400.0 eV) ratio, decreased from 31.8 to 10.9 after addition of 0.36% BET, indicating that the protonation effect of the nitrogen atoms was significantly weakened and more neutral nitrogen atoms were generated. Other works have also analyzed the doping level using XPS technique by a close inspection of the N 1s region [49, 55–57]. Liu *et al.* [55] have shown that formation of complexes between nitrogen atoms of amine groups and metal copper ions has improved after reduction of the doping level. The surface complexes are formed because nitrogen atoms share a lone pair of electrons with the electron-withdrawing metal ions. A decrease of nitrogen protonation reduces electrostatic repulsion and results in more neutral amine groups available for metal adsorption. Therefore, after addition of 0.36% BET, as more neutral nitrogen atoms are available, stronger nitrogen absorption on the metal surface should be favored.

When a second layer of fluorinated polyoxadiazole is applied to the DPE-HF coated sample containing 0.36% BET, a significant decrease in corrosion current and increase in the corrosion potential was observed. The significant improved results have been ascribed to the inhibition effect of the BET. In the monolayer constituted only of poly(hydrazide oxadiazole) copolymer DPE-HF, because of the high hydrophilicity of this coating conferred by the sulfonated groups, the water permeates through the coating. After addition of a second hydrophobic layer, the water is avoided to penetrate though the coating. The thickness values of both bilayer and monolayer containing fluorinated polyoxadiazole were similar, 29 ± 4 μm and 28 ± 6 μm, respectively. Figure 2.11 shows the electrochemical impedance spectra of bare metal, fluorinated polyoxadiazole and bilayer polyoxadiazole coated AZ31 magnesium alloy. As it can be seen the bilayer coated sample showed a very high coating resistance, about three orders of magnitude higher than the monolayer of fluorinated polyoxadiazole coated sample.

The significant improved results have been ascribed to the inhibition effect of the BET as well as to the high polyoxadiazole hydrophobic second layer, avoiding water permeation though the coating.

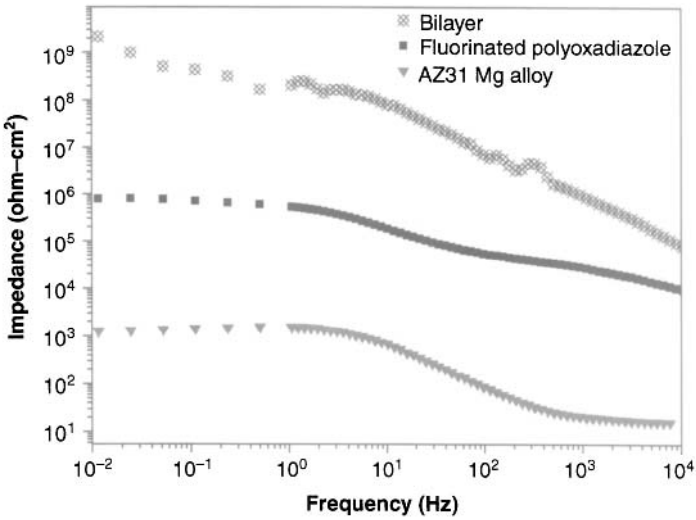

Figure 2.11 Electrochemical impedance spectra of bare metal, fluorinated polyoxadiazole (POD-6F) and bilayer polyoxadiazole (DPE-HF) coated AZ31 magnesium alloy.

Fuel Cell Menbranes

Polymers containing heterocyclic rings with basic character have been shown to be quite interesting for polymer electrolyte for fuel cells application, since they are able to transport protons above 100°C when doped with phosphoric acid [6]. Sulfonated oxadiazole-based materials for fuel cells have been reported by Gomes *et al.* [6, 7, 44]. They have shown that the presence of (C = N) pyridine-like N sites favor additional points for proton jumps, contributing to the proton conductivity [6, 7, 44, 58, 59]. Thus, the use of polyoxadiazoles as polymer material for fuel cell presents two advantages: it offers a new alternative for proton transport, and opens the possibility to operate the fuel cells at temperatures above 100°C. It is expected that the availability of materials for operation at such condition will be an important step for the establishment of the fuel cell in large-scale deployment in the sector of energy conversion for automotive and stationary applications. By 2050 the reserves of fossil fuel will be critical and alternative energy carriers will be essential. It has been predicted that hydrogen will then be dominant in the market, powering about 50% of automobiles. In this scenario, the fuel cell will be a breakthrough technology path for future transportation applications.

Recently, it was demonstrated that during the synthesis of polyoxadiazole by reaction between dicarboxylic acid and a salt of hydrazine a partial sulfonation occurs [44]. This fact had been overseen in the previous papers describing or applying this synthesis route [13, 60, 61]. However, the recognized level of functionalization, i.e. the ion-exchange capacity (IEC) of 1.26 mequiv g^{-1}, was too low to result in a polyoxadiazole with acceptable proton conductivity. The polyoxadiazole "dopping" by treatment with sulfuric acid in mild conditions [43] led to higher proton conductivity values (order of magnitude of 10^{-2} S cm^{-1} at 50–80°C), but covalently bonding sulfonic groups to the polyoxadiazole chain should potentially be a much more effective strategy to increase the polymer applicability in fuel cells. Optimized synthesis methods for the synthesis of sulfonated polyoxadiazoles (SPODDPE) with molecular weight in the order of magnitude of 10^5 g/mol and ion-exchange capacity (IEC) higher than 1.26 mequiv g^{-1} were then later successfully been reported [7]. Figure 2.12 shows the proton conductivity of SPODDPE membranes with different IEC as a function of relative humidity (RH) measured at 80°C. As expected, the conductivity of SPODDPE membranes has a strong dependence on the level of hydration. The high proton conductivity values at RH = 100% sharply decrease upon dehydration. The high proton conductivity

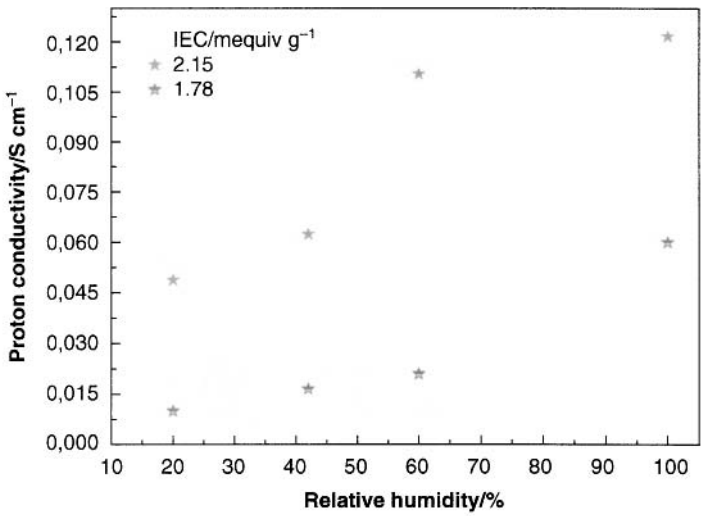

Figure 2.12 Proton conductivity of SPOD-DPE membranes with different IEC as a function of relative humidity (RH) measured at 80°C.

for the SPODDPE membrane with IEC equal to 2.15 mequiv g^{-1} may be attributed to the high water retention capacity of this membrane, keeping a minimum hydration level in the membrane. As one may see, for all membranes high proton conductivity in the order of magnitude of 10^{-2} S cm^{-1} at 20% RH were obtained. Taking into account the low level of external humidification under this condition, this result can be attributed first to the fact of the $-SO_3H$ groups are not much separated from each other and also to the presence of additional sites for protonation which strengthen the mechanism of proton transport by the diffusion of protons within a hydrogen bonded structure. Due to the high number of interaction sites not only the transport is favored but the water is also better retained. In polymers with lower functionalization the hydrogen bond structure for the proton transport can not be well formed and the proton conductivity is much reduced at low humidity level. The high proton conductivity values at low humidity conditions are the main advantage of the sulfonated polyoxadiazole in comparison with the (sulfonated poly(ether ether ketone), SPEEK. It has been shown in literature that the conductivity of the SPEEK is only in the order of magnitude 10^{-2} S cm^{-1} at high levels of hydration, at low levels of hydration the conductivity is significantly lower (order of magnitude 10^{-5} S cm^{-1} at 40% RH) [62].

Addition of sulfonated dense silica particles containing oxadiazole groups has shown promissory results at conditions of high relative humidity (100% RH) when added to a SPEEK and attributed to the amphoteric character of the sulfonated oxadiazole oligomeric segments containing both sulphonic acid groups and basic nitrogen sites [58]. This result motivates further develop of new polymers containing both acidic ($-SO_3H$ group) and basic sites (basic nitrogen) in the repeating unit. Addition of hydrophilic sulfonated silica to a non-functionalized hydrophobic fluorinated polyoxadiazole resulted in porous membrane and very low proton conductivity in the order of magnitude of 10^{-8} S cm^{-1} was obtained at low humidity condition (20% RH) [6]. Taking into account the high proton conductivity values in the order of magnitude of 10^{-2} S cm^{-1} at low humidity conditions (20% RH) [7] as well as its excellent thermal and mechanical stability, sulfonated polyoxadiazole was then further tested as the polymeric matrix [63]. The ionic conductivity data at 120°C and under 5–25% RH for the polyoxadiazole plain mebrane and for the polyoxadiazole composite membrane are shown in Figure 2.13. As expected, the composite membrane had

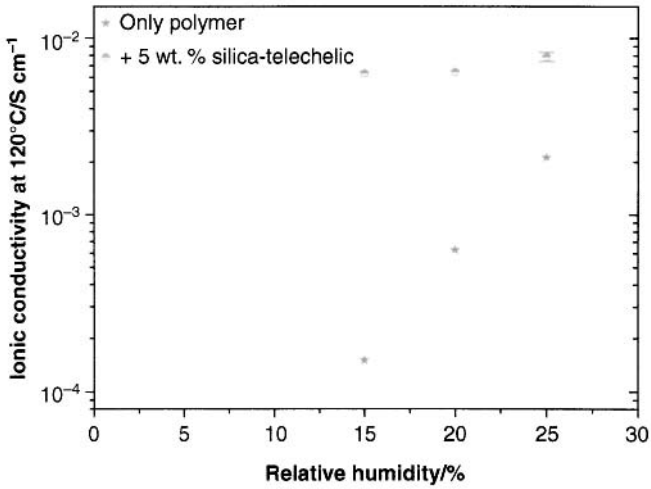

Figure 2.13 Ionic conductivity data at 120°C and under 5–25% RH for the polyoxadiazole plain membrane and for the polyoxadiazole composite membrane.

higher proton conductivity than the pristine polymer membrane in all range of relative humidity. The significant difference between conductivity data of composite membranes and the pristine polymer membrane at low relativity humidity (e.g. 15 RH%) is probably a consequence of the better water retention capacity of the composite membrane conferred by the sulfonated silica. The membrane containing 5 wt.% silica-telechelic exceeds the value obtained for the pristine polymer membrane by one order of magnitude.

Nanocomposites can offer advantages when dealing with the following fuel cell key issues: optimization of the membrane-electrode-catalyst interface, preparation of membranes able to effectively operate above 100°C and under external low humidification in fuel cells fed with hydrogen and preparation of membranes with low alcohol crossover [64, 65]. Above 100°C and under external low humidification most of the available membranes starts to dehydrate, requiring more complex operating conditions to compensate the consequent conductivity decrease. The motivations for operating at high temperatures are improved reaction kinetics, minimization of catalyst poisoning by CO, simplification of the heat and water (humidification) management in the cell, improved gas transport and other issues associated with catalyst and design [64, 65].

Polymer Matrices for Composites

In recent years, high temperature resistant engineering polymers have gained acceptance for use as matrices in advanced polymer composites for aerospace structural applications, including military aircraft and missiles [39, 66]. Recent applications of reinforced polymers in aircraft propulsion systems have resulted in substantial reductions in both engine weight and manufacturing costs. Unfortunately, the low thermal-oxidation stability of these materials severely limits the extent of their application. Commercially available state-of-the-art high-temperature fiber-reinforced polymers, such as graphite fiber/PMR-15 polyimide, can be used at temperatures between 290 and 345°C. Continued improvements in the stability of polymer matrices coupled with improvements in polymer/fiber interfaces, composite processing, and oxidation-resistant coatings will yield fiber-reinforced polymers for use at high temperatures. A major effort underway in this area is the development of high-temperature fiber-reinforced polymers to 425°C.

Poly(1,3,4-oxadiazole)s have been the focus of considerable interest with regard to the production of high-performance materials, particularly owing to their high thermal stability [39]. In-situ polymerizations of sulfonated polyoxadiazole through a polycondensation reaction of hydrazine sulphate and aromatic dicarboxylic acid monomers with carbon nanotubes (CNTs) in poly(phosphoric acid) were recently successfully performed [67]. Against what could be expected taking into account that polycondensation reactions could be draw backed in the presence of CNTs, which could act as an "impurity", innumerous works have shown that polymer composites can be successfully in-situ polymerized with CNTs [68–71]. High molecular weights in the order of magnitude of 10^5 g/mol with polydispersity around 2 for the CNT-based composites were obtained.

The composites show electrical conductivity in the order of magnitude 10^{-5} S m^{-1}, indicating that they can be used as antistatic materials and at temperatures as high as 470°C [67]. The sulfonated polyoxadiazole itself is a semiconductor material with an electrical conductivity of 2.3 x10^{-7} S m^{-1} [67], higher than insulating polymers with the order of magnitude in the range 10^{-16}–10^{-8} S m^{-1} [72–74]. The semiconductor behavior of the sulfonated polyoxadiazole samples is a consequence of the conjugated and aromatic character of the polyoxadiazole chains as well as of the sulfonation level once the

introduction of sulfonic acid groups and the consequent presence of mobile metal counter-ions might increase the electron transport [75]. Therefore, the electrical conductivity of the sulfonated polyoxadiazole samples depends not only on the content of CNT in the composite but also on the content of sulfonic acid groups acting as a self doping agent.

Thermal degradation behavior of polyoxadiazole composites was analyzed by TGA and the results are shown in Table 2.4. CNT-based polyoxadiazole composites exhibits excellent thermal stability, showing 5% weight loss (T_{d5}) in the range of 465–472°C with residue at 700°C in the range of 57–63%.

High storage modulus values up to 3.6 GPa at 300°C were obtained for composite films with similar T_g (tan δ around 430°C) of the pristine sulfonated polyoxadiazole, exhibiting 44% increment compared with the polymer. The T_g values of the composites are affected both by the sulfonation level as well as by the CNT content. These composites exhibit 44% increment in the storage modulus compared with the pristine sulfonated polyoxadiazole. The significant improvement in the storage modulus can be attributed to the high performance and well dispersion of CNTs in the sulfonated polyoxadiazole matrix. SEM images show a uniform distribution of CNTs in the sulfonated polyoxadiazole matrix, indicating that the CNTs are well dispersed in the composites (Figure 2.14).

Lim *et al.* [38] have proposed bow-type SWCNTs based on dot-like structures observed by AFM top-view images with dot diameter of 20–30 nm and 7–8 nm in height. Figure 2.15 shows AFM images of the sulfonated polyoxadiazole nanocomposite film surfaces containing 1 wt.% of CNT. The particles shown in the images are 20–60 nm in width and 9–11 nm in height. Similarly, Phang *et al.* [76] have also observed CNT composites with dot-like structures by AFM with diameter of 25–66 nm.

The development of high-performance polymers has been a demand from the aerospace industries seeking for new materials. Particularly polyoxadiazoles have a great potential as structural material because of their superior mechanical and thermal properties. With proper control of synthesis, it has been shown that polyoxadiazoles with molecular weight in the order of magnitude of 10^5 g/mol and with excellent reproducible tensile properties (tensile strength up to 200 MPa, elastic modulus around 4 GPa and elongation at break in the range 40–60%) can be obtained.

Table 2.4 Thermal degradation behavior of polyoxadiazole composites.

Polyoxadiazole + CNT	T_g (°C)[a]		T_{d5} (°C)[b]	Residue (%)[c]	S/C[d]	Storage Modulus (GPa)	
	E″	Tan δ				at 100°C	at 300°C
–	415	429	465	65	0.098–0.085	4.1	2.5
0.1 wt.%	405	425	472	61	0.075	4.8	3.1
0.2 wt.%	410	429	469	63	0.087	3.3	2.5
0.5 wt.%	395	415	472	59	0.081	4.7	2.6
1 wt.%	415	435	465	57	0.091	3.9	2.6
5 wt.%	415	430	465	57	0.081	5.6	3.6
15 wt.%	380	410	465	61	0.059	4.9	3.2

[a]Glass Transition temperature measured by DMTA, [b]5% weight loss temperature measured by TGA, [c]Residue weight at 700°C in N_2, [d]determined by elemental analysis.

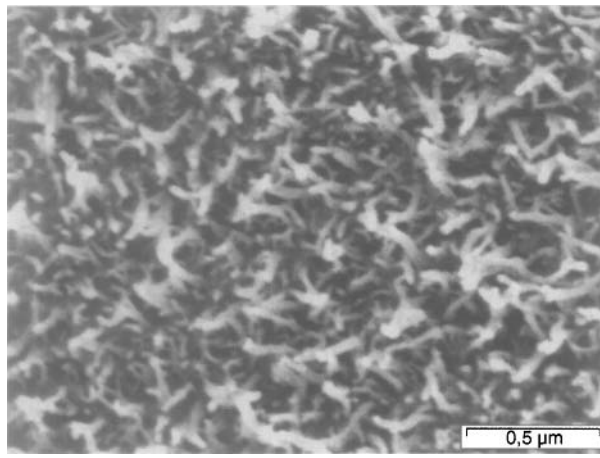

Figure 2.14 SEM image of polyoxadiazole composite containing 1 wt.% CNT.

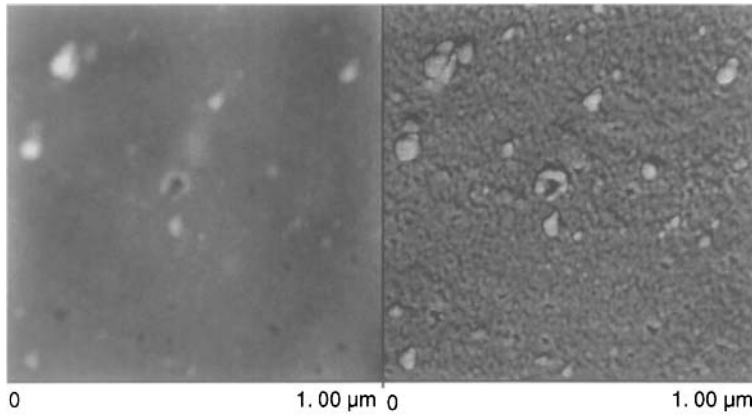

Figure 2.15 AFM images of the sulfonated polyoxadiazole nanocomposite film surfaces containing 1 wt.% CNT. (Left) Tapping mode AFM topography. (Right) Phase mode AFM image of the same area.

Due to their outstanding thermal stability, i.e. degradation temperatures about 500°C and glass transition temperatures up to 442°C and high chemical stability, polyoxadiazoles have a great potential for engineering applications requiring thermally and chemically resistant polymers.

2.5 References

1. Y. Iwakura, K. Uno, and S. Hara, *Journal of Polymer Science, Part A*, Vol. 3, p. 45, 1965.
2. B. Gebben, Thermally Stable and Chemically Polymer Membranes-Aromatic Polyoxadiazoles and Polytriazoles, Ph.D. Thesis, Twente University, Enschede, Holland, 1988.
3. E.R.Hensema, Polyoxadiazole and Polytriazole Gas Separation Membranes-Synthesis and Properties, Ph.D. Thesis, Twente University, Enschede, Holland,1991.
4. D.F. Gomes, Síntese do Poli(difenil éter oxadiazol) visando o Preparo de Fibras Ocas Anisotrópicas para separação de Gases por Extrusão Tripla, Ph.D. Thesis, COPPE/UFRJ, Rio de Janeiro, Brazil, 2002.
5. D. Gomes, C.P. Borges, and J.C. Pinto, *Polymer*, Vol. 45, p. 4997, 2004.
6. D. Gomes, and S. Nunes, *Journal of Membrane Science*, Vol. 321, p. 114, 2008.
7. D. Gomes, J. Roeder, M.L. Ponce, and S.P. Nunes, *Journal of Power Sources*, Vol. 175, p. 49, 2008.
8. A.H. Frazer, and F.T. Wallenberger, *Journal of Polymer Science, Part A*, Vol. 2, p. 1137, 1964.
9. P.M. Hergenrother, B.J. Jensen, and S.J. Havens, *Polymer*, Vol. 29, p. 358, 1988.
10. D. Gomes, C.P. Borges, and J.C. Pinto, *Polymer*, Vol. 42, p. 851, 2001.
11. A.H. Frazer, and F.T. Wallenberger, *Journal of Polymer Science, Part A*, Vol. 2, p. 1147, 1964.
12. A.H. Frazer, W. Sweeny, and F.T. Wallenberger, *Journal of Polymer Science, Part A*, Vol. 2, p. 1157, 1964.
13. E.R. Hensema, J.P. Boom, M.H.V. Mulder, and C.A. Smolders, *Journal of Polymer Science, Part A*, Vol. 32, p. 513, 1994.
14. D. Gomes, S.P. Nunes, J.C. Pinto, and C.P. Borges, *Polymer*, Vol. 44, p. 3633, 2003.
15. D. Gomes, J.C. Pinto, and C.P. Borges, *Polymer*, Vol. 44, p. 6223, 2003.
16. G. Odian, *Principles of Polymerization*, New York, John Wiley & Sons, 1991.
17. P.J. Flory, *Principles of Polymer Chemistry*, New York, Cornell University Press, 1953.
18. D. Gomes, and M.R. Loos, Verfahren zur Herstellung eines Polyoxadiazol-Polymers, DE102008009068A.
19. A.H. Frazer, *High Temperature Resistant Polymers*, John Wiley & Sons, New York, 1968, Vol. 17.
20. Y. Iwakura, K. Uno, and S. Hara, *Die Makromolekulare Chemie*, Vol. 94, p. 103, 1966.
21. Y. Iwakura, K. Uno, and S. Hara, *Die Makromolekulare Chemie*, Vol. 108, p. 160, 1967.
22. D. Gomes, Functionalized polyoxadiazole and polytriazole for fuel cell applications, GKSS internal report, 2007.
23. S.H. Hsiao, and J.H. Chiou, *Journal of Polymer Science, Part A*, Vol. 39, p. 2271, 2001.
24. E.I. Lozinskaya, A.S. Shaplov, and M.V. Kotseruba, *Journal of Polymer Science, Part A*, Vol. 44, p. 380, 2006.
25. S.H. Hsiao, and M.H. He, *Macromolecular Chemistry and Physics*, Vol. 202, p. 3579, 2001.

26. J.W. Connell, P.M. Hergenrother, and P. Wolf, *Polymer*, Vol. 33, p. 3507, 1992.
27. C. Hamciuc, E. Hamciuc, M. Bruma, *et al.*, *Polymer*, Vol. 42, p. 5955, 2001.
28. M.D. Iosip, M. Bruma, I. Ranova, *et al.*, European Polymer Journal, Vol. 39, p. 2011, 2003.
29. M.R. Loos, and D. Gomes, *High Performance Polymers*, Vol. 21, p. 697, 2008.
30. A. Noshay, and L.M. Robeson, *Journal of Applied Polymer Science*, Vol. 20, p. 1885, 1976.
31. C. Iojoiu, M. Maréchal, F. Chabert, *et al.*, *Fuel Cells*, Vol. 5, p. 344, 2005.
32. L.M. Nicholson, K.S. Whitley, and T.S. Gates, *International Journal of Fatigue*, Vol. 24, p. 185, 2002.
33. X. Zhang, S. Liu, and J. Yin, *Journal of Membrane Science*, Vol. 275, p. 119, 2006.
34. R.G. Bryant, *High Performance Polymers*, Vol. 8, p. 607, 1996.
35. H.F. Mark, *Encyclopedia of Polymer Science and Technology*, New York, John Wiley & Sons, 2004.
36. H.H. Yang, *Aromatic High-Strength Fibers*, New York, John Wiley&Sons, 1989.
37. M.J. Nanjan, *Encyclopedia of Polymer Science and Engineering*, Vol. 12, New York, John Wiley & Sons, 1987.
38. H.C. Bach, F. Dobinson, K.R. Lea, and J.H. Saunders, *Journal of Applied Polymer Science*, Vol. 23, p. 2125, 1979.
39. P.E. Cassidy, *Thermally Stable Polymers: Synthesis and Properties*, New York, Marcel Dekker Inc., 1980.
40. S. Janietz, and S. Anlauf, *Macromolecular Chemistry and Physics*, Vol. 203, p. 427, 2002.
41. E.R. Hensema, M.E.R. Sena, M.H.V. Mulder, and C.A. Smolders, *Gas Separation & Purification*, Vol. 38, p. 149, 1994.
42. D. Gomes, I. Buder, and S.P. Nunes, *Journal of Polymer Science, Part B*, Vol. 44, p. 2278, 2006.
43. J. Roeder, D. Gomes, M.L. Ponce, *et al.*, *Macromolecular Chemistry and Physics*, Vol. 208, p. 467, 2007.
44. D. Gomes, M.L. Ponce, J. Roeder, and S.P. Nunes, *Journal of Membrane Science*, Vol. 295, p. 121, 2007.
45. M.B. Mathan, D. Gomes, W. Dietzel, *et al.*, *Surface & Coatings Technology*, Vol. 202, p. 4598, 2008.
46. J.E. Gray, and B. Luan, *Journal of Alloys and Compounds*, Vol. 336, p. 88, 2002.
47. J. Yano, K. Nakatani, Y. Harima, and A. Kitani, *Materials Letters*, Vol. 61, p. 1500, 2007.
48. L.J. Berchmans, V. Sivan, and S.Venkata, *Materials Chemistry and Physics*, Vol. 98, p. 395, 2006.
49. F. Bentiss, M. Traisnel, L. Gengembre, and M. Lagrene, *Applied Surface Science*, Vol. 152, p. 237, 1999.
50. S. Ramesh, S. Rajeswari, and S. Maruthamuthu, *Applied Surface Science*, Vol. 229, p. 214, 2004.
51. R. Ravichandran, S. Nanjundan, and N. Rajendran, *Applied Surface Science*, Vol. 236, p. 241, 2004.
52. R. Agrawal, and T.K.G. Namboodhiri, *Corrosion Science*, Vol. 30, p. 37, 1990.
53. M. Lagrenee, B. Mernari, N. Chaibi, *et al.*, *Corrosion Science*, Vol. 43, p. 951, 2001.
54. D. Gomes, Polymer coatings on magnesium and its alloys, GKSS internal report, 2008.

55. C. Liu, R. Bai, and L. Hong, *Journal of Colloid and Interface Science*, Vol. 303, p. 99, 2006.
56. N. Kohut-Svelko, S. Reynaud, and J. François, *Synthetic Metals*, Vol. 150, p. 107, 2005.
57. W. Zhang, G. Li, Y. Fang, and X. Wang, *Journal of Membrane Science*, Vol. 295, p. 130, 2007.
58. M.L. Ponce, M. Boaventura, D. Gomes, *et al., Fuel Cells*, Vol. 8, p. 209, 2008.
59. M.L. Ponce, D. Gomes, and S.P. Nunes, *Journal of Membrane Science*, Vol. 319, p. 14, 2008.
60. S. Krongauz Ye, V.V. Korshak, Z.O. Virpsha, *et al., Vysokomol Soyed*, Vol. A12, p. 135, 1970.
61. E.R. Hensema, M.E.R. Sena, M.H.V. Mulder, *et al., Journal of Polymer Science, Part A*, Vol. 32, p. 527, 1994.
62. J.S. Park, P. Krishnan, S.H. Park, *et al., Journal of Power Sources*, Vol. 178, p. 642, 2008.
63. D. Gomes, R. Marschall, S.P. Nunes, *et al., Journal of Membrane Science*, Vol. 322, p. 406, 2008.
64. Q. Li, R. He, J.O. Jensen, *et al., Chemistry of Materials*, Vol. 15, p. 4896, 2003.
65. W.H.J Hogarth, J.C. Diniz da Costa, and G.Q. Lu, *Journal of Power Sources*, Vol. 142, p. 223, 2005.
66. P.M. Hergenrother, *Encyclopedia of Polymer Science and Engineering*, New York, Wiley-Interscience, 1988.
67. D. Gomes, M.R. Loos, M.H.G. Wichmann, *et al., Composites Science and Technology*, Vol. 69, p. 220, 2009.
68. S.J. Oh, H.J. Lee, D.K. Keum, *et al., Polymer*, Vol. 47, p. 1132, 2006.
69. J.B. Baek, C.B. Lyons, and L.S. Tan, *Macromolecules*, Vol. 37, p. 8278, 2004.
70. D.H. Wang, P. Mirau, B. Li, *et al., Chemistry of Materials*, Vol. 20, p. 1502, 2008.
71. H.C. Kuan, C.C.M. Ma, W.P. Chang, *et al., Composites Science and Technology*, Vol. 65, p. 1703, 2005.
72. F.H. Gonjny, M.H.G. Wichmann, B. Fiedler, *et al., Composites Part A: Applied Science and Manufacturing*, Vol. 36, p. 1525, 2005.
73. E.N. Konyushenko, J. Stejskal, M. Trchová, *et al., Polymer*, Vol. 47, p. 5715, 2006.
74. Z. Ounaies, C. Park, K.E. Wise, *et al., Composites Science and Technology*, Vol. 63, p. 1637, 2003.
75. K. Meerholz, *Nature*, Vol. 437, p. 327, 2005.
76. I.Y. Phang, T. Liu, W. Zhang, *et al., European Polymer Journal*, Vol. 43, p. 4136, 2007.

3

Conjugated Polymers Based on Benzo[1,2-*b*:4,5-*b*′]dithiophene for Organic Electronics

Huaxing Zhou and Wei You

University of North Carolina at Chapel Hill, NC, USA

Abstract

Conjugated polymers based on benzo[1,2-*b*:4,5-*b*′]dithiophene (BDT) are one of the most important classes of polymers for applications in organic electronics. The BDT monomer has a rigid, planar and symmetric structure, which imparts a few unique features to BDT based polymers. The spectral and electronic properties of the BDT based polymers, such as highest occupied molecular orbital (HOMO) and lowest unoccupied molecular orbital (LUMO) energy levels, as well as the band gaps, can be tuned by the copolymerization of the BDT unit with different chromophores (co-monomers) or through the attachment of substituents or even side chains. In this chapter, we summarized the synthetic methods of BDT monomers and BDT based polymers. A few unique features of BDT based polymers were discussed, including planar polymer backbone, high crystallinity and high mobility. All these have contributed to the tremendous development in BDT based materials for applications in organic electronics over the past decade.

Keywords: Conjugated polymers, polymer solar cells, organic field effect transistors, molecular orbital

3.1 Introduction

Conjugated polymers based on benzo[1,2-*b*:4,5-*b*′]dithiophene (BDT) are one of the most important classes of polymers for

Vikas Mittal (ed.) High Performance Polymers and Engineering Plastics, (49–80)
© Scrivener Publishing LLC

applications in organic electronics (Scheme 3.1). The BDT monomer has a rigid, planar and symmetric structure, which imparts a few unique features to BDT based polymers, such as a planar polymer backbone, high crystallinity and high mobility. The spectral and electronic properties of the BDT based polymers, such as highest occupied molecular orbital (HOMO) and lowest unoccupied molecular orbital (LUMO) energy levels, as well as the band gaps, can be tuned by the copolymerization of the BDT unit with different chromophores (co-monomers) or through the attachment of substituents or even side chains. These unique features enable wide-spread usage of BDT based conjugated polymers in organic electronics, especially in organic field effect transistors (OFET) [1, 2] and polymer solar cells (PSC) [3–5]. For example, BDT based polymers have been demonstrated with OFET mobility up to 0.4 $cm^2/(V \cdot s)$ [6] and power conversion efficiency over 7%, [7–10] which are among the highest mobility and efficiency in OFET and PSC fields, respectively. The first half of this chapter will be focused on the syntheses of monomers and polymers. We will first summarize the synthetic methods for the BDT monomer, followed by a discussion of advantages and drawbacks of different polymerization methods used to prepare BDT based polymers. The second half of this chapter is dedicated to the applications of BDT based polymers for OFET and PSC. We will first introduce basic concepts of OFET and PSC, and then further elaborate the development of the BDT based polymers for OFET and PSC applications with a focus on the design strategies.

3.2 General Synthetic Methods for BDT Monomers and Polymers

The first synthesis of BDT molecule was reported in as early as 1971 [11]. However, the early synthetic approach was rather

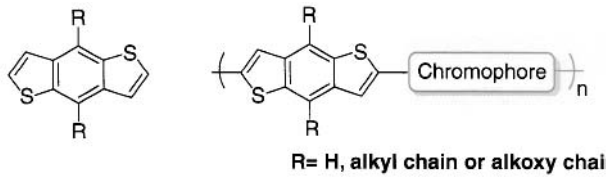

Scheme 3.1 General structures of benzo[1,2-*b*:4,5-*b'*]dithiophe (BDT) unit (left) and BDT based copolymers (right).

lengthy and accompanied with low yields. In 1986, Beimling *et al.* summarized several improved synthetic routes of preparing BDT monomers [12]. The polymers based on BDT monomers emerged much later, with the first soluble BDT based polymers with high molecular weight synthesized by Yamamoto *et al.* in 2002. The same authors also studied the electronic and stacking properties at solid state of these materials [13–15]. The following decade witnessed different polymerization methods applied to achieve numerous BDT based copolymers with different chromophores.

3.2.1 Synthesis of BDT Monomers

The report in 1971 by MacDowell and Wisowaty on the synthesis of BDT unit started from thiophene derivatives [11, 16], which was further improved by Beimling *et al.* in 1986 (Scheme 3.2) [12, 17]. Instead of using 3-thiophenecarboxaldehyde and 2,3-dibromothiophene as starting materials in the original report, the improved method started with only 3-bromothiophene. It was first converted to 3-bromothiophene-2-carbaldehyde, which was then treated with 3-thienyllithium to afford compound **1**. The newly formed hydroxyl group was reduced off to afford compound **2**. The bromine on the 3 position of compound **2** was lithiated and quenched by *N,N*-dimethylformamide (DMF) to yield compound **3**, which underwent a cyclization in 48% hydrobromic acid solution to complete the synthesis of BDT monomer **4** with high yield.

However, the aforementioned syntheses not only require thiophene derivatives as key starting materials, also are rather lengthy

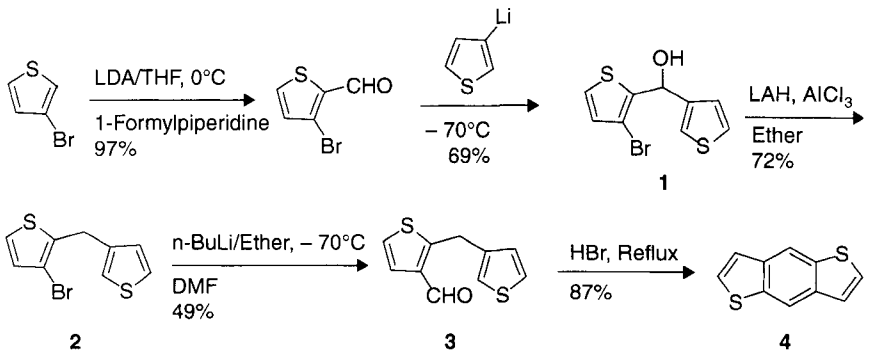

Scheme 3.2 Synthetic route of BDT monomer **4**.

with low overall yield of the BDT monomer. An significantly improved synthesis was reported by Takimiya and coworkers [18], which started with a readily prepared benzene derivative **5**. The intermediate **6** with sulfur anion was generated by halogen-lithium exchange and quenching with sulfur (Scheme 3.3). A final intramolecular cyclization reaction formed BDT core **7** with a reasonable yield. In addition, this method is particularly useful to make benzo[1,2-*b*:4,5-*b*']dichalcogenophenes because of the limited availability of selenophene and tellurophene derivatives (Scheme 3.3).

The rigidity and planarity of the BDT unit usually helps its polymers exhibit enhanced interchain packing. However, this strong stacking – though desirable for applications such as OFET and PSC – often introduce concomitant issues such as limited solubility and low molecular weight of BDT based polymers [19]. One popular and very effective solution is to attach solubilizing side chains onto the center benzo unit. BDT units with side chains are usually made from benzo[1,2-*b*:4,5-*b*']dithiophene-4,8-dione **(10)**, whose synthesis was first reported by Gierer *et al.* and later improved by Yang and coworkers [20, 21]. As shown in Scheme 3.4, *N,N*-diethylthiophene-3-carboxamide (**9**) was first prepared from acyl chloride and diethylamine almost quantitatively (95% yield), and compound **10** was obtained by compound **9** reacting with *n*-buyllithum with a yield of 75%.

Compound **10** serves as a key intermediate towards any further functionalization of the center benzo unit. For example, BDT unit with alkoxy side chains (**11**) was prepared from dione **10** through the reduction with zinc dust in aqueous sodium hydroxide solution followed by the alkoxylation with alkyl bromide or alkyl toluenesulfonate [12, 21]. The synthesis of alkylated BDT unit **13** was first reported by Ong *et al.* (Scheme 3.4c). In their approach, reacting

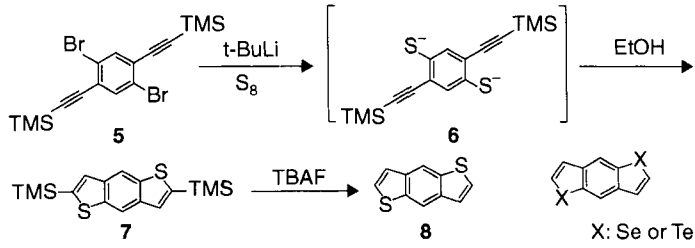

Scheme 3.3 Synthetic route of BDT monomer **8**.

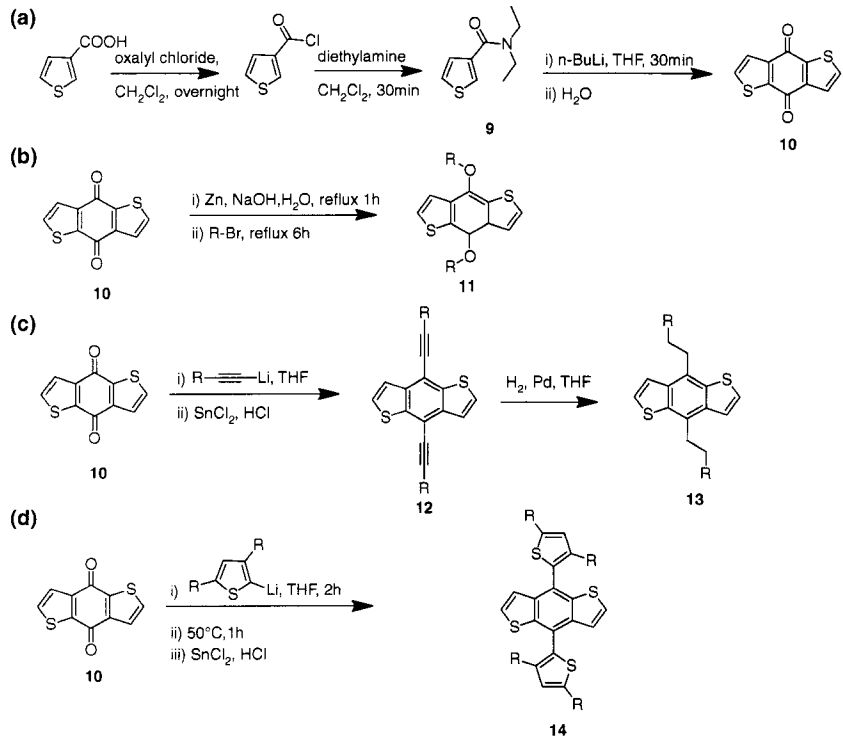

Scheme 3.4 Synthesis of BDT monomers with various side chains.

alkynylmagnesium chloride or alkynyllithum with dione **10** followed by a reduction with $SnCl_2$ under acidic conditions afforded dialkynyl-substituted intermediate **12**. Dialkylated BDT unit **13** was then prepared readily from Pd catalyzed hydrogenation of **12** with hydrogen gas [22]. With a similar methodology, Yang *et al.* reported the synthesis of BDT unit bearing alkylated thiophene as side chains (Scheme 3.4d) [23]. Instead of acetylene, alkylated thiophene derivatives were first lithiated and then reacted with dione **10**. The BDT unit with alkyl thiophene side groups **14** was then isolated in 44% yield.

3.2.2 Polymerization Methods of Polymers Incorporating BDT Unit

Two main polymerization methods have been employed disproportionally towards the synthesis of these BDT based copolymers.

Oxidative coupling: A few simple BDT copolymers were prepared by oxidative coupling of the monomers with iron(III) chloride [17, 24, 25]. As exemplified in Scheme 3.5, a homopolymer would be obtained if only one type of monomer were used, whereas employing two different monomers would lead to a random copolymer.

The disadvantages of this method include: (a) the degree of polymerization is usually low; (b) a high level of defects along polymer backbones due to coupling reactions occurring at positions other than 2-position of thiophenes; (c) oxidative polymerization with ferric chloride can result in doping the polymer by residual catalyst [26, 27]. This inevitable doping, which changes electronic properties of semiconducting polymers, is detrimental to the application of polymers as semiconductors in FET and solar cells. As a result, this method is much less favored in preparing polymers for organic electronics.

Transition metal catalyzed coupling polymerization: The most popular method for the synthesis of BDT based conjugated polymers takes advantage of the well-developed transition-metal mediated coupling reactions, featuring mild reaction conditions, remarkable functional group tolerance and high yields (Scheme 3.6).

Stille coupling polycondensations have been used in the synthesis of most BDT based copolymers [28–32]. Monomers for Stille coupling polymerizations are relatively stable and usually remain as solids at room temperature, a feature that allows easy purifications of the monomers (e.g., via recrystallization). These ultra-pure monomers of solid state are beneficial in achieving an accurate stoichiometry of the two constituting monomers, a general requirement to obtain high molecular weights via polycondensations. The major

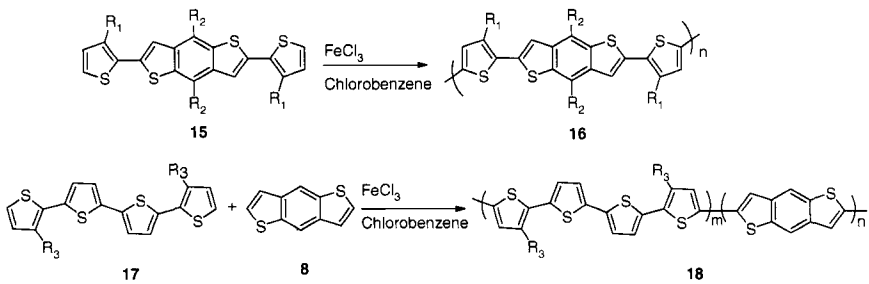

Scheme 3.5 Oxidative coupling polymerization.

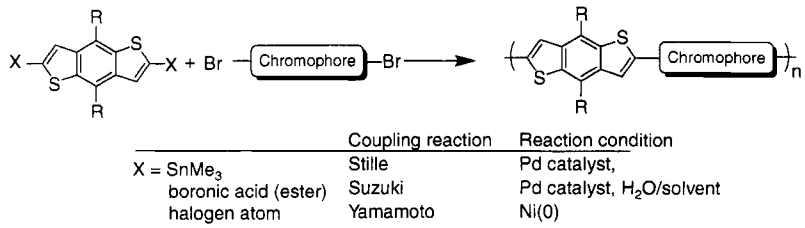

Scheme 3.6 Transition metal catalyzed coupling polymerization.

drawback of Stille coupling reaction resides in the use of toxic trialkyl tin chloride during the monomer preparation. Compared with the Stille coupling, Suzuki coupling is a greener alternative [23], because organo-boron compounds are usually non-toxic, environmentally-friendly and insensitive to moisture. However, it is relatively difficult to control the stoichiometry of the two co-monomers for the polymerization, due to the well-known problems in purifying the monomers containing boronic acids. Finally, Yamamoto-type polycondensation has also been used to prepare BDT based copolymers [14]. Though this method is experimentally simpler than Suzuki/Stille couplings, the rather expensive nickel(0) reagent must be used stoichiometrically. In addition, the scope of monomers polymerizable via the Yamamoto-type polycondensation is rather limited.

Although transition metal-mediated coupling reactions have received great successes in the syntheses of conjugated polymers, there are still a few outstanding issues. First, it is generally difficult to completely remove residual metal particles formed during the polymerization and trapped within conjugated polymers. Common practices such as extraction of polymers by soxhlet extraction and/or purification by passing the polymer solution through a silica gel column can remove most of the metal particles. However, for the application in organic electronics, even a very low level of metal residue could be catastrophic. Complete removal of those residual metal particles usually requires the addition of chelating reagents, followed by precipitation and soxhlet extraction to remove chelating reagents [33]. Second, monomers containing functional groups that can bind to the metal catalysts cannot undergo transition-metal mediated coupling methods to achieve polymers of high molecular weights: usually no polymerization or oligomers of low molecular weights would be obtained instead.

Microwave assisted coupling reactions have been developed to significantly accelerate the reaction time and suppress side reaction, mainly because of the direct transfer of energy to reactants. Similarly, in microwave assisted polymerizations, polymers can be prepared with much shorter reaction time with high purity. In addition, polymers with ultra-high molecular weight and low polydispersity can be accomplished through this method. Since polymers with high molecular weight, and low defect level usually exhibit enhanced performance in organic electronics, microwave assisted transition metal-mediated polycondensation is increasingly adopted in synthesizing high performance conjugated polymers [9, 10, 34].

3.3 Application of BDT-Based Polymers in OFET and PSC

Organic semiconductors have been widely applied as active materials for organic light emitting diode (OLED), organic thin film transistors (OFET) and organic solar cells (OSC) [35]. Compared with small organic molecules such as rubrene or pentacene, polymeric materials offer notable advantages such as tunable electro-optical properties, solution processability, and excellent mechanical properties. In addition, BDT based polymers usually have planar polymer backbones, strong polymer chain interactions and the further tunability of material properties – including solubility, opto-electric and photophysical properties – by different functional groups and side chains. Therefore BDT based polymers have attracted significant amount of attention in OFET and PSC fields. In this section, we will first introduce basic concepts of OFET and PSC and then focus on the design strategy and development of the BDT based polymers tailored for OFET and PSC applications.

3.3.1 Introduction of OFET

As a low-cost alternative to traditional inorganic semiconductors based transistors, organic field effect transistors are ideally positioned for applications such as radio frequency ID tags, sensors, and smart banknotes [36–40]. An archetypical structure of a *bottom-gate top-contact* OFET is shown in Scheme 3.7a. Other device architectures have also been employed depending on the relative

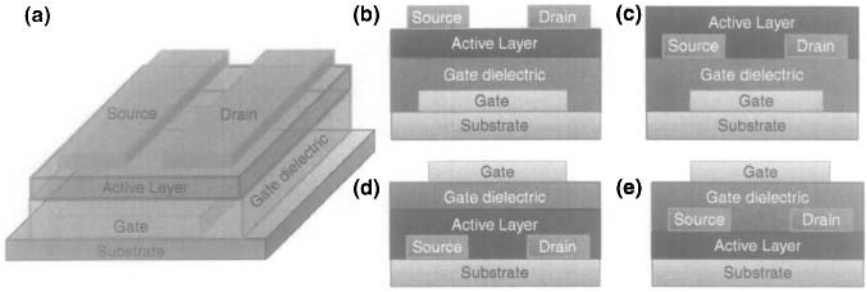

Scheme 3.7 a) a typical structure of bottom-gate top-contact OFET; b) bottom-gate top-contact; c) bottom-gate bottom-contact; d) top-gate bottom-contact; e) top-gate top-contact.

position of the contacts to the dielectric/semiconductor layers (Scheme 3.7c–3.7e) [2]. A typical OFET device includes three electrodes (source, drain and gate), a gate dielectric layer, and a polymer semiconductor layer. Desirable properties of OFET devices include a high field-effect mobility (μ), a large current on/off ratio (I_{on}/I_{off}) and a low threshold voltage (V_T).

In general, polymer based FETs exhibit much smaller hole mobility than that of small molecules based OFET devices (esp. single crystals OFET devices). However, a few unique advantages exist for using polymeric materials. First, polymeric materials are generally soluble in appropriate organic solvents to form polymer "inks" with large viscosity. This allows easy and cheap processing of polymers into smooth and uniform films by spin-coating, doctor-blading or other printing techniques, which are adaptable to roll-to-roll fabrication on large flexible substrates. Second, polymer crystalline domains are typically much smaller than the length scale of organic electronic devices and randomly oriented. These result in less variability of device performance and an isotropic charge transport characteristic, which is especially important for real world applications.

With the increasing demand for polymer based FETs of higher performance, the search for newer and better polymeric materials – the core part of polymer FETs – has accelerated. In addition to the desired high mobility, a few other criteria have emerged from the perspective of the manufacturing [41–45], including (a) good solution processability especially on flexible polymer substrates, (b) short time or no annealing to enable high-speed mass production of OFET, (c) high operational stability under ambient conditions

without a costly protective barrier layer, (d) ability to self-organize into a higher structural order to achieve high charge-carrier mobilities, and (e) facile and economically feasible syntheses which can be scaled up for mass production.

3.3.2 BDT Based Polymers in OFET Application

The first application of BDT based polymers in OFET was reported by Ong *et al.* in 2006 [22]. At that time, only a few polymeric semiconductors offered OFET mobility over 0.01 $cm^2/(V \cdot s)$. The highest mobility of 0.1 $cm^2/(V \cdot s)$ was obtained by regioregular poly(3-hexylthiophene) (P3HT) [46]. However, the mobility of P3HT is significantly affected by the structure (the higher the regioregularity of P3HT, the higher the mobility [47]) and the operational condition/air stability (e.g., measured under ambient conditions leads to much lower mobility than in inert atmosphere [48]). The homopolymer of BDT unit (**P1**) was therefore synthesized [22] as an attempt to solve the regioregularity and stability issues obsessing P3HT [23]. Compared with asymmetric 3-hexylthiophene, the repeating unit of P3HT, the BDT unit features a C_{2h} symmetry, thereby eliminating any potential regio-irregularity. In addition, BDT unit has elevated oxidation stability ascribed to the center benzo unit fused into the bithiophene unit. This center benzo unit also offers two positions for anchoring solubilizing chains with a minimum impact on the planarity of the conjugated backbone and promoting stacking of polymer chains at the solid state. Although a low molecular weight of 2.1 kg/mol was obtained for such a homopolymer even with two dodecyl side chains per repeating unit, a good hole mobility of 0.012 $cm^2/(V \cdot s)$ was still observed in Ong's report [22]. Indeed, XRD study indicated a high crystallinity of **P1** and a high molecular order in the solution-cast thin film. Additionally, the stability of **P1** was much improved from P3HT with the decomposition temperature around 450°C.

Further improvement was achieved from copolymerizations of BDT unit with more thiophene unit (**P2** in Figure 3.1) [24]. The incorporation of two thienyl units in between the BDT monomer units of **P1** extended the effective π-conjugation and widened the spacing of pendant alkyl side chains along the polymer backbone. Thus polymer chain packing and molecular ordering through intermolecular interdigitation were much improved [44, 49]. In addition, a short methyl group on the 4 position of thiophene was used to ensure regioselective polymerization on C-5 via the oxidative polymerization. Compared

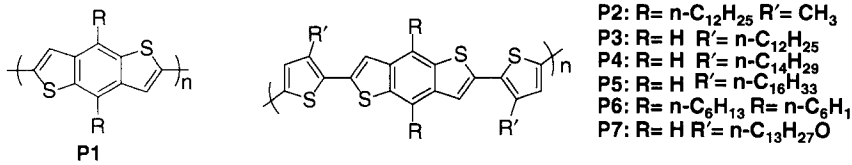

Figure 3.1 Chemical structures of BDT based polymers as OFET materials.

with **P1**, **P2** with a high molecular weight of 16 kg/mol exhibited a higher mobility of 0.15 $cm^2/(V \cdot s)$. It is worth noting that the post-deposition thermal annealing – a process required for P3HT based OFET devices to reach higher mobility – was not needed for OFET devices based on **P2**. This annealing-free feature of **P2** is extremely attractive to the mass production of OFET devices.

Shortly after the successful introduction of **P2**, several groups performed detailed studies on the positions and lengths of side chains on the thiophene-BDT-thiophene backbone in order to fine-tune polymer properties. **P3** with no side chains on BDT unit and long dodecyl groups on thiophene unit was reported by Kwon and coworkers [17], attempting to enhance stability and film orderness. However, the oxidative polymerization resulted in crosslinking of polymer chains. This was attributed to the oxidative coupling of other active sites in the monomer, such as the benzene ring or 4-position of the thiophenes. This ill-defined polymer structure failed to achieve an effective packing of polymer chains and an efficient charge transport. As a result, a very low mobility (on the order of 10^{-5} $cm^2/(V \cdot s)$) was obtained. However, when the same polymer was synthesized using the Stille coupling polymerization to overcome the problems caused by oxidative polymerization [50], a number-average molecular weight over 20 kg/mol was reported and the hole mobility was enhanced by a factor of 100. The impact of the length of side chains on material performance was investigated further with polymers with longer alkyl chains on thiophene units (**P4** and **P5**). It was observed that polymers with shorter chains exhibited higher hole mobility. The authors argued that the longer the side chain, the larger the influence of the insulating side chains on film formation and on film morphology at interfaces where the charge transport occurs. In the meantime, a strong molecular weight dependent of the OFET performance was also discovered for BDT based polymers [50]. Different molecular weight fractions were separated by the soxhlet extraction and

characterized. In general, the mobility of high molecular weight polymers was one order of magnitude higher than that of lower molecular weight polymers, though both with identical conjugated backbone.

P6 with alkyl chains evenly distributed along the polymer backbone was synthesized by Ong *et al.* using oxidative polymerization [6]. A high molecular weight of 16.3 kg/mol and a very high mobility up to 0.4 $cm^2/(V \cdot s)$ were successfully demonstrated. Furthermore, **P6** not only required no post-deposition thermal annealing, also exhibited relatively stable performance over 30 days in ambient environment at 20% relative humidity. Assisted by the Grazing-incidence X-ray diffraction (GIXRD) measurement, the authors discovered a well-organized lamellar layered structure of **P6** thin films which was oriented normal to the silicon substrate pre-modified with octyltrichlorosilane (OTS-8) [51, 52].

All these above-mentioned polymers exhibited HOMO levels around – 5.7 eV, which would increase the oxidation stability and current on/off ratio of related OFET devices. However, such a low HOMO energy level would also introduce a large barrier for hole injection into conjugated polymer and large threshold voltages. To achieve a better energetic match with the commonly employed Au contact electrodes (work function of – 5.1 eV), the HOMO energy level of conjugated polymers would need to be increased. In this regard, electron donating alkoxy side chains would be a better choice than alkyl chains. Additionally, oxygen atom can interact with sulfur atoms in neighboring thiophene units and the smaller van der Waals radius of oxygen atom over a methylene group would also lead to a smaller steric hindrance. **P7** was thus designed and synthesized by the Stille coupling polymerization. Indeed, the introduction of alkoxy side chains decreased the band gap by 0.18 eV and moved HOMO level up to – 5.1 eV. However, thermal stability of **P7** was largely decreased because alkoxy side chains are thermally less stable than alkyl side chains [53]. The as-fabricated OFET devices showed an ideal injection from gold electrodes into the polymer, with a hole mobility of 2×10^{-3} $cm^2/(V \cdot s)$ and an on/off ratio over 10^6 achieved with annealing. Even with the reduced thermal stability of **P7**, it is worth noting that the **P7** based OFET devices showed no significant degradation over 5 weeks.

BDT isomers and related polymers have recently been developed by Müllen and co-workers [41, 42]. Depending upon the geometrical arrangement of the thiophene units and the benzo unit in the fused

BDT monomer, a varying degree of curvature could be introduced into the polymer backbone, as exemplified by the five isomeric polymers shown in Figure 3.2. The monomer angle is defined by the angle introduced by the benzodithiophene unit with two flanking thiophene units. From **P3** to **P11**, as the monomer angle decreased, both amplitudes and wavelengths of the sine-shaped contour lines increased. (Table 3.1) Their study showed that the optical band gap

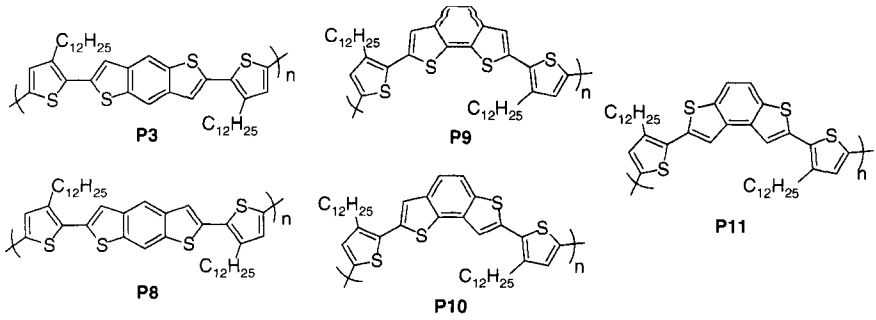

Figure 3.2 Chemical structures of **P3** and its analogs with different geometric arrangements.

Table 3.1 Geometry of polymers [41].

Polymer	Monomer Angle	Backbone	Amplitude	Wave Length
P3	180°		0.14 nm	1.47 nm
P8	169°		0.29 nm	2.82 nm
P9	127°		0.31 nm	2.83 nm
P10	113°		0.59 nm	2.75 nm
P11	106°		0.88 nm	2.32 nm

increased with increasing curvature from **P3**, **P9** to **P11**, probably because of a reduced effective conjugation length of the polymers. Similar band gap increase was observed for **P8** and **P10**, where the sulfur atoms arranged meta to the benzene unit also resulted in a less effective conjugation. XRD study showed the film ordering in bulk was suppressed with increased curvature, however, the π-stacking distance was unaffected. Additionally, the mobility did not show strong correlation with the polymer backbone curvature.

3.3.3 Introduction of PSC

Polymer solar cells (PSC) have attracted significant research attention, due to their unique features including low-cost, flexibility, solution processability and light weight. As a rather young research field – less than 20 years since the first discovery of the efficient and rapid charge transfer between conjugated polymers and fullerenes [54, 55], polymer solar cells have witnessed significant improvements in both device performances and the understanding of the underlying physical mechanisms. With the state-of-the-art efficiency already over 8% [56, 57] and newer and better materials emerging in an accelerated speed, the realization of commercial applications of polymer solar cells appears extremely promising.

The single most important performance parameter of a solar cell is the power conversion efficiency (PCE or η), which is related with the open circuit voltage (V_{oc}), short circuit current (J_{sc}) and fill factor (*FF*) through equation (**1**). All of those parameters can be extracted from the J-V curves under the 1 sun condition (100 mW/cm^2, simulated AM1.5 solar illumination) (Scheme 3.8). The PCE is calculated by the following equation:

$$\mathrm{PCE} = \frac{\mathrm{V_{oc}} \times J_{sc} \times FF}{\mathrm{P_{1n}}} \tag{1}$$

And FF is defined as:

$$\mathrm{FF} = \frac{\mathrm{V_{mpp}} \times J_{mpp}}{\mathrm{V_{oc}} \times J_{sc}} \tag{2}$$

Where $\mathrm{V_{mpp}}$ and J_{mpp} are the voltage and current at the maximum power point in the J-V curve, respectively (Scheme 3.9).

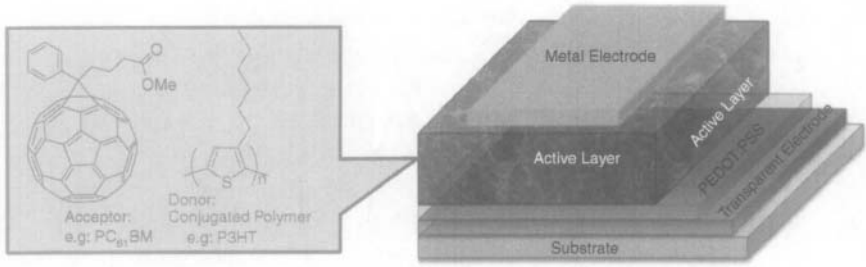

Scheme 3.8 Schematic illustration of the structure of a typical bulk heterojunction polymer solar cell device.

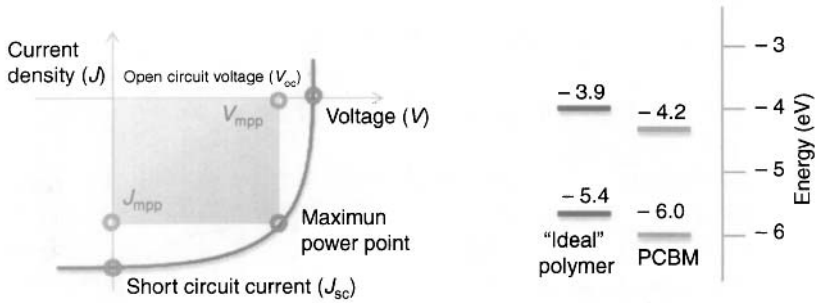

Scheme 3.9 An illustration of current density-voltage (J-V) curve of a polymer solar cell (left) and energy levels of "ideal polymer" and PCBM (right).

To date, the most successful method to construct the active layer of a polymer solar cell is to blend a photoactive polymer and an electron acceptor in a bulk-heterojunction (BHJ) configuration to maximize the interfacial contact and surface area (Scheme 3.8). Typical acceptors are generally soluble fullerene derivatives such as $PC_{61}BM$, which does not absorb light efficiently. Therefore, the conjugated polymer of the active layer not only serves as the main absorber to solar photon flux, also must transport the holes effectively. Design and synthesis of high performance conjugated polymers to optimize these two functions is, therefore, of great importance.

Specifically, to improve the power conversion efficiency of polymer-based BHJ photovoltaic cells, one has to carefully address the following three issues:

a. Open circuit voltage (V_{oc}). V_{oc} is correlated with the energy difference between the HOMO energy level

of the donor polymer and the LUMO of the acceptor. Therefore, the HOMO and LUMO energy levels of the donor and acceptor components need to have an optimal offset to maximize the attainable V_{oc}. Furthermore, it is estimated that a minimum energy difference of 0.3 eV between the LUMO of the donor and that of the acceptor is required to facilitate exciton splitting and charge dissociation. Since the most successful acceptor material $PC_{61}BM$ has a LUMO energy level of – 4.2 eV, the lowest possible LUMO level of the donor polymer would be near – 3.9 eV (Scheme 3.9). Generally, the lower the HOMO level of the donor, the higher the V_{oc}; however, a lower HOMO level would lead to an increased band gap of the donor polymer and less efficient light absorption.

b. Short circuit current (J_{sc}). The theoretical upper limit for J_{sc} of a polymer solar cell is set by the number of excitons created during solar illumination. The absorption of the active layer should be compatible to the solar spectrum to maximize exciton generation. Lower band gap polymers absorb more light, which would potentially increase the J_{sc}; however, lowering the band gap would require an increase of the HOMO level of the donor polymer (since the LUMO level of the donor polymer cannot be lower than – 3.9 eV), which would reduce the V_{oc}. Thus, an optimal band gap of 1.5 eV is proposed to be a compromise between these two contradictory factors [58, 59], which would thereby position the HOMO of the "ideal" polymer around – 5.4 eV.
c. Fill factor (*FF*). The morphology of the active layer governs the physical interaction between the donor polymer and the acceptor. It should be optimized to promote charge separation and favorable transport of photogenerated charges, thereby maximizing the *attainable* J_{sc} and *FF*.

To summarize, in order to exhibit high photovoltaic properties, the "ideal" polymer should have (a) good solubility; (b) high molecular weight; (c) HOMO level around – 5.4 eV; (d) a narrow band gap around 1.5 eV; (e) a high hole mobility; and (f) an optimized

active layer morphology [3, 58, 60]. Therefore, designing new polymers with all these properties presents a daunting challenge to the research community.

3.3.4 BDT Based Polymers for High performance PSC

BDT based polymers have witnessed even more successes in organic solar cells than in organic field effect transistors. In fact, more than half of the high performance polymers for PSC with power conversion efficiency over 6% incorporate the BDT unit as part of their conjugated backbones [61].

There are several structural advantages associated with the BDT unit. First, BDT has a large planar conjugated structure and easily forms strong π-π stacking, which can improve the mobility of related conjugated polymers. For example, previous discussion already showed that polymers based on BDT have exhibited a hole mobility as high as 0.4 $cm^2/(V \cdot s)$ [6]. Second, the benzo core of BDT unit renders BDT a relatively electron-deficient unit (compared with bithiophene or thiophene), which could lead to a low-lying HOMO level for BDT based copolymers (and a higher V_{oc} of related BHJ solar cells) [62]. Third, it is well documented that the band gap of conjugated polymers is very sensitive to the conjugated backbone twisting between repeating units. The smaller the chain twist, the lower the band gap. Since the solubilizing chains on the BDT based polymers can be anchored on the center benzo unit which is flanked by the relatively small sized thiophene units, the steric hindrance between BDT and other chromophores (co-monomers) is very small, which leads to a more effective conjugation and thereby a smaller band gap. Finally, BDT unit can be easily alkylated or alkoxylated. This allows not only additional control on the HOMO energy level of BDT based conjugated polymers, also fine-tuning these side chains (length and branching) of conjugated polymers to further optimize solar cell performances [63].

Since the homopolymer of the BDT unit has a wide band gap, [22, 57] incorporation of other chromophores (usually electron-accepting moieties) as co-monomers is necessary to tune the band gap and energy levels of the BDT based copolymers. These copolymers of BDT with other chromophores can be readily prepared

by the transition metal-mediated copolymerization as discussed earlier (Section 3.2.2).

For example, Yang and coworkers have synthesized and characterized a series of BDT based copolymers **P12 to P19** [21](Figure 3.3). Their study showed that the polymers **P13**, **P14** and **P15** with electron-rich chromophores such as ethylene, thiophene, and ethylenedioxythiophene (EDOT) exhibited similar band gap in regard to the homopolymer **P12**. However, when electron-deficient units were employed, these D-A type copolymers exhibited noticeable band gap reductions (**P16-P19**), which was ascribed to the internal charge transfer (ICT) between these D-A units [64, 65]. The observed smaller band gaps of **P18** was mainly due to the elevated HOMO level compared with that of the homopolymer of **P12**. This much elevated HOMO level led to instability of the copolymer **P18**. On the contrary, the benzo[c][1,2,5]thiadiazole (BT) unit (**P17**) or the benzo[c][1,2,5]selenadiazole (BSe) unit (**P19**) lowered the band gap by mainly reducing the LUMO levels. These authors further studied the photovoltaic properties of these polymers based BHJ devices. The lower the HOMO levels of the copolymers, generally the higher the V_{oc} of the BHJ devices. But J_{sc} seemed independent of the band gap of these polymers, which indicated the significant contribution of other factors in addition to energy levels and band gaps. The highest efficiency of 1.6% was obtained from devices based on **P14**:$PC_{61}BM$.

Li *et al.* also studied the copolymer of BDT unit with a simple vinylene linkage (**P20**) [66], which has an identical conjugated backbone as that of **P13**, but with different side chains (2-ethylhexyloxy

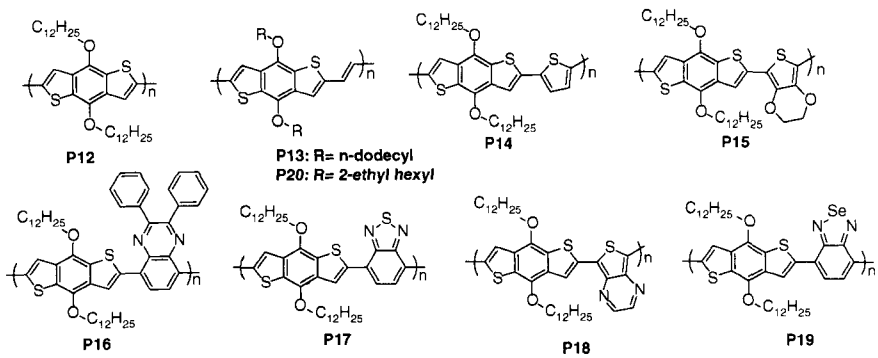

Figure 3.3 Structures of **P12** to **P20**.

on **P20** vs. n-dodecyloxy on **P13**). With the help of $PC_{71}BM$, which has better light absorption than $PC_{61}BM$, a PCE of 2.63% was achieved in **P20** based BHJ devices, over ten times higher than the efficiency obtained by **P13** based devices. This study underscores the great influence of the side chain selection on photovoltaic properties of conjugated polymers.

Because BDT is generally regarded as an electron-rich "donor", a number of electron-deficient "acceptor" units have been employed to construct the D-A copolymers with smaller band gaps via the ICT. One such "acceptor" is the diketopyrrolopyrrole (DPP) unit, which was polymerized with the BDT unit to offer copolymers **P21** through **P23** in Figure 3.4. The DPP unit has an extended conjugation which would lead to strong polymer chain-chain interactions, in addition to its strong electron-withdrawing ability offered by the electron-deficient lactam subunit. Therefore, **P21** synthesized by Yang *et al.* exhibited a small band gap of only 1.31 eV [67]. Its BHJ devices fabricated with $PC_{71}BM$ reached a PCE of 2.53%. More recently, Patil and coworkers replaced these thiophene units flanking DPP with benzene units, converting **P21** into **P22** [68]. A much larger band gap of 1.70 eV was observed due to the steric hindrance introduced by the benzene unit with adjacent BDT and DPP units. However, incorporating benzene units effectively decreased the HOMO level of **P22**, leading to a higher V_{oc} of 0.78 V in BHJ devices compared with that of **P21** based devices. Unfortunately, the J_{sc} was significantly lower, which concluded a total PCE of 1.51% of its BHJ device with $PC_{61}BM$ as the acceptor.

Another excellent electron-accepting building block is the newly developed thieno[3,4-*c*]pyrrole-4,6-dione (TPD) unit, which was first incorporated in BDT copolymers by Leclerc *et al.* (**P24** in Figure 3.5) [69]. When TPD is co-polymerized with BDT, the

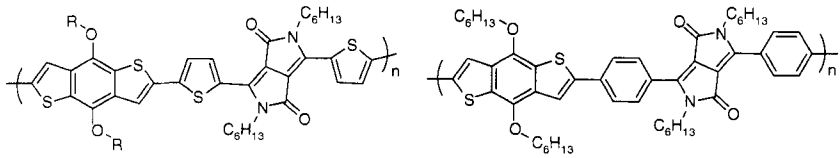

Figure 3.4 Structures of DPP containing polymers **P21** to **P23**.

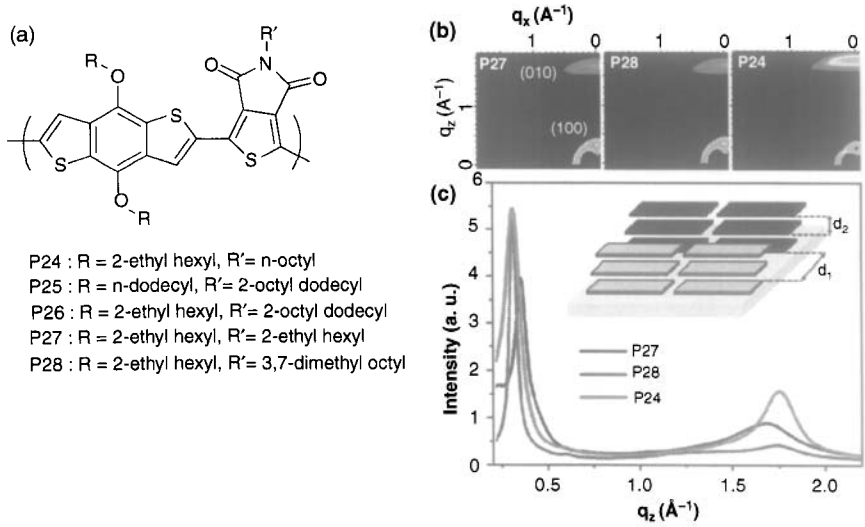

Figure 3.5 (a) TPD containing polymers **P24** to **P28**, (b) 2D grazing incidence X-ray scattering (GIXS) patterns of films of **P24**, **P27**, and **P28**. (c) Out-of-plane linecuts of GIXS. Inset: Schematic illustration of the face-on orientation of the polymers with the backbone parallel to the substrate. The lamellar spacing and the π-stacking distance are labeled d1 and d2, respectively [72].

resulting copolymer not only has a small band gap for a high J_{sc}, also maintains a low HOMO energy level which is desirable to increase the V_{oc}. **P24** exhibited a high number average molecular weight of 13 kg/mol measured via GPC in trichlorobenzene (TCB) running at 140°C. The UV–vis absorption spectrum of **P24** in solution was very similar to that obtained in the solid state, indicating a similar rigid-rod conformation in both states. The HOMO and LUMO energy levels determined by cyclic voltammetry were – 5.56 eV and – 3.75 eV, respectively. Therefore, a high V_{oc} of 0.85 V was demonstrated in the solar cell device with $PC_{71}BM$ as the acceptor. Along with a J_{sc} of 9.81 mA/cm^2 and a fill factor (*FF*) of 0.66, a PCE of ~5.5% was obtained. It is particularly worth mentioning that Leclerc *et al.* obtained these impressive values from devices with an active area of 1.0 cm^2. Achieving high efficiencies on devices of large area is advantageous for real world application of PSC, because efficiencies obtained on areas smaller than 0.2–0.3 cm^2 may become strongly substrate size-dependent, in addition to the possible over-estimation of the J_{sc} due to a very small device area. Similar polymers with identical conjugated backbone but

having different solubilizing chains were independently reported by Xie *et al.* and Jen *et al.* (**P25** and **P26**). These polymers showed similar band gaps and energy levels with those of **P24**. PCEs of related BHJ devices with $PC_{71}BM$ varied from 3.42% to 4.79% after some optimization [70, 71].

Realizing the important role of these side chains on the photovoltaic properties of conjugated polymers based solar cells, Fréchet and coworkers carefully studied the impact of these side chains on the TPD-BDT copolymer [72]. **P24** and two other copolymers (**P27** and **P28**) with different alkyl side chains on the TPD unit were synthesized and PCEs between 4% and 6.8% were reported. It is also worth noting that the photovoltaic properties of these polymers were investigated with $PC_{61}BM$ as the acceptor. High boiling-point additive 1,8-diiodooctane (DIO) was attempted to optimize the performance [73–75]. Simply by modifying side chains on the TPD unit, the PCE increased from 3.9% for BHJ devices based on **P27** with an ethylhexyl side chain, to 5.4% for **P28** with a dimethyloctyl side chain, whereas the elimination of branching on the side chain of TPD in **P24** further enhanced PCE to 6.8%. The addition of DIO greatly improved the performance of **P27** and **P28**, but only observed slight enhancement for **P24**. Further investigation of the active layers by grazing incidence X-ray scattering (GIXS) (Figure 3.5) showed that the use of high-boiling-point additives promoted the packing of these polymers while avoiding excessive crystallization of the fullerene. This optimized morphology was believed to account for the large enhancement in the device performance of **P27** and **P28**. In addition, the (010) peak corresponding to the π-stacking of the polymers was more prominent in the out-of-plane direction for all three polymers, which suggests that most of the polymer backbones were oriented parallel to the substrate (inset, Figure 3.5). This face-on orientation is beneficial for charge transport in the PSC device, and the effect would be further enhanced by reducing the π stacking distance between polymer backbones (d_2 in Figure 3.5c). Therefore by replacing the bulky ethylhexyl side chain on **P24** with less bulky dimethyloctyl and straight octyl chains on **P27** and **P28**, the value of d_2 decreased from 3.8Å to 3.6Å, which correlated well with the increased J_{sc} due to the improved charge transport.

An interesting electron-deficient heterocycle, pyrido[3,4-*b*]pyrazine (PP), was also copolymerized with BDT unit (**P29**) by Wei *et al.*[76] (Figure 3.6). Compared with the quinoxaline in **P16**, the extra electron-withdrawing nitrogen atom in the PP unit would

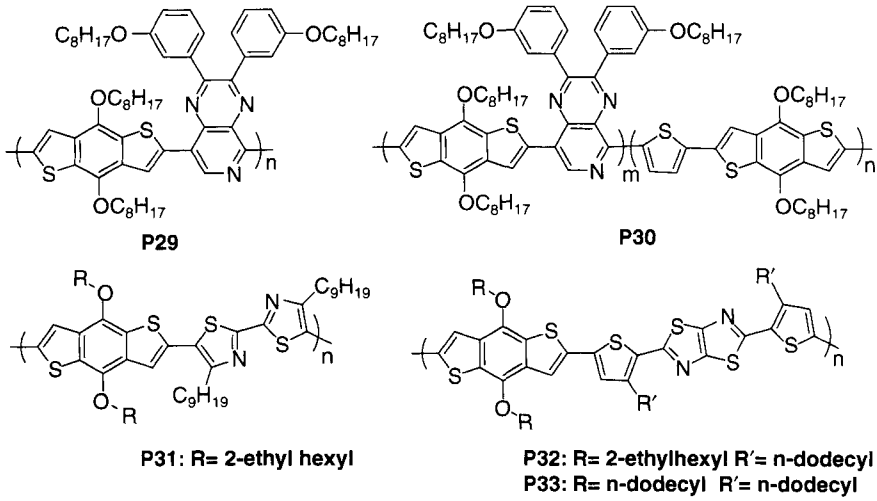

Figure 3.6 Structures of copolymers **P29** to **P33.**

render the PP more electron deficient. Thus the internal charge transfer from BDT unit to PP unit would be stronger [77, 78], resulting the red-shift of the absorption and lower HOMO level of **P29** relative to those of **P16**. Therefore, both of the J_{sc} and V_{oc} of **P29** based devices fabricated with $PC_{71}BM$ were improved compared with those of **P16**. And a total PCE of 1.2% was demonstrated. In order to broaden the light absorption of the conjugated polymer **P29**, the same authors attempted a random copolymer approach by combining BDT, PP and thiophene units into the conjugated backbone (**P30**). This new polymer was able to absorb the solar spectrum from the visible to the near infra-red region. As a result, improved photocurrents were achieved with **P30** based BHJ devices, leading to an improved PCE of 2.35%.

Very recently, Li and co-workers reported several new BDT based copolymers (**P31** and **P32**) incorporating bithiazole (BTz) or thiazolothiazole (TzTz) [79] (Figure 3.6). Thiazole is a well-known electron-deficient unit because of the electron-withdrawing nitrogen in the form of the imine (C = N). Conjugated polymers bearing BTz or TzTz units have demonstrated high mobilities (hole or electron) in OFET devices [80, 81]. Moreover, low HOMO energy levels were observed for these polymers containing BTz or TzTz, which led to relatively high voltages of 0.73 V and 0.77 V for BHJ devices based on **P31** and **P32**, respectively. However, **P31** and **P32** exhibited large

band gaps around 2 eV, which limited the efficient absorption of solar flux. Thus preliminary studies on photovoltaic devices of **P31** and **P32** only showed efficiencies over 2%. Interesting, when the branched side chains of **P32** were replaced with straight dodecyl chains in **P33** [82, 74], the PCE was improved to 2.72% with $PC_{71}BM$.

Di-2-thienyl-2,1,3-benzothiadiazole (DTBT) has been widely used as the acceptor unit to create "donor-acceptor" low band gap polymers with high performance, due to a few structural features of the DTBT. First, the two flanking thienyl units relieve the otherwise possibly severe steric hindrance between adjacent units. Thus, the synthesized donor-acceptor polymers would adopt a more planar structure, thereby reducing the band gap. In addition, a more planar conjugated backbone would facilitate the chain-chain interactions among polymers, improving the charge carrier mobility. Second, while the electron accepting BT unit maintains the low band gap, the two electron rich, flanking thienyl units would help improve the hole mobility. For example, Yang *et al.* recently demonstrated efficiencies up to 5.66% for BHJ devices based on a copolymer combining BDT with novel thienyl side chains and the DTBT unit (**P34**) [23] (Figure 3.7). The thienyl side chains which are not coplanar with the BDT unit did not contribute to any possible polymer backbone twist and a small band gap of 1.75 eV was still obtained. The observed high V_{oc} of 0.92 V was attributed to the lower HOMO level of the polymer and a larger π-π interaction distance between polymers caused by these thienyl side groups.

There is one catch with the incorporation of the DTBT unit: due to the excellent stacking ability of the DTBT unit [60], DTBT based polymers usually exhibit low molecular weights and limited solubility

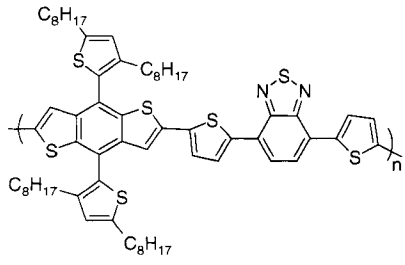

P34

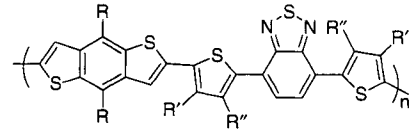

P35:R=2-ethylhexyl R'=H R''= n-hexyl
P36:R= 2-ethylhexyl R'=H R'= n-hexyloxy
P37:R= 3-butylnonyl R'= n-hexyl R''= H
P38:R= 3-hexylundecyl R'= H R''= H

Figure 3.7 Structures of copolymers **P34** to **P38** based on DTBT acceptor unit.

in organic solvents. Therefore, side chains are commonly anchored on the DTBT unit to improve the solubility of related polymers. Compared with the BDT-DTBT copolymer **P38** with no solubilizing chains on the DTBT, polymers of identical conjugated backbone but with more side chains showed much higher molecular weights, as reported by Yang *et al.* and You *et al.* [19, 83] (Figure 3.7). However, the anchoring position of these extra side chains on the DTBT had a significant impact on the band gaps and energy levels of these polymers, as well as photovoltaic properties of related devices. When alkyl chains on the DTBT unit were positioned close to the BT core (**P35**), the polymer backbone was twisted at the linkage between the thienyl and the BT, leading to a large band gap (1.85 eV) and weak chain-chain interactions. Switching to electron-rich alkoxy side chains yielded a lower band gap polymer **P36** (E_g = 1.55 eV), but at the cost of an elevated HOMO level (−4.8 eV). Only through anchoring the alkyl chains on the 4th position of the thienyl units (**P37**) could one simultaneously achieve the desired good solubility, high molecular weight, small band gap and low HOMO level with **P37**. Moreover, the enhanced solubility led to a better mixing of **P37** with $PC_{61}BM$ to form a smooth active layer. A PCE of 4.31% was thereby achieved for **P37**.

A few BDT based copolymers with DTBT derivatives were recently explored by You and coworkers (Figure 3.8) [9, 10, 84]. In one study, a strong acceptor unit di-2-thienyl thiadiazolo[3,4-*c*] pyridine (DTPyT) was synthesized by replacing the benzene unit

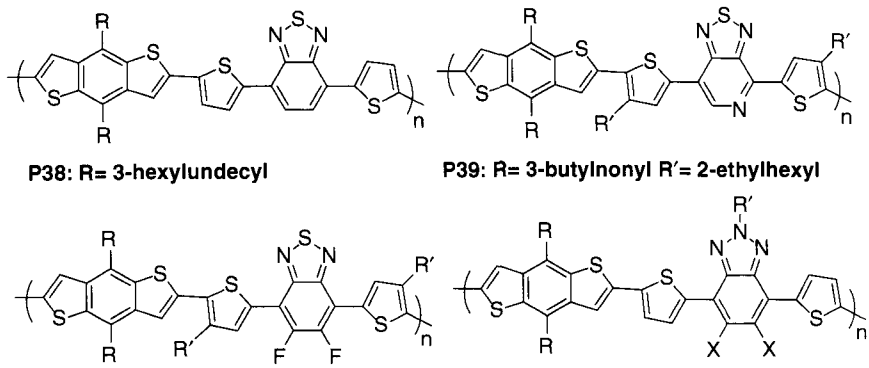

Figure 3.8 Structures of copolymers **P38** to **P42** with DTBT derivatives.

in the acceptor DTBT with a more electron-deficient pyridine unit [84]. The resulting polymer (**P39**) showed lower LUMO level and slightly reduced HOMO level than those of **P38**. More importantly, the enhanced ICT between adjacent BDT unit and DTPyT unit led to a smaller band gap of 1.51 eV of **P39** compared with that of **P38** (1.7 eV). With additional 2-ethyl hexyl chains on the DTPyT unit, **P39** also exhibited good solubility and ultra-high molecular weight via microwave assisted Stille coupling polymerization. All these contributed to a PCE over 6% observed in initial solar cell studies.

In another study, You *et al.* incorporated fluorine substitutions on the BT unit and carefully studied the impact of the fluorine substitution [9]. Fluorinated organic molecules exhibit a series of unique features such as great thermal and oxidative stability [85], elevated resistance to degradation [86], enhanced hydrophobicity and high lipophobicity in perfluorinated substances [87]. In addition, these fluorine atoms often have a great influence on inter- and intramolecular interactions via C-F···H, F···S and C-F···π_F interactions [86, 88]. Therefore fluorinated benzothiadiazole (ffBT) was developed as a novel structural unit for high performance solar cell materials [9]. Interesting, the difluorinated polymer (**P40**) showed decreased HOMO and LUMO levels and a similar band gap when compared with its non-fluorinated analog (**P38**). Preliminary tests on **P40** BHJ device demonstrated both increased V_{oc} (0.91 V) and J_{sc} (12.9 mA/cm^2). With an also enhanced fill factor of 0.61, an impressive PCE of 7.2% was thus obtained without special treatments.

In another related study, BDT based copolymers with di-2-thienyl-2,1,3-triazole (TAZ) (**P41**) or its difluorinated derivative (**P42**) as the acceptor unit were synthesized [10]. Both of the polymers exhibited medium band gaps of 2.0 eV compared with that of the DTBT based polymer (**P38**). This is because that the lone pair on the nitrogen atom of the triazole unit is more basic than the lone pairs on the sulfur of the benzothiadiazole and is thereby more easily donated into the triazole ring, making it more electron-rich compared with the original benzothiadiazole. Thus the ICT between BDT unit and TAZ unit would be reduced, leading to the observed wider band gap. Surprisingly, in spite of a medium band gap of ~2.0 eV, the currents of both polymers were larger than 10 mA/cm^2, which can be explained by ultra-high molecular weights and large hole mobilities of both polymers. A PCE of 4.3% was reported for **P41** based photovoltaic devices with $PC_{61}BM$ as the acceptor. More interesting results came from the di-fluorinated

P42. The application of the two fluorine atoms had a minimal effect on the optical and electrochemical properties of the polymer, but had a profound effect on the hole mobility of **P42** and thus the photovoltaic performance of its devices. BHJ devices based on **P42** consistently showed a higher *FF* and J_{sc} than those of devices based on **P41** at comparable thicknesses. A peak PCE of 7.1% was obtained in BHJ devices of **P42**:$PC_{61}BM$ without annealing and additives. Remarkably, **P42**:$PC_{61}BM$ solar cells can still achieve over 6% effciency even at an unprecedented thickness of 1 μm (of the active layer), which makes **P42** an excellent polymer for tandem solar cells.

Besides copolymerizing electron-deficient chromophores to construct "donor-acceptor" type low band gap polymers (since BDT is electron-rich), BDT based copolymers of small band gaps designed by the "quinoid" approach have also been investigated and received significant successes [7, 8, 89–93]. Yu *et al.* first reported such a polymer by alternating the thieno[3,4-*b*]thiophene (TT) unit with the BDT unit in the conjugated backbone (**P43**) [89], which had a very small band gap of 1.48 eV. Such a small band gap was attributed to the unusual stability of the quinoid form of the TT unit, which can be better understood through a schematic comparison of the possible quinoid stabilization for both TT and BT (Figure 3.9). In the quinoid structure of the TT unit, the five-member ring on the top can form a stable thiophene unit, whereas there is no such extra stability when the BT unit adopts the quinoid form. Therefore the TT unit would stabilize the quinoid structure far better that the BT unit, leading to a smaller band gap of **P43** compared with that of **P17**. A PCE of 5.6% was demonstrated in devices fabricated from a 1:1.2 (by weight) blend of **P43** and $PC_{71}BM$.

The relatively high HOMO level of the original BDT-TT polymers resulted in a small V_{oc} (0.58 V). In order to lower the HOMO level and enhance the V_{oc} of BHJ devices, an electron-withdrawing

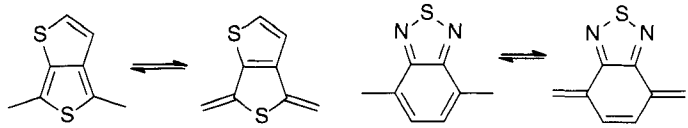

TT BT

Figure 3.9 Aromatic and quinoid forms of TT and BT units.

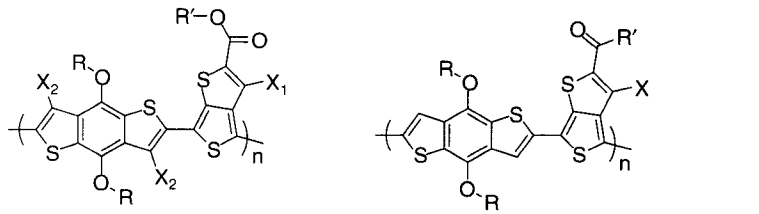

P43: X_1= H X_2= H R=C_8H_{17} R'= $C_{12}H_{25}$
P44: X_1= F X_2= H R= R'= 2-ethylhexyl
P47: X_1= H X_2= F R= R'= 2-ethylhexyl
P48: X_1= F X_2= F R= R'= 2-ethylhexyl

P45: X= H R= C_8H_{17} R'= $C_{12}H_{25}$
P46: X= F R= 2-ethylhexyl R'=n-C_7H_{15}

Figure 3.10 Structures of copolymers **P43** to **P48** containing TT or its derivatives.

fluorine atom was introduced onto the TT unit [90] (Figure 3.10). By further fine-tuning the length and shape of side chains, PCE up to 7.4% has been achieved in single layer photovoltaic devices of **P44** when $PC_{71}BM$ is used as the acceptor [7]. Grazing-incidence wide-angle X-ray scattering studies showed the polymer chain was stacked on the substrate in the face-on conformation which favors charge transport [91, 94].

Alternatively, Li and coworkers replaced the electron-donating alkoxy group on the TT unit with the alkyl group (**P45**) [93] (Figure 3.10). As expected, HOMO level of **P45** was 0.2 eV lower than that of **P43**, which was largely converted into the observed 0.12 V increase on the V_{oc} of BHJ devices based on **P45** compared with that of **P43** based devices. The average PCE obtained from more than 200 devices reached 6.3%. The subsequent introduction of the fluorine onto the TT unit further lowered both HOMO and LUMO levels. Therefore, **P46** based devices exhibited efficiencies as high as 7.7% by taking advantages of a low HOMO level and long wavelength absorption [8].

Yu *et al.* further showed that the incorporation of the fluorine on various positions of the polymer backbone significantly affected the performance of related solar cells [92]. Depending upon which hydrogen of the conjugated backbone was substituted with the fluorine, PCE of corresponding BHJ devices could vary from 2.3% to 7.2%. They also observed that fluorination of the BDT unit lowered both the HOMO and LUMO levels of **P47** but widened the band gap. Further, perfluorination of the polymer backbone led to a poor compatibility of **P48** with the $PC_{71}BM$ molecule, thus poor solar cell performance was observed. In addition, perfluorination of the

polymer backbone resulted in poor photochemical stability against singlet oxygen attack [92].

3.4 Outlook

In this chapter, we summarized the synthetic methods of BDT monomers and BDT based polymers. A few unique features of BDT based polymers were discussed, such as planar polymer backbone, high crystallinity and high mobility. All these have contributed to the tremendous development in BDT based materials for applications in organic electronics over the past decade. We believe more and better materials incorporating BDT as the structural unit still remain to be discovered.

3.5 References

1. H. Dong, C. Wang, and W. Hu, *Chemical Communications*, Vol. 46, p. 5211, 2010.
2. A. Facchetti, *Materials Today*, Vol. 10, p. 28, 2007.
3. J. Chen, and Y. Cao, *Accounts of Chemical Research*, Vol. 42, p. 1709, 2009.
4. O. Inganas, F. Zhang, and M.R. Andersson, *Accounts of Chemical Research*, Vol. 42, p. 1731, 2009.
5. J. Peet, A.J. Heeger, and G.C. Bazan, *Accounts of Chemical Research*, Vol. 42, p. 1700, 2009.
6. H. Pan, Y. Li, Y. Wu, P. Liu, B.S. Ong, S. Zhu, and G. Xu, *Journal of American Chemical Society*, Vol. 129, p. 4112, 2007.
7. Y. Liang, Z. Xu, J. Xia, S.-T. Tsai, Y. Wu, G. Li, C. Ray, and L. Yu, *Advanced Materials*, Vol. 22, p. E135, 2010.
8. H.-Y. Chen, J. Hou, S. Zhang, Y. Liang, G. Yang, Y. Yang, L. Yu, Y. Wu, and G. Li, *Nature Photonics*, Vol. 3, p. 649, 2009.
9. H. Zhou, L. Yang, A.C. Stuart, S.C. Price, and W. You, *Angewandte Chemie International Edition*, Vol. 50, p. 2995, 2011.
10. S.C. Price, A.C. Stuart, L.Q. Yang, H. Zhou, and W. You, *Journal of the American Chemical Society*, Vol. 12, p. 4625, 2011.
11. D.W.H. MacDowell and J.C. Wisowaty, *Journal of Organic Chemistry*, Vol. 36, p. 4004, 1971.
12. P. Beimling, and G. Koβmehl, *Chem. Ber.*, Vol. 119, p. 3198, 1986.
13. K. Shiraishi, and T. Yamamoto, *Japanese Journal of Applied Physics, Part 1*, Vol. 42, p. 6619, 2003.
14. K. Shiraishi, and T. Yamamoto, *Synthetic Metals*, Vol. 130, p. 139, 2002.
15. K. Shiraishi, and T. Yamamoto, *Polymer Journal (Tokyo, Japan)*, Vol. 34, p. 727, 2002.
16. J.G. Laquindanum, H.E. Katz, A.J. Lovinger, and A. Dodabalapur, *Advanced Materials*, Vol. 9, p. 36, 1997.

17. T.T.M. Dang, S.-J. Park, J.-W. Park, D.-S. Chung, C.E. Park, Y.-H. Kim, and S.-K. Kwon, *Journal of Polymer Science, Part A: Polymer Chemistry*, Vol. 45, p. 5277, 2007.
18. K. Takimiya, Y. Konda, H. Ebata, N. Niihara, and T. Otsubo, *The Journal of Organic Chemistry*, Vol. 70, p. 10569, 2005.
19. S.C. Price, A.C. Stuart, and W. You, *Macromolecules*, Vol. 43, p. 4609, 2010.
20. D.W. Slocum, and P.L. Gierer, *Journal of Organic Chemistry*, Vol. 41, p. 3668, 1976.
21. J. Hou, M.-H. Park, S. Zhang, Y. Yao, L.-M. Chen, J.-H. Li, and Y. Yang, *Macromolecules*, Vol. 41, p. 6012, 2008.
22. H. Pan, Y. Li, Y. Wu, P. Liu, B.S. Ong, S. Zhu, and G. Xu, *Chemistry of Materials*, Vol. 18, p. 3237, 2006.
23. L. Huo, J. Hou, S. Zhang, H.-Y. Chen, and Y. Yang, *Angewandte Chemie International Edition*, Vol. 49, p. 1500, 2010.
24. H. Pan, Y. Wu, Y. Li, P. Liu, B.S. Ong, S. Zhu, and G. Xu, *Advanced Functional Materials*, Vol. 17, p. 3574, 2007.
25. F. Jaramillo-Isaza, and M.L. Turner, *Phys. Status Solidi C*, Vol. 4, p. 4092, 2007.
26. X. Qiao, X. Wang, and Z. Mo, *Synthetic Metals*, Vol. 122, p. 449, 2001.
27. T.D. McCarley, Noble, C.J. DuBois, and R.L. McCarley, *Macromolecules*, Vol. 34, p. 7999, 2001.
28. J. Chen, M.-M. Shi, X.-L. Hu, M. Wang, and H.-Z. Chen, *Polymer*, Vol. 51, p. 2897, 2010.
29. N. Hundt, K. Palaniappan, J. Servello, D.K. Dei, M.C. Stefan, and M.C. Biewer, *Organic Letters*, Vol. 11, p. 4422, 2009.
30. B. Carsten, F. He, H.J. Son, T. Xu, and L. Yu, *Chemical Reviews*, Vol. 111, p. 1493, 2011.
31. Z. Bao, W. Chan, and L. Yu, *Chemistry of Materials*, Vol. 5, p. 2, 1993.
32. Z. Bao, W.K. Chan, and L. Yu, *Journal of the American Chemical Society*, Vol. 117, p. 12426, 1995.
33. K.T. Nielsen, K. Bechgaard, and F.C. Krebs, *Macromolecules*, Vol. 38, p. 658, 2005.
34. R.C. Coffin, J. Peet, J. Rogers, and G.C. Bazan, *Nature Chemistry*, Vol. 1, p. 657, 2009.
35. C. Li, M. Liu, N.G. Pschirer, M. Baumgarten, and K. Müllen, *Chemical Reviews*, Vol. 110, p. 6817, 2010.
36. T. M. Swager, *Accounts of Chemical Research*, Vol. 41, p. 1181, 2008.
37. R.S. Dudhe, J. Sinha, A. Kumar, and V.R. Rao, *Sensors and Actuators B: Chemical*, Vol. 148, p. 158, 2010.
38. V. Subramanian, P.C. Chang, J.B. Lee, S.E. Molesa, and S.K. Volkman, *Components and Packaging Technologies, IEEE Transactions*, Vol. 28, p. 742, 2005.
39. H.E. Katz, X.M. Hong, A. Dodabalapur, and R. Sarpeshkar, *Journal of Applied Physics*, Vol. 91, p. 1572, 2002.
40. H.E. A. Huitema, G.H. Gelinck, J.B.P.H. van der Putten, K.E. Kuijk, C.M. Hart, E. Cantatore, and D.M. de Leeuw, *Advanced Materials*, Vol. 14, p. 1201, 2002.
41. R. Rieger, D. Beckmann, A. Mavrinskiy, M. Kastler, and K. Müllen, *Chemistry of Materials*, Vol. 22, p. 5314, 2010.
42. R. Rieger, D. Beckmann, W. Pisula, W. Steffen, M. Kastler, and K. Müllen, *Advanced Materials*, Vol. 22, p. 83, 2010.
43. H. Sirringhaus, *Advanced Materials*, Vol. 17, p. 2411, 2005.

44. B.S. Ong, Y. Wu, P. Liu, and S. Gardner, *Journal of the American Chemical Society*, Vol. 126, p. 3378, 2004.
45. I. McCulloch, M. Heeney, C. Bailey, K. Genevicius, I. MacDonald, M. Shkunov, D. Sparrowe, S. Tierney, R. Wagner, W. Zhang, M.L. Chabinyc, R.J. Kline, M.D. McGehee, and M.F. Toney, *Nature Materials*, Vol. 5, p. 328, 2006.
46. Z. Bao, A. Dodabalapur, and A.J. Lovinger, *Applied Physics Letters*, Vol. 69, p. 4108, 1996.
47. Y.-K. Han, Y.-J. Lee, P.-C. Huang, L.A. Majewski, J.W. Kingsley, C. Balocco, and A.M. Song, *Journal of The Electrochemical Society*, Vol. 156, p. K37, 2009.
48. L.A. Majewski, J.W. Kingsley, C. Balocco, and A.M. Song, *Applied Physics Letters*, Vol. 88, p. 222108, 2006.
49. Y. Wu, P. Liu, S. Gardner, B.S. Ong, *Chemistry of Materials*, Vol. 17, p. 221, 2004.
50. M.A.M. Leenen, F. Cucinotta, W. Pisula, J. Steiger, R. Anselmann, H. Thiem, and C.L. De, *Polymer*, Vol. 51, p. 3099, 2010.
51. H. Sirringhaus, P.J. Brown, R.H. Friend, M.M. Nielsen, K. Bechgaard, B.M.W. Langeveld-Voss, A.J.H. Spiering, R.A.J. Janssen, E.W. Meijer, P. Herwig, and D.M. de Leeuw, *Nature*, Vol. 401, p. 685, 1999.
52. Y. Kim, S. Cook, S.M. Tuladhar, S.A. Choulis, J. Nelson, J.R. Durrant, D.D.C. Bradley, M. Giles, I. McCulloch, C.-S. Ha, and M. Ree, *Nature Materials*, Vol. 5, p. 197, 2006.
53. X. Hu, and L. Xu, *Polymer*, Vol. 41, p. 9147, 2000.
54. G. Yu, J. Gao, J.C. Hummelen, F. Wudl, A.J. Heeger, *Science*, Vol. 270, p. 1789, 1995.
55. N.S. Sariciftci, L. Smilowitz, A.J. Heeger, and F. Wudl, *Science*, Vol. 258, p. 1474, 1992.
56. "http://www.konarka.com/".
57. "http://www.solarmer.com/".
58. M.C. Scharber, D. Mühlbacher, M. Koppe, P. Denk, C. Waldauf, A.J. Heeger, and C.J. Brabec, *Advanced Materials*, Vol. 18, p. 789, 2006.
59. C. Soci, I.W. Hwang, D. Moses, Z. Zhu, D. Waller, R. Gaudiana, C.J. Brabec, and A.J. Heeger, *Advanced Functional Materials*, Vol. 17, p. 632, 2007.
60. H. Zhou, L. Yang, S. Xiao, S. Liu, and W. You, *Macromolecules*, Vol. 43, p. 811, 2010.
61. A. Facchetti, *Chemistry of Materials*, Vol. 23, p. 733, 2010.
62. H. Zhou, L. Yang, S. Stoneking, and W. You, *ACS Applied Materials & Interfaces*, Vol. 2, p. 1377, 2010.
63. L. Yang, H. Zhou, and W. You, *The Journal of Physical Chemistry C*, Vol. 114, p. 16793, 2010.
64. J. Roncali, *Macromolecular Rapid Communications*, Vol. 28, p. 1761, 2007.
65. J. Roncali, *Chemical Reviews*, Vol. 97, p. 173, 1997.
66. Y. He, Y. Zhou, G. Zhao, J. Min, X. Guo, B. Zhang, M. Zhang, J. Zhang, Y. Li, F. Zhang, and O. Inganaes, *Journal of Polymer Science, Part A: Polymer Chemistry*, Vol. 48, p. 1822, 2010.
67. L. Huo, J. Hou, H.-Y. Chen, S. Zhang, Y. Jiang, T.L. Chen, and Y. Yang, *Macromolecules*, Vol. 42, p. 6564, 2009.
68. C. Kanimozhi, P. Balraju, G.D. Sharma, and S. Patil, *Journal of Physical Chemistry B*, Vol. 114, p. 3095, 2010.
69. Y. Zou, A. Najari, P. Berrouard, S. Beaupre, A.B. Reda, Y. Tao, and M. Leclerc, *Journal of the American Chemical Society*, Vol. 132, p. 5330, 2010.

70. Y. Zhang, S.K. Hau, H.-L. Yip, Y. Sun, O. Acton, and A.K.Y. Jen, *Chemistry of Materials*, Vol. 22, p. 2696, 2010.
71. G. Zhang, Y. Fu, Q. Zhang, amd Z. Xie, *Chemical Communications*, Vol. 46, p. 4997, 2010.
72. C. Piliego, T.W. Holcombe, J.D. Douglas, C.H. Woo, P.M. Beaujuge, and J.M.J. Frechet, *Journal of the American Chemical Society*, Vol. 132, p. 7595, 2010.
73. J. Peet, N.S. Cho, S.K. Lee, and G.C. Bazan, *Macromolecules*, Vol. 41, p. 8655, 2008.
74. J. Peet, J.Y. Kim, N.E. Coates, W.L. Ma, D. Moses, A.J. Heeger, and G.C. Bazan, *Nature Materials*, Vol. 6, p. 497, 2007.
75. J.K. Lee, W.L. Ma, C.J. Brabec, J. Yuen, J.S. Moon, J.Y. Kim, K. Lee, G.C. Bazan, and A.J. Heeger, *Journal of the American Chemical Society*, Vol. 130, p. 3619, 2008.
76. M.-C. Yuan, M.-Y. Chiu, C.-M. Chiang, and K.-H. Wei, *Macromolecules*, Vol. 43, p. 6270, 2010.
77. B.-L. Lee, and T. Yamamoto, *Macromolecules*, Vol. 32, p. 1375, 1999.
78. M. Jonforsen, T. Johansson, L. Spjuth, O. Inganäs, and M.R. Andersson, *Synthetic Metals*, Vol. 131, p. 53, 2002.
79. M. Yang, B. Peng, B. Liu, Y. Zou, K. Zhou, Y. He, C. Pan, and Y. Li, *Journal of Physical Chemistry C*, Vol. 114, p. 17989, 2010.
80. I. Osaka, R. Zhang, J. Liu, D.-M. Smilgies, T. Kowalewski, and R.D. McCullough, *Chemistry of Materials*, Vol. 22, p. 4191, 2010.
81. M. Mamada, J. Nishida, D. Kumaki, S. Tokito, and Y. Yamashita, *Chemistry of Materials*, Vol. 19, p. 5404, 2007.
82. Q. Shi, H. Fan, Y. Liu, W. Hu, Y. Li, and X. Zhan, *Journal of Physical Chemistry C*, Vol. 114, p. 16843, 2010.
83. J. Hou, H.-Y. Chen, S. Zhang, and Y. Yang, *Journal of Physical Chemistry C*, Vol. 113, p. 21202, 2009.
84. H. Zhou, L. Yang, S.C. Price, K.J. Knight, and W. You, *Angewandte Chemie International Edition*, Vol. 49, p. 7992, 2010.
85. S. Wong, H. Ma, A.K.Y. Jen, R. Barto, and C.W. Frank, *Macromolecules*, Vol. 36, p. 8001, 2003.
86. K. Reichenbacher, H.I. Suss, and J. Hulliger, *Chemical Society Reviews*, Vol. 34, p. 22, 2005.
87. M. Pagliaro, and R. Ciriminna, *Journal of Materials Chemistry*, Vol. 15, p. 4981, 2005.
88. Y. Wang, S.R. Parkin, J. Gierschner, and M.D. Watson, *Organic Letters*, Vol. 10, p. 3307, 2008.
89. Y. Liang, Y. Wu, D. Feng, S.-T. Tsai, H.-J. Son, G. Li, and L. Yu, *Journal of the American Chemical Society*, Vol. 131, p. 56, 2009.
90. Y. Liang, D. Feng, Y. Wu, S.-T. Tsai, G. Li, C. Ray, and L. Yu, *Journal of the American Chemical Society*, Vol. 131, p. 7792, 2009.
91. Y. Liang, and L. Yu, *Accounts of Chemical Research*, Vol. 43, p. 1227, 2010.
92. H.J. Son, W. Wang, T. Xu, Y. Liang, Y. Wu, G. Li, and L. Yu, *Journal of the American Chemical Society*, Vol. 133, p. 1885, 2011.
93. J. Hou, H.-Y. Chen, S. Zhang, R.I. Chen, Y. Yang, Y. Wu, and G. Li, *Journal of the American Chemical Society*, Vol. 131, p. 15586, 2009.
94. J. Guo, Y. Liang, J. Szarko, B. Lee, H.J. Son, B.S. Rolczynski, L. Yu, and L.X. Chen, *Journal of Physical Chemistry B*, Vol. 114, p. 4746, 2010.

This page intentionally left blank

4

Polysulfone-Based Ionomers

Cristina Iojoiu and Rakhi Sood

LEPMI, CNRS-Grenoble INP – UJF, Saint Martin d'Hères, France

Abstract

This chapter is a review focussed on the development of ionomers based on aromatic polysulfones for their application as Polymer Electrolyte Membrane (PEM) in Proton Exchange Membrane Fuel Cells (PEMFC) or in Direct Methanol Fuel Cells (DMFC). Different types of synthesis routes have been discussed in this chapter in order to obtain ionomers based on polysulfones with variation in structural designs. Special attention is given to the impact of the structural design of the ionomer on various properties such as membrane morphology, thermo-mechanical stability and protonic conductivity of the membranes for their utilization as PEMs.

Keywords: Ionomers, fuel cells, membranes, polysulfones, sulfonation, phosphonation, nano-structuration

4.1 Introduction

Polymer Electrolyte Membrane Fuel Cells (PEMFC) have attracted considerable attention as candidates for alternative power sources due to their high power density, good energy conversion efficiency, and zero emissions levels [1–3]. Perfluorosulfonic acid (PFSA) based polymers such as Nafion® (DuPont) are the most promising and state-of-the-art Polymer Electrolyte Membranes (PEM) for PEMFC. However, the PFSA polymers have several shortcomings which limit their utility and performance, such as low proton conductivity at elevated temperatures (>80°C), high methanol crossover, high gas diffusion, environmental incompatibility (poor recyclability), and significant manufacturing costs [4–6]. Hence, finding an alternative is essential for the commercialization of PEMFC technology

Vikas Mittal (ed.) High Performance Polymers and Engineering Plastics, (81–110)
© Scrivener Publishing LLC

for energy production and consequently, a lot of effort has been put to develop novel hydrocarbon PEMs based on aromatic polymers, which have enough good physical properties and are inexpensive.

The cheapest alternative is sulfonated polystyrene [7, 8] but, due to the high sensitivity of its benzylic sites to free-radicals and oxidants, it cannot be used as a PEM.

Recently, the most widely investigated PEMs include sulfonated derivatives of poly(arylene ether sulfone)s (SPSU), [9, 10] poly-(arylene ether ether ketone)s (SPEEK), [11–13] poly(arylene sulphide sulfone)s (SPSS), [14, 15] polyimides (SPI), [16, 17], polyphenylenes (PP) [18, 19], etc.

The PEM are usually based on thin ionomer (polymer functionalised with acidic function) films. The main roles served by membrane are to separate the electrodes, to allow proton transportation from anode to cathode and to create a barrier against the passage of gases or fluids (e.g. methanol). Nevertheless the ionomer itself does not provide any appreciable conductivity and so must be swollen by molecules, e.g. water, to ensure proton conductivity. Water uptake by the membrane is therefore one of the most essential parameters in obtaining high conductivity levels.

The proton conductivity of ionomers is proportional to the IEC (Ion Exchange Capacity) and it often increases abruptly at some specific IEC in relation with the ionomer structure and percolation limit [20–22]. Many ionomers show sufficiently high conductivities only at high IECs and high IECs cause extensive water uptake above a critical temperature and consequently a dramatic loss of mechanical properties due to dimensional swelling is observed that renders them unsuitable for practical PEM applications. The dimensional stability and proton conductivity of aromatic ionomers are crucial issues that require improvement through careful structural design. These issues can be sorted out by fine-tuning several parameters such as acidity, number and position of ionic groups, main-chain and/or side chain structures, composition and sequence of hydrophilic and hydrophobic components, and membrane morphology.

Among these, acidity of ionic groups and membrane morphology appear to be crucial, and they are inter-related. Kreuer *et al.* [23] reported that typical sulfonated aromatic polymers are unable to form defined hydrophilic domains, as the rigid aromatic backbone prevents the formation of continuous conducting channels. Thus, various strategies have been pursued to obtain efficient ionic networks for enhancing the proton conductivity.

Presently, there has been a lot of interest generated for the production of polysulfones based ionomers for their utilization as polymer electrolyte membrane in High Temperature-PEMFCs (HT-PEMFC) due to their very high thermo-mechanical and chemical stability which are required for HT-PEMFC application.

The polysulfone ionomers are obtained by chemical modification of commercial polysulfone or by polymerization of ionic monomers using step-growth polymerization. In order to enhance their performance as a PEM, different approaches (enlisted below) have been reported which will be discussed thoroughly in this chapter.

1. One approach is to increase the acidity and the stability of acidic function by moving the acid function from the ortho-to-ether position to the ortho-position of a strongly electron-withdrawing units i.e. ortho-to-sulfone position connecting the phenyl rings in the case of polyether sulfone (UDEL).
2. Another approach is to induce distinct phase separation between the hydrophilic region containing acidic ionic function and the hydrophobic region composed of polymer main-chain by positioning the acid groups on side chains grafted onto the polymer main-chain. If the polymer structure consists of flexible pendant side chains carrying ionic function moieties linked to the polymer main-chain, nano-phase separation between hydrophilic and hydrophobic domains might be improved.
3. A third approach is to induce nano-phase separation through block copolymer architecture, whereby acidic ionic groups are concentrated in one of the blocks along the polymer chain. In this regard, multiblock acidic polymers were prepared with a promising morphological structure by polycondensation.

4.2 Polysulfone Backbone and Selection of the Ionic Function

The polysulfone are amorphous thermoplastics polymers possessing unique high performance properties such as high thermal, chemical

and mechanical stability, wide electrochemical stability window over wide temperature range, self-extinguishing properties, transparency and resistance to greases. From the chemical point of view, usually, the polysulfones are the polymers containing aryl groups linked by sulfonyl (-SO_2-) and ether (-O-) groups (Scheme 4.1). The different segments in the structure of polysulfones impart different properties to this polymer. The arylene ether segment and isopropylidene groups are electron-donating and non-polar in nature and provides chain flexibility. On the other hand, the arylene sulfone segment is strongly electron-withdrawing and polar in nature and hence provides rigidity to the polymer along with resistance to heat and oxidation.

These polymers have high glass-transition temperatures while their solubility in usual organic solvents enabling chemical modifications, is an indisputable asset. Moreover, as contrary to other aromatic polymers such as polyetherketone, polyether ether ketone, the polysulfone are fully amorphous; their mechanical strength does not depend on crystallinity ratios and melting temperatures which are very sensitive to the nature of chemical modifications and to their extent.

Concerning polysulfone functionalised with acidic function, special attention has to be paid to the selection of the anionic group which must be both electrochemically stable and must provide high proton conductivity. By definition, acidic solid-state ionomers, even if swollen by water, have a cationic transport number T^+ equal to 1. As in any electrolyte the conductivity depends on the concentration of charge carriers and their mobility, the proton concentration is proportional to the acid concentration and its dissociation in PEM. In order to optimize the dissociation, the organic anions have to be selected from among the conjugated bases of strong acids to superacids. The various acidic functions which can be easily attached to the polysulfone backbone include carboxylic acid, alkyl, aryl or perfluoro sulfonic acid, phosphoric acid, perfluorosulfonyl imide acid.

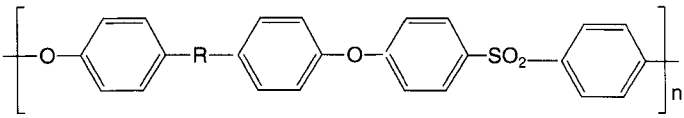

RADEL;R= -
UDEL;R= $C(CH_3)_2$

Scheme 4.1 Widely studied commercially available polysulfones.

The acidity and stability of carboxylic acid is not enough high for this kind of application and therefore will not be discussed here. Among the other acidic function, the sulfonic acid units have been by far the acidic moiety of choice. This is due to the wide range of reactants that are commercially available for sulfonation and also due to their enough high acidity and stability. Another ionic function i.e. phosphonic acid is largely described in the literature while any work on the polysulfone functionalised with perfluorosulfonyl imide acid has not been reported. The main advantage of phosphonic acid moieties is the increased chemical and thermal stability in comparison to sulfonic acid moieties [24, 25]. Also, they show greater ability to retain water than sulfonic acid units [26] along with higher degree of self-dissociation and hydrogen bonding [27], and this is crucial for maintaining high conductivities at elevated temperatures.

4.3 Ionomer Synthesis and Characterization

In order to attach the acidic ionic function on the polysulfone main-chain, two main approaches have been developed:

1. *Chemical modification of commercially available polysulfones*

Among the available commercial polysulfones, UDEL has been largely reported in the literature. The advantage of this polymer is its better solubility in organic solvents compared to other polysulfone (i.e. RADEL) which enables to use different reactions for the chemical modification i.e. (i) electrophilic substitution which lead to chloromethylation, halogenation, and sulfonation, (ii) nucleophilic substitution by use of lithiation chemistry.

Although this approach has been widely developed, there are certain shortcomings of this approach as follows (i) the limitation in chemical backbone structure, (ii) the random distribution of ionic function (iii) the side reactions during the modification, i.e. sulfonation may lead to main-chain breaking and reticulation (iv) the reaction reproducibility.

2. *Polymerisation of ionic monomers by step- growth polymerisation*

This approach is complementary to chemical modification of available commercial polysulfone and its main advantages include

(i) a high diversity in the chemical structure of the backbone; (ii) synthesis of hydrophobic-hydrophilic block copolymers that allow separation between the mechanical and conduction properties and (iii) control of the polymer molecular weight.

4.3.1 Chemical Modification of Commercially Available Polysulfones

The ionic function can be added by (i) electrophilic substitution in ortho-to-ether position on arylene ether segment due to its electron-donating nature or by (ii) aromatic nucleophilic substitution in ortho-to-sulfone position. Due to the electron withdrawing nature of sulfonyl link present in arylene sulfone segment, the acidic character of hydrogen atom present ortho-to-sulfone link is quite high and hence, activated for nucleophilic substitution using lithiation chemistry.

4.3.1.1 Acidic Ionic Function Attached Directly at Ortho-to-Ether Position of the Polymer

By electrophilic substitution the sulfonic acid and phosphonic acid groups were grafted on the backbone (Scheme 4.2 and Scheme 4.3). It is well known that the acidity of phosphonic acids is lower than that of sulfonic acids.

The electrophilic sulfonation of polysulfones can be achieved by many ways such as by using fuming sulphuric acid or by trimethylsilyl chlorosulfonate [28, 29] or by chlorosulfonic acid [30, 31] (shown in Scheme 4.2). Since trimethylsilyl chlorosulfonate is milder in nature compared to chlorosulfonic acid, it is preferred since the latter one requires proper attention and also leads to significant chemical degradation of the polymer [32]. The degree of sulfonation (DS) depends on the molar ratio of sulfonating agent and polymer-repeating units. The membranes obtained form the sulfonated polysulfone (IEC = 1.2 meq /g) show the conductivity in the range of 1–10 S/cm at 100°C, 98% RH (relative humidity) [29]. But the membranes with high IEC value lose mechanical stability due to extensive swelling at temperature above 80°C and the membranes with IEC = 1.6 meq/g become water-soluble [33].

The electrophilic phosphonation of polysulfones is achieved by a two-step reaction (i) bromination (ii) phosphonation of brominated polymer. Brominated sites located ortho to ether linkage

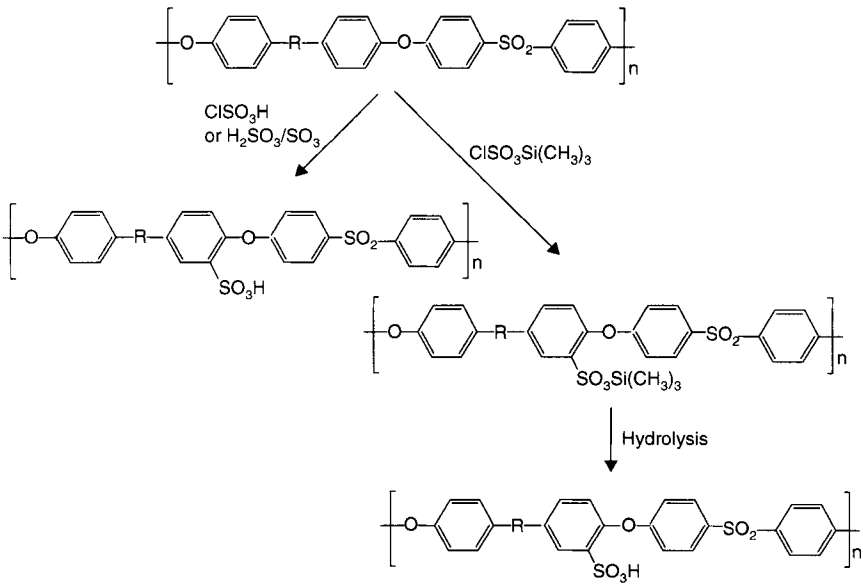

Scheme 4.2 Sulfonation of UDEL and RADEL.

can be selectively metalized in a second step reaction followed by phosphonation [34] as shown in Scheme 4.3a. Though in order to achieve monosubstitution of phosphoric acid unit and avoid crosslinking, one has to select the reaction parameters (i.e. reactivity of the nucleophile, nature of electrophile, solvent, reaction time and temperature) carefully. A study by Allock *et al.* [35, 36] showed that the phosphonating agents had to be added very quickly and a lot more in excess to effectively quench all the lithiated sites and to suppress any coupling reaction between already grafted phosphonic ester units and lithiated sites resulting in the displacement of the phenoxy- or ethoxy- groups. Jannasch *et al.* [34] prepared the ortho-to-ether phosphonated polysulfones as shown in Scheme 4.3(a) with the phosphonation degree achieved up to 50% which was not very high due to competing crosslinking side reaction. The phosphonated polysulfone showed very high thermal stability up to 350°C (and high T_g as well) under nitrogen atmosphere but also showed bad membrane forming properties which is possibly due to the reduced mobility of the flexible ether segment of the polymer due to substitution of phophonate unit at ortho-to-ether position in the ether segment [34].

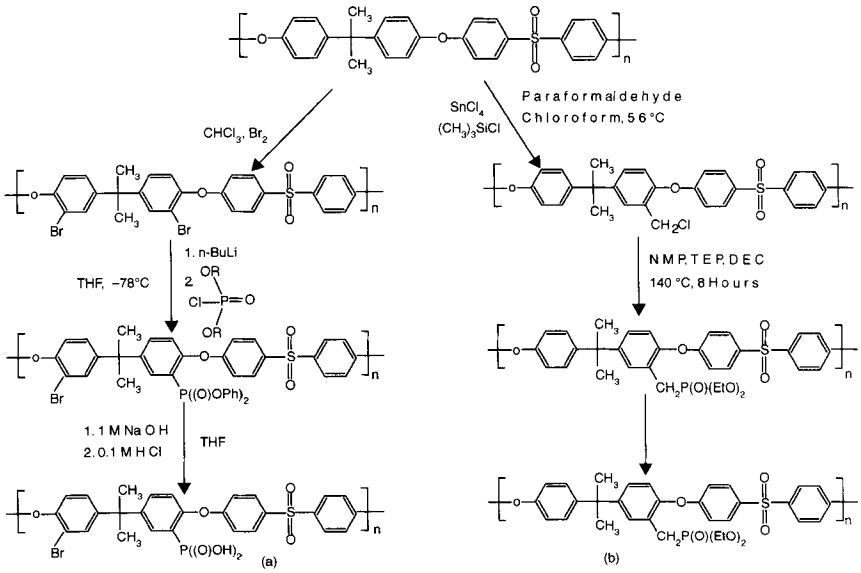

Scheme 4.3 Phosphonation of polysulfones at ortho-to-ether position.

Thabit *et al.* [37] also proposed the utilization of chlormethylated polysulfones for the preparation of phosphonic acid functionalized polysulfones with high degree of phosphonation (Scheme 4.3(b)). The reaction involved phosphonation of chloromethylated polysulfone by using Diethyl Carbitol (DEC) and Triethyl Phophite (TEP) in N-Methyl-2- Pyrrolidone (NMP) as solvent followed by hydrolysis. The phosphonated PSU membrane obtained with a DP (Degree of Phosphonation) of 0.4 and IEC = 0.9meq/g took up 18 wt% of water under immersed conditions. The highly phosphonated membrane with a DP of 1.5 and IEC = 3.8meq/g took up 52 wt% water. The highest phosphonic acid content membrane with DP of 1.5 reached a conductivity of 12mS/cm at 100°C under fully hydrated conditions. Furthermore, the synthesized membranes possessed high thermal stability up to 252°C and low methanol permeability compared to the sulfonic acid based ionomers such as Nafion which is advantageous in case of operation of direct methanol fuel cell.

Although the sulfonic acid-based polysulfones show better proton conductivity, they are highly susceptible to hydrolytic desulfonation (i.e. loss of sulfonic acid unit through hydrolysis) at elevated temperatures [39]. Hence, it is required to either find a solution of this critical issue or develop phosphonic acid based

membranes with improved architecture to enhance their water-uptake and hence water-assisted conductivities.

4.3.1.2 *Ionic Function Attached Directly to Ortho-to-Sulfone Position of the Polymer*

Kerres *et al.* [38] reported that the sulfonation close to electron-donating substituents (i.e. ortho-to-ether position) of the main aromatic polymer chain is normally more easily activated for hydrolytic desulfonation in acidic media compared to sulfonation close to electron-withdrawing substituents (i.e. ortho-to-sulfone position). An electrophilic route does not allow acidic ionic groups to be located on the ortho-to-sulfone position in the arylene sulfone segment where it should be, at least slightly, more dissociated than an acidic ionic function located at the ortho-to-ether position in the arylene ether segment.

The sulfonation at ortho-to-sulfone position involves three successive steps, metalation–sulfination–oxidation as reported by Kerres *et al.* [38] (Scheme 4.4).

The polymer lithiation is performed, under argon, by treatment of THF solution of the polymer with highly concentrated n-butyl lithium. Lithiation is followed by SO_2 addition which leads to an

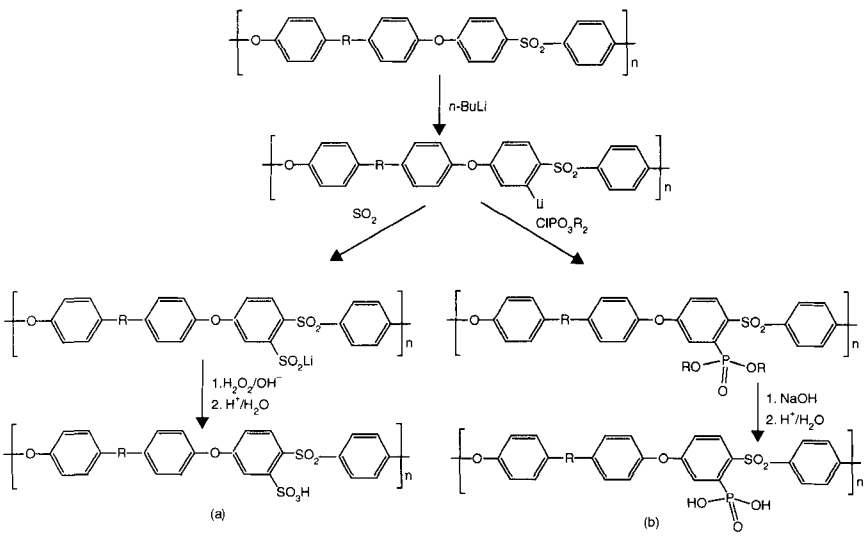

Scheme 4.4 Sulfonation and phosphonation of polysulfone in ortho-to-sulfone position.

arylsulfinate, whose oxidation leads to the sulfonate. Although highly sensitive to oxidants, lithium sulfinated polysulfone may be used as nucleophilic agents. Thus, some of them may therefore be used to insure the membrane crosslinking, while most of them are converted into sulfonates [42]. The membrane with IEC = 1.15 showed T_g of 180°C and T_d of 432°C in sodium form (the temperature at which polymer had lost 5% of its original weight was taken as the degradation temperature T_d using thermo-gravimetric analysis) with water uptake of 22% at 25°C under immersed state and 60% at 80°C along with proton conductivity of 10^{-1}S/cm at 100°C. Increase in IEC from 1.15 to 1.83 meq/g increased T_g from 180°C to 328°C (in sodium form) and water uptake from 22% to 77% at room temperature but similar proton conductivity were reported by Jannasch *et al.* [40]. The high uptake of water led to compromise of mechanical properties due of high degree of swelling which is explained very well by the SAXS measurements done by Kreuer *et al.* [23]. The SAXS profiles of the main-chain sulfonated PSUs showed much broader ionomer peaks shifted to higher q values, as compared to the profile of Nafion®. This indicated a smaller cluster separation, d ≈ 25 Å, with a significantly wider distribution. The polymer main-chain is far less hydrophobic and the sulfonic acid groups far less acidic than in Nafion®, leading to less regular phase domains in the main-chain sulfonated PSU membranes.

Phosphonated PSU by nucleophilic substitution was reported by Jannasch *et al.* [34] using directly metalation-phosphonation method shown in Scheme 4.4(b) and these membranes showed even higher thermal stability than membranes phosphonated at ortho-to-ether position (up to 375°C) under nitrogen atmosphere. This may be explained by both the lower phosphonation degree (around 45%) and the stabilization effect because of the location of the phosphonic acid units on the electron-poor segments of the polysulfone main-chain. This membrane gained insignificant amount of water (<2%) due to its high Tg value and low phosphonation degree, thereby unable to reach high levels of water-assisted conductivities.

4.3.1.3 Ionic Function Attached to Main-Chain Through Side Chains

The studies on above mentioned directly sulfonated polysulfones in context of PEMFC application show that these are water soluble at high degree of sulfonation i.e. 0.8 sulfonic acid group per repeating

unit (high degree of sulfonation required to ensure enough good proton conductivity) and hence not having dimensional stability required for the PEMFC application. This is explained on the basis of the fact that there is very small spatial separation between hydrophilic sulfonic acid groups and hydrophobic polymer main-chain as the sulfonic acid groups are substituted directly on the main-chain. So when the swelling pressure becomes too high, the polymer loses morphology and hence mechanical stability. In order to overcome this problem, there have been certain approaches in the literature recently which involve (i) cross linking of the sulfonated-polysulfones to acquire enough good dimensional stability (though covalent cross linking imparts brittleness to the membrane [41, 42] and weakening of ionic cross links at high temperature was observed [43]) (ii) placement of pendant groups carrying terminal acid moiety away from the main-chain (iii) concentration of the ionic function on the specific chain segments in order to have nano-scale separation between hydrophobic and hydrophilic regions of the polymer to achieve enough good dimensional stability along with high proton conductivity.

Jannasch *et al.* [40, 44] synthesized and studied various types of aromatic poly (arylene ether sulfone) ionomers functionalized with mono-, di- and tri- sulfonic acid groups isolated on different aromatic/aliphatic short side chains to enhance hydrophilic-hydrophobic separation (Scheme 4.5(a) and 4.5(b), Table 4.1).

The SAXS measurements of sulfobenzoyl functionalized PSU (sb-PSU) showed very weak ionomer peaks meaning no significant ionic clustering of acid groups. The reason behind this could be the reduced mobility of the acid moieties due to ortho-position to ketone link and close to main-chain. A rather narrow ionomer peak (resembling that of Nafion®) was observed for the membrane prepared from sulfonaphthoxybenzoyl functionalized PSU (6snb-PSU and 7snb-PSU) indicating the formation of ionic clusters. The SAXS profile of disulfonaphthoxybenzoyl functionalized PSU (dsnb-PSU) showed an ionomer peak corresponding to lower inter-ionic cluster distances (d) indicating formation of larger ionic clusters in the polymer membrane. Also, the ionomer peak shifted to even lower d values with increasing IEC values meaning reduced distance between the ionic domains with increasing concentration of sulfonic acid groups [40]. The PSU membrane functionalized with trisulfonaphthoxybenzoyl side chains (tsnb-PSU) showed similar behavior. The results of the SAXS study demonstrated that

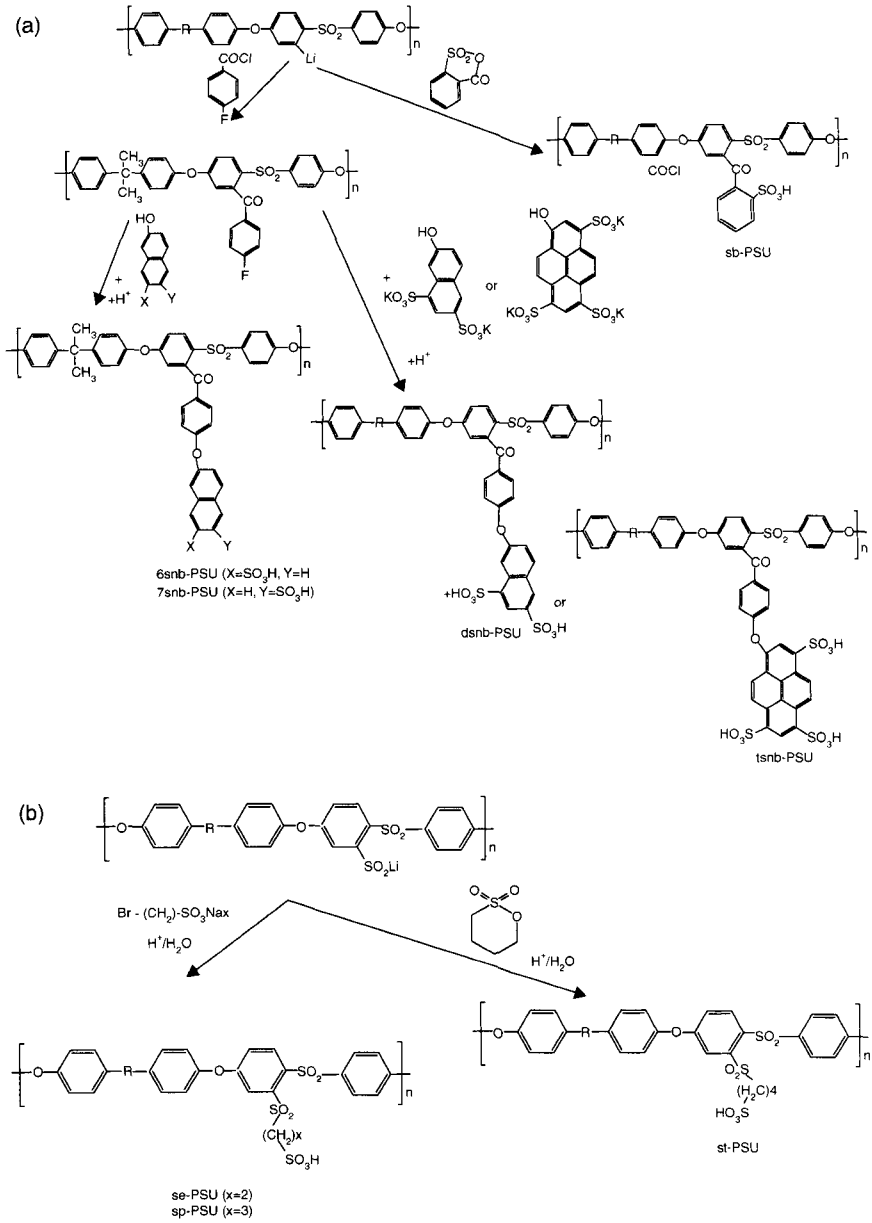

Scheme 4.5 Different sulfonic acid groups attached to main-chain through aromatic/aliphatic side chains.

Table 4.1 Water up-take, IEC, conductivity and thermal characteristics of different sulfonic acid functionalized polysulfone ionomers.

Membrane	IEC (meq/g)	% W_{water} [1]	σ (S/cm) [2]	T_g (°C) in sodium form	T_d (°C) [3] in sodium form;N_2 atm.
se-PSU	1,1	24	$18 \times 10^{-2*}$	na	370
sp-PSU	1,5	37	$40 \times 10^{-2*}$	na	350
st-PSU	1,2	25	$22 \times 10^{-2*}$	na	340
sb-PSU	1,12	21	1×10^{-2}	173	310
6-snb-PSU	0,77	13	1×10^{-2}	270	404
7-snb-PSU	0,8	15	$2,5 \times 10^{-3}$	309	431
dsnb-PSU	1,18	27	6×10^{-2}	194	442
tsnb-PSU	1,27	44	1×10^{-1}	199	431

(*): *membranes humidified until equilibrated in liquid water and proton conductivity measured under humidifying conditions in an air-tight cell.*

([1]): *% W_{water} - % uptake water when immersed in water at room temperature;* $\% W_{water} = [(W_{wet} - W_{dry})/W_{dry}]*100$

([2]): *σ – Proton conductivity at 120°C with membranes fully immersed in water.*

([3]): *The temperature at which polymer loses 5% of its original weight after the pre-dry at 150°C for 10 minutes.*

the concentration of the acidic groups to side chains promoted a high degree of phase separation and ionic clustering in the membranes. However, the case of the sulfobenzoyl functionalized PSUs showed that the side chains need to have a proper configuration for the ionic clustering to be efficient. In conclusion, the study showed that highly phase separated ionomer membranes may be achieved with side chain sulfonated polymers with a proper macromolecular design.

The TGA analysis of these membranes showed T_g in the range of 175–300°C and T_d in the range of 300–400°C depending on the structure shown in Table 4.1. It can be said that these membranes show enough good thermal properties required for the PEMFC application.

The water uptake by membranes (shown in Table 4.1) in immersed state in water at room temperature shows that tsnb-PSU

took maximum amount of water which must be due to the highest concentration of hydrophilic sulfonic acid moieties and sb-PSU (with similar IEC value) took minimum amount of water which must be due to poor ionic clustering as observed in SAXS measurements. While comparing sulfoalkylated PSUs, it can be seen that sp-PSU gained maximum amount of water probably due to higher IEC value than other two [44]. Moreover, all these membranes swell up to limited extent at elevated temperature (80–100°C) except tsnb-PSU which swells extensively leading to membrane disintegration [40].

It can be seen from the Table 4.1 that all the membranes have comparable conductivities with tsnb-PSU showing the maximum value at 120°C. The reason must be the higher concentration of sulfonic acid units thereby higher water gain and hence higher water-assisted conductivity [40]. But this membrane also observed morphological disintegration at elevated temperatures.

It is assumed that dissociation of aryl sulfonic acids is probably higher than that of alkyl sulfonic acids. However, similar conductivities (as shown in Table 4.1) have been reported for polymers bearing either a dangling alkyl sulfonic acid or an aryl sulfonic acid located on the main-chain of an ionomer [40, 44].

Another type of modification involving placement of a perfluorinated sulfonic acid group as side chain on the PSU main-chain has been achieved by Yoshimura *et al.* [47]. PES-PSA was synthesized by a coupling reaction at 120°C using copper (Scheme 4.6). The obtained polymer had an IEC of up to 1.58 meq/g with water uptake of 157% under immersed state and showed proton conductivity of up to 0.12 S/cm at 80°C under 90% relative humidity. They also compared various characteristics of Nafion® and PES-PSA (IEC = 1.34 meq/g) as both carry similar side chains. It was observed with the help of SAXS measurements that the latter did not show any significant peak in dry state contrary to former but formation of cluster channels took place in wet state (water content = 38%) with 3.7 nm as cluster size. However, the cluster size for PES-PSA was smaller than for Nafion®112 (cluster size ~ 4.2 nm, water content 23%) which could be due to the rigid main-chain in PES-PSA preventing aggregation of the side-chain. The DMA measurements showed that PES-PSA (188°C) had higher α-relaxation temperature than Nafion®112 (126°C). The in-plain proton conductivity for PES-PSA (IEC = 1.34meq/g, thickness = 47 μm) was 0.077 S/cm at 80°C under 90% RH as compared to 0.089 S/cm for Nafion® 112 under

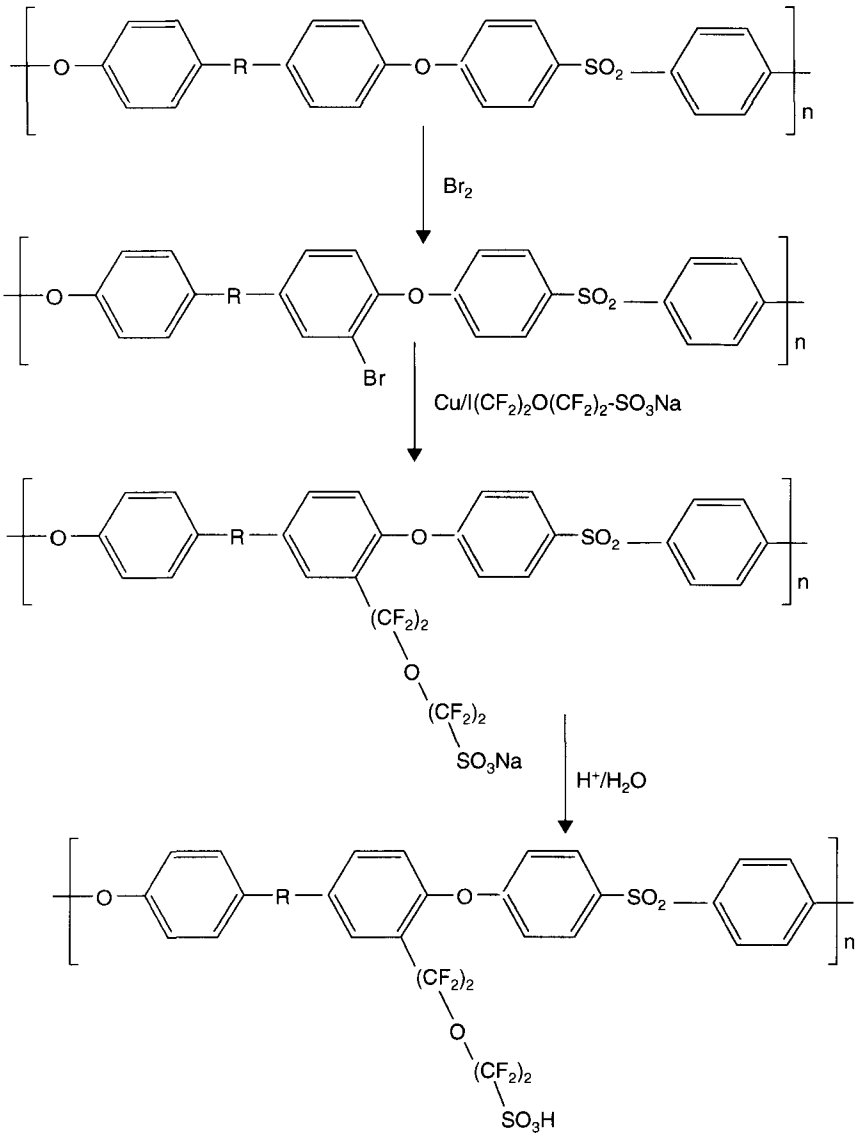

Scheme 4.6 Ionic function attached to main-chain through perfluorinated side chains.

similar conditions. The through-plain proton conductivities of Nafion®112 and PES-PSA were 0.060 and 0.063 S/cm, respectively. The difference in proton conductivity might account for ambiguous micro-phase separation/anisotropy in PES-PSA.

Lafitte *et al.* [45] reported polysulfone ionomers functionalized with benzoyl(difluoromethylenephosphonic acid) side chain (bfp-PSU) as an alternative to sulfonic acid based PSU ionomers shown in Scheme 4.8(a) and Table 4.2. The degree of phosphonation (DP) was achieved up to 53% and this membrane took higher amount of water (6%) under immersed state at room temperature compared to membrane with phosphonic acid directly attached to main-chain at ortho-to-sulfone position taking 2% water as discussed before. The probable reason is the increased acidity of the phosphonic acid unit. The thermal stability was found to be inferior to sulfonated derivatives due to the presence of aryl $-CF_2$-P linkage [45].

Jannasch *et al.* [27] also tried to further increase the acidity of the phophonated PSUs by preparing PSUs with short alkyl chains carrying diprotic phosphonic acid (mp-PSU) and tetraprotic (bisphosphonic acid) (dp-PSU) to promote water assisted conductivity as shown in Scheme 4.7(a) and 4.7(b) respectively and Table 4.2. mp-PSU with IEC = 0.8 meq/g showed water uptake of 8% under immersed conditions while dp-PSU having higher acidity and IEC gained more water (water uptake = 28%; IEC = 3.4meq/g).

Table 4.2 Water uptake, IEC, conductivity and thermal characteristics of different polysulfone ionomers functionalized phosphonic acid.

Membrane	DP	IEC (meq/g)	% W_{water} [1]	σ (mS/cm)[2]	T_d (°C)[3] In acid form; N_2 atm.
bfp-PSU	0,53	1,79	6	5 (at 100°C)	227*
mp-PSU	0,8	1,4	8,2	4	337
dp-PSU	1,4	3,4	28	25	248
PSU-PVPA (32% PVPA content)	0,1	2,9	31	32	320

(1): *% W_{water} - % uptake water when immersed in water at room temperature;* *% $W_{water} = [(W_{wet} - W_{dry})/W_{dry}]*100$.*

(2): *σ – Proton conductivity at 120°C with membranes fully immersed in water.*

(3): *The temperature at which polymer loses 5% of its original weight after the pre-dry at 150°C for 10 minutes.*

(*): *The temperature at which polymer loses 2% of its original weight after the pre-dry at 150°C for 10 minutes.*

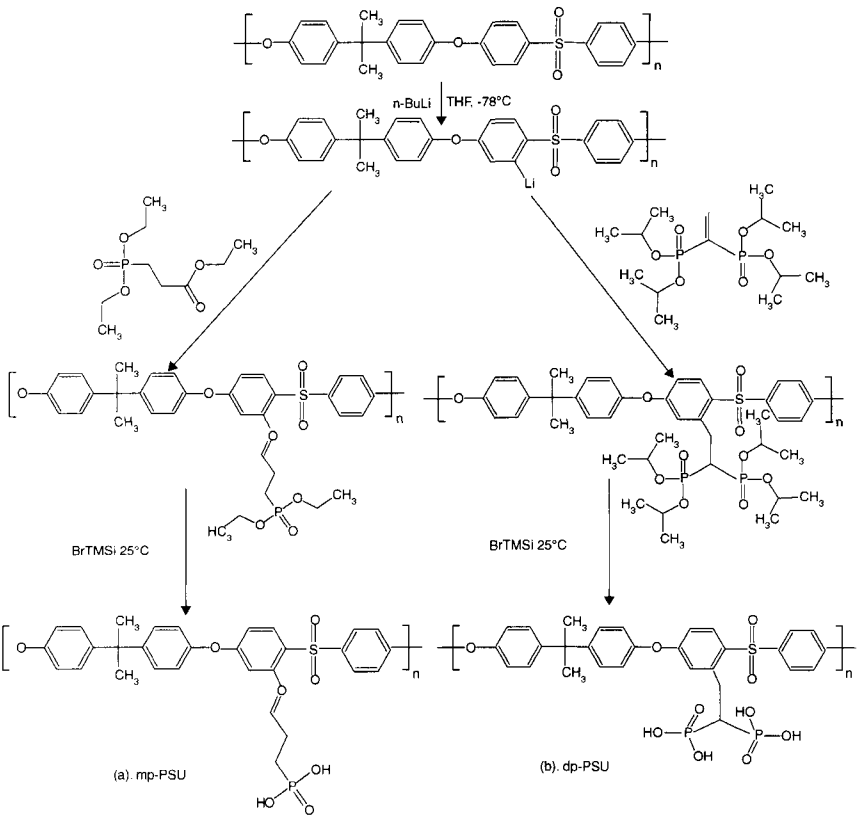

Scheme 4.7 Different chemical modifications to synthesize phosphonated-polysulfones with mono- & di- phosphonic acid goups attached away from the polymer main-chain.

The TGA results showed that C–P bond was weaker in the bisphosphonic acid, as compared to the monophosphonic acid and hence lower T_d was observed for dp-PSU compared to mp-PSU. This was expected because the arrangement of two electron withdrawing phosphonate units bonded to the same carbon decreases the strength of the C–P bonds [27].

Parvole *et al.* [46] have synthesized multifunctional membranes with phase separated morphology to achieve high proton conductivity under dry and wet conditions along with good mechanical properties. The work involved anionic grafting of polyvinyl (phosphonic acid) side chains as phosphonated component onto polysulfones (PSU-PVPA) shown in Scheme 4.8(b) and Table 4.2.

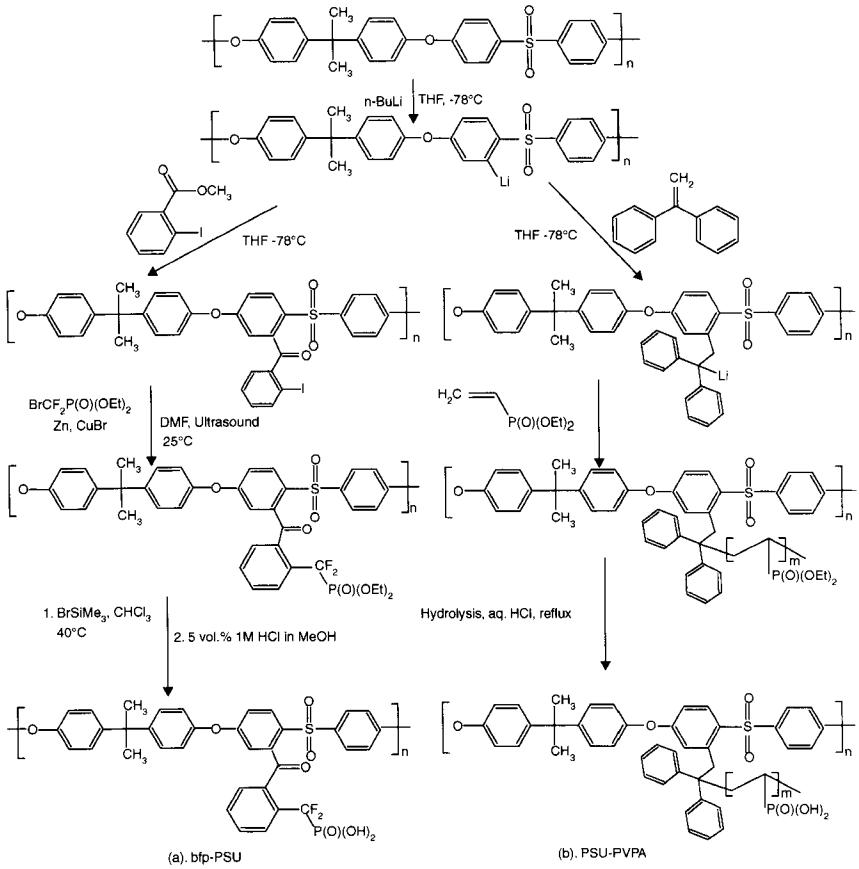

Scheme 4.8 Different chemical modifications to synthesize phosphonated-polysulfones with phosphonic acid attached away from the polymer main-chain.

Due to higher local phosphonic acid group concentration and morphology with presumably larger phosphonated phase domain, it had greater ability to take up and accommodate more water and there must be formation of large H-bonded aggregates (due to high local phosphonic acid group concentration) to higher anhydrous proton conductivity. Hence, overall there was an increase in water uptake compared to other phosphonic acid based PSUs but still restricted one compared to sulfonated PSUs helping in avoiding mechanical disintegration of membrane. The thermal stability of the membranes was sufficiently high under air with T_d at 260–340°C, depending on IEC and DP. The membrane with the highest PVPA

content in the study (57 wt %) & IEC = 5.3meq/g reached a conductivity of 4.6 mS/cm under nominally dry conditions and 93 mS/cm under 100% RH at 120°C. However, at high temperatures the performance of this membrane was limited by condensation reactions under dry conditions and, especially, by high levels of water uptake under immersed conditions [46].

4.3.2 Polymerisation of Ionic Monomers by Step Growth

The synthesis of polysulfones by polycondensation using specifically designed monomers can act as an asset in comparison to the chemical modification of the commercially available Polysulfone in certain ways such as (i) designing of new and more stable main-chains than commercially available polysulfone (ii) incorporation of specific functional groups on the polymer main-chain (iii) additionally, the synthesis from ionic and non-ionic monomers allows the ionomer to be separated between hydrophobic and hydrophilic blocks, whereas the chemical modification of commercial polymers results in functional groups that are randomly distributed along the macromolecular backbone. As a result, this synthesis route, which should restrict the swelling of the membrane to the hydrophilic domains, improves both the dimensional stability and the tensile strength of the membranes.

4.3.2.1 Ionomers Containing Hexafluoro-Isopropylidene or/and Polar Functions

The most studied commercial polymer in the chemical modification, Udel polyethersulfones are based on bis-phenol A, in which the electron-donating isopropylidene moiety increases the electronic density of the whole phenoxy sites and, in particular, increases the ether basicity. This may favour chain breaking during the sulfonation step [29, 32] the former may favour free-radical attacks on the aromatic rings.

Moving from bis-phenol A (BPA) to its fluorinated form (BHFPA) (by replacing iso-propylidene by hexafluoro- isopropylidene), is one of the ideas to overcome both drawbacks. In addition, due to the perfluorinated moiety of BHFPA, a decrease in the hydrophilic character of the related ionomer can be expected. Kim *et al.* [48] reported the effects induced by BHFPA and non-ionic polar monomers in

sulfonated polysulfones. The properties of poly(arylene ether sulfone) copolymers prepared from BHFPA, biphenol and non-ionic polar monomers, based on benzonitrile and tri-phenyl phosphine oxide, were compared (Scheme 4.9) [48].

In spite of the decrease in the basicity of BHFPA that should lower their reactivity in nucleophilic aromatic substitution, the ionomer synthesis was successful. Surprisingly, the water uptake dependence of the ionomers on IEC was found to be almost unaffected by the presence of the BHFPA repeat unit. This result, in agreement

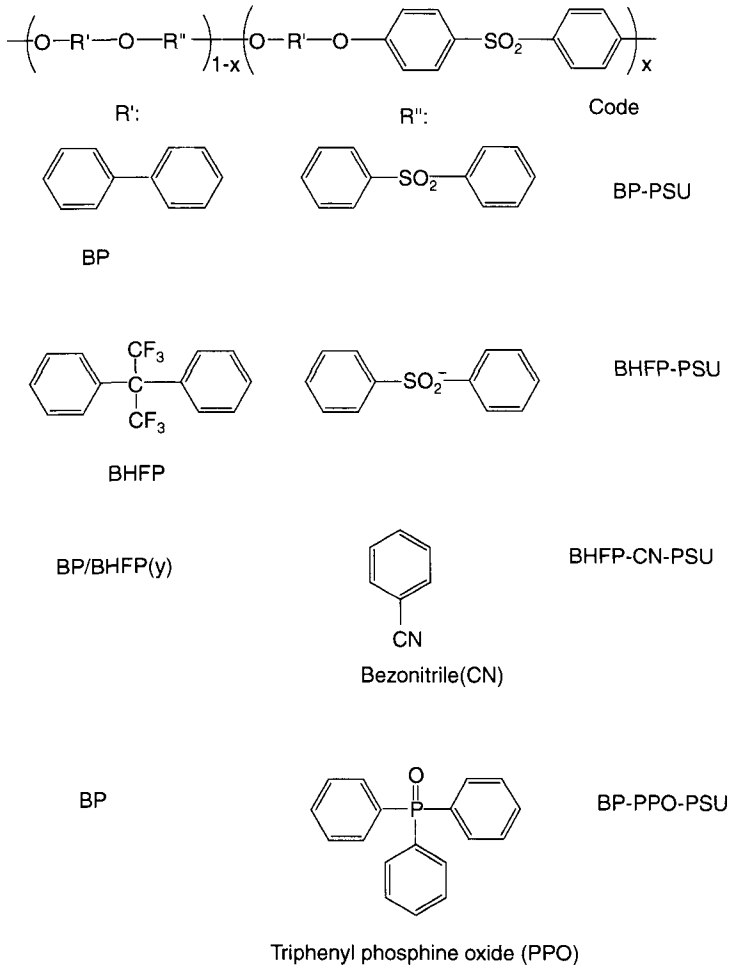

Scheme 4.9 Structure of different main-chain, containing specific functional groups, obtained by polycondensation.

with other data obtained with similar materials, [49–51] is probably related to the dominating effect of the ionomer structures in blocks. The authors claimed conductivity that was twice as high as the unfluorinated ionomers at the same IEC (Table 4.3).

In contrast to the fluorine moiety, the presence of polar functions such as CN or P = O induces a decrease in both water uptake and conductivities. Both nitrile and phosphine oxide groups are known to be strongly polar and have a fairly high donor number (DN) (Lewis basicity) that favours strong interactions with aprotic and protic polar groups. Table 4.3 presents data on a variety of ionomers. Although it was expected that these polar groups may, according to the IEC, improve the conductivity of ionomers, to the contrary they strongly decrease both water uptake and conductivity. Furthermore, interactions between polar groups and acidic ones should be significantly favored in acidic ionomers. Whatever be the kind of inter-chain interaction, it acts as a physical cross-link, thus restraining free-volume and water uptake.

While the conductivity decrease is a shortcoming of polar groups, their incorporation may lead to advantages in terms of (i) mechanical performance, (ii) decrease in membrane–electrode interfacial resistance, and (iii) decrease in methanol crossover, which is an asset for an implementation in direct methanol fuel cells (DMFC), provided high selectivity (ratio of proton conductivity to methanol permeability) is retained [52]. While comparing the effects of polar groups, it appears that phenylphosphine incorporation,

Table 4.3 Effect of polar groups on water uptake and proton conductivity [48].

Membrane	IEC (meq/g)	% W_{water} [1]	σ (mS/cm)[2]
BP-PSU	1.11	23	23
BP-PSU	1.34	31	40
BHFP-PSU	1.12	23	55
BHFP-PSU	1.3	31	92
BHFP-CN-PSU	1.16	18	35
BHFP-CN-PSU	1.33	24	58
BP-PPO-PSU	1.4	26	35

([1]): *% W_{water} - % uptake water when immersed in water at room temperature.*

([2]): *σ – Proton conductivity at 80°C with membranes fully immersed in water.*

although significantly lowering methanol permeability, did not improve the selectivity with respect to the bisphenol-based copolymers. The incorporation of benzonitrile, on the other hand, led to the most selective copolymer, BPCN, as presented in Table 4.4. Thus, both fluorinated (BHFP-PSU) and unfluorinated polymers (BP-PSU) exhibited increase in selectivity because of the benzonitrile incorporation.

4.3.2.2 *Multi-block Ionomeric Polycondensates Based on Medium to Long Blocks*

To synthesize multiblock copolymers, there are usually two approaches. In one approach, a terminal-activated oligomer is first synthesized. The oligomer is then copolymerized with other monomers to prepare multiblock copolymers [53]. Another approach uses the reaction between different types of terminal-activated oligomers [54, 55].

However, this reaction has to be performed at high reaction temperature when chloride end-capped oligomers are used [56] and can induce an ether–ether interchange reaction that could lead to randomized polymer architectures, multi-block copolymers therefore not being obtained. McGrath and co-workers solved this problem, using highly reactive fluorine end-capped oligomers instead of chloride end-capped ones, and successfully prepared sulfonated multiblock poly (arylene ether) copolymers under milder conditions

Table 4.4 Polycondensation from ionic and usual monomers.

Membrane	PPO (or benzonitrile) content (wt%)	σ (mS/cm)[1]	Methanol permeability (x10) (cm^2/s)	Methanol selectivity (x10^2) (S m/s)
BP-PPO-PSU	17.2	21	0.55	3.8
BP-PPO-PSU	10.5	38	1.02	3.7
BP-CN-PSU	(17.2)	78	1.44	5.4
BHFP-CN-PSU	(14.1)	58	1.32	3.6
BHFP-PSU	0	55	1.66	3.3
BP-PSU	0	72	1.55	4.7
Nafion®	0	111	4.2	2.6

([1]): σ – *Proton conductivity at 80°C with membranes fully immersed in water.*

[57, 58]. Nakabayashi *et al.* used DecaFluoroBiphenyl (DFB) as a chain extender because of its high reactivity in nucleophilic aromatic substitution reaction [59, 60]. They demonstrated an easy synthesis method of sulfonated multiblock copoly(ether sulfone)s by the coupling reaction, at low reaction temperature, between hydroxyl end-capped poly(ether sulfone) oligomers and hydroxyl end-capped sulfonated poly(ether sulfone) oligomers, DFB acting as the chain extender and leading to high molecular weight multiblock copolymers with *Mw* of 100 000 g mol/1 (Scheme 4.10, Table 4.5).

While equal hydrophobic and hydrophilic block lengths were selected to perform the multi-blocks synthesis, the authors performed a wide investigation on the impact of the block lengths on the membrane properties that are gathered in Table 4.5.

Proton conductivities higher than the Nafion® were reported at 95% relative humidity (10^{-1} S cm^{-1}) for all membranes. The effect of the oligomer lengths on proton conductivity was, however, clearly observed under low relative humidity (50% relative humidity). The membrane BP-PSU14 showed good conductivity of 7.1 × 10^{-3} S cm^{-1} at 50% relative humidity. On the other hand, the conductivity of the BP-PSU 6 membrane was 3.0 × 10^{-3} S cm^{-1} at 50% relative humidity. The same behaviour was observed for the membranes based on BP-BHF-PSU. These data demonstrate that there

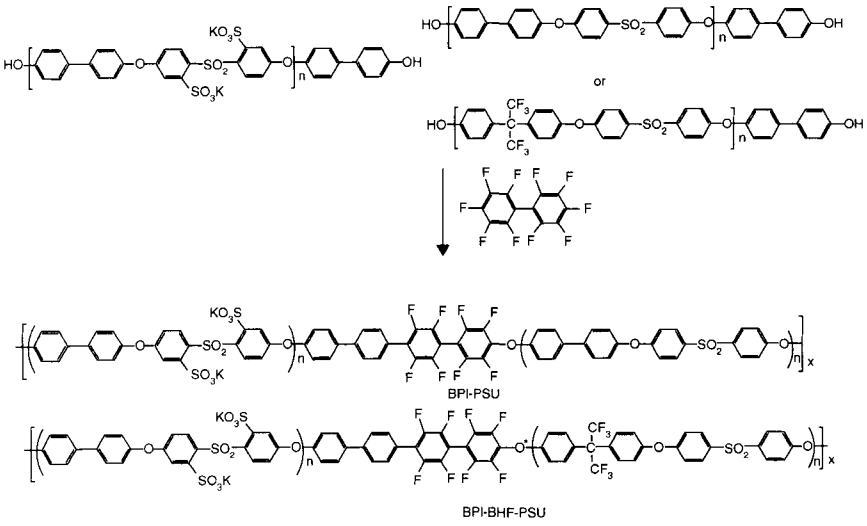

Scheme 4.10 Synthesis of multi-block ionomeric Polysulfones [59].

Table 4.5 Molecular weights of the oligomers and block copolymers.

Copolymer	Mn (SEC) of each oligomer (g/mol)	IEC (meq/g))	Mn (g/mol)	Mw/Mn
BP-PSU$_{14}$	14 000/14 000	2	68 000	2.5
BP-PSU$_{10}$	10 000/10 000	2	74 000	3.3
BP-PSU$_{6}$	6 000/6 000	1.99	55 000	4.4
BP-BHF-PSU$_{14}$	14 000/14 000	1.95	70 000	4.1
BP-BHF-PSU$_{10}$	10 000/10 000	1.97	60 000	3.5
BP-BHF-PSU$_{6}$	6 000/6 000	1.99	84 000	4.9

is a strong relation between proton conductivity and block lengths. The membranes with the longest block lengths exhibited, in agreement with the water uptake behaviour, the highest conductivity at 50% relative humidity. It may be assumed that, thanks to their longest block lengths, the hydrophilic blocks allow maintaining high water uptake, in particular at 50% relative humidity. In addition, by increasing the lengths of hydrophilic and hydrophobic blocks, a better phase separation into hydrophobic/hydrophilic domains is obtained. Besides, Atomic Force Microscopy (AFM) observations of the multiblock copolymer membranes supported the formation of a surface hydrophilic/hydrophobic, phase-separated structure [59, 60]. In particular, the hydrophilic domains of high block length-based copolymers are larger and better interconnected, thus resulting in the highest conductivities for the longest block lengths.

4.3.2.3 *Multi-block Copolymers and Random- Ionomeric Copolymers*

A lot of works reported that multiblock copolymer showed higher water uptake, proton conductivity, proton/methanol selectivity, thermal stability, etc. than a similar random copolymer [61–63]. Liang *et al.* [64] have shown recently the morphology differences between random and multiblock copolymers (Scheme 4.11, Table 4.6) and the effects of the membrane morphology on the properties of the membranes.

The effects of the microstructures of the copolymers on the membrane morphology, water uptake, proton conductivity, and

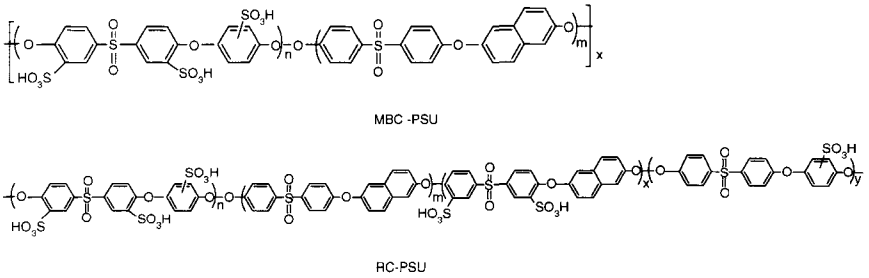

Scheme 4.11 Structure of a multiblock and random copolymers compared by Liang *et al.* [64].

methanol permeability and selectivity of the membranes are gathered in Table 4.6. At similar IECs, the water uptake and conductivity of the multiblock MBC-PSU membranes were higher than that of the random RC-PSU membranes. For random SPAES copolymers, the sulfonic acid groups would be randomly distributed in the copolymer chain [65]. Unlike random RD-PSU copolymers, the multiblock MBC-PSU copolymers had repeated hydrophilic and hydrophobic units. These (repeated units) were thought to be able to assemble into cluster like structures or spherical or cylindrical micelles [66] as also confirmed by AFM and SAXS measurements. These kinds of structures made the hydrophilic domains well connected and tended to effectively keep more water in the membranes.

By SAXS measurements they observed intensity peaks at q values of approximately 1.64 and 4.30 nm^{-1} for the Nafion® 117 and multiblock MBC-PSU3 membranes, respectively. These peaks were supposed to be caused by the clustering of the ionic groups in the polymer matrix [67, 68]. The Bragg spacing (d) for the Nafion® 117 and multiblock MBC-PSU3 membranes were determined to be 3.8 and 1.5 nm, respectively. For the random RC-PSU2 membrane, no obvious peak was observed. These SAXS investigations suggested that the multiblock MBC-PSU3 membrane had nanoscale clusters. Both the random and multiblock polysulfone membranes showed higher proton/methanol selectivity than the Nafion® 117 membrane. The random copolymers had similar IECs, the multiblock PSU membrane showed slightly higher methanol permeability while the multiblock membranes showed quite high selectivities. In particular, because of the low methanol permeability, the MBC-PSU1 membrane exhibited the highest methanol selectivity among these membranes.

Table 4.6 Molecular characteristics, water uptake, IEC, conductivity of MBC-PSU and RC-PSU.

Copolymer	IEC (meq/g)	Mn (g/mol)	Mw/Mn	% Water uptake[1]	σ (mS/cm)[2]	Methanol permeability (cm^2/s)	Methanol selectivity ($S.s/cm^3$)
MBC-PSU1	0.52	32 000	5.9	39	2.10^{-3}	0.1×10^{-7}	26×10^{-3}
MBC-PSU2	1.22	59 000	3.3	45	5.10^{-2}	2×10^{-7}	15×10^{-3}
MBC-PSU3	1.77	69 000	2.8	98	23.10^{-2}	10×10^{-7}	12×10^{-3}
RC-PSU1	0.77	70 000	6.6	20	1.10^{-3}	0.1×10^{-7}	–
RC-PSU2	1.76	60 000	6.1	45	8.10^{-3}	3×10^{-7}	9×10^{-3}

([1]): *% Wwater - % uptake water when immersed in water at room temperature.*

([2]): σ *– Proton conductivity at 50°C and 90% RH.*

4.4 Conclusion

Due to their high thermo-mechanical perfomance, wide electrochemical stability window and good chemical inertness, high-performance polysulfone ionomers are excellent candidates among the alternative membranes to perfluorinated membranes for their implementation as PEMs in fuel cells. Despite the fact that sulfonated polysulfones show lower stability compared to the phosphonated polysulfones, they are more promising due to their higher conductivity and easier synthesis route. Among the ionomers functionalised with sulfonic acid function, the block copolymers seem to be more promising than chemically modified commercial polysulfones. However, these alternative membranes face many harsh challenges as follows: (i) they have to acquire enough good thermo-mechanical properties along with required conductivities to allow PEMFCs and DMFCs to be operated at least up to 120°C, and (ii) their lifespan has to be improved markedly and their cost should be reduced as well.

4.5 References

1. M.R. Tant, K.A. Mauritz, and G.L. Wilkes, *Ionomers*, New York, Chapman & Hall, 1997.
2. L. Carrette, K.A. Friedrich, and U. Stimming, *Fuel Cells*, Vol. 1, p. 5, 2001.
3. P. Costamagna, and S.J. Srinivasan, *Power Sources*, Vol. 102, p. 253, 2001.
4. J. Roziere, and D.J. Jones, *Annual Reviews in Materials Research*, Vol. 33, p. 503, 2003.
5. B. Lakshmanan, W. Huang, D. Olmeijer, and J.W. Weidner, *Electrochem. Solid-State Letters*, Vol. 6, p. A282, 2003.
6. M.F. Mathias, R. Makharia, H.A. Gasteiger, J.J. Conley, T.J. Fuller, C.J. Gittleman, S.S. Kocha, D.P. Miller, C.K. Mittelsteadt, T. Xie, S.G. Yan, and P.T. Yu, *Interface*, Vol. 14, p. 24, 2005.
7. J. Yu, B. Yi, D. Xing, F. Liu, Z. Chao, Y. Fu, and H. Zhang, *Phys. Chem. Chem. Phys.*, Vol. 5, p. 611, 2003.
8. J.M. Amarilla, R.M. Rojas, J.M. Rojo, M.J. Cubillo, A. Linares, and J.L. Acosta, *Solid State Ionics*, Vol. 127, p. 133, 2000.
9. F. Wang, M. Hickner, Y.S. Kim, T.A. Zawodzinski, J.E. McGrath, *Journal of Membrane Science*, Vol. 197, p. 231, 2002.
10. Y. Chikashige, Y. Chikyu, K. Miyatake, and M. Watanabe, *Macromolecules*, Vol. 38, p. 7121, 2005.
11. P. Xing, G.P. Robertson, M.D. Guiver, S.D. Mikhailenko, K. Wang, and S. Kaliaguine, *Journal of Membrane Science*, Vol. 229, p. 95, 2004.
12. M. Gil, X. Ji, X. Li, H. Na, J.E. Hampsey, and Y. Lu, *Journal of Membrane Science*, Vol. 234, p. 75, 2004.

13. X. Shang, S. Tian, L. Kong, and Y. Meng, *Journal of Membrane Science*, Vol. 266, p. 94, 2005.
14. M. Schuster, K.-D. Kreuer, H.T. Andersen, and J. Maier, *Macromolecules*, Vol. 40, p. 598, 2007.
15. Z. Bai, and T.D. Dang, *Macromolecular Rapid Communications*, Vol. 27, p. 1271, 2006.
16. C. Genies, R. Mercier, B. Sillion, N. Cornet, G. Gebel, and M. Pineri, *Polymer*, Vol. 42, p. 359, 2001.
17. K. Miyatake, H. Zhou, T. Matsuo, H. Uchida, and M. Watanabe, *Macromolecules*, Vol. 37, p. 4961, 2004.
18. T. Kobayashi, M. Rikukawa, K. Sanui, and N. Ogata, *Solid State Ionics*, Vol. 106, p. 219, 1998.
19. C.H. Fujimoto, M.A. Hickner, C.J. Cornelius, and D.A. Loy, *Macromolecules*, Vol. 38, p. 5010, 2005.
20. S.M.J. Zaidi, S.D. Mikhailenko, G.P. Robertson, M.D. Guiver, and S. Kaliaguine, *Journal of Membrane Science*, Vol. 173, p. 17, 2000.
21. D.S. Kim, B.L. Michael, and D. Guiver, Vol. 47, p. 7871, 2006.
22. Y.A. Elabd, E. Napadensky, J.M. Sloan, D.M. Crawford, and C.W. Walter, *Journal of Membrane* Science, Vol. 217, p. 27, 2003.
23. K.D. Kreuer, M. Ise, A. Fuchs, J. Maier, *Journal of Physics IV*, Vol. 10, p. 279, 2000.
24. R. Nolte, K. Ledjeff, M. Bauer, R. Muelhaupt, *BHR Group Conf Ser Publ.*, Vol. 3, p. 381, 1993.
25. S.V. Kotov, S.D. Pedersen, W.M. Qiu, Z.M. Qiu, D.J, Burton, Journal of Fluorine Chemistry, Vol. 82, p. 13, 1997.
26. J.C. Lassegues, J. Grondin, M. Hernandez, and B. Maree, *Solid State Ionics*, Vol. 145, p. 37, 2001.
27. J. Parvole, and P. Jannasch, Journal of Materials Chemistry, Vol. 18, p. 5547, 2008.
28. P. Genova-Dimitrova, B. Baradie, D. Foscallo, C. Poisignon, and J.Y. Sanchez, *Journal of Membrane Science*, Vol. 185, p. 59, 2001.
29. C. Iojoiu, P. Genova-Dimitrova, M. Marechal, and J.Y. Sanchez, *Electrochimica Acta*, Vol. 51, p. 4789, 2006.
30. A. Linkous, H.R. Anderson, R.W. Kopitzke, and G.L. Nelson, *Journal of Hydrogen Energy*, Vol. 23, p. 525, 1998.
31. J.F. Blaco, Q.T. Nguyen, and P. Schatzel, *Journal of Applied Polymer Science*, Vol. 84, p. 2461, 2002.
32. C. Iojoiu, M. Marechal, F. Chabert, and J.Y. Sanchez, *Fuel Cells*, Vol. 5, p. 344, 2005.
33. R. Nolte, K. Ledjeff, M. Bauer, and R. Mulhaupt, *Journal of Membrane Science*, Vol. 83, p. 211, 1993.
34. B. Lafitte, and P. Jannasch, *Journal of Polymer Science, Part A: Polymer Chemistry*, Vol. 43, p. 273, 2005.
35. H.R. Allcock, M.A. Hofmann, and R.M. Wood, *Macromolecules*, Vol. 34, p. 6915, 2001.
36. H.R. Allcock, M.A. Hofmann, C.M. Ambler, and R.V. Morford, *Macromolecules*, Vol. 35, p. 3484, 2002.
37. N.Y.A. Thabit, S.A. Ali, S.M. Javed, *Journal of Membrane Science*, Vol. 360, p. 26, 2010.

38. J.A. Keres, W. Cui, S. Reichle, *Journal of Polymer Science, Part A: Polymer Chemistry*, Vol. 34, p. 2421, 1996.
39. H. Cerfontain, Interscience Monographs on Organic Chemistry, New York, Interscience, 1968.
40. E.P. Jutemar, and P. Jannasch, *Journal of Membrane Science*, Vol. 351, p. 87, 2010.
41. J. Kerres, W. Zhang, and W. Cui, *Journal of Polymer Science*, Vol. 36, p. 1441, 1998.
42. J. Kerres, W. Cui, and M. Junginger, *Journal of Membrane Science*, Vol. 139, p. 227, 1998.
43. J. Kerres, A. Ullrich, F. Meier, and T. Häring, *Solid State Ionics*, Vol. 125, 243–249, (1999).
44. LE. Karlsson, and P. Jannasch, *Journal of Membrane Science*, Vol. 230, p. 61, 2004.
45. B. Lafitte, and P. Jannasch, *Journal of Polymer Science: Part A: Polymer Chemistry*, Vol. 45, p. 269, 2007.
46. J. Parvole, and P. Jannasch, *Macromolecules*, Vol. 41, p. 3893, 2008.
47. K. Yoshimura, and K. Iwasaki, *Macromolecules*, Vol. 42, p. 9302, 2009.
48. Y.S. Kim, B. Einsla, M. Sankir, W. Harrison, and B.S. Pivovar, *Polymer*, Vol. 47, p. 4026, 2006.
49. F. Wang, M. Hickner, Y.S. Kim, T.A. Zawodzinski, and J.E. McGrath, *Journal of Membrane Science*, Vol. 197, p. 231, 2002.
50. W.L. Harrison, F. Wang, J. Mecham, V. Bhanu, M. Hill, and Y.S. Kim, *Journal of Polymer Science: Part A: Polymer Chemistry*, Vol. 41, p. 2264, 2003.
51. B.R. Einsla, Y.S. Kim, M.A. Hickner, Y.T. Hong, M.L. Hill, and B.S. Pivovar, *Journal of Membrane Science*, Vol. 255, p. 141, 2005.
52. R. Langner, and G.F. Zundel, *Journal of Physical Chemistry*, Vol. 99, p. 12214, 1995.
53. C. Genies, R. Mercier, B. Sillion, N. Cornet, G. Gebel, and M. Pineri, *Polymer*, Vol. 42, p. 359, 2001.
54. M. Shibata, J. Cao, and R. Yosomiya, *Polymer*, Vol. 38, p. 3103, 1997.
55. H. Ghassemi, G. Ndip, and J.E. McGrath, *Polymer*, Vol. 45, p. 5855, 2004.
56. Z. Wang, T. Chen, and J. Xu, *Polymer International*, Vol. 50, p. 249, 2001.
57. H. Ghassemi, J.E. McGrath, and T.A. Zawodzinski, *Polymer*, Vol. 47, p. 4132, 2006.
58. H.S. Lee, A. Roy, O. Lane, S. Dunn, and J.E. McGrath, Polymer, Vol. 49, p. 715, 2008.
59. K. Nakabayashi, K. Matsumoto, and M. Ueda, *Journal of Polymer Science: Part A: Polymer Chemistry*, Vol. 46, p. 3947, 2008.
60. K. Nakabayashi, K. Matsumoto, T. Higashihara, and M. Ueda, *Journal of Polymer Science: Part A: Polymer Chemistry*, Vol. 46, p. 7332, 2008.
61. J.-I. Ishikawa, S. Fujiyama, K. Inoue, T. Omi, and S. Tamai, *Journal of Membrane Science*, Vol. 298, p. 48, 2007.
62. C. Zhao, X. Li, Z. Wang, Z. Dou, S. Zhong, and H. Na, *Journal of Membrane Science*, Vol. 280, p. 643, 2006.
63. A. Roy, M.A. Hickner, X. Yu, Y. Li, T.E. Glass, and J.E. McGrath, *Journal of Polymer Science, Part B: Polymer Physics*, Vol. 44, p. 2226, 2006.
64. C. Liang, T. Maruyama, Y. Ohmukai, T. Sotani, and H. Matsuyama, *Journal of Applied Polymer Science*, Vol. 114, p. 1793, 2009.

65. Y. Li, A. Roy, A.S; Badami, M. Hill, J. Yang, S. Dunn, and J.E. McGrath, *Journal of Power Sources*, Vol. 172, p. 30, 2007.
66. H. Ghassemi, J.E. McGrath, and T.A. Zawodzinski, *Polymer*, Vol. 47, p. 4132, 2006.
67. B. Yang, and A. Manthiram, *Journal of Power Sources*, Vol. 153, p. 29, 2006.
68. N. Takimoto, L. Wu, A. Ohira, Y. Takeoka, and M. Rikukawa, *Polymer*, Vol. 50, p. 534, 2009.

5

High-Performance Processable Aromatic Polyamides

S Banerjee and S Maji

Materials Science Centre, Indian Institute of Technology Kharagpur, India

Abstract

Aromatic polyamides (PAs) are classes of high performance polymers owing to their outstanding set of thermal and mechanical properties. This class of polymers is used for different advanced military applications in ballistic composites to membrane based separation applications. However, these classes of polymers suffer from their poor processability by solution or melt processing routes that restricts their application in many of the field. Many approaches have been taken to prepare solution or melt processable PAs and polyimides by incorporating different flexible groups in the polymer backbone or by incorporating bulky substituents. Great amounts of research have been directed towards synthesis of $-CF_3$ substituted diamine monomers and their polymerization followed by property evaluations of the resulting polymers. The present article provides a comprehensive review on processable and $-CF_3$ substituted aromatic PAs that have been developed in the last decade. A major effort towards development of novel PAs that have been devoted by our group for the last few years thoroughly covered in this article.

Keywords: Aromatic polyamides, diamine, separation applications, melt processing, solution processing, hyperbranched

5.1 Introduction

In contrast to conventional polymeric materials, high performance polymeric materials are categorized by specific criteria, exhibit a number of interesting properties, such as high thermal stability,

Vikas Mittal (ed.) High Performance Polymers and Engineering Plastics, (111–166)
© Scrivener Publishing LLC

chemical resistance, low flammability, and excellent mechanical properties which make them useful for advanced technologies. Among high performance materials wholly aromatic polyamides (PAs) (aramids) exhibit all these properties. Aromatic PAs are considered to be high performance polymers due to their outstanding set of properties and they find wide applications in many of the advanced technologies, particularly, in aerospace and military applications. However, their extremely high transition temperatures, which lie above their decomposition temperatures, and their poor solubility in common organic solvents give rise to processing difficulties and limit their many of the applications. As a consequence, basic and applied research is being conducted to enhance their processability and solubility, in order to broaden the scope of their industrial applications.

According to the US Federal Trade Commission (FCT), wholly aromatic PAs are synthetic PAs in which at least 85% of amide groups are bound directly to two aromatic rings [1]. Aromatic PAs were first introduced in commercial applications in the early 1960s by DuPont under the tradename Nomex®. It is used extensively in the production of protective apparel, air filtration, thermal and electrical insulation as well as a substitute for asbestos. Later para-aramid called Kevlar® was introduced in also market by DuPont in 1973. The chemical structure of the poly(p-phenylene terephtalamides) (PPPT) and the poly(m-phenylene isophtalamides) (PMPI), which are commercial aramids of great economic relevance are shown in Figure 5.1.

Since the commercialization of Nomex® and Kevlar® a great number of PAs have been reported that covers a wide rage of properties. However the properties of Kevlar®, the PA fibre made from terephthalic acid and p-phenyle diamine are still unique in terms properties-price balance. Thus all the efforts dedicated to design and produce novel aromatic PAs have concentrated to improve the

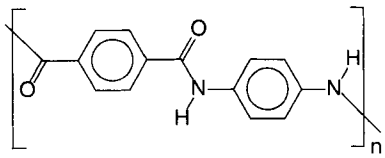

Poly(p-phenylene terephtalamides) (PPPT)

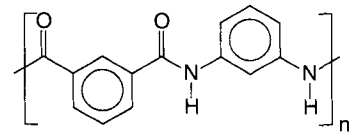

Poly(m-phenylene isophtalamides) (PMPI)

Figure 5.1 Chemical structure of the PPPT and the PMPI.

processability and to improve some properties that are crucial to specific end use application. The enhanced solubility of aromatic PAs in common organic solvents is targeted through different structural modifications [2]. The various approaches that have been used to design novel processable PAs are:

- use of diamines, diacids, or both, that contain flexible ether linkages, that reduces chain stiffness;
- introduction of bulky substructures, or side groups that help for separation of polymer chains and hinder molecular packing and crystallization;
- introduction of fluorine as trifluoromethyl groups, that helps in solubilization of the aromatic PAs by reducing interchain interaction and increases optical clarity;
- introduction of linear aliphatic and non-linear rigid alicyclic structures, or a mixture of thereof;
- use of 1,3 substituted instead of 1,4- substituted monomers and/or asymmetric monomers that lower regularity and molecular ordering.

In this chapter we will highlights the recent developments in aromatic PAs, broad range of structures possibility to make processable aromatic PAs with specific characteristics for various possible applications.

5.2 Monomers

The wholly aromatic processable PAs is achieved by modifying diamines, diacids, or both structures. The modification of the monomers can be broadly categorized in the four pathways to get the processable aromatic PA (i) incorporation of flexible spacers (ii) incorporation of bulky substructures as side substituent, (iii) incorporation of non-linear rigid alicyclic structures and cardo moieties and (iv) incorporation of fluorine as trifluoromethyl or a mixture of thereof. A short discussion on the monomers for the processable PAs has been described below.

5.2.1 Monomers Containing Flexibilizing Spacers

Much effort has been made to prepare aromatic PAs having increased solubility and processability with retention of their high

thermal stability. The solubility of PAs is often increased when flexible bonds such as [-O-, -SO_2-, -CH_2-, -$C(CF_3)_2$-] are incorporated into the PA backbone. These groups helps in altering crystallinity and intermolecular interactions. García *et al.* reported aminophenyl-terminated oxyethylene oligomers (Figure 5.2a) to synthesize processable aromatic PAs [3]. Nasr-Isfahani *et al.* reported short trimethylene aliphatic flexible spacer (Figure 5.2b) in the backbone containing aromatic diacid to obtain soluble PA [4]. Ferreiro *et al.* described that the incorporation of aliphatic pendent groups as substituents on the aromatic rings (Figure 5.2c) [5].

5.2.2 Monomers with Bulky Side Substituents

Inclusion of bulky pendent groups can provide advantage towards solubility of the PAs. These groups increases the inter chain distances, weakens the hydrogen bonding, lowers the chain packing and subsequently increase in free volume. These bulky side groups also restrict molecular mobility, so that the overall effect is an increase in glass transition temperature (T_g). Espeso *et al.* designed

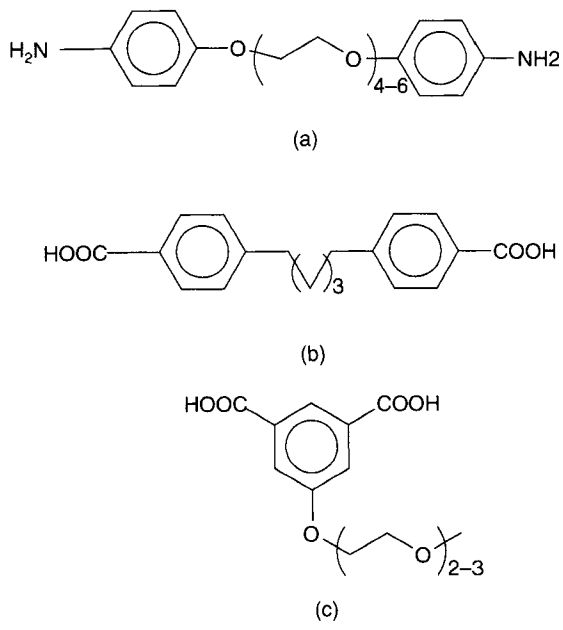

Figure 5.2 Structure of monomer containing flexibilizing spacers (a) (from [3]), (b) (from [4]) and (c) (from [5]).

and synthesized some linear bulky pendent group containing aromatic diacid and diamine monomers (Figure 5.3) for the synthesis of soluble aromatic PAs [6].

5.2.3 Monomers Containing Cardo Moieties

The cardo groups containing diacid or diamine monomers were widely used for the synthesis of high performance and processable aromatic PAs. The introduction of cardo groups in the polymer backbone created amorphous polymers with characteristic features such as improved solubility and enhanced thermal stability and mechanical properties [7]. Wu and Shu reported the synthesis of soluble aromatic PAs derived from a diacid monomer with a spiro core, 2,2′-bis(4-carboxyphenoxy)-9,9′-spirobifluorene (Figure 5.4a) [8]. Srivastava *et al.* reported cyclo aliphatic cage like diacid monomer (Figure 5.4b) for the synthesis of high temperature stable and soluble PAs [9]. We have reported trifluoromethyl and phthalimidine cardo group containing aromatic diamine monomer (Figure 5.5) for the synthesis of processable aromatic PAs [10, 11].

5.2.4 Monomers Containing Trifluoromethyl Groups

The introduction of fluorine in the form of trifluoromethyl groups ($-CF_3$) in polymer lead to great benefits for improving polymer solubility. This is due to the increase of fractional free volume that limits chain packing density and hence increases solubility and processability. We have reported several new aromatic diamine monomers containing trifluoromethyl groups for the synthesis of soluble and

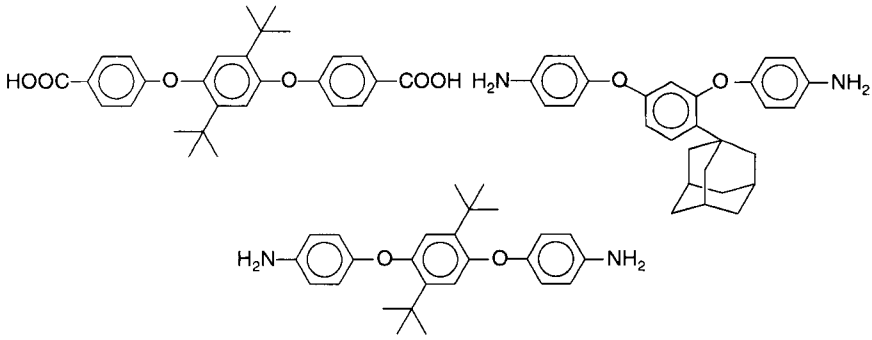

Figure 5.3 Structure of monomer containing bulky side substituents (from [6]).

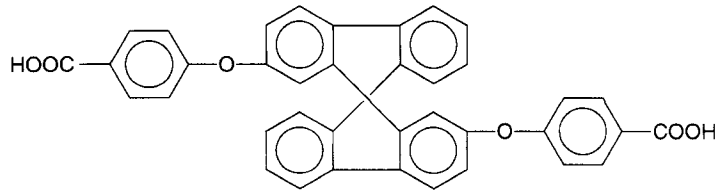

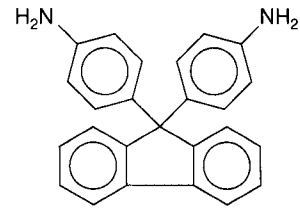

(a)

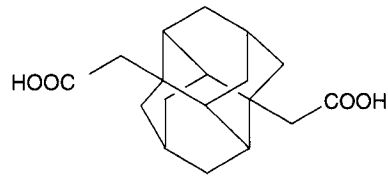

(b)

Figure 5.4 Structure of cardo diacid and diamine monomers (a) (from [8]) and (b) (from [9]).

processable aromatic PAs [10–15]. Moreover, we have taken other aspects into consideration viz. flexible ether linkage, bulky side substituents and cardo moiety in the monomer to get soluble and processable PAs. The structure of the diamine monomers is given below in Figure 5.5.

5.3 Polymerization

In general aromatic PAs can be synthesized by two different pathways. The most common methods for the preparation of aromatic PAs are the reaction of diacid dichlorides with diamines at low temperatures or direct condensation reactions in solution of aromatic diacids with diamines at high temperatures.

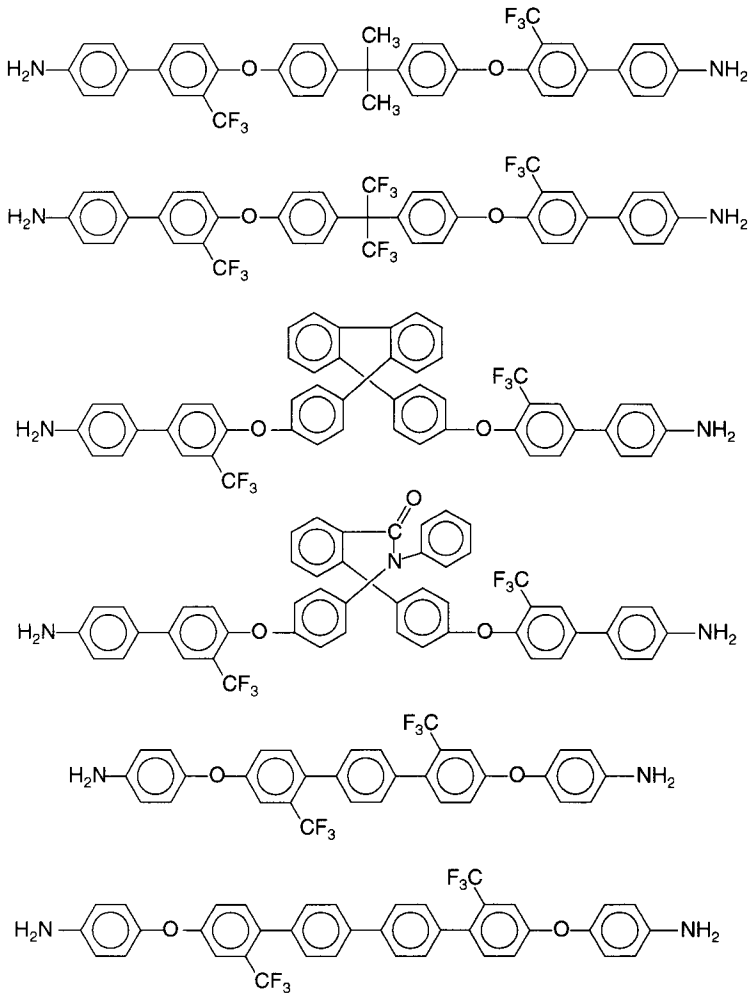

Figure 5.5 Structure of semifluorinated aromatic diamine monomers (from [10–15]). (Continued)

5.3.1 Low Temperature Solution Polycondensation

The first low-temperature solution processable PAs from acid chlorides were carried out in halogenated hydrocarbons. Piperazines and aliphatic or aromatic diacid based polymers were the first attempted polymers. Now this is not a preferred route to synthesize wholly aromatic PAs [16]. The solvents used are polar aprotic solvents like N,N-dimethylformamide (DMF), N,N-dimethylacetamide (DMAc), hexamethyl phosphoramide

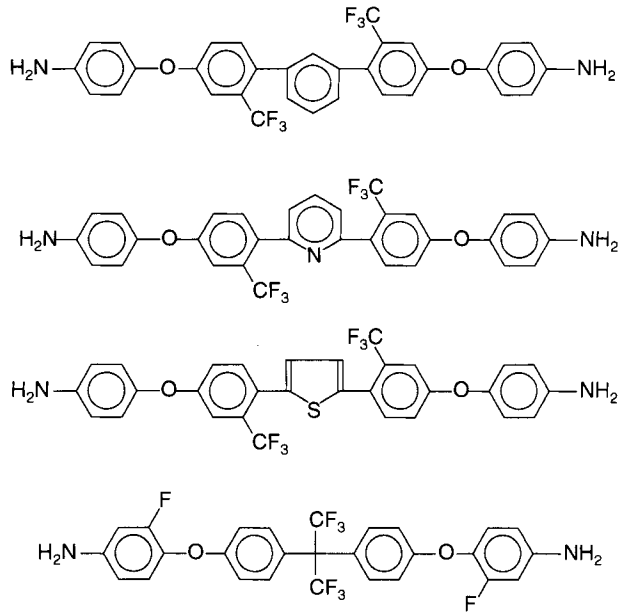

Figure 5.5 Structure of semifluorinated aromatic diamine monomers (from [10–15]). (Continued)

(HMPA) and N-methyl-2-pyrrolidone (NMP). Salts, such as LiCl, $CaCl_2$, or a mixture of both, are often used as solubility promoters because the cations interact with the amide groups, diminishing the strength of the interchain hydrogen bonds. The low temperature solution method is generally preferred when the diacid chloride can be easily obtained from the corresponding aromatic diacid. Extremely high monomer purity is the criteria in order to obtain high molecular weight polymers. The polydispersity (PD) of the polymers obtained by this method is around two. A modification of this method includes the silylation of the diamines to increase the reactivity of the amino groups. The silylation-polymerization procedure is usually performed in situ to avoid the isolation and purification of the moisture sensitive silylated diamines [17].

The polycondensation reaction can also be carried out in a two-phase system at room temperature, via the so-called interfacial polymerization [18]. The diamine and the acid dichloride monomers are dissolved in water and a water-immiscible solvent, respectively. A base and a surfactant are generally added to the aqueous media. The mixture of immiscible solutions, upon rapid stirring, gives rise

to a polymer precipitate in seconds. The reaction is extremely fast and occurs in the interphase on the organic solvent side. The stoichiometry cannot easily be controlled in the interphase because the instantaneous concentration is controlled by diffusion and depends only in part on the concentration of the monomers. Precipitation of the growing polymer chains usually produces polymers having a broad molecular weight distribution that are considered to be unsuitable for fibers or film-forming materials [19]. The tuning of the polymerization conditions in terms of the organic solvent type, solvent volume, monomer concentration, and stirring rate yields aromatic PAs that have more similar properties than those prepared via solution polycondensation methods. In addition, water insoluble diamines can be used as monomers upon polymerization of their water-soluble dihydrochloride derivatives [20]. This polycondensation has not achieved commercial importance.

5.3.2 High Temperature Phosphorylation Polyamidation Reaction

The direct condensation between aromatic diacids and diamines is another route for synthesis of PAs. In 1974, Yamazaki *et al.* [21] reported a procedure for the synthesis of aromatic PAs, which involved the complexation of a dicarboxylic acid with triphenyl or diphenyl phosphite (TPP/DPP) and pyridine in a solvent consisting of NMP containing $LiCl/CaCl_2$. The reaction may proceed via an acyloxy N-phosphonium salt of pyridine (I) formed by dephenoxylation of triphenyl phosphite, as has been proposed by Yamazaki *et al.* (Figure 5.6) [22]. In this case, high-purity monomers are required and an extra drawback is the side reactions occurred at the high temperatures. To obtain an aromatic PA with side chains containing sensitive functional groups it is important to that there should not be side reactions in the polymerization conditions. This can be verified by making model compounds prior to actual polymerization.

The high-temperature solution procedure was recently modified by the introduction of microwave-assisted (MW) polycondensation. This technique now widely used in organic chemistry, employed to promote chemical reactions in extremely fast and sometimes unconventional ways. The MW-assisted synthesis of PAs was performed to promote the condensation of aromatic diacids and diamines under Yamazaki conditions. The conventional heating system, i.e., temperature control oil bath, is replaced by the MW system, which

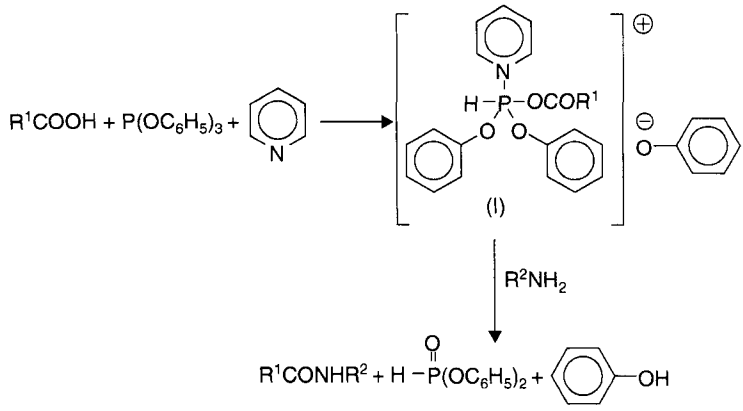

Figure 5.6 Reaction mechanism of the PA formation proposed by Yamazaki *et al.* (from [22]).

reduces the reaction time from 4 h to approximately 2 min [23]. The polymers obtained by both methods have comparable inherent viscosities (η_{inh}s).

Recent efforts have also been directed to the greener promotion of polycondensation under low or high temperature solution methods. The replacement of organic solvents by more environmental friendly versions is a topic of current interest. In this approach, the mixture of solvents used in the usual low temperature polycondensation (DMF, DMAc, NMP) and in the Yamazaki polyamidation method (NMP and pyridine) can be replaced by ionic liquids (IL). The ionic liquids have high thermal stability, low vapor pressure, are highly polar, and have a high dielectric constant, which makes them suitable to dissolve the aromatic PAs. Thus, eco-friendly aramids have been prepared using ionic liquids with TPP to promote the direct condensation of the acid and amide groups. The technique avoids the use of harmful solvents like pyridine and NMP This approach promote the reaction of diacid dichlorides and diamines at low temperatures [24]. Moreover, the polycondensation can be carried out by a conventional high-temperature heating method, using TPP as the condensation promoter, or employing MW, thus diminishing the reaction times from hours to minutes. The polymers having identical chemical structures and comparable inherent viscosities are obtained from both two heating methods, suggesting that their molecular weights are similar.

5.4 Major Problem with Aromatic Polyamides

Wholly aromatic PAs are considered to be high performance organic materials due to their outstanding thermal and mechanical resistance [25]. Their properties arise from their aromatic structure and amide linkages, which result in stiff rod-like macromolecular chains that interact with each other via strong and highly directional hydrogen bonds. These bonds create effective crystalline microdomains, resulting in a high-level intermolecular packing and cohesive energy. Owing to their rigid chemical structure they exhibit extremely high transition temperatures viz. T_g and T_m (melting temperature) that lie above their decomposition temperatures. These polymers are sparingly soluble in common organic solvents and that restricts their solution processability. Ongoing research efforts are therefore to take the advantage of their properties, enhance their processability and solubility, and incorporate new chemical functionalities in the PA backbone or lateral structure, so that their applicability is expanded and remains on the forefront of scientific research. As outlined earlier, aromatic PAs are difficult to process, and this fact restricts the development of new applications. Conventional linear aramids, i.e., PPPT and PMPI, are highly crystalline and cannot be processed by conventional methods like extrusion or injection because they do not melt. This is because their decomposition temperature is below their melt temperature. Thus, PPPT is wet spun into fibers from a lyotropic solution in concentrated sulfuric acid (H_2SO_4). The solubility of a less rigid and linear structure like PMPI is higher, and can be processed into fibers or coatings upon solution in polar aprotic solvents, such as NMP, DMAc and DMF. The solubility of PMPI was significantly improved over PPPT, since the nonlinear chemical structure exhibited all meta orientation of the phenylene moieties of the PMPI main chain, compared with the rigid rod all-para orientations of PPPT. The varity of application of the wholly aromatic PAs involves increasing polymer solubility without a dramatic loss in the chemical, thermal, and mechanical properties.

5.5 Approaches to Processable Polyamides

Several approaches have been taken to improve the processability of the aromatic PAs. The most important approaches are to impart

chain flexibility by incorporating flexible ether linkages through preparation of PAs and by diminishing the cohesive energy through lowering the interchain interactions. The use of meta substitution in the main chain phenylene residues, introduction of bulky side groups to the main chain, by employing non-symmetric monomers to the polymer backbone are the important approaches to achieve soluble PAs. Much work has been done in these areas, and several published papers report PAs with increasing solubility. A critical evaluation of this property indicates that most of the PAs are somewhat soluble in polar aprotic solvents such as NMP, DMAc, DMF, and dimethyl sulfoxide (DMSO). Whereas, a number of aromatic PAs were also found to be soluble in common organic solvents, like tetrahydrofuran (THF), cyclohexanone, chloroform ($CHCl_3$), acetone, or dioxane [26]. Approximately 30% of the published PAs are soluble in THF, 5% in $CHCl_3$, acetone, and cyclohexanone, and 2% in dioxane. The enhanced solubility of PAs in organic solvents is achieved using diamines, diacids, or both, that contain flexible ether linkages, bulky substructures, trifluoromethyl groups, cardo moieties, non-linear rigid alicyclic and linear aliphatic structures, or a mixture of thereof [26]. A discussion on the chemical structure, characterization, and properties of soluble aromatic PAs in the last 10 years can be found in the review by García *et al.* [26].

5.6 Processable Linear Aromatic Polyamides

5.6.1 Polyamides Containing Flexibilizing Spacers

Polyamides with short trimethylene aliphatic flexible sequences were described by Nasr-Isfahani *et al.* [4]. The polycondensation of the diacid 1,3-(4-carboxy phenoxy)propane with various aromatic diamines by direct polycondensation provide PAs with moderate yield. These PAs were found to be soluble in polar aprotic solvents and soluble even in acetone and in THF. Ferreiro *et al.* [5] described the effect of lateral oxyethylene moieties on the properties of aromatic polyisophthalamides. Several polyisophthalamides containing short sequences of oxyethylene as pendent substituents were synthesized by the reaction of three aromatic diamine monomers and four novel diacid monomers containing pendent oxyethylene units by the phosphorylation method of polycondensation. The polymers were prepared in high yield and high molecular weight.

All of the polymers were soluble in organic aprotic solvents at room temperature, which gave flexible films upon casting from solution. The mechanical properties of the films were reasonably good, with tensile strengths in the range of 70–100 MPa and moduli around 2.5 GPa. García *et al.* [3] synthesized and characterized segmented block thermotropic aromatic PAs (**PA-1**$_{a\text{-}b}$) from aminophenyl-terminated oxyethylene oligomers and terephthaloyl dichloride or 4,4′-biphenyl dicarboxylic acid dichloride (Figure 5.7). The polymers were produced in high yield and exhibited high molecular weight. The PAs showed solubility in organic solvents, viz. NMP, DMF and DMAc.

Mohamed and Fahmy have described four novel wholly para-oriented aromatic PA-hydrazides, containing flexibilizing sulfone-ether linkages in their main chains. The polymers were synthesized from 4-amino-3-hydroxy benzhydrazide (4A3HBH) with either 4,4′-sulfonyldibenzoyl chloride (SDBC), 4,4′-[sulfonylbis(1,4-phenylene)dioxy] dibenzoyl chloride (SODBC), 4,4′-[sulfonylbis(2,6-dimethyl-1,4-phenylene)dioxy] dibenzoyl chloride (4MeSODBC), or 4,4′-(1,4-phenylenedioxy) dibenzoyl chloride (ODBC) via low-temperature solution polycondensation [27]. The intrinsic viscosities of the reported PAs ranged from 2.85 to 4.83 dL/g in DMAc at 30°C. All the polymers were soluble in DMAc, DMF, and NMP, and the solution cast films showed good mechanical strengths. Both solubility and hydrophilicity were increased due to the flexibilizing linkages. The unoriented polymer films showed elastic moduli, tensile strengths, and elongation to break in the range of 6.45–3.54 GPa, 319.51–182.53 MPa, and 53–116%, respectively [27].

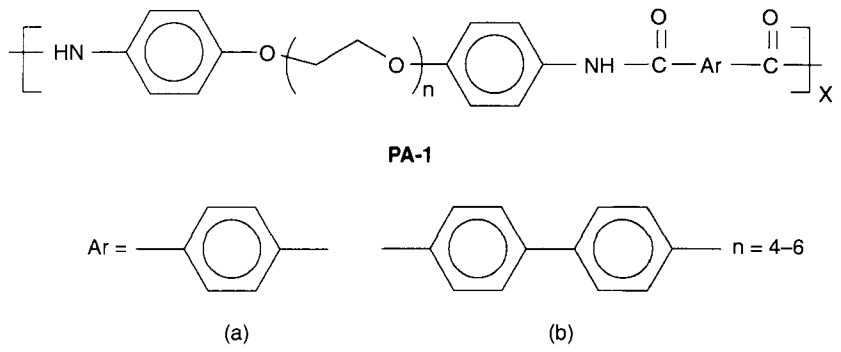

Figure 5.7 Chemical structure of the PAs containing flexibilizing spacers (from [3]).

Zulfiqar and Sarwar reported the synthesis of soluble and high mmolecular weight linear aromatic PA (**PA-2**) by condensing 4-aminophenylsulfone with isophthaloyl chloride in DMAc under an inert atmosphere (Figure 5.8) [28]. The structure elucidation of the resulting PA was carried out using infrared (IR) and nuclear magnetic resonance (NMR) spectroscopy. This PA was found to be soluble in various organic solvents. The T_g of the polymer was found to be 78°C measured by differential scanning calorimetry (DSC). The PA showed a maximum tensile strength of 35.6 MPa, elongation at break point 0.13 and Young modulus of 578.8 MPa [28].

5.6.2 Polyamides with Bulky Side Substituents

The incorporation of bulky pendent groups can provide advantage towards solubility. These groups increases the inter chain distances, a weakening of hydrogen bonding, and a lowering of chain packing with in crease in free volume. This chain separation effect improves the solubility (processability). Liaw and Liaw [29] described the synthesis and characterization of poly(amide imide)s (PAIs) containing adamantyl pendant groups. Diimide-dicarboxylic acid, and 4-(1-adamantyl)-1,3-bis(4-trimellitimidophenoxy) benzene, which contains pendent adamantyl groups was synthesized in three steps starting from adamantyl resorcinol. The reaction of the direct condensation of the diacid with aromatic diamines yielded a series of amorphous PAs. The PAs were soluble in polar aprotic solvents, cyclohexanone, and THF. In general transparent, flexible, and tough films were casted from DMAc solution. Espeso *et al.* [30] described aromatic PAs (**PA-3**$_{a-h}$) based on 1,4-bis(4-carboxyphenoxy)-2,5-di-*t*-butylbenzene, which is a linear diacid monomer constituted by three aromatic rings linked by a flexible ether group and substituted by two bulky *t*-butyl groups in the central ring (Figure 5.9).

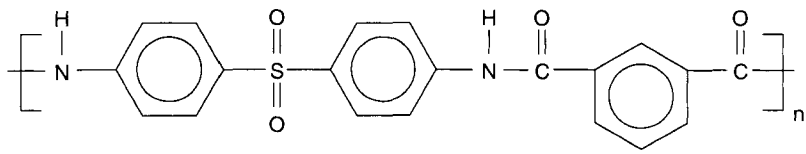

PA-2

Figure 5.8 Structure of the aromatic PA bearing sulfone linkages (from [28]).

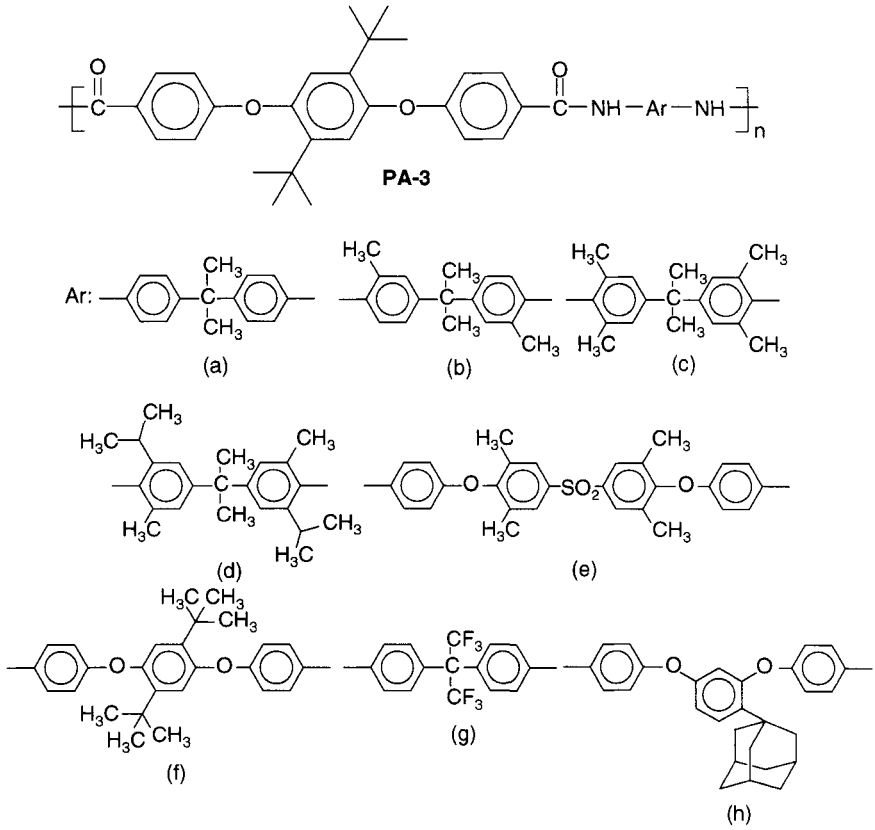

Figure 5.9 Chemical structure of the PAs based on bulky 1,4-bis (4-carboxyphenoxy)-2,5-di-*t*-butyl benzene (from [30]).

The monomer was combined with various diamines containing flexible linkages and side substituents to produce a set of eight aromatic PAs. As reported all the polymers were soluble in DMF, DMAc and NMP at room temperature, except one. Moreover some polymers were reported as soluble in cyclohexanone, and two polymers containing trifluoromethyl and adamantly group as pendent group were soluble even in THF and dioxane. The same research group [31] reported on the preparation of aromatic PAs based on an aromatic diamine with an adamantyl moiety in the lateral structure. The direct reaction under phosphorylation condensation of this diamine with various diacids produced amorphous polymers. The PAs were soluble in a variety of solvents, including cyclohexanone and THF.

Liou and Lin reported [32] a triphenylamine-based PA (**PA-4**), prepared by direct polycondensation of AB-type monomer, 4-amino-4′-carboxy-4″-methoxytriphenylamine in the presence of TPP and pyridine as condensation agents (Figure 5.10). The PA showed excellent solubility in aprotic solvents such as NMP, DMAc, DMF, DMSO and m-Cresol and could be cast into transparent film. The high solubility could be attributed to the introduction of the bulky pendent methoxysubstituted triphenylamine (TPA) moiety into the repeat unit. The M_w and PDI was found to be 63.4×10^3 and 1.79 respectively. The **PA-4** exhibited relatively high T_g (282°C), with good thermal stability T_{d10} above 470°C under a nitrogen atmosphere, and high char yield (> 64%) at 800°C in nitrogen.

Liou and Yen reported [33] a series of novel PAs (**PA-5**$_{a-e}$) with pendent naphthylamine units prepared via direct phosphorylation polycondensation from various diamines and a naphthylamine-based aromatic dicarboxylic acid, 1-[N,N-di(4-carboxyphenyl) amino] naphthalene (Figure 5.11). The inherent viscosities of the PAs were in the range of 0.15–1.02 dL/g. These light-colored polymers exhibited good solubility in a variety of solvents, such as NMP, DMAc, DMF, and m-cresol. The attempt has been taken by the research group to enhance solubility by the introduction of the bulky, asymmetric, and noncoplanar 1-naphthyldiphenylamine group into the repeat unit, which reduces interchain interactions

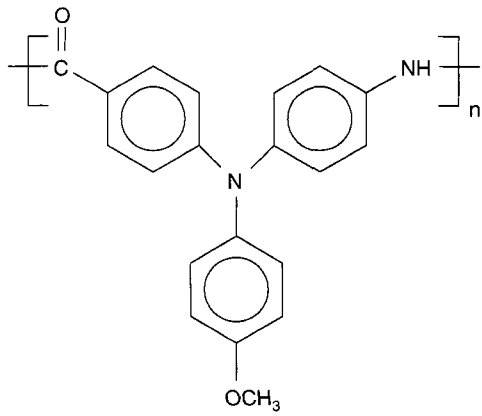

PA-4

Figure 5.10 Chemical structure of the PA based on bulky 4-amino-4′-carboxy-4″-methoxytriphenylamine (from [32]).

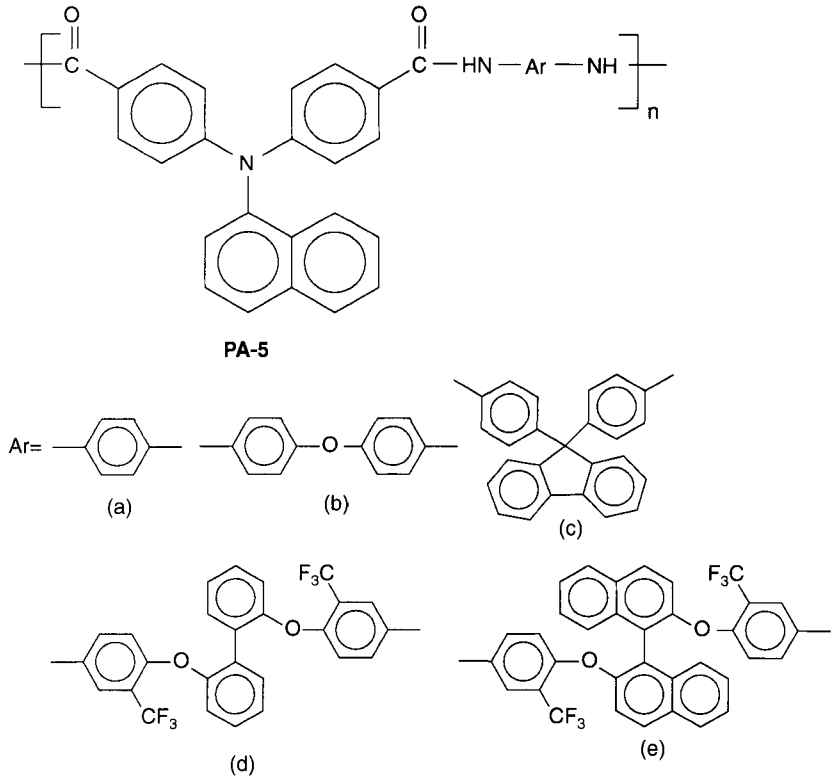

Figure 5.11 Chemical structure of the PAs based on bulky 1-[N,N-di (4-carboxyphenyl)amino]naphthalene (from [33]).

and increases free volume. The excellent solubility makes these polymers good candidates for practical applications by spin- or dip-coating processes. The aromatic PAs (**PA-5**$_{a\text{-}e}$) showed high T_g (268–355°C) and thermal stability (T_{d10}>480°C), and char yields at 800°C in nitrogen higher than 60%.

Wang and Hsiao have prepared [34] a series of electroactive di-*t*-butyl-substituted N,N,N′,N′-tetraphenylphenylenediamine (TPPA) bearing aromatic PAs, (**PA-6**$_{a\text{-}g}$) from a newly synthesized dicarboxylic acid monomer, N,N-bis(4-carboxyphenyl)-N′,N′-bis(4-*t*-butylphenyl)-1,4-phenylenediamine, with various aromatic diamines via the phosphorylation polyamidation reaction (Figure 5.12). Most of these polymers exhibited good solubility in highly polar organic solvents because of the introduction of the three-dimensional TPPA moiety and bulky pendent *t*-butyl

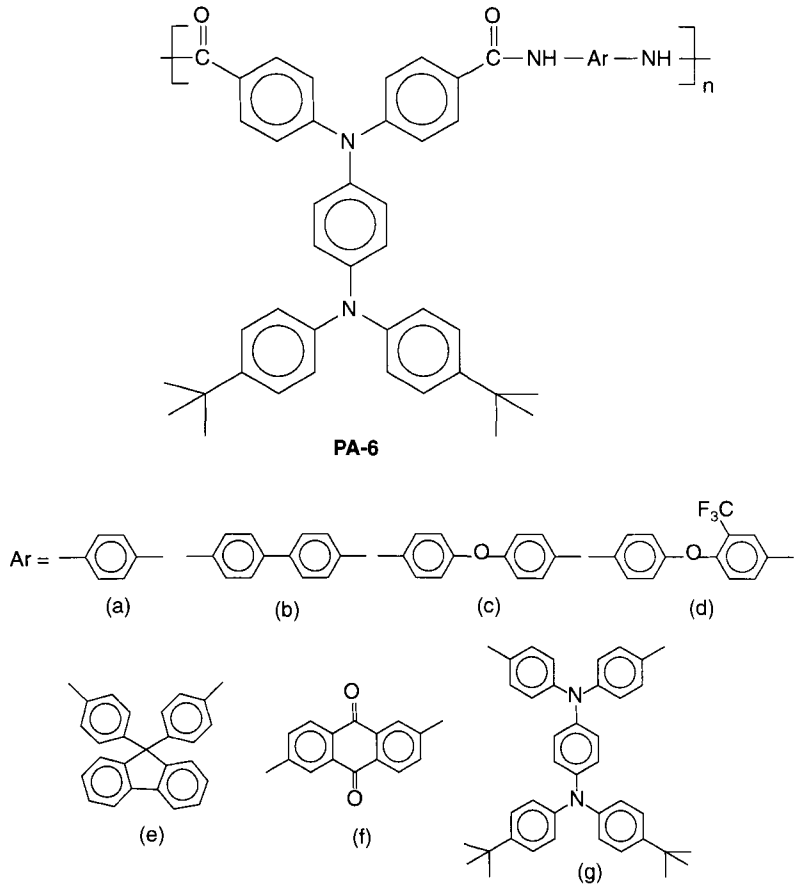

Figure 5.12 Chemical structure of the PAs (from [34]).

substituents into the repeat unit. Among these **PAs,** -CF_3 substituted **PA-6d** showed the best solubility. Except for **PA-6f,** flexible and tough films were obtained from the other polymers [34]. The PAs exhibited high T_g's in the range of 247–293°C and high thermal stability (T_{d10}> 500°C).

Mallakpour *et al.* [24, 35–41] have investigated the synthesis of PAs **[PA-(7A-7E$_{a-d}$)]** (Figure 5.13) from chiral diacids; 5-(4-methyl-2-phthalimidylpentanoylamino) isophthalic acid, (2S)-5-(3-phenyl-2-phthalimidyl pro-panoylamino)isophthalic acid, 5-(3-methyl-2-phthalimidyl pentanoyl amino) isophthalic acid, (2S)-5-[4-(4-methyl-2-phthalimidylpentanoyl-amino) benzoyl amino] isophthalic acid and 5-[3-methyl-2-(1,8-naphthalimidyl)-butanoylamino] isophthalic acid with several aromatic and

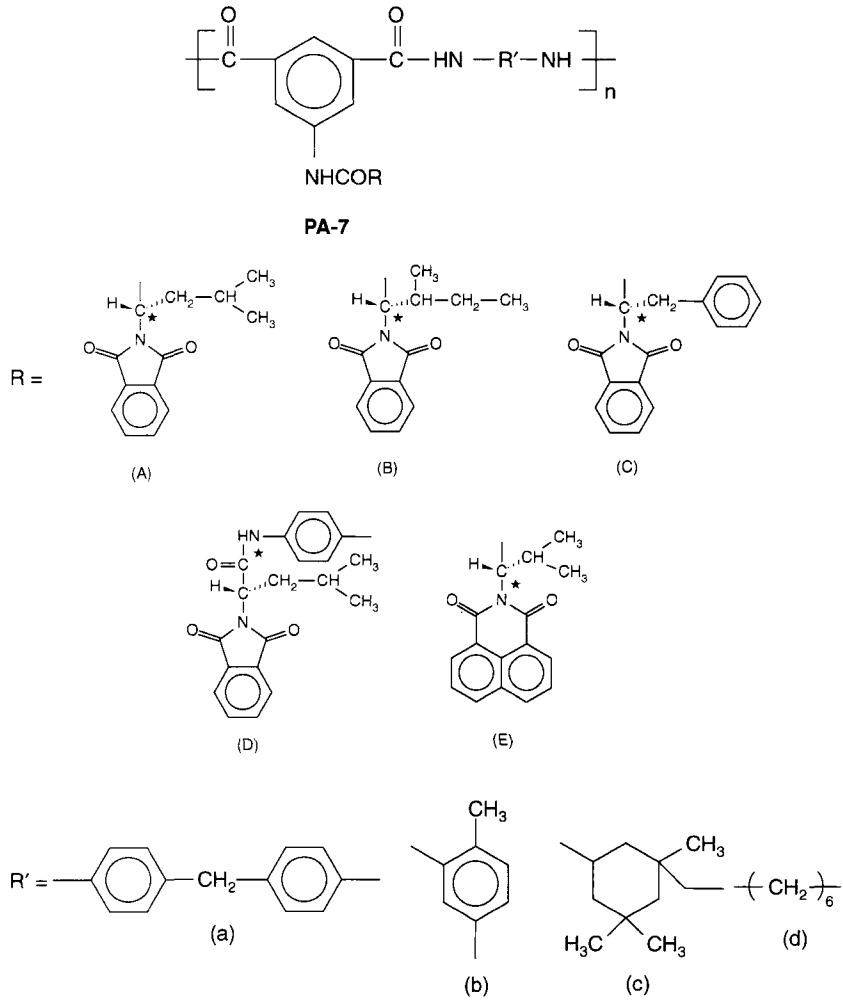

Figure 5.13 Chemical structure of the PAs (from [24, 35–41]).

aliphatic diisocyanates such as 4,4′-diphenylmethane diisocyanate (MDI), toluylene-2,4-diisocyanate (TDI), isophorone diisocyanate (IPDI) and hexamethylene diisocyanate (HDI) under microwave irradiation as well as conventional technique (Figure 5.13). The polymerization reactions were also carried out in the presence of tetrabutylammonium bromide (TBAB) as a molten ionic liquid (IL) or traditional solvent like1-methyl-2-pyrrolidone (NMP) under microwave irradiation. The resulting optically active PAs (**PA-7A**$_{a\text{-}d}$) have moderate inherent viscosities in the range of 0.32–0.57 dL/g

when synthesized in IL. The inherent viscosities of the same polymers were in the range of 0.25–0.63 dL/g when microwave step-growth polymerization technique was used. The PAs were soluble in amide-type solvents. Aromatic PAs **PA-7B**$_{a\text{-}d}$ synthesized under MW technique showed good yields and moderate inherent viscosities. Some of the reported PAs showed good solubility and are readily soluble in organic solvents. Another series of PAs (**PA-7C**$_{a\text{-}d}$) were also soluble in polar aprotic solvents. Aromatic PAs; **PA-7D**$_{a\text{-}d}$ [40] also were obtained in high yields and high inherent viscosities. Incorporation of the bulky side chain in the PAs cause an increase in the solubility organic solvents such as DMF, DMSO, DMAc, NMP, pyridine and in H_2SO_4 at room temperature. The unsymmetric diisocyanates such as TDI and IPDI gave polymers with lower inherent viscosities compared to the symmetric MDI and HDI [41]. This is attributed to the better possibility of chain arrangement and chain growth, when a step-growth polymerization reaction mechanism is performed during a defined reaction time. The inherent viscosities of the resulting polymers (**PA-7E**$_{a\text{-}d}$) under microwave irradiation were in the range of 0.26–0.54 dL/g and the yields were 75–91%.

The same research group also reported a series of thermally stable and optically active PAs (**PA-8A**$_{a\text{-}h}$) (Figure 5.14) prepared via an oil bath heating method using a mixture of 1,3-dipropylimidazolium bromide (as IL) and triphenyl phosphite (TPP) both as reaction media and activator [42]. The reaction proceeded efficiently with IL/TPP as condensing agent without the need of any additional promoters as necessary in case of traditional organic solvents like NMP. The incorporation of tetrabromophthalimide, and L-phenylalanine groups into PAs backbone gave polymers with good solubility in common organic solvents. These PAs showed high thermal stability, with the decomposition temperature above 400 °C, which is slightly lower compared to related aromatic PAs which do not contain any pendant groups (Figure 5.14).

In another study, Mallakpour and Rafiee [43] synthesized several optically active aromatic PAs (**PA-8B**$_{a\text{-}h}$) (Figure 5.14) from the reaction of new diacid monomer, 5-[3-phenyl-2-(9,10-dihydro-9,10-ethanoanthracene-11,12-dicarboximido)propanoylamino] isophthalic acid which was successfully synthesized starting from cis-9,10-dihydro-9,10-ethanoanthracene-11,12-dicarboxylic acid anhydride and L-phenylalanine and different aromatic diamines by MW assisted and conventional heating polyamidation reaction (Figure 5.14).

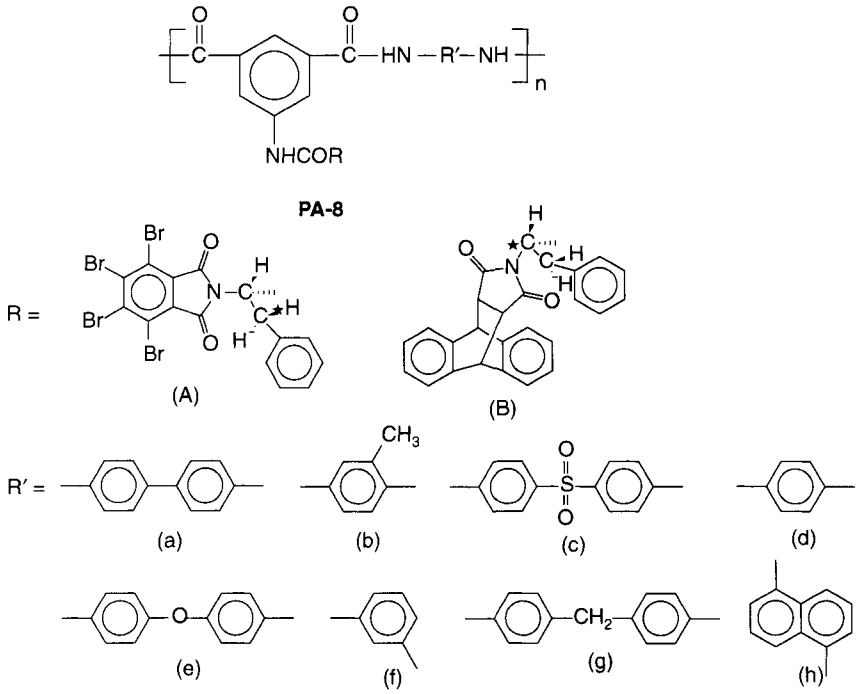

Figure 5.14 Chemical structure of the PAs (from [42, 43]).

As described earlier in this case also better yields were obtained under faster and cleaner reactions compared to those from conventional heating. All of these polymers having bulky anthracenic and amino acid functionality in the side chain showed excellent solubility in various organic solvents. PAs were thermally stable, with T_{d10} at 385°C in the nitrogen atmosphere, T_g above 180°C and char yields at 800°C higher than 50%.

5.6.3 Polyamides with Cardo Moieties

The cardo fluorene moiety was extensively studied to improve the solubility of PAs. Hu *et al.* [44] synthesized several PAs with fluorenyl-cardo moieties in the main chain. Most of the polymers were readily soluble in polar aprotic solvents, and some were soluble in THF. PAs exhibited better solubility when alkyl substituents were incorporated. Wu and Shu [45] described the synthesis of soluble aromatic PAs derived from a diacid monomer with a spiro core, 2,2′-bis (4-carboxyphenoxy)-9,9′-spirobifluorene (Figure 5.15). The direct

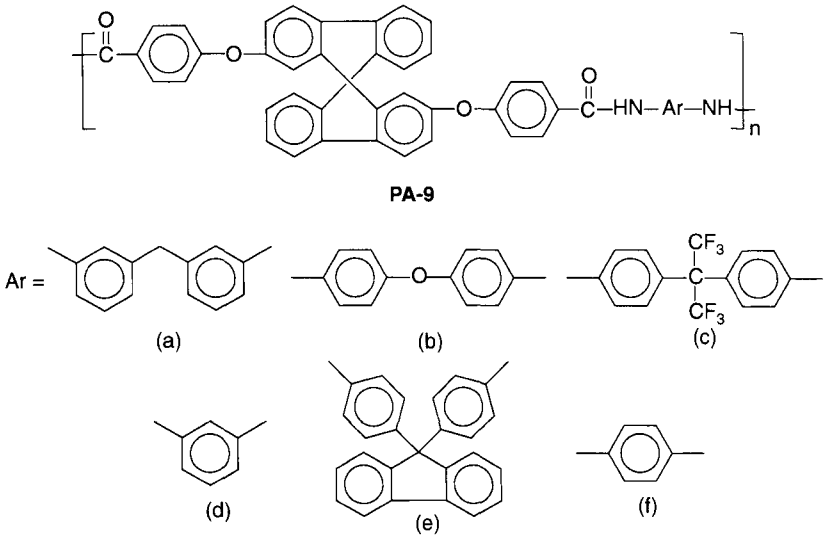

Figure 5.15 Chemical structure of the PAs based on cardo 2,2′-bis (4-carboxyphenoxy)-9,9′-spirobifluorene (from [45]).

phosphorylation polycondensation of this diacid monomer with various aromatic diamines gives amorphous aromatic PAs. The presence of the spiro segment in the main chain restricts the packing density of the polymer chains thereby decreases interchain interactions and resulting in PAs with enhanced solubility. All the PAs (**PA-9**$_{a\text{-}f}$) were soluble in THF and in polar aprotic solvents. Sagar *et al.* [46] reported on the synthesis and characterization of aromatic PAs containing *s*-triazine rings and fluorene "cardo" groups by low-temperature interfacial polycondensation of *s*-triazine ring containing diacyl chlorides with a cardo diamine. The PAs were amorphous and soluble at room temperature in polar aprotic solvents, but not in acetone. Korshak and coworkers [47] reported that the polymer chains having cyclic side cardo groups (for e.g., a fluorene group) can cause a significant increase in both T_g and thermo-oxidative stability while providing good solubility.

5.6.4 Polyamides Containing Trifluoromethyl Groups

Recently, considerable attention has been devoted to the fluorinated aromatic PAs. It was found that the incorporation of fluorinated groups into PA backbones resulted in great benefits for improving polymer solubility. This is attributed to the small dipole and the

low polarizability of the C–F band as well as the increase in free volume. The presence of $-CF_3$ groups and the substitution of fluorine for hydrogen, causes a remarkable change of properties. The C–F bond is a high energy bond, so that PAs containing fluorine are in general polymers with high T_g and better thermal properties, comparable to those of the conventional aromatic PAs. Fluorinated PAs showed improved properties, such as; increased solubility, excellent mechanical properties and low moisture absorption. The fluorinated PAs are very attractive for applications in advanced technologies, such as in high performance structural resins, thermally stable coatings and films, polymeric membranes for gas separation and pervaporation applications due to their excellent balances in properties. Zhu *et al.* [48] described the preparation of novel soluble fluorinated azo-PAs by reacting 2-trifluoromethyl-4,4′-diaminodiphenyl ether with various azodibenzoyl chlorides. Sheng *et al.* [49] reported on fluorinated aramids derived from an asymmetric monomer, 2-(4-trifluoromethylphenoxy)terephthaloyl chloride, polymerized with various aromatic diamines. The PAs were amorphous and readily soluble in polar aprotic solvents. Hsiao *et al.* [50] synthesized fluorinated PAs that had a isomeric diamine, 1,4-bis(4-amino-2-trifluoromethyl phenoxy)naphthalene. All the PAs were soluble in THF. Yang and Su [51] prepared fluorinated PAs with 4,4′-bis(4-amino-2-trifluoro methylphenoxy) biphenyl monomers. The main characteristics of these polymers are their excellent solubility even in THF and thermal and mechanical properties. Hsiao and Chang [52] prepared two types PAs containing flexible ether linkages and laterally attached side rods, which were synthesized from two diamine monomers; 2′,5′-bis(4-aminophenoxy)-[1,1′;4′,1″]terphenyl and 2′,5′-bis(4-amino-2-trifluoro methylphenoxy)-[1,1′;4′,1″] terphenyl. The polymers were readily soluble in aprotic polar solvents, and the PAs derived from diamine with the two trifluoromethyl substituents were soluble in THF. We have reported a series of fluorinated aromatic PAs (**PA-10**$_{a\text{-}d}$) (Figure 5.16) [15]. The reported PAs were soluble in polar aprotic solvents such as DMF, DMAc, NMP, DMSO, THF, pyridine, and chloroform.

Later, we have reported several $-CF_3$ group containing aromatic PAs (**PA-11a**$_{1\text{-}4}$, **PA-11b**$_{1\text{-}4}$ **and PA-11c**$_{1\text{-}4}$) for the pervaporation of benzene (Bz)-cyclohexane (Chx) mixture (Figure 5.17) [53–55]. The PAs were very much soluble in polar aprotic solvents and some of the polymers were even soluble in THF [53].

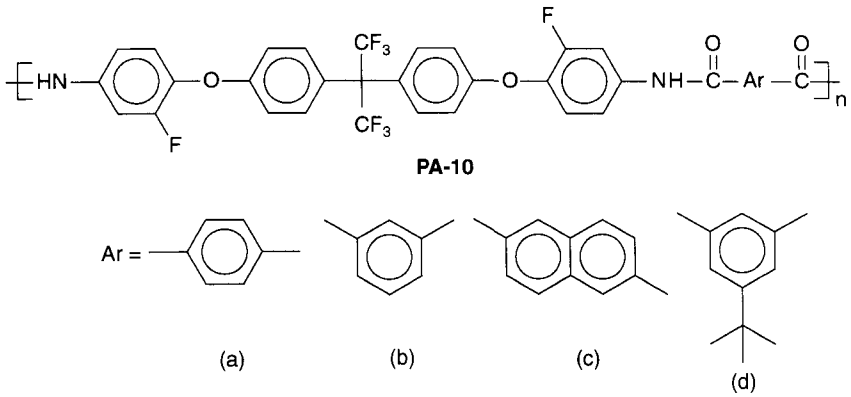

Figure 5.16 Chemical structures of the fluorinated aromatic PAs soluble in THF (from [15]).

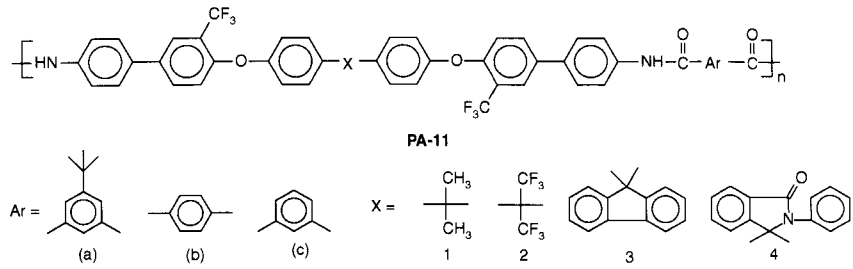

Figure 5.17 Chemical structures of the fluorinated aromatic PAs (from [53–55]).

Recently, we have described a series of new semifluorinated aromatic PAs (**PA-12**$_{a\text{-}e}$) where variation of rigidity, bond angle and polarity has been taken into consideration (Figure 5.18). Moreover, the effect of heterocyclic moiety in the polymer backbone was taken into consideration on its properties. These PAs were soluble in different organic solvents e.g. DMF, DMAc, NMP, pyridine and also in THF [56].

5.7 Processable Hyperbranched Aromatic Polyamides

Hyperbranched polymers (HBPs) have received great attention owing to their unique combination of low viscosity, excellent solubility, and facile synthesis. The preparation of HBPs from AB_2 monomers emerged with the initial report by Flory in 1952 [57].

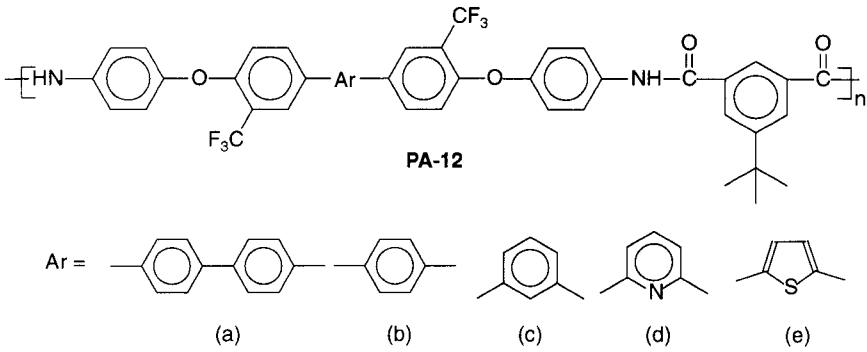

Figure 5.18 Chemical structures of the semifluorinated aromatic PAs (from [56]).

Jikei and co-workers [58] described the synthesis of aromatic hyperbranched polyamides (HBPAs), derived from aromatic diamines (A_2) and trimesic acid (B_3). Furthermore, Jikei and co-workers, [59] as well as Voit and co-workers [60] have explored these HBPs in more detail. polyamide dendrimers were first reported by Miller and Neenan in 1990 [61]. The synthetic pathway was based on a convergent approach. 1,3,5-Benzenetricarbonyl trichloride and 5-nitroisophthaloyl chloride were used as the core and building blocks, respectively [62].

Baek and Harris reported aromatic HBPAs [63], synthesized by the self-polymerization of AB_2 amide monomers containing hydroxyl and two fluoro groups. The reported polymers were amorphous in nature and were very much soluble in common organic solvents such as THF, $CHCl_3$, DMF, DMAc, DMSO, NMP, and m-cresol. The aryl-fluoride-terminated, amorphous polymers had intrinsic viscosities of 0.34 and 0.24 dL/g (30.0 ± 0.1°C in m-cresol) and T_g's of 210–269°C.

Liou *et al.* reported [64] a series of electrochromic aromatic HBPAs **PA-(13-15)** with electroactive triphenylamine (TPA) units, prepared from the phosphorylation polyamidation reactions of a newly A_2B type monomer, 4-amino-4′,4″-dicarboxytiphenylamine, with AB monomer and end-capping agent, respectively (Figure 5.19). Most of the reported PAs are readily soluble in polar aprotic organic solvents such as NMP, DMAc, DMF, DMSO and THF. Thus, the excellent solubility makes these polymers potential candidates for practical applications by spin-coating or inkjet-printing processes to afford high performance thin films for optoelectronic devices. The PAs showed good thermal stability associated with high T_g's (201–221°C) and higher than 71% char yield at 800°C in nitrogen.

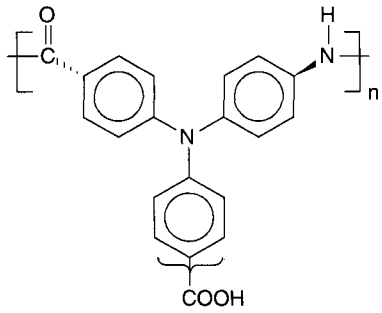

PA-13

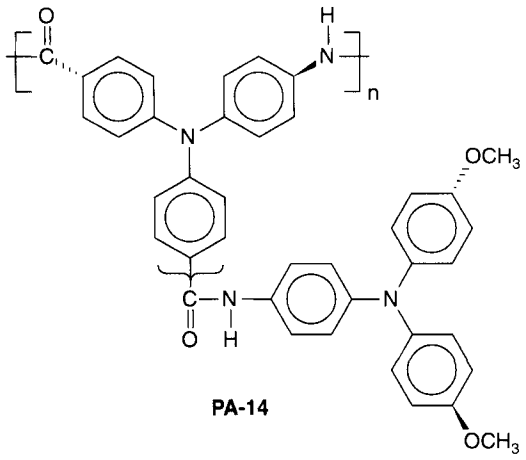

PA-14

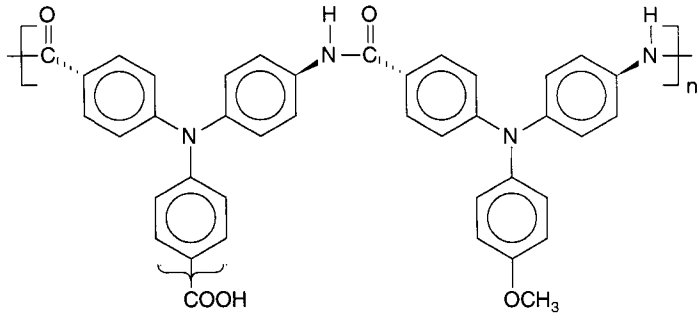

PA-15

Figure 5.19 Chemical structures of the aromatic HBPAs (from [64]).

Shabbir *et al.* reported the synthesis of an amide group containing aromatic triol and polycondensation of the aromatic triol monomer with various diacid chlorides that resulted in a series of hydroxy-terminated hyperbranched poly(amide esters) (HBPAEs) (**PA-16**$_{a\text{-}d}$)

(Figure 5.20) without gelation [65]. Polymer back bone structure and degree of branching of the resulting polymers were confirmed by FTIR, ^{1}H and ^{13}C-NMR spectroscopy. η_{inh} and T_g values of the HBPAEs lie in the range of 0.15–0.21 dL/g and 74–112°C, respectively. These thermally stable polymers were found to be good soluble in polar aprotic solvents including DMF, DMAc, NMP, and DMSO and to some extent in THF. The presence of alkyl groups in the semi-aromatic HBPAEs derived from aliphatic acid chlorides caused enhancement of solubility in comparison to fully aromatic HBPAEs. The presence of alkyl group caused improved solubility of **PA-16c** and **16d** and showed the highest solubility among the prepared HBPs.

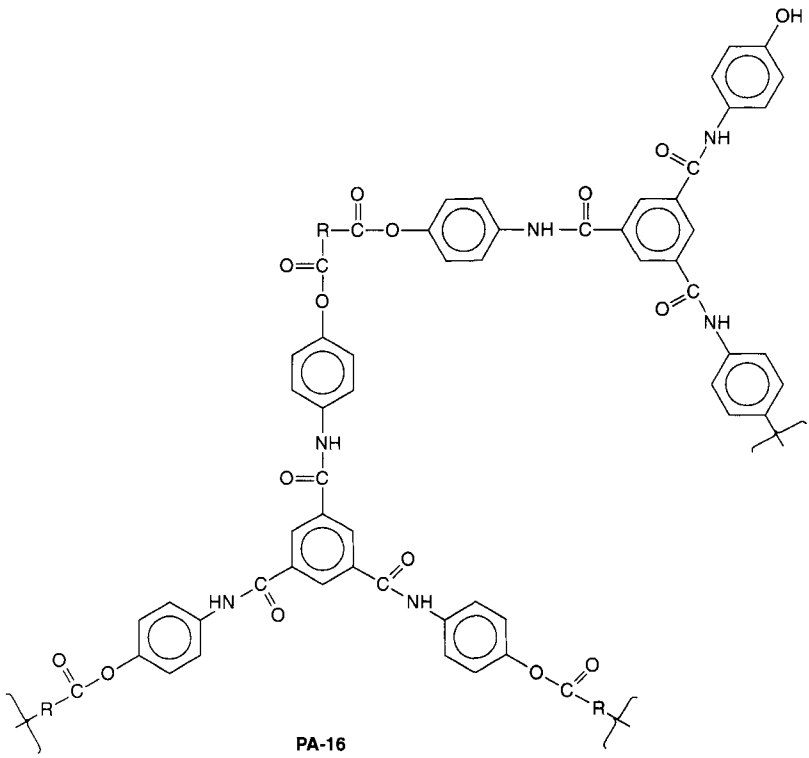

Figure 5.20 Chemical structures of the aromatic HBPAEs (from [65]).

Ishida *et al.* reported three aromatic HBPAs, synthesized by the direct polycondensation of 3,5-diaminobenzoic acid (AB_2), first generation (G1) dendron (AB_4), and second generation (G2) dendron (AB_8). The degrees of branching (DB) of the polymers from monomers were 0.32, 0.72, and 0.84, respectively, as determined by ^{1}H-NMR spectroscopy [66]. All aromatic HBPAs prepared from the three different monomers by direct polymerization were soluble in DMF, DMAc, NMP, and DMSO. The M_w of the resulting polymers measured by GPC based on polystyrene standards were in the range of $10 \times 10^4 - 20 \times 10^4$. The fifth generation (G5) dendron was soluble in aprotic polar solvents and THF, whereas both the end-capped HBPAs from AB_2 and AB_4 were insoluble in THF. The authors assume that the difference in solubility is caused by the difference in architecture of the molecule: random for the HBPs and spherical for the G5 dendron.

In and Kim described the synthesis of hyperbranched poly(arylene ether amides) (HBPAEAs) (**PA-17,18**) (Figure 5.21) with fluorine or hydroxy end groups from AB_2 or A_2B type monomers via a nucleophilic aromatic substitution reaction [67]. The reported HBPAEAs showed highly branched characteristics (DB = 0.43–0.53), high T_g (>220°C), and high thermal stability (T_{d10}>420°C). All HBPs were readily soluble in aprotic polar solvents such as DMF, DMSO, and NMP regardless of the end groups.

Li *et al.* reported a fast and highly efficient approach of synthesis to prepare aromatic and semiaromatic HBPEAs (Figure 5.22) via the polycondensation of AA′ and CB*x* monomers [68]. 2,2-Diphenic anhydrides (AA′ monomers) with aromatic or aliphatic multihydroxyl primary amine (CB*x* monomers) were thermally polycondensed to prepare aromatic and semiaromatic HBPEAs (**PA-19**) with multihydroxyl end groups without any catalyst. The DBs of the polymers were determined to be 0.53-0.63 by ^{1}H-NMR. These polymers exhibit excellent solubility in a variety of solvents such as DMAc, DMSO, THF, and $CHCl_3$ and possess moderate molecular weights with broad distributions determined by size exclusion chromatography (SEC). The decomposition temperature of the polymers at T_{d10} ranging from 333 to 397°C in nitrogen.

Jikei *et al.* have described the synthesis of aromatic HBPA copolymers by direct polycondensation of 3-(4-aminophenoxy)benzoic acid (AB monomer) and 3,5-bis(4-aminophenoxy)benzoic acid (AB_2 monomer) in the presence of TPP and pyridine as condensation agents [69]. The structure of resulting polymers was confirmed

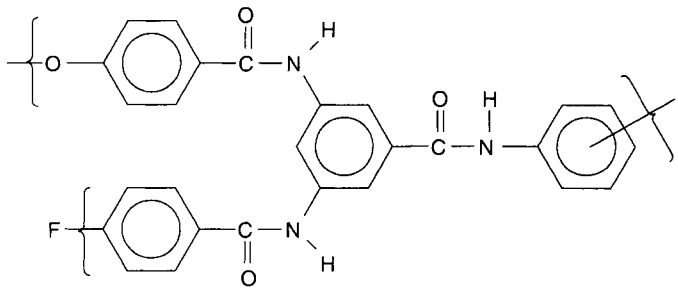

PA-17

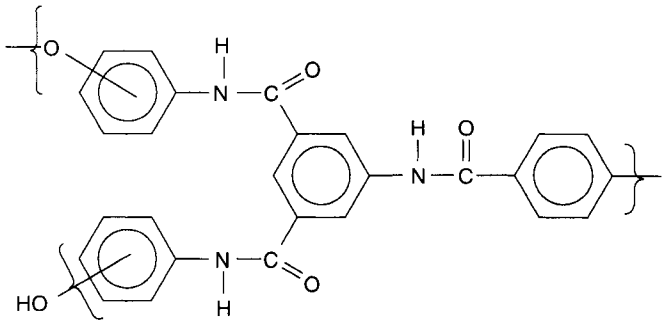

PA-18

Figure 5.21 Chemical structures of the aromatic HBPAEAs (from [67]) Vol. 38, p. 8235, 2005.

by IR, ^{1}H, and ^{13}C-NMR measurements. The resulting copolymers were soluble in aprotic polar solvents such as DMF, NMP, and DMSO, and transparent yellow films were prepared from DMF solution of the copolymers. The 5% weight loss (T_{d5}) temperature determined by TGA was over 400°C for all copolymers. The feed ratio of the monomers affected the T_g's and the softening points (T_s's). A minimum T_g was observed at a 50% of the AB_2 monomer whereas T_s's gradually decreased with increasing the AB_2 monomer and became constant over a 60%. Young's modulus determined by the tensile test decreased from 2.4 to 1.6 GPa with increasing amount of the AB_2 monomer in the range 0–60%.

Chang and Shu reported a aromatic hyperbranched poly(amide-imide) (HBPAI) (**PA-20**) (Figure 5.23), prepared by the copolymerization of 4-(3,5-dicarboxyphenoxy)phthalic anhydride, a $B'B_2$ type

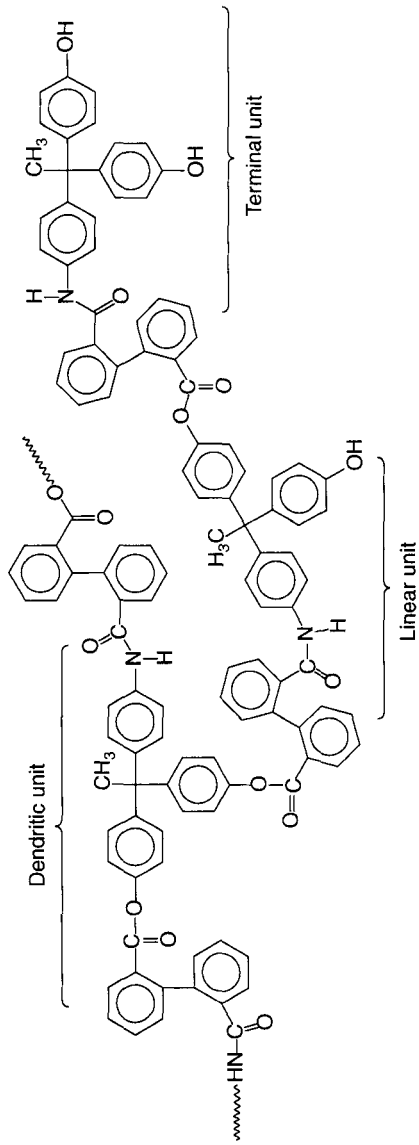

PA-19

Figure 5.22 Chemical structures of the aromatic HBPEAs (from [68]).

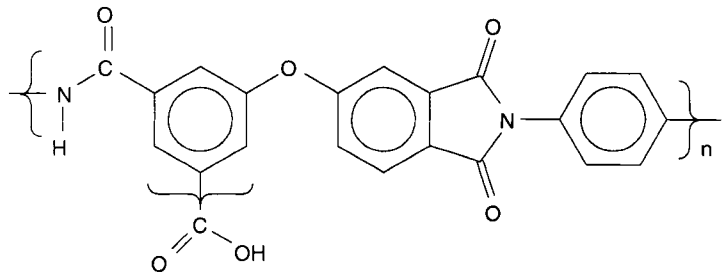

PA-20

Figure 5.23 Chemical structures of the aromatic HBPAI (from [70]).

monomer and 1,4-phenylenediamine and an A_2 type monomer [70]. The rapid reaction between the anhydride and amino group led to the formation of the dominant imide intermediate, regarded as a new AB_2 type of monomer. The intermediate, without isolation, was subjected to further polymerization in the presence of TPP and pyridine, as condensing agents, to give the HBPAI, containing carboxylic acid chain ends. For comparison they prepared an AB_2 monomer separately and the conventional self-polymerization of this monomer was also studied. The structures of the obtained polymers were characterized by FTIR and ^{1}H NMR spectroscopy. The DB of the HBPAIs was estimated to be 60–61%. The terminal carboxylic acid groups were modified by reaction with a variety of aromatic amines to give the corresponding amide derivatives. These PAIs have enhanced solubility in organic solvents and are highly soluble in polar solvents such as DMAc, NMP, and pyridine and the different chain ends led to solubility differences.

Jikei and Kakimoto have prepared the aromatic HBPAs and copolymers by direct polycondensation in the presence of condensation agents by (i) self-polycondensation of ABx-type monomers, (ii) copolymerization of AB_2 and AB monomers and (iii) polymerization of A_2 and B_3 monomers [71]. The self-polycondensation of ABx monomers proceeded without gelation to form soluble polymers. Spectroscopic measurements revealed that the copolymers were composed of five kinds of repeating units. The inherent viscosity of the resulting PAs was low, in the range 0.2–0.4 dL/g. All of the resulting PAs were soluble in aprotic polar solvents, such as DMF, NMP and DMSO. The good solubility and adequate solution viscosity of the copolymers allowed the preparation of transparent

yellow films by casting the copolymer solution onto a glass plate. The polymerization of A_2 and B_3 monomers was also investigated as a novel route to prepare HBPAs without using AB*x*-type monomers.

Shabbir *et al.* have reported carboxylic acid terminated aromatic and semiaromatic HBPAEs (**PA-21**$_{a\text{-}d}$) containing pyrimidine moieties (Figure 5.24). The polymers were prepared by polycondensation of 4-hydroxy-2,6-diaminopyrimidine (CBB') to a double molar ratio of various diacid chlorides (A_2) without any catalyst [72]. The products were soluble in organic solvents, such as DMF, NMP and showed T_g between 180 and 244°C. The polymerization products have been investigated with FTIR, ^{1}H and ^{13}C-NMR analyses and the degree of branching was higher than 60%. Amorphous polymers had inherent viscosity (η_{inh}) ranging between 0.21–0.28 dL/g and had excellent thermal stability with T_{d10} at 346–508°C.

Yu *et al.* reported aromatic HBPA grafted nano-silica particles (**PA-22**), successfully prepared via "onepot" melt polycondensation [73] (Figure 5.25). The silica particles were firstly treated with a silane coupling agent to introduce amine groups as the growth points, and then grafting of the HBPs started from the modified surface. The percentage grafting can be as high as 32.8%. All the aromatic HBPAs prepared by either grafting or homopolymerization are soluble in DMF, DMAc, NMP and DMSO. They also investigated the

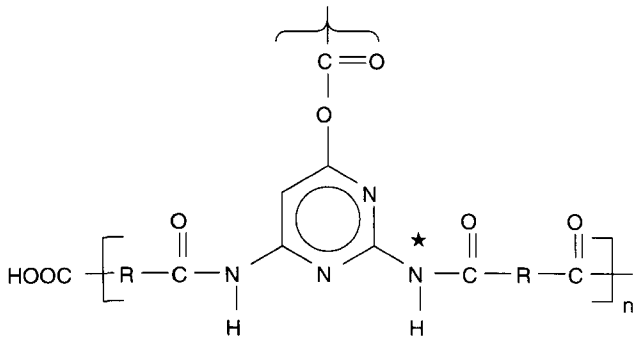

PA-21

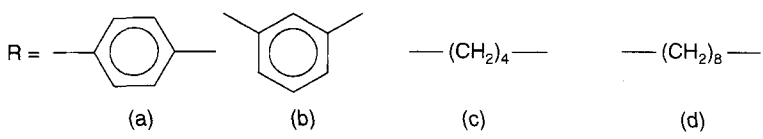

Figure 5.24 Chemical structures of the aromatic HBPAEs (from [72]).

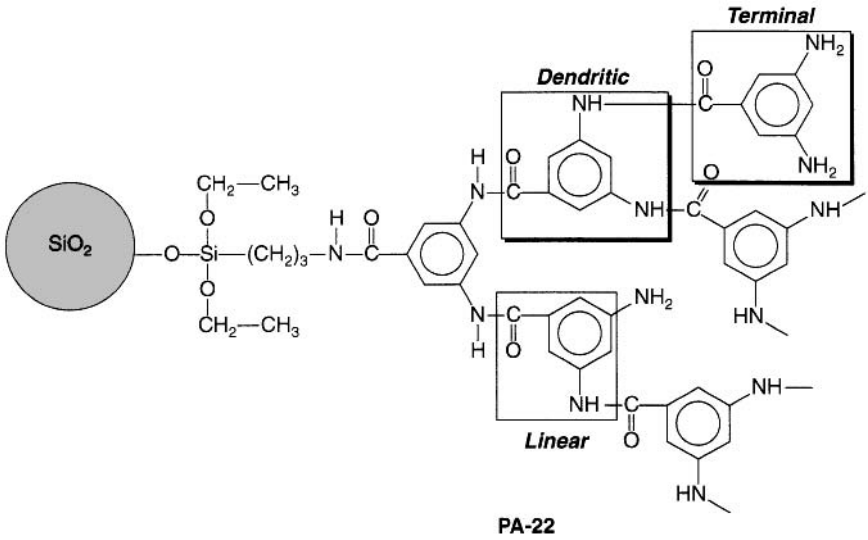

Figure 5.25 Chemical structures of the aromatic HBPA grafted nano-silica particles (from [73]).

role of terminal group in the HBP; all the PAs are soluble in DMSO, whereas they become partially soluble in DMF and DMAc.

Ohishi *et al.* have reported homopolymer-arm, block-arm, and miktoarm star polymers consisting of poly(N-octylm-benzamide) and poly(N-H-m-benzamide) by means of a core cross-linking method [74]. The ^{1}H-NMR spectra of the star polymers in DMSO revealed that the poly(N-octyl-m-benzamide) segments and arms of the block-arm and miktoarm star polymers, respectively. Star 2 and star 3 before deprotection showed rather similar solubility, and they were soluble in many kinds of organic solvents, except for alcohols. After deprotection, star 4 was only soluble in polar aprotic solvents, such as DMF and DMSO, whereas star5 was soluble in dichloromethane (DCM), $CHCl_3$, and DMF and insoluble in DMSO. Hence, the character of the external segment of the arms dominates the solubility and aggregability of the block-arm star polymers.

5.8 Properties

The thermal and mechanical properties of the PAs depends on their aromatic structure and amide linkages, which result in stiff rod-like macromolecular chains that interact with each other via

strong and highly directional hydrogen bonds. Moreover, main chain sp^3 carbon as a constitutive part of a lateral rings generally brings about polymers with excellent thermal and chemical stability, good mechanical and dielectric properties. García *et al.* described a number of aromatic PAs in a recent review on high-performance aromatic PAs [26]. Where the author nicely arrange all the PAs based on PAs with heterocyclic rings in the main chain, PAs with heteroaromatic pendant rings, cardo, fluorinated and chlorinated PAs, crown ether containing PAs, PAs with bulky pendant structures, segmented block PAs and unclassified PA structures. Moreover, pointed out all the properties of aromatic PAs e.g., thermal, mechanical etc. In our group we have reported a series of fluorine containing aromatic PAs prepared by the direct polycondensation of fluorine-containing aromatic diamines [15] and different commercially available aromatic dicarboxylic acid (Table 5.1). The PAs had inherent viscosity between 0.422 and 0.591 dL/g. These PAs showed reasonably good thermal stability, as indicated by T_{d10}s values upto 460°C in air. The PAs synthesized from 5-*t*-butyl isophthalic acid and isophthalic acid were amorphous and exhibited low T_g of 217 and 185°C, respectively, and the PAs derived from terephthalic acid and 2,6-naphthalene dicarboxylic acid were semicrystalline and showed $T_{m's}$ of 319 and 385°C, respectively. The solution casting film had tensile strengths of upto 82 MPa and moduli of upto 2.3 GPa. Further, we have synthesized another series of PAs containing pendent trifluoromethyl group [53]. These PAs had medium-to-high inherent viscosities and the highest value was found to be 0.93 dL/g and M_w value was determined to be 152×10^3 (GPC). The PAs exhibited good thermal stability upto 489°C (T_{d10} in nitrogen) and T_gs values upto 273°C (DSC) and 283°C (DMA). The PAs gave flexible films, which exhibited moderate mechanical properties (tensile strength upto 72 MPa, and modulus upto 1.39 GPa) (Table 5.2). Later, many other processable aromatic PAs have reported by us [11, 54, 55] and all the properties of the PAs we have tabulated in Table 5.2. Recently, we have reported another series of PAs and their properties have been compared in terms of rigidity, bond angle and polarity of the diamines used in the synthesis [56]. Moreover, the effect of heterocyclic moiety in the polymer backbone was taken into consideration on its properties. The properties we have tabulated in Table 5.3.

Table 5.1 Properties of the PAs containing $-CF_3$ substituent, ether linkage and bulky pendent groups (from [15]).

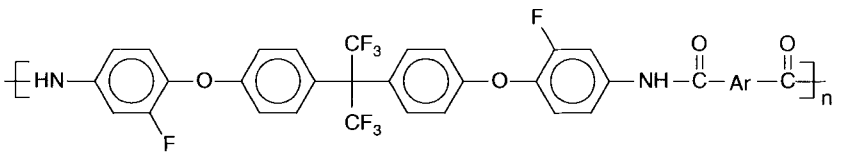

PA-10

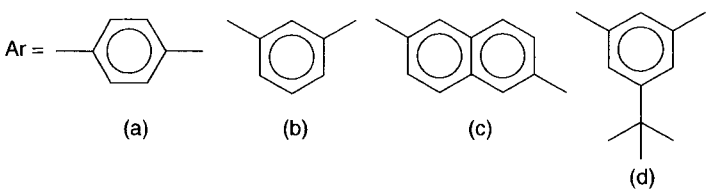

Polymer	η_{inh} (dL/g)	M_n (g/mol)	PDI	T_g (°C)	T_{d10} (°C) in air	Tensile strength (MPa)	Elongation at break (%)
PA-10a	0.423	18600	1.4	–	435	82	9
PA-10b	0.465	17200	1.3	185	440	65	6
PA-10c	0.422	13400	1.6	–	460	73	4
PA-10d	0.591	16100	1.8	217	432	71	7

Table 5.2 Properties of the poly(ether amide)s containing $-CF_3$ substituent, ether linkage, bulky pendent groups and cardo moieties in the main chain (from [11,53–55]).

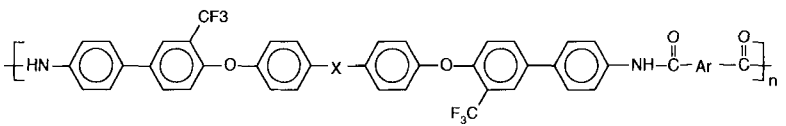

PA-11

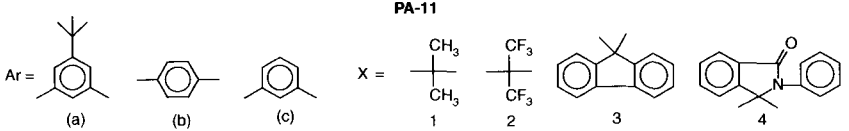

Sl. No.	η_{inh} (dL/g)	M_n (g/mol)	PDI	T_g (°C)	T_{d10} (°C) in air	Tensile strength (MPa)	Elongation at break (%)	Normalized flux (kgμm/ m^2h) at 50°C	Separation factor (α)	PSI (g/m^2 h) at 50°C
PA-11a1	0.93	61,000	2.49	250	475*	58 ± 2	10 ± 0.5	23.66	4.7	2087
PA-11a2	0.80	60,000	2.43	252	489*	72 ± 1	14 ± 1	29.89	4.4	2421
PA-11a3	0.88	42,000	2.71	273	481*	69 ± 0.5	09 ± 0.5	31.42	3.9	2169
PA-11a4	0.59	37,000	2.70	310	491	91 ± 3	11 ± 1	30.85	5.9	3601

PA-11b1	–	37,000	2.6	233	443	76 ± 1.0	9 ± 0.6	13.41	6.9	1888
PA-11b2	–	38,000	2.7	240	486	78 ± 0.5	11 ± 1.2	21.77	6.5	2849
PA-11b3	–	44,000	2.7	294	477	99 ± 1.3	13 ± 0.5	23.91	5.9	2788
PA-11b4	–	47,000	2.6	300	489	82 ± 1.5	10 ± 0.7	23.03	7.6	3616
PA-11c1	0.57	37,500	2.5	230	439	68 ± 1.2	8 ± 0.6	18.04	6.2	2236
PA-11c2	0.61	43,000	2.5	233	462	74 ± 1.5	12 ± 1.2	24.86	5.7	2782
PA-11c3	0.71	47,000	2.6	285	465	71 ± 0.8	10 ± 0.7	27.31	5.0	2600
PA-11c4	0.65	45,000	2.5	290	483	78 ± 1.4	9 ± 0.4	26.04	7.1	3782

*in nitrogen.

Table 5.3 Properties of the PAs containing $-CF_3$ substituent, ether linkage and bulky pendent groups (from [56]).

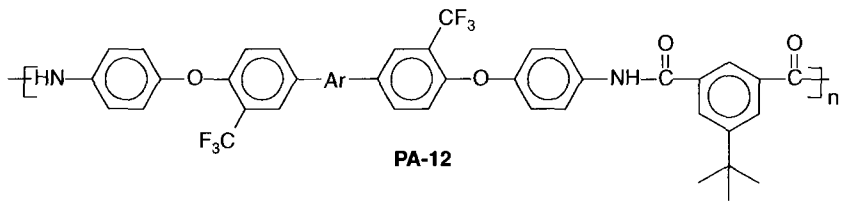

PA-12

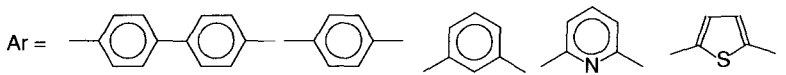

(a) (b) (c) (d) e

Polymer	η_{inh} (dL/g)	M_n (g/mol)	PDI	T_g (°C)	T_{d10} (°C)	Tensile strength (MPa)	Elongation at break (%)
PA-12a	0.59	83,400	2.8	261	475	88 ± 2.6	26 ± 2
PA-12b	0.42	73,000	2.5	255	412	84 ± 2.5	10 ± 1
PA-12c	0.63	77,500	3.0	245	445	75 ± 4.1	14 ± 2
PA-12d	0.45	69,500	2.8	259	458	86 ± 2.2	21 ± 3
PA-12e	0.47	70,300	2.7	244	409	81 ± 3.1	15 ± 2

5.9 Applications

The aramids are used mainly in heat-protection products; cut-protection products; ballistic-protection products; tires; hoses; transmission belts; friction product; sealing materials (gaskets and braided packings); adhesives, sealant and coatings; specialty paper products; ropes and cables; thermoplastic pipes; aramid-rubber composites; hot gas filtration; composites etc.

In the recent year PAs are used for optically devices, electronic devices, pervaporation membranes, gas separation membranes; ion exchange membranes; selective receptors and with environmental applications; packaging application, materials medical applications of biomaterials etc. These results are extracted from patent claims that have been approved over the last ten years [75].

5.9.1 Aromatic Polyamides for Membrane Application

5.9.1.1 Aromatic Polyamides for Pervaporation Application

Membrane-based technology is currently regarded as a new frontier of chemical engineering that has been developed in the past few decades and recently emerged as an additional category for separation processes which has been widely used for the purification, concentration, and fractionation of liquid mixtures. The needs for searching new polymeric materials for applications have been a continuous research challenge. For instance, with regard to the development of new materials, the U.S. Department of Energy identified "pervaporation membrane for organic separations" and "reverse osmosis oxidation-resistant membrane" as two of the highest ranking research priorities [76].

Chan *et al.* carried out pervaporation experiments through membranes comprising of different poly(amide-sulfonamides) (PASA's) [76]. They found that the best separation factor was achieved with a membrane based on N,N',-bis(4-aminophenylsulfonyl)-1,3-diaminopropane and isophthaloyl chloride. However, since they produced dense membranes by solvent evaporation the fluxes for all of the membranes prepared were very low in the region of 0.007–0.034 kg/m^{2}h.

Wang *et al.* reported a series of novel aromatic PAs (**PA-23A**$_{a\text{-}c}$ and **PA-23B**$_{a\text{-}c}$) based on the 2,2-bis[4-(4-aminophenoxy)phenyl]propane and 2,2-bis[4-(4-aminophenoxy)phenyl]hexafluoro-propane with

various aromatic diacids (Figure 5.26) for the pervaporation separation of benzene (Bz)/cyclohexane (Chx) binary system [77]. The aromatic PA membranes exhibited a Bz-permselectivity for all the feed compositions and the permeation rate increased with increasing Bz in the feed solution. The fluorine-containing PA membranes were swollen in Bz but only slightly in Chx. A separation factor toward Bz, a permeation rate, and a pervaporation separation index (PSI) value through the fluorine-containing PA membrane (**PA-23Bc**) for a 50 wt.% feed Bz concentration were 4.0, 1470 and 5903 g/m^{2}h, respectively. The permeation rate and the PSI value of fluorine-containing PA membranes based on (B) were higher than that of the aromatic PA membranes based on the (A) [77].

We have reported a number of new aromatic PAs for the application in pervaporation of Bz/Chx (50/50 wt%) mixture. Pervaporation study of Bz/Chx (50/50 wt%) mixture at three different temperatures have been successfully investigated using these PA membranes. The pervaporation study of Bz/Chx mixture indicates that the membranes are Bz selective in nature. In general, PAs containing phthalimidine moiety showed higher selectivity and **PA-11b4** showed the highest selectivity of 7.6 among all the polymers. PAs containing fluorene moiety showed higher permeation flux due to the more π-π interaction with benzene.

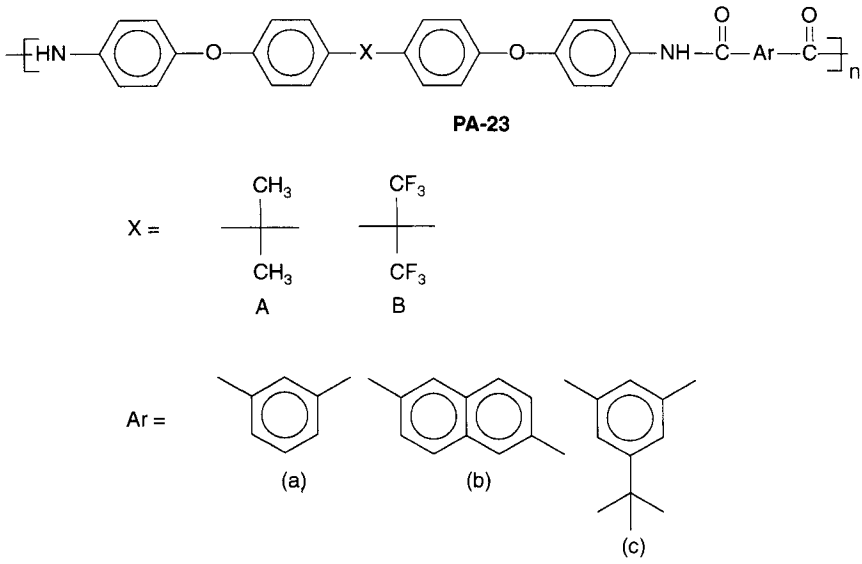

Figure 5.26 Chemical structures of the aromatic PAs (from [77]).

PA-11a3 showed the highest normalized permeation flux of 31.42 kgμm/m²h and **PA-11c4** showed the highest PSI of 3782 g/m² h at 50°C. These behaviors of the polymers were explained on the basis of the bulkiness, fractional free volume, T_g's and catenation angle. The pervaporation results are tabulated in (Table 5.2). Pervaporation of Bz/Chx mixture through various polymeric membrane materials were studied by Lue *et al.* [78]. They deduced the relationship between Bz/Chx selectivity and benzene flux to plot an upper bound tradeoff curve. The pervaporation result (Bz/Chx selectivity and benzene flux) of the synthesized PAs lies near to the upper bound trade-off curve in comparison to the many of the reported polymers (Figure 5.27).

5.9.1.2 *Aromatic Polyamides for Gas Separation Application*

There are current environmentally friendly processes for separation and purification methods by gas separation membrane technologies that are cost-effective for selective applications. Aromatic PAs

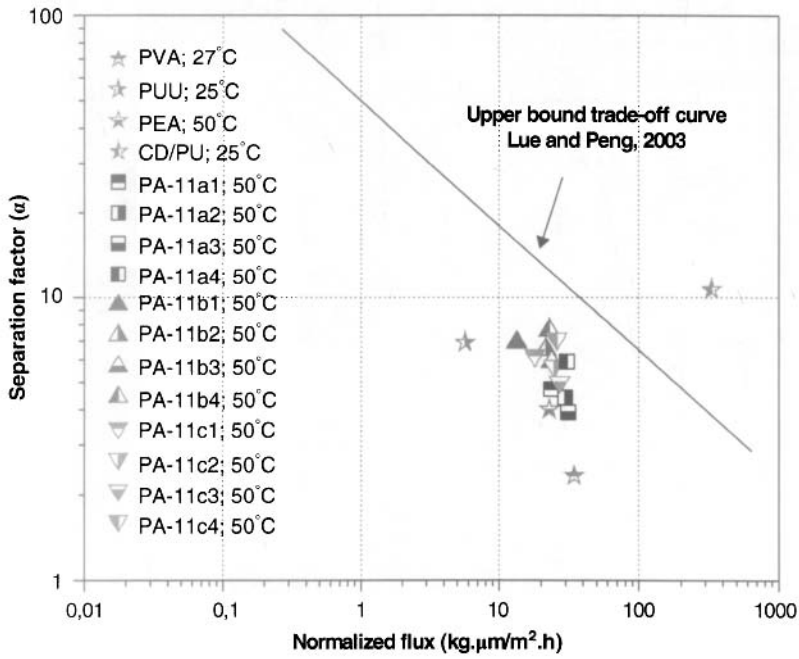

Figure 5.27 Lue and Peng plot for relationship between Bz/Chx selectivity and normalized permeation flux (Bz) using various membranes given in literatures and our synthesized PAs studied at 50°C.

have been traditionally considered to be very efficient barrier materials due to their high selectivity for gas separation. However, the high cohesive energy associated with the high packing density of the PA chains of the traditional aramids, such as PPPT and PMPI, produces extremely low gas permeability. Thus, research efforts are directed toward the reduction of this cohesive energy, by means of lowering the efficiency of the interchain hydrogen bonds, consequently increasing the free volume to yield materials with better processability and improved gas permeability.

Carrera-Figueiras and Aguilar-Vega [79, 80] studied the gas transport properties of benzophenone and hexafluoroisopropylidene containing aromatic polyisophthalamides and co-PAs derived from the copolymerization of isophthalic and 5-*t*-butyl-isophthalic acids with 4,4'-diaminebenzophenone or 2,2-bis(4-aminophenyl)hexafluoropropane (Figure 5.28). The gas permeability coefficients for **PA-24Aa** is around 10^{-2} barrers for O_2, which classifies this polymer as a barrier polymer. The inclusion of a bulky *t*-butyl group in ring position five of the isophthalic residue significantly increases the permeability (**PA-24Ba** is up to 15 times that of **PA-24Aa**, depending on the gas being considered and **PA-24Bb** is upto six times more

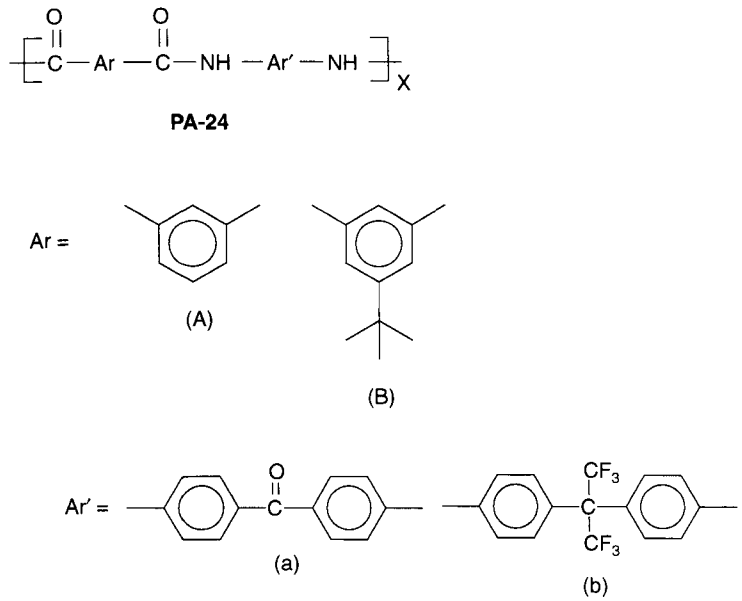

Figure 5.28 Chemical structures of the aromatic PAs (from [79, 80]).

permeable than **PA-24Ab**). This is attributed to an increase in the fractional free volume and interchain spacing, and a concomitant rise in the gas permeability and diffusion coefficients. However, a decrease in the selectivity of gas pairs is generally observed.

Ding and Bikson described prepared the dens membranes from aromatic PAs containing 2,3-dihydro-1,1,3-trimethyl-1H-indene moieties in the main chain and investigated their gas transport properties [81]. The membranes showed high gas permeability coefficients and gas separation factors. The nonsymmetric and nonplanar diacid residue results in desirable gas transport properties. However, PAs containing 1,1,1,3,3,3-hexafluoro-2,2-diphenylpropane exhibited higher gas permeability coefficients and modestly lower gas separation factors.

Recently, Ekiner and Simmons reported on membranes for the production of oxygen-enriched air, nitrogen-enriched air, for the separation of carbon dioxide from hydrocarbons, and the separation of hydrogen from various petrochemical and oil refining streams [82]. The membranes are made with blends of PAs, PIs and PI-PAs. They show high strength, chemical resistance, and are suitable for high pressure and temperature applications.

5.9.1.3 *Aromatic Polyamides as Reverse Osmosis and Nanofiltration Application*

Reverse osmosis (RO) is a water purification technique that reduces the quantity of dissolved solids in solution [83]. The technology depends mainly on complex polymer semipermeable membranes having a dense barrier layer where separation occurs. In general the membrane is designed to allow only water to pass through this dense layer while preventing the passage of solutes (such as salt ions). One of the most important applications of RO is the production of drinking water from saline or seawater. Aromatic PAs have been used for many years in RO membranes. Aromatic PAs usually form the active layer, and exhibit high salt rejection, water permeability, and fouling tolerance.

Konagaya *et al.* [84] prepared co-PAs from the diamine comonomers 3,3- or 4,4-diaminodiphenylsulfone, piperazine, and isophthaloyl or terephthaloyl diacid dichlorides. The asymmetric membranes prepared from the co-PAs not only have better reverse osmosis performance, but also have higher chlorine resistance properties than NOMEX-type aromatic PAs.

Mohamed and Al-Dossary [85] prepared flat sheet asymmetric RO membranes comprised of a wholly aromatic PA–hydrazides. The PA was prepared from 4-amino-3-hydroxybenzhydrazide or 3-amino-4-hydroxybenzhydrazide having equimolar amounts of terephthaloyl or isophthaloyl dichloride, or mixtures of both. The effects of various processing parameters on membrane transport properties were investigated by varying the temperature and the solvent evaporation time of the cast membranes, the coagulation temperature of the thermally treated membranes, the annealing of the coagulated membranes, casting solution composition, membrane thickness, and the operating pressure. The salt rejection was measured above 80% within the required level of permeability. Polymers having a higher content of meta-phenylene rings exhibited higher salt rejection.

Buch *et al.* [86] prepared aromatic–cycloaliphatic PA thin film composite membranes to measure the chlorine stability. The nanofiltration (NF) membranes contained the PA skin layer on a reinforced polyethersulfone ultrafiltration membrane, and were prepared by in situ interfacial polymerization of 1,3-cyclohexanebis(methylamine) in water with trimesoyl chloride in hexane under different conditions. As expected, the performance, i.e., salt rejection and water flux, of the membranes was strongly dependent on the PA skin layer preparation conditions, including monomer concentrations, reaction time, and curing temperature. They reported upon exposure of the membrane to 1, 3, or 5 ppm NaOCl solution containing 2000 ppm NaCl for different time periods, the smooth granular structure of the PA skin layer transformed to a rough granular nature. This they explained due to the conversion of the hydrogen bonding amide N–H group to the non-hydrogen bonding amide N–Cl. The membrane salt rejection decreased from the initial 78% to 63–65%, and water the flux decreased from 73 L/hm^2 to 32–38 L/hm^2. The amount of decrease was dependent upon the chlorine concentration and exposure time.

5.9.1.4 Aromatic Polyamides as Ion Exchange Membrane

In different scientific fields and technological process viz. chemical synthesis, mass separation, energy conversion, storage in fuel cell and electrical batteries, ion exchange membranes are useful. PAs have excellent mechanical and thermal properties. However, these materials have not been extensively studied for ion exchange membrane.

Taeger *et al.* examined the ion exchange capacity based on the sulfonated moieties in the backbone of aromatic homo- and both random and block co-PA [87]. Mechanically stable dense PA membranes were prepared and depending on the block length (higher than 20), a phase separation between sulfonated and nonsulfonated domains was observed. The water uptake and the methanol crossover of the PA membranes could be controlled by adjusting the block length. Materials showing phase separation exhibited enhanced properties with respect to methanol permeability and water uptake (swelling) in comparison to Nafion®. The materials have a theoretical ion exchange capacity of up to 3.14 mequiv./g.

Similar sulfonated PAs structures as proton exchange membranes in fuel cells have been recently proposed by Jo *et al.* [88]. One of the PAs had a comparable proton conductivity (105 mS/cm) to that of Nafion® 117 at 80°C.

5.9.2 Polyamides with Special Properties

5.9.2.1 Optically Active Polyamides (OAPs)

Naturally occurring polymers, such as proteins, DNA, and polysaccharides, are optically active. Consequently, the design, characterization, and preparation of chiral polymers are of particular interest [89]. The methods of preparing OAPs involve the polymerization of optically active monomers and asymmetric polymerization, which produces OAPs starting from optically inactive monomers. Concerning the aromatic PA synthesis, the simplest approach, starting with chiral monomers, is commonly used.

Mallakpour *et al.* have been prepared several aromatic PAs having a lateral L-isoleucine core group by adopting two polymerization methods (conventional high-temperature solution method, and MW method) using aromatic diacids and diisocyanates [38, 39]. Both methods were employed using different catalysts (dibutyltin dilaurate: DBTDL, pyridine, triethylamine (TEA), or no catalysts). The best results were obtained with DBTL, under MW radiation as well as conventional heating polymerization. Polymers prepared by different methods showed different optical rotation, and this fact was attributed to the dependence of the optical rotation on the overall structure and regularity of the resulting polymer chains. Surprisingly, polymers of the same chemical structure obtained by the same method with different catalysts resulted in different values of $[\alpha]$, i.e., the $[\alpha]_D^{25}$ is −28.5 and +28.5 for one of the polymer

PA-7A$_a$ (Figure 5.13) polymers obtained employing DBTL and TEA as catalysts, respectively. The authors claim that since these polymers are optically active and have amino acids in the polymer architecture, they are likely biodegradable, and are therefore classified as environmentally friendly polymers. Potential application can be found for the amino acid based polymers as the chiral stationary phases for the resolution of enantiomers in chromatographic techniques, drug delivery and biomaterials.

The same research group [90] reported the preparation of OA (PAIs) derived from N,N-(4,4'-oxydiphthaloyl)-bis-(s)-(+)-valine diacid chloride. The polymers were prepared by the reaction of aromatic diamines with the diacid by classical low-temperature solution polycondensation (reaction time: 2 h at −5°C and 8 h at rt), high-temperature polycondensation (reflux conditions, reaction time: 1min), and MW polycondensation reaction (reaction time: 6min). Comparable results were obtained for all polycondensation processes.

The authors further synthesized another series of PAIs derived from trimellitylimido-L-phenylalanine [91]. The direct polycondensation reaction of the monomer imide–diacid with different diamines rendered high yield PAIs with relatively low η_{nh} values between 0.21 and 0.45 dL/g. All the above compounds were fully characterized by IR spectroscopy and elemental analyses, the $[\alpha]_D^{25}$ varied between −1.0 and −3.6 °.

5.9.2.2 Luminescent and Electrochromic PAs

The demand for lighter, thinner and more compact electrical and electronic devices is increasing day by day. Polymers, or polymer composites, are suitable materials for these applications, which moreover require high-performance materials that can undergo injection molding and have sufficient heat resistance to withstand surface mounting technology. The inclusion of chromogenic and fluorescent chemical moieties in the lateral aromatic PA chains gives rise to luminescent converter (LUCO) materials.These polymers used for preparation of LEDs with tremendous potential in lighting and backlighting applications [92].

Light-emitting phenomena are a characteristic of luminescence materials. Among the different types of luminescence, light-emitting aromatic PAs are of importance that produces electroluminescence (EL) or photoluminescence (PL) phenomena upon exposure to an electric current or due to absorption of photons

causing re-radiation [93, 94] respectively. The physics underlying luminescence have been extensively described in the literature, and are beyond the scope of this study.

Additionally, the film formation properties and outstanding mechanical properties of aramids make these polymers suitable for the production of organic light emitting diodes (OLEDs), and specifically polymer light emitting diodes (PLEDs). Despite this, classical condensation polymers are rarely studied for these applications. Moreover, some luminescence materials also show electrochromism (EC), a phenomenon in which materials exhibit a reversible change in optical properties when they are oxidized and reduced. Electrochromic materials are now been exploited in diverse applications such as mirrors, displays, windows, and earth-tone chameleon materials [95].

Estevez *et al.* prepared and analyzed a chemically modified co-PA consisting of 90% of structural units of poly(m-phenylene isophthalamide) (NOMEX®) and 10% of structural units containing the pendant fluorene groups (**PA-25**$_{a\text{-}f}$) (Figure 5.29). The authors used the copolymer to maintain the outstanding mechanical and thermal properties of NOMEX® to give rise to dense membranes to be used as colorimetric or fluorescence sensing materials [92].

Hsiao *et al.* reported [96] a series of new PAs (**PA-26**$_{a\text{-}f}$) with *t*-butyl-substituted triphenylamine units were successfully prepared (Figure 5.30). The PAs exhibit good solubility and film-forming capability and high thermal stability, and all of them are

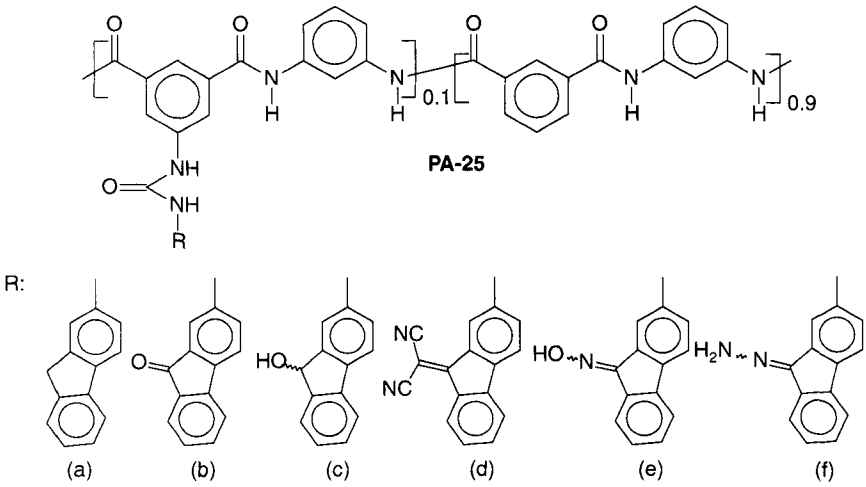

Figure 5.29 Chemical structures of the modified co-PAs (from [92]).

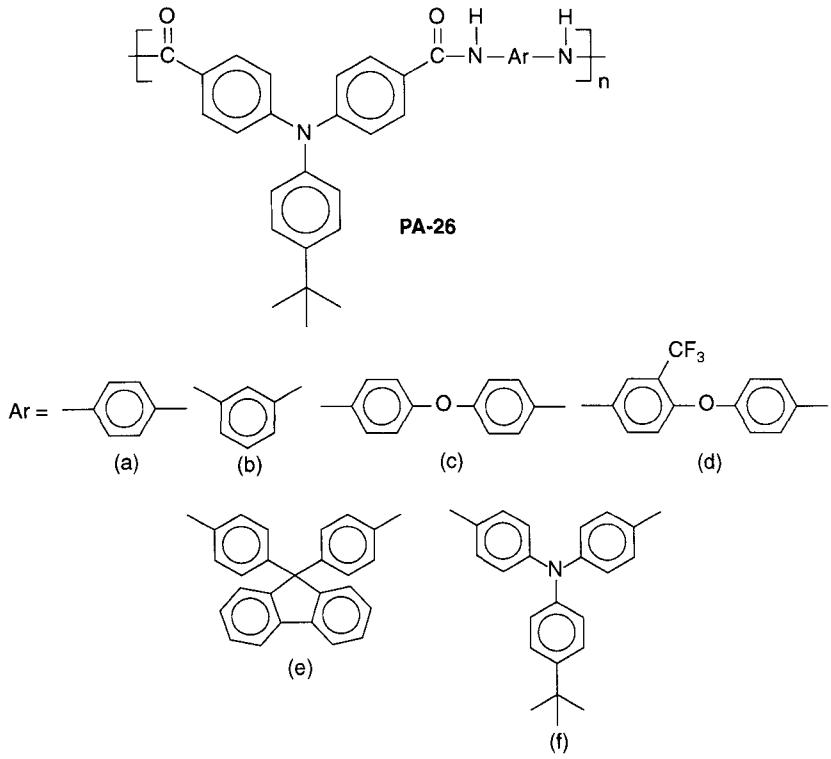

Figure 5.30 Chemical structures of the PAs (from [96]).

fluorescent with blue-light emission. The polymers display very well-defined and reversible redox processes in acetonitrile solutions. Furthermore, they possess electrochomic behavior. The **PA-26f** containing the *t*-butyl-triphenylamine unit in both diacid and diamine components shows multielectrochromic behaviour; colorless in the neutral state, green in the semioxidized state, and purple in the fully oxidized state. Good redox and electrochromic stability, moderate fluorescence intensity, and proper HOMO values of these PAs make them promising candidates for optoelectronic applications.

Nechifor [97] examined a monomer diacid having two coumarin moieties in the main chain and in the pendant structure, namely 6,6′-methylene bis{2-oxo-8-{2-[(2-oxo-2H-chromen-7-yl)oxy] acetoxy}-2H-chromene-3-carboxylicacid} (Figure 5.31). This was polymerized with various aromatic diamines to give a series of new aromatic PAs (**PA-27**$_{a\text{-}g}$) with photosensitive coumarin pendent

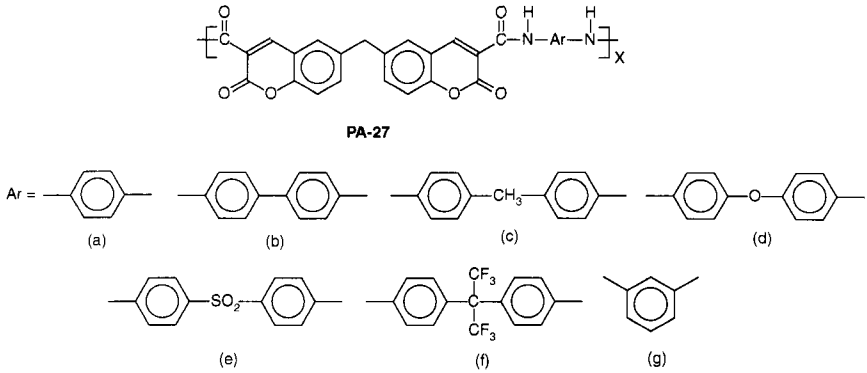

Figure 5.31 Chemical structures of the PAs (from [97]).

groups. The bulkiness of the side lateral structure creates amorphous PAs having increased solubility, and is soluble in aprotic polar solvents as well as less polar solvents like THF. Polymer films were prepared via induced crosslinking between PA molecules through a [2π+2π] photo-cycloaddition at the double bond of coumarin moieties and irradiated (η > 300 nm). The emission spectra of polymer solutions showed a band with a maximum at 387 nm. The fluorescence spectra of the films showed red shifts of 18 nm in the emission maxima.

Liou and Yen reported [33] a series of PAs with pendent naphthylamine units (Figure 5.11). These polymers showed maximum UV–visible absorption at 350–358 nm and exhibited fluorescence emission maxima around 435–458 nm in NMP solutions with fluorescence quantum yields ranging from 0.4 to 15.0%. The hole-transporting and electrochromic properties were examined with electrochemical and spectro-electrochemical methods. Cyclic voltammograms of the PA films cast onto an indium tin oxide coated glass substrate exhibited one oxidative redox couple around 1.08–1.16 V (oxidation onset potential) versus Ag/AgCl in an acetonitrile solution and revealed good stability of the electrochromic characteristics, with a color change from colorless to green at applied potentials ranging from 0 to 1.6 V.

Liou *et al.* [98] also prepared aromatic PAs (**PA-28**$_{a\text{-}c}$) with cardo fluorene moieties in the main chain (Figure 5.32). The introduction of the cardo fluorine moiety into the polymer backbone enhanced the solubility, film-formation capability, and the thermal stability (T_gs between 318 and 366°C; T_{d5}s in N_2 between 525 and 540°C). The polymer showed UV–vis absorption bands at 286–348 nm in

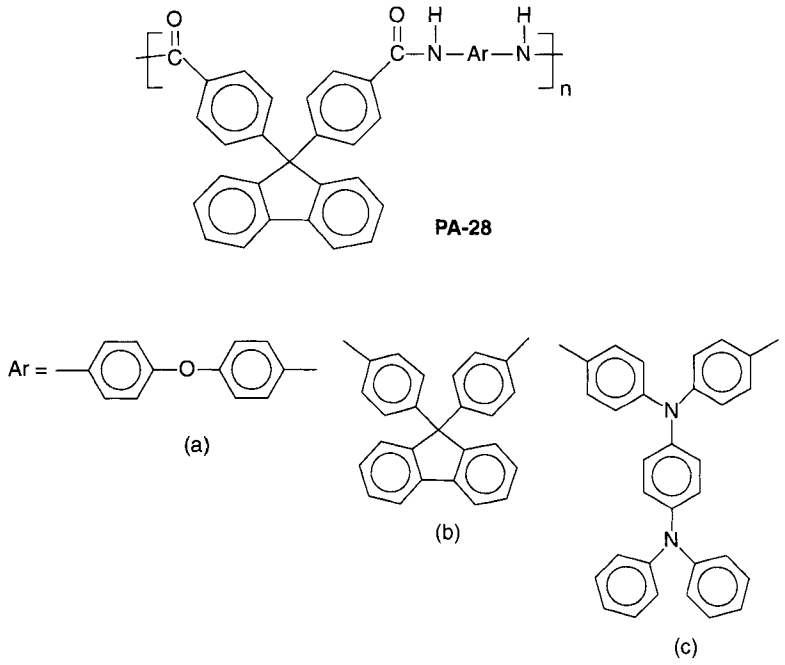

Figure 5.32 Chemical structures of the PAs (from [98]).

DMA solution and 295–345 in the solid (film) state, and their PL spectra exhibited maximum bands at 452–456 nm in the purple-to-green region in DMA solution, and 451–520 in the films. The films showed high optical transparency, with cut-off wavelengths in the range of 296–391 nm. Moreover, the **PA-28c** exhibited excellent electrochromic contrast and coloration efficiency, changing from the colorless neutral form to green, and then to dark blue upon oxidation (potentials from 0.00 to 1.35 V).

There has been further work on triarylamine-containing aromatic PAs (**PA-29**$_{a\text{-}e}$). Green-light-emitting polymers bearing anthrylamine chromophores, 9-[N,N-di(4-carboxyphenyl)amino] anthracene, were studied by Yen and Liou (Figure 5.33) [99]. The aromatic PAs were amorphous and had significantly high thermal stability due to the high softening temperatures (T_s) (290–300°C), a T_{d5}s up to 505°C, and char yields over 60% at 800°C in nitrogen. The polymers show good solubility, and **PA-29d and PA-29e** were even soluble in THF. All PAs exhibited high optical transparency as indicated by the UV–vis transmittance measurement with cut-off

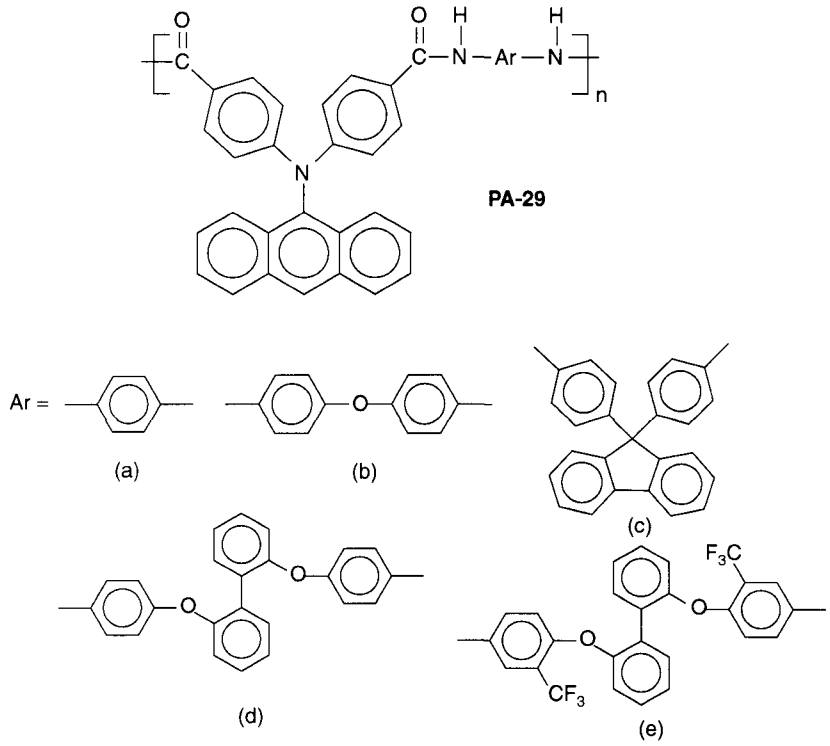

Figure 5.33 Chemical structures of the PAs (from [99]).

wavelengths between 423 and 433 nm, and exhibited a green emission maximum around 478–484 nm in the solid state. The PAs exhibited a high PL quantum yield in NMP solution (from 55% to 74%), and had one oxidation and reduction couple (E_{onset}) nearly 1.10 and −1.50 V versus Ag/AgCl in acetonitrile and DMF solutions, respectively.

The same research group reported [32] a new triphenylamine-based PA (**PA-4**). It showed maximum UV-vis absorption at 362 nm and exhibited fluorescence emission maxima at 493 nm in NMP solution with fluorescence quantum yield 4.4%. Cyclic voltammogram of PA-4 film cast onto an indium tin oxide coated glass substrate exhibited one oxidative redox couple at 0.72 V (oxidation onset potential) versus Ag/AgCl in acetonitrile solution and revealed good stability of the electrochromic characteristic with a color change from colorless to green at applied potentials ranging from 0.00 to 1.10 V.

San-José investigated fluorescent aromatic PAs with bulky dansyl, fluorine pendant, or fluorine moieties in the main chain [100]. The fluorescent signals of the dansyl or fluorine moieties are chemically associated with the main polymer chains through a urea group, a well-known supramolecular binding site. They also fluorescence yellowish-green or blue both in solution and solid state depending on the signaling unit. The PAs had high T_gs values upto 331°C, and low T_ds values around 300°C, due to the moderate thermal stability of the urea group.

5.10 Conclusion

Wholly aromatic PAs are unique materials in relating to their thermal and mechanical behavior. However, their extremely high transition temperatures and their poor solubility in common organic solvents give rise to processing difficulties and limit their applications. As a result, fundamental and applied research is being carried out to enhance their processability and solubility in order to broaden the technological scope of application associated with these materials. Many novel species have been prepared by polycondensation of diacids and diamines specially designed to overcome the traditional processing problems. Thus, fully aromatic PAs have been used in many novel applications.

5.11 References

1. Rules and Regulations Under the Textile Fiber Products Identification Act http://www.ftc.gov/os/statutes/textile/rr-textl. pdf), Part 303.7 (Generic names and definitions for manufactured fibers), US Federal Trade Commission (FCT) 2002.
2. C.P. Yang, and J.H. Lin, *Journal of Polymer Science Part A: Polymer Chemistry*, Vol. 31, p. 2153, 1993.
3. J.M. García, J.G. de la Campa, G. Schwarz, and J. de Abajo, *Macromolecular Chemistry and Physics*, Vol. 202, p. 1298, 2001.
4. H. Nasr-Isfahani, K. Faghihi, and N. Valikhani, *Journal of Applied Polymer Science*, Vol. 111, p. 1769, 2009.
5. J.J. Ferreiro, J.G. de la Campa, A.E. Lozano, J. de Abajo, and J. Preston, *Journal of Polymer Science Part A: Polymer Chemistry*, Vol. 45, p. 4671, 2007.
6. J.F. Espeso, E. Ferrero, J.G. de la Campa, A.E. Lozano, and J. de Abajo, *Journal of Polymer Science Part A: Polymer Chemistry*, Vol. 39, p. 475, 2001.
7. S.S. Vibhute, M.D. Joshi, P.P. Wadgaonkar, A.S. Patil, and N.N. Maldar, *Journal of Polymer Science Part A: Polymer Chemistry*, Vol. 35, p. 3227, 1997.

8. S.C. Wu, and C.F. Shu, *Journal of Polymer Science Part A: Polymer Chemistry*, Vol. 41, p. 1160, 2003.
9. M.K. Mukul, and P.K. Srivastava, *E-Journal of Chemistry*, Vol. 5, p. 257, 2008.
10. V. Kute, and S. Banerjee, J *Journal of Applied Polymer Science*, Vol. 103, p. 3025, 2007.
11. S. Maji, S.K. Sen, B. Dasgupta, S. Chatterjee, and S. Banerjee, *Polymers for Advanced Technologies*, Vol. 20, p. 384, 2009.
12. S. Banerjee, M.K. Madhra, A.K Salunke, and D.K. Jaiswal, *Polymer*, Vol. 44, p. 613, 2003.
13. S. Banerjee, M.K. Madhra, A.K. Salunke, and G. Maier, *Journal of Polymer Science Part A: Polymer Chemistry*, Vol. 40, p. 1016, 2002.
14. M.K. Madhra, A.K. Salunke, S. Banerjee, and S. Prabha, *Macromolecular Chemistry and Physics*, Vol. 203, p. 1238, 2002.
15. P.K. Gutch, S. Banerjee, and D.K. Jaiswal, *Journal of Applied Polymer Science*, Vol. 89, p. 691, 2003.
16. P.W. Morgan, *Macromolecules*, Vol. 10, p. 1381, 1977.
17. Y. Imai, and Y. Oishi, *Progress in Polymer Science*, Vol. 14, p. 173, 1989.
18. P.W. Morgan, "Condensation polymers by interfacial and solution methods", Interscience, New York, 1965.
19. J. Preston, Encyclopedia of Polymer Engineering. Vol 1. New York: Wiley-Interscience, p. 381, 1988.
20. J.M. García, J.C. Álvarez, J.G. de la Campa, and J. de Abajo, *Macromolecular Chemistry and Physics*, Vol. 198, p. 727, 1997.
21. C.P. Yang, R.S. Chen, and C.S. Wei, *European Polymer Journal*, Vol. 38, p. 1721, 2002.
22. N. Yamazaki, and F. Higasi, *Tetrahedron*, Vol. 30, p. 1323, 1974.
23. P. Carretero, R. Sandin, R. Mercier, A.E. Lozano, J.G. de la Campa, and J. de Abajo, *Australian Journal of Chemistry*, Vol. 62, p. 250, 2009.
24. S. Mallakpour, and M. Dinari, *Journal of Applied Polymer Science*, Vol. 112, p. 244, 2009.
25. K.P. Park, M.A. Kakimoto, and Y. Imai, *Journal of Polymer Science Part A: Polymer Chemistry*, Vol. 33, p. 1031, 1995.
26. J.M. García, F.C. García, F. Serna, and J.L. de la Peña, *Progress in Polymer Science*, Vol. 35, p. 623, 2010.
27. N.A. Mohamed, and M.M. Fahmy, *Journal of Applied Polymer Science*, Vol. 113, p. 767, 2009.
28. S. Zulfiqar, and M.I. Sarwar, *High Performance Polymers, Vol.* 21, p. 3, 2009.
29. D.J. Liaw, and B.Y. Liaw, *Polymer*, Vol. 42, p. 839, 2001.
30. J.F. Espeso, E. Ferrero, J.G. de la Campa, A.E. Lozano, and J. de Abajo, *Journal of Polymer Science Part A: Polymer Chemistry*, Vol. 39, p. 475, 2001.
31. J.F. Espeso, J.G. de la Campa, A.E. Lozano, and J. de Abajo, *Journal of Polymer Science Part A: Polymer Chemistry*, Vol. 38, p. 1014, 2000.
32. G.S. Liou, and K.H. Lin, *Journal of Polymer Science Part A: Polymer Chemistry*, Vol. 47, p. 1988, 2009.
33. G.S. Liou, and H.J. Yen, *Journal of Polymer Science Part A: Polymer Chemistry*, Vol. 44, p. 6094, 2006.
34. H.M. Wang, and S.H. Hsiao, *Journal of Polymer Science Part A: Polymer Chemistry*, Vol. 49, p. 337, 2011.

35. S. Mallakpour, and S. Sepehri, *Designed Monomers and Polymers*, Vol. 11, p. 535, 2008.
36. S. Mallakpour, and S. Sepehri, *Reactive and Functional Polymers*, Vol. 68, p. 1459, 2008.
37. S. Mallakpour, and M. Taghavi, *Journal of Applied Polymer Science*, Vol. 109, p. 3603, 2008.
38. S. Mallakpour, and M. Taghavi, *European Polymer Journal*, Vol. 44, p. 87, 2008.
39. S. Mallakpour, and M. Dinari, *Polymers for Advanced Technologies*, Vol. 19, p. 1334, 2008.
40. S. Mallakpour, and A. Zadehnazari, *Journal of Macromolecular Science Part A: Pure and Applied Chemistry*, Vol. 46, p. 783, 2009.
41. S. Mallakpour, and M. Taghavi, Polymer, Vol. 49, p. 3239, 2008.
42. S. Mallakpour, and M. Taghavi, *Reactive and Functional Polymers*, Vol. 69, p. 206, 2009.
43. S. Mallakpour, and Z. Rafiee, *Reactive and Functional Polymers*, Vol. 69, p. 252, 2009.
44. Z. Hu, S. Li, and C. Zhang, *Journal of Applied Polymer Science*, Vol. 106, p. 2494, 2007.
45. S.C. Wu, and C.F. Shu, *Journal of Polymer Science Part A: Polymer Chemistry*, Vol. 41, p. 1160, 2003.
46. A.D. Sagar, R.D. Shingte, P.P. Wadgaonkar, and M.M. Salunkhe, *European Polymer Journal*, Vol. 37, p. 1493, 2001.
47. M. Aggarwal, S. Maji, S.K. Sen, B. Dasgupta, S. Chatterjee, A. Ghosh and S. Banerjee, *Journal of Applied Polymer Science*, Vol. 112, p. 1226, 2009.
48. Q. Zhu, L. Dong, Y. Niu, C. Xiong, Y. Liu, J. Liu, L. Liu, and B. Shu, *Polymer Bulletin*, Vol. 61, p. 569, 2008.
49. S.R. Sheng, X.L. Pei, Z.Z. Huang, X.L. Liu, and C.S. Song, *European Polymer Journal*, Vol. 45, p. 230, 2009.
50. S.H. Hsiao, C.P. Yang, and S.C. Huang, *Journal of Polymer Science Part A: Polymer Chemistry*, Vol. 42, p. 2377, 2004.
51. C.P. Yang, and Y.Y. Su, *Macromolecular Chemistry and Physics*, Vol. 206, p. 1947, 2005.
52. S.H. Hsiao, and Y.H. Chang, *European Polymer Journal*, Vol. 40, p. 1749, 2004.
53. S. Maji, and S. Banerjee, *Journal of Applied Polymer Science*, Vol. 108, p. 1356, 2008.
54. S. Maji, and S. Banerjee, *Journal of Membrane Science*, Vol. 349, p. 145, 2010.
55. S. Maji, and S. Banerjee, *Journal of Membrane Science*, Vol. 360, p. 380, 2010.
56. D. Bera, B. Dasgupta, S. Chatterjee, S. Maji, and S. Banerjee, *Polymers for Advanced Technologies*, In Press (2010).
57. P.J. Flory, *Journal of American Chemical Society*, Vol. 74, p. 2718, 1952.
58. M. Jikei, S.H. Chon, M. Kakimoto, S. Kawauchi, T. Imase and J. Watanabe, *Macromolecules*, Vol. 32, p. 2061, 1999.
59. J.J. Hao, M. Jikei and M.A. Kakimoto, *Macromolecules*, Vol. 36, p. 3519, 2003.
60. H. Komber, B.I. Voit, O. Monticelli and S. Russo, *Macromolecules*, Vol. 34, p. 5487, 2001.
61. T.M. Miller, and T. X. Neenan, *Chemistry of Materials*, Vol. 2, p. 346, 1990.
62. M. Jikei, and M.A Kakimoto, *Journal of Polymer Science Part A: Polymer Chemistry*, Vol. 42, p. 1293, 2004.
63. J.B. Baek, and F.W. Harris, *Journal of Polymer Science Part A: Polymer Chemistry*, Vol. 41, p. 2374, 2003.

64. G.S. Liou, H.Y. Lin, and H.J. Yen, *Journal of Materials Chemistry*, Vol. 19, p. 7666, 2009.
65. S. Shabbir, S. Zulfiqar, Z. Ahmad, M. I. Sarwar, *Tetrahedron*, Vol. 66, p. 1389, 2010.
66. Y. Ishida, A.C.F. Sun, M. Jikei, and M. Kakimoto, *Macromolecules*, Vol. 33, p. 2832, 2000.
67. I. In, and S.Y. Kim, *Macromolecular Chemistry and Physics*, Vol. 206. p. 1862, 2005.
68. X. Li, J. Zhan, Y. Lin, Y. Li, and Y. Li, *Macromolecules*, Vol. 38, p. 8235, 2005.
69. M. Jikei, K. Fujii, G. Yang, and M. Kakimoto, *Macromolecules*, Vol. 33, p. 6228, 2000.
70. Y.T. Chang, and C.F. Shu, *Macromolecules*, Vol. 36, p. 661. 2003.
71. M. Jikei, and M. Kakimoto, *High Performance Polymers*, Vol. 13, p. S33. 2001.
72. S. Shabbir, S. Zulfiqar, Z. Ahmad, M. I. Sarwar, *Tetrahedron*, Vol. 66, p. 7204, 2010.
73. Y. Yu, M. Z. Rong, and M.Q. Zhang, *Polymer*, Vol. 51, p. 492, 2010.
74. T. Ohishi, T. Masukawa, S. Fujii, A. Yokoyama, and T. Yokozawa, Macromolecules, Vol. 43. p. 3206, 2010.
75. M.T. López, P. Estévez, N.S. José, A.G. Valdemoro, F.C. García, F. Serna, J.L. de la Peña, and J.M. García, *Recent Patents on Materials Science*, Vol. 2, p. 190, 2009.
76. W.H. Chan, C.F. Ng, S.Y.L. Leung, X. He, and O.C. Cheung, *Journal of Applied Polymer Science*, Vol. 65, p. 1113, 1997.
77. Y.C. Wang, C.L. Li, J. Huang, C. Lin, K.R. Lee, D.J. Liaw, and J.Y. Lai, *Journal of Membrane Science*, Vol. 185, p. 193, 2001.
78. S.J. Lue, and S.H. Peng, *Journal of Membrane Science*, Vol. 222, p. 203, 2003.
79. C. Carrera-Figueiras, and M. Aguilar-Vega, *Journal of Polymer Science Part B: Polymer Physics*, Vol. 45, p. 2083, 2007.
80. C. Carrera-Figueiras, and M. Aguilar-Vega, *Journal of Polymer Science Part B: Polymer Physics*, Vol. 43, p. 2625, 2005.
81. Y. Ding, and B. Bikson, *Polymer*, Vol. 43, p. 4709, 2002.
82. O.M. Ekiner, and J.W. Simmons, *US20087393389*, 2008.
83. J. Kucera, *Chemical Engineering Progress*, 54–61, 1997.
84. S. Konagaya, H. Kuzumoto, and O. Watanabe, *Journal of Applied Polymer Science*, Vol. 75, p. 1357, 2000.
85. N.A. Mohamed, and A.O.H. Al-Dossary, *European Polymer Journal*, Vol. 39, p. 1653, 2003.
86. P.R. Buch, D. Jagan Mohan, and A.V.R. Reddy, *Journal of Membrane Science*, Vol. 309, p. 36, 2008.
87. A. Taeger, C. Vogel, D. Lehmann, D. Jehnichen, H. Komber, J. Meier-Haack, N.A. Ochoab, S.P. Nunesc, and K.V. Peinemannc, *Reactive and Functional Polymers*, Vol. 57, p. 77, 2003.
88. T.S., Jo, C.H. Ozawa, B.R. Eagar, L.V. Brownell, D. Han, and C. Bae, *Journal of Polymer Science Part A: Polymer Chemistry*, Vol. 47, p. 485, 2009.
89. S. Itsuno, *Progress in Polymer Science*, Vol. 30, p. 540, 2005.
90. S. Mallakpour, and E. Kowsari, *Polymer Engineering & Science*, Vol. 46, p. 558, 2006.
91. S.E. Mallakpour, A.R. Hajipour, and S. Habibi, *Polymer International*, Vol. 50, p. 331, 2001.
92. P. Estévez, H. El-Kaoutit, F.C. García, F. Serna, J.L. de la Peña, and J.M. García, *Journal of Polymer Science Part A: Polymer Chemistry*, Vol. 48, p. 3823, 2010.

93. D.Y. Kim, H.N. Cho, and C.Y. Ki, *Progress in Polymer Science,* Vol. 25, p. 1089, 2000.
94. L. Akcelrud, *Progress in Polymer Science,* Vol. 28, p. 875, 2003.
95. C.W. Chang, and G.S. Liou, *Journal of Material Chemistry,* Vol. 18, p. 5638, 2008.
96. S.H. Hsiao, G.S. Liou, Y.C. Kung, and Y.M. Chang, *Journal of Polymer Science Part A: Polymer Chemistry,* Vol. 48, p. 2798, 2010.
97. M. Nechifor, *Reactive and Functional Polymers,* Vol. 69, p. 27, 2009.
98. G.S. Liou, H.J. Yen, Y.T. Su, and H.Y. Lin, *Journal of Polymer Science Part A: Polymer Chemistry,* Vol. 45, p. 4352, 2007.
99. H.J. Yen, and G.S. Liou, *Journal of Polymer Science Part A: Polymer Chemistry,* Vol. 46, p. 7354, 2008.
100. N. San-José, A. Gómez-Valdemoro, P. Estevez, F.C. García, F. Serna, and J.M. García, *European Polymer Journal,* Vol. 44, p. 3578, 2008.

6

Phosphorus-Containing Polysulfones

Oana Petreus[1] and Tudor Petreus[2]

[1] *"Petru Poni" Institute of Macromolecular Chemistry, 4 Iasi, Romania*
[2] *"Gr. T. Popa" University of Medicine and Pharmacy Iasi (Faculty of Molecular Biology), Iasi, Romania*

Abstract

Aromatic polysulfones are a family of amorphous, thermoplastic polymers with phenylene, sulfone (-SO_2-), ether (-O-), and in some cases, other groups in the chain, that possess remarkable thermal and chemical stability, excellent strength and flexibility, transparency, as well as high glass transition temperature and good film forming properties. In addition they are mainly important as high-quality semipermeable membranes, as an alternative to cellulosic ones in separation processes, due to the high resistance in extreme pH conditions. Furthermore, polysulfones are soluble in chloroform and dimethylformamide, and membranes can easily prepared by conventional phase inversion technique. Its porosity allows it to be used in micro-ultrafiltration and reverse osmosis processes as well as in the development of composite membranes to facilitate transport.

Keywords: Polysulfones, polysulfonylation, electrophilic aromatic substitution, post-polymerization, chemical modification

6.1 Introduction

Aromatic polysulfones are a family of amorphous, thermoplastic polymers with phenylene, sulfone (-SO_2-), ether (-O-), and in some cases, other groups in the chain, that possess remarkable thermal and chemical stability, excellent strength and flexibility, transparency, as well as high glass transition temperature and good film forming properties. In addition they are mainly important as high-quality semipermeable membranes, as an alternative to cellulosic

Vikas Mittal (ed.) High Performance Polymers and Engineering Plastics, (167–204)
© Scrivener Publishing LLC

ones in separation processes, due to the high resistance in extreme pH conditions. Furthermore, polysulfones are soluble in chloroform and dimethylformamide, and membranes can easily prepared by conventional phase inversion technique. Its porosity allows it to be used in micro-ultrafiltration and reverse osmosis processes as well as in the development of composite membranes to facilitate transport. Since 1965, they were continuous commercialized through different name, but three basic types could be selected in connection with their chemical structure (Table 6.1).

Despite these enumerate benefits, however, polysulfones have also some disadvantages in practical uses, such as their rather hydrophobic nature, the non-resistance to low polar organic solvents or to UV radiations. For this reason, there is a high interest in the chemical modification of polysulfones, which alter their chemical nature to some degree, but do not scarify their excellent physical, chemical and mechanical properties.

The synthesis of polysulfones (PSF) can be performed by two main routes: a polysulfonylation process, which is a classical electrophilic aromatic substitution [1], or a polyether synthesis, which is a nucleophilic substitution of activated aromatic dihalides [2, 3].

One of main routes to achieve new characteristics of polysulfones is polymer modification. There are two ways to functionalize PSFs. The first way is post-polymerization modification, in which the polymer is functionalized after polymerization. PSF can be chemically modified by both electrophilic and nucleophilic reactions to yield new polymers with specific properties. Electrophilic reactions (for example sulfonation, chloromethylation followed by aminolysis) take place in the electron-rich bisphenol A part of PSFs [4–9], whereas nucleophilic reactions (in example lithiation with Li-organic compounds followed by reaction with aldehydes, ketones or carboxylic acid esters) can be performed in the electron-deficient diarylsulfone [10–17].

The second way involves direct copolymerization of functionalized monomers. Modification of monomers is a fundamentally different approach from modification of polymer in that modification of monomer makes feasible control of the molecular structures. Both diphenols and dihalide aryl sulfones can be modified to incorporate functional groups or new counterparts.

Using bisphenols with pendant carboxylic group as comonomer, some polysulfones with pendant carboxylic groups were successfully synthesized [18–22]. The functional groups can be used for

Table 6.1 Commercial aromatic polysulfones.

Chemical structure	Trade name	Abbreviation	Year for starting production	Producer
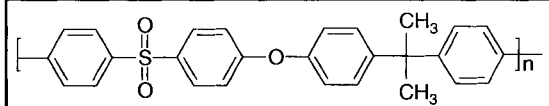	Udel	PSF	1965	Union Carbide
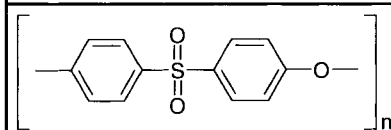	Victrex	PES	1972	Corp. ICI America Inc.
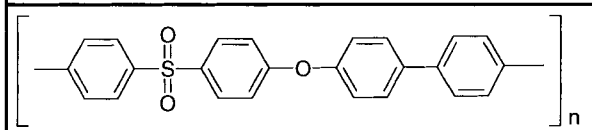	Radel Radel R	PPSF	1976 1990	Union Carbide Corp. Amoco Corp.

the preparation of graft copolymers. If the monomer contains copper (II), it would be also used to synthesize the electrically conductive polysulfone [23]. These polysulfones with reactive functional groups can be used also to prepare polymer networks by thermal curing.

The diaryl sulfone monomers could be nitrated and then reduced to amine functionalized monomers [24–26], or sulfonated, afterwards used to copolymerize with different bisphenols [27, 28].

An increasing topic of interest concerns cooperation of PSFs with epoxy resins via end group functionalization or blending. Engineering thermoplastics based on PSF have been widely used to overcome the problems associated with the brittleness or flame resistance of epoxy resins [29–33].

The functionality of the end groups itself is important. When such groups are bifunctional (e.g. vinyl groups) they can participate in polymerization reactions, yielding graft copolymers or networks; such telechelic polymers are called macromolecular monomers, macromonomers [34, 35].

Introducing phosphorus-containing groups into the structure of polysulfone (either into backbone or main chain) the new modified polymers display high thermal stability with inherent flame retardant quality and could also be used as high temperature matrix resins and toughness modifiers in curable high performance epoxy resins.

Polyethersulfone has been widely used in production of high quality membrane in protein separation and purification. However, in many cases, the nonspecific protein adsorption on the membrane surface and in the membrane pores due to the inherent hydrophobic characteristics of PES, often causes serious membrane fouling and thus rapid decline of permeation flux. This exerts severe limitation for industrial applications. Many investigations have revealed that increasing membrane surface hydrophilicity could effectively reduce membrane fouling therefore, incorporation of hydrophilic polymer through blending, coating and surface grafting has been subsequently developed to improve the protein adsorption-resistance and permeation property of PES membrane. Among many hydrophilic polymers, those containing phosphorylcholine (PC) groups have been proved to be extremely effective in reducing protein adsorption [36].

6.2 Synthesis of Phosphorus Containing Polysulfones

6.2.1 Functionalization of Preformed Polysulfones

Polysulfones can be chemically modified by both electrophilic and nucleophilic reactions to yield polymers with specific properties. Electrophilic reactions take place in the electron-rich bisphenol part of PSFs, whereas nucleophilic reactions can be performed in the electron-deficient diarylsulfone part of polysulfones. For example, sulfonation with chlorosulfonic acid or the SO_3/triethylphosphate complex leads to sulfonated PSF, which can be used as a cation-exchange membrane [37, 38] and chloromethylation, followed by aminolysis with tertiary amines, leads to anion-exchange polymers [9]. To obtain phosphorus containing polysulfones, one of the attractive strategy is to phosphonate the existing polysulfones. When polysulfone consists of alternating bisphenol A and biphenyl sulfone segments, the strong electron-withdrawing effect of the sulfone units gives a slight acidic character to the ortho-to-sulfone aromatic hydrogens.

6.2.1.1 Functionalization of Sulfone Moiety

Polysulfone possesses aryl sulfone groups in the structure which is strongly activate towards ***ortho-lithiation***, making this polymer a particularly suitable substrate. The carbons at ortho-to-sulfone positions may be metalized by the use of a strong base such as *n*-BuLi [12] (Scheme 6.1). Lithiated polysulfone could be reacted with various electrophiles in convenient one- or two-step reactions, without rise to chain scission or any other degradation of the polysulfone main chain In an example, the more acidic difluoromethylenephosphonic acid units cold be grafted onto PDF main chains, using lithiated polysulfone and methyl 2-iodobenzoate followed by the reaction with diethyl (bromo difluoromethyl)phosphonate. So, an increase in the acidity and a separation of the acidic moiety from the polymer main chain by benzoyl spacers were realized [39] (Scheme 6.1 way A). Phosphonated PSFs with the acid units attached directly to the polymer main chain have been prepared by lithiation and subsequent reactions with chlorophosphonic acid esters without the use of a catalyst [40] The reaction parameters

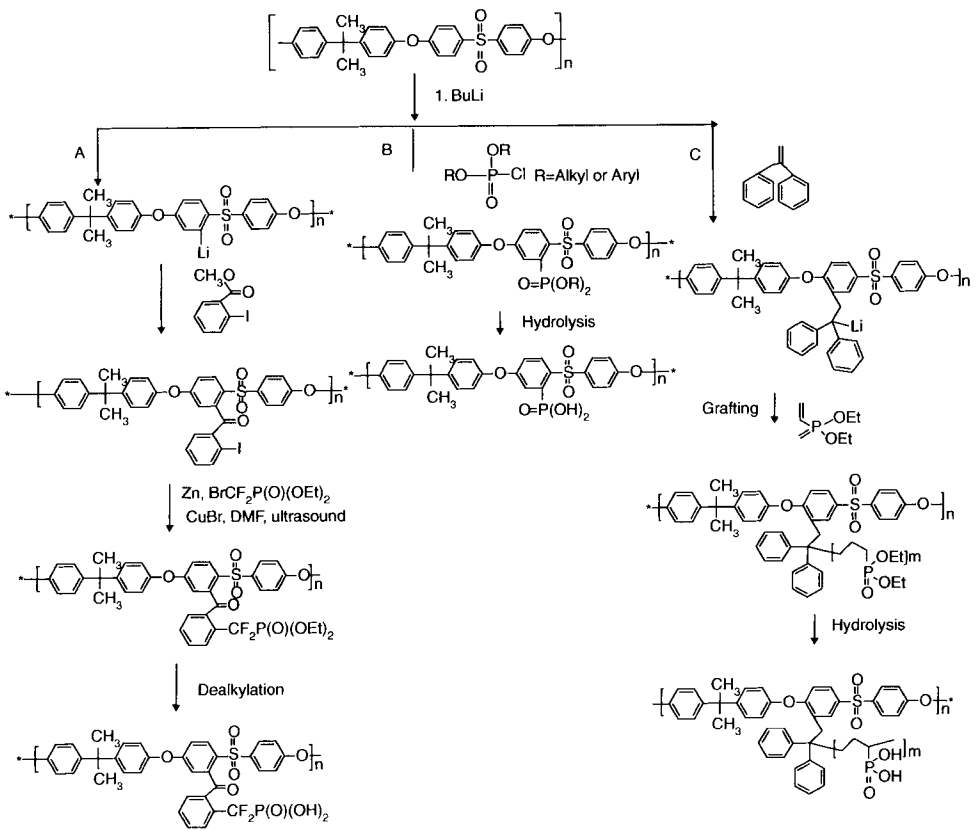

Schema 6.1 Functionalization by lithiation of sulfone moiety and subsequent reactions with different phosphorus containing electrophiles.

(including the reactivity of the nucleophile, the nature of the electrophile and solvent, the relative amounts of each reactant, the reaction temperature and time), were carefully selected to avoid cross linking reactions (Scheme 6.1 way B). A well-defined copolymer grafted with polyvinylphosphonic acid was prepared by anionic polymerization of diethylvinylphosphonate from polysulfone macroinitiators, followed by hydrolysis of the ester groups of the units of diethylvinylphosphonate. In the first step, diphenylethylene was added to the lithiated sites to form the initiating 1, 1-diphenylalkyl anion, that is capable of initiating polymerization of diethylvinylphosphonate. Hydrolysis of the ester groups produced soluble graft copolymers with different contents of poly (vinylphosphonic) acid (Scheme 6.1 way C) [41].

6.2.1.2 *Functionalization of the Bisphenol A Moiety*

The electron-donating effect of the ether linkages of the main chain activates the phenylene rings of the bisphenol A part toward nucleophilic attack, and they may thus be used as positions for halogenation, such as ***bromination*** [14]. Brominated sites located ortho to the ether linkages can be selectively metalized in a second reaction step because the halogen–lithium exchange is favored over the proton–lithium exchange at low temperatures. The subsequent reaction with an electrophil does not produce scission or any other degradation of polysulfone main chain (Scheme 6.2).

An efficient synthetic procedure for the phosphonation of polyphenylsulfone involved also the brominating in excess (Scheme 6.2, way A) of the polymer and the subsequent bromine-phosphorus exchange by means of a $PdCl_2$ catalyst (alone or with dibenzylidenacetone as ligands) and subsequent P–C coupling reaction [42]. In the resulting product, the phosphonate ester pendant groups were attached to aromatic rings of the polymer chain without alkylene spacer units. A substitution degree of almost one phosphonate moiety per repeating unit of the polymer was achieved. Polymers with free phosphonic acid groups were prepared by ester hydrolysis. Using a monobrominated polysulfone and the subsequent reaction with tris(trimethylsilyl)phosphate on $Ni\ Cl_2$ catalyst, a soluble, halogen-free and highly functionalized polyelectrolyte could be obtained [43]. The silylated phosphonates are readily cleaved in the presence of methanol, which simultaneously removes the residual catalyst residues (Scheme 6.2, way B).

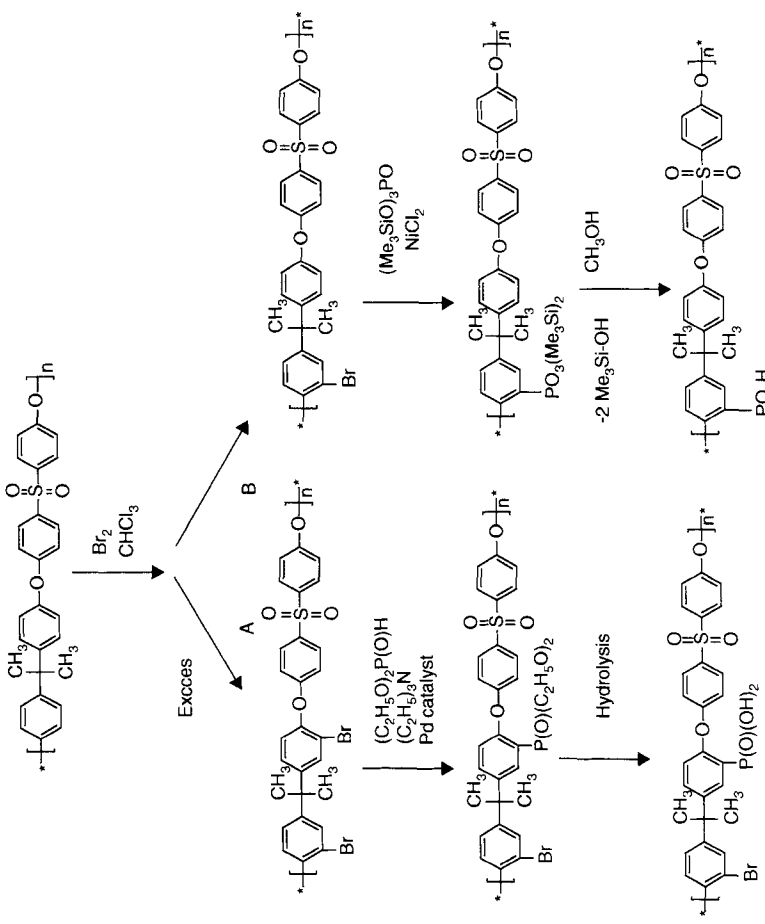

Schema 6.2 Functionalization by bromination of bisphenol A moiety of polysulfone and subsequent reactions with phosphorus compounds.

Another modification of bisphenol A part of polysulfone structural unit is the ***chloromethylation*** reaction. The reactive chloromethyl group can be readily modified by a reaction with various nucleophilic reactants. The reaction with an aliphatic phosphine (triethylphosphite in the presence of diethylcarbitol) leads to phosphonate ester groups, which can be hydrolyzed in aqueous acid to phosphonic acid pendant groups [44]. If the aliphatic phosphine is replaced with an aromatic one (triphenyl-phosphine or it derivative), the quaternary phosphonium polysulfone would also obtained [45, 46]. Using an aromatic bulky reactant with P-H reactive group (9, 10-dihydro-oxa-10-phosphophenanthrene-10-oxide) (DOPO), another type of phosphorus modified polysulfone could be obtained [47]. The substitution of chlorine with the bulky cyclic phosphorus compound was carried out at elevated temperature, using a large excess of phosphorus reactant. The reactive P-H group interacts with CH_2Cl group of chloromethylated polysulfone. The occurrence of HCl evolved from the reaction proved the substitution and could also offer kinetic data about the process (Scheme 6.3).

6.2.2 Polycondensation of Phosphorus Containing Diols with Dihalogen Substituted Aromatic Sulfones

New phosphorus containing polysulfones could be obtained by using different phosphorus containing diols in the classical synthesis of PSF (Scheme 6.4). Diols can contain phosphorus in main chain position or incorporate in a phenanthrene-type ring as side chain. These different phosphorus-containing diols form aromatic polyethers by polycondensation with dihalogen-substituted aromatic sulfones [48]. The chain structure of the polymer (aromatic or aliphatic) and the position of phosphorus in the chain influence the polymer properties (electroluminescence [49, 50], flame retardancy [51], liquid crystal properties [52]).

Another approach in the synthesis of phosphorus containing polysulfones is the reaction between bisphenol S and a halogenated phosphorus containing derivative (Scheme 6.5). When spirocyclic pentaerythritol di-(phosphate monochloride) was used as monomer [53], triethyl amine was added to cap the resulted HCl. The obtained copolymer blended with an epoxy resin increased

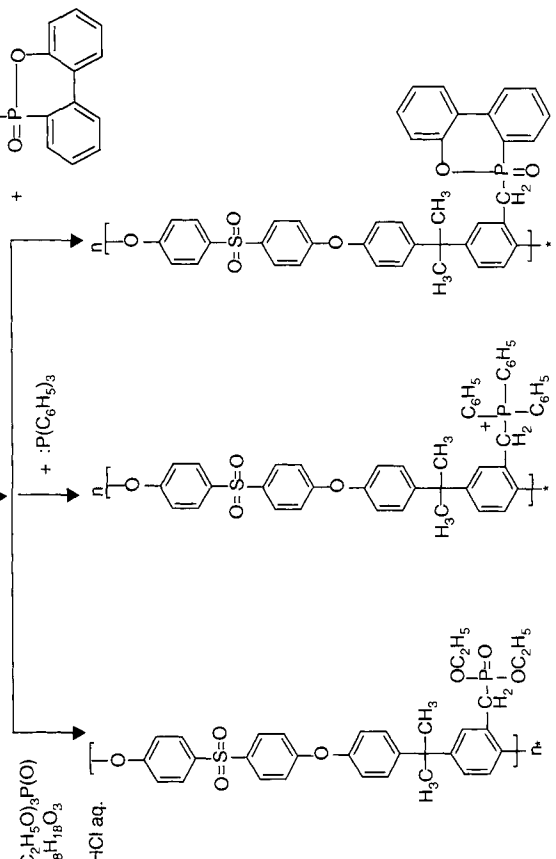

Schema 6.3 Reaction between chloromethylated polysulfone and different phosphorus compounds.

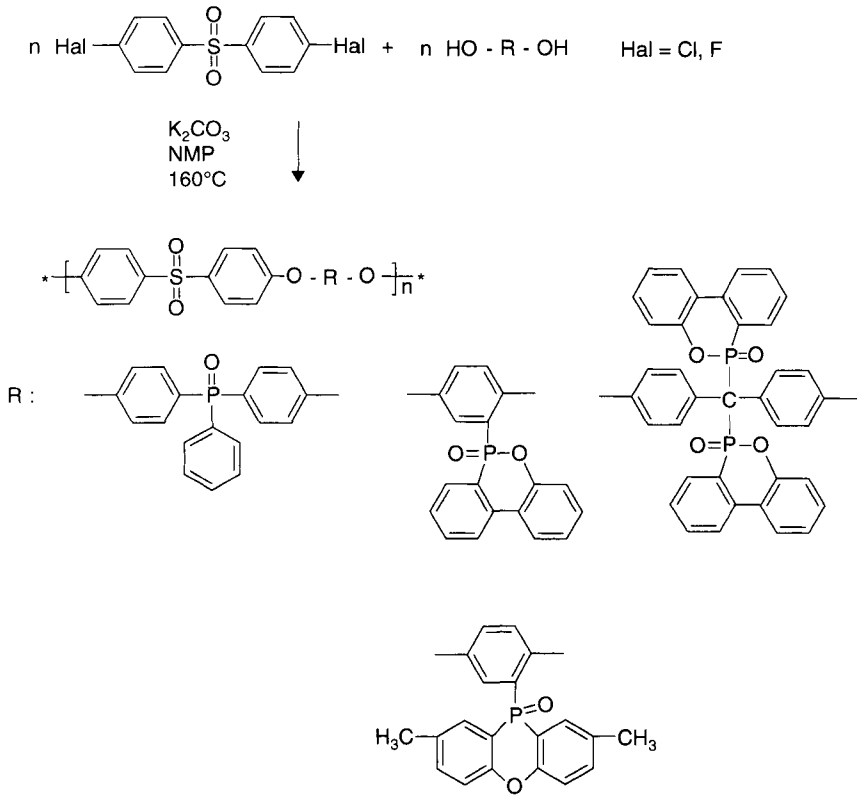

Schema 6.4 Polycondensation of substituted dihalogen aromatic sulfones with phosphorus containing diols.

it thermal and fire resistance. Bis[4-(4-fluorobenzoyl)phenyl] phenylphosphine oxide was obtained and reacted with bisphenol S via nucleophilic substitution reaction to synthesize a soluble phosphorus-containing poly(ether ketone). The tetrahedral geometry of the phosphine oxide group may have disrupted the crystal packing, reducing intermolecular interactions and enhancing the solubility of the semicrystalline, insoluble commercial poly(ether sulfone) –Victrex [54]. The incorporation of phenylphosphine oxide moieties also could increase the adhesion, resistance to atomic oxygen, and flame resistance of the parent polymer. The attachment of phenyl pendent groups may have increased the glass-transition temperature by restricting segment mobility.

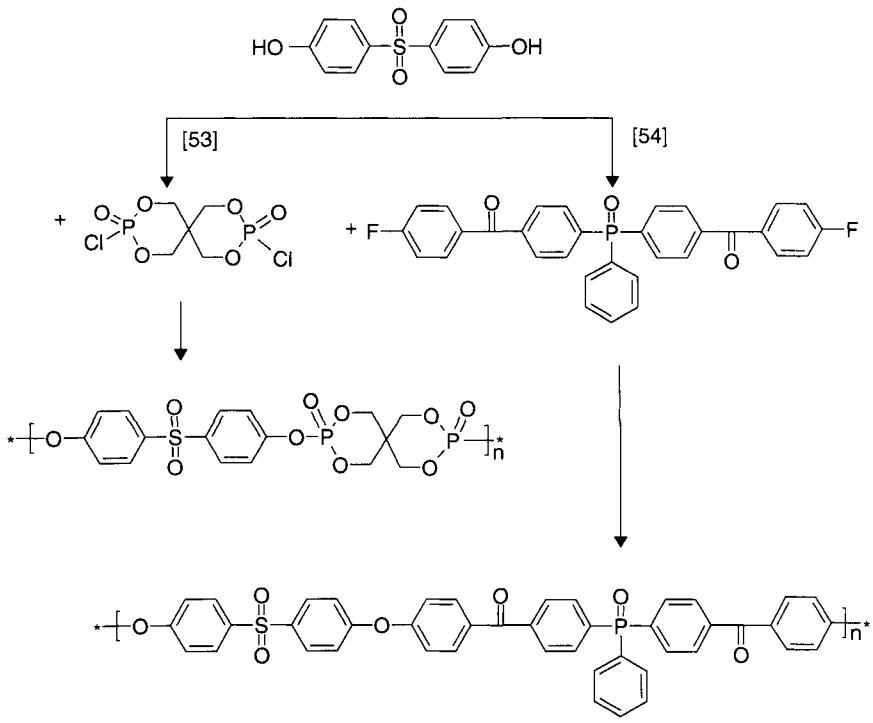

Schema 6.5 Synthesis of phosphorus containing polysulfones from bisphenol S and halogenated phosphorus derivatives.

6.3 Properties of Phosphorus-Containing Polysulfones (P-PSF)

6.3.1 Spectral Features

FTIR and NMR (^{1}H, ^{13}C and ^{31}P) spectra give informations concerning the structure of phosphorus-containing polysulfones, the substitution degree of sulfone or bisphenol moiety with a phosphorus compound and the position of substituted groups.

The FTIR spectra of phosphorus-containing polysulfones usually show the following absorption bands:

1. The phosphoryl linkage stretching is found to absorb at 1320–1200 cm^{-1}. However, the considerable overlap between absorptions bands originating from the

asymmetric stretches of the SO_2 and phenyl ether linkages at 1292–1326 and 1238 cm^{-1}, respectively, did not allow a clear identification.

2. P-O-Alkyl and P-O-Aryl group absorbs at 1030–1050 and 1190–1240 cm^{-1} respectively. In a particular case of phosphorus bulky group substitute, the P-CH_2 group presents a strong absorption at 910cm^{-1}

^1H NMR spectroscopy and elemental analysis were applied for the determination of the degree of phosphonation (DS) [42]. In the case of ^1H NMR spectroscopy, the DS was calculated from the signal ratio of the ethyl ester protons and the aromatic protons. In the case of elemental analysis, the DS could be calculated also from the P/S ratio. A comparison of the obtained DS values from this two methods shows that data are always in good agreement with each other. When chloromethylated PSF was modified with aliphatic phosphite [46], the degree of phosphonation could be calculated from area for two protons of C***H***$_2$-P– at $\delta = 3.0$–3.1 ppm, those for six protons of (CH_3CH_2O)$_2$– at 1.25 ppm and for four protons of (CH_3CH_2O)$_2$– at 4.0 ppm versus the area for six protons of the two methyl groups of diol.

Both the ^1H and ^{13}C NMR spectra alone are too complex for a detailed structure analysis of bulky aromatic phosphorus substitute of PSF [47] because of the large number of different aromatic protons and carbons. ^1H-^{13}C #MQCgs-QNP-34 NMR and the ^{31}P NMR resolved these problems. The characteristic peaks associated to protons of -CH_2Cl group situated at 4.64 ppm in chloromethylated PSF spectrum disappeared and the characteristic peak associated to protons of -CH_2-P-bulky group was moved at 3.5 ppm. Aromatic domain in ^1H-^{13}C-NMR spectra is quite different for chloromethylated and phosphorylated PSF caused by the additional number of protons and carbon atoms provided by phosphorus group structure.

The ^{31}P NMR spectra of the phosphorous-containing PSF with DS between 0.62 and 0.74 indicated the existence of one phosphorous bulky group attached to the diol. When the substitution degree increased, the signal for the single peak at 33.17 ppm slightly moved to 33.20 ppm. Two peaks were observed to a higher substitution degree, one at 33.27 and the second at 31.92, probably related to the incomplete substitution of the two chloromethylated groups in diol ring.

6.3.2 Solubility

Phosphorus-modified polysulfones with side bulky groups were soluble in polar-aprotic solvents (N-methyl-2-pyrrolidone, dimethylacetamide, dimethylformamide), but also in some non-polar solvents as chloroform and 1, 4 dioxane [48]. The solubility increases only in a certain extent with the substitution degree. In the graft copolymers with poly(vinyl phosphoric)acid [41], the well-separated poly(phosphoric) acid side chains along stiff and hydrophobic PSF main chains could produced membranes with interesting water uptake. The solubility of polyethersulfone with a bis(4-carboxyphenyl)phenyl phosphine oxide in main chain [54] were readily soluble at room temperature in polar, aprotic solvents, such as N-methyl-2-pyrrolidone, dimethylacetamide, dimethylformamide, and dimethyl sulfoxide. They were also soluble in chloroalkylenes and in tetrahydrofuran at elevated temperatures. The good solubility can be attributed to the phosphine oxide moiety, which reduced the regularity of the main chain and led to the amorphous nature of the polymers. The excellent solubility makes the polymers potential candidates for practical applications in casting processes.

6.3.3 Thermal Stability

In many cases, between the thermal stability and flammability there are some connections. The great majority of organic polymers are flammable, therefore research and development of polymers with reduced flammability is an area of continuing scientific interest. Flame retardant properties of such organic polymers can be achieved by introducing "flame retardant" groups. Among these, phosphorus containing groups, either pendant (as substituent on the polymer backbone) or built-in into the backbone, are of high interest with respect to halogen-free flame retardance. Just as for organophosphorus flame retardant additives, the flame retardant action of these groups may be expected in the gas phase due to flame inhibition of the fuel, and/or in the condensed phase due to involving of the macromolecules in charring processes. The flame inhibition increases with decreasing the oxidation state of phosphorus, which plays a significant role for the fire performance of materials [55]. The thermal decomposition behavior of phosphorus containing polymers and analysis of pyrolysis products give information on the possibilities of their flame inhibition.

6.3.3.1 *Thermal Gravimetric Aspects*

It is well known that polysulfone gives outstanding polymer membranes with a high glass transition temperature (195°C), good thermal and oxidative stability (decomposition range between 400 and 550°C regardless of environment (under air, argon or vacuum) [56]. The chemical modification of polysulfones with phosphorus compound incites a great interest with respect to their thermal behavior, especially in connection to the flame retardant properties. The decrease or increase of thermal stability of phosphorus-containing polysulfones could be correlated with the position of phosphorus group in PSF structure. Table 6.2 resumes some examples.

The TG data show that phosphorus containing groups incorporated into polysulfones structure generally decreases their thermal stability. Some particularities were remarked. The thermal decomposition for polymers containing phosphonic acid exhibited a first weight loss in most cases being interpreted as a loss of water molecules in connection with the formation of P-O-P bonds. In addition, the cleavage of the C-P bond has been reported to occur at temperatures above 320–350°C for most studied systems. However, in the case of structure 4, the first weight loss started at T decomposition = 230°C. It has previously been reported that alkyl-P bonds are usually weakened by the presence of electron-withdrawing units, whereas aryl-P bonds are weakened by electron-donating units [57]. This might explain the lower thermal stability of the phosphonic acid unit in this case because of the strong electron-withdrawing character of the CF_2 group. In line with this observation, Miyatake K. *et al.* [58] reported the loss of phosphonic acid units at 260°C in phosphonated poly(arylene ether)s, for which the phosphonic acid units were located on electron-rich aromatic rings.

The copolymer with poly(phosphonic) acid in the ester form (structure 5) showed a first degradation step between 250 and 350°C. The magnitude of the step was directly correlated with the phosphonate ester content. This degradation was ascribed to the decomposition of the ester units to form ethylene and phosphonic acid units, possibly followed by a subsequent formation and loss of water, by self-condensation at these high temperatures. A second degradation step was noted between 350 and 400°C, most probably connected with the cleavage of the C-P bond. The copolymers in the acid form showed a small initial weight loss already from 150°C, ascribed to reversible self-condensation and desorption of

Table 6.2 Thermal stability of some phosphorus-containing polysulfones.

Nr	Structure	T_{onset}	T_{peak}	Char residue at 650°C In inert atmosphere	References
1	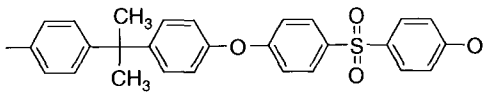	442	529	44	[56]
2	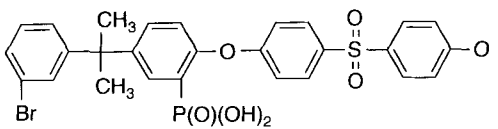	250	350	25	[42]
3	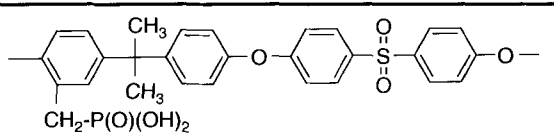	100–300	400	18–20	[46]
4	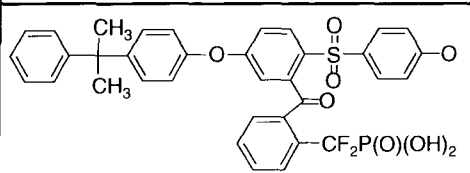	230	270	47	[39]

5		250–320	350–400	30	[41]
6			557	38	[55]
7			470	38	[55]

(Continued)

Table 6.2 Thermal stability of some phosphorus-containing polysulfones. (Continued)

Nr	Structure	T_{onset}	T_{peak}	Char residue at 650°C In inert atmosphere	References
8	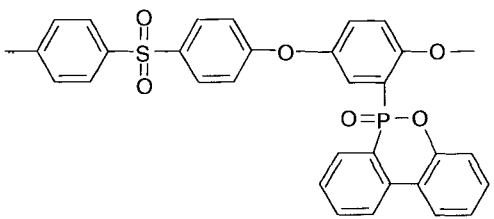		455	45	[48]
9	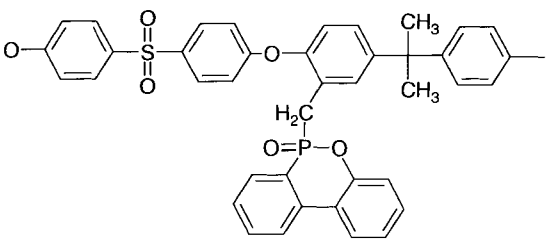	431–466	321–511	38–45.94 function of DS	[47]

water. A large degradation step at 340°C was connected with the cleavage of C-P bonds, and then polymer backbone degradation occurred at higher temperatures [41].

By means of TG experiments and evolved gas analysis it was demonstrated that polysulfones containing phosphorus in the main chain or as pendant group decompose in different ways [55]. Phosphorus-oxygen bonds in the polymer backbone (structure 7) showed a lower thermal stability than phosphorus-carbon bonds (structure 6). The sulfone group does not control the decomposition temperature. The incorporation of biphenylene-phosphinate as side groups of the polymer backbone (structure 8 and structure 9) triggered the decomposition of the polymer chain at lower temperatures than for the non-phosphorous PSF. Although in structure 7, parts of the phosphorus is vaporized, in structure 6, 8 and 9, phosphorus mainly remained in the residue. The altered bond nature between phosphorus and adjacent atoms (oxygen and carbon) provoked different thermal stability and consequently changed the degradation mechanism. All P-PSfs were char-forming [59].

6.3.3.2 Glass Transition and Mechanical Properties

It was observed that incorporation of phosphorus pendant bulky group slight decreased the thermal stability of PSF, but increased the glass transition T_g. This increase is higher for a higher substituted PSFs. Phosphorus-modified polysulfone exhibited also a good solubility and a higher Tg, indicated that the bulky cyclic group produced a decrease in interchain attraction existing in starting PSF. This group imparts also a skeleton rigidity. The dynamic storage modulus (E′) and tension loss tangent (tan δ) versus temperature for PSF and P-PSF in the range of temperature between 150 and 220°C illustrated the superior mechanical properties of phosphorus modified PSFs (Figure 6.1). The magnitude of tan δ at Tg is a measure of the energy-damping characteristic of a material and is related with the impact strength of the material [47]. The impact strength increases with the addition of tan δ value at Tg. Value of tan δ at Tg for PSF was 2.83 and that of phosphorus modified one is 12.84, respectively. This results that the energy-damping characteristics and mechanical properties were superior for P-PSF. It is well known that glass transition temperature is associated with crank-shafting movement of the main chain, whereas the secondary transitions are associated with the movements of side groups.

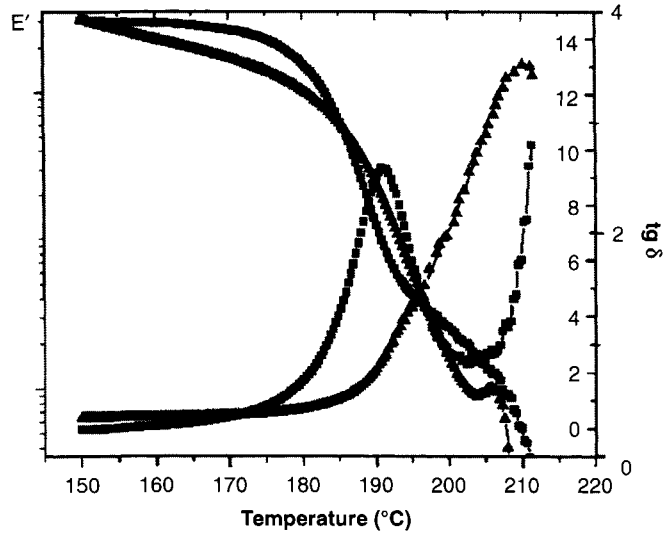

Figure 6.1 Dynamic storage modulus (E') and tension loss tangent (tan δ) versus temperature for PSF (-■-) and P-PSF (-▲-) in the range of temperature between 150–220°C.

The appearance of glass transition at higher temperature for P-PSF in comparison with PSF was assigned to chains of reduced mobility. Another observation was relied to the increase of β transition temperature which could indicate that a higher energy barrier exists for molecular motions, caused by bulky structure of phosphorus containing side chain.

6.3.3.3 *Differences Between Thermal and Thermo-Oxidative Degradation of Phosphorus Containing Polysulfones*

The thermal degradation in nitrogen was quite different from the usual thermo-oxidative behavior of polysulfones and phosphorus-containing polysulfones [60]. Chemical modifications of PSFs with bulky phosphorous compound essentially changed their thermal behavior. The thermal stability was not so different in nitrogen and air atmospheres up to 410°C, although in nitrogen, a slight decrease was observed when the substitution degree increased (Table 6.3). The thermal degradation of P-PSFs with substitution degree between 0.64 and 0.72 in nitrogen occurred in one degradation step; only P-PSP with DS=1.72 exhibited two steps.

Table 6.3 Thermal and thermo-oxidative characteristics of phosphorus modified polysulfones.

Sample	Stage of thermal degradation	Nitrogen atmosphere			Air atmosphere		
		T_{peak}	Mass loss (%)	Weight loss after decomposition (%)	T_{peak}	Mass loss (%)	Weight loss after decomposition (%)
PSF	I	517	51.23	48.77	515	27.06	23.46
	II	–	–		–	49.48	
P-PSF DS=0.62	I	511	62.08	37.92	424	31.14	13.34
	II	–	–		567	55.52	
P-PSF DS=0.74	I	466	54.06	45.94	404	7.77	27.69
	II	–	–		479	18.45	
	III	–	–		565	21.81	
	IV	–	–		–	24.28	
P-PSF DS=1.30	I	321	11.16	45.94	404	13.96	31.45
	II	488	43.48		468	9.50	
	III	–	–		556	20.78	
	IV	–	–		–	24.31	

Thermal degradation in air exhibited an additional degradation stage (one or three steps) in comparison with thermal degradation in nitrogen. In air, the degradation mechanism was more complex. In this case, all chemically modified PSFs showed a DTG peak at a low temperature, which probably mainly corresponded to the loss of some aliphatic groups. After the elimination of these groups, a less stable structure than PSF appeared with a peculiar decomposition pathway as a function of the modified polymer structure and the atmosphere employed in the TG apparatus.

A relation between the substitution degree and residue percentages was observed: in nitrogen, the residue increased when the substitution degree increased from 0.62 to 0.72 .When the substitution degree increased to 1.3, the residue, instead of being higher, remained close to that of P-PSF with DS = 0.62. This unusual behavior could be related to the possible substitution of the structural unit by two bulky groups, which affected the heat stability and could have led to the breaking of some fragments below 300°C. In air, a continuous increase in the residue percentage was observed when the substitution degree was enhanced. In air, the phosphorus pendent group promoted the formation of a more compact char residue, which could prevent the attack of heat. Oxidation of the unsaturated char residue reduced the quantity of decomposition residues in comparison with those resulting after pyrolysis in nitrogen. Porous and open structures of the PSF indicated that it decomposition released a lot of gaseous products that penetrated the char. The compact char structure (even an ordered one) observed for P-PSF confirmed the increased resistance to heat and oxygen.

6.4 High Performance Applications of Phosphorus-Containing Polysulfones

6.4.1 Membrane Materials in Proton exchange Membrane Fuel Cell

For many years, several polymers have been investigated intensively for their potential as membrane materials in proton exchange membrane fuel cell. Research groups have sought to improve the existing material and to find alternative polymer that possess similar performance as the standard Nafion membrane. Among the other polymers, polysulfone was considered to be the

most interesting polymer due to its low cost, commercial availability and ease of processing. Unfortunately, polysulfone has rather hydrophobic nature. It was observed that sulfonation process have significantly improving the water uptake of the sulfonated membrane compared to the origin polymer by the introduction of hydrophilic sulfonic acid group in the polymer skeleton. The water uptake and ion exchange capacity value of the obtained membrane increases with the temperature of sulfonation and when the sulfonation degree is increased. However, a higher degree of sulfonation could negatively influences the membranes properties [61]. Another type of functionalization was used in order to obtain flexible and mechanically tough membranes with higher acidity, higher thermal stability and at same time a high proton conductivity [62]. Access to these membranes promises important benefits concerning the complexity, cost and performance of the fuel cell system. In this context, membranes functionalized with covalently linked phosphonic acid may potentially show some crucial advantages in relation to the commonly employed sulfonated membranes [42, 58, 63–73]. Because of the hydrogen bonding and more amphoteric character of the phosphonic acids, the former membranes may transport protons through structure diffusion under low-humidity conditions. At high water contents the protons may instead be transported through the dynamics of the water, much in the same way as in conventional sulfonated membranes. Furthermore, phosphonated polymers generally show a high hydrolytic, thermal stability, due to the strength of the carbon-phosphorus bond, and oxidation resistance, which is especially critical under high-temperature operation. However, it is clear that the molecular architecture of the phosphonated polymers will require a very careful design in order to reach these advantageous membrane properties. In addition, phosphonated polymers are in general more complicated to prepare than the corresponding sulfonated ones [74]. Poly(arylene ether sulfone)s have been functionalized with alkyl side chains carrying phosphonic acid and bis(phosphonic acid) in order to investigate their properties as membrane materials. The significantly higher acidity and acid concentrations of the membranes containing the tetraprotic bis(phosphonic acid) led to higher conductivities in comparison to the membranes containing the diprotic phosphonic acid. Membranes containing 1.7 mmol of bis(phosphonic acid)/g of dry polymer absorbed 28 wt% water when immersed at room temperature, and a conductivity of 25 mS/cm was measured at 120°C.

Moreover, the bisphosphonated membranes did not decompose at temperatures of up to 240°C under air. The study also showed that high degrees of hydrolysis of the bisphosphonate units were crucial in order to reach the thermal stability necessary for fuel cell applications.

Parvole and Jannach [41] successfully grafted PSF with poly(vinyl phosphonic acid) using an anionic grafting strategy. The graft copolymers displayed a number of important features for use as fuel cell membranes. They were prepared from inexpensive starting materials and were all soluble and nicely film-forming from solution. The resulting membranes were phase-separated because of the inherent immiscibility of the stiff and hydrophobic backbone polymer and the strongly hydrogen-bonding side chains. The poly(vinyl phosphonic acid) side chains thus formed separate phases in the membranes with very high local concentrations of interacting phosphonic acid units, giving rise to large hydrogen-bonded aggregates. These aggregates are essential for efficient proton conduction in the nominally dry state. The thermal stability of the membranes was sufficiently high under air, with $T_{decomp.}$, 5% at 260–340°C, depending on ion exchange capacity and DS. However, at high temperatures the performance of this membrane was limited by condensation reactions under dry conditions and, especially, by high levels of water uptake under immersed conditions. Yet, by adding small concentrations of perfluorosulfonic acid polymer to the phosphonated membranes with the highest poly (vinyl phosphonic acid) contents, the water uptake was efficiently reduced under immersed conditions. At the same time the conductivity was enhanced, especially at low temperatures. The conductivity under nominally dry conditions could be enhanced only by additions of small amounts of perfluorosulfonic acid polymer. The presence of the perfluorosulfonate polymer in these membranes may further increase the compatibility with Nafion-impregnated electrode layers which will facilitate the preparation of membrane electrode assemblies.

On the other part, the incorporation of bulky aromatic phosphorus pendant group into PSF's side chain influenced their reological properties. The maximum hydrophobicity of the polysulfones with bulky phosphorus pendant groups, in which the work of water adhesion is very low comparatively with the work of cohesion, correlated with low adhesion to interfaces, would be advantageous for dielectric performance in different biological applications. Atomic force microscopy showed that the increase of density of the bulky phosphorus pendant groups determine the formation of domains

with pores whose dimensions increase, while roughness decreases, confirming the poor adhesion of modified polysulfone films [75, 76].

6.4.2 Protein-Adsorption-Resistant Membranes

Ultrafiltration, as a novel and powerful pressure-driven separation technology, is often used to concentrate or fractionate protein solutions. However, the adsorption and deposition of biomacromolecules on membrane surfaces and/or pore walls (the so-called membrane fouling), often cause severe decrease of flux, substantial increase of energy consumption and operation cost. The application of ultrafiltration is seriously limited by membrane fouling. In the last years, many researchers have revealed that increasing the hydrophilicity of the membrane surfaces and pore surfaces can remarkably reduce or suppress membrane fouling [77–83]. Accordingly, hydrophilic molecules, such as poly(ethylene glycol) (PEG) and zwitterionic molecules, have been widely used to modify the ultrafiltration membranes [84–86].

Several methods, including adsorption, coating, and grafting polymerization, constitute the prevalent methods for ultrafiltration membranes modification. However, the adsorbed or coated modification agents may not reside on the membrane surfaces permanently and lead to a decrease of flux. Chemically or radiation induced grafting polymerization suffers from the drawback of requiring additional complicated steps and rigorous conditions. They can obtain only two-dimensional modification instead of three-dimensional modification, namely, the inner surfaces of membranes cannot be modified [83]. In comparison, surface segregation seems to be a promising method because of its facile operation, high efficiency, and low cost [85]. The surface segregation method can be briefly described as follows: amphiphilic additive is blended into membrane casting solution, and during the subsequent phase inversion process, the hydrophilic segments of the additive are segregated spontaneously to the membrane surfaces while the hydrophobic parts of the additive are firmly entrapped in the membrane bulk matrix. One of the most effective methods of making a blood-compatible polymer is to modify conventional materials with polymers having a phospholipid polar group mimicking a biomembrane surface.

The ***phosphorylcholine*** (PC), an electrically neutral zwitterionic head group, which represents the dominant property of the phospholipids existing on the external surfaces of cell membranes, can

play an important role as a surface group for biomedical devices to reduce undesirable interaction with proteins. Protein adsorption on the material surfaces causes serious biological reactions such as thrombus formation, immune response, complement activation, capsulation, etc. Recently, synthesis of 2-methacryloyloxyethyl phosphorylcholine (MPC) [87–91] had been conducted to a variety of polymer and copolymers, as is shown in Scheme 6.6. These polymers had different methylene chain lengths between the phospholipid polar group and the backbone, which enhances the affinity of the MPC polymer for phospholipids in blood. To understand the blood-compatibility of surfaces, it is necessary to determine not only the amount of adsorbed protein but also the species of the protein, e.g. cells, plasma protein, phospholipids, and water. The homopolymer of MPC is soluble in water and the solubility of MPC copolymers can be easily controlled by changing the structure and fraction of the co-monomer. The copolymer of MPC with n-butylmethacrylate (PMB) adsorbs in preference on surface proteins and platelets, while the MPC unit in the polymer has affinity for the phospholipids. Activation and aggregation of the cells and clot formation were observed on the hydrophobic poly(n-butyl methacrylate). In contrast, the copolymer PMB with 30 mol% MPC effectively suppressed cell adhesion. The adherent platelets readily detach from the surface, but are strongly activated in contact with the polymer surface, which induces embolization. It is, therefore, necessary to evaluate the activation of platelets just coming into contact with the polymer surface and those adhering to the surface to understand true blood-compatibility. The adsorbed phospholipids on the PMB surface form a biomimetic surface. The highly water-free content of hydrated PMB also contributes to the demonstrable excellent blood compatibility. Chen *et al.* have prepared the self-assembly PC monolayer on gold films which displayed the excellent antifouling property [92]. An artificially synthesized monomer of 2-methacryloyloxyethylphosphorylcholine (MPC) has received increasing attention in recent years; many MPC-based materials bearing the PC groups in the side chains are demonstrated to be capable of effectively inhibiting protein adsorption and platelet adhesion [93–98].

Phosphatidylcholine is an integral component of the lipoproteins. On the other hand, it is less often found in bacterial membranes, perhaps 10% of species. It is a neutral or zwitterionic phospholipid over a pH range from strongly acid to strongly alkaline. Because of

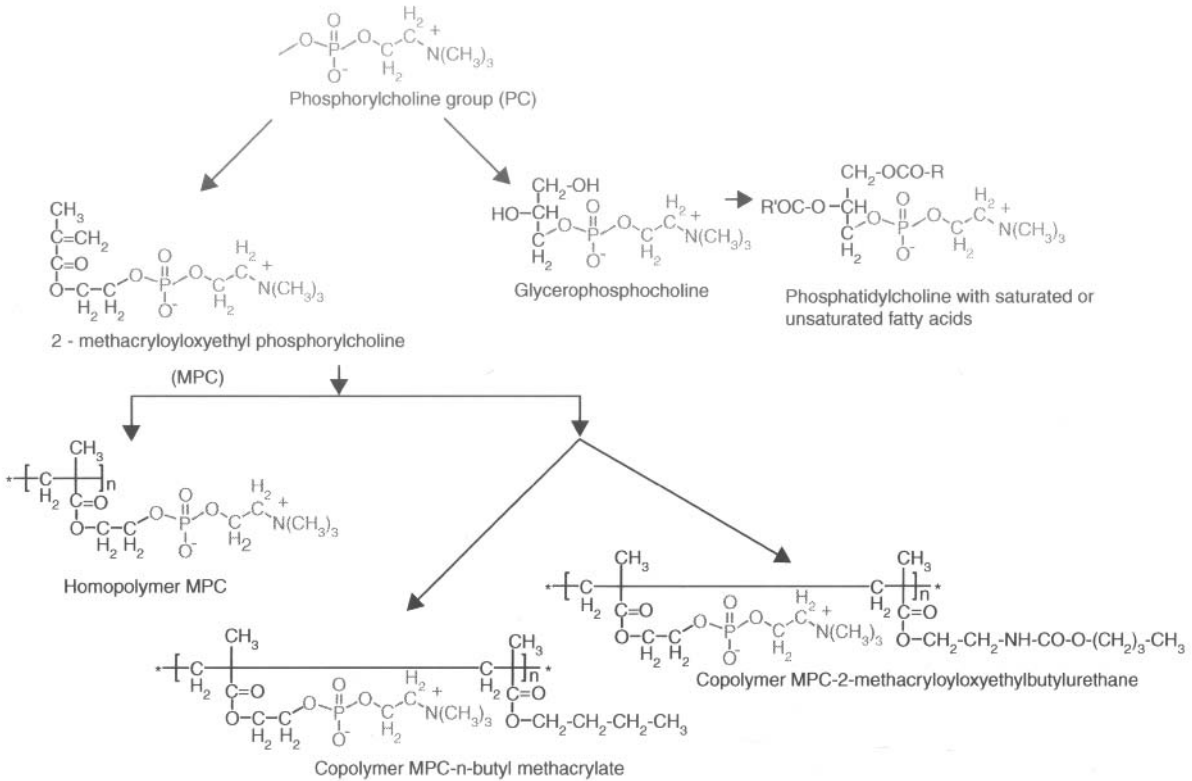

Schema 6.6 Synthesis of some copolymers containing phosphorylcholine group.

the generally cylindrical shape of the molecule, phosphatidylcholine spontaneously organizes into bilayers, so it is ideally suited to serve as the bulk structural element of biological membranes. The unsaturated acyl chains are kinked and confer fluidity on the membrane. Such properties are essential to act as a balance to those lipids that do not form bilayers or that form specific micro-domains such as rafts. While phosphatidylcholine does not induce curvature of membranes, as may be required for membrane transport and fusion processes, it can be metabolized to form lipids. Phosphatidylcholine is obtained combining a choline head group and glycerophosphoric acid with a variety of fatty acids. Many researchers have employed lipidlike molecules for modifying surfaces in order to enhance their non-specific protein adsorption resistivity. The synthetic process of phospholipid polymers is difficult and sophisticated, which limits their wide application in large scale [99]. Soybean phosphatidylcholine, from versatile biosources has the following advantages: easy of availability, low cost and good biocompatibility. If it can be effectively introduced to membrane, it will be more suitable for industrial application.

Polysulfone possesses excellent membrane-forming property, as well as mechanical strength and physicochemical stability [100]. However, due to its inherent hydrophobic nature, there are serious membrane fouling processes and thus rapid decline of permeation flux in many application situations. Since there are no functional groups on phosphatidylcholine or MPC-copolymer, it will be quite difficult to immobilize them at a polysulfone membrane surface through chemical approach. So, blending seems to be a more feasible method. Ye *et al.* have reported that blending with the MPC copolymer was an effective treatment for both improving hemocompatibility and reducing protein fouling on the cellulose acetate (CA) flat membranes and hollow fiber membranes [101–103].

Ishihara *et al.* also investigated that polysulfone/MPC polymers blend membranes could improve blood compatibility and reduce protein adsorption and platelet adhesion [104–108]. Based on these results, the addition of the MPC polymer to the polysulfone should be a very useful method to improve the functions and blood compatibility. Ultrafiltration antifouling membranes were successfully prepared blending polyethersulfone with 2-methacryloyloxyethylphosphorylcholine (MPC) and n-butyl methacrylate (BMA) copolymer, by phase inversion method. Due to the high hydrophilicity and electric neutrality of MPC–BMA copolymer, the

antifouling property of the modified membranes was remarkably improved with increasing MPC–BMA copolymer content between 7–15%. The incorporation of MPC groups substantially reduced total membrane fouling, especially irreversible membrane fouling. In a wide pH range from 4.5 to 9.0, the MPC-modified PES membranes exhibited superior antifouling property. The adsorption experiments indicated that the adsorption amounts of bovine serum albumin (BSA) on the MPC-modified PES membranes were dramatically decreased in comparison with the control PES membrane. In addition, the MPC-modified PES membranes could run several cycles without substantial flux loss. By analogy, polysulfone (PSF) membranes were modified with 2-methacryloyloxyethyl phosphorylcholine (MPC) and protein adsorption and platelet adhesion from human plasma on polymer membrane were studied. The amount of protein adsorbed on the PSF/MPC polymer blend membrane was significantly decreased with an increase in the composition of the blended MPC polymer. The distribution of the specific proteins adsorbed on the membrane surface was also determined. Albumin, γ-globulin and fibrinogen were observed on every membrane surface after contact with plasma. However, for the blended composition membrane, the density of the adsorbed proteins decreased compared with that of original PSF membrane. That is, the MPC polymer blended in the membrane could function as a protein-adsorption-resistant additive. The number of platelets adherent on the PSF membrane was reduced, and change in the morphology of adherent platelets was also suppressed by the modification with the MPC polymer. Therefore, the PSF/MPC polymer blend membrane had improved blood compatibility compared with the PSF membrane.

6.4.3 Flame Resistant Materials

Polysulfones are self-extinguishing resin. Polysulfones with no flame retardant additives has been given 94V-0 under the UL Standards. The value of limited oxygen index (around 0.40) points out their excellent flame retardancy [109]. Furthermore, exposed to flame, polysulfones emit very little smoke or toxic volatiles. However, the high flameproof properties of polysulfones are scanty when they are used as electrical parts or in an epoxy resins network. Poly(sulfone) (PSF) and poly(ether sulfone) (PES) are commonly used for high performance applications such as advanced

injection molded engineering parts and as toughness modifiers in epoxy resins (EP) [110–114].

Recently, it was proposed to incorporate phosphorus-containing diols into the polymer to further improve the fire behaviour of poly(ether sulfone) [48] and hence to use these new materials not only as toughness modifier for epoxy resins, but also as flame retardant at the same time. It should be noted that fire retardants containing phosphorus – regardless of whether an additive or reactive approach is used, show different mechanisms in the condensed and gas phase [115]. The main mechanisms reported in the literature [116] are char formation and flame inhibition, respectively. The fire behavior of the phosphorus modified epoxy resins was compared to non-fire-retarded epoxy resin cured with 4,4'-diamine-diphenylsulfone as a hardener. It turned out that this comparison is not perfectly systematic, as the -SO2- group, in particular, increases the intrinsic fire retardancy of the polymeric structure in fire performance. However, this system serves as an interesting reference value for an established system. The main results based on systematic investigation of various hardeners containing phosphorus are summarized as follows:

- Phosphorus-containing groups alter the decomposition of the epoxy resins, resulting in a multi-step decomposition. Mass losses between around 15 and 20 wt.% occur for the decomposition subsequent to the main decomposition step. The high temperature residue is increased.
- Phosphorus-phenoxy groups incorporated in the structure of the epoxy resins decrease the decomposition temperature, enhance water elimination, and reduce mass loss during the main decomposition step.
- Phosphorus-containing acids are formed and enhance charring. Apart from carbonaceous char, PxOy and PxNyOz occur in the high-temperature residue. The condensed phase effects are strongest for phosphate and decrease with the decreasing oxidation state of the phosphorus. They are of minor importance for phosphine oxide.
- Volatile decomposition products containing phosphorus are released in a little extent into the gas phase.

However, it was shown that the mechanisms and their efficiency depend on such factors as the chemical structure of the

phosphorus-containing compounds, their interactions with the matrix or additional additives, the water content and the pH value during decomposition [117–120]. Indeed, the understanding of mechanisms and their controlling interactions is as yet limited. A concept for tailoring the materials properties is encouraged by comparable approaches such as incorporating poly(sulfonyl-diphenylene phenylphosphate) in poly(butylene terephthalate) (PBT) [121] or polycarbonates (PC) [122, 123].

Braun *et al.* [55, 59, 124–126] have shown that a cured bisphenol-A based epoxy resin can simultaneously be equipped with both an enhanced toughness and improved flame retardancy by adding a new type of polysulfone containing phosphorus in the backbone (structure 8-Table 6.2). These performance improvements were achieved without sacrificing the stiffness and the glass transition temperature of the resulting material. Furthermore, owing to the chemical structure of the phosphorus-modified polysulfone, an interlocked epoxy thermoplastic network can be created under certain curing conditions, providing the cured epoxy resin with a higher glass transition temperature. It was demonstrated by means of temperature-modulated DSC that the reaction-induced phase separation is suppressed when curing the material at temperatures equal or less than 180°C and higher than 220°C when using the phosphorus modified polysulfone. An enhanced reaction rate, the occurrence of secondary reactions and an earlier vitrification of the reacting mixture were found to prevent any morphology development in the materials cured under these conditions. Hence, only about a 20% improvement in the fracture toughness was observed in samples cured at 180°C. Nevertheless, the absence of phase separation contributed to a high interpenetration of the thermoplastic and thermoset networks, which significantly increased the glass transition temperature of the final material. Modification of the epoxy with blends of a commercially available and the phosphorus-modified polysulfone indicated another interesting approach towards increasing the fracture toughness of the resulting material while maximizing the total phosphorus content in the system. Such blends were found to be more effective to increase the toughness of the epoxy than the neat thermoplastics, at a concentration of 20 wt %, owing to the particular resulting microstructures. By increasing the amount of the phosphorus-modified polysulfone in the blend, the viscosity of the reactive mixture also increased. This, in turn, contributed to "lock in" the observed morphologies. The microstructure change upon curing of the material was found

to be crucial for the fracture toughness improvement, in agreement with the majority of the studies in the literature. A combination of polymer interpenetration and phase separation appears to be an efficient way to simultaneously improve the toughness and glass transition temperature as well as the flame retardancy of thermosetting materials for modern-day applications.

6.5 References

1. M.E.A. Cudby, R.G. Feasey, B.E. Jennings, M.E.B. Jones, and J.B. Rose, *Polymer*, Vol. 6, p. 589, 1965.
2. J.L. Hedrick, D.K. Mohanty, B.C. Johnson, R. Viswanathan, J.A. Hinkley, and J.E. McGrath, *Journal of Polymer Science, Part A: Polymer Chemistry*, Vol. 24, p. 287, 1986.
3. J.L. Hedrick, J.J. Dumais, L.W. Jelinski, R.A. Patsiga, and J.E. McGrath, *Journal of Polymer Science, Part A: Polymer Chemistry*, Vol. 25, p. 2289, 1987.
4. F. Lufrano, G. Squadrito, A. Patti and E. Passalacqua, *Journal of Applied Polymer Science*, Vol. 77, p.1250, 2000.
5. F. Lufrano, V. Baglio, P. Staiti, A.S. Arico, and V. Antonucci, *Journal of Power Sources*, Vol. 179, p.34, 2008.
6. E. Avram, C. Luca, S. Petrovan, and C. Mihailescu, *Polymer-Plastics Technology and Engineering*, Vol. 35, p. 757, 1996.
7. E. Avram, I. Druta, E. Butuc, and C. Luca, *Journal of Macromolecular Science A*, Vol. 34, p. 1701, 1997.
8. E. Avram, *Polymer-Plastics Technology and Engineering*, Vol. 40, p. 275, 2001.
9. M.D. Guiver, *Dissertation*, Carletown University, Ottawa–Ontario, Canada, 1987.
10. Y. Nagase, A. Naruse, and K. Matsui, *Polymer*, Vol. 30, p. 1931, 1989.
11. M.D. Guiver, J.W. ApSimon, and O. Kutowy, *Journal of Polymer Science, Part C*, Vol. 26, p. 123, 1988.
12. M.D. Guiver, and O. Kutowy, Aromatic polysulfone compounds and their manufacture. U.S. Patent 4,999,415, 1991.
13. M.D, Guiver, O. Kutowy, and J.W. ApSimon, *Polymer*, Vol. 30, p. 1137, 1989.
14. M.D. Guiver, A.Y. Tremblay, and C.M. Tam, Method of manufacturing a reverse osmosis membrane and the membrane so produced. U. S. Patent 4,894,159, 1990.
15. M.D. Guiver, P. Black, C.M. Tam, and Y. Deslandes, *Journal of Applied Polymer Science*, Vol. 48, p. 1597, 1993.
16. M.D. Guiver, H. Zhang, G.P. Robertson, and Y. Dai, *Journal of Polymer Science, Part A: Polymer Chemistry*, Vol. 39, p. 675, 2001.
17. A.R. Bader, and A.D. Kontowicz, *Journal of American Chemical Society*, Vol. 76, p. 4465, 1954.
18. J.A. Mikroyannidis, *European Polymer Journal*, Vol. 21, p. 1031, 1985.
19. A. Warshawsky, and O. Kedem, *Journal of Membrane Science*, Vol. 53, p. 37, 1990.

20. I.C.H.M. Esser, and I. Parsons, *Polymer*, Vol. 34, p. 2836, 1993.
21. T. Koch, and H. Ritter, *Macromolecular Chemistry and Physics*, Vol. 195, p. 1709, 1994.
22. C.G. Herbert, and A.S. Hay, *Journal of Polymer Science, Polymer Chemistry Edition*, Vol. 35, p. 1095, 1997.
23. M. Rusu, A. Airinei, E. Butuc, G.G. Rusu, C. Baban, and G.I. Rusu, *Journal of Macromolecular Science, Physics*, Vol. 37, p. 73, 1998.
24. F.A. Bottino, A. Mamo, A. Recca, J. Brady, A.C. Street, and P.T. McGrail, *Polymer*, Vol. 34, p. 2901, 1993.
25. S.J. Park, G.D. Lyle, R. Mercier, and J.E. McGrath, *Polymer*, Vol. 34, p. 885, 1993.
26. S.J. Park, *Ph. D. Thesis*, Virginia Polytechnic Institute and State University, Blacksburg, United State, 1992.
27. M. Ueda, H. Toyota, T. Ouchi, J-I. Sugiyama, K. Yonetake, T. Masuko, and T. Teramoto, *Journal of Polymer Science, Polymer Chemistry Edition*, Vol. 31, p. 853, 1993.
28. F. Wang, Q. Ji, W. Harrison, J. Mecham, R. Formato, R. Kovar, P. Osenar, and J.E. McGrath, *Polymer Preprints*, Vol. 41, p. 237, 2000.
29. H.T. Lin, C.H. Lin, Y.M. Hu, and W.C. Su, *Polymer*, Vol. 50, p. 5685, 2009.
30. E. Scamporrino, P. Mineo, A. Scamporrino, S. Dattilo, D. Vitalini, and R. Alicata, *Journal of Polymer Science, Part A: Polymer Chemistry*, Vol. 47, p. 5682, 2009.
31. K. Mimura, H. Ito, and H. Fujioka, *Polymer*, Vol. 41, p. 4451, 2000.
32. R.A. Pethrick, E.A. Hollins, I. McEwan, A.J. MacKinnon, D. Hayward, and L.A. Cannon, *Macromolecules*, Vol. 29, p. 5208, 1996.
33. A. Bonnet, J.P. Pascault, H. Sautereau, J. Rogozinski, and D. Kranbuehl, *Macromolecules*, Vol. 33, p. 3833, 2000.
34. M. Sawamoto, and M. Kamigaito, in J.R. Ebdon and G.C. Eastmond, eds., New Methods of Polymer Synthesis, Vol. 2. Blackie, Glasgow, pp. 37–68, 1995.
35. Y. Yagci, O. Nuyken, and V.-M. Graubner, Telechelic Polymers, in J.I. Kroschwitz, ed., *Encyclopedia of Polymer Science and Technology*, Vol. 12, 3rd ed., Wiley and Sons, New York, pp. 57–130, 2005.
36. Y. Ishihara, S. Iwasaki, Y. Ebihara, N. Shindo, and N. Nakabayashi, *Colloids and Surfaces B: Biointerfaces*, Vol. 18, p. 325, 2000.
37 A. Noshay, and L.M. Robeson, *Journal of Applied Polymer Science*, Vol. 20, p. 1885, 1976.
38. B.C. Johnson, I. Yilgör, C. Tran, M. Iqbal, J.P. Wightman, D.R. Lloyd, and J.E. McGrath, *Journal of Polymer Science, Polymer Chemistry Edition*, Vol. 22, p. 721, 1984.
39. B. Lafitte, and P. Jannasch, *Journal of Polymer Science, Part A: Polymer Chemistry*, Vol. 45, p. 269, 2007.
40. B. Laffite, and P. Jannasch, (2005) *Journal of Polymer Science, Part A: Polymer Chemistry*, Vol. 43, p. 273, 2005.
41. J. Parvole, and P. Jannasch, *Macromolecules*, Vol. 41, p. 3893, 2008.
42. K. Jakoby, K.V. Peinemann, and S.P. Nunes, *Macromolecular Chemistry and Physics*, Vol. 204, p. 61, 2003.
43. T. Bock, R. Mülhaupt, and H. Möhwald, *Macromolecular Rapid Communications*, Vol. 27, p. 2065, 2006.
44. N.Y. Abu-Thabit, S.A. Ali, and S.M.J. Javaid-Zaidib, *Journal of Membrane Science*, Vol. 360, p. 26, 2010.

45. S. Gu, R. Cai, T. Luo, and Y. Yan, Synthesis and characterizations of quaternary phosphonium polysulfone anion exchange membrane for alkaline fuel cell. *214th ECS Meeting B8-PEM fuel cells*, October 12–17, Honolulu, HI, Abstract 1107, 2008.
46. S. Gu, R. Cai, T. Luo, Z. Chen, M. Sun, Y. Liu, G. He, and Y. Yan, *Angewandte Chemie International Edition*, Vol. 48, p. 1, 2009.
47. O. Petreus, E. Avram and D. Serbezeanu, *Polymer Engineering and Science*, Vol. 50, p. 48, 2010.
48. T. Hoffmann, D. Pospiech, L. Haüßler, H. Komber, D. Voigt, C. Harnisch, C. Kollann, M. Ciesielski, M. Döring, R. Perez-Graterol, J. Sandler, and V. Altstädt, *Macromolecular Chemistry and Physics*, Vol. 206, p. 423, 2005.
49. O. Petreus, T. Vlad-Bubulac, and C. Hamciuc, *European Polymer* Journal, Vol. 41, p. 2663, 2005.
50. O. Petreus, T. Vlad-Bubulac, and C. Hamciuc, *High Performance Polymers*, Vol. 20, p. 588, 2008.
51. O. Petreus, E. Avram, and D. Serbezeanu, *Journal of Applied Polymer Science*, Vol. 115, p. 2084, 2010.
52. T. Vlad-Bubulac, C. Hamciuc, O. Petreus, and M. Bruma, *Polymers for Advanced Technologies*, Vol. 17, p. 647, 2006.
53. H.-J. Xu, F-L. Jin, and S-J. Park, *Bulletin of Korean Chemical Society*, Vol. 30, p. 2643, 2009.
54. X-T. Chen, H. Sun, X.D. Tang and C-Y Wang, *Journal of Applied Polymer Science*, Vol. 110, p. 1304, 2008.
55. U. Braun, A.I. Balabanovich, B. Schartel, U. Knoll, J. Artner. M. Ciesielski, M. Döring, R. Perez, J.K.W. Sandler, V. Altstädt, T. Hoffmann, and D. Pospiech, *Macromolecular Chemistry and Physics*, Vol. 207, p. 1501, 2006.
56. G. Molnár, A. Botyay, L. Pöppl, K. Torkos, J. Borossay, A. Máthé, and T. Török, *Polymer Degradation and Stability*, Vol. 89, p. 410, 2005.
57. L.D. Freedman, and G.O. Doak, *Chemical Reviews*, Vol. 57, p. 479, 1957.
58. K. Miyatake, and A.S. Hay, (2001). *Journal of Polymer Science, Part A: Polymer Chemistry*, Vol. 39, p. 3770, 2001.
59. T. Hoffmann, D. Pospiech, K. Haüßler, L. Sahre, H. Komber, C. Harnisch, M. Landwehr, A. Schäfer, and M. Döring, *High Performance polymers*, Vol. 22, p. 715, 2010.
60. O. Petreus, G. Lisa, E. Avram, and D. Rosu, *Journal of Applied Polymer Science*, Vol. 120, p. 3233, 2011.
61. F. Wang, M. Hickner, Y.S. Kim, T.A. Zawodzinski, and J.E. McGarth, *Journal of Membrane Science*, Vol. 197, p. 231, 2002.
62. M. Schuster, T. Rager, A. Noda, K.D. Kreuer, and J. Maier, *Fuel Cells*, Vol. 5, p. 355, 2005.
63. X. Xu, and I. Cabasso, *Polymeric Materials Science and Engineering*, Vol. 68, p. 120, 1993.
64. S.V. Kotov, S.D. Pedersen, W. Qiu, Z-M. Qiu, and J. Burton, *Journal of Fluorine Chemistry*, Vol. 82, p. 13, 1997.
65. C. Stone, T.S. Daynard, L-Q. Hu, C. Mah, and A.E. Steck, *J. New Mater. Electrochem. Syst.*, Vol. 3, p. 43, 2000.
66. M. Yamabe, K. Akiyama, Y. Akatsuka, and M. Kato, *European Polymer Journal*, Vol. 36, p. 1035, 2000.

67. Y.Z. Meng, S.C. Tjong, A.S. Hay and S.J. Wang, *Journal of Polymer Science, Part A: Polymer Chemistry*, Vol. 39, p. 3218, 2001.
68. H.R. Allock, M.A. Hoffmann, and R.M. Wood, *Macromolecules*, Vol. 34, p. 6915, 2001.
69. H.R. Allock, M.A. Hoffmann, C.M. Ambler, S.N. Lvov, X.Y. Zhou, E. Chalkova, and J. Weston, *Journal of Membrane Science*, Vol. 201, p. 47, 2002.
70. Y.M. Li., and K. Hinokuma, *Solid State Ionics*, Vol. 150, p. 309, 2002.
71. H.R. Allcock, M.A. Hofmann, C.M. Ambler, and R.V. Morford, *Macromolecules*, Vol. 35, p. 3484, 2002.
72. Y.Z. Meng, S.C. Tjong, A.S. Hay, and S.J. Wang, *European Polymer Journal*, Vol. 39, p. 627, 2003.
73. S. Yanagimachi, K. Kaneko, Y. Takeoka, and M. Rikukawa, *Synthetic Metals*, Vol. 135–136, p. 69, 2003.
74. B. Lafitte, and P. Jannach, On the prospects for phosphonate polymers as proton-exchange fuel cell membranes, in T.S. Zjao, K.D. Kreuer, and T.V. Nguyen, eds., *Advances in Fuel*, Vol. 1, Chap., Elsevier , pp. 119–185, 2007.
75. S. Ioan L.I. Buruiana, E. Avram O. Petreus, and V.E. Musteata, *Journal of Macromolecular Science, Part B*, Vol. 99999, p. 1, 2011.
76. S. Ioan, L.I. Buruiana, O. Petreus, E. Avram, I. Stoica, and G. Ioanid, *Polymer-Plastics Technology and Engineering*, Vol. 50, p. 36, 2011.
77. Z.M. Liu, Z.K. Xu, L.S. Wan, J. Wu and M. Ulbricht, *Journal of Membrane Science*, Vol. 249, p. 21, 2005.
78. A.V.R. Reddy, D.J. Mohan, A. Bhattacharya, V.J. Shah, and P.K. Ghosh, *Journal of Membrane Science*, Vol. 214, p. 211, 2003.
79. M. Taniguchi, and G. Belfort, *Journal of Membrane Science*, Vol. 231, p. 147, 2004.
80. E. Kiss, J. Samu, A. Toth, and I. Bertoti, *Langmuir*, Vol. 12, p. 1651, 1996.
81. J. Pieracci, J.V. Crivello, and G. Belfort, *Journal of Membrane Science*, Vol. 156, p. 223, 1999.
82. H. Chen, and G. Belfort, *Journal of Applied Polymer Science*, Vol. 72, p. 1699, 1999.
83. L.F. Hancock, S.M. Fagan, and M.S. Ziolo, *Biomaterials*, Vol. 21, p. 725, 2000.
84. Y.W. Kim, W.S. Ahn, J.J. Kim, and Y.H. Kim, *Biomaterials*, Vol. 26, p. 2867, 2005.
85. Q. Sun, Y. Su, X. Ma, Y. Wang, and Z. Jiang, *Journal of Membrane Science*, Vol. 285, p. 299, 2006.
86. S. Kang, A. Asatekin, A.M. Mayes, and M. Elimelech, *Journal of Membrane Science*, Vol. 296, p. 42, 2007.
87. Y. Iwasaki, K. Kurita, K. Ishihara, and N. Nakabayashi, *Journal of Biomaterials Science, Polymer Edition*, Vol. 6, p. 447, 1994.
88. K. Ishihara, A. Fujiike, Y. Iwasaki, and N. Nakabayashi, *Journal of Polymer Science, Part A: Polymer Chemistry*, Vol. 34, p. 199, 1996.
89. K. Sugiyama, K. Ohga, and H. Aoki, *Macromolecular Chemistry and Physics*, Vol. 196, p. 1907, 1995.
90. K. Sugiyama, and K. Ohga, *Macromolecular Chemistry and Physics*, Vol. 200, p. 1439, 1999.
91. T. Oishi, H. Uchiyama, K. Onimura, and H. Tsutsumi, *Polymer Journal*, Vol. 30, p. 17, 1998.
92. S. Chen, J. Zheng, L. Li, and S. Jiang, *Journal of the American Chemical Society*, Vol. 127, p. 14473, 2005.

93. W. Feng, S. Zhu, K. Ishihara, and J.L. Brush, *Langmuir*, Vol. 21, p. 5980, 2005.
94. K. Ishihara, Y. Iwasaki, S. Ebihara, Y. Shindo, and N. Nakabayashi, *Colloids and Surfaces B*, Vol. 18, p. 325, 2000.
95. R. Iwata, P. Suk-In, V.P. Hoven, A. Takahara, K. Akiyoshi, and Y. Iwasaki, *Biomacromolecules*, Vol. 5, p. 2308, 2004.
96. J.R. Lu, E.F. Murphy, and T.J. Su, *Langmuir*, Vol. 17, p. 3382, 2001.
97. K. Ishihara, H. Nomura, T. Mihara, K. Kurita, Y. Iwasaki, and N. Nakabayashi, *Journal of Biomedical Materials Research*, Vol. 39, p. 323, 1998.
98. K. Ishihara, H. Hanyuda, and N. Nakabayashi, *Biomaterials*, Vol. 16, p. 873–879.
99. T. Wang, Y-Q. Wang, Y-I. Su, and Z-Y. Jiang, *Colloids and Surfaces B*, Vol. 46, p. 233, 2005.
100. N.A. Hoenich, C. Woffindin, S. Stamp, S.J. Roberts, and J. Turnbull, *Biomaterials*, Vol. 18, p. 1299, 1997.
101. S.H. Ye, J. Watanabe, Y. Iwasaki, and K. Ishihara, *Journal of Membrane Science*, Vol. 210, p. 411, 2002.
102. S.H. Ye, J. Watanabe, Y. Iwasaki, and K. Ishihara, *Biomaterials*, Vol. 24, p. 4143, 2003.
103. S.H. Ye, J. Watanabe, and K. Ishihara, *Journal of Biomaterials Science, Polymer Edition*, Vol. 15, p. 981, 2004.
104. Y. Su, C. Li, W. Zhao, Q. Shi, H. Wang, Z. Jiang, and. S. Zhu, *Journal of Membrane Science*, Vol. 322, p. 171, 2008.
105. K. Ishihara, K. Fukumoto, Y. Iwasaki, and N. Nakabayashi, *Biomaterials*, Vol. 20, p. 1545, 1999.
106. K. Ishihara, K. Fukumoto, Y. Iwasaki, and N. Nakabayashi, *Biomaterials*, Vol. 20, p. 1553, 1999.
107. T. Hasegawa, Y. Iwasaki, and K. Ishihara, *Biomaterials*, Vol. 22, p. 243, 2001.
108. T. Hasegawa, Y. Iwasaki, and K. Ishihara, *Journal of Biomedical Materials Research*, Vol. 63, p. 333, 2002.
109. D.W. Van Krevelen, *Polymer*, Vol. 16, p. 615, 1975.
110. R.J.Varley, J.H. Hodgkin, and G.P. Simon, *Polymer*, Vol. 42, p. 3847, 2001.
111. P.A.Oyanguren, M.J. Galante, K. Andromaque, P.M. Frontini and R.J.J. Williams, *Polymer*, Vol. 40, p. 5249, 1999.
112. S. Zheng, J. Huang, Q. Guo, and W. Zhu, *Polymer*, Vol. 38, p. 5565, 1997.
113. Y. Liu, A. Bhatnagar, Q. Ji, J.S. Riffle, J.E. McGrath, J.F. Geibel, and T. Kashiwagi, *Polymer*, Vol. 41, p. 5137, 2000.
114. I. Martinez, M.D. Martin, A. Eceiza, P. Oyanguren, and I. Mondragon, *Polymer*, Vol. 41, p. 1027, 2000.
115. B. Schartel, A.I. Balabanovich, U. Braun, U. Knoll, J. Artner, M. Ciesielski, M. Döring, R. Perez, J.K.W. Sandler, V. Altstädt, T. Hoffmann, and D. Pospiech, *Journal of Applied Polymer Science*, Vol. 104, p. 2260, 2007.
116. B. Schartel, *Materials*, Vol. 3, p. 4710, 2010.
117. B. Schartel, R. Kunze, and D. Neubert, *Journal of Applied Polymer Science*, Vol. 83, p. 2060, 2002.
118. B. Schartel, R. Kunze, D. Neubert, and U. Braun, Mechanistic Studies on PA-66 Fire Retarded with Red Phosphorus, in M. Lewin, ed., *Recent Advances in Flame Retardancy of Polymeric Materials*, Vol. 13, BCC, Norwalk, pp. 93, 2002.
119. U. Braun, and B. Schartel, *Journal of Fire Science*, Vol. 23, p. 5, 2005.

120. U. Braun, and B. Schartel, *Macromolecular Chemistry and Physics*, Vol. 205, p. 2185, 2004.
121. S.V. Levchik, D.A. Bright, G.R. Alessio, and S. Dashevsky, *Polymer Degradation and Stability*, Vol. 77, p. 267, 2002.
122. A.I. Balabanovich, and J. Engelmann, *Polymer Degradation and Stability*, Vol. 79, p. 85, 2003.
123. Y.-Z. Wang, B. Yi, B. Wu, B. Yang, and Y. Liu, *Journal of Applied Polymer Science*, Vol. 89, p. 882, 2003.
124. A. Schäfer, S. Seibold, W. Lohstroh, O. Walter, and M. Döring, *Journal of Applied Polymer Science*, Vol. 105, p. 685, 2007.
125. R.M. Perez, J.K.W. Sandler, V. Altstädt, T. Hoffmann, D. Pospiech, M. Ciesielski, M. Döring, A.I. Balabanovich, U. Braun, and B. Schartel, *Polymer*, Vol. 48, p. 778, 2007.
126. U. Braun, A.I. Balabanovich, B. Schartel, U. Knoll, J. Artner, M. Ciesielski, M. Döring, R. Perez, J.K.W. Sandler, V. Altstädt, T. Hoffmann, and D. Pospiech, *Polymer*, Vol. 47, p. 8495, 2006.

This page intentionally left blank

7

Synthesis and Characterization of Novel Polyimides

Atsushi Morikawa

Department of Biomolecular Functional Engineering, Ibaraki University, Ibaraki, Japan

Abstract

Polyimides are known as reliable high temperature polymers with superior mechanical and electrical properties. Polyimides can be easily prepared by reactions between dianhydrides and diamines, and many types of polyimides have been prepared by structural modification of the monomers to obtain the polyimides having desirable properties. This chapter introduced the synthetic methods for polyimides and the relationship between their structures and properties. The properties of polyimides are affected by internal rotation around bond in molecules, sweep volume, free volume, molecular packing, and molecular ordering. These factors are mainly dependent on the structure of polyimides, but also on the preparation condition. In particular, the molecular packing and the molecular ordering of some polyimides were reported to be extremely dependent on the preparation condition (preparation procedure, imidation conditions, annealing conditions and film thickness, etc). In future, high performance polyimides are expected to be developed on the basis of knowledge about the effect of the structures and the preparation conditions on properties, taking into consideration the polyimide characteristic, the cost, the convenience of operation and the environment.

Keywords: Polyimides, synthetic methods, properties of polyimides, structural modification, preparation condition

7.1 Introduction

Polyimides, possessing the cyclic imide groups and aromatic groups in the main chain, are recognized as very high performance

Vikas Mittal (ed.) High Performance Polymers and Engineering Plastics, (205–242)
© Scrivener Publishing LLC

polymers due to their excellent heat resistance and toughness; they were developed in the 1960s by Du Pont as materials for the aerospace industry. The most familiar polyimide is poly-*N,N'*-(oxydi-*p*-phenylene)pyromellitimide, which is synthesized from bis(4-aminophenyl) ether and pyromellitic dianhydride, and is widely known as Kapton (Figure 7.1) [1]. Polyimides are stable over a wide range of temperatures from very low temperatures to temperatures above 300°C, so they are suitable for severe space environments. Polyimides were originally developed for the aerospace industry, are now also used in airplanes and in machinery for various other industries, and are indispensable in the electronics industry as heat-resistant insulators suitable for soldering processes.

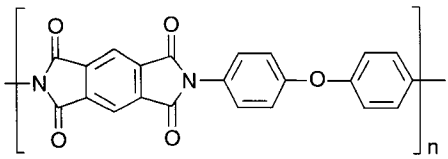

Figure 7.1 Kapton-type polyimide.

With the rapid development of electronics, devices such as semiconductors, displays and the computers, the characteristics demanded from the electronic parts progressed, and it became necessary for polyimides to have other characteristic properties, such as processability, low dielectric constants (ε), low water absorption (WA), low coefficients of thermal expansion (CTE), and high radiation resistance, as well as their excellent thermal stability and good mechanical properties. After the marketing of the Kapton-type polyimide, many other polyimides, such as biphenyl-type polyimides and polyimides with a connecting group (-X-) between the phthalimides, were developed (Figure 7.2) [2, 3]. More types of polyimides have been synthesized to investigate the relationship between their structures and these properties.

This chapter introduces the synthetic methods for polyimides and the relationship between their structures and properties. In order to show the remarkable effects of polyimide structures on their properties, the properties of polyimides from characteristic monomers are mainly described.

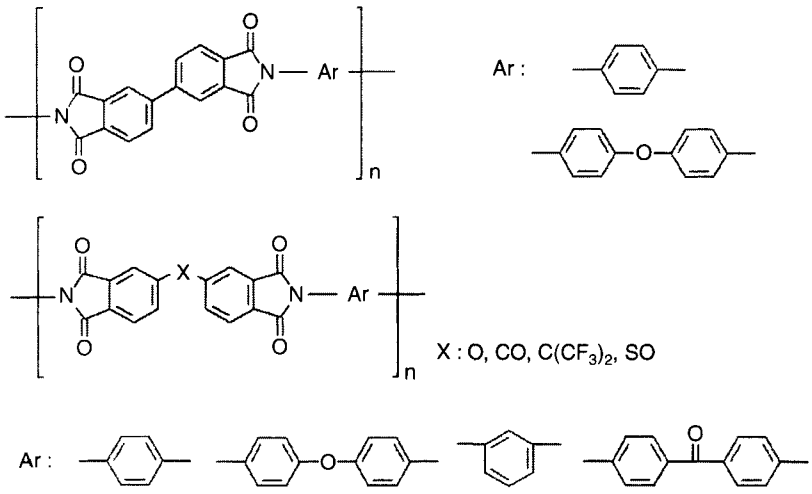

Figure 7.2 Biphenyl-type polyimides and polyimides with a connecting group (-X-) between the phthalimides.

7.2 Synthesis of Polyimides

Polyimides are synthesized by polycondensation of tetracarboxylic dianhydrides with diamines, and the synthetic procedure is roughly classified into three methods: a two-step procedure, a one-step procedure and a three-step procedure.

7.2.1 Two-step Procedure

Most polyimides are difficult to process because of their insolubility and high melting temperatures, so polyimides are synthesized by a two-step procedure via a soluble polyamic acid, precursor of the polyimide (Eq. 1) [4–6]. In the first step, ring-opening polyaddition of a diamine to a tetracarboxylic dianhydride is carried out in an amide type solvents, for example, *N*-methyl-2-pyrrolidinone (NMP) and *N,N'* -dimethylacetamide (DMAc), at room temperature, leading to formation of a polyamic acid solution. After processing from the polyamic acid solution, the thermal conversion of the polyamic acid to the polyimide is performed by heating a at about 300°C or by chemical treatment with a mixture of carboxylic dianhydride and tertiary amine in the second step [7].

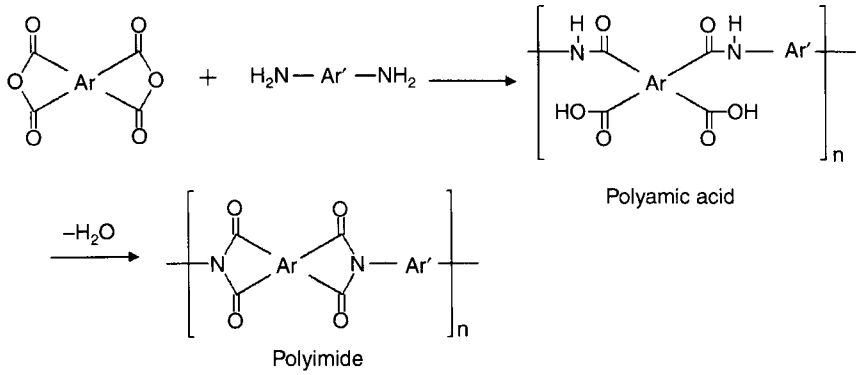

(1)

As solutions of polyamic acids are difficult to be store for long periods because of their low stability [8], procedures using derivatives of polyamic acids, such as polyamic acid alkyl esters [9, 10], polyamic acid trimethylsilyl esters [11, 12] and polyamic acid amides [13], have been investigated. Although the solutions of these derivatives are more stable than those of polyamic acids, synthesis of polyimides via these polyamic acid derivatives is not attractive for large-scale mass production and industrial applications because more steps are involved, and the cost is high.

Polymerization of polyamic acids derived from aliphatic diamines often suffers from strong salt formation or gelation in the initial reaction stage because the basicities of aliphatic diamines are much higher than those of aromatic diamines, and polymerization is prevented. Several methods, such as gradual addition of the aliphatic diamine to the dianhydride solution and dissociation of the formed salt by stirring for a long time, are used to avoid the salt formation [14–16]. Polyimides having low dielectric constants have been developed from aliphatic monomers.

7.2.2 One-step Procedure

Most polyimides are insoluble in organic solvents, but some are soluble. Soluble polyimides can be synthesized in one-step (Eq. 2) [17–22]. The polyimide solution is obtained by reacting a diamine with a tetracarboxylic dianhydride in a high boiling point solvents (phenolic solvent, for example, *m*-cresol) at 150–200°C. As the polyamic acid is formed and converted to the polyimide in solution, the water formed during imidation is removed as an azeotrope with toluene to obtain high molecular weight polyimide.

It was reported that the molecular weights of polyimides prepared in one-step procedure were higher than those of polyimides prepared in two-step procedure [21] and the polyimides prepared in one-step procedure showed higher strength than those prepared in two-step procedure [18], and the one-step procedure is thought to be more suitable for the synthesis of soluble polyimides. The solubility of some polyimides prepared by the one-step procedure was reported to be higher than that of polyimides prepared by two-step procedure in spite of the same structures [22]. Thermoplastic polyimides and polyimide adhesives are prepared by this method.

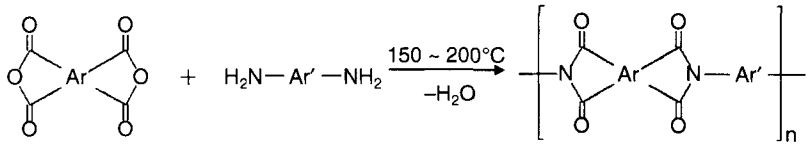

(2)

Soluble polyimides are also synthesized by using diisocyanates instead of diamines (Eq. 3) [23–25]. The polyimide solution is obtained by reacting a diisocyanate with a tetracarboxylic dianhydride in NMP or DMAc at 100–150°C. The soluble polyimide "PI-2080" (Figure 7.3) is produced by the one-step procedure using diisocyanate.

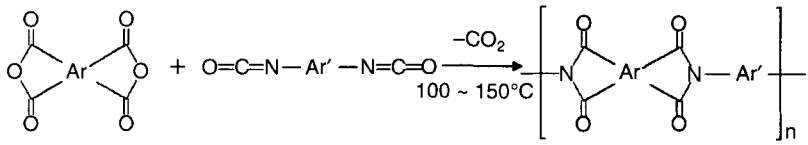

(3)

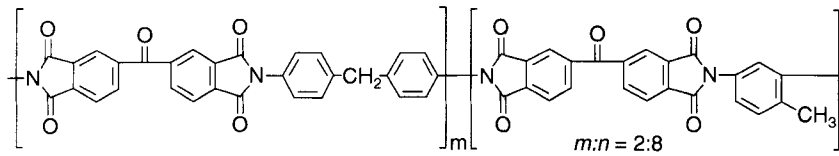

Figure 7.3 PI-2080.

Synthesis using tetracarboxylic dithioanhydrides [26, 27] instead of tetracarboxylic dianhydrides and the high-pressure synthesis from nylon-salt-type monomers composed of diamines and tetracarboxylic acids [28–32] have also been reported.

7.2.3 Three-step Procedure

Polyimides can be synthesized via a three-step procedure, the synthesis of a polyamic acid, conversion of the polyamic acid to a polyisoimide (a polyimide isomer), and conversion of the polyisoimide to the polyimide (Eq. 4) [33, 34]. The polyisoimide solution is obtained by addition of a dehydrating agent, for example, *N,N'*-dicyclohexylcarbodiimide, to the polyamic acid solution, and the conversion of the polyisoimide to the polyimide is performed at a lower temperature (about 200°C) than that used for conversion of polyamic acid to polyimide. As no water is formed in the conversion to the polyimide, the production is smooth. The thermosetting polyimide oligomer "Thermid PI-600" (Figure 7.4) [33] is prepared by the three-step procedure.

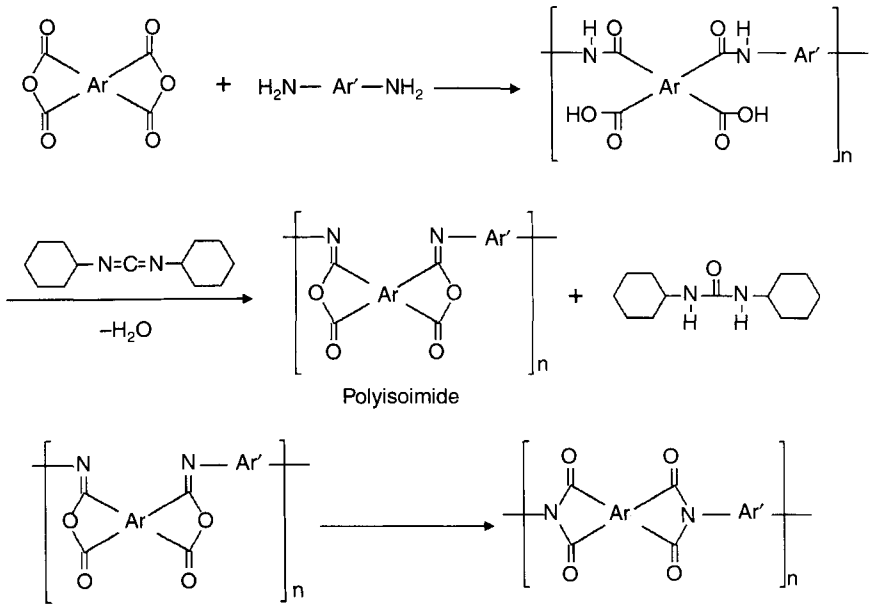

(4)

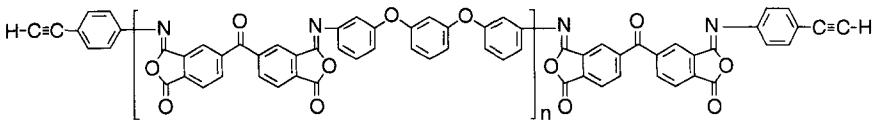

Figure 7.4 Thermid PI-600.

In spite of the instability of polyamic acid solutions, the two-step procedure via polyamic acid has been the most frequently used because of its high utility and the low cost.

7.3 Properties of Aromatic Polyimides

The relationship between the structures and properties of polyimides must be clarified in order to design the polyimides suitable for application of some fields. In this section, the properties of characteristic polyimides are introduced.

1. Kapton-type polyimide
2. Biphenyl-type polyimides and polyimides with a connecting group (-X-) between the phthalimides
3. Polyimides from characteristic monomers

   - Polyimides from isomeric biphenyltetracarboxylic dianhydrides
   - Polyimides from isomeric oxydiphthalic anhydride
   - Polyimides containing *p*-phenylene units, $-(C_6H_4)_m-$ (m = 2, 3, 4), between phthalimides
   - Polyimides containing ester linkages, $-COOC_6H_4OCO-$, between phthalimides
   - Polyimides containing ether linkages, -O-Ar-O- (Ar: Bulky moiety)

7.3.1 Kapton-type Polyimide

Kapton type polyimide, poly-*N*,*N*′-(oxydi-*p*-phenylene)pyromellitimide (Figure 7.1), has a high glass transition temperature (T_g) (400°C) because of the rigid the pyromellitimide structure and the large sweep volume (conformational change on rotation around ether linkages) [1]. The high T_g was also reported to be caused by strong intermolecular interactions, which originated in the charge transfer interaction between the electron-withdrawing part of pyromellitimide and the electron-donating part of diphenyl ether [35].

Kapton-type polyimide is thermally stable as a result of their high T_g, but the values of CTE, ε and WA are 47 ppm, 3.22 (10 GHz) and 2.5%, respectively, so they are not suitable for use in all fields of electronics [36, 37]. The polyimide is insoluble in organic solvents and unprocessable after conversion from polyamic acid.

When polyimide films are formed on a metal substrate via thermal imidation after the solution casting of a polyamic acid, polyimide/metal laminates undergo thermal stress arising from CTE mismatches (40–80 ppmK^{-1} for polyimides, and 17 ppm ppmK^{-1} for copper) during cooling from the imidation temperature to room temperature. Serious problems such as curling, cracking and detaching of polyimide films occur [36].

When polyimides are used in interlayer dielectronics, the signal propagation speed and wiring density in the semiconductor devices are dependent on the dielectric constant (ε) of the substrate [38].

Water absorbed in the polyimides corrodes the wiring and etch metal substrate [36].

7.3.2 Biphenyl-type Polyimides and Polyimides with a Connecting Group (-X-) between the Phthalimides

The *T*g of the polyimide prepared from 3,3′,4,4′-biphenyltetracarboxylic dianhydride (BPDA) is lower *T*g (306°C) due to an increase in the rotational bonds between the phthalimides as well as rotational bonds around the ether linkages. Polyimides with connecting groups (-X-: -O-, -CO-, -SO_2-, -$C(CF_3)_2$-) between phthalimides have much lower *T*g values because of the further increase in rotational bonds between phthalimides [3] . The bulk and rigidity of -X- have also influence the *T*g value of polyimides, and the *T*g value of polyimides where -X- is a long group, such -O-C_6H_4-$C(CF_3)_2$-C_6H_4-O- and -O-C_6H_4-CO-C_6H_4-O-, are much lower due to the further increase in rotational bonds in -X- (Table 7.1).

Although the *T*gs of these polyimides are lower than that of Kapton-type polyimide, some polyimides are soluble in organic solvents.

7.3.3 Polyimides from Characteristic Monomers

7.3.3.1 Polyimides from Isomeric Biphenyltetracarboxylic Dianhydrides

There are three isomers, 3,3′,4,4′-biphenyltetracarboxylic dianhydride (s-BPDA), 2,3,3′,4′-biphenyltetracarboxylic dianhydride (a-BPDA) and 2,2′,3,3′-biphenyltetracarboxylic dianhydride (i-BPDA) in biphenyltetracarboxylic dianhydride. Many polyimides

Table 7.1 Glass transition temperatures (Tg) of polyimides.

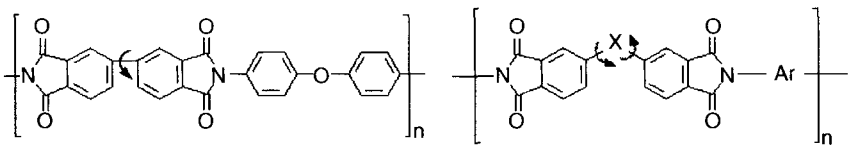

X/Ar	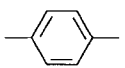	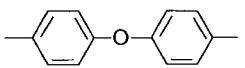	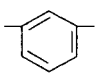	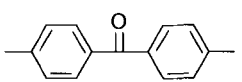
None	360	306		
O	342	270	313	280
CO	333	280	300	288
$C(CF_3)_2$	349	307	303	311
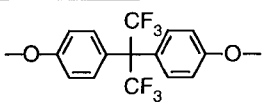	254	237	240	248
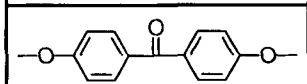	226	221	224	221

have been prepared from 3,3′,4,4′-biphenyltetracarboxylic dianhydride and various diamines. Polyimides have been prepared from s-BPDA, a-BPDA and i-BPDA, and their properties have been compared [39–41]. The syntheses of polyimides from these biphenyltetracarboxylic dianhydrides and various diamines were performed by the conventional two-step procedure using NMP as the solvent, and the polyimides were obtained by thermal imidation (150°C/1 h, 200°C/1 h, 350°C/1 h) (Eq. 5).

The solubility of these polyimides is shown in Table 7.2. PI-(s-BPDA/4,4′-ODA) was almost insoluble in any aprotic solvents,

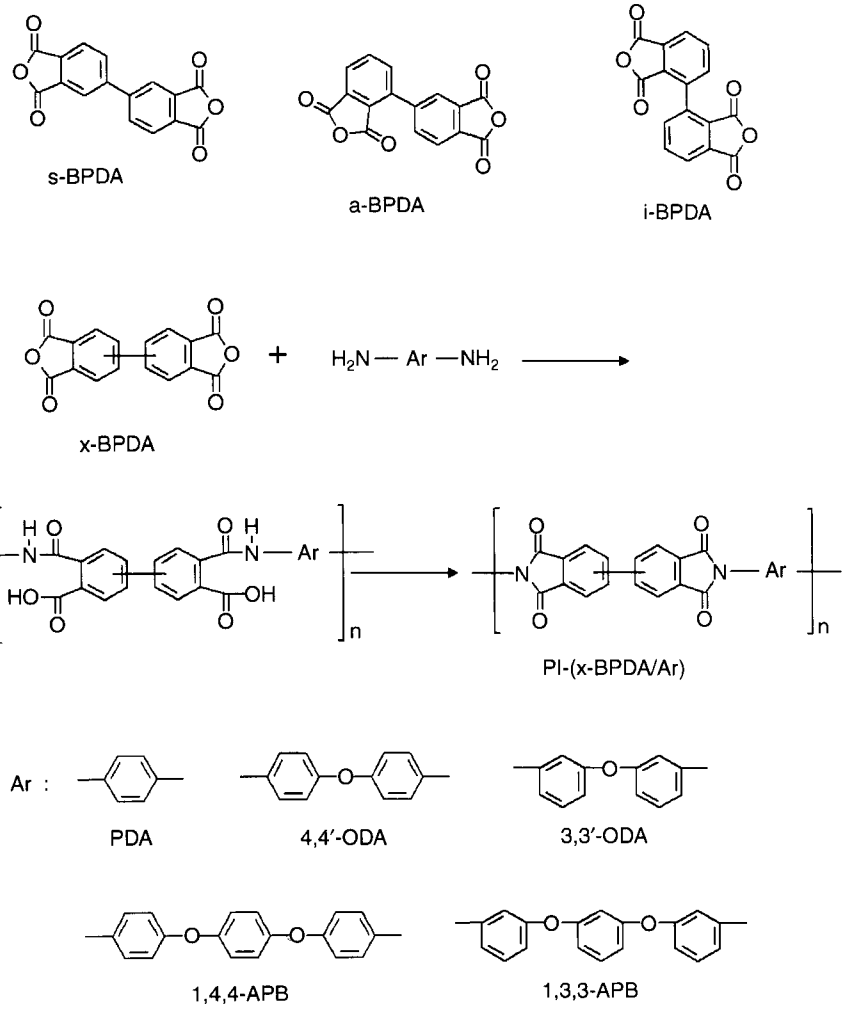

(5)

whereas PI-(a-BPDA/4,4'-ODA) was partially soluble in NMP. PI-(i-BPDA/4,4'-ODA) was soluble in NMP; the solubility in NMP was PI-s-BPDA<PI-a-BPDA< PI-i-BPDA.

Table 7.2 Solubility of polyimides from biphenyltetracarboxylic dianhydrides.

	NMP	DMAc	DMF	$CHCl_3$	MEK	Dioxane
PI-(s-BPDA/4,4'-ODA)	–	–	–	–	–	–
PI-(a-BPDA/4,4'-ODA)	±	–	–	–	–	–
PI-(i-BPDA/4,4'-ODA)	+	–	–	–	–	–
PI-(s-BPDA/3,3'-ODA)	±	–	–	–	–	–
PI-(a-BPDA/3,3'-ODA)	±	±	±	–	–	–
PI-(i-BPDA/3,3'-ODA)	+	+	±	±	–	–

+, soluble on heating; ±, partially soluble on heating; –, insoluble.

The *Tg* values of the prepared polyimides were determined from the inflection temperature of the storage modulus *E'*, measured by dynamic mechanical analysis (DMA). The *Tg* values moved towards higher temperature in the order of PI-s-BPDA < PI-a-BPDA < PI-i-BPDA; for example, *Tg* values of PI-(s-BPDA/4,4'-ODA), PI-(a-BPDA/4,4'-ODA) and PI-(i-BPDA/4,4'-ODA) from 4,4'-ODA were 262°C, 319°C and 330°C, respectively (Figure 7.5).

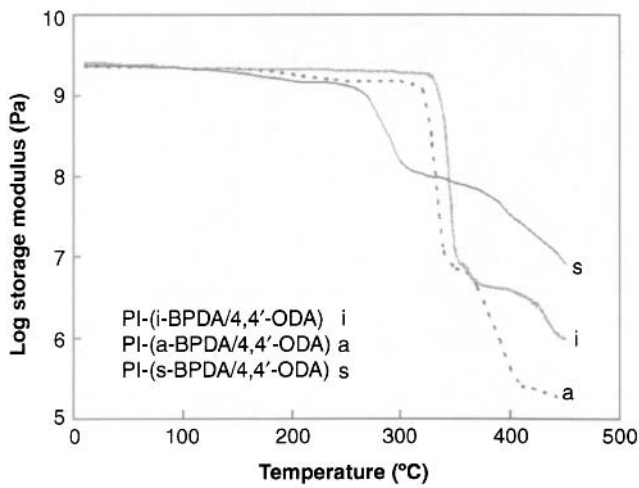

Figure 7.5 Temperature dependence of storage modulus for PI-(BPDA/4,4'-ODA).

This order of the *Tg* values is rationalized in terms of the steric restriction of internal rotation around the biphenyl linkages. The restriction of internal rotation around the biphenyl linkages increases in the order of s-BPDA< a-BPDA< i-BPDA. Table 7.3 shows the properties of polyimides from BPDA. In contrast to those of PI-(BPDA/4,4'-ODA), the *Tg* values of PI-(s-BPDA/3,3'-ODA), PI-(a-BPDA/3,3'-ODA) and PI-(i-BPDA/3,3'-ODA) from 3,3'-ODA were 243°C, 245°C and 246°C, respectively; those of PI-(BPDA/3,3'-ODA) were almost constant. The independence of the *Tg* is

Table 7.3 Thermal properties of polyimide from biphenyltetracarboxylic dianhydride.

	Tg (°C)[a]	T_5 (°C) (N_2)[b]	T_5 (°C) (Air)[b]	CTE[c] ($ppmK^{-1}$)
PI-(s-BPDA/PDA)	354	599	596	12
PI-(a-BPDA/PDA)	405	557	541	58
PI-(i-BPDA/PDA)	–	–	–	
PI-(s-BPDA/4,4'-ODA)	262	567	566	56
PI-(a-BPDA/4,4'-ODA)	319	545	538	62
PI-(i-BPDA/4,4'-ODA)	330	534	515	
PI-(s-BPDA/3,3'-ODA)	243	545	531	
PI-(a-BPDA/3,3'-ODA)	245	520	518	
PI-(i-BPDA/3,3'-ODA)	246	515	508	
PI-(s-BPDA/1,4,4-APB)	257	532	517	
PI-(a-BPDA/1,4,4-APB)	283	524	509	
PI-(i-BPDA/1,4,4-APB)	293	524	508	
PI-(s-BPDA/1,3,3-APB)	200	531	521	
PI-(a-BPDA/1,3,3-APB)	205	514	507	
PI-(i-BPDA/1,3,3-APB)	206	474	489	

[a]Measured by DMA.
[b]5% weight loss temperature.
[c]Measured by thermal mechanical analysis (TMA).
–not measured since the film was very brittle.

thought to be due to more easier internal rotation around the ether linkages in polyimides from 3,3'-ODA than that in polyimides from 4,4'-ODA.

The *Tg* values of the polyimides were discussed on the basis of the sweep volume (conformational changes in rotation of around the biphenyl linkages). The sweep volume of the PI(i-BPDA) is the largest, and that of the PI(s-BPDA) is the smallest among the three kinds of PIs. The decrease in E' at the *Tg* follows the order PI-(s-BPDA/4,4'-ODA) < PI-(a-BPDA/4,4'-ODA) < PI-(i-BPDA/4,4'-ODA), and this tendency is also interpreted in terns of the size of the sweep volume. The decrease in E' at the *Tg* of polyimides from PDA was smaller (Figure 7.6).

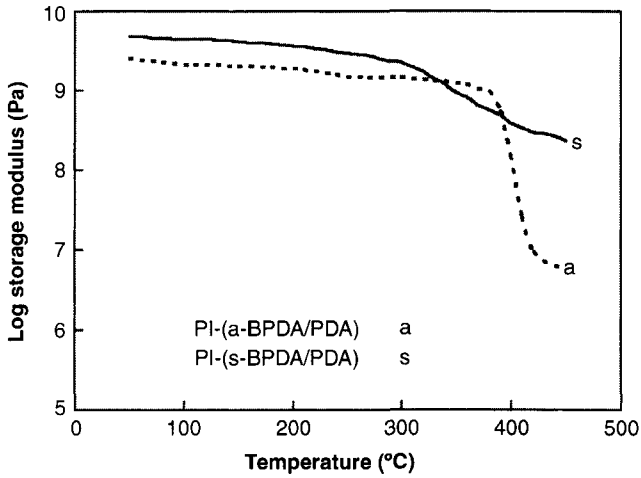

Figure 7.6 Temperature dependence of storage modulus for PI-(sBPDA/PDA) and PI-(aBPDA/PDA).

The CTE values for polyimides from PDA were lower than those of polyimides from 4,4'-ODA, and that of PI-(s-BPDA/PDA) (12 ppmK^{-1}) was lower than that of PI-(a-BPDA/PDA) (58 ppmK^{-1}), due to the rigid linear structure (Table 7.3). PI-(i-BPDA/PDA) was not obtained as a film.

7.3.3.2 *Polyimides from Isomeric Oxydiphthalic Anhydride*

Isomers of 3,3',4,4'-oxydiphthalic anhydride(3,3',4,4'-ODPA), i.e., 2,2',3,3'-oxydiphthalic anhydride (2,2',3,3'-ODPA) and 2,3,3',4'-oxydiphthalic anhydride (2,3,3',4'-ODPA) were synthesized. Polyimides were prepared from these dianhydrides, and their

properties were compared with those of polyimides prepared from 3,3',4,4'-oxydiphthalic anhydride [42, 43].

The polyimides from these dianhydrides and diamines, 4,4'-ODA and 1,4-bis(4aminophenoxy)benzene (1,4,4-APB), were synthesis by the two-step procedure in DMAc. The polyimides from 2,2',3,3'-ODPA were obtained by chemical imidation and the polyimides from 2,3,3',4'-ODPA and 3,3,4',4'-ODPA were obtained by thermal imidation (40°C/12 h, 80°C/1 h, 220°C/1 h, 300°C/0.5 h) (Eq. 6).

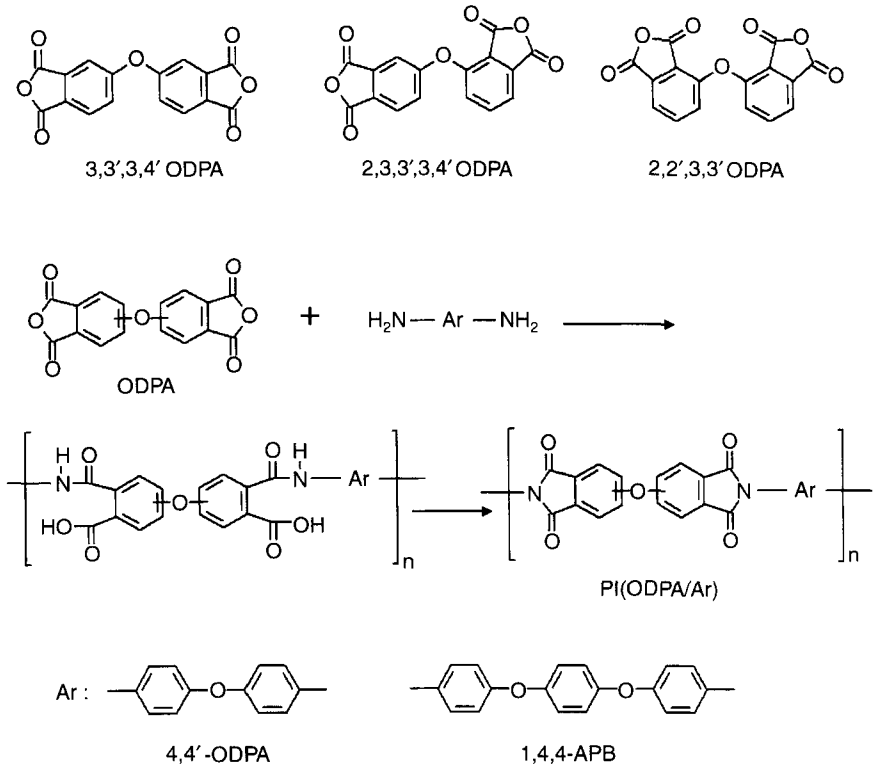

(6)

The solubility of these polyimides is shown in Table 7.4. The polyimides from 2,2',3,3'-ODPA and 2,3,3',4'-ODPA were soluble in phenols and polar aprotic solvents, and their solubility was higher than that of the polyimides from 3,3,4',4'-ODPA.

The thermal properties of these polyimides are shown in Table 7.5. The *Tg* values of these polyimides were determined by the peak temperatures in tanδ spectra (Figure 7.7) and differential scanning calorimetry (DSC).

Table 7.4 Solubility of polyimide from oxydiphthalic dianhydride.

	$CHCl_3$	THF	DMF	DMAc	DMSO	NMP	*m*-cresol	PCP[a]
PI-(2,2,3′,3′-ODPA/4,4′-ODA)	±	–	+	+	±	+	+	+
PI-(2,3,3′,4′-ODPA/4,4′-ODA)	+	–	+	+	±	+	+	+
PI-(3,3′,4,4′-ODPA/4,4′-ODA)	±	–	±	±	–	±	+	+
PI-(2,2,3′,3′-ODPA/1,4,4-APB)	+	–	+	+	±	+	+	+
PI-(2,3,3′,4′-ODPA/1,4,4-APB)	+	–	+	+	±	+	+	+
PI-(3,3′,4,4′-ODPA/1,4,4-APB)	–	–	–	–	–	–	±	+

+; fully soluble, ±; partially soluble, –; insoluble on heating.
[a]*p*-Chlorophenol.

Table 7.5 Thermal properties of polyimides from oxydiphthalic dianhydrides.

	Tg (°C)[a] (DMA)	*Tg* (°C)[b] (DSC)	T_5 (°C)[c] in air
PI-(2,2′,3,3′-ODPA/4,4′-ODA)	295	290	500
PI-(2,3,3′,4′-ODPA/4,4′-ODA)	282	272	505
PI-(3,3′,4,4′-ODPA/4,4′-ODA)	272	262	493
PI-(2,2′,3,3′-ODPA/1,4,4-APB)	263	253	493
PI-(2,3,3′,4′-ODPA/1,4,4-APB)	253	245	488
PI-(3,3′,4,4′-ODPA/1,4,4-APB)	245	238	477

[a]Measured by DMA.
[b]Measured by DSC.
[c]5% weight loss temperature.

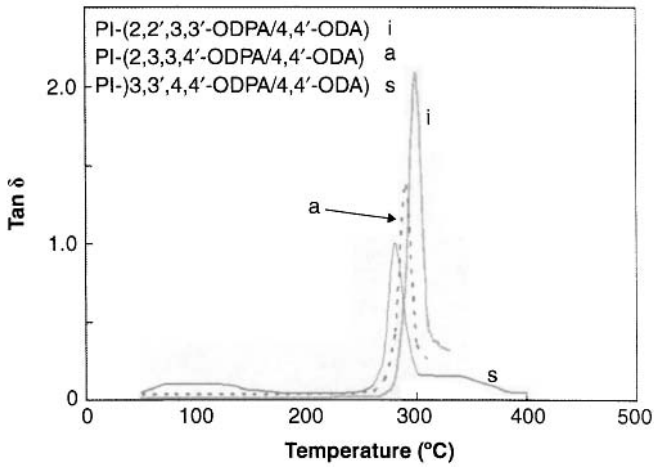

Figure 7.7 Tan δ curves of PI-(ODPA /4,4′-ODA).

The *Tg* values move towards higher temperatures in the order of PI(3,3,4′,4′-ODPA)< PI(2,3,3′,4′-ODPA)< PI(2,2′,3,3′-ODPA). This is rationalized in terms of restriction of internal rotation around the ether linkage between the phthalimides, as seen in the polyimides from BPDA. The rotation axes of the two aromatic rings of 2,2′,3,3′-ODPA are nearly perpendicular, and the rotation is strongly resisted. The polyimide structure is therefore nonlinear; nonlinear

molecular backbones make the molecular packing looser, but the rotation restriction effect is larger. The rotation restriction was explained by the existence of *cis-trans* isomers in 2,3,3′,4′-ODPA and 2,2′,3,3′-ODPA (Figure 7.8).

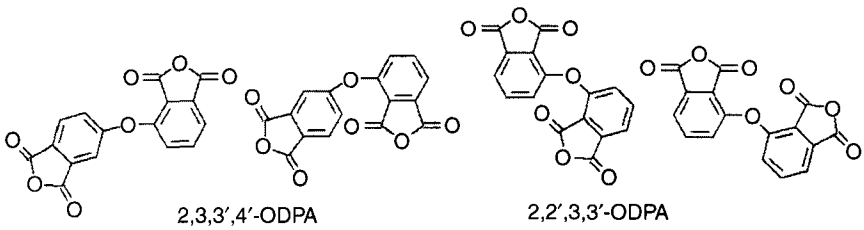

Figure 7.8 Cis-trans isomers in 2,3,3′,4′-ODPA and 2,2′,3,3′-ODPA.

The effect of rotation around the ether linkages on the *T*g value was observed in PI-[s-BPDA/bis(4-amino-2-biphenyl)ether] [44]. The *T*g value of PI-[s-BPDA/bis(4-amino-2-biphenyl)ether], which was determined by DSC, was 253°C; that is higher than that of PI-(s-BPDA/4,4′-ODA) (234°C). The higher *T*g value is explained by resistance to internal rotation around the ether linkages by phenyl groups at the 2,2′-positions of the diphenyl ether moiety (Figure 7.9).

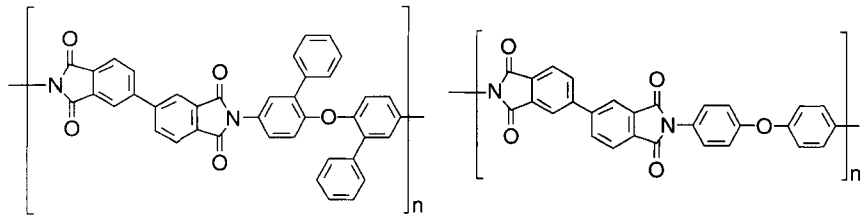

Figure 7.9 PI-[s-BPDA/bis(4-amino-2-biphenyl)ether] and PI-(s-BPDA/4,4-ODA).

The *T*g values of PI(2,3,3′,4′-ODPA/4,4′-ODA) and PI(2,2,3′,3′-ODPA/4,4′-ODA) were lower than those of the corresponding the polyimides from BPDA due to the presence of the ether bonds between the phthalimides.

The temperature dependence of the *E′* values for PI(ODPA/4,4′-ODA) is shown in Figure 7.10. The decrease in *E′* at the *T*g for

PI(3,3′,4′,4′-ODPA/4,4′-ODA) was the smallest, as shown in the polyimides from BPDA and E' was maintained at 10^7 Pa at 400°C as a result of crystallization. The E' values of PI(2,3,3′,4′-ODPA/4,4′-ODA) and PI(2,2,3′,3′-ODPA/4,4′-ODA) decreased drastically at the Tg, and showed high thermoplasticity. PI(2,3,3′,4′-ODPA/4,4′-ODA) could be prepared as thin film because of its high thermoplasticity [43, 45]. As the thin film maintained high strength even after molten adhesion, PI(2,3,3′,4′-ODPA/4,4′-ODA) was used with APICAL®AH (Kapton-type polyimide) as the thin film on the Small Solar Power Sail Demonstrator "IKAROS". Wholly aromatic polyimides without aliphatic moietes have electron-beam-resistant and proton-beam-resistant characteristics in space environments.

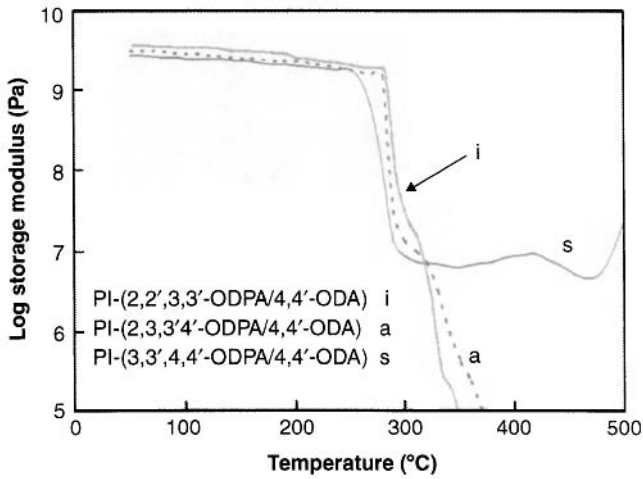

Figure 7.10 Temperature dependence of storage modulus for PI-(ODPA/4,4′-ODA).

7.3.3.3 *Polyimides Containing p-Phenylene Units, -(C_6H_4)m- (m = 2, 3, 4), between Phthalimides*

In polyimides containing a connecting group (-X-), for example, -C=O, -O-, -SO_2-, -$C(CF_3)_2$-, between phthalimides, the Tg values are affected by -X-. Polyimides containing *p*-phenylene units as the connecting group (-X-) were prepared, and the properties were discussed. Three kinds of dianhydride, 3,3‴,4,4‴-*p*-quaterphenyltetracalboxylic dianhydride (m = 2), 3,3⁗,4,4⁗-*p*-quinquephenyltetracalboxylic

dianhydride (m = 3) and 3,3''''',4,4''''-p-sexiphenyltetracalboxylic dianhydride (m = 4), were synthesized (Figure 7.11). The properties of polyimides from these dianhydrides were compared on the basis of the number (m) of p-phenylene units [46–50]. The structure of polyimides was thought to beome more rigid with increasing m.

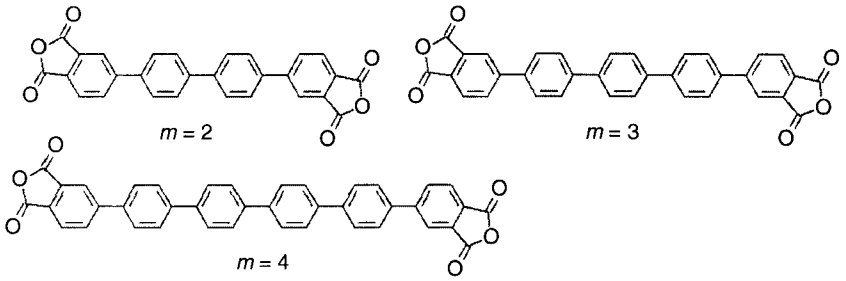

Figure 7.11 3,3''',4,4'''-p-Quaterphenyltetracalboxylic dianhydride (m = 2), 3,3''''',4,4'''''-p-quinquephenyltetracalboxylic dianhydride (m = 3) and 3,3''''',4,4''''''-p-sexiphenyltetracalboxylic dianhydride (m = 4).

The polyimides from these dianhydrides and various diamines were synthesized by the two-step procedure in NMP, and the polyimides were obtained by thermal imidation (100°C/1 h, 200°C/1 h, 300°C/1 h) (Eq. 7). The properties of polyimides from 4,4'-ODA and PDA were compared with those of polyimides from s-BPDA (m = 0) and 3,3'',4,4''-p-terphenyl tetracarboxylic dianhydride (m = 1) (Table 7.6).

The Tg values and 10% weight loss temperatures (T_{10}) corresponding to thermal stability increased slightly with increasing number m of phenylene units. The reason why the Tg values are hardly dependent on m can be explained in terms of the restriction of internal rotation around phenylene linkages and the sweep volume. In these polyimides, the restriction of internal rotation and the sweep volume are independent of m. The influence of m was observed in the temperature dependence of the E' (Figure 7.12). The decrease in E' at the Tg decreaseed with increasing m, and the degree for PI-4-4,4'-ODA was the smallest.

In DSC measurements, the polyimides showed exothermic peaks (Texo) above their Tgs. As the Texos were due to the formation of ordered structures, the E's of the polyimides increased on annealing at 350°C (Figure 7.13). The crystalline orders in annealed PI-2-4,4'-ODA and PI-3-4,4'-ODA could be detected by X-ray diffraction,

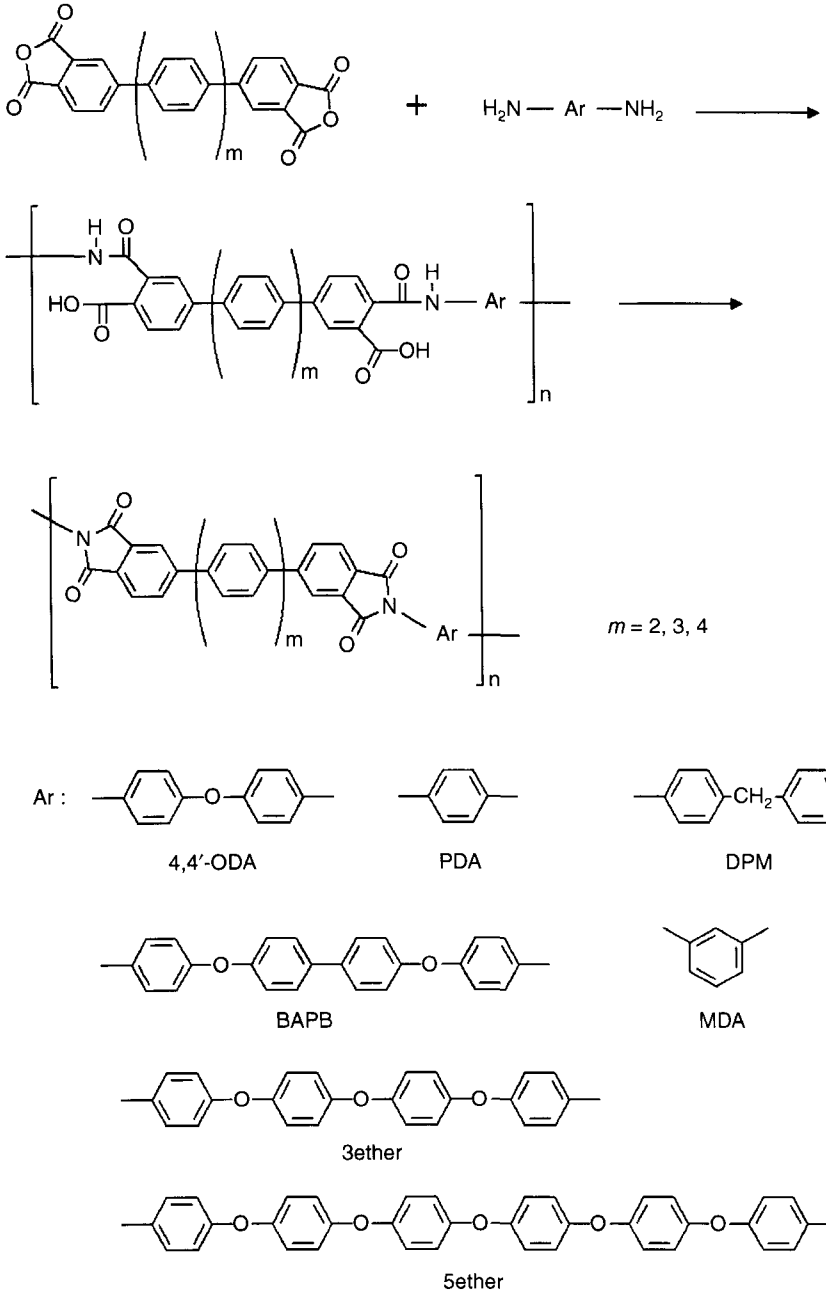

(7)

Table 7.6 Properties of polyimides from PI-*m*-4,4′-ODA and PI-*m*-PDA.

	Tg (°C)[a]	*Texo* (°C)[a]	*Tm* (°C)[a]	T_{10}(°C)[b] in N_2	T_{10} (°C) [b]in air	CTE[c] ($ppmK^{-1}$)	WA[d] (%)
PI-*0*-4,4′-ODA	234	275–304	–	565	558	56	1.3
PI-*1*-4,4′-ODA	232	265–303	–	570	545	43	1.0
PI-*2*-4,4′-ODA	236	275–297	415–456	638	585	25	0.9
PI-*3*-4,4′-ODA	243	326–341	–	635	575	7.7	0.6
PI-*4*-4,4′-ODA	244	377–421	–	640	585	3.1	0.4
PI-*0*-PDA	281	325–390	–	590	570	12	1.5
PI-*1*-PDA	278	360–470	–	592	568	3.0	1.1
PI-*2*-PDA	282	345–470	–	645	600	3.6	0.9
PI-*3*-PDA	263	332–371	–	637	565	3.0	0.7
PI-*4*-PDA	281	385–450	–	645	595		

[a]Measured by DSC.
[b]10% weight loss temperature.
[c]Measured by TMA.
[d]Water absorption.
–Not detected by DSC.

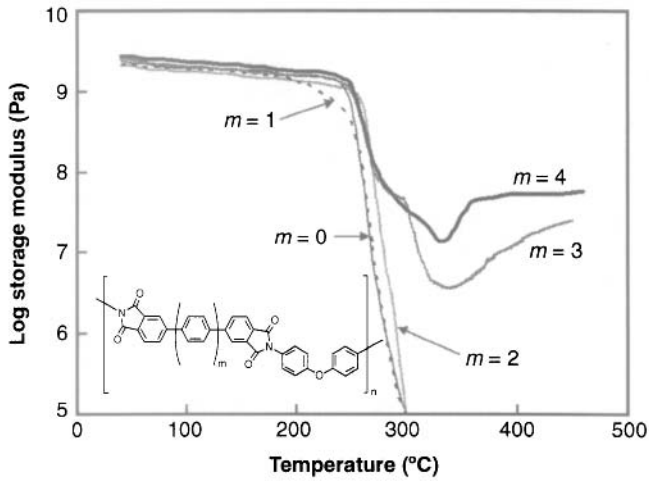

Figure 7.12 Temperature dependence of storage modulus for PI-*m*-4,4′-ODAs.

but that in annealed PI-4-4,4′-ODA could not be detected. As the imide content decreased with increasing m, the water absorptions decreased. The CTE values were also lower with increasing m, and that of PI-4-4,4′-ODA was 3.0 ppm K^{-1} in spite of the polyimide from 4,4′-ODA.

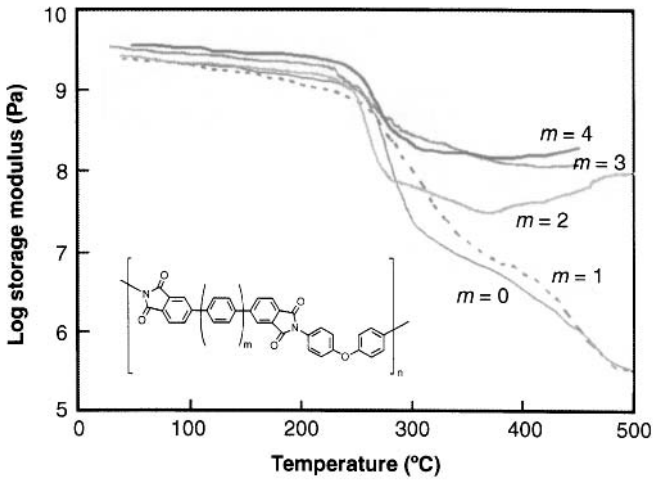

Figure 7.13 Temperature dependence of storage modulus for PI-m-4,4′-ODAs annealed at 350°C.

The Tg values of PI-m-PDAs were also hardly dependent on m, and were about 280°C. The p-phenylene unit content was very high in PI-4-PDA, and the Tg value was approximately equal to that for poly-p-phenylene. The decreases in E' for PI-m-PDAs decreased with increasing m as did those of PI-m-4,4′-ODA. The E' values were higher than those for PI-m-4,4′-ODA, the E' value of PI-3-PDA at 400°C was 10^9 Pa (Figure 7.14), and the E' values increased on annealing (Figure 7.15). PI-4-PDA was not obtained as a film.

The CTE values of PI-m-PDAs were lower than those of PI-m-4,4′-ODA, because of their rigid linear structures. This rigid linear structure is thought to be indispensable for the polyimides with low CTE [51, 52], and the CTE values decreased with increasing m in these polyimides (PI-m-4,4′-ODA and PI-m-PDA). However, the CTE values for polyimides have been reported to be dependent on the method for film preparation [53, 54]. For example, partially

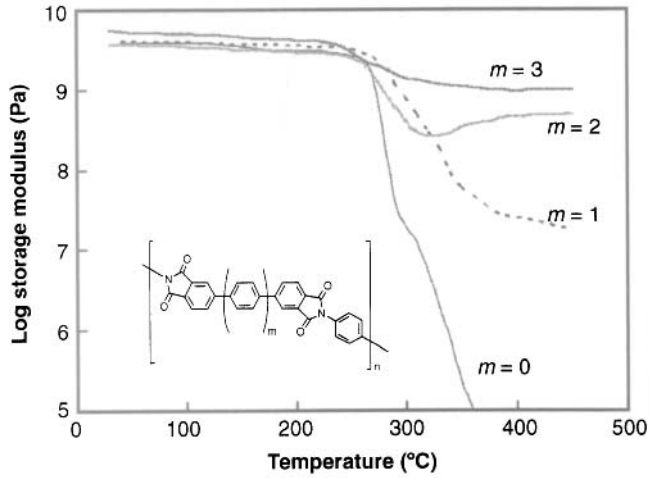

Figure 7.14 Temperature dependence of storage modulus for PI-*m*-PDAs.

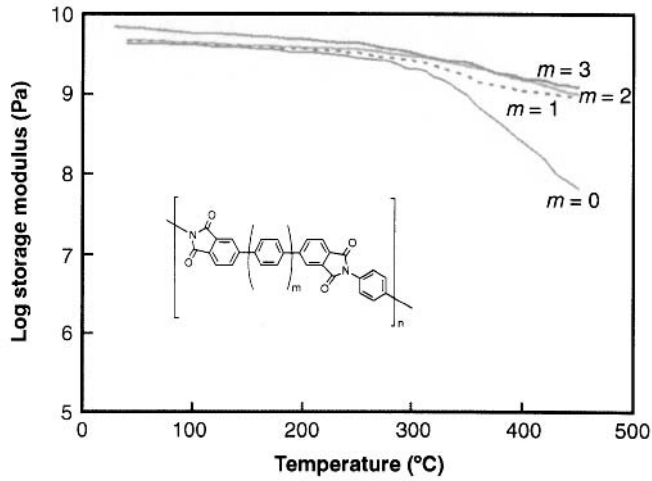

Figure 7.15 Temperature dependence of storage modulus for PI-*m*-PDA annealed at 350°C.

imidized polyamic acid prepared from diamino-BPDI formed an ordered liquid crystal structure in NMP solution, and a polyimide film with a CTE (3.5 ppmK^{-1}), which was the same structure as PI-0-PDA, was obtained from the ordered solution (Eq. 8) [54]. The imidation method was also reported to have great influences

on the CTE, and the degree of in-plain orientation of the chain axis on thermal imidation was reported to be an important factor [54].

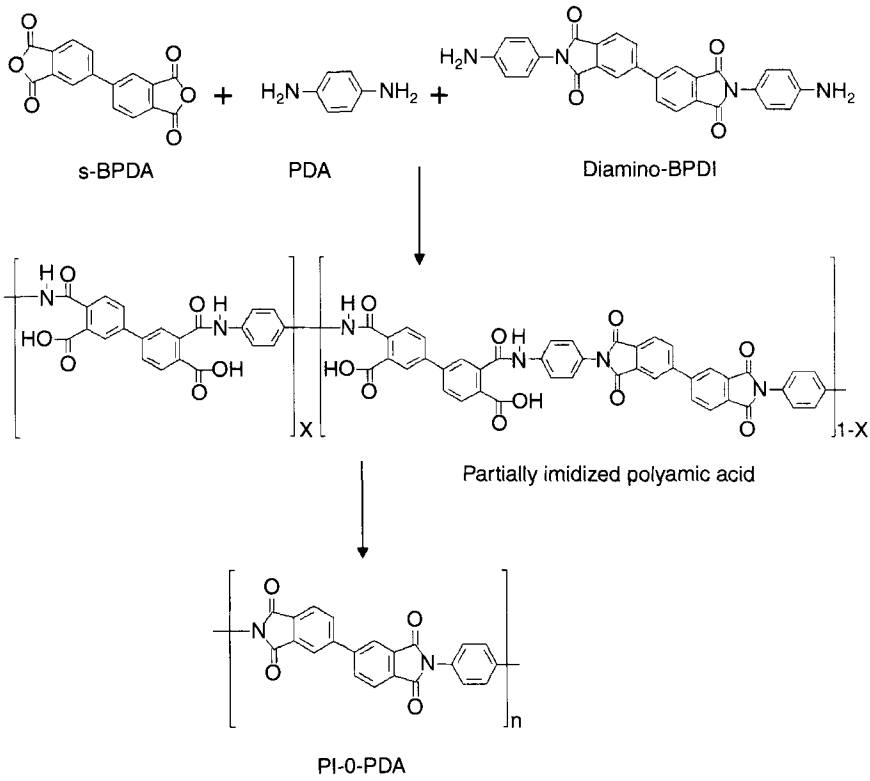

(8)

Almost all the polyimides from other diamines showed similar thermal properties. The *Tg* values were hardly dependent on *m* (Table 7.7). The decrements in *E'* at *Tg* decreases with increasing *m*, and *E'*s above the *Tg* increase on curing above *Tg*. The valves of the *E'* above the *Tg* for the polyimides were in order of PI-2-Ar < PI-3-Ar < PI-4-Ar.

Only the temperature dependence of *E'* for PI-*m*-3ether was differed [50]. Figure 7.16 displays the temperature dependence of *E'* for PI-*m*-3ether. The decrements in *E'* at the *Tg* were larger than those for PI-m-4,4'-ODA because of the three flexible rotational ether linkages; the decrements decreased with increasing *m* as observed in other polyimides (Figure 7.16). However, the *E'*s of PI-m-3ether

Table 7.7 Properties of polyimides from PI-*m*-Ar.

	Tg (°C)[a]	*Texo* (°C)[a]	*Tm* (°C)[a]	T_{10}(°C) [b] in N_2	T_{10} (°C) [b] in air	CTE[c] ($ppmK^{-1}$)
PI-2-DPM	252	300–322	420–462	600	570	
PI-3-DPM	260	326–363	–	605	560	
PI-4-DPM	244	330–385	–	637	580	
PI-2-MDA	253	277–328	417–458	625	585	
PI-3-MDA	260	345–453	–	610	570	
PI-4-MDA	237	335–380	385–425	600	590	
PI-2-BAPB	220	276–322	413–465	612	575	
PI-3-BAPB	233	–	–	610	550	
PI-4-BAPB	232	325–455	–	635	580	
PI-2-3ether	205	290–360	–	630	580	36.0(16.5)[d]
PI-3-3ether	206	380–405	405–435	631	582	34.8(15.0)[d]
PI-4-3ether	208	–	–	631	582	30.7(12.6)[d]
PI-2-5ether	180	–	390–405	628	581	69.1(38.0)[d]
PI-3-5ether	182	–	390–408	630	582	49.3(48.7)[d]
PI-4-5ether	182	–	390–430	632	584	34(31.6)[d]

[a]Measured by DSC.
[b]10% weight loss temperature.
[c]Measured by TMA.
[d]CTE value of polyimide films cured at 350°C.
–Not detected by DSC.

increased greatly on annealing above the *Tg*s and the order of the *E′* values above the *Tg* is PI-4-3ether < PI-3-3ether < PI-2-3ether (Figure 7.17). The high *E′* values of annealed PI-*m*-3ether were due to the formation of highly ordered structures (formation of a crystalline structure), and the degree of crystallization for PI-2-3ether was thought to be the highest.

The CTE values of PI-*m*-3ether were not higher than those of PI-*m*-4,4′-ODA due to the more flexible rotational ether linkages, but the values decreased with increasing *m*. The values were drastically lowered by annealing, and crystallization had a great influence on CTE.

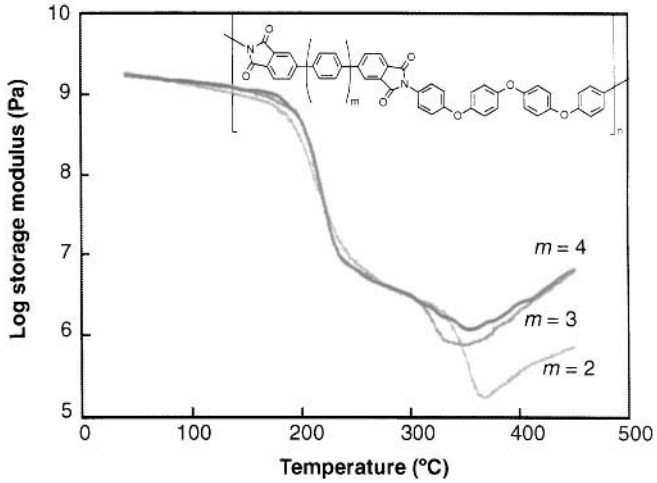

Figure 7.16 Temperature dependence of storage modulus for PI-m-3ether.

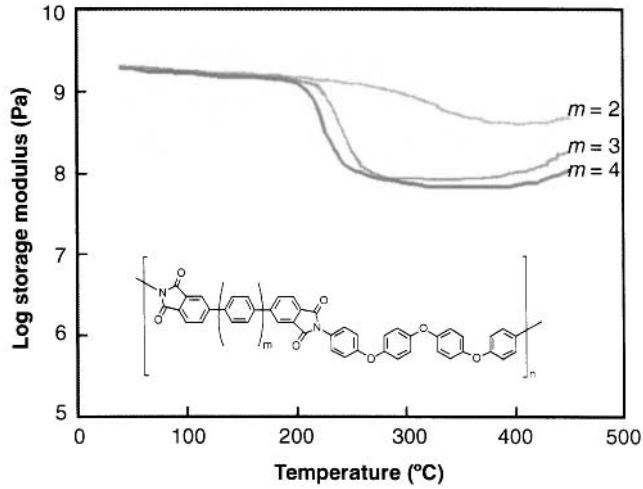

Figure 7.17 Temperature dependence of storage modulus for PI-m-3ether annealed at 350°C.

7.3.3.4 *Polyimides Containing Ester Linkages, -COOC$_6$H$_4$OCO-, between Phthalimides*

The extent of water absorption is about 2.5% for Kapton-type polyimide, and 0.4% for poly (ethylene terephthalate). As the ester

linkages do not contribute to water absorption in comparison with the contribution of imide groups, polyimides with ester linkages as the connecting group (-X-) were designed. Bis(trimellitic acid anhydride)phenyl ester (TAHQ) was synthesized, and polyimides were prepared from this dianhydride and various diamines by the two-step procedure in DMAc or NMP (Eq. 9) [36, 55, 56]. The polyimides were obtained by thermal imidation (PPD and TFMB: 250°C/2 h + 350°C/1 h, CHDA: 250°C/2 h + 300°C/1h + 350°C/1 h, 4,4'ODA; 250°C/2 h + 300°C/1 h). PDA, TFMB, and CHDA were used as the diamines to prepare polyimides with low CTE values as well as low water absorption. For a comparison, 4,4'-ODA was also used.

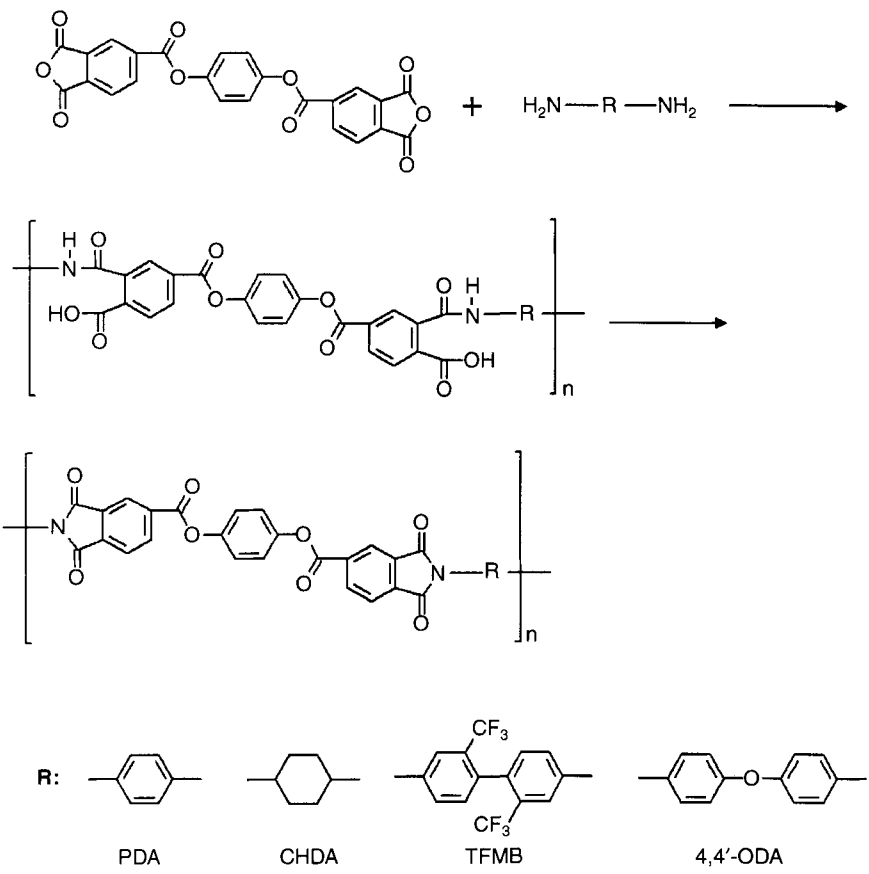

(9)

The properties of the polyimides from TAHQ are summarized in Table 7.8. These polyimides exhibited low CTEs, and the value for PI-TAHQ-PDA was 3.2 ppm K^{-1}. In contrast, the value for PI-TAHQ-4,4'-ODA was high (51.2 ppmK^{-1}).

Table 7.8 Properties of polyimides from PI-(TAHQ/Ar).

	Tg (°C)[a]	T_5 (°C)[b] in N_2	T_5 (°C)[b] in air	ε cal	WA[c] (%)	CTE[d] (ppmK^{-1})
PI-(TAHQ/PDA)	–	481	463	3.22	1.6	3.2
PI-(TAHQ/CHDA)	360	471	428	3.04	1.2	12.7
PI-(TAHQ/TFMB)	–	487	479	2.99	0.7	31.5
PI-(TAHQ/4,4'-ODA)	320	462	433	3.16	0.6	51.2

[a]Measured by DMA.
[b]5% weight loss temperature.
[c]Water absorption.
[d]CTE value of polyimide films cured at 350°C.
–Not detected by DMA.

A *Tg* of only PI-(TAHQ-4,4'-ODA) was observed at 320°C, and the value was much higher than that (245°C) of the corresponding ether-linked PI-(HQDA-4,4'ODA) from hydroquinone diphthalic anhydride. The high *Tg* was explained by suppression of internal rotation around the ester linkages (Figure 7.18).

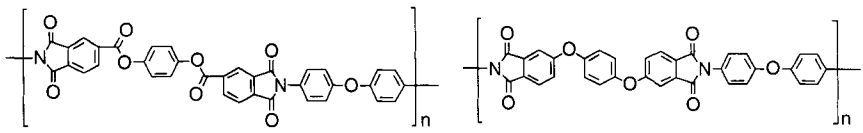

Figure 7.18 PI-(TAHQ-4,4'-ODA) and PI-(HQDA-4,4'ODA).

All the polyimides showed lower water absorptions as a result of introduction of ester linkages, and the value of even PI-(TAHQ-PDA) (the highest imide content) was 1.6%.

The 5% weight loss temperature showed that the thermal stabilities were relatively high in spite of the introduction of ester linkages, and the polyimides displayed low water absorption values and high thermal stabilities.

Polyimides were also synthesized from an ester-containig diamine, 4-aminophenyl-4-aminobenzoate (APAB) (Eq. 10).

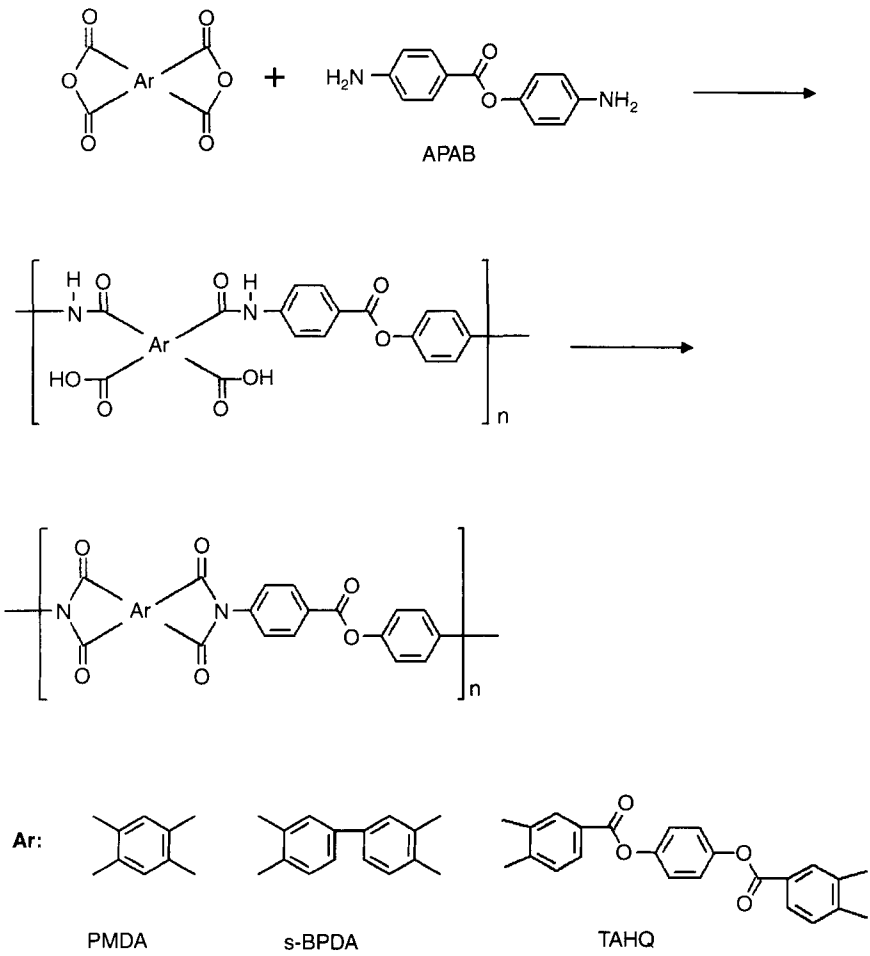

(10)

The properties of the polyimides from APAB are summarized in Table 7.9. Like the polyimides from TAHQ, these polyimides showed low water absorption, and the CTE values were lower than those of the polyimides from TAHQ. The low CTE values were explained by the imidation-induced in-plane orientation induced by the *p*-aromatic ester linkage.

For comparison, polyimides were synthesized from an amide-containing diamine, 4,4'-diaminobenzanilide (DABA) (Eq. 11).

Table 7.9 Properties of the polyimides from APAB.

	Tg (°C)[a]	T_5 (°C)[b] in N_2	T_5 (°C)[b] in air	ε cal	WA[c] (%)	CTE[d] ($ppmK^{-1}$)
PI-(PMDA/APAB)	–	531	501	3.29	1.6	2.0
PI-(s-BPDA/APAB)	–	534	525	3.28	0.7	3.4
PI-(TAHQ/APAB)	–	471	452	3.26	0.7	3.3

[a]Measured by DMA.
[b]5% weight loss temperature.
[c]Water absorption.
[d]CTE value of polyimide films cured at 350°C.
–Not detected by DMA.

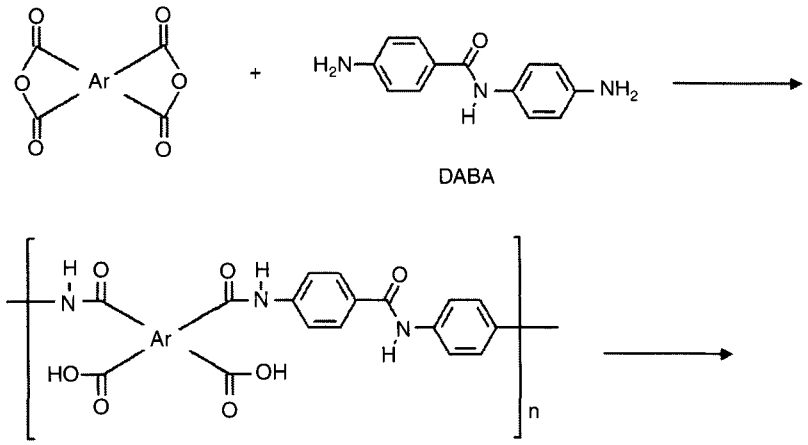

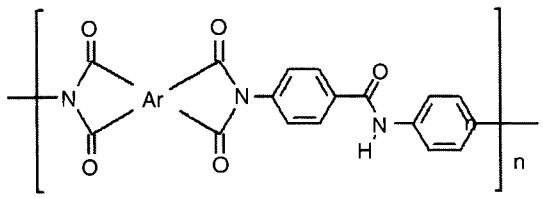

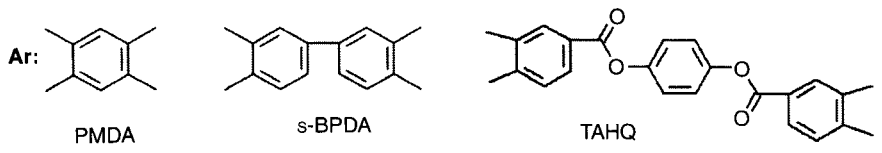

(11)

The properties of polyimides from DABA are summarized in Table 7.10. The CTE values were lower than those of polyimides from APAB, and the polyimides from PMDA and s-BPDA showed extremely low CTE values. However, the water absorptions of polyimides from DABA were higher than those of polyimides from APAB as the amide group is hydrophilic.

Table 7.10 Properties of the polyimides from DABA.

	Tg (°C)[a]	T_5 (°C[b] in N_2	T_5 (°C)[b] in air	ε cal	WA[c] (%)	CTE[d] ($ppmK^{-1}$)
PI-(PMDA/DABA)	–	522	489	3.17	3.4	0.2
PI-(s-BPDA/DABA)	–	540	507	3.28	2.3	1.6
PI-(TAHQ/DABA)	–	480	470	3.27	2.1	6.0

[a]Measured by DMA.
[b]5% weight loss temperature.
[c]Water absorption.
[d]CTE value of polyimide films cured at 350°C.
–Not detected by DMA.

Polyimides with longer ester linkages as connecting groups (-X-) were also prepared, and their properties were investigated (Table 7.11) [56]. The water absorptions of all the polyimides were lower than those of PI-TAHQ because of the higher ester content. The CTE values for polyimide films from PDA were low, but the films were not flexible. Copolyimides which had the flexibility, without increasing the CTE, were prepared by copolymerization with 4,4'-ODA.

The dielectric constants of polyimides with ester linkages were not so lower than those of polyimides without ester linkage. This may be due to the presence of polar ester carbonyl groups.

7.3.3.5 *Polyimides Containing Ether Linkages, -O-Ar-O- (Ar: Bulky Moiety)*

Polyimides with ether linkage (-O-Ar-O-) as connecting groups (-X-) between the phthalimides were prepared, and their properties were investigated. As the content of polar imide groups decreased as a result of the introduction of ether linkages, the values of ε for the polyimides became low. For example, ε (3.02) of PI-(HQDA-4,4'ODA) (-Ar-:-pC_6H_4-) was lower than that (3.50) of PI-(s-BPDA/4,4'-ODA) (-Ar-: None) [37]. However, *Tg* (245°C)

Table 7.11 Properties of ester containing polyimides.

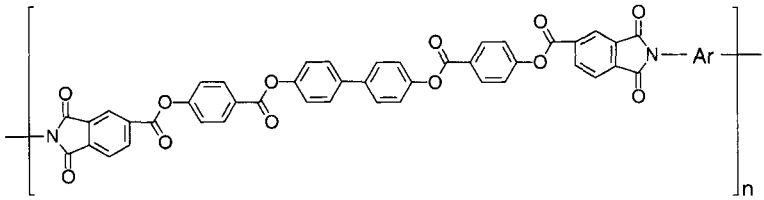

-Ar-	*Tg* (°C)[a]	T_5 (°C)[b] in air	ε[b](%)	WA[c] (%)	CTE[d] ($ppmK^{-1}$)
PDA	359	459	6.5	0.43	−5.0
4,4′-ODA	331	479	42.9	0.35	37.6
PDA(75) + 4,4′-ODA(25)	361	474	23.1	0.47	2.2

[a] Measured by DMA.
[b] 5% weight loss temperature.
[c] Water absorption.
[d] CTE value of polyimide films cured at 350°C.

of PI-(HQDA-4,4′ODA) was much lower, as internal rotation of the ether bond is not suppressed [36].

If the -Ar- is a bulky moiety, rotation is suppressed, as described in section 7.3.3.1 and 7.3.3.2, and the *Tg* of the polyimide is not significantly lower than that of PI-s-BPDA/4,4′-ODA (306°C). Polyimides with bulky fluorene moieties as -Ar- have been developed [36, 57].

Four kinds of polyimides with low ε (2.60–2.80) were prepared from 9,9-bis[(3,4-dicarboxyphenoxy)phenyl]fluorene derivatives, FLDA1 and FLDA2, and 9,9-bis[(4-(amino-phenoxy)phenyl)fluorine derivatives, DAFL1 and DAFL2 (Figure 7.19), by the two-step procedure using *N,N*-dimethylformamide as a solvent. The polyimides were obtained by thermal imidation (80°C/20 min, 140°C/20 min, 200°C/20 min, 250°C/20 min, 300°C/20 min).

The *Tg*s (253–284°C) of these polyimides were higher than that of PI-(HQDA-4,4′ODA) (Table 7.12). As aromatic bulky fluorene moieties combined short aromatic π–conjugation with a cardo structure, the ε values of the polyimides were lower without decreasing thermal stability. Asymmetric bulky groups such as fluorene disturb the chain packing and enhance the free volume in the polyimides. However, as internal rotation of the ether bonds is suppressed, the thermal stability of the polyimides does not decrease greatly.

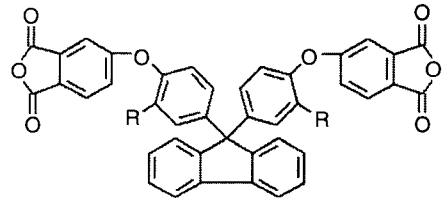

FLDAI (R:H), FLDA2(R:-C_6H_5)

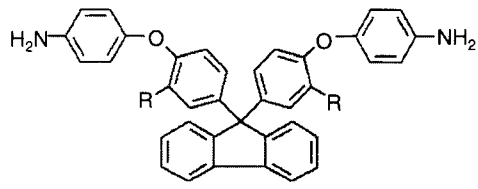

DAFLI (R:H), DAFL2(R:-C_6H_5), DAFL3(R: -CF_3)

Figure 7.19 Fluorene containing dianhydrides and diamines.

Table 7.12 Properties of the polyimides from FLDA1, FLDA2, DAFL1 and DAFL2.

Diamine	Dianhydride	*Tg* (°C)[a]	T_5 (°C)[b] in N_2	ε[c]
DAFL1 (R:H)	FLDA1 (R:H)	284	542	2.80
DAFL1 (R:H)	FLDA2 (R:-C_6H_5)	266	525	2.77
DAFL2 (R:-C_6H_5)	FLDA1 (R:H)	263	558	2.61
DAFL2 (R:-C_6H_5)	FLDA2 (R:-C_6H_5)	253	554	2.61

[a]Measured by DMA.
[b]5% weight loss temperature.
[c]Measured with a LCR meter at 1MHz with parallel plate.

The diamines, DAFL1 and DAFL2 were reacted with PMDA, s-BPDA, 3,3′,4,4′-ODPA and 4,4′-(hexafluoroisopropylidene)diphthalic anhydrtde (6FDA), and polyimides with low ε values were also prepared without decreasing their thermal stability (Table 7.13).

Polyimides with low ε values were prepared by introducing of fluorine as fluorine substitution lowered the electron polarization and close packing of the polyimide. The ε values of polyimides with trifluoromethyl groups along with fluorene moieties were lower (2.51–2.69), and the effects of fluorine atoms on the dielectric constant were also observed in the polyimides containing fluorene (Table 7.13).

Table 7.13 Properties of the polyimides from DAFL1, DAFL2 and DAFL3.

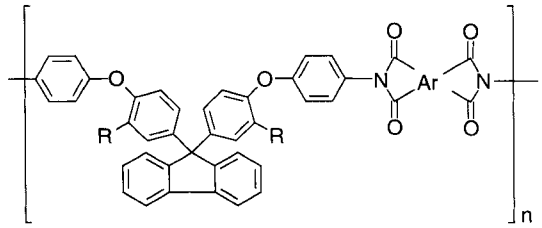

Diamine	Dianhydride	Tg (°C)[a]	T_5 (°C)[b] in N_2	ε[c]
DAFL1 (R:H)	PMDA	358	546	2.91
DAFL1 (R:H)	s-BPDA	302	567	2.95
DAFL1 (R:H)	3,3',4,4'-ODPA	293	540	2.93
DAFL1 (R:H)	6FDA	293	534	2.65
DAFL2 (R:-C_6H_5)	PMDA	293	544	2.82
DAFL2 (R:-C_6H_5)	s-BPDA	272	543	2.86
DAFL2 (R:-C_6H_5)	3,3',4,4'-ODPA	253	539	2.80
DAFL2 (R:-C_6H_5)	6FDA	268	539	2.65
DAFL3 (R:-CF_3)	PMDA	307	460	2.62
DAFL3 (R:-CF_3)	6FDA	281	454	2.51

[a]Measured by DMA.
[b]5% weight loss temperature.
[c]Measured with a LCR meter at 1 MHz with parallel plate.

As the introduction of asymmetric bulky groups was the method to improve the solubility of the polyimides, soluble polyimides with norbornene [58], phenylphthalide [59], and adamantine moieties [60] were prepared (Figure 7.20).

7.4 Conclusions

Polyimides are known as reliable high temperature polymers with superior mechanical and electrical properties. Polyimides can be easily prepared by reactions between dianhydrides and diamines, and many types of polyimides have been prepared by structural modification of the monomers to obtain the polyimides having desirable

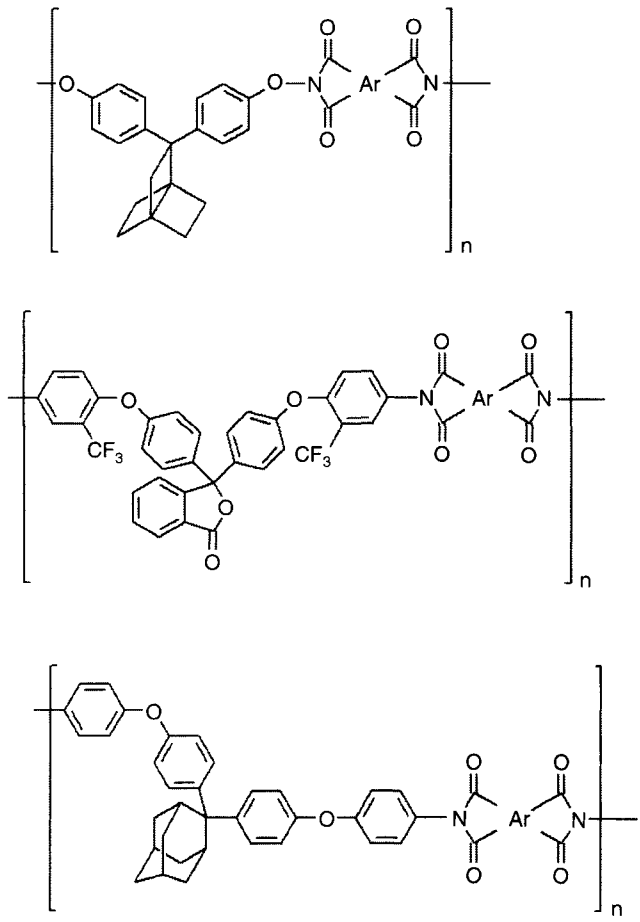

Figure 7.20 The polyimides with norbornebe, phenylphthalide, and adamantine moiety.

properties. This chapter introduced the synthetic methods for polyimides and the relationship between their structures and properties. The properties of polyimides are affected by internal rotation around bond in molecules, sweep volume, free volume, molecular packing, and molecular ordering. These factors are mainly dependent on the structure of polyimides, but also on the preparation condition. In particular, the molecular packing and the molecular ordering of some polyimides were reported to be extremely dependent on the preparation condition (preparation procedure, imidation conditions, annealing conditions and film thickness, etc). In future, high performance

polyimides are expected to be developed on the basis of knowledge about the effect of the structures and the preparation conditions on properties, taking into consideration the polyimide characteristic, the cost, the convenience of operation and the environment.

7.5 References

1. C.E. Sroog, A.L. Endrey, S.V. Abramo, C.E. Berr, W.M. Edward, and K.L. Olivier, *Journal of Polymer Science, Part A*, Vol. 3, p. 1373, 1965.
2. W.R. Shiang, and P.E. Woo, *Journal of Polymer Science, Polymer Chemistry Edition*, Vol. 31, p. 2081, 1993.
3. S.-S.A. Pavlova, G.I. Timofeeva, and I.A. Ronova, *Journal of Polymer Science, Polymer Physics Edition*, Vol. 18, p. 1175, 1980.
4. C.E. Sroog, *Journal of Polymer Science, Macromolecular Reviews*, Vol. 11, p. 161, 1976.
5. C.E. Sroog, *Progress in Polymer Science*, Vol. 16, p. 561, 1991.
6. W. Volksen, *Advances in Polymer Science*, Vol. 117, p. 111, 1994.
7. V.L. Bell, B.L. Stump, and H. Gager, *Journal of Polymer Science, Part A*, Vol. 14, p. 2275, 1976.
8. G.M. Bower, and L.W. Frost, *Journal of Polymer Science, Part A*, Vol. 1, p. 3135, 1963.
9. W. Huang, Y. Tong, J. Xu, and M. Ding, *Journal of Polymer Science, Part A*, Vol. 35, p. 143, 1997.
10. F.M. Houlihan, B.J. Bachman, C.W. Wilkins Jr., and C.A. Pryde, *Macromolecules*, Vol. 22, p. 4477, 1989.
11. Y. Oishi, M. Kakimoto, and Y. Imai, *Macromolecules*, Vol. 24, p. 547, 1991.
12. Y. Oishi, and Y. Imai, *Progress in Polymer Science*, Vol. 14, p. 173, 1989.
13. Y. Imai, M. Ueda, and T. Takahashi, *Journal of Polymer Science, Part A*, Vol. 14, p. 2391, 1976.
14. M. Hasegawa, *High Performance Polymers*, Vol. 13, p. S93, 2001.
15. T. Matsumoto, *Macromolecules*, Vol. 32, p. 4933, 1999.
16. H. Seino, A. Mochizuki, and M. Ueda, *Journal of Polymer Science, Part A*, Vol. 37, p. 3584, 1999.
17. C.A. Arnold, J.D. Summers, Y.P. Chen, R.H. Bott, D. Chen, and J.E. McGrath, *Polymer*, Vol. 30, p. 986, 1989.
18. H. Inoue, Y. Sasaki, and T. Ogawa, *Journal of Applied Polymer Science*, Vol. 60, p. 123, 1996.
19. T. Kaneda, T. Katsura, K. Nakagawa, and H. Makino, *Journal of Applied Polymer Science*, Vol. 32, p. 3157, 1986.
20. Z. Shi, M. Hasegawa, Y. Shindo, R. Yokota, F. He, H. Yamaguchi, and H. Ozawa, *High Performance Polymers*, Vol. 12, p. 377, 2000.
21. F.W. Harris, and S.L.–C. Hsu, *High Performance Polymers*, Vol. 1, p. 3, 1989.
22. A. Morikawa, T. Furukawa, and Y. Moriyama, *High Performance Polymers*, Vol. 18, p. 593, 2006.
23. P.S. Carleton, W.J. Farrissey, Jr., and J.S. Rose, *Journal of Applied Polymer Science*, Vol. 16, p. 2983, 1972.

24. N.D. Ghatge, and U.P. Mulik, *Journal of Polymer Science, Part A*, Vol. 18, p. 1905, 1975.
25. M. Kakimoto, R. Akiyama, Y.S. Negi, and Y. Imai, *Journal of Polymer Science, Part A*, Vol. 26, p. 99, 1988.
26. Y. Imai, and K. Kojima, *Journal of Polymer Science, Part A-1*, Vol. 10, p. 2091, 1972.
27. Y. Oishi, M. Ishida, M. Kakimoto, Y. Imai, and T. Kurosaki, *Journal of Polymer Science, Part A*, Vol. 30, p. 1027, 1992.
28. Y. Imai, T. Fueki, T. Inoue, and M.-A. Kakimoto, *Journal of Polymer Science, Part A*, Vol. 36, p. 1341, 1998.
29. Y. Imai, H. Nemoto, and M.-A. Kakimoto, *Journal of Polymer Science, Part A*, Vol. 34, p. 701, 1996.
30. T. Inoue, Y. Kumagai, M.-A. Kakimoto, Y. Imai, and J. Watanabe, *Macromolecules*, Vol. 30, p. 1921, 1997.
31. K. Itoya, Y. Kumagai, M. Kakimoto, and Y. Imai, *Macromolecules*, Vol. 27, p. 4101, 1994.
32. Y. Imai, T. Fueki, T. Inoue, and M.-A. Kakimoto, *Journal of Polymer Science, Part A*, Vol. 36, p. 1031, 1998.
33. J.S. Wallace, L. Tan, and F.E. Arnold, *Polymer*, Vol. 31, p. 2411, 1990.
34. A. Mochizuki, T. Teranishi, and M. Ueda, *Polymer Journal*, Vol. 32, p. 315, 1994.
35. M. Hasegawa, and K. Horie, *Progress in Polymer Science*, Vol. 26, p. 259, 2001.
36. M. Hasegawa, and K. Koseki, *High Performance Polymers*, Vol. 18, p. 697, 2006.
37. J.O. Simpson, A.K. St.Clair, *Thin Solid Films*, Vol. 308–309, p. 480, 1997.
38. K. Goto, Y. Inoue, and M. Matsubara, *J. Photopolym. Sci. Tech.*, Vol. 14, p. 33, 2001.
39. M. Hasegawa, N. Sensui, Y. Shindo, and R. Yokota, *Macromolecules*, Vol. 32, p. 387, 1999.
40. C. Chen, R. Yokota, M. Hasegawa, M. Kochi, K. Horie, and P. Hergenrother, *High Performance Polymers*, Vol. 17, p. 317, 2005.
41. M. Kochi, C. Chen, R. Yokota, M. Hasegawa, and P. Hergenrother, *High Performance Polymers*, Vol. 17, p. 335, 2005.
42. Q. Li, X. Fang, Z. Wang, L. Gao, and M. Ding, *Journal of Polymer Science, Part A*, Vol. 41, p. 3249, 2003.
43. M. Suzuki, Y. Ishida, M. Miyauchi, and R. Yokota, *Polyimides and Advanced Aromatic Polymers*, p. 34, 2008.
44. A. Morikawa, T. Furukawa, and Y. Moriyama, *Polym. J.*, Vol. 37, p. 759, 2005.
45. M. Suzuki, M. Iwata, Y. Ishida, M. Miyauchi, and R. Yokota, *Polyimides and Advanced Aromatic Polymers*, p. 38, 2008.
46. A. Morikawa, *Polymer Journal*, Vol. 32, p. 275, 2000.
47. A. Morikawa Hosoya, Y., *Polymer Journal*, Vol. 34, p. 544, 2002.
48. A. Morikawa, and K. Ono, *Polymer Journal*, Vol. 32, p. 948, 2000.
49. A. Morikawa, and K. Ono, *High Performance Polymers*, Vol. 13, p. S73, 2001.
50. A. Morikawa, Y. Hosoya, and A. Umezawa, *Polyimides and Advanced Aromatic Polymers*, p. 48, 2004.
51. M. Ree, K. Kim, S.H. Woo, and H. Chang. *Journal of Applied Physics*, Vol. 81, p. 698, 1997.
52. S. Numata, S. Oohara, J. Imaizumi, and N. Kinjo, *Polymer Journal*, Vol. 17, p. 981, 1985.
53. T. Takeich, M. Zuo, and M. Hasegawa, *Journal of Polymer Science, Part B*, Vol. 39, p. 3011, 2001.

54. S. Ebisawa, J. Ishii, M. Sato, L. Vladimirov, and M. Hasegawa, *European Polymer Journal*, Vol. 46, p. 283, 2010.
55. M. Hasegawa, *Polyimides and Advanced Aromatic Polymers*, p. 37, 2007.
56. T. Saito, and M. Hasegawa, *Polyimides and Advanced Aromatic Polymers*, 2009.
57. K. Goto, M. Kakuta, Y. Inoue, and M. Matsubara, *J. Photopolym. Sci. Tech.*, Vol. 13, p. 313, 2000.
58. D.-J. Liaw, and B.-Y. Liaw, *Polymer Journal*, Vol. 31, p. 1270, 1999.
59. C.-P. Yang, H.-C. Chiang, and Y.-Y. Su, *Polymer Journal*, Vol. 36, p. 979, 2004.
60. S.-H. Hsiao, and C.-T. Li, *Macromolecules*, Vol. 31, p. 7213, 1998.

8

The Effects of Structures on Properties of New Polytriazole Resins

Farong Huang, Liqiang Wan, Lei Du, Yanhong Hu, Yanpeng E and Yujing Li

Key Laboratory for Specially Functional Polymeric Materials and Related Technology of the Ministry of Education, School of Materials Science and Engineering, East China University of Science and Technology, Shanghai, PR China

Abstract

This article reviews the researches on the relationship between structures and properties of a new kind of polytriazole resins. After introduction to the preparation of the resins, the thermal behaviour and reactivity of crosslinkable polytriazole resins are discussed. The effects of the chains rigidity, polarity of chain units, functionality of monomers, grid size of crosslinked network on glass transition temperatures of the polytriazole resins are described. Furthermore, the effects of structures of the polytriazole resins on the mechanical properties, dielectric properties, thermal stabilities are demonstrated. The researches show that the curing reaction of the resins would take place at about 75°C. The glass transition temperatures of the resins change with the chains rigidity, polarity of chain units, and crosslinking degree. The highest one reaches 324°C. The mechanical properties, dielectric properties, thermal stabilities of polytriazole resins are also influenced to some extent by the structures of the polytriazole resins. The flexural strength of a crosslinkable polytriazole resin, A_2B_4, arrives at 200 MPa. The polytriazole resins are expected to be used in advanced polymeric composites.

Keywords: Polytrizole, thermal behaviour, crosslinking, transition temperature, dielectric properties, thermal stability

Vikas Mittal (ed.) High Performance Polymers and Engineering Plastics, (243–268)
© Scrivener Publishing LLC

8.1 Introduction

1,3-Dipolar cycloaddition reaction of azides and alkynes produces 1,4-disubmitted and 1,5-disubmitted 1,2,3-triazole compounds with interesting biological properties [1–4], such as anti-allergic [5–7], anti-bacterial [8], and anti-HIV activity [9] as shown in Scheme 8.1. The reaction is highly exothermic reaction and usually occurs at a low temperature, even at room temperature.

In 2002, Sharpless *et al.* popularized 1,3-dipolar cycloaddition of azides and terminal alkynes, catalyzed by copper(I), in organic synthesis and first defined the addition as "click" reaction [10]. The reaction was proven to be very practical and effective because it can be performed in high yield in multiple solvents (including water) to give 1,4-substituted products in high regioselectivity whether or not in the presence of other functional groups [11–12]. Due to the efficiency and simplicity of the cycloaddition, "click" chemistry has greatly attracted intensive interest in polymer science. Recently, a lot of researches have concerned with the application of the "click" reaction in the synthesis of dendrimers, connection of preformed polymer segments, reparation of new polymers, or post-functionalization of polymer backbones [13–21].

In fact, utilization of the cycloaddition of azides and alkynes to polymerization dates back to 1960s. In 1966, Johnsons *et al.* first reported the synthesis of linear polytriazoles through 1,3-dipolar cycloaddition reaction of monomers with both an azide and an alkyne group [22, 23]. The formed linear polytriazoles exhibited good thermal stability. However, they were unsoluble in any organic solvent and unmeltable under heating. The further characterization of the structures and properties of the formed polytriazoles was unfeasible. Thereby, the application of the polytriazoles is impossible.

Recently, our laboratory has been developing a new series of crosslinkable polytriazole resins with low temperature curing

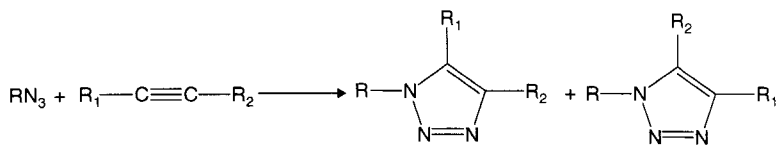

Scheme 8.1 1,3-dipolar cycloaddition reaction of an azide and an alkyne.

character, good processability, excellent mechanical and thermal properties through specialty design of molecular structures on the basis of the preparation and investigation of processable linear polytriazole resins. These polytriazole resins could be expected to be used as polymer matrices for advanced composites. This article focuses on some relationship between the structures and properties of these new polytriazole resins [24–31].

8.2 The Preparation of Polytriazole Resins

Linear polytriazole resins ($A_2B_2^k$ or $A'_2B_2^k$, k = 1, 2, 6, 7, ..., 10) have been synthesized from diazides (A_2 or A'_2) and dialkynes (B_2^k, k = 1,2) or dialkyne macromonomers (B_2^k, k = 6, 7, 8, ..., 10) which contains imide units in molecular chains as shown in Table 8.1 through 1,3-dipolar cycloaddition reactions in melt or solution at 70°C. The measured molecular weight (MW) and inherent viscosity of the synthesized linear polytriazole resins are shown in Table 8.2. As shown in Table 8.2, the synthesized linear polytriazole resins have high MW with the magnitude of 10^4.

Crosslinkable polytriazole resins have been prepared by prepolymerization of multifunctional azides with multifunctional alkynes. A variety of multifunctional azide (A_i or A'_i, i = 2, 3) and alkyne monomers (B_j, j = 3, 4; or B_j^k, j = 2, k = 1, 2, 3,...5) used in the synthesis or preparation of the polytriazole resins are also listed in Table 8.1. The produced polytriazole resins made from the multifunctional azide (A_i or A'_2) and alkyne monomers (B_j, or B_2^k) are separately designated as A_iB_j or A'_iB_j or $A_iB_j^k$ or $A'_iB_j^k$. The crosslinkable polytriazole resins could be cured at 70°C for 6–12 h. Thereafter, the solid resins were further postcured at 120°C for 2 h, 150°C for 2 h, and 180°C for 2 h to obtain well-cured resins.

A series of triazole oligomers capped with alkyne groups (B'_2^m, m = 1, 2, 3, ..., 7) were synthesized by thermal cycloaddition of A_2 and B_2^1 monomers with various molar ratios of functional groups $[N_3]/[C \equiv C](<1)$ at 80°C for 18 h as shown in Figure 8.1. The obtained triazole oligomers B'_2^m were characterized. MWs of the alkyne-capped oligomers calculated and measured are listed in Table 8.3. The results demonstrate that the designed MW values of the oligomer B'_2^m correspond with those measured by NMR technique.

Table 8.1 *Monomers for a variety of polytriazole resins.*

Resin	Azide Monomer	Alkyne Monomer
$A_2B_2^1$	1,4-diazidomethyl benzene (A_2) 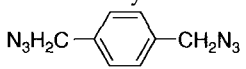	4,4′-dipropargyloxydiphenylpropane (B_2^1) 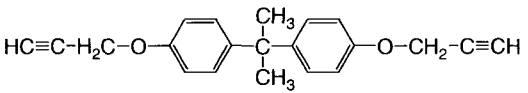
$A_3B_2^1$	1,3,5-tris(azidomethyl)-2,4,6-trimethyl-benzene(A_3) 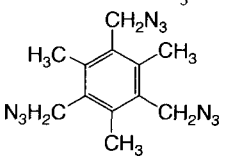	4,4′-dipropargyloxydiphenylpropane (B_2^1)
$A'_2B_2^2$	4,4′-diazidomethyl biphenyl (A'_2) 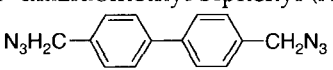	1,3-dipropargyloxybenzene (B_2^2) 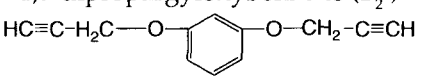
$A_3B_2^2$	1,3,5-tris(azidomethyl)-2,4,6-trimethyl-benzene(A_3)	1,3-dipropargyloxybenzene (B_2^2)
$A_3B_2^3$	1,3,5-tris(azidomethyl)-2,4,6-trimethyl-benzene(A_3)	4,4′-diproparyloxydiphenylether (B_2^3) 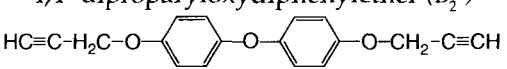

$A_3B_2^4$	1,3,5-tris(azidomethyl)-2,4,6-trimethyl-benzene(A3)	4,4′-diproparyloxybenzophenone (B_2^4) 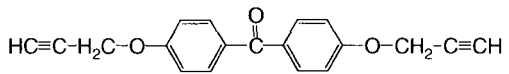
$A_3B_2^5$	1,3,5-tris(azidomethyl)-2,4,6-trimethyl-benzene(A_3)	4,4′-dipropargyloxydiphenylhexafluoropropane (B_2^5) 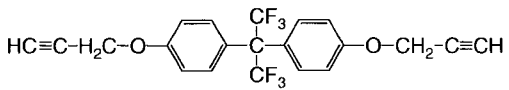
$A'_2B_2^6$	4,4′-diazidomethyl biphenyl (A'_2)	diethynylbenzene (B_2^6) 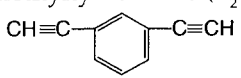
$A_2B_2^7$	1,4-diazidomethyl benzene (A_2)	2,2-bis-{4- [*N*- (3-ethynylphenyl) phthalimide-4-oxy-] phenyl} propane (B_2^7). 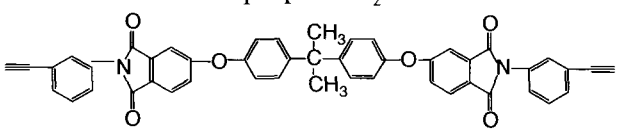
$A_2B_2^8$	1,4-diazidomethyl benzene (A_2)	3, 3-bis [*N*- (3-ethynylphenyl) phthalimide-4-] ether (B_2^8) 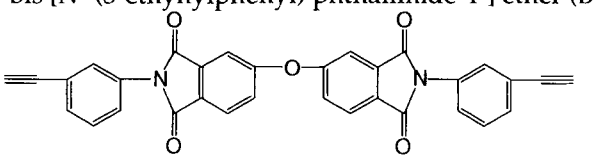

(Continued)

Table 8.1 Monomers for a variety of polytriazole resins. (Continued)

Resin	Azide Monomer	Alkyne Monomer
A_2B_2[9]	1,4-diazidomethyl benzene (A_2)	3, 3-bis -[*N*- (3-ethynylphenyl) phthalimide-4-] ketone (B_2[9]) 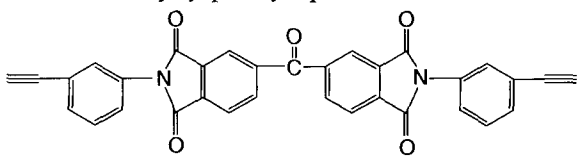
A_2B_2[10]	1,4-diazidomethyl benzene (A_2)	2, 2-bis- [*N*-(3-ethynylphenyl) phthalimide-4-] hexafluoropropane (B_2[10]) 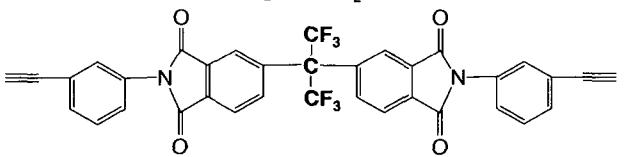
A'_2B_2[7]	4,4′-diazidomethyl biphenyl (A'_2)	2,2-bis- {4- [*N*- (3-ethynylphenyl) phthalimide-4- oxy-]phenyl} propane (B_2[7])
A'_2B_2[8]	4,4′-diazidomethyl biphenyl (A'_2)	3, 3-bis- [*N*- (3-ethynylphenyl) phthalimide-4-] ether (B_2[8])
A'_2B_2[9]	4,4′-diazidomethyl biphenyl (A'_2)	3, 3-bis- [*N*- (3-ethynylphenyl) phthalimide-4-] ketone (B_2[9])

$A'_2B_2^{10}$	4,4′-diazidomethyl biphenyl (A'_2)	2,2-bis-[N-(3-ethynylphenyl) phthalimide-4-] hexafluoropropane (B_2^{10})
A_2B_3	1,4-diazidomethyl benzene (A_2)	*N,N*-dipropargyl-4-propargyloxyaniline (B_3) 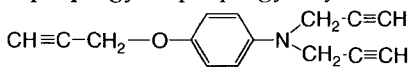
A_3B_3	1, 3, 5-tris(azidomethyl)-2, 4, 6-trimethyl-benzene(A_3)	*N,N*-dipropargyl-4-propargyloxyaniline (B_3)
A_2B_4	1,4-diazidomethyl benzene (A_2)	*N,N,N′,N′*-tetrapropargyl-4,4′-diaminodiphenylmethane (B_4) 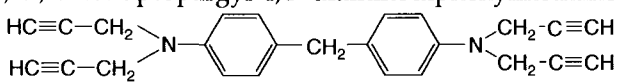
A'_2B_4	4,4′-diazidomethyl biphenyl(A_2')	*N,N,N′,N′*-tetrapropargyl-4,4′-diaminodiphenylmethane (B_4)
A_3B_4	1,3,5-tris(azidomethyl)-2,4,6-trimethyl-benzene(A_3)	*N,N,N′,N′*-tetrapropargyl-4,4′-diaminodiphenylmethane (B_4)

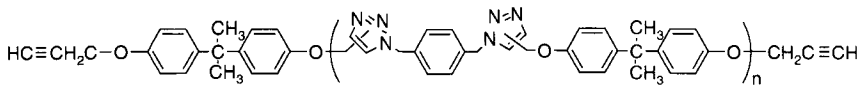

Figure 8.1 Structure of the alkyne-capped triazole oligomers.

Table 8.2 Molecular weight and viscosity of linear polytriazole resins.

Resin	$A_2B_2^1$	$A'_2B_2^2$	$A_2B_2^7$	$A_2B_2^8$	$A_2B_2^9$	$A'_2B_2^7$	$A'_2B_2^8$
$\overline{M_n}$ ($\times 10^{-4}$)	9.77	4.22	–	–	–	–	–
[η] (dL/g)*	0.41	–	0.58	0.42	0.48	0.51	0.39

* [η]: the inherent viscosity of polytriazoles in DMF solvent.

Table 8.3 Molecular weights of the alkyne-capped triazole oligomers.

Oligomer $B'_2{}^m$	Molar Ratio ($[N_3]$/ $[C \equiv C]$)	$\overline{M_n}{}^a$	$\overline{M_n}{}^b$	
			(I)	(II)
$B'_2{}^1$	1/2	796	834	835
$B'_2{}^2$	2/3	1288	–	–
$B'_2{}^3$	4/5	2272	–	–
$B'_2{}^4$	6/7	3256	3306	3322
$B'_2{}^5$	9/10	4732	–	–
$B'_2{}^6$	19/20	9652	9582	9619
$B'_2{}^7$	29/30	14572	–	–

a: The designed $\overline{M_n}$ is calculated by the equation $\overline{M_n} = 188r + 304/1 - r$, where r is the molar ratio of group $[N_3]$ to $[C \equiv C]$.

b: $\overline{M_n}$: obtained by ^{1}H NMR analyses on the basis of different groups[30].

The polytriazole resins($A_3B'_2{}^m$, m = 1, 2, 3, ..., 7) for crosslinked networks with various grid sizes were prepared from the alkyne-capped triazole oligomers and 1,3,5-tris(azidomethyl)-2,4,6-trimethyl-benzene by "click" cycloaddition with the equivalent moles of groups N_3 and C ≡ C(i.e., $[N_3]/[C \equiv C] = 1$). The curing procedure of the polytriazole resins was considered as follows: the resins were kept at 70°C for 12 h, followed by at 110°C for 2 h, at 150°C for 2h, at 180°C for 2 h, and finally at 200°C for 2 h to obtain polytriazole networks with different grid sizes.

8.3 Reactivity of Crosslinkable Polytriazole Resins

The thermal behavior of crosslinkable polytriazole resins (A_iB_j, A'_iB_j, $A_iB_j^k$, $A'_iB_j^k$) were traced by DSC technique. Figure 8.2 shows typical DSC curves of some polytriazole resins. There is an exothermal peak on the DSC curves. As shown in the figure, the initial temperatures of the exothermal peaks for all resins are located at about 75°C. This indicates that the curing reaction of the crosslinkable polytriazole resins could take place at about 75°C. The top temperatures (T_ps) of those peaks for the resins are tabulated in Table 8.4. T_ps of the peaks range from 130°C to 150°C. As shown in the table,

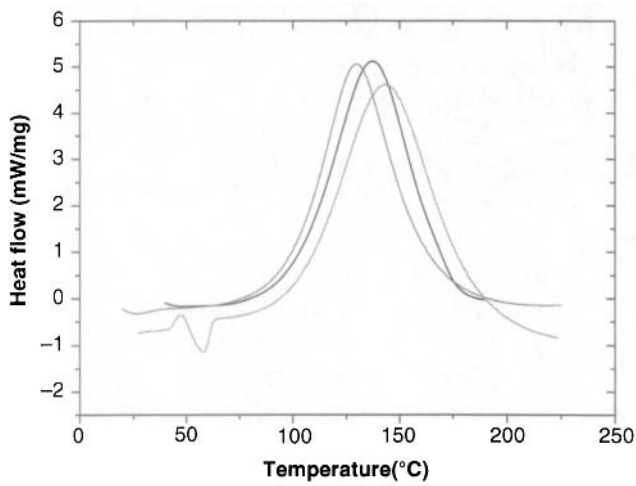

Figure 8.2 DSC curves of crosslinkable polytriazole resin A_3B_4(—), A_2B_4(—), and A_3B_3(—).

Table 8.4 DSC analysis results for some crosslinkable polytriazole resin.

Resin	A_2B_4	A'_2B_4	A_2B_3	A_3B_2[1]	A_3B_3	A_3B_4
T_p(°C)	137	139	134	140	143	130
Resin	A_3B_2[1]	A_3B_2[2]	A_3B_2[3]	A_3B_2[4]	A_3B_2[5]	–
T_p(°C)	150	143	147	148	149	–

Note: T_p stands for a top temperature for the exothermal peak on a DSC curve.

Table 8.5 The apparent activation energy of alkyne-azide curing reactions for various resins.

Resin	A'_2B_2	A'_2B_2[6]	A_2B_4	A'_2B_4	A_3B_4
Apparent reaction activation energy (kJ/mol)	84.7	94.1	80.7	82.9	92.1

the peak temperatures seem to be not related with the structures of monomers too much though A'_2B_4 resin with high rigidity exhibits a bit high peak temperature as compared with that of A_2B_4 resin and A_3B_4 resin with high functionality displays lowest curing temperature among the resins.

The azide-alkyne reaction kinetics were studied by DSC analysis technique and the apparent kinetic parameters of the curing reactions were obtained by Kissinger's method [26, 31–32]. The apparent activation energies are tabulated in Table 8.5. As shown in the table, there are differences among the activation energies of different resins. The apparent reaction energies are related with the structures and the functionality of monomers. A_3B_4 resin with high functionality has higher activation energy as compared with A'_2B_2, A_2B_4, and A'_2B_4 resins. A'_2B_4 resin with high rigidity exhibits a bit high energy as compared with that of A_2B_4 resin. This probably results from the reaction activity of functional groups in the resin. The higher the functionality of monomer is, the higher the steric effect is, and thus the more difficult the reaction is. The higher the rigidity of monomer molecules, the lower the collision probablity of the reactive groups, and then the more difficult the reaction is. In addition, A'_2B_2[6] resin has higher energy than that of A'_2B_2 resin. This illustrates that the reaction of the aromatic alkyne with azide is more difficult than that of aliphatic alkyne with azide.

8.4 Glass Transition Temperatures of Polytriazole Resins

8.4.1 The Effect of Molecular Rigidity and Polarity on the Glass Transition Temperature (T_g)

The glass transition temperature (T_g) of linear polytriazole resins was measured by DMA and DSC techniques. The typical DMA and DSC analysis diagrams are respectively shown in Figure 8.3 and Figure 8.4. All analysis results are tabulated in Table 8.6. As seen from Figure 8.3, T_gs of $A_2B_2^1$ and $A'_2B_2^2$ are 94 and 130°C, respectively. T_g of $A'_2B_2^2$ is higher than that of $A_2B_2^1$ because the molecular chain of $A'_2B_2^2$ resin is more rigid than $A_2B_2^1$ resin.

As shown in Table 8.6, the glass transition temperatures (T_gs) of $A_2B_2^k$ resin system(k = 7,..., 10) are located in the range of 220–262°C. T_gs of $A_2B_2^k$ resins depend on the structures of the diazide units, dialkyne units, and imide units. $A_2B_2^k$ resins series containing imide units have obviously much higher T_gs than those of $A_2B_2^1$ and $A'_2B_2^2$ resins. Imide units in the molecular chains play an important role in increase of T_g due to high rigidity and polarity of imide units which prevent chains from movement. $A_2B_2^7$ and $A'_2B_2^7$ resins exhibit lower T_gs as compared with other resins in $A_2B_2^k$

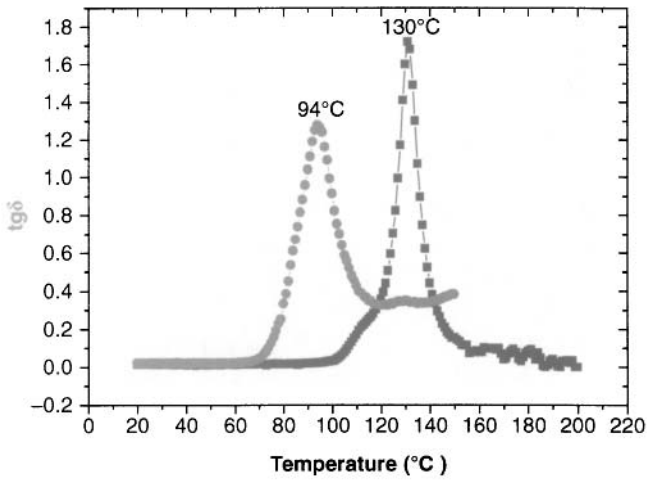

Figure 8.3 Typical DMA diagrams of linear polytriazole resins $A_2B_2^1$ (●)and $A'_2B_2^2$(■).

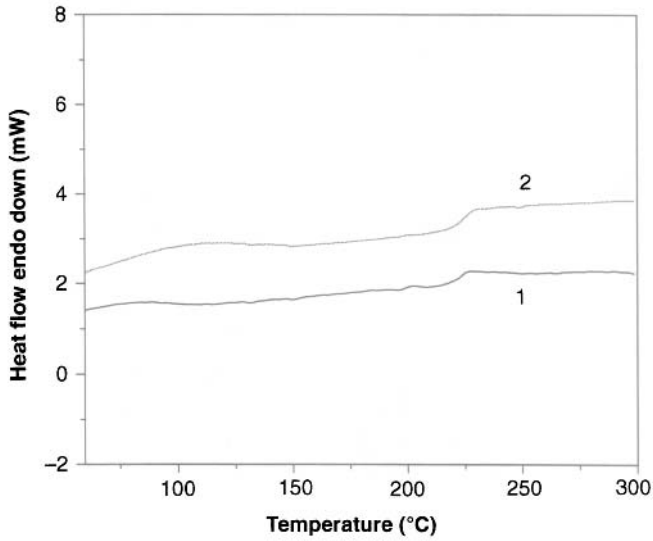

Figure 8.4 Typical DSC curves of linear resin $A_2B_2^7$(1) and $A'_2B_2^7$(2).

Table 8.6 The glass transition temperatures of various polytriazole resins.

Resin	$A_2B_2^1$	$A'_2B_2^2$	$A_2B_2^7$	$A_2B_2^8$	$A_2B_2^9$	$A'_2B_2^7$	$A'_2B_2^8$	$A'_2B_2^{10}$
Glass transition temperature T_g(°C)	94	130	221	249	253	224	250	262

derivatives. This might result from the presence of a flexible linkage like ether and propylidene between the phthalimide and phenyl units. Obviously, T_g of polytriazoles decreases with increase in the flexibility of molecular backbones.

DMA technique was also used to determine T_g of cured $A_3B_2^k$ polytriazole resins (k = 1,2,..., 5). The typical DMA diagrams are shown in Figure 8.5. T_gs of all cured resins are listed in Table 8.7. As shown in Table 8.7, the cured $A_3B_2^5$ resin has the highest T_g of 226°C. T_g of the cured $A_3B_2^1$ resin is 216°C and lower than that of the cured $A_3B_2^5$ resin. T_gs of other cured resins are all 204°C. For $A_3B_2^1$, $A_3B_2^3$, $A_3B_2^4$ and $A_3B_2^5$ resins, they have almost same cosslinking density. However, —CF_3 and —CH_3 side groups in $A_3B_2^5$ and $A_3B_2^1$

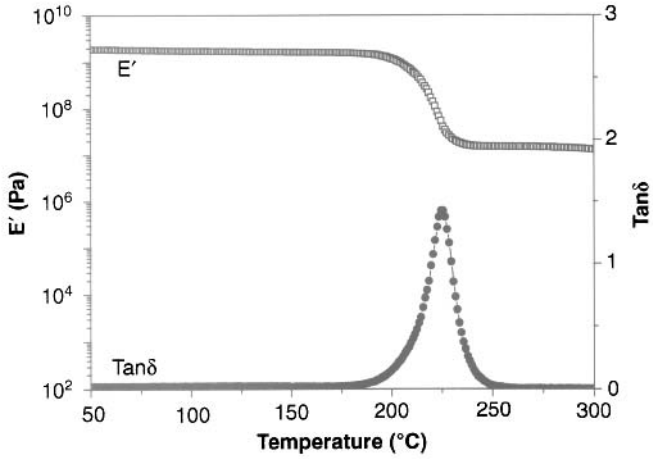

Figure 8.5 DMA diagrams of $A_3B_2^5$ resin.

Table 8.7 Glass transition temperature of cured A_3B_2k resins.

Resin	$A_3B_2^1$	$A_3B_2^2$	$A_3B_2^3$	$A_3B_2^4$	$A_3B_2^5$
Glass transition temperature T_g(°C)	216	204	204	204	226

resins have high steric effect. This increases the difficulty of chain movements of $A_3B_2^5$ and $A_3B_2^1$ resins. Therefore, T_gs of $A_3B_2^5$ and $A_3B_2^1$ resins are higher than those of $A_3B_2^3$ and $A_3B_2^4$ resins. Besides, because —CF_3 groups have larger volume and stronger polarity than —CH_3 groups, $A_3B_2^5$ resin has higher T_g than $A_3B_2^1$ resin. As for $A_3B_2^2$ resin, although it has higher crosslinking density than that of other resins, the flexible -CH_2- links in $A_3B_2^2$ resin is far more than those in other resins. Herewith, T_g of the cured $A_3B_2^2$ resin is low.

8.4.2 The Effect of Monomer Functionality on T_g

Figure 8.6 shows the glass transition tanδ peaks of the cured polytriazole resin A_2B_3, A_3B_2, A_2B_4, A'_2B_4, A_3B_3, and A_3B_4 in DMA diagrams. As shown in the figure, T_gs of cured A_2B_3, A_3B_2, A_2B_4, A'_2B_4, A_3B_3, and A_3B_4 resins are 181°C, 216°C 218°C, 250°C, 311°C, and

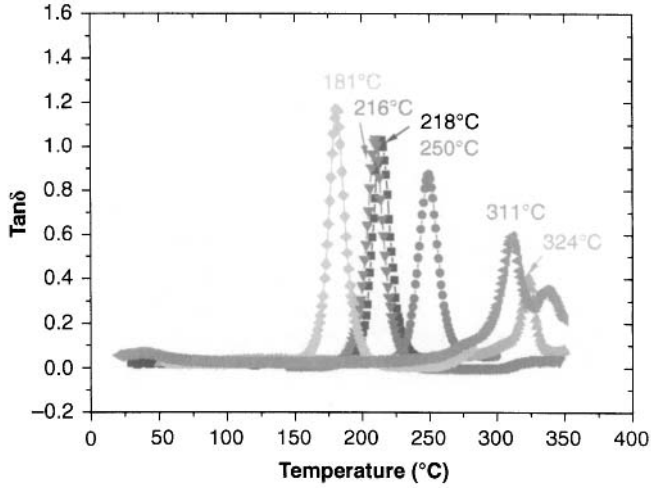

Figure 8.6 DMA of Cured polytriazole resin A2B3(◆), A3B2(▼), A2B4(■), A'2B4(●), A3B3(◀), and A3B4(▲).

324°C, respectively. The results show that T_gs of the cured polytriazole resins increase with the average functionality increases. The higher the average functionality of the monomers is, the higher the crosslinking density of the cured resin and thereby the higher T_g is. Although the resin A_2B_4 and A'_2B_4 possess the same average functionality, T_g of cured A_2B_4 resin is lower than cured A'_2B_4 resin. This change could be explained by that the rigidity of the molecular chain of A'_2B_4 resin is higher than that of A_2B_4 resin.

8.4.3 The Effect of Crosslinked Network Grid Size on T_g

As usual, the crosslinked structures of a resin have a great influence on its properties. Investigation on the effect of the molecular structure and crosslinking character of a crosslinked network on properties would give an effective guide for the design and preparation of a new crosslinkable resin. The influence of crosslinked structures on properties of crosslinkable polytriazole resins with different network grid sizes is further investigated.

The glass transition temperatures of $A_3B'^{m}_2$ resins (m = 1,2,3....7) with different chain lengths between two crosslinking sites are

characterized by DSC technique under nitrogen at a heating rate of 20°C/min. The DSC analysis results of the $A_3B'_2{}^m$ resins with different network grid sizes are tabulated in Table 8.8.

The grid size of $A_3B'_2{}^m$ resins(determined by M_n of $B'_2{}^m$) would have a significant influence on its T_g. T_gs of $A_3B'_2{}^m$ resins as a function of M_n of the oligomer $B'_2{}^m$ is shown Figure 8.7. As shown in Figure 8.7, an initially rapid and then slow decreasing curve is observed. The critical point of the curve is found at M_n 2000(*ca.*), which shows a critical molecular weight of $B'_2{}^m$. If $M_n < 2000$, the size of the network grids has a significant influence on the T_g; while $M_n > 2000$, the influence is not obvious.

In general, the increasement of crosslinking density of a network would result in enhancement of thermal properties. We consider the molecular weight of two adjacent crosslinking sites as a crosslinking density. Based on the theory of glass transition, T_g can often

Table 8.8 DSC analysis results of $A_3B'_2{}^m$ resins.

Resin	$A_3B_2{}^1$	$A_3B'_2{}^1$	$A_3B'_2{}^2$	$A_3B'_2{}^3$	$A_3B'_2{}^4$	$A_3B'_2{}^5$	$A_3B'_2{}^6$	$A_3B'_2{}^7$
T_g /°C	216	141	140	134	128	128	121	123

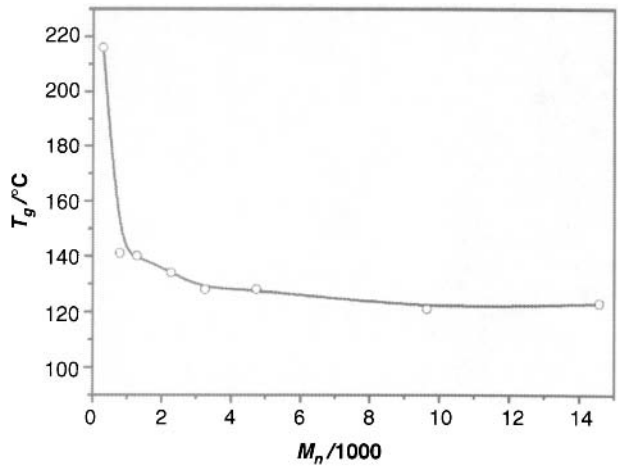

Figure 8.7 Tg of $A_3B'_2{}^m$ resins as a function of Mn of oligomer $B'_2{}^m$ (m = 1,2,3...7).

be expressed as a function of crosslinking density by the following equation:

$$T_g = T_{g\infty} + \frac{k}{M_c} \tag{8.1}$$

where T_g is the glass transition temperature of the crosslinked polytriazole, $T_{g\infty}$ the glass transition temperature of the oligomer $B'_2{}^m$ with a nearly infinite high molecular weight, k a constant associated with the average functionality of crosslinking system and M_c the molecular weight between two adjacent crosslinking sites. For the studied polytriazoles system, M_c can be calculated by the following equation:

$$M_c = M_n + M' \tag{8.2}$$

where M_n is the molecular weight of $B'_2{}^m$ and M' (=190) the revised value determined by a crosslinking monomer.

The relationship between T_g and $1/M_c$ of $A_3B'_2{}^m$ resins is shown in Figure 8.8. The relationship between T_g and M_n of $B'_2{}^m$ for the $A_3B'_2{}^m$ resins could be expressed as follows:

$$T_g = 122 + \frac{21600}{(M_n + 190)} \tag{8.3}$$

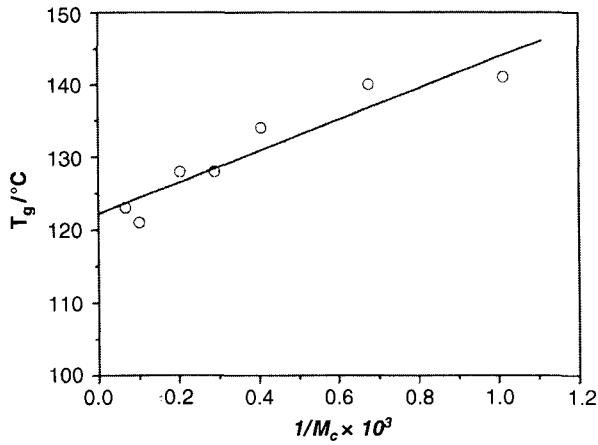

Figure 8.8 T_g of $A_3B'_2{}^m$ resins as a function of the crosslinking density.

From the results front, we can conclude that the size of the network grids has an effective influence on T_gs of polytriazoles: small network grids of polytriazoles would result in a high T_g.

8.5 Mechanical Properties of Polytriazole Resins

8.5.1 The Effect of Structures On Mechanical Properties of Polytriazole Resins

Tensile property of a polytriazole resin film was measured by a mechanical tester. The tensile strength and tensile modulus of $A_2B_2^1$ polytriazole film are 72.9 MPa and 2.95 GPa, respectively. The elongation at break is 4.36%. This indicates that $A_2B_2^1$ resin possesses good mechanical properties. The tensile properties of $A_2B_2^k$ resin films containing imide units in main molecular chains are listed in Table 8.9. The $A_2B_2^k$ films exhibit high mechanical properties. As shown in the table, $A_2B_2^7$ and $A'_2B_2^7$ resins have the highest values among these resins. It is because of the contribution of two bulky methyl or trifluoromethyl in molecular structure to toughness of the resin. As compared with $A_2B_2^1$ resin, the resin series $A_2B_2^k$ (k = 7, 8, ... , 10) containing imide units in the molecular chains exhibit higher mechanical properties.

8.5.2 The Effect of Crosslinking on Mechanical Properties of Polytriazole Resins

Mechanical properties of the cured polytriazole resins are tabulated in Table 8.10. As shown in the table, the mechanical properties of the cured polytriazole resins are excellent. The tensile and flexural strengths of cured A_2B_4 resin reach as high as 99.0 and 200 MPa, respectively. Flexural strength of the cured A'_2B_4 resin is a bit lower

Table 8.9 The tensile properties of linear polytriazole resin film.

Resin	$A_2B_2^1$	$A_2B_2^7$	$A_2B_2^8$	$A_2B_2^9$	$A'_2B_2^7$	$A'_2B_2^8$
Tensile Strength (MPa)	72.9	92.4	76.2	83.1	89.4	84.6
Elongation (%)	4.4	6.4	6.4	4.8	6.4	6.9

Table 8.10 Mechanical properties of cured polytriazole resins.

Resin	Tensile Strength (MPa)	Tensile Modulus (GPa)	Tensile Elongation(%)	Flexural Strength (MPa)	Flexural Modulus (GPa)
A_2B_4	99.0	3.60	3.49	200	3.34
A'_2B_4	93.7	3.53	4.10	185	3.42
A_3B_4	89.3	3.51	4.04	153	3.10
$A_3B_2^1$	–	–	–	168	3.60
$A_3B_2^2$	–	–	–	201	3.80
$A_3B_2^5$	–	–	–	169	3.30
A_2B_3	–	–	–	156	3.50
A'_2B_3	–	–	–	155	2.70
A_3B_3	–	–	–	150	3.30

than that of cured A_2B_4 resin, whereas the modulus is a bit higher than that of cured A_2B_4 resin. This probably results from that the rigidity of the molecular chain of A'_2B_4 resin is higher than that of A_2B_4 resin. Flexural strength of the cured A_3B_4 resin is much lower than cured A_2B_4 resin. The main reason is that the crosslinking density of A_3B_4 resin is higher, which probably leads to the brittleness of the cured resin. $A_3B_2^2$ resin shows the highest flexural strength and modulus. The possible explanation would be the resin with suitable crosslinking degree and chain flexibility combined. Anyway, all resins exhibit excellent flexural strengths with the value of higher than 150 MPa.

8.6 Dielectric Properties of Polytriazole Resins

Dielectric properties of cured $A_3B_2^1$, $A_3B_2^2$, $A_3B_2^3$, $A_3B_2^4$, and $A_3B_2^5$ resins are shown in Figure 8.9. As shown in Figure 8.9, when the measuring frequency ranges from 10^2 to 10^6 Hz, dielectric constant (ε') of $A_3B_2^5$ resin is in the range 2.99–2.79 which is lowest in all the cured resin. Although C—F bonds in $A_3B_2^5$ resin have high bond moment, the symmetric structure of $C(CF_3)_2$ leads dipole moment

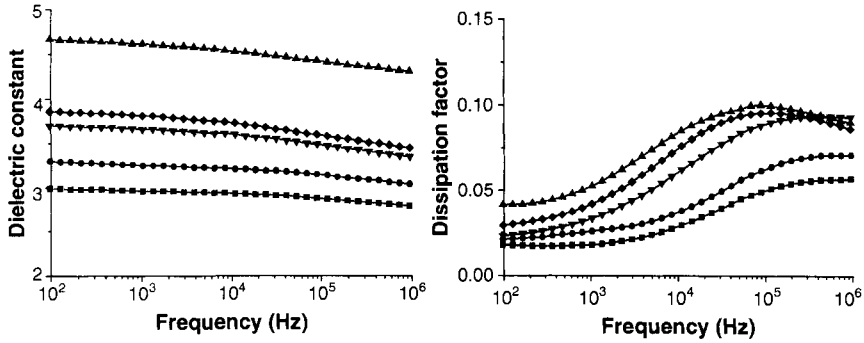

Figure 8.9 Dielectric contant and dissipation factor as a function of frequency for the cured polytriazole resins. $A_3B_2^5$ (■); $A_3B_2^1$ (●); $A_3B_2^3$ (▼); $A_3B_2^2$ (♦); $A_3B_2^4$ (▲).

of the whole molecular chains to be near zero. Besides, due to the presence of rigid —CF_3 side groups, molecular chains in $A_3B_2^5$ resin are more difficult to move than those of other resins. Therefore, ε′ of $A_3B_2^5$ resin is lowest. Similarly, dielectric constant ε′ of $A_3B_2^1$ resin is lower than those of $A_3B_2^2$, $A_3B_2^3$ and $A_3B_2^4$ resins due to the existence of similar symmetric —CH_3 side groups. It can be known from the DMA results that T_gs of $A_3B_2^2$ and $A_3B_2^3$ resins are equal, which indicates their molecular chains have similar chain segment mobility. The symmetric structure of $A_3B_2^3$ provides lower ε′ in spite of the presence of the polar ether (-O-). ε′ values of $A_3B_2^2$ and $A_3B_2^3$ resins are close. However, ε′ of $A_3B_2^4$ resin is higher than those of $A_3B_2^3$ and $A_3B_2^2$ resins and highest among these resins mainly because $A_3B_2^4$ resins have strong polar C=O group in the molecular chains.

The relationship between dissipation factor ε″ of the cured resins and frequency is shown in Figure 8.9. As shown in Figure 8.9, the cured $A_3B_2^5$ resin has the lowest ε″ among all $A_3B_2^k$ resins (k = 1, 2, 3, ..., 5). The change of ε″ is similar to that of ε′. ε″ values of $A_3B_2^4$, $A_3B_2^3$ and $A_3B_2^2$ resins are higher than those of $A_3B_2^5$ and $A_3B_2^1$ resins probably because their molecular chains are easier to move than those of $A_3B_2^5$ and $A_3B_2^1$ resins.

8.7 Thermal Stabilities of Polytriazole Resins

Thermogravimetric curves of the cured A_3B_3 and A_3B_4 resins under nitrogen and air atmospheres are shown in Figure 8.10 and the

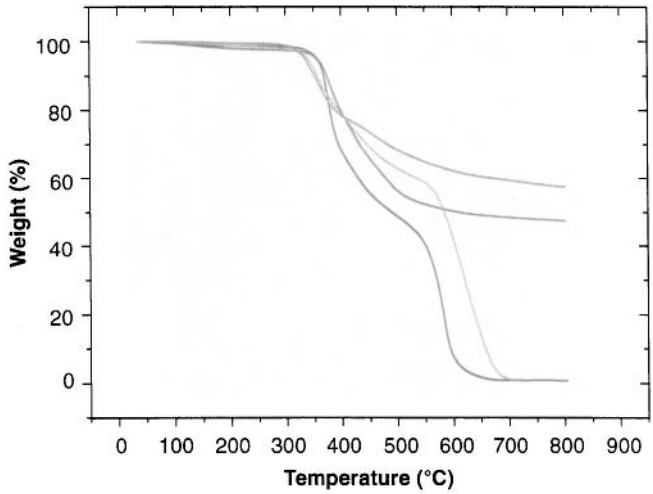

Figure 8.10 TGA thermograms of the cured A_3B_3 and A_3B_4 resins under nitrogen and air. 1: A_3B_3 (—N_2;— air); 2: A_3B_4 (—N_2;—air).

analysis results are tabulated in Table 8.11. As shown in Figure 8.10, the degradation process for the cured A_3B_3 and A_3B_4 resins are performed in one stage under nitrogen but in two stages under air. For the cured A_3B_3 and A_3B_4 resins, the degradation temperature T_{d5}s (the degradation temperature at 5% weight loss) under air and nitrogen are almost the same. This indicates that thermal oxidative degradation is not the main process for the degradation of the cured resin in the initial stage and the cleavage of weak bonds in the cured resin should be the main degradation mechanism. The conclusion is further demonstrated by other series of resins $A_3B_2^k$ (k = 1,2,..., 5). For all cured resins, their T_{d5}s under nitrogen are near. This is because that the main chains in all cured resin have the same weak bonds H_2C—N [33]. Thermogravimetric curves of some other resins including a linear polytriazole resin in nitrogen are shown in Figure 8.11 and all results are listed in Table 8.11. As shown in Figure 8.11 and Table 8.11, all T_{d5}s arrives at around 350°C regardless of linear and crosslinked structures except for the resins with imide units which show a bit higher T_{d5} value. This indicates that the cured resins possess good thermal stability. The degradation of all cured resins initiates at H_2C—N bond and their T_{d5} values under nitrogen or air are near the same. Besides, the degradation residue of the cured $A_3B_2^5$ and $A_3B_2^1$ resins are much lower than those of other resins under nitrogen. This is because that $C(CF_3)_2$

Table 8.11 TGA analysis results for cured polytriazole resins.*

Resin	Under N_2		Under Air	
	T_{d5}(°C)	Y_c (%)	T_{d5}(°C)	Y_c (%)
$A_2B_2^1$	351	46.1	–	–
$A'_2B_2^2$	353	50.5	–	–
$A_2B_2^7$	365	53.9	–	–
$A_2B_2^8$	369	57.0	–	–
$A_2B_2^9$	369	53.8	–	–
$A'_2B_2^7$	377	60.2	–	–
$A'_2B_2^8$	376	56.3	–	–
$A_3B_2^1$	361	32.4	360	0
$A_3B_2^2$	361	50.4	359	0
$A_3B_2^3$	358	51.8	356	0
$A_3B_2^4$	358	49.9	356	0
$A_3B_2^5$	356	35.1	356	0
A_2B_3	326	54.0	–	–
A_3B_3	333	57.4	338	0
A_2B_4	348	47.7	–	–
A'_2B_4	351	46.9	–	–
A_3B_4	355	47.4	357	0

*T_{d5}: the decomposition temperature at 5% weight loss; Y_c: Char yield of decomposition at 800°C .

and $C(CH_3)_2$ groups in $A_3B_2^5$ and $A_3B_2^1$ resins are easy to decompose into small molecules at high temperature.

8.8 Conclusions

The polytriazole resins with various structures were prepared after fine design of molecular structures of monomers and polymers.

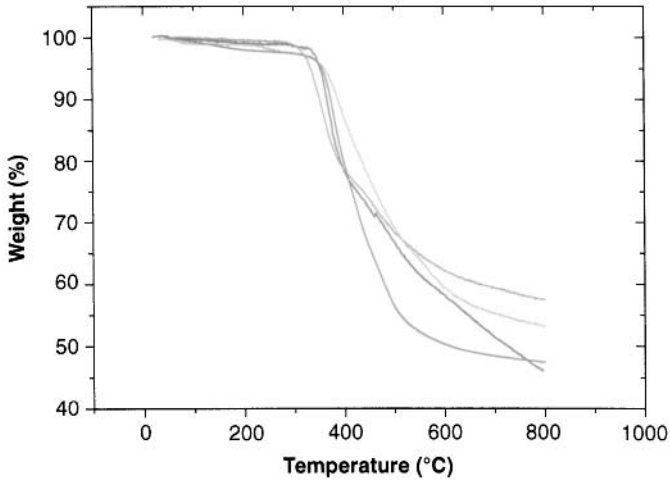

Figure 8.11 TGA diagrams of polytriazole resins under nitrogen A_3B_3(—), A_3B_2[1] (—), A_3B_4 (—), and A_2B_2[7](—).

The effects of the structures on the properties of the polytriazole resins are discussed in this article. From the above discussion, we reach the following conclusion points:

1. Reactivity of resins is influenced by the molecular structure, but the effect is not obvious. The cycloaddition of an aromatic alkyne with an azide is more difficult than that of an aliphatic alkyne with an azide. The curing reactions of the resins start at around 75°C.
2. The glass transition temperatures of polytriazole resins change with the rigidity of molecular chains, polarity, and crosslinked degree of network(related with functionality of monomers and grid size of crosslinked network formed). The higher the rigidity, polarity, and crosslinking degree, the higher the T_g of the resin is. Polytriazole resins containing imide units show higher glass transition temperatures than polytriazole resins without imide units. Crosslinked polytriazole resins demonstrate much higher glass transition temperatures than linear polytriazole resins. The grid size of the crosslinked network has an effective effect on the T_g of the polytriazole resins. Small network grids of polytriazole resins would

result in a high T_g, especially when the grid size is less critical one(M_n ~ 2000).

3. The mechanical properties also vary with the structures of polytriazole resins. The crosslinked polytriazole resins have higher mechanical properties than linear polytriazole resins. The polytriazole resins with higher polarity exhibit higher mechanical properties. In addition, the mechanical properties of polytriazole resins are complicatedly influenced by crosslinking degree, chain flexibility, etc. The tensile and flexural strengths arrive at 99.0 MPa and 200 MPa, respectively. The polytriazole resins are a kind of high performance resins.
4. Dielectric properties of polytriazole resins are obviously influenced by their structures. The polytriazole resins with a symmetry structure and low polarity show low dielectric constant and dielectric loss.
5. The degradation temperature (T_{d5}) for all resins is around 350°C. Thermal stabilities of polytriazole resins are obviously not affected by the structures. The polytriazole resins possess excellent thermal and thermooxidative stabilities.

8.9 Acknowledgement

Our special thanks go to previously graduated students Dr Jianjun Tian, Dr Xiaoan Zhou, Dr Xiaofei Wang, Mr Yonghong Luo, Mr Jianzhi Huang for their laboursome and pioneering research work. We gratefully acknowledged the financial support of the National High Technology Research and Development Program (Grant No.: 305103) and the National Research Program of China (Grant No 5131101).

8.10 References

1. R. Huisgen, *1,3-Dipolar Cycloaddtion Chemistry*, Wiley, New York, 1984.
2. H. Wamhoff, *Comprehensive Heterocyclic Chemistry*, Pergamon, Oxford, 1984.
3. T. Sheradsky, *The Chemistry of the Azido Group*, Interscience, London, 1971.
4. S.T. Abu-Orabi, M.A. Atfah, and I. Jibril, *Journal of Heterocyclic Chemistry*, Vol. 26, p. 1461, 1989.

5. D.R. Buckle, and C.J.M. Rockell, *Journal of Chemical Society, Perkin Transactions*, Vol. 1, p. 627, 1982.
6. D.R. Brukle, D.J. Outred, C.J.M. Rockell, H. Smith, and B.A. Spicer, *Journal of Medicinal Chemistry*, Vol. 26, p. 251, 1983.
7. D.R. Brukle, C.J.M. Rockell, H. Smith, and B.A. Spicer, *Journal of Medicinal Chemistry*, Vol. 29, p. 2262, 1986.
8. M.J. Genin, D.A. Allwine, D.J. Anderson, M.R. Barbachyn, D.E. Emmert, S.A. Garmon, D.R. Graber, K.C. Grega, J.B. Hester, D.K. Hutchinson, J. Morris, R.J. Reischer, C.W. Ford, G.E. Zurenko, J.C. Hamel, R.D. Schaadt, D. Stapert, and B.H.Yagi, *Journal of Medicinal Chemistry*, Vol. 43, p. 953, 2000.
9. R. Alvarez, S. Velazquez, A. San-Felix, S. Aquaro, E. De Clercq, C.-F. Perno, A. Karlsson, J. Balzarini, and M.J. Camarasa, *Journal of Medicinal Chemistry*, Vol. 37, p. 4185, 1994.
10. V.V. Rostovtsev, L.G. Green, V.V. Fokin, K.B. Sharpless, *Angewandte Chemie International Edition*, Vol. 41, p. 2596, 2002.
11. A.J. Link, M.K.S. Vink, and D.A. Tirrell, *Journal of the American Chemical Society*, Vol. 126, p. 10598, 2004.
12. H.C. Kolb, M.G. Finn, and K.B. Sharpless, *Angewandte Chemie International Edition*, Vol. 40, p. 2004, 2001.
13. B. Helms, J.L. Mynar, C.J. Hawker, and M.J. Fréchet, *Journal of the American Chemical Society*, Vol. 126, p. 15020, 2004.
14. R.J. Thibault, K. Takizawa, P. Lowenheilm, B. Helms, J.L. Mynar, M.J. Fréchet, and C.J. Hawker, *Angewandte Chemie International Edition*, Vol. 44, p. 6384, 2005.
15. J. Pyun, C. Tang, T. Kowalewski, M.J. Fréchet, and C.J. Hawker, *Macromolecules*, Vol. 38, p. 2674, 2005.
16. R.J. Thibault, K. Takizawa, P. Lowenheilm, B. Helms, J.L. Mynar, M.J. Fréchet, and C.J. Hawker, *Journal of the American Chemical Society*, Vol. 128, p. 12084, 2006.
17. H. Nandivada, X. Jiang, and J. Lahann, *Advanced Materials*, Vol. 19, p. 2197, 2007.
18. D. Fournier, R. Hoogenboom, U.S. Schubert, *Chem. Soc. Rev*, Vol. 36, p. 1369, 2007.
19. B.L. Droumaguet, and K. Velonia, *Macromolecular Rapid Communications*, Vol. 29, p. 1073, 2008.
20. W.H. Binder, and R. Sachsenhofer, *Macromolecular Rapid Communications*, Vol. 29, p. 952, 2008.
21. Y. Tang, C.K.W. Jim, Y. Liu, L. Ye, A. Qin, J.W.Y. Lam, C. Zhao, and B.Z. Tang, *Appl. Mater. Interfaces*, Vol. 2, p. 566, 2010.
22. K.E. Johson, J.A. Lovinger, C.O. Parker, and M.G. Baldwin, *Journal of Polymer Science, Part B*, Vol. 4, p. 977, 1966.
23. M.G. Baldwin, K.E. Johson, J.A. Lovinger, C.O. Parker, *Journal of Polymer Science, Part B*, Vol. 5, p. 803, 1967.
24. L. Wan, J. Tian, J. Huang, Y. Hu, F. Huang, and L. Du, *Journal of Macromolecular Science, Part A-Pure and Applied Chemistry*, Vol. 44, p. 175, 2007.
25. L. Wan, Y. Luo, L. Xue, J. Tian, Y. Hu, H. Qi, X. Shen, F. Huang, L. Du, and X. Chen, *Journal of Applied Polymer Science*, Vol. 104, p. 1038, 2007.
26. L. Wan, J. Tian, J. Huang, Y. Hu, F. Huang, and L. Du, *Journal of Applied Polymer Science*, Vol. 106, p. 2111, 2007.

27. J. Tian, L. Wan, J. Huang, Y. Hu, F. Huang, L. Du, *Polymer Bulletin*, Vol. 60, p. 457, 2008.
28. J. Tian, X. Wang, L. Wan, Y. Hu, F. Huang, and L. Du, *High Performance Polymers*, Vol. 22, p. 198, 2010.
29. X. Zhou, L. Wan, Y. E, Y. Hu, F. Huang, and L. Du, *Polymer Journal*, Vol. 42, p. 216, 2010.
30. X. Wang, Y. E, L. Wan, F. Huang, and L. Du, *Journal of Applied Polymer Science*, Vol. 120, p. 419, 2011.
31. Y. Luo, Y. Hu, L. Wan, F. Huang, L. Du, *et al.*, *Chem. J. Chinese U.*, Vol. 27, p. 170, 2006.
32. J. Huang, L. Wan, J. Tian, Z. Zhao, X. Wang, Y. Hu, F. Huang, and L. Du, *Acta Chim. Sinica*, Vol. 65, p. 2629, 2007.
33. L. Xue, L. Wan, Y. Hu, F. Huang, L. Du, *et al.*, *Thermochimica Acta*, Vol. 430, p. 147, 2006.

This page intentionally left blank

9

High Performance Fibers

Mehdi Afshari[1,2], Richard Kotek[1], Peng Chen[3]

[1]Textile Engineering Chemistry and Science Department, College of Textiles, North Carolina State University, Raleigh, NC, USA
[2]Fiberweb Inc., Old Hickory, TN, USA
[3]Ningbo Institute of Materials Technology and Engineering, Chinese Academy of Sciences, Ningbo, Zhejang, China

Abstract

This chapter reviews recent developments in the production of well-established high tenacity and high modulus (HT-HM) fibers known as high performance fibers such as Kevlar, PBO, Spectra, and M5 fibers. The new generation of high performance fibers "smart fibers" go beyond the scope of this chapter and did not discussed. All the polymers in HT-HM fibers have strong axial chemical bonding. The polymer chain could be linear and flexible such as polyethylene used in Spectra/Dyneema. The linear polymer chain could be stiff like Kevlar. Carbon fiber is another HT-HM fiber which graphitic sheets oriented parallel to the fiber axis. We also review advances in improving performance of conventional melt spun fibers by manipulating fiber structure, i.e., molecular orientation and crystallization via novel technology.

Keywords: High performance fibers, M5, Zylon, Kevlar, Dyneema, Spectra, PEN

Introduction

In recent years significant progress has been made in high performance fibers that are produced from rigid and flexible polymers. Each subchapter describes in details advances in major fibers namely, M5, Zylon, Kevlar, Dyneema/Spectra, and carbon fibers.

Vikas Mittal (ed.) High Performance Polymers and Engineering Plastics, (269–340)
© Scrivener Publishing LLC

9.1 PIPD or "M5" Rigid Rod

9.1.1 A New HM-HT Fiber

As a result of research in Akzo-Nobel laboratories a new high-performance fiber, known as M5, has been produced. Akzo-Nobel has spun off its fiber activities, and the M5 project has been taken up by Magellan Systems International. DuPont de Nemours has taken a majority interest in Magellan. The polymer is poly {2,6-diimidazo[4,5-b:4',5'-e]pyridinylene-1,4-(2,5-dihydroxy)phenylene} or PIPD, with the formula shown in Scheme 9.1.

Two methods have proved effective in preparing high modulus, high tenacity polymer fibers:

a. perfecting the drawing technique of precursor fibers to attain draw ratios far above ten, as in the well-known polyethylene Dyneema and Spectra yarns [1–3] described in Section 4 and
b. manipulating rigid rod-like molecules into fibers that are already very highly oriented in the as-spun state, as in PPTA fibers [4–6] described in Section 3.

Work has been directed at much stiffer rigid rod like materials in an effort originating with the U.S. Air Force culminating in the PBO fiber (Section 2) that is now commercially available from Toyobo after much development at Wright-Patterson AFB, at SRI International and at Dow Chemical [4, 7, 8]. Although PBO shows very impressive tensile properties, its performance under compression has been disappointing, and much work has been done in various ways to correct the problem, without making much headway. Various schemes have been tried to increase lateral strength in PBO after fiber formation, [9–15] often by crosslinking. One attempt at introducing hydrogen bonds in such a polymer did not afford the improved compression performance hoped for; its

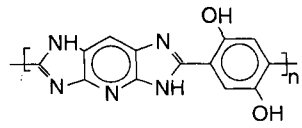

Scheme 9.1 Poly{2,6-diimidazo [4,5-b:4',5'-e]pyridinylene-1,4-(2,5-dihydroxy) phenylene} (PIPD).

lack of success in attaining improved compression properties was attributed to the hydrogen bonds being formed intra rather than inter-molecularly [16].

It has been the aim of one of the researchers (Doetze J Sikkema) to create polymers as rigid rod-like as PBO, with strong intermolecular hydrogen bonds. After much experimentation, some of which has been reported [17–20], scientists turned their attention to the well-proven (albeit experimentally challenging – cf. Ref. [9–15]) polymerization of one-ring aromatic tetrafunctional nucleophiles. An example of high merit appeared to be 2,3,5,6-tetraaminopyridine: 2,6-pyridinediamine, a commercial product, is fairly simply accessible by Chichibabin amination [21] (they found a more economical route to 2,6-diaminopyridine) and, importantly, nitration was expected to be highly selective to produce the 3,5-dinitro isomer. Literature reports existed on this nitration, albeit with low yield after purification, [22, 23] as well as on polymerization of the tetraamine HCl salt (along the USAF-SRI lines [9–15] for PBO), with isophthalic acid to prepare a thermally stable polymer [21, 24].

9.1.2 Monomer Selection and Syntheses

Synthesis of 2,3,5,6-tetraaminopyridine (TAP) along the lines of Refs. [21] and [24], with low yield after nitration, and including reduction with tin/hydrochloric acid afforded early samples of TAP (Scheme 9.2).

In early work, researchers isolated TAP as the hydrochloride salt and used it in the polymerization, cf. Ref. [9–15] The nitration problems were soon corrected by modifying the nitration medium- changing from concentrated sulfuric acid [21, 24] to oleum [25]. Thus, they could isolate high purity products at 90–95% from the nitration and 85% yield of polymer grade purity crystal ($TAP \cdot 3HCl \cdot 1H_2O$) from the reduction with hydrogen. Having a sufficient supply of TAP in hand, they tackled the polymerization. Reaction according to the method developed in Refs. [9–15] with terephthalic acid produced almost instantaneous precipitation of very low MW oligomer.

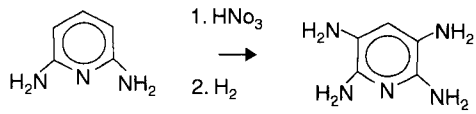

Scheme 9.2 Structure 2,3,5,6-tetraaminopyridine (TAP).

Polymerization with 2,5-dihydroxyterephthalic acid seemed desirable in itself because the hydroxyl groups could contribute to the hydrogen bond network envisioned (even though disappointing results were reported in Refs. [17–20] with this monomer); the reaction led to high molecular weight products, in contrast with the results with unsubstituted terephthalic acid. Thus, not only an enhanced-polarity polymer proved accessible, in fact the analog with fewer active protons could not be prepared in a usable form. Concentrations of almost 20 wt.% of polymer in solution in PPA could be attained. By contrast, 1,2,4,5-tetraaminobenzene [26] (which likewise gives insoluble very low MW material with terephthalic acid, note that reasonable MW was reached in polymerizing a tosylated monomer) [27] proved to have a solubility limit in its high MW polymer with 2,5-dihydroxyterephthalic acid of about 8.5%, in related work in laboratory (at 8–9% of polymer in PPA consisting, at the end of the polymerization, of 81.0% of P_2O_5 and 19.0% of water, η_{rel} values of about 100, 0.25 g/dl in methanesulfonic acid, could be reached when starting with tetraaminobenzene — DHTA 1:1 complex. Lower MW products of this type were described in Ref. 28) [28].

2,5-Dihydroxyterephthalic acid (DHTA) is described (Scheme 9.3) in the literature as the product of bromine/sulfuric acid mediated aromatization [29] of diethyl succinoylsuccinate, a commercial product, followed by hydrolysis. The aromatization can also be effected with sulfur: succinoyl succinate is boiled with slight excess of sulfur in NMP for 20–30 min as the temperature rises from about 150°C (H_2S evolution) to about 200°C. Dilution with water precipitates dimethyl dihydroxyterephthalate which is hydrolyzed with hot aqueous NaOH. Alternatively, aromatization can be done with S and a Pd/C catalyst [17–20]. Sikkema *et al.* found a convenient and non-noxious procedure in aromatizing the succinoylsuccinate in acetic acid at reflux with 30% aqueous hydrogen peroxide with

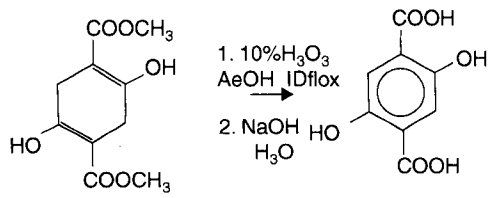

Scheme 9.3 Structure of 2,5-dihydroxyterephthalic acid(DHTA).

a sodium iodide catalyst. After hydrolysis, >90% of polymer grade DHTA [30] from succinoylsuccinate can be isolated upon acidification. Alternatively, the sodium salt of DHTA can be crystallized from the hydrolysis reaction mixture in high purity and somewhat lower yield (abt. 87%).

With a view to improved economics in the case of scaling up, Sikkema *et al.* developed syntheses of the monomers based on epichlorohydrin, HCN and ammonia for 2,6-diaminopyridine [21] and for DHTA based on hydroquinone and CO_2 [30].

9.1.3 Polymerization

Right from the outset of work with TAP hydrochloride and DHTA (Scheme 9.4), scientists avoided the experimental difficulties inherent in the traditional [9–15] method of adding most of the phosphorus pentoxide, and the organic diacid only after driving off the hydrochloric acid by heating in ("weak") polyphosphoric acid (PPA). When working at a small scale at least, they could add all ingredients at the outset of a heating cycle that involved (cf. Ref. [9–15]) many hours of heating at about 100°C while evacuating, to eliminate the hydrochloric acid. An important improvement was found in isolating TAP as its phosphoric acid salt, resulting not only in a much faster polymerization cycle, but also eliminating the corrosion-type difficulties implicit in the earlier route. A further convenience improvement was achieved by the synthesis of the TAP.DHTA 1:1 complex, or TD complex. This complex is significantly more stable against oxidation than TAP phosphate and it precipitates in a high yield from the combination of (alkaline) aqueous solutions of TAP and DHTA Na or K salt upon neutralization. A fast polymerization cycle (typically 4–8 h) rather than 24 h according to Ref. [9–15] now yields high MW polymer with high consistency: relative viscosities (0.1 g/dl in methane sulfonic acid) of 8 and above could be reached routinely. Others did not succeed in preparing the terephthalic acid salt of TAP, curiously, Rosenberg,

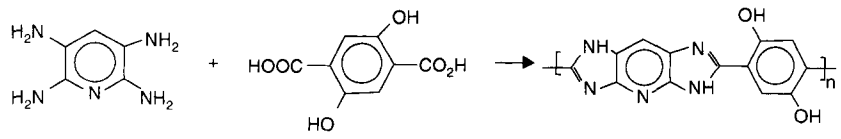

Scheme 9.4 Polymerization TAP and DHTA.

Krauss, and Kleiss describe a facile preparation of the terephthalate salt of 4,6-diaminoresorcinol [31]. Thus, copolymers employing both DHTA and terephthalic acid (TPA) necessitated use of TAP phosphate and TPA next to TD complex. Such copolymers showed lower relative viscosities when more TPA was used as a comonomer, and became insoluble in the polymerization medium when more than 50% of DHTA was substituted by TPA.

The polymerization of homopolymer consists of taking TD complex, polyphosphoric acid and P_2O_5 with a trace of tin powder into the reactor, displacing air by nitrogen, homogenizing the thick slurry, and raising the reaction temperature to 130–140°C. Mixing for at least 1.5 h at that temperature before taking the mixture to 180°C and stirring for another 1–2 h yields the spinning solution. The solution becomes liquid crystalline when it reaches 140°C. Work on the mechanism of PBO polymerization has been reported. [32, 33] Sikkema's view is different [34].

The P_2O_5 content of the solvent system impacts the final molecular weight, and obviously only the highest purity TD complex will deliver the highest MW polymers. Conveniently, the final phosphoric pentoxide content of the solvent system is 82%, the balance being water. Solubility limit of high MW homopolymer in 80.5–83% PPA (i.e., a PPA consisting of 80.5–83% of P_2O_5 and the balance being water) is 19 wt.%. At 180°C, the solution (18 wt.% of polymer) is a nematic solution with long relaxation times of orientation; upon cooling it crystallizes at about 110°C; the crystallized solution melts at about 140°C. A further thermal transformation can be seen at about 80°C in DMA. Crystallosolvate fibers of astoundingly high and perfect crystallinity could be prepared under special conditions [35].

9.1.4 Fiber Spinning and Fiber Properties

Conventional air gap wet spinning of the as-polymerized solutions of polymers with Mw 60,000–150,000 (Twaron aramid calibration SEC in methane sulfonic acid) at 180°C into a water or dilute phosphoric acid bath, proceeded readily; spindraw ratios attainable depend on spinning orifice diameter and the result normally delivers filaments with a diameter of about 10 mm, which are further washed to a low phosphorus content and drawn (by a few percent at most) at high temperature (>400°C) to produce the final, high modulus product. It is unclear whether the crystal solvate can form

in the air gap – the process being characterized by very fast cooling. The XRD patterns of solidified polymer solution in PPA showed the existence of two different crystal solvate phases. The crystal solvate phase 1 in the polymer solution at room temperature changed to crystal solvate 2 which starts at 85°C and is completed at 115°C. It disappears above 135°C and a nematic phase appeared. The transition from nematic phase to the crystal solvate can happen by cooling. The crystallinity of crystal solvates of PPID is higher than PBO and PBT. The coagulated and washed fiber is isolated as a crystal hydrate and the hot drawing process transforms this into the final high modulus "M5" crystal structure [35]. The as-spun fiber already shows attractive mechanical properties, comparable to para-aramid fibers, although the modulus is higher (about 180 GPa). The as spun fiber excels in flame resistance [36]. The crystal-to-crystal transformation during the hot drawing leads to a much higher modulus, due to a more slender effective chain and stronger interchain bonding, coupled with an improvement of the orientation [35]. Note that the fiber modulus depends on the shear modulus through nonperfect orientation of the molecules [37].

Evolution of fiber structure and morphology, and its properties, during the manufacturing process is discussed in detail in Ref. [35]. The final crystal structure is analyzed in Ref. [38] and illustrated in Figure 9.1. The rod like polymer molecules feature internal hydrogen bonds between -O-H groups and imidazole N atoms, and a network in both directions perpendicular to the rodlike chains between imidazole N-H atoms and the — O-H groups [38]. For the determination of this hydrogen bond structure, it was not sufficient to ascertain the precise arrangement of the heavier atoms, but further measurements were needed. The fact that over a very large temperature range, both directions perpendicular to the polymer chain direction showed that the same thermal expansion was the final lock on the proof of the 3-dimensional network character of the hydrogen bond system (as opposed to a sheetlike character), [38] as an independent observation in addition to the very high shear modulus determined from the relation [37] between molecular orientation and fiber properties [35].

The as-spun PIPD fiber is a crystal hydrate, which transforms into a bidirectional hydrogen bonded structure during heat treatment. This transition results in an increase in crystalline modulus along the chain direction due to a decrease of the cross-sectional area per chain, and in an increase in shear modulus due to stronger

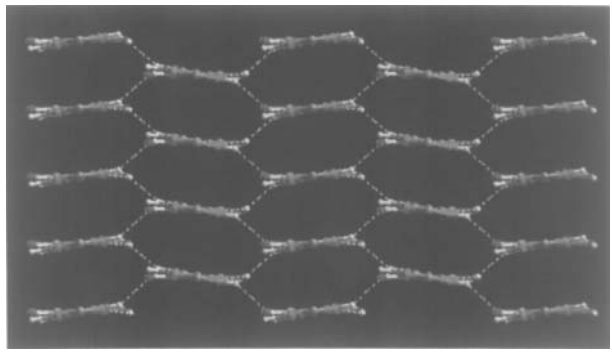

Figure 9.1 The crystal structure of M5-HT seen along the chain axis. Note the bidirectional hydrogen-bonded network between the chains resembling a honeycomb and reinforcing the lateral chain - chain interaction. This leads to a high shear modulus and shear strength and thus to good compressive properties of the M5 fiber. We speculate that this honeycomb-like structure may be involved in the explanation of the impact and damage tolerance properties of M5 products (reprinted from ref. 38 with permission from Elsevier).

interaction between the chains caused by hydrogen bonds. During heat treatment of PIPD fiber improvement of orientation of the fiber and change in crystal structure happened. The heat treated fiber has a bidirectional hydrogen bonded network which causes a strong interaction between polymer chains and results in a high shear modulus (Figure 9.2). Figure 9.3 shows the change of structure during processing of PIPD fibers [35].

The crystal structure of as-spun PPID fiber is a two-dimensional ordered crystal hydrate. At high temperatures a three dimensional crystalline order is developed. The heat-treated PIPD fiber has a monoclinic symmetry structure. The good compression performance of heat-treated PIPD fiber can be explained by the monoclinic crystal structure with its bi-directional hydrogen bonding network [38].

Even though much optimization remains to be done, Sikkema *et al.* soon achieved promising mechanical properties and structure data in new "M5" fibers, even from bench scale operations using improvised machinery. Moduli well over 300 GPa, tenacities of well over 2.3 N/tex (4 GPa), elongation at or above 1.5% and compressive strength of 1.7 GPa (onset of plastic deformation) were recorded – the highest compressive yield strength by far shown by

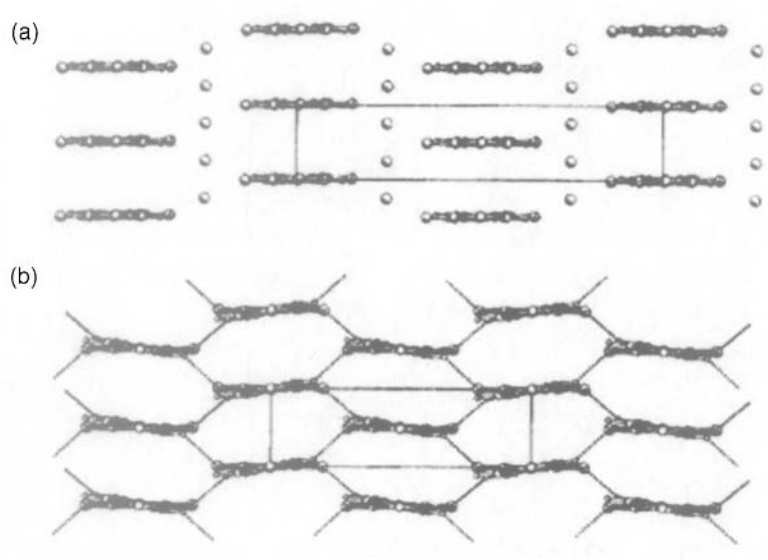

Figure 9.2 Projection of (a) as-spun PIPD fiber and (b) heat-treated PIPD fiber (reprinted from ref. 35 with permission from Elsevier).

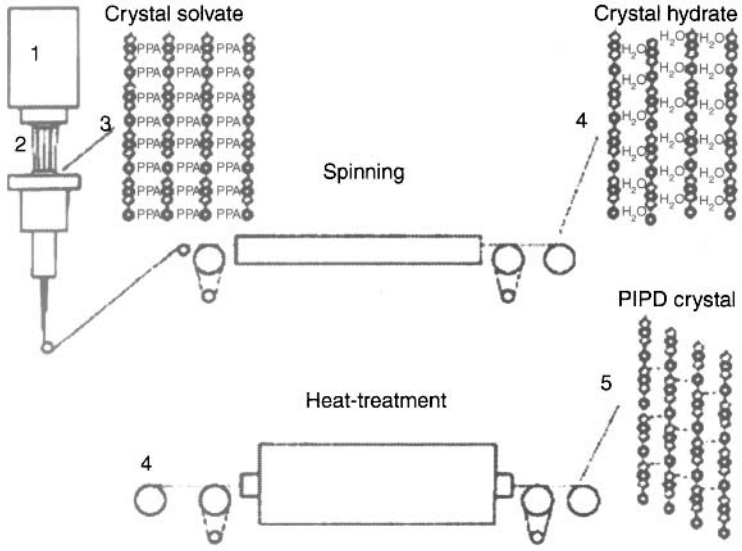

Figure 9.3 Structure development during fiber fabrication process: 1-nematic phase; 2-oriented nematic phase; 3-crystal solvate; 4-crystal hydrate; 5-water-free structure (reprinted from ref. 35 with permission from Elsevier).

any polymer fiber [35]. Tensile and compressive deformations were investigated by micro-Raman spectroscopy, with qualitatively the same conclusions [39]. The good compressive properties are coupled to a very high internal shear modulus of 7 Gpa [35]. The first composite test bars that were tested for longitudinal compressive strength confirmed the high compressive properties of the new fiber in composite form [40]. Three point bending tests of composite bars indicated a compressive yield stress of 1.75 GPa in the fiber (onset of plastic deformation at the most-stressed surface of the test bar) [40].

Ab initio calculations were performed on the M5 molecule and crystal [41]. A chain modulus of 553–578 GPa was concluded (depending on details in the unit cell), in good agreement with the experimental chain modulus from WAXS measurements of 510 GPA [35]. The internal hydrogen bond contributes to this particularly high value.

Work is proceeding to spin fibers with properties exceeding the values given in Table 9.3 for early experimental samples of the new [42] fiber. Details on convenient laboratory scale procedures to prepare the monomers and the polymer have been published [34], alternative routes intended for scaling up were worked out as well [21, 25, 30].

9.1.5 Applications and Outlook

The mechanical properties of the new fiber make it competitive with carbon fiber in most applications – in light, slender, load bearing stiff advanced composite components and structures. Very promising indications were obtained pointing to a ductile failure mode of (bending and compression) test pieces notwithstanding the high stiffness. Similarly, such very stiff composite test pieces showed outstanding impact properties in scouting experiments. This suggests the possibility to design, for instance, vehicle parts substantially lighter than can now be done on the basis of brittle reinforcing fibers. The ductile (as opposed to brittle) properties of the fiber under (bending; compression) overload conditions also explain the easy processability of the new fiber in textile type operations (weaving, knitting, braiding, and so on). Exploratory evaluation of the UV stability of M5 indicated excellent performance in that field. The high electrical resistance of the new fiber would enable it to perform in areas where carbon fiber presents problems (corrosion in metal contacts) or is unsuitable, such as in electrical

and electronic contexts. The high polarity of M5 aids in easy adhesion to a variety of matrix materials, judging by bundle pull-out tests performed with various epoxy, unsaturated polyester, and vinyl ester resins. These gratifying results were obtained without any optimization, suggesting further possibilities of even higher or (if needed) specifically tailored adhesion levels, depending on the application. The very good UV-resistance should be helpful in many fields – this is a particular strength of M5 where many other organic fibers show a weakness.

Other than the composites field, flame-resistant textiles appear to be another interesting field of applications. Table 9.1 lists observations in a cone calorimeter, when standard construction fabrics were challenged with an air stream at 900°C. Table 9.2 compares the mechanical properties of M5 with aramid, carbon, and PBO fibers.

9.2 "Zylon" PBO Rigid Rod Polymer Fibers

9.2.1 Introduction

PBO fiber was commercialized by Toyobo Co. in 1998 after about 20 years research in United States and Japan with the trade name Zylon. Poly {benzo [1,2-*d*:5, 4-*d'*]bisoxazole-2,6-diyl-1,4-phenylene} (PBO) (Scheme 9.5) belongs to the class of high performance fibers commonly known as rigid-rod polymers. Rigid rod polymers are classified into lyotropic and thermotropic liquid crystalline polymers. Lyotropic and thermotropic polymers show liquid crystallinity in

Table 9.1 Flammability of high performance fibers.

Material	Time to ignition (Seconds)	Peak heat release rate	Light extinction in Smoke column	Residue (%)
FR M5	77	44	224	61
HT M5	48	54	844	62
PBO	56	48	2144	72
Twaron/ Kevlar	20	205	70816	11
Nomex	14	161	38670	24

Table 9.2 Provisional characterization of M5 fiber, spun at bench scale, compared with commercial fibers.

	p-Aramid HM	Carbon HS[a]	PBO[b]	M5 Exper.
Tenacity, GPa	3.2	3.5	5.5	5
Elongation, %	2.9	1.5	2.5	1.5
E modulus, GPa	115	230	280	330
Compr. str., GPa[c]	0.58	2.1	0.4	1.6
Compr. strain, %[c]	0.5	0.9	0.15	0.5
Density	1.45	1.8	1.56	1.7
Water regain, %	3.5	0	0.6	2
LOI,% O_2	29	68	>50	
Onset of thermal degradation, air	450	800	550	530
UV resistance	–	++	–	++
Electr. conduction	–	++	–	–
Impact resistance	++	–	++	++
Damage tolerance	+	–	++	
Weaving props	+	–	+	+
Knot strength	+	–	0	0

[a]Mechanical properties of carbon fibers are evaluated in resin impregnated strands to protect the material against premature brittle failure in the tensile testing machine. The organic fibers are tested as such: filament averages at 10 cm gauge length are presented.

[b]Toyobo data.

[c]Measured in UD composite test bars, 3-point bending test, onset of deflection for the organic fiber reinforced composites; catastrophic failure for the carbon composites. M5 composites proved to be able to carry much higher loads than the load at onset of deflection in these tests, and to absorb much energy at high strains in a mode analogous to the ductile behavior in steel structures being overloaded.

solution and in the melt, respectively. PBO and Kevlar polymers both show lyotropic behavior.

The chemical structure of PBO is similar to that of poly {2,6-diimidazo[4,5-b:4′,5′-e]pyridinylene-1,4-(2,5-dihydroxy) phenylene} (PIPD), the new 'M5' fiber. PBO has great thermal stability and does not exhibit softening behavior prior to thermal

Table 9.3 Unit cell parameters of PBO [77, 79] (reprinted from Ref. 73 with permission of Wiley).

Crystal					
system	a (nm)	b (nm)	c (nm)	g (degrees)	References
Monoclinic	1.1201	0.3540	1.205	101.3	77
Monoclinic	0.5651	0.3570	0.603	101.4	79

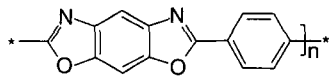

Scheme 9.5 Structure of Poly {benzo[1,2-*d*:5, 4-*d'*]bisoxazole-2,6-diyl-1, 4-phenylene} (PBO).

degradation (above 600°C in air) [43]. PBO fiber has outstanding tensile modulus (352 GPA) and tensile strength (5.6 GPA) compared to other commercially available high performance fibers and its specific strength and specific modulus 9 and 9.4 times that of steel [44, 45]. For PBO, with great performance came great problems. The resistance of PBO to UV light and visible radiation is notoriously poor. PBO also lack axial compressive strength. The tensile strength of PBO fiber also reduces in hot and humid environments. Considerable effort has been devoted to chemical modifications of PBO fiber to enhance axial compressive strength.

9.2.2 Monomer Synthesis

The first challenge to be overcome in the production of PBO is the high purity synthesis of the monomer 4,6-diamino-1,3-benzenediol dihydrochloride (DABDO) (Scheme 9.6). The long-established method developed by Wolfe *et al.* [46] involved reacting diacetyl-1,3-benzenediol with concentrated nitric acid containing less than 2% water. This method required multiple recrystallizations to remove undesirable byproducts. The expense of the starting materials and the purification process has lead to the abandonment of this method of DABDO production in favor of a process developed by Lysenko [47] at the Dow Chemical Company. This method involves nitrating 1,2,3-trichlorobenzene under acid conditions to produce 1,2,3-trichloro-4,6-dinitrobenzene. Sodium hydroxide is

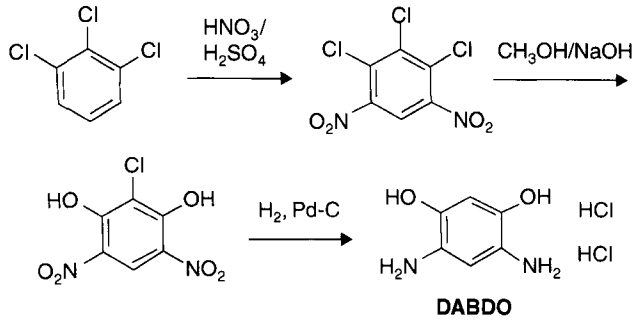

Scheme 9.6 Synthesis of 4,6-diamino-1,3-benzenediol dihydrochloride (DABDO).

then used to displace the chlorines in the 1 and 3 positions. The final step involves the use of hydrogen and a palladium catalyst to remove the 2-chlorine and reduce the nitro groups to amino groups [47]. Great care must be taken once the DABDO is produced as the monomer will rapidly decompose if it is exposed to oxygen or water [48].

The other monomer needed for the traditional production of PBO is terephthalic acid (TA) or a similar TA derivative. The TA must have extremely high purity and small particle size (50–100 μm) and is easier to handle than the acid chloride; [49, 50] suitable TA is commercially available. However, the particle size must be reduced to less than 10 μm in order to ensure complete dissolution in poly phosphoric acid (PPA) for the polymerization. Recently, TA has been used as a starting material for the synthesis of 1,4-bis (1-chloro-2,2-dicyanovinyl)benzene (CCB) (Scheme 9.7). Using CCB for PBO polymerization yields a more soluble precursor.

The cost of monomer synthesis has been a major consideration in the potential commercial production of PBO. A cost effective synthetic approach to PBO monomer, 4, 6 - diamino-1,3-benzenediol dihydrochloride has been reported. This synthetic method uses 1,2,3-trichlorobenzene as a starting material for nitration, which guarantees that only dinitration occurs at positions 4 and 6 in the benzene ring with no possibility of trinitration. After displacement of 1,3-dichloro groups by hydroxyl groups, the final catalytic hydrogenation step combined reduction of nitro to amine groups and hydrogenolysis of the 2-chlorine atom, and yielded the high quality monomer [51].

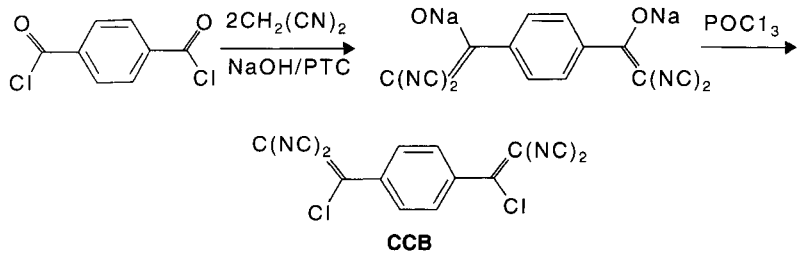

Scheme 9.7 Synthesis 1,4-bis(1-chloro-2,2-dicyanovinyl)benzene (CCB).

9.2.3 Polymerization

The role of polyphosphoric acid (PPA) in the polymerization of PBO is complex (Scheme 9.8). PPA acts as a solvent, catalyst, and dehydrating agent. The three functionalities of PPA allow formation of polybenzobisazoles in situ without any separation. The functions of PPA are controlled by adjusting the concentration of P_2O_5 during a two stage polymerization process. During the first stage lower viscosity is favored because it allows the hydrogen chloride protecting groups to leave the solution more easily as they are removed. Low viscosity during this dehydrochlorination step is maintained by using PPA with low P_2O_5 concentration (75–80%). To begin the second stage the P_2O_5 concentration is raised to 88%.

As the polymerization proceeds, the amount of P_2O_5 decreases to the optimal final concentration of 83% [52]. PBO is a lyotropic polymer meaning that is displays liquid crystalline behavior which is dependent upon the concentration in solution [53]. The two stage method of adjusting the P_2O_5 concentration allows the production of PBO at high polymer concentrations.

Extensive research has been carried out to understand PBO polymerization mechanism [54]. Observations have been made which indicate that PBO is formed through an unusual polymerization mechanism. Step-growth polymerization with AA and BB monomers usually requires equal proportions of each monomer type to achieve high molecular weights. Oligomers isolated during step-growth polymerization are expected to have a statistical distribution of each monomer type on the chain ends. Surprisingly, unlike the conventional step-growth polymerization reactions, in PBO polymerization only oligomers containing DABDO on the ends are observed. This is a result of poor solubility of TA in PPA.

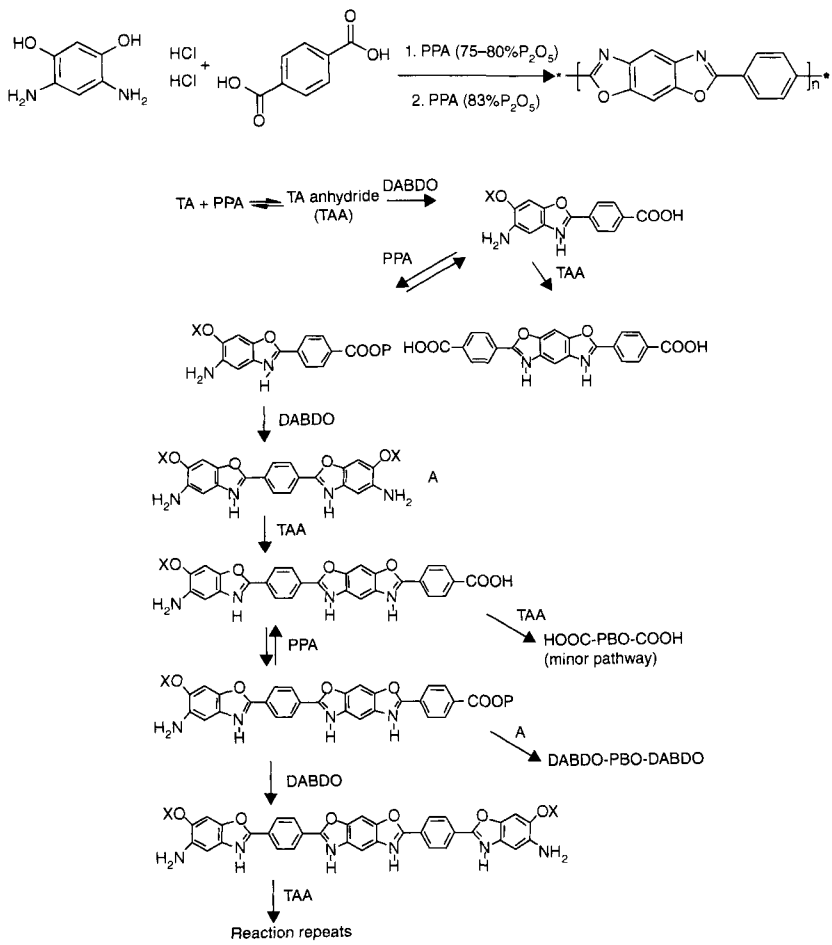

Scheme 9.8 Synthesis of PBO.

PBO polymerization can proceed to high molecular weights even when there is a 5% excess of TA. The high degree of polymerization that can be obtained with an excess of one monomer can be explained by the low of solubility of TA in PPA. The solubility at 140°C is 0.0006 g TA per 1 g PPA [44].

The polymerization kinetics of PBO has been studied by several researchers, but it is difficult to draw a unanimous conclusion from these researches due to complexity of the reaction system involving an isotropic-nematic phase transition [55–57]. The polymerization rate for PBO was found to decrease sharply

with the increase of the molecular weight in the isotropic state, [58] which implied a diffusion-controlled polymerization process. However, the polymerization in the nematic phase appeared to be independent of the degree of polymerization [57]. This result suggests that for well-mixed reaction mixtures, translational diffusion does not appear to control the polymerization rates of PBO in the nematic phase.

9.2.4 Solution Properties

PBO is soluble in some strong acids such as PPA, methanesulfonic acid (MSA), chlorosulfonic acid, and trifluoroacetic acid [59] via backbone protonation, which weakens intermolecular interaction and reduces chain stiffness [60, 61]. The Mark-Houwink equation of PBO in MSA at 308°C is given by [49]:

$$[\eta] = 2.77 \times 10^{-7} \overline{Mw}^{1.8}$$

The Mark-Houwink exponent of 1.8 indicates the high polymer chain rigidity. The persistence length of cis-PBO in MSA reported about 20–30 nm [62] and 50 nm [63], whereas the theoretical persistence calculated in the range of 22–65 nm [64–66]. By comparison, the persistence length of flexible polymers such as PE is much shorter (1 nm or less).

PBO can also be dissolved in aprotic organic solvents such as nitroalkanes and nitrobenzene in the presence of Lewis acids such as BCl_3, $AlCl_3$, and $GaCl_3$ because of electron donor-acceptor complex formation [67–69]. The average effective diameter of the polymer chains by complex formation decreases the L/D ratio. The higher critical concentration and the utilization of organic solvents are attractive from industrial point of view, compared with the protonated PBO using protic strong acids. However, fibers could not be processed from these solutions.

9.2.5 Fiber Spinning

The question of how to spin a lyotropic liquid crystalline polymer which has high thermal stability and degrades before it melts presented a major challenge. Fortunately for the makers of PBO this question had already been answered during the development of Kevlar. PBO is spun directly from the PPA solution used

in polymerization via the dry jet wet-spinning technique without polymer precipitation and re-dissolution (Figure 9.4). The fibers that are spun from this solution have maximal strength and modulus when the viscosity of the spinning solution is 30 dL/g [50]. Figure 9.4 is a schematic illustration of a fiber preparation line [70]. As the fiber emerges from the spinneret it travels through an air-gap before reaching the coagulation bath. The air gap is another technique which was developed for processing Kevlar in the 1960s before being applied to PBO production. Because of liquid crystalline behavior, the orientation of the PBO fiber is greatly improved by the use of the air gap. The orientation of PBO is also improved by heat treatment under tension in a nitrogen environment following coagulation and washing [71]. The concentration of polymer in the spin dope is 10–15 wt% and the temperature can range from 100°C to 170°C [49].

The common coagulation bath consists of water at room temperature. Coagulation speed depends on temperature and coagulation media. Acidic (dilute phosphoric acid solution [72]), basic (ammonium hydroxide [73]), and organic (methanol [73]) coagulants are used for PBO. Coagulation conditions significantly affect the ultimate fiber structure and mechanical properties. In the post processing step, coagulated fiber is washed, dried, and heat-treated under tension. Heat treatment under tension is a key step for obtaining

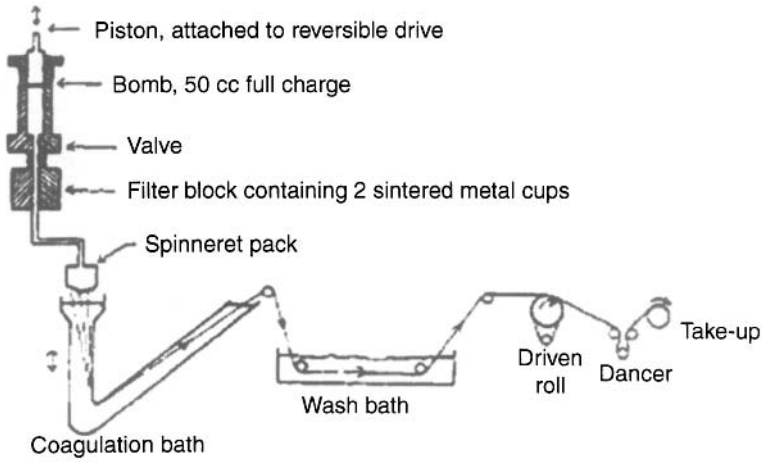

Figure 9.4 Schematic picture of producing line of fibers (Reprinted from ref. 50 with permission of MRS).

high molecular orientation in order to enhance mechanical properties of fibers. Typically for high tensile strength fiber, the PBO solution with the intrinsic viscosity 50 dL/g and molecular weight of the order of 40,000 g/mol was used [49].

9.2.6 Structure and Morphology

The liquid crystalline polymeric fibers exhibit high degree of order and orientation (greater than 0.9) compare to commodity polymeric fibers such as polyester, nylon, and polypropylene. The structure of commodity fibers is highly defective and contains chain folds and low amorphous orientation and typically crystallinity 30–65%, while the crystalline orientation is in the range of 0.9–0.98.

The crystal structure of PBO is monoclinic (Table 9.3 [74, 75, 115] and Figure 9.5 [76]). The crystal size of PBO fibers from WAXD increased with heat treatment along the fiber axis and c-axis in agreement with TEM studies [77–79], and the crystal perfection also improved by heat treatment. There is a limited growth of the crystallites along the c-axis after heat treatment which indicates that a high degree of axial order in PBO fiber has already existed in the as-spun state. WAXD patterns show PBO-PPA complex when fiber

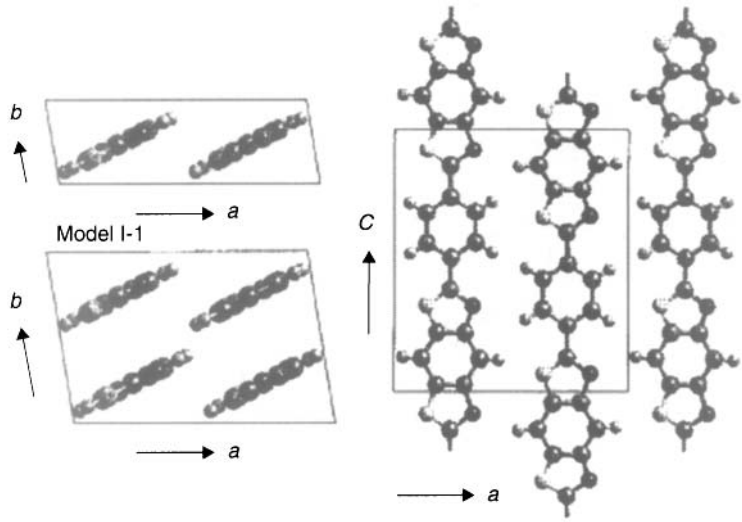

Figure 9.5 Crystal structure PBO (reprinted from ref. 107 with permission from ACS).

coagulated for 2 s in water at room temperature and formation of pure PBO crystals after long coagulation times (30 min). Diffraction patterns of PBO fiber show layer line streaking indicative of axial disorder similar to PBZT. However, with increasing heat treatment the scattering becomes more localized and an off-meridian reflection on the second layer line becomes well-defined and intense. Therefore, there is a three dimensional crystalline order in the heat treated PBO fiber [77–79]. Adams *et al.* [73] studied heat treated PBO fiber by TEM bright field lattice imaging. Fratini *et al.* [75] determined a non-permitive monoclinic unit cell with two chains per cell by using X-ray. They proposed a model in which neighboring polymer chains packed side by side are displaced by discrete axial translations. SAXS showed the presence of voids elongated along the fiber axis due to large volume reduction during coagulation. The Northolt's plot of PBO fibers showed inhomogeneity along the fiber axis within the fibrils (four point pattern) in as spun fibers and homogenous structure (without four point pattern) along the fiber axis in high modulus fibers (Figure 9.6) [76, 80]. Figures 9.7 and 9.8 show the structural model of PBO fiber and TEM images showing elongated microvoid structure in the fiber [80].

The SEM images of PBO fibers show fibrillar structure. A hierarchical structure model [81] was proposed for oriented liquid crystalline polymers, in which a fiber is made up of macrofibrils,

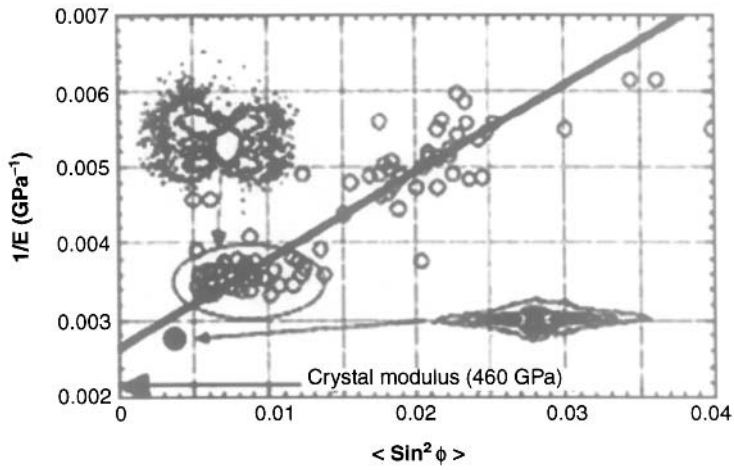

Figure 9.6 Northolt's plot for PBO fibers with SAXS patterns (reprinted from ref. 76 with permission from ACS).

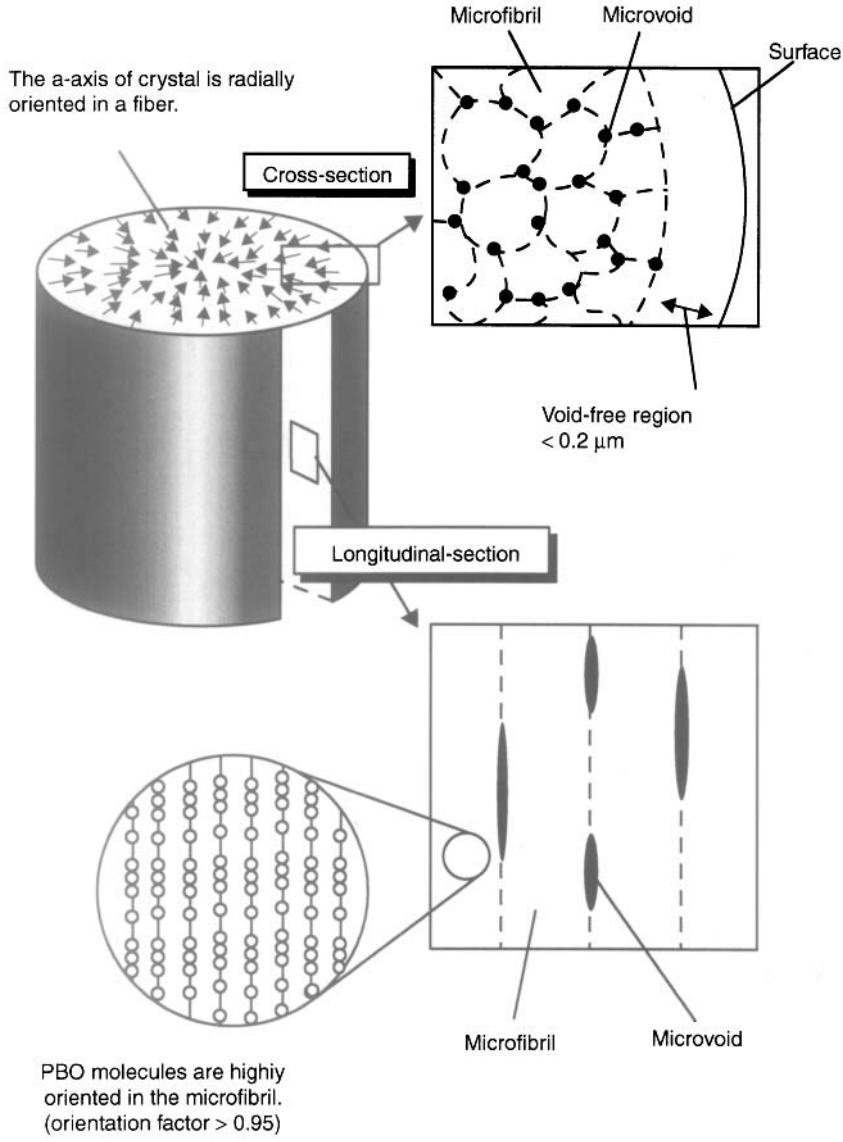

Figure 9.7 PBO structure model (reprinted from ref. 77 with permission from ACS).

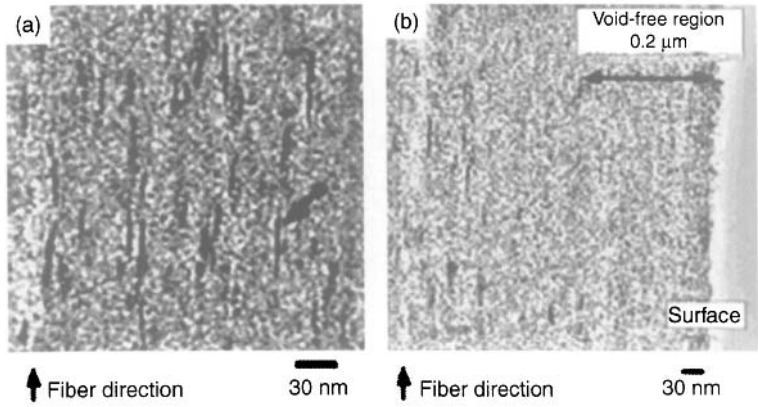

Figure 9.8 TEM image of capillary microvoids focusing on core region of the fiber. Mean micro-voids diameter is approximately 30 A°, (b) TEM image of capillary microvoids in surface region (reprinted from ref. 77 with permission from ACS).

fibrils, and microfibril. The typical diameters of these entities are suggested to be 5, 0.5, and 0.05 μm, respectively.

9.2.7 Fiber Properties

9.2.7.1 Mechanical Properties

Table 9.4 summarizes properties of various fibers. The tensile strength and modulus of PBO fibers were reported to be 5.8 and 352 GPA, respectively [82, 83]. The mechanical properties of PBO fibers depend on polymer molecular weight, processing and post processing conditions [84, 85]. The modulus of PBO fiber from X-ray diffraction was measured to be in the range of 460–480 GPA [86, 87]. Figure 9.9 shows crystal modulus versus fiber modulus of various high performance fibers.

PBO is currently sold under the trade name Zylon® [88]. Toyobo produces Zylon® AS (as spun) and Zylon® HM (high modulus) (Tables 9.5 and 9.6).

The lack of compressive strength seen in PBO fibers is responsible for driving the development of PIPD fibers. Comparisons between Zylon®AS, Kevlar 29, and Spectra 1000 have been conducted to determine the differences in cut resistance and failure mode of these materials. The effects of cut angle, blade sharpness,

Table 9.4 Mechanical properties of various fibers (reprinted from ref. 85 with permission of Wiley).

	Density (g/cm^3)	Tensile strength (GPa)	Tensile modulus (GPa)	Elongation at break (%)	Moisture regain (%)	Decomposition temperature (°C)	LOI
Zylon AS	1.54	5.8	180	3.5	2	650	68
Zylon HM	1.56	5.8	270	2.5	0.6	650	68
Kevlar 49	1.44	3.6–4.1	130	2.8	4.5	550	28
Kevlar 149	1.47	3.4	185	2	3	550	30
Nomex 45O	1.38	0.65	17	22	4.5	400	30–32
Technora	1.39	3.4	71	4.5	3.5–5	500	25
PIPD (M5)	1.7	3.5–4.5	330	2.5	4.5	500	.50
Steel	7.8	2.8	200	1.4	–	–	–
Spectra 900	0.97	2.4	70	4	–	150	16
Spectra 1000	0.97	3.1	105	2.5	–	150	16
Vectran	1.4	2.85	65	3.3	<0.1	400	.30
PBI	1.4	0.4	5.6	30	15	550	41
Polyester	1.38	1	15	20	0.4	260	17

LOI – Limiting Oxygen Index (the minimum % of oxygen in an atmosphere for a burning event to be self-sustaining under well-defined conditions).

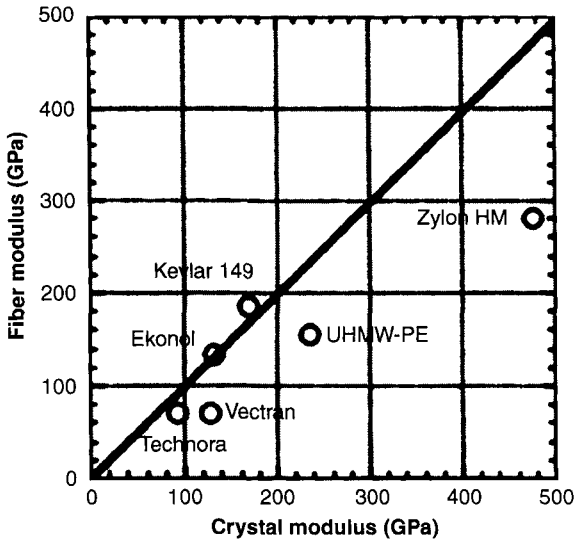

Figure 9.9 Comparison between fiber modulus and crystal modulus of different fibers (reprinted from ref. 74 with permission from Wiley).

Table 9.5 Mechanical properties of Zylon AS and Zylon HM (reprinted from Ref. 85 with permission of Wiley).

	Zylon® AS	Zylon®HM
Tensile strength (GPa)	5.8	5.8
Tensile modulus (GPa)	180	270
Elongation at the break (%)	3.5	2.5
Decomposition temp. (°C)	650	650

Table 9.6 Mechanical properties of Zylon and Vectran (reprinted from Ref. 85 with permission of Wiley).

	Tensile	Tensile	Compressive	Density
Fiber	Modulus, GPa	Strength, GPa	Strength, GPa	$(kg/m^3) \times 1023$
PBO (Zylon)	360	6.0	0.2–0.4	1.58
Vectran	65	2.9		1.4

and pre-tension on cut resistance were investigated. Cut angle had the greatest effect on cut resistance. All three fibers demonstrated the greatest resistance to cutting when the blade angle was held at 90°. When the angle was reduced to 82.5° the energy required to cut Zylon was reduced by 75%. Scanning electron microscope images of Zylon fiber ends cut at angles of 90° (a) and 82.5° (b) are shown in Figure 9.10. The Zylon fiber flows opposite to the movement of the cutting blade and forms a protuberance along the side of the fiber where the blade entered. The size of the protuberance varies, but is generally proportional to the cut energy. Figure 9.11 illustrates the decrease in deformation of the Zylon fibers with decreasing cut angle. The energy required to cut Zylon at an angle of 90° was 4.5 times greater than the energy required to cut Kevlar and 3.2 times higher than the energy required to cut Spectra. At lower angles, the difference in cut energy for Zylon was approximately 2.7 times greater than Kevlar and 1.7 times greater than Spectra [89].

At 250°C with saturated steam, the strength retention in PBO is less than 20% of its room temperature value. Therefore, PBO fibers should be stored in humid-free environment. PBO tensile strength also drops sharply with UV exposure. Exposure to visible light also affects PBO strength [85]. PBO fiber has excellent chemical resistance to various organic solvents, acids, and bases [49]. Abrasion resistance of PBO on metal is higher than aramid fiber, while both the PBO and aramid show much lower abrasion resistance than nylon or UHMW-PE [49]. Shear modulus of PBO fibers at room temperature is 1 GPA and for commodity textile fibers are generally

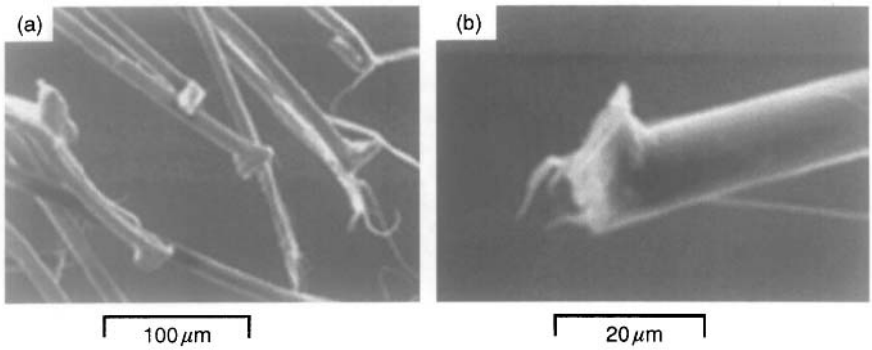

Figure 9.10 SEM micrographs of Zylon fibers ends cut (a) 90°, (b) 82.5° [83] (reprinted from ref. 83 with permission from Sage Publications).

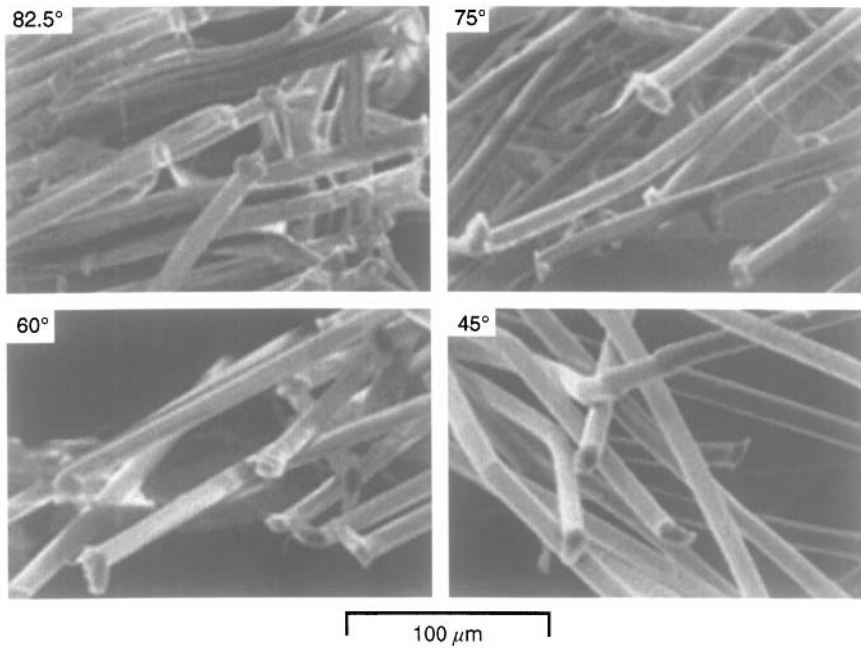

Figure 9.11 SEM micrographs of Zylon fiber ends cut at different angles (reprinted from ref. 83 with permission from Sage Publications).

0.5–1 GPA, whereas for carbon fibers in the range of 4–16 GPA [49]. The compressive strength of PBO fiber is 200–300 MPa, which is only a small fraction of its tensile strength. Different theoretical models have been proposed to explain compressive failure in high performance fibers. One model proposed the elastic instability of perfectly oriented rigid rod chains. This model suggested that the compressive failure is dominated by fibrillar instability rather than molecular instability [90, 91]. The other theories concerned the misalignment between fibrils, crystals, or domains of well oriented molecules and applied force direction [92]. PIPD (M5) shows the highest compressive strength (1 GPa) of any polymer (bulk or fiber). However, compressive strength of carbon fiber is in the range of 1–3 GPa, and those of Boron, Al_2O_3, and SiC fiber can reach 7 GPa [49].

9.2.7.2 Thermal Properties

Thermal decomposition of PBO in air is about 650°C and under nitrogen or argon more than 700°C which is 100°C higher than Kevlar [49]. TG-mass spectra analysis and TG-Fourier transformed

infrared spectroscopy [93–95] showed small molecules such as H_2O, CO, CO_2, and NH3 were released during thermal degradation. Coefficient of thermal expansion of PBO fiber is –6 ppm/°C. PBO fiber showed the highest limiting oxygen index (LOI) among the polymeric fibers [96, 97]. In addition, exceptional flame resistance of PBO was also reported [98].

9.2.7.3 Ballistic Properties

The combination of high strength, modulus, and toughness are some of the key factors for the candidate materials for high performance applications. The results of ballistic experiments showed that the required energy for penetrating PBO fabric was approximately twice that of Kevlar fabric [79].

9.2.7.4 Applications and Outlook

PBO fibers are used for fire fighters' clothing, heat resistant clothing, high temperature cut resistant gloves, gloves for high voltage electrical work, body armor, sail cloth, aircraft engine fragment barrier [49, 99]. PBO has also attracted attention as a potential reinforcement fiber for composites due to its strength and resistance to heat where compressive strength is not a requirement. PBO is not an ideal reinforcement fiber because its smooth and chemically inactive surface causes it to have poor adhesion to the matrix. Adhesion is one of the primary factors influencing stress transfer between the components in the composite. For improving the adhesion of high performance fibers through surface modification were used plasma, electron beam, chemicals, electrolytic oxidation, and coupling agents have been used. The PBO fiber was subjected to proton, electron, and gamma radiation. The proton radiation increased the compressive strength over 140% while gamma and electron irradiation showed 84 and 83% improvement, respectively [100]. Recent work has been conducted concerning the use of O_2 plasma to activate the surface of PBO. Wu [101] investigated the effect of oxygen plasma treatment on a Zylon®AS/Epon 828 bisphenol-A diglycidyl ether epoxy composite. PBO which was exposed to 70 W oxygen plasma for 5 min. had a surface free energy increase of 41% and a composite interfacial shear strength increase of 29%. The decrease in the tensile strength of the fiber was merely 3%. Oxygen plasma treatment appears to be an effective method for modifying the surface of PBO fibers for use in composites without compromising the mechanical strength [101].

A variety of chemical modifications have been made in rigid rod polymers such as including bulky side groups [102, 103] and introducing a small fraction of a multifunctional monomer [104, 105]. The modified PBO referred to as poly(aryl ether benzoxazoles) was synthesized by using the nucleophilic aromatic displacement of an aryl halide with a phenoxide in polar aprotic solvents [106, 107].

PBO also has been used in space exploration. Prototype Mars exploration balloon tested in 2002 utilized PBO tendons [108]. PBO fiber is used as reinforcement for producing high magnetic field at the National High Magnetic Field Laboratory in Tallahassee, Florida [109]. PBO fiber is also used for high temperature gas chromatography in a fused silica capillary [110].

Efforts to improve compressive strength of PBO fiber include incorporation of inorganic materials to provide lateral support to fibrils, [111–113] including morphological changes for interfibrillar entanglement, [111] covalent crosslinking by radiation [107]. However, crosslinking make the fiber more brittle and decrease the tensile strength. Using carbon nanotube in polymers improved compressive strength [114].

So far, the tensile strength of PBO fibers that has been achieved is only about 15% of the theoretical tensile strength, while modulus of fibers is up to 50–80% of the theoretical modulus. The modulus (low strain property) is not very sensitive to defects, whereas tensile strength is highly dependent on defects including chain ends. Thus, molecular weight has an affect on tensile strength of high modulus fibers. Due to difficulties in polymerization and processing, there is a limit for molecular weight with current technologies. The typical PBO molecule length is about 200 nm which is longer than PET (100 nm). Adding single wall carbon nanotubes (1–100 μm) improved the tensile strength of PBO fibers by 60% [114]. Therefore, probably in future we can produce PBO or PBO/carbon nanotube fiber with tensile strength and modulus more than 10 and 400 GPA, respectively [49].

9.3 Aromatic Polyamide-Rigid Rod "Kevlar" Poly(p-Phenylene Terephthalamide) Fibers

9.3.1 Introduction

Nomex® (a DuPont registered trademark for aromatic polyamide fibers) was available in early 1960s and became breakthrough

material in the field of the thermal and electrical insulation. Kevlar®, a much higher tenacity and modulus fibers, is the marketed name for the aramid based on poly(p-phenylene terephthalamide) developed by DuPont and commercially introduced in 1972. Scientists who were in the field of liquid crystals, polymers, rheology, and fiber processing had spent many years during the early stage of its market introduction. While working for DuPont in 1965 Stephanie Kwolek was attempting to develop a polymer to be used in strengthening tires and happened to find that p-aminobenzoic acid could be polymerized into a spinnable fiber. Soon poly (p-phenylene terephthalamide) was discovered [116, 117]. Poly (p-phenylene terephthalamide) (PPTA) is an aromatic polyamide that in fiber form exhibits highly crystalline structure and high tensile strength. In addition to Kwolek [117–120], there were many others such as Blades, [121, 122] Tanner, and coworkers, [123–125] Gabara and co-workers, [126] and Yang [127, 128] who took an active part at DuPont to bring above this achievement. The four books entitled "High modulus wholly aromatic fibers", Black and Preston [129] (1973), "The strength and stiffness of polymers", Schaefgen [130] (1983), "High performance aramid fibers", Jones and Jaffe [131] (1985), and "Aromatic high-strength fibers", Yang [127] (1989) were the initial important sources for the literature on the matter. The US Federal Trade Commission defines an aramid as "a manufactured fiber in which the fiber forming substance is a long-chain synthetic polyamide in which at least 85% of the amide linkages are attached directly to two aromatic rings". Weight for weight, Kevlar is significantly stronger than steel. Kevlar is flame resistant, does not melt, soften, or flow. The fiber also has a high modulus, high tensile properties, resistance to chemicals and environmental exposure, excellent thermal properties, is not flammable, and has good dimensional stability. These properties make Kevlar useful in a variety of applications such as strengthening cables and ropes, and the well-known bulletproof vests (Table 9.7). Twaron® from Teijin is also an aromatic copolyamide, similar to Kevlar®, appeared on the market at the end of 1980s. Teijin later produced Technora® from aromatic copolyamide polymers which exhibit high tensile strength properties as well as high resistance to hydrolysis.

Kevlar is a carbon based aramid polymer, which is similar in structure to nylons. When nylons are at high concentration in solution their flexible chains become highly entangled. Due to this entanglement when the solution is spun it produces only moderately extended chains negatively affecting the fiber properties.

Table 9.7 Physical properties of Kevlar 29 (reprinted from Ref. 127 with permission of Wiley & Sons).

Physical Properties of Kevlar	
Density (g/cc)	1.45
Young's modulus (GPa)	130
Tensile modulus (g/den)	1100
Tensile strength (GPa)	3.6
Electrical resistance (mohm-m)	.1015
Thermal conductivity (watts/m-K)	0.04–0.08
Melting point (°C)	Decomposes at 460°C
Compressive strength (MPa)	393

Unlike nylon, the para-directed groups attached to the benzene rings in Kevlar give it a rigid rod structure [132]. When put in solution at high concentration these rigid structures must align closely to optimize the solvent volume [133]. The secret to Kevlar's strength lays in these first stages of polymerization. As the molecular weight increases the critical concentration is passed and the polymer develops liquid crystalline characteristics [121]. A liquid crystal is a thermodynamically stable phase characterized by anisotropic properties without the existence of a 3-D crystal lattice. During the spinning process the polymer chains' rod-like structures aggregate into ordered clumps running parallel to the flow. While passing through the spinneret the liquid-crystalline solution remains highly oriented creating high crystalline fibers with excellent strength, however, only in the longitudinal direction. In the microstructure of Kevlar linear molecular chains aline along the fiber axis and are held together by hydrogen bonds. The polar amide groups form bonds with the carboxyl oxygen in the transverse direction (Figure 9.12).

When bonded the polymer molecules form planar sheets. Within the sheets the chains are offset slightly due to the steric hindrance of the benzene rings. Large electromagnetic structures such as these rings repel each other, and thus the chains become offset. These molecular sheets are aligned radially creating a near perfect longitudinal and radial order never seen before [134–136]. Kevlar's excellent properties are due to its internal structure. Its high modulus has

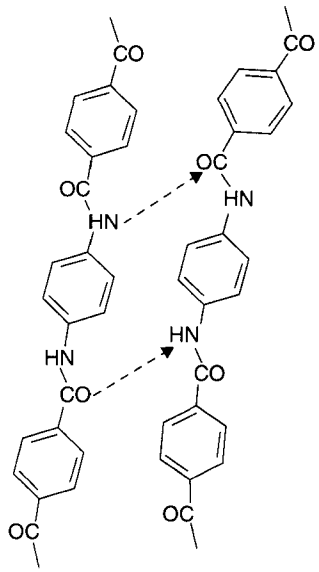

Figure 9.12 Kevlar molecular structure showing transverse bonds.

been the topic of much research and the verdict is that the modulus is determined by the mis-orientation, the paracrystalline parameter, and c-plane dimension. According to Rao, Waddon, and Farris, [137] the trend is with increasing modulus there is decreasing mis-orientation angle and paracrystalline parameter, and increasing c-dimension. Through diffraction studies they also determined that the ability to develop Kevlar of increasing strength such as Kevlar 149 eliminates "cis" conformation in the structure. This creates more order in the sheets making for a more perfect crystalline structure [137].

9.3.2 Polymer Synthesis

PPPTA can be prepared by solution polycondensation of p-phenylenediamine (PPD) and terephthaloyl (TCL) chloride at low temperatures. In the reaction -NH2 reacts with -Cl, producing HCl. An alternate reaction involves -NH2 reacting with an -OH group attached at the same position that the -Cl group was attached in the original reaction (Figure 9.13).

One of the methods involves the dissolution of appropriate quantities of PPD in a mixture of hexamethylphosphoramide (HMPA)

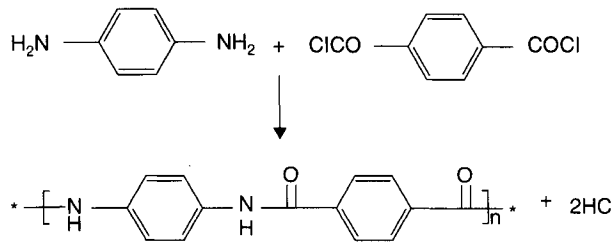

Figure 9.13 Polycondensation reaction of PPTA from p-phenylenediamine and terephthaloyl chloride.

and N-methylpyrrolidone (NMP). After cooling is done in an ice/acetone bath to 258 K (–15°C) in a nitrogen atmosphere, TCL is added with rapid stirring. The result is a thick, paste-like gel product. Stirring is discontinued and the reaction mixture stands overnight followed by slow warming to room temperature. In order to wash away solvent and HCl, the reaction mixture is agitated with water in a blender. The polymer is then collected by filtration. In determining the molar mass of the final product, the stoichiometry of the solvent and reactant mixture is very important. Blair and Morgan [138, 139] reported that a 2:1 ratio by volume of HMPA:NMP produced PPTA having the highest inherent viscosity (and hence largest molar mass). Reactant concentration of PPD and TCL was found to be best at ca 0.25 M. If reactant concentration was less than 0.25 M then the inherent viscosity was shown to decrease quite rapidly. If reactant concentration was greater than 0.3 M, the inherent viscosity falls but gradually. Herlinger *et al.* [140] who examined the solution polymerization of aromatic diamines and aromatic dicarboxylic acid chlorides in N,N-dimethylacetamide (DMAc) said that the viscosity falls at a low reactant concentration due to the occurrence of competitive side-reactions. The reason behind the fall in viscosity at higher values of the reactant concentration is the decrease in reactant mobility due to the onset of gelation before a high value of inherent viscosity could be attained. As we know that the polymerization reaction is exothermic and with greater reactant concentrations greater quantity of heat would be produced and this could lead to an increased rate in side-reactions and this would hence decrease the value of inherent viscosity attainable.

Other methods in Higashi and co-workers [141–144] include the reactions between aromatic dicarboxylic acids and diamines since the diacids are comparatively cheaper. Here solvent mixtures/salt systems are utilized. In Higashi, [144] high molecular mass of PPTA

is obtained. Here polycondensation of TPA and PPD was carried out in NMP which contained dissolved $CaCl_2$ and LiCl in the presence of pyridine.

The manufacturing process of Technora® reacts PPD and 3,4'-diaminodiphenylether (3,4'-ODA) with terephthaloyl chloride in an amide solvent such as N-methyl-2-pyrrolidone/$CaCl_2$ (10% concentration), to complete the polymerization (see Scheme 9.9). The reaction mixture is neutralized and subjected to spinning into an aqueous coagulation bath. The as-spun fiber is then brought to extraction of solvent, super-drawn at high temperature and passed through finishing steps to give the final product. This process is simple and use only one solvent which simplifies the solvent recovery process and free of residual acid and avoid later difficulties in the spinning process. Technora® is spun from an isotropic solution compared to Kevlar® is spun from a liquid crystalline.

9.3.3 Fiber Spinning

Difficulty was faced when researchers attempted to form fibers from the polymer. It was originally not thought possible to spin the polymer because when put in solution it could not be clarified leading to the belief that there was inert matter in the solution that would block the spinneret during extrusion. Further studies showed that the opaque solution was due to the formation of liquid crystals [116]. Another potential problem was that PPTA is a lyotropic polymer and degrades well below its melting point, making it impossible to form fibers through any melt-extrusion process [135]. PPTA is also not soluble in most common polymer solvents, preventing it from forming fibers through solution spinning. Blades discovered that PPTA could dissolve in highly concentrated solutions of greater than 18% in extremely strong acid solutions, 98–100% sulfuric acid. The resulting crystalline solution could then be spun at relatively low temperature using an air gap spinning process called dry jet-wet

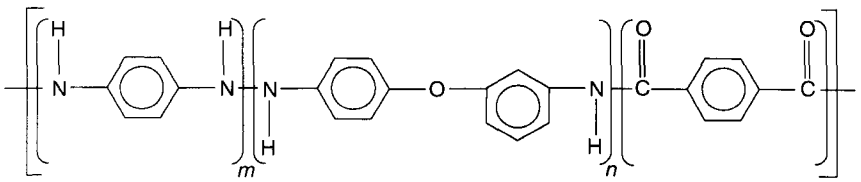

Scheme 9.9 Polymer chemical structure of Technora® 131.

spinning. Dry jet-wet spinning employed involves dissolving PPTA in strong acid and removing the air from the solution. The solution is then extruded through a spinneret, exposed to air, and washed with water and NaOH to remove the acid. The water is then removed by drying the fiber under a small stress [122, 123] (Figure 9.14).

To increase the modulus (stiffness) and crystallinity of an aramid fiber, it can be hot drawn. For fiber from PPTA, this involves subjecting the fibers to a bath at around the glass transition temperature (400°C). The fibers are then stretched to produce a stronger, stiffer fiber. As the fibers cool they retain their higher orientation, which produces a high degree of crystallinity. Kevlar 29, when subjected to this process, forms Kevlar 49 which has 1.5 times the tensile strength and is most common in cloth applications. This process can also produce Kevlar 149 from the hot-drawing of Kevlar 49.

9.3.4 Structure and Properties

In poly (p-phenylene terephthalamide), there are very stiff polymer chains and this is due to the bonding of rigid phenylene rings in the para position. The other advantage of PPTA is the presence of

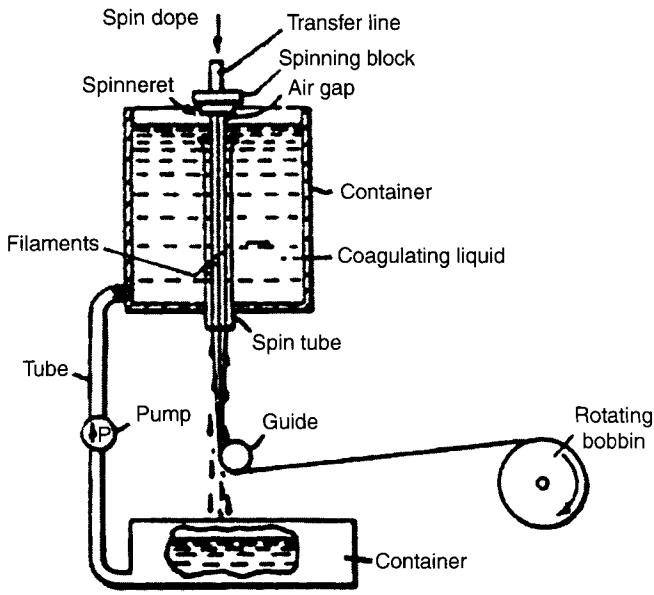

Figure 9.14 Air-gap spinning schematic from Blades [121].

amide groups at regular intervals along the linear macromolecular backbone and due to this extensive hydrogen bonding in a lateral direction between adjacent chains is achieved and this leads to efficient chain packing and high crystallinity. Structural studies on PPTA fibers have been described by Northolt, [145] Haraguchi *et al.* [146] and Yabuki *et al.* [147] According to Haraguchi *et al.* [146] two crystal modifications of PPTA are observed. Northolt and Chapoy [148] worked on an X-ray diffraction analysis of PPTA fibers and proposed a model for the crystal and molecular structure of the PPTA. By spinning the polymer from a highly concentrated anisotropic solution, the chains form an essentially mono-clinic unit cell with associated parameters a = 0.787 nm, b = 0.518 nm, c (fiber axis) = 1.29 nm, there are two molecular chains per unit cell.

One through the center, the other through a corner and two monomeric units in the axial repeat. When the fiber is formed from an anisotropic solution of lower concentration, it exhibits a different packing arrangement that is equivalent to a lateral displacement (b/2) of chains along alternate 200 planes. However, both crystallographic forms coexist in fibers spun from solutions of intermediate concentration.

Before Kevlar fibers can be used in cloth applications such as body armor, they must be first twisted into yarn structures and coated with a plastic resin to increase the rigidness of the already high modulus fibers. These coated fibers are then woven tightly to produce an effective cloth and layered with plastic film to add additional rigidness and strength. The layers are the reason for the impact resistance because each layer absorbs some degree of energy, spreading the force evenly throughout the material [135]. In ballistic situations most layered materials will "mushroom" and stop before exiting the other side. This impact resistance is due to the structural ductile compressive failure mode. A compressive strain of about 0.5% causes buckling of the PPTA molecule. This is possible with a rotation of the molecule between the carbon and nitrogen bonds creating more of a trans shape conformational change rather than the cis form commonly seen. The change in conformation folds the molecule in an accordion-like fashion allowing the material to compress without breaking any bonds [149]. Other failure modes of PPTA include intracrystalline slip, gauche-trans transitions, deformation of entanglement network, and molecular scissions [150].

In Kevlar there are regularly positioned amide segments which help in proper load transfer between the chains. These hydrogen

bonded chains forms sheets which are stacked parallel into crystallites. Between these adjacent hydrogen bonded planes, the interaction largely takes place by Van der Waal's forces with some pi-bond overlap of the phenylene segments. As a result, the hydrogen bonded planes function as slipplanes in a manner analogous to close-packed planes in metals. Due to the aromatic rings and the double bond nature of the amide group arising from resonance effects, the bond rotation and the molecular flexibility are inhibited.

The fibers are generally characterized by intense but diffuse small-angle scattering features on the equator of the X-ray diffraction (XRD) patterns. This is due to the presence of microvoids. According to electron microscopy and X-ray data, the voids are rod shaped with their long axis parallel to the fiber axis. The typical width of the void is in the range of 5–10 nm and length about 25 nm. The effect of microvoids in para-aramid fibers was explored by Dobb *et al.*, [151] using the original method designed by Allen [152]. The surface microstructure of an aramid fiber was also observed directly by atomic force microscopy [153, 154] (Figure 9.15).

The supermolecular structure of Kevlar 49 has been reported by Dobb *et al.* [149] Here both electron diffraction and electron

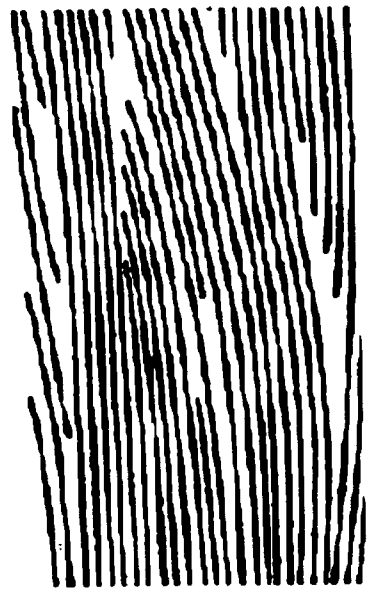

Figure 9.15 Schematic representation of the microstructure of PPTA (fiber axis vertical) (reprinted from ref. 147 with permission from Springer).

microscope dark field image techniques were utilized. Analysis showed that there was a uniform distribution of ordered crystalline material throughout the fiber and the dark field banding shows changes in crystalline orientation and not of crystalline order. The result provided strong evidence for a regular pleated structure with the alternating components of each sheet arranged at approximately equal but opposite angles to the plane of the section. The angle between adjacent components of the pleat is about 170° (Figure 9.16).

Kevlar is highly anisotropic giving the high modulus and tensile strength only in one direction. Weak hydrogen bonds in the transverse direction result in low shear moduli, poor transverse properties, and low compressive strength [155, 156]. In response to this, composite designs have been introduced, and studies have been conducted on treatments to improve the interfacial properties. Yue and Padmanabhan [157] suggest the possibility of chemically treating the surface of Kevlar/epoxy composites with an organic solvent to improve the interfacial shear strength. They found that surface treating with acetic anhydride followed by a three minute methanol wash improved the strength by 60%. They believe this is due to a high oxygen surface content adding to the bonding ability to the matrix [157]. Another surface treatment uses a size that is common with treating glass fibers combined with a new processing method. First PPTA was processed slightly different than that of usual Kevlar. An open-gap system was used in spinning to create gaps between the crystal lattice while keeping the high degree of crystallization intact. The idea includes three steps: one, to introduce low molecular size, made of a combination of silane coupling agents and film formers, into the gaps. Two, heat the system to polymerize

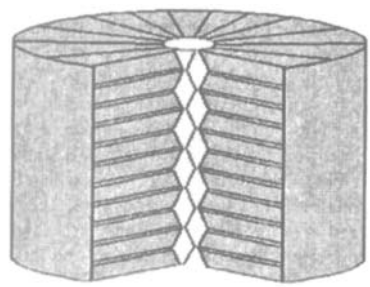

Figure 9.16 Radial pleated structure model of PPTA fiber [147] (Reprinted with permission from Springer).

in the gaps. And three, close the gaps with heat to swell the crystals closing the gaps and further network the size. Tests showed that before heating the gapped system had similar interfacial strength to the non-gapped PPTA. After heat was added the gapped fibers increased in interfacial strength by 67% while retaining the same fiber strength [158].

9.3.5 Application and Outlook

Kevlar has many practical end uses including but not limited to protective armor, ropes, cords, tires, and heat/abrasion resistant gloves. The use of PPTA in high temperature situations is a topic of study. As stated earlier PPTA is a lyotropic fiber but due to the rod like structure of the molecule the melting point is very high, 500°C [135]. For long exposure to high temperatures fibers are not effective because of decomposition and loss of elongation. However, for short length exposure and temperatures not exceeding 300°C Kevlar holds its strength at a tenacity of 0.88 N/tex. According to TGA and DSC data obtained, there was minimal weight loss (1%) due to thermooxdative degradation at <400°C but at temperatures >450–500°C there was significant degradation (4%). Suggestions for temperature limits should be noted for products made from these fibers. Note, although there is degradation with exposure to high heat the fiber is still resistant to flame [159]. This flame resistance can further be increased with the addition of phosphorus to fibers that are not highly drawn [135]. More recently with the development of M5 fiber comparison shows Kevlar lacking in the area of thermal stability. Based on its limiting oxygen index of 27–29% Kevlar is considered a flame resistant fiber but in comparison M5 is reported to have LOI of 50%. In laboratory tests of brief encounters to a filament, PPTA fibers perform adequately; however, in real situations the fiber would be woven into fabric and possibly exposed to continuous flames. In this same study woven Kevlar fabric was compared to M5 in areas of smoke production, heat release, and thermal stability and in each area M5 greatly surpassed Kevlar; however, the thermooxidative degradation properties were comparatively similar [160].

Kevlar finds its application in composites which are used for ship building, pressure vessels, sports goods, etc. This is due to its light weight, high strength, high modulus, good impact strength, and

wear resistance. Kevlar finds its application in protective apparels such as heat resistance work wear, fire blankets, flame retardant textiles, cut protective gloves, and seat cover layers due to its good heat resistance, flame retardation, and cut resistance.

Kevlar is used in high speed tires such as truck, aircraft, and motorcycle because of its low density, weight saving, high tenacity, dimensional stability, low shrinkage, and puncture resistance. Kevlar is used in mechanical rubber goods such as conveyor belts, transmission belts, hoses for automotive, and hydraulic hoses because of its high strength, high modulus, dimensional stability, thermal resistance, and chemical resistance.

Kevlar is used in friction products and gaskets such as brake linings, clutch facings, thixotropic additive and industrial paper because of fiber fibrillation, heat resistance, chemical resistance, low flammability, and good mechanical performance. Kevlar is used in ropes, and cables such as aerial optical fiber cable, electrocable, mechanical construction cable, and mooring ropes because of its high strength, high modulus, dimensional stability, low density, corrosion resistance, good dielectric properties, and heat resistance.

Kevlar is used for life protection by finding its application in bullet proof vests, helmets, property protection panels, vehicle protection, and strategic equipment shielding due to its high tenacity, high energy dissipation, low density and weight reduction, and comfort.

9.4 Spectra, Dyneema UHMWPE Flexible Polymer Chain

9.4.1 Introduction

In the past two decades, significant progress has been made in developing ultimate mechanical properties of fibers. Amongst the various developments in the area of high performance fibers, two major routes can be distinguished which are completely different in the respect to the starting materials. That is intrinsically rigid chain polymers such as Kevlar (PPTA), PIPD (M5), and PBO (Zylon) as opposed to flexible chain polymers such as ultrahigh molecular weight polyethylene [161]. High performance polyethylene fibers are commercially produced under the trade names Dyneema by DSM High Performance Fibers in the Netherlands and

by Toyobo/ DSM joint venture in Japan, and Spectra by Honeywell (formerly Allied Signal or Allied Fibers) in the USA.

High performance polyethylene fibers are produced through gel spinning of ultra high molecular weight polyethylene (UHMWPE). The early work of Albert J. Pennings suggested it was possible to create an ultra-strong fiber from flexible polyethylene chains and that it was not necessary to include a liquid crystalline state as was previously thought required for the strong aramids [162]. Through the work of many researchers and numerous hours of laboratory experiment an ultra strong polyethylene fiber was created. The first company to officially introduce a product was DSM under trade name Dyneema, by researchers Smith and Lemstra patented in the U.S. on August 17, 1982 [163]. Soon after, Allied Signal produced Spectra and Kavesh patented this technology on November 1, 1983 [164]. The difference in these two products can be seen in their production and in their DSC data but both have similar end properties.

The theoretical tensile modulus of polyethylene is 180–340 GPa. [165, 166] The extremely high tensile modulus of polyethylene is due to the small cross-sectional area of the chain, no side groups, and the planar zig-zag conformation in the orthorhombic crystal lattice. The theoretical tensile strength calculated from the C-C bond energy is in the order of 20–60 GPa. These theoretical values for polyethylene can happen if all the C-C bonds fracture simultaneously. This requires defect free, chain-extended structure, and infinite polymer chains which is a completely different situation from which is encountered [167].

In an array of completely paralleled and extended finite polymer chains, the stress transfers through intermolecular bonds. Therefore, in order to transfer load through the system, chain overlap is also needed [167]. The difference between polyethylene and aramid is weak Van der Waals intermolecular interaction in polyethylene and strong hydrogen bonds in aramid fibers. So, in order to make high strength fibers from polyethylene, a high molecular weight, high degree of chain extension, and sufficient chain overlap are needed to build up sufficient intermolecular interactions along the chains [167]. It was found that molecular weight has a great effect on fracture mechanism and theoretical tensile strength [168–170]. It was shown that polymers with strong intermolecular bonds need lower molecular weight to obtain high tenacity. However, hydrogen bonds in aliphatic polyamides (nylon 6 and nylon 6,6) also exist in crystals which provides a barrier for ultra drawing in order to obtain high tenacity fibers [168].

9.4.2 Polymerization

Ethylene, or known by the systematic name ethene, is the simplest and the most common organic monomer (CH2 = CH2). A free radical polymerization of ethylene generally leads to branching but a linear polyethylene can be produced by using organometallic catalysts developed by Ziegler and others. Low density (branched) polyethylene with the melting point of 105 to 115°C is an ideal material for making films and nonwovens. Linear polyethylenes exhibit higher melting points in the range of 120–130°C.

Tubular reactors and high pressures of 120–300 MPa (17,000–43,000 psi) are commercially used to polymerize ethylene and produce low-density polyethylene (LDPE) [171]. The process was first invented by ICI Laboratories in the early 1930's. The branched polymer is usually produced due to intermolecular chain transfer or "backbiting". Consequently, long and short branches are formed. In the latter the propagating radical abstract hydrogens from the fifth, sixth and seventh methylene groups to form n-hexyl, n-amyl and n-Butyl branches respectively (Figure 9.17) [171]. n-butyl branches generally dominate.

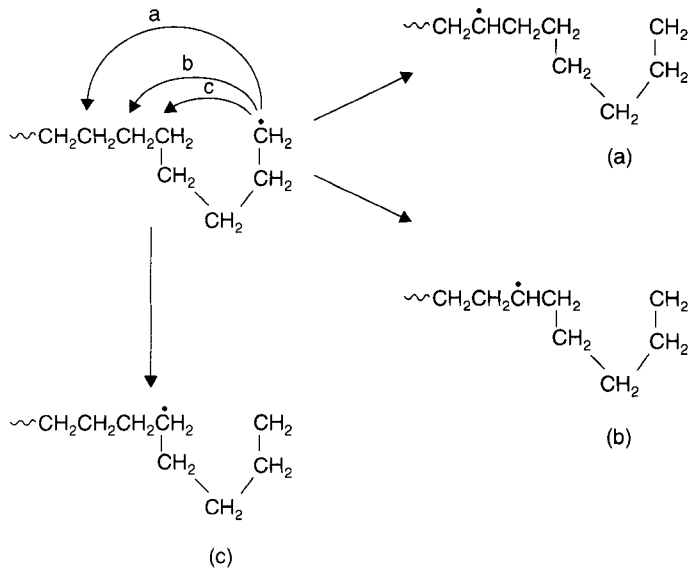

Figure 9.17 Mechanisms of short branching in LLDPE (reprinted from ref. 171 with permission from Wiley-Interscience).

In a typical industrial polymerization process (Figure 9.18), ethylene is initially compressed to a higher pressure. Traces of oxygen with alkyl or acyl peroxide are then injected to initiate the polymerization. To control the degree of polymerization simple alkanes (propane, butane etc.), ketones (acetone) or alcohols (isopropanol) are used as chain-transfer agents. The polymerization process is carried out as a bulk polymerization. Compressed liquid ethylene serves as a solvent for polyethylene if the pressure is above 200 MPa. Thus, homogenous polymerization occurs. Lower pressures result in a suspension polymerization. Low molecular weight waxes and oils usually dissolve in the liquid ethylene and later are separated. Tubular reactors have an inner diameter of 2–6 cm and a length of 0.5 to 1.5 km. The polymer residence time does not exceed 2 minutes as the process is carried to a low conversion about 30%. The highest process temperatures reach 300–325°C. The polyethylene is extruded into pellets at 250–275°C [172]. A number-average molecular weight of commercial LDPE does not exceed 100,000 g/mole

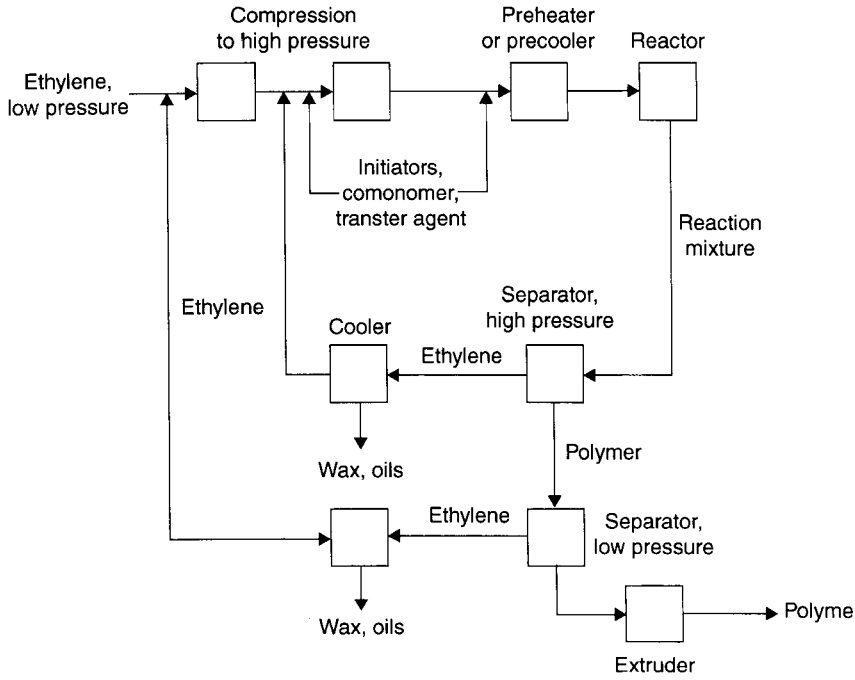

Figure 9.18 Flow diagram of a high-pressure polyethylene process (reprinted from ref. 171 with permission from Wiley-Interscience).

and could have a high polydispersity index from 3 to 20 [171]. The polymer has low density of 0.91–0.93 g/cm^3 [162] and the degree of crystallinity of 40–60%.

Due to good film properties LDPE is extensively used for film making and nonwovens accounting for about 60% of polymer consumption [173]. Poltrusion and paper coating account for about 15%. Over 8 billion pounds of the polymer were produced in 2001 in the United States.

Linear high-density polyethylene (HDPE) is mainly manufactured by using traditional Ziegler-Natta and metal oxide Philips-type initiators in suspension polymerization [173]. More expensive metallocene catalysts are also used but accounted for less than 5% of the total HDPE production in 2002 [172]. About 14 billion pounds of high density polyethylene was produced in the United States in 2001.

Since HDPE is nearly a linear polymer it has a higher density of 0.94–0.96 g/cm^3, the melting point of 133–138°C as well as improved tensile strength, bending stiffness and chemical resistance.

Polymerization of UHMWPE was commercialized in the 1950s by Ruhrchemie AG, by using a Ziegler-Natta catalyst made from titanium chloride and organo-aluminium compounds (triethyl aluminum or diethyl aluminum chloride). Polymerization takes place at 65–85°C under 0.5–2 MPa. Because of sensitivity of these materials to air and moisture, the synthesis steps are carried out in an inert gas environment. Pure ethylene and a suspending agent without polar impurities are important prerequisties for successful synthesis. The molecular weight of polyethylene can be controlled by adding very small amounts of hydrogen to the ethylene gas or by changing the polymerization temperature. In chain polymerization, the ethylene molecules attached to the active sites of the catalyst particles. The polyethylene grows around these particles until the polymer encapsulates them. The molecular weight of polymer cannot be more than 6–7 $\times$ 10^6 g/mol. The final product is a fine white powder; the diameter of most of the powder particles is less than 300 μm. Adding very small amounts of fine calcium stearate can eliminate the residual catalysts. It also acts as a lubricant and helps the powders have white color.

In some literature UHMWPE is referred to as high density polyethylene. However, there are many differences between these two polymers such molecular weight, melting point, and density [174].

Recently, new techniques of solvent free routes have been proposed for the production of high modulus/strength UHMWPE fiber. Porter *et al.* [175, 176] showed that UHMWPE reactor powder

could effectively be drawn by solid state extrusion [175] and coextrusion [176]. Smith *et al.* [177, 178] proposed a technique based on tensile drawing of virgin (the UHMWPE reactor powders, often referred to as virgin or nascent) UHMWPE films, which were prepared by depositing a vanadium catalyst system on a glass slide, followed by polymerization of ethylene at relatively low temperatures. It was shown by Smith [179] that reactor powders, after compacting below the melting temperatures, could easily be drawn into high modulus structures. Kanamoto *et al.* [180, 181] have proposed a two stage drawing technique, which consists of the initial state coextrusion to a low draw ratio, followed by tensile drawing at controlled temperatures and rates.

9.4.3 Spinning and Fiber Properties

The strength of high performance polyethylene fiber is attributed to a high degree of parallel orientation greater than 95% and crystallinity exceeding 85% [181]. This differs from polyethylene fibers with low orientation degree and less than 60% crystallinity. The ultradrawing during a gel spinning process is responsible for this high crystallinity. First ultra-high molecular weight polyethylene is dissolved in a solvent then spun through a spinneret [182]. This is where the primary difference between Dyneema and Spectra can be seen. DSM's Dyneema uses a volatile solvent and approximately 5% HMWPE (high molecular weight polyethylene) solution of 2–3 $\times$ 10^6 Mw. In a quench stack or heated chamber the solvent is partially removed. With decreasing solvent concentration the fibers are drawn though increasing temperature and a very high degree of molecular orientation is achieved and maintained through cooling. Allied Signal's Spectra uses a non-volatile solvent of paraffin oil and HMWPE in the spinning process. The solvent is then removed using a volatile solvent. Fibers with high tenacity and modulus are achieved through both processes; however the later process is the more cost effective and it is more easily controlled [182, 183].

The gel-spinning process (Figure 9.19) is to date the most effective means of producing a high strength polyethylene fiber. The process includes three basic transformations: polymer to gel, gel to Xerogel, and orientation drawing. Gel-spinning can improve the mechanical properties of HMWPE by one order of magnitude, but this is only 10% of what is calculated to be the theoretical limit. Pakhomov *et al.* are of the opinion that the only way to improve this percentage is to

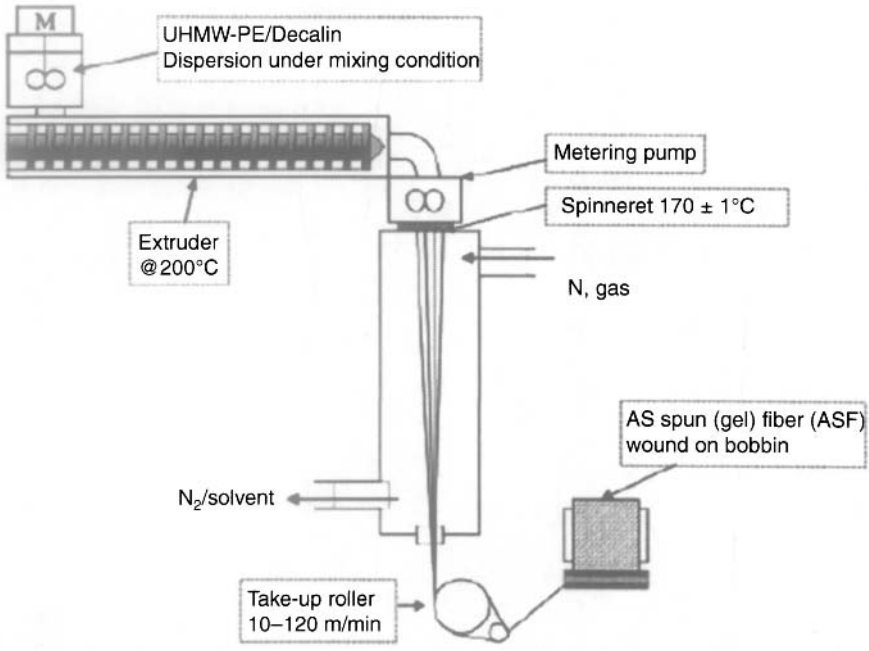

Figure 9.19 Gel-spinning process schematic (reprinted from ref. 186 with permission of Wiley).

understand the relationship between the structure of the molecule and its properties. Their study shows that during the first step of the spinning process when transitioning from solution to gel the shear modulus is increased 3 or 4 order of magnitudes. Elastic properties are increased as well. During this step structurally there are formations of lamellar crystallites of 4–5 nm thick and 20–40 nm in transverse size that forms a gel network. The second step forms clusters of these lamellar crystallites in a coplanar arrangement. The third step draws out the folds of crystallites increasing uniformity along the fiber axis and improving elastic strength [184].

Gel-spinning gained its popularity because of its ability to attain such a high molecular orientation of the fibers. This orientation is achieved during the drawing process through elongation of the gel fiber. Based on Griffith theory there is a relationship between fiber diameter and modulus. The smaller the diameter the higher the modulus, leading to the statement that drawing is just a process to decrease the diameter (Figure 9.20). The reason for the higher

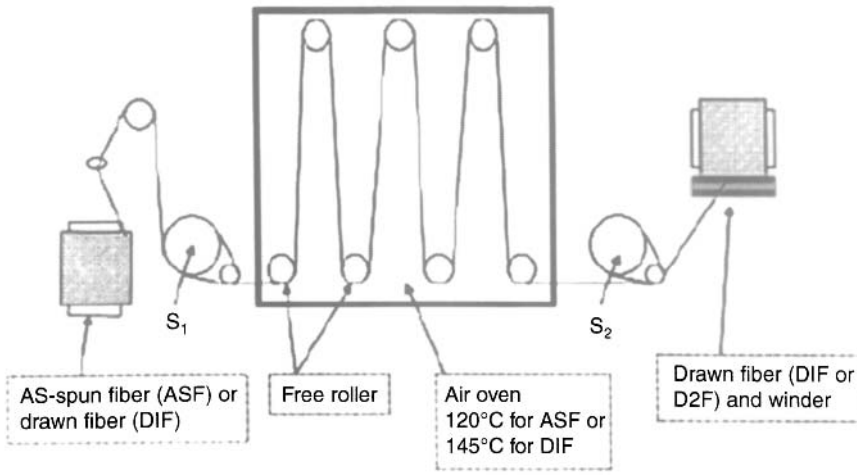

Figure 9.20 Drawing process schematic (reprinted from ref. 186 with permission of Wiley).

modulus at a smaller diameter is thought to be due to higher defects at the surface in larger fibers. Below the spinneret evaporation of solvent causes an increase in polymer concentration, negatively effecting the molecular orientation. A larger diameter gives more surface area to be affected. With an increased spinning speed and smaller diameter there is less time for evaporation and therefore less deformation and higher modulus. The inhomogeneous structure from low speed is made up of a "skin" of interlocked shish-kebab morphology (the "shish" refers to extended chain crystals and the "kebab" refers to folded chain crystals) and a "core" of lamella stacking crystals. This inhomogeneous structure hinders drawability because of stress at the surface. The smaller diameter has a more homogeneous shish-kebab structure that allows for smooth drawing [185].

The final properties of the fiber in gel spinning of UHMWPE are achieved in the drawing step. The maximum attainable draw ratio depends to the molecular weight and concentration. Lemstra and Smith found that the maximum achievable draw ratio (λmax) relates to the square root of the inverse of the polymer concentration ($\Phi^{-0.5}$) [175, 186]. But, for each molecular weight there is a minimum concentration. Below this concentration, there is no sufficient molecular entanglement for drawing. HMWPE is an extremely linear molecule with high orientation due to the drawing and cooling

procedure. HMWPE fibers are unique in their linearity. Individual fibers have macrofibrils that contain many microfibrils whose finite lengths have been measured to be 1000 to 2000 nm [187]. Along the microfibrils are crystal regions with lengths of about 100 nm. It is not, however, perfectly crystalline. Along the linear direction are entanglements and chain end terminals creating disordered areas that comprise about 25% of the fiber and are about 3–4 nm in length. At ambient temperature these disordered areas are elastomeric giving the molecule rubbery and stiff regions covalently bonded to each other. The regularly interchanging rubbery and stiff regions are what give Spectra its reputation of being so strong and impact resistant. When made into a composite structure the alternating regions are layered in a lattice structure held together by strong covalent bonds [181].

Work by Prevorsek shows that the modulus of HMWPE is strain dependent in that with high impact it actually increases in modulus. At standard deformation rates Spectra 900 and 1000 are 120 and 170 GPa but at ballistic rates it can reach up to 300 GPa [188] (Tables 9.8 and 9.9). At these ballistic rates the material absorbing the energy of a projectile is proportional to the modulus of the material, thus making this material popular for the end use of bullet protection apparel [189].

Table 9.8 Physical properties of Dyneema SK60, SK65, SK75, SK76 [188].

	Physical Properties of Dyneema			
	SK 60	**SK 65**	**SK 75**	**SK 76**
Density (g/cc) Strength	0.97	0.97	0.97	0.97
Tenacity (N/tex)	2.8	3.1	3.5	3.7
Tenacity (g/den)	32	35	40	42
Tensile strength (GPa)	2.7	3.0	3.4	3.6
Modulus				
Specific modulus (N/tex)	91	97	110	120
Specific modulus (g/den)	1025	1100	1250	1350
Modulus (GPa)	89	95	107	116
Elongation (%)	3.5	3.6	3.8	3.8

Table 9.9 Physical properties of Spectra 900, Spectra 1000, Spectra 2000 [189].

	Physical properties of Spectra					
Weight/unit length (den) (decitex)	**900**		**1000**		**2000**	
	650	4800	215	2600	75	180
Ultimate tensile strength	722	5333	239	2888	83	200
(g/den)	30.5	27.4	38	34	41	38
(GPa)	2.61	2.34	3.25	2.91	3.51	3.25
Breaking strength (lbs)	44	290	18	195	6.8	15.0
Modulus (g/den)	920	885	1320	1135	1450	1350
(GPa)	79	75	113	97	124	116
Elongation (%)	3.6	3.6	2.9	3.4	2.9	2.9
Density						
(g/cc)	0.97	0.97	0.97	0.97	0.97	0.97
(lbs/in^3)	0.035	0.035	0.035	0.035	0.035	0.035
Filament/tow	60	480	60	480	40	60
Filament (dpf)	10.8	10.0	3.6	5.4	1.9	3.0

Thermal stability of HMWPE was tested and the results as reported by Xiaoyan and Weidong [189] show that with increasing annealing temperatures properties of tensile tenacity, modulus, and extension at break decrease. They subjected samples of Dyneema SK65 to different temperatures and aging times and found that Dyneema can be used and keep its mechanical properties at constant temperatures under 70°C [190]. Mechanical properties that vary with temperature are thus the topic for much study. Tensile and creep tests preformed at different temperatures show a higher temperature dependence at temperatures between 5°C and 140°C [191]. This is most likely due to a solid phase change from orthorhombic to hexagonal. In the orthorhombic phase the molecular chains do not slide freely as they do in the hexagonal phase and the fiber failure is due only to the primary bonds. Therefore the temperature dependence of mechanical properties in the orthorhombic phase is much lower than in the hexagonal phase [192]. With no stress applied the phase change occurs

slightly below the melt (146°C) at 140°C. It is possible to lower the phase change temperature with applied stress. The stress required to lower the change increases with lowering temperature until a point is reached where the stress to change equals the failure stress of 2.74 GPa. This critical stress is reached at 5°C below which it is not possible to have a phase change [191]. To show the stress dependence on creep strain a mathematical expression was developed:

$$E^c = C_0 \sigma^{c1} t^{c2} e^{\frac{(-ct/T)}{T}}$$

where: E^c is the creep strain, s is the applied stress, the C's are the constants for the model. The constants were generated at five temperatures and 2 different loads. The solution to this model verifies the work completed on phase change control of tensile and creep behavior [193].

Smith and Lemstra [186] studied the effect of molecular weight on the tensile strength of melt and solution spun, ultra drawn PE fibers. They showed that the tensile strength (s) and tensile modulus (E) of drawn fibers increases with molecular weight (Mw) based on an empirical relationship [186]:

$$\sigma_t \propto E^n M_W{}^m \quad n = 0.7; m = 0.4$$

They [186] also found that decreasing polydispersity (Mw/Mn) enhances the tensile strength at specific molecular weight and tensile modulus.

Methods to improve the thermal stability of polyethylene include crosslinking and zone drawing. Crosslinking by radiation can cause scission in the polymer backbone leading to lowered tensile strength and modulus. Crosslinking by peroxide is effective but must be introduced to the system before chain orientation occurs. Zone drawing creates a necking effect using heat to orient the chains. Combining cross linking by peroxide (dicumyl peroxide in decaline) with a zone drawing technique keeps high modulus at high temperature but it showed negative drawability. Sung *et al.* achieved maximum storage modulus of 65 GPa at 25°C and a draw ratio of 150 using this method. Comparatively uncrosslinked fibers had a storage modulus of 165 GPa at 25°C and a draw ratio of 324. At high temperatures reaching 190°C, it was possible for the crosslinked PE to retain a modulus of 0.77 GPa where the uncrosslinked PE melted at 150°C. Considering this high temperature stability the peroxide-zone drawing method was an effective treatment for

thermal stability [194]. The negative drawability could be due to the increased defects added by the crosslinking discussed previously.

The UHMWPE fibers show an orthorhombic crystalline structure with low levels of non-orthorhombic crystals [196–99]. Tension along the fiber axis and lateral compression in UHMWPE fibers make crystal transformation from the orthorhombic to the monoclinic form [199, 200]. At high temperatures and temperatures near to melting point, crystal transformation happens through a solid state phase transformation from orthorhombic to pseudohexagonal crystals [195–197, 200].

9.4.4 Application and Outlook

The tensile strength and modulus of UHMWPE fibers are relevant in a large number of applications such as composites, ropes, and fishing nets. The UHMWPE fibers also have favorable properties such as high impact resistance, cutting resistance, low dielectric constant, high heat conductivity, high sonic modulus, and low stretch. These properties are important for applications such as ballistic (bullet proof vests), helmets (impact), gloves (cutting resistance), hybrid composites (impact), loudspeaker cones (sonic modulus), and radomes/sonar domes (dielectric properties).

9.5 Carbon Fibers

9.5.1 Introduction

It has been more than 50 years that carbon fibers have been under development from rayon, polyacrylonitrile (PAN), isotropic and mesophase pitches. PAN-based technologies are most commercial production of carbon fibers and rayon-based carbon fibers are no longer in production. Pitch-based carbon fibers currently account for niche markets. Isotropic pitch-based carbon fibers have modest level of strength and modulus and are the least expensive carbon fibers. PAN and mesophase-based carbon fibers heat treated to improve modulus. Both PAN and mesophase pitch-based carbon fibers are not subject to creep or fatigue failure and set them apart from other material which is critical for application such as tension leg platforms for deep sea oil production [201]. The new generation of carbon based fibers is carbon nanotube (single and multi-walled). There are different synthesis methods for carbon

nanotubes include arc-discharge, laser ablation, gas phase catalytic growth from carbon monoxide, and chemical vapor deposition (CVD) from hydrocarbon [202].

9.5.2 PAN-Based Carbon Fibers

Polyacrylonitrile (PAN) fibers are produced by dry and wet spinning process. Although the preferred process for high strength fiber is wet spinning. Impurities and voids in the PAN fibers have significant effect on strength of carbon fibers. It is believed spinning PAN precursor under clean room conditions in order to remove small impurities which can act as crack initiators is critical for producing high strength carbon fibers such as Toray's T800 and T1000. The PAN for textile application modified by introducing co-monomers to assist processing and eliminating impurities to avoid reduction in tensile strength [201].

The chemistry of conversion of PAN to carbon fibers is complex and the most details of the manufacturing processes are the proprietary. The steps of producing PAN-based carbon fibers are: a) Cyclize the pendant nitrile groups. This step is exothermic and activation temperature depends on type and amount of co-monomer in PAN fibers. The fibers are under tension at this step. b) Oxidize the fibers by adding oxygen atoms to the polymer by heating in air (>600°C for tens of minutes). At this step decynisation and dehydrogenation take place. The PAN fibers lose ~50% weight and the carbon fibers structure contain longitudinal voids (see Figure 21) [201] .

9.5.3 Pitch-Based Carbon Fibers

The low strength carbon fibers made from isotropic pitch. These fibers produced by centrifugal and melt blowing process. High performance carbon fibers are produced from mesophase pitch by melt spinning process. Three common elements in pitch preparation are: highly aromatic feedstock, polymerization, and separating the unreacted molecules. In polymerization step the pitch molecules aggregate and will form 'Brooks and Taylor' spheres. As polymerization continues a continuous nematic liquid crystalline phase (mesophase) will form. Mochida *et al.* (24) showed strong Lewis acid combination (HF/BF_3) can act as solvent for aromatic molecules and catalyst for polymerization of mesophase pitch. HF/BF_3 is gas at atmospheric pressure and can be removed completely from

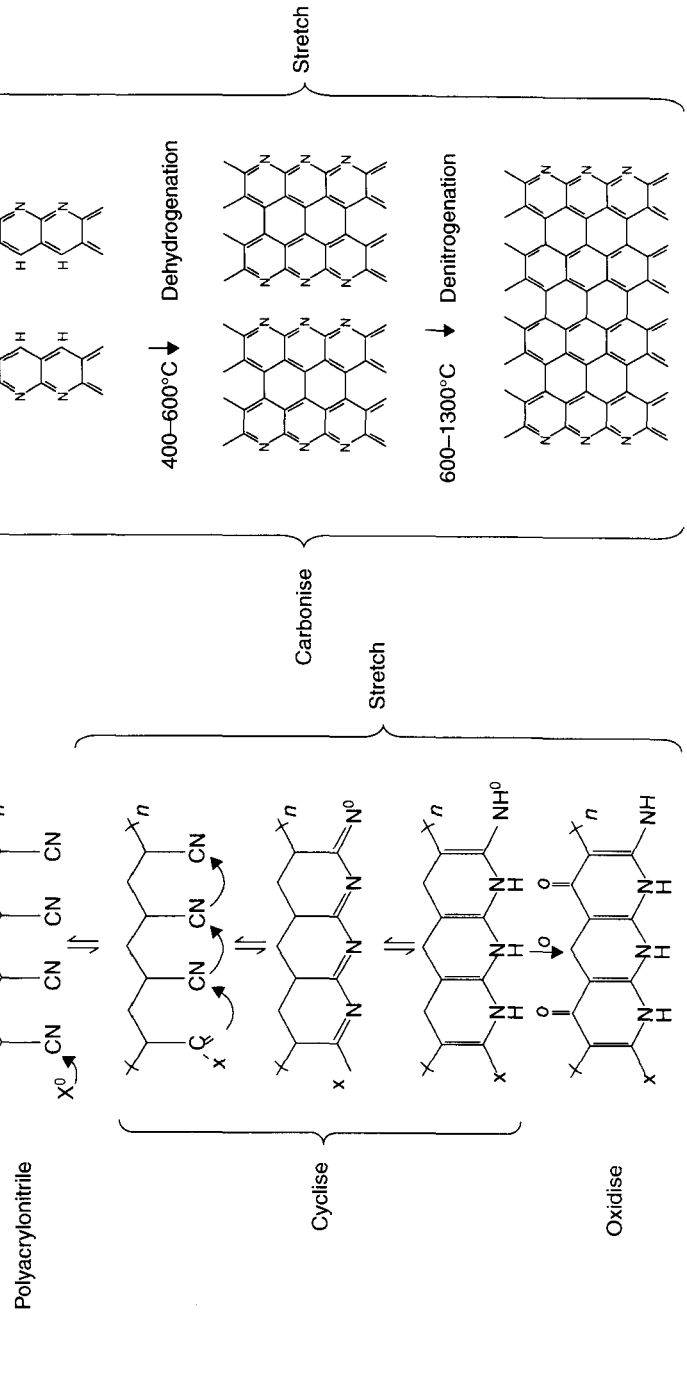

Figure 9.21 PAN-based carbon fibers chemistry.

the product. Another progress in producing pitch-based carbon fibers is development of solvated mesophase pitch which consist a heavy aromatic pitch fraction and a volatile solvent with more than one aromatic ring. The high amount of solvent acts as plasticizers and allows the spinning of very high molecular weight pitches. The fibers can produce from fibers using melt blowing process [201].

Melt spinning is the preferred method for producing fibers from mesophase pitch. The next step is removing hydrogen from melt spun fibers by heating at 450–600°C. We can avoid this step by stabilization by air oxidation. Two chemical reactions at stabilization process are increasing melting or boiling point and bridge two pitch molecules by oxygen. The great advantage of pitch-based carbon fiber is that carbonization and graphitization (>1600°C) can be accomplished with the relaxed fiber. The heat treatment improves the modulus of pitch fibers [201].

9.5.4 Vapor-Grown Carbon Fibers

In this method, pure carbon fibers produce by a catalytic process from carbon containing gases. The most common process the catalyst is a metal supported on a ceramic. This process produces long fibers which tangled together in a ball which is difficult to break up. The other method, the catalyst is an organometallic, injected into a chamber containing the gas mixture. The fibers produced by this method are short and straight. The vapor-grown carbon fibers have limited reinforcing capabilities [201].

9.5.5 Carbon Nanotubes

Since nearly two decades ago that Iijima [203] reported the observation of carbon nanotubes, numerous researchers studied physical and chemical properties of this new form of carbons. From unique electronic properties and a thermal conductivity higher than diamond to mechanical properties (stiffness, strength, resilience) higher any current material, carbon nanotubes offer tremendous opportunities for the development of new materials.

Carbon nanotubes can be imagined as a sheet of graphite that has been rolled into a tube. The properties of nanotubes depend on atomic arrangement, the diameter and length of the tubes, and the morphology, or nano structure. Nanotubes exist as either single-walled (SWCNT) or multi-walled (MWCNT) structures. The MWCNTs are composed of concentric SWCNTs [202].

The primary synthesis methods for single and multi-walled carbon nanotubes include arc-discharge [203, 204], lase ablation [205], gas-phase catalytic growth from carbon monoxide [206], and chemical vapor deposition (CVD) from hydrocarbons [207–209]. The scale-up limitation of arc discharge and laser ablation methods would make them cost prohibitive. One unique aspect of CVD technique is its ability to synthesize aligned arrays of carbon nanotubes with controlled diameter and length. The details on these methods go beyond the scope of this chapter.

The exceptional mechanical and physical properties of carbon nanotubes along with low density make this new form of carbon an excellent candidate for composite reinforcement. The understanding thermo-mechanical properties of nanotube-based composite require knowledge of the elastic, fracture, and interface interaction of nanotube.

9.5.6 Applications

According to wide range of properties of carbon fibers, they are suited to different applications. The properties of some commercially available fibers are given in Table 9.10.

Table 9.10 Mechanical properties of carbon fibers [201].

Type	Manufacturer	Product name	Tensile strength (GPa)	Young's modulus (GPa)	Strain to failure (%)
PAN	Toray	T300	3.53	230	1.5
		T100	7	294	2.0
		M55J	3.92	540	0.7
	Hercules	IM7	5.3	276	1.8
GP-Pitch	Kureha	KCF 200	0.85	42	2.1
HP-Pitch	BP-Amoco	Thornel P25	1.4	140	1.0
		Thornel P75	2.00	500	0.4
		Thornel P120	2.20	820	0.2

During the 1980s, the development of PAN-based carbon fibers was driven by use in composites for military aircraft. Due to reduction in weight and improvement of performance, the carbon fibers used into sporting goods, medical devices, industrial applications, and infrastructure. Electrical and thermal conductivity of carbon fibers are also important in many applications. By increasing modulus electrical resistivity (μΩ.cm) and thermal conductivity (W/mK) decrease and increase, respectively [201].

9.6 Advances in Improving Performance of Conventional Fibers

9.6.1 Introduction

With the increasingly fierce competition in the synthetic fiber market, it is extremely important to operate at a high performance to cost ratio. This has been done before by: a) improving the fiber properties by the development of the dry jet wet-spinning (aramid) or gel-spinning (UHMWPE) or b) reducing the production cost via high-speed spinning in the traditional melt-spinning process. As a result, the ever successfully developed fibers can be divided into two groups: high performance fibers such as carbon, aramid and UHMWPE, and conventional fibers such as PP, PET and nylon. The performance (tenacity) is plotted against cost ($/lb) for these fibers in Figure 9.22, where the most intriguing feature may be the big gap between the two

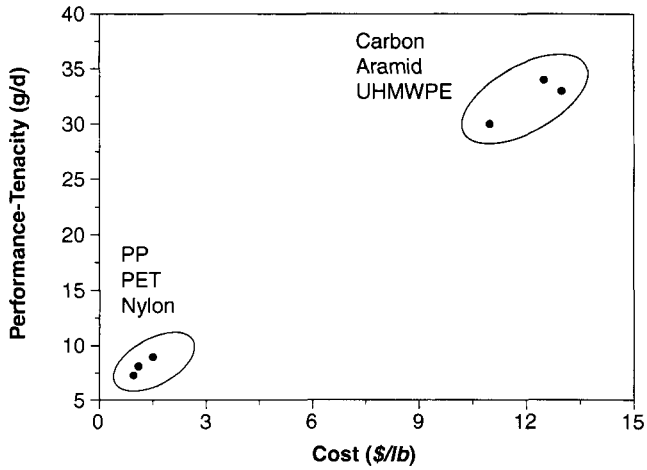

Figure 9.22 Performance vs. cost for various fibers.

groups. Since the difference is minor between the theoretically predicted ultimate tenacity values of various fibers (e.g., 232 g/d for PET and 235 g/d for aramid) [210], it is generally believed that the gap can be filled up by improving the fiber formation process.

In the book *Structure Formation in Polymeric Fibers*, Cuculo *et al.* [210] demonstrated the substantial potential of enhancing fiber properties by judiciously controlling the threadline dynamics. In other words, the enhanced fiber properties result not only from higher quality of raw materials but also from improved fiber structures. Hence in this Section, focus will be on advances in improving performance of conventional fibers by manipulating fiber structures, i.e., molecular orientation and crystallization.

9.6.2 Conventional Methods

The general idea [211] that the polymer undergoes stress-induced orientation (SIO) and crystallization (SIC) has been used for a long time to guide the conventional fiber formation process. However, it seems insufficient to further improve the process.

Various conventional methods have been used to control the SIO/SIC process. One of the typical examples may be the solid-state drawing of PET above T_g. It was observed [212–215] that drawing PET at different strain rates led mainly to three types of results. When the strain rate was higher than that of chain retraction, there was only a development of molecular orientation with the crystallization delayed until the end of drawing. The presence of highly-oriented but noncrystalline molecule chains or chain segments was related to the precursor for crystallization [216–218]. When the strain rate is between those of chain retraction and reptation, the concurrence of SIO and SIC was observed, resulting in not well aligned but tilted crystals. When the strain rate is slower than that of chain reptation, there was no significant molecular orientation but an isotropic crystallization occurred.

Cooling rate also plays a critical role in controlling the SIO/SIC process. This can be clearly illustrated by using "Continuous Cooling Transformation (CCT)" curves (Figure 9.23) [219]. As Figure 9.23 shows, the threadline starts to crystallize when the cooling curve crosses the "c-curve" for crystallization. SIC moves the "c-curve" to less time and higher temperature. This leads the crystallization to occur at higher temperatures and much wider range of time (strain rate). Under both quiescent and stressed conditions,

cooling at a rate that misses the "nose" of the "c-curve" will result in solidification of the threadline without crystallization.

Although various strategies, such as altering strain rate or cooling rate, have been conventionally used to control the SIO/SIC process, it is usually difficult to avoid massive crystallization especially with a high degree of orientation achieved. In the solid-state drawing process, SIC produces crystallites which act as rigid crosslinks inhibiting further drawing. These crystallites, associated with the intense chain entanglements built during the solidification process prior to drawing, make the achievable draw ratios far below the predicted maximum values [210]. This forms an insuperable barrier for substantially improving molecular orientation via the solid-state drawing process.

9.6.3 Innovative Liquid Isothermal Bath (LIB) Method

The liquid isothermal bath (LIB) was first applied in producing PET fibers by NCSU researchers in early 1990s. The initial motivation was quite straightforward, i.e., to produce high tenacity/high modulus fibers via a one-step high-speed spinning process.

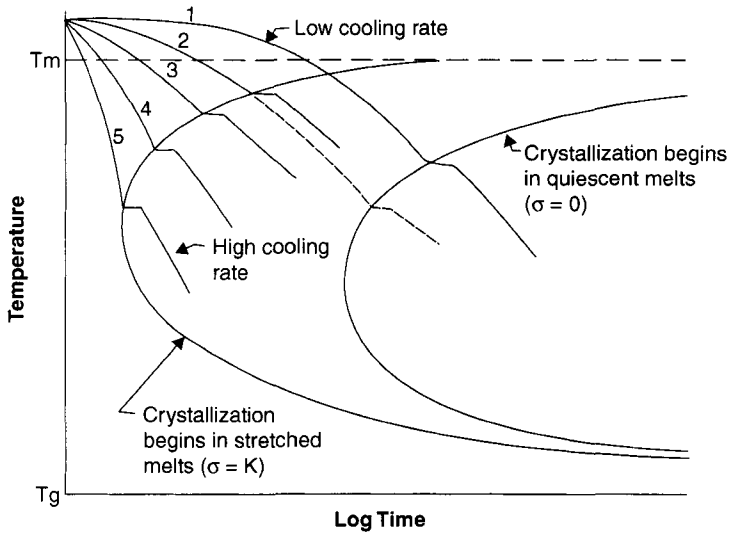

Figure 9.23 Schematic of "Continuous Cooling Transformation (CCT)" curves [219] (Reprinted with permission of Wiley).

The results turned out fairly encouraging, as the maximum tenacity of the PET fibers were improved from 9.5 g/d to 11.8 g/d [220–224]. It was also surprisingly found that the fibers spun with LIB showed unique morphology [224–232].

9.6.3.1 Liquid Isothermal Bath (LIB)

The traditional melt spin-draw process consists of melt-extrusion/spinning and solid-state drawing processes, as shown on the left hand in Figure 9.25. Apparently, the threadline in the melt-spinning stage undergoes changing parameters, such as time (strain rate), temperature, and tension. The solid-state drawing is usually carried out under constant temperature and tension, but changing strain rate, which has been widely studied [210].

To optimize the threadline dynamics, a liquid isothermal bath (LIB) has been designed as shown on the right hand in Figure 9.24. Note that several forms of LIB have been designed but only one is present here because all the forms have proven equivalent in the general effect. When the threadline passes through the bath at high speeds (>1000 m/min), the polymer molecules are subjected to a combined effect of enhanced tension and constant temperature for a longer time in state of fluid or semi-fluid. This endows the polymer molecules with a great freeness or flexibility to reach a highly-oriented state. Meantime, the SIC process can be effectively suppressed by the judicious selection of processing parameters,

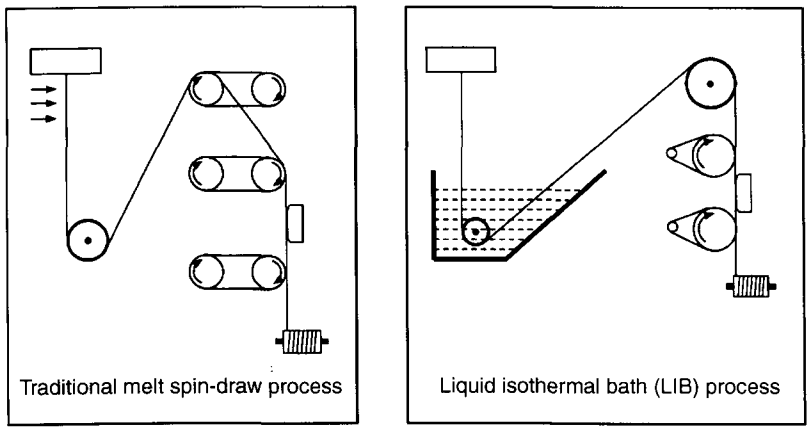

Figure 9.24 Schematic of traditional melt spin-draw process and liquid isothermal bath (LIB) process.

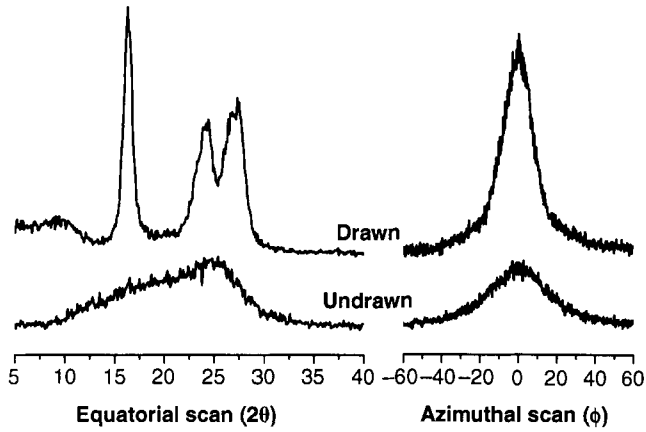

Figure 9.25 Equatorial and azimuthal X-ray diffraction profiles of undrawn (lower) and drawn (upper) PEN fibers spun with LIB.

such as bath temperature and take-up speed (strain rate). As a result, the polymer molecules are locked in a highly-oriented but noncrystalline state which acts as precursor to crystallization.

9.6.3.2 Properties of LIB Fibers

Numerous studies [220–232] have shown that superior properties were obtained for fibers spun with LIB. Tables 9.1 and 9.2 show typical results for PET and PEN fibers spun with LIB, with the experimental details described in Ref. [233]. As shown in Tables 9.1 and 9.2, the LIB fibers are featured by high tenacity but low modulus and high elongation. The tenacity of PET and PEN fibers spun with LIB is ca. 30–40% higher than that of fibers spun with the conventional meltspinning process. After a mild hot-drawing with draw ratio (DR) of 1.40, the tenacity and the modulus are increased by almost 50% and 90%, and the elongation is decreased by 40%, respectively, for the LIB fibers. Table 9.3 gives the maximum properties for PET and PEN fibers spun with LIB achieved in preliminary studies. As a result, the highest tenacity reaches 11.4 g/d for PET fibers and 12.3 g/d for PEN fibers spun with LIB and drawn at a low DR of less than 2.0, respectively, compared with 9.2 g/d for PET commercial fibers and 9.5 g/d for PEN commercial fibers by using large DRs of 5.0–7.0.

The LIB fibers also show interesting properties in orientation and crystallization, as shown in Tables 9.11 and 9.12. To be specific,

Table 9.11 Properties of PET Fibers Spun at 4000 m/min.

Fiber sample		Tenacity (g/d)	Modulus (g/d)	Elongation (%)	X_c^1 (%)	X_c^2 (%)	f_c	f_a
Undrawn	w/o LIB	4.90	76.6	27.2	26.4	29.7	0.91	0.70
	LIB	6.41	72.5	26.5	0	5.2	0.93	0.81
Drawn (DR = 1.40)	w/o LIB	6.76	113.0	15.4	37.3	38.5	0.96	0.77
	LIB	9.55	135.7	9.8	51.8	53.4	0.96	0.88

The crystallinity is calculated by using [1] density and [2] WAXD data.

Table 9.12 Properties of PEN Fibers Spun at 4000 m/min.

Fiber sample		Tenacity (g/d)	Modulus (g/d)	Elongation (%)	X_c^1 (%)	X_c^2 (%)	f_c	f_a
Undrawn	w/o LIB	5.35	126.2	11.7	27.0	30.5	0.92	0.72
	LIB	7.27	114.5	12.8	0	7.4	0.93	0.82
Drawn (DR = 1.40)	w/o LIB	7.31	173.0	8.7	35.2	39.4	0.95	0.78
	LIB	10.75	216.7	7.6	49.6	51.3	0.97	0.90

The crystallinity is calculated by using [1] density and [2] WAXD data.

Table 9.13 Maximum properties of polyester fibers.

Polymer Description		Tenacity (g/d)	Modulus (g/d)	Elongation (%)
PET	Commercial	9.2	n/a	14.0
	LIB	11.4	n/a	9.0
PEN	Commercial	9.5	156.7	12.8
	LIB	12.3	217.2	7.0

the undrawn fibers spun with LIB always have very low crystallinity and relatively high amorphous orientation, compared with the fibers spun without LIB. After a mild hot-drawing, the LIB fibers gain highly improved crystallinity (>50%) and high orientation in both crystalline and amorphous phases. Apparently, the improved crystallinity and the high amorphous orientation are credible for the superior mechanical properties for the LIB fibers. It may be expected to further improve the fiber properties by increasing the crystallinity as well as the amorphous orientation to higher levels.

9.6.3.3 Morphology of LIB Fibers

The superior fiber properties have inspired a great curiosity on the morphology of the LIB fibers. Of most interests is the highly-oriented but noncrystalline characteristic of the undrawn fibers spun with LIB, which is clearly indicated in Tables 9.11 and 9.12 and confirmed by wide angle X-ray diffraction (WAXD) data in Figure 9.25. Microscopy analysis showed that the undrawn LIB fibers was featured by a banded structure not only on their surface but also inside (The images can be found in Ref. [233]). When the LIB fibers were subjected to hot-drawing, the banded structure gradually disappeared and was finally transformed into a fibrillar crystalline structure, showing a transient and mesomorphic characteristic.

Moreover, profuse microvoids were found in the LIB fibers by using a focus ion beam (FIB) method (The images can be found in Ref. [233]). Other than the crazes usually observed in the plastic deformation of glassy polymers, the microvoids in the LIB fibers were empty and aligned in the fiber direction. Such microvoids were similar to those observed during deforming semicrystalline

polymers at high strains which were related to the negative pressure generated between crystalline lamellae [234, 235]. However, there was a lack of crystalline lamellae in the undrawn LIB fibers. This implied that the necessary condition for cavitation might not be the existence of crystalline lamellae, but formation of any ordered/rigid structures, such as the precursor for crystallization, between which the negative pressure could be generated [233].

9.7 Conclusions

While great challenges still exist, a promising way has been opened up for improving performance of conventional fibers via the newly developed liquid isothermal bath (LIB) technology. The LIB technology provides a feasible and economical way to manipulate the principle factors, i.e., time, tension, and temperature, during the melt-spinning process. This makes possible to disentangle the stress-induced orientation and crystallization of the polymer molecules. Further, a highly-oriented but noncrystalline precursor phase, acting as a hinge connecting the unoriented amorphous state and the oriented crystalline state, is produced and plays a key role in controlling orientation and crystallization of polymers. As a result, the fiber properties have been significantly improved for polyesters (PET, PEN). Work is still to be done to extend the application of the LIB technology to other semicrystalline polymers and to fill up the gap between the high performance fibers and the conventional fibers.

9.8 Acknowledgments

The authors gratefully acknowledge the cooperation of Dr. Sikkema and Katelyn Lee, and Mary Bogle in writing parts of this chapter.

9.9 References

1. B.Kalb, A.J. Pennings, *Polymer Bulletin*, Vol. 1, p. 871, 1979.
2. P. Smith, P.J. Lemstra, B. Kalb, and A.J. Pennings, *Polymer Bulletin*, Vol. 1, p. 733, 1979.
3. P. Smith, P.J. Lemstra, *Journal of Materials Science*, Vol. 15, p. 505, 1980.

4. M.G. Northolt and D.J. Sikkema, *Liquid Crystal Polymers, from Structures to Applications;* Collyer, A. A., Ed.; Elsevier Applied Science, 1992.
5. M.G. Northolt and D.J. Sikkema, *Advances in Polymer Science,* Vol. 98, p. 115, 1991.
6. L. Vollbracht In *Comprehensive Polymer Science;* Allen, G. Ed.; Pergamon Press: Oxford, 1989, Vol. 5, Chapter 22.
7. J.F. Wolfe, In *Encyclopedia of Polymer Science and Engineering,* 2nd edn; Wiley-Interscience: New York, 1988, Vol. 11, p. 601.
8. W.W. Adams, R.K. Eby, D.E. McLemore, The Materials Science of Rigid-Rod Polymers. In The Materials Research Society Symposium Proceedings; 1989, p. 134.
9. W. Sweeny, *Journal of Polymer Science, Part A: Polymer Chemistry,* Vol. 30, p. 1111, 1992.
10. M.A. Rakas, R.J. Farris, *Journal of Applied Polymer Science,* Vol. 40, p. 823, 1990.
11. M. Sahafeyan, S. Kumar, *Journal of Applied Polymer Science,* Vol. 56, p. 517, 1995.
12. M. Dotrong, M.H. Dotrong, and R.C. Evers, Polymer Preprints, Vol. 34, p. 408, 1993.
13. T.D. Dang, F.E. Arnold, Polymer Preprints, Vol. 36, p. 455, 1995.
14. F.J. McGarry, J.E. Moalli, *Polymer,* Vol. 32, p. 1816, 1991.
15. V.V. Kozey, H. Jiang, V.R. Mehta, and S. Kumar, *Journal of Materials Research,* Vol. 10, p. 1044, 1995.
16. L.S. Tan, F.E. Arnold, T.D. Dang, H.H. Chuah, K.H. Wei, *Polymer,* Vol. 35, p. 3091, 1994.
17. D.J. Sikkema, *Synthesis,* Vol. 12, p. 1211, 1993.
18. A. Duindam, V.L. Lishinsky, D.J. Sikkema, *Synthetic Communications,* Vol. 23, p. 2605, 1993.
19. D.J. Sikkema, J. Reichwein, *Macromolecular Chemistry and Physics,* Vol. 195, p. 273, 1994.
20. D.J. Sikkema, D.B. Van Guldener, *Polymer,* Vol. 34, p. 4373, 1993.
21. A.M. Reichwein, D.J. Sikkema, Process for preparing pyridine-2,6-diamines, US Patent 5,939,553, assigned to Akzo Nobel N.V., Aug. 17, 1999.
22. A.H. Gerber, *Journal of Polymer Science,* Polymer Chemistry Edition, Vol. 11, p. 1703, 1973.
23. R.L. Williams, S.A. Cohen, *Journal of Heterocyclic Chemistry,* Vol. 8, p. 841, 1971.
24. A.H. Gerber, Liquid crystalline polymer compositions, process and products, U.S. Patent 4533692, assigned to SRI International, Aug. 6, 1985.
25. D.J. Sikkema, Nitration of pyridine-2,6-diamines, US Patent 5,945,537, assigned to Akzo Nobel N.V., Aug. 31, 1999.
26. R. Nietzki, A. Schedler, *Berichte der Deutschen Chemischen Gesellschaft,* Vol. 30, p. 1666, 1897.
27. R.F. Kovar, F.E. Arnold, *Polymer Chemistry Edition,* Vol. 14, p. 2807, 1976.
28. T.D. Dang, L.S. Tan, F.E. Arnold, *Polymeric Materials Science and Engineering,* Vol. 62, p. 86, 1990.
29. T.D. Dang, H.H. Chuah, L.S. Tan, F.E. Arnold, US Patent 5041552, 1991.
30. D.J. Sikkema, A.M. Reichwein, Process for dicarboxylating dihydricphenols, US Patent 6,040,478, assigned to Akzo Nobel N.V., Mar. 21, 2000.
31. S. Rosenberg, R.C. Krauss, L.R. Kleiss, WO Patent 93/08156.
32. Y.H. So, J.M. Zaleski, C. Murlick, A. Ellaboudy, *Macromolecules,* Vol. 29, p. 2783, 1996.

33. Y.H. So, J.P. Heeschen, *Journal of Organic Chemistry*, Vol. 62, p. 3552, 1997.
34. D.J. Sikkema, *Polymer*, Vol. 39, p. 5981, 1998.
35. M. Lammers, E.A. Klop, M.G. Northolt, D.J. Sikkema, *Polymer*, Vol. 39, p. 5999, 1998.
36. M.G. Northolt, D.J. Sikkema, EU Patent 97203642.
37. M.G. Northolt, R.V.D. Hout, *Polymer*, Vol. 26, p. 310, 1985.
38. E.A. Klop, M. Lammers, *Polymer*, Vol. 39, p. 5987, 1998.
39. J. Sirichaisit, R.J. Young, *Polymer*, Vol. 40, p. 3421, 1999.
40. O.C. Van der Jagt, A. Beukers, *Polymer*, Vol. 40, p. 1035, 1999.
41. J.C.L. Hageman, J.W. Van der Horst, R.A.de Groot, *Polymer*, Vol. 40, p. 1313, 1999.
42. D.J. Sikkema, V.L. Lishinsky, Rigid rod polymer based on pyridobisimidazole, US Patent 5,674,969, assigned to Akzo Nobel N.V., Oct. 7, 1997.
43. T. Kuroki, Y. Tanaka, *Journal of Applied Polymer Science*, Vol. 65, p. 1031, 1997.
44. Y.H. So, *Progress in Polymer Science*, Vol. 25, p. 137, 2000.
45. T. Kitagawa, K. Yabuki, R.J. Young, *Polymer*, Vol. 42, p. 2101, 2001.
46. J.F. Wolfe, P.D. Sybert, J. R. Sybert, U. S. Patent 4,533,692, 4,533,693, and 4,533,724, 1987.
47. Z. Lysenko, High purity process for the preparation of 4,6-diamino-1, 3-benzenediol, U.S. Patent No. 4,766,244, assigned to DOW, Aug. 23, 1988.
48. H.F. Mark, *Encyclopedia of Polymer Science and Technology*, 3rd Edn.; Hoboken, N. J. John Wiley & Sons, Inc., 2003, p. 710.
49. H.G. Chae, S. Kumar, *Journal of Applied Polymer Science*, Vol. 100, p. 791, 2006.
50. H.D. Ledbetter, S. Rosenberg, C.W. Hurtig, The Materials Science and Engineering of Rigid-Rod Polymers; Adams, W. W., Eby, R. K., McLemore, D. E. Eds.; MRS: Boston, 1989, Vol. 134, p. 253.
51. E.W. Choe, D.E. McLemore, *Macromolecules*, Vol. 14, p. 920, 1981.
52. J.F. Wolfe, "The Materials Science of Rigid-Rod Polymers" Adams, W. W., Eby, R. K. McLemore, D. E., Eds.; Materials Research Society Symposium proceedings, 1989, 83.
53. X.J. Wang, Q.F. Zhou, *Liquid Crystalline Polymers*; World Scientific Publishing Co.: MA, 2004, p. 25.
54. Y.H. So, J.P. Heeschen, B. Bell, P. Bonk, M.Briggs, R. DeCaire, *Macromolecules*, Vol. 13, p. 5229, 1998.
55. A.W. Chow, J.F. Sandell, J.F. Wolfe *Polymer*, Vol. 29, p. 1307, 1988.
56. C.P. Spencer, G.C. Berry, *Polymer*, Vol.33, p. 1909, 1992.
57. D.B. Roitman, L.H. Tung,M. Serrano, R.A. Wessling, P.E. Pierini, *Macromolecules*, Vol. 26, p. 4045, 1993.
58. D.B. Cotts, G.C. Berry, *Macromolecules*, Vol. 14, p. 930, 1981.
59. X.D. Hu, S.E. Jenkins, B.G. Min, M.B. Polk, S. Kumar, *Macromolecular Materials and Engineering*, Vol. 288, p. 823, 2003.
60. P.M. Cotts, G.C. Berry, *Journal of Polymer Science, Polymer Physics Edition*, Vol. 21, p. 1255, 1983.
61. C.C. Lee, S.G. Chu, G.C. Berry, *Journal of Polymer Science, Polymer Physics Edition*, Vol. 21, p. 1573, 1983.
62. D.B. Roitman, R.A. Wessling, J. McAlister, *Macromolecules*, Vol. 26, p. 5174, 1993.
63. C.P. Wong, H. Ohnuma, G.C. Berry, *Journal of Polymer Science*, Polymer Symposia, Vol. 65, p. 173, 1978.
64. R. Zhang, W.M. Mattice, *Macromolecules*, Vol. 25, p. 4973, 1992.

65. R. Zhang, W.M. Mattice, *Macromolecules*, Vol. 26, p. 4384, 1993.
66. D.B. Roitman, M. McAdon, *Macromolecules*, Vol. 26, p. 4381, 1993.
67. S.A. Jenekhe, P.O. Johnson, *Macromolecules*, Vol. 23, p. 4419, 1990.
68. M.F. Roberts, S.A. Jenekhe, *Polymer Communications*, Vol. 31, p. 215, 1990.
69. M.F. Roberts, S.A. Jenekhe, *Chemistry of Materials*, Vol. 5, p. 1744, 1993.
70. S.R. Allen, A.G. Filippov, R.J. Farris, E.L. Thomas, C.P. Wong, G.C. Berry, E.C. Chenevey, *Macromolecules*, Vol. 14, p. 1135, 1981.
71. H.F. Mark, *Encyclopedia of Polymer Science and Technology;* 3rd Edn.; John Wiley & Sons, Inc.: Hoboken N.J., 2003, Vol. 4, p. 111.
72. Y. Cohen, E.L. Thomas, *Molecular Crystals and Liquid Crystals*, Vol. 153, p. 375, 1987.
73. S. Kumar, *International Encyclopedia of Composites*; Lee, S. M. Ed.; VCH: New York, 1990, Vol. 4, p. 51.
74. A.V. Fratini, P. G. Lenhert, T.J. Resch, W.W. Adams, W. W. "Molecular packing and crystalline order in polybenzobisoxazole and polybenzobisthiazole fibers", Materials Research Society Symposium Proceedings, Vol. 134, p. 431, 1989.
75. Y. Takahashi, H. Sul, *Journal of Polymer Science, Part B: Polymer Physics*, Vol. 38, p. 376, 2000.
76. T. Kitagawa, M. Ishitobi, K. Yabuki, *Journal of Polymer Science, Part B: Polymer Physics*, Vol. 38, p. 1605, 2000.
77. S.J. Krause, T.B. Haddock, D.L. Vezie, P.G. Lenhert, W.F. Hwang, G.E. Price, T.E. Helminiak, J.F. O'Brion, W.W. Adams, *Polymer*, Vol. 29, p. 1354, 1988.
78. W.W. Adams, S. Kumar, D.C. Martin, K. Shimamura, *Polymer Communications*, Vol. 30, p. 285, 1989.
79. D.C. Martin, E.L. Thomas, *Macromolecules*, Vol. 24, p. 2450, 1991.
80. T. Kitagawa, H. Murase, K. Yabuki, *J. Polym. Sci. Part B: Polym Phys.*, Vol. 36, p. 39, 2000.
81. L.C. Sawyer, M. Jaffe, *Journal of Materials Science*, Vol. 21, p. 1897, 1986.
82. T. Kitagawa, K. Yabuki, R.J. Young, *Polymer*, Vol. 42, p. 2101, 2001.
83. Y.H. So, *Progress in Polymer Science*, Vol. 25, p. 137, 2000.
84. H.D. Ledbetter, S. Rosenberg, C.W. Hurtig, Materials Research Society Symposium Proceedings, Vol. 134, p. 253, 1989.
85. L.A. Pottick, R.J. Farris, *Polymer Engineering and Science*, Vol. 31, p. 1441, 1991.
86. K. Tashiro, M. Kobayashi, *Macromolecules*, Vol. 24, p. 3706, 1991.
87. P.G. Lenhert, W.W. Adams, Materials Research Society Symposium Proceedings, Vol. 134, p. 329, 1989.
88. C.L. So, J.A. Bennett, J. Sirichaisit, R.J. Young, *Plastics, Rubber and Composites*, Vol. 32, p. 199, 2003.
89. H.S. Shin, D.C. Erlich, J.W. Simons, D.A. Shockey, Textile Research Journal, Vol. 76, p. 607, 2006.
90. S.J. DeTeresa, R.S. Porter, R.J. Farris, *Journal of Materials Science*, Vol. 20, p. 1645, 1985.
91. S.J. DeTeresa, R.S. Porter, R.J. Farris, *Journal of Materials Science*, Vol. 23, p. 1886, 1988.
92. M.G. Northolt, J.J.M. Baltüssen, B. Schaffers-Korff, *Polymer*, Vol. 36, p. 3485, 1995.
93. J.E. Grant, D.L. Pedrick, Materials Research Society Symposium Proceedings, Vol. 134, p. 407, 1989.

94. S. Liebman, M.B. Wasserman, A.P. Snyder, R.A. Pesce-Rodriguez, R.A. Fifer, L. Denny, T. Helminiak, Polymer Preprints, Vol. 32, p. 276, 1991.
95. C.A. Nielsen, P. Pierini, S. Fuh, *Journal of Fire Sciences*, Vol. 11, p. 156, 1993.
96. P.K. Kim, P. Pierini, R. Wessling, *Journal of Fire Sciences*, Vol. 11, p. 296, 1993.
97. J.F. Wolfe, Materials Research Society Symposium Proceedings, Vol. 134, p. 83, 1989.
98. S. Bourbigot, X. Flambard, M. Ferreira, F. Poutch, *Journal of Fire Sciences*, Vol. 20, p. 3, 2002.
99. H.S. Shin, D.C. Erlich, D.A. Shockey, *Journal of Materials Science*, Vol. 38, p. 3603, 2003.
100. R.F. Kovar, J. Richard, M. Druy, S. Tripathy, E.L. Thomas, A. Anwar, *Polymer Preprints*Vol. 35, p. 900, 1994.
101. G.M. Wu, *Materials Chemistry and Physics*, Vol. 85, p. 81, 2004.
102. J. Burkett, F.E. Arnold, *Polymer Preprints*, Vol. 28, p. 278, 1987.
103. C.S. Wang, J. Burkett, S. Bhattacharya, H.H. Chuah, F.E. Arnold, *Polymeric Materials Science and Engineering*, Vol. 60, p. 767, 1989.
104. D.R. Dean, D.M. Husband, M. Dotrong, C.S. Wang, M.H. Dotrong, W.E. Click, R.C. Evers, *J. Polym. Sci. Part A: Polym. Chem.*, Vol. 35, p. 3457, 1997.
105. F. Yang, Y. Bai, B.G. Min, S. Kumar, M.B. Polk, *Polymer*, Vol. 44, p. 3837, 2003.
106. J. Hilborn, J. Labadie, J.L. Herdrick, *Macromolecules*, Vol. 23, P.2854, 1990.
107. J.L. Hedrick, *Macromolecules*, Vol. 24, p. 6361, 1991.
108. L. Seely, M. Zimmerman, J. McLaughlin, *Advances in Space Research*, Vol. 33, p. 1736, 2004.
109. H. J. Schneider-Muntau, K. Han, N.A. Bednar, C.A. Swenson, R. Walsh, *IEEE Transactions on Applied Superconductivity*, Vol. 14, p. 1153, 2004.
110. Y. Saito, A. Tahara, M. Imaizumi, T. Takeichi, H. Wada, K. Jinno, *Analytical Chemistry*, Vol. 75, p. 5525, 2003.
111. K.E. Newman, P. Zhang, L.J. Cuddy, D.L. Allara, *Journal of Materials Research*, Vol. 6, p. 1580, 1991.
112. R.F. Ovar, R.R. Haghighat, R.W. Lusignea, Materials Research Society Symposium Proceedings, Vol. 134, p. 389, 1989.
113. C. Lietzau, R.J. Farris, Materials Research Society Symposium Proceedings, Vol. 305, p. 141, 1993.
114. S. Kumar, T.D. Dang, F.E. Arnold, A.R. Bhattacharyya, B.G. Min, X.F. Zhang, R.A. Vaia, C. Park, W.W. Adams, R.H. Hauge, R.E. Smalley, S. Ramesh, P.A. Willis, *Macromolecules*, Vol. 35, p. 9039, 2002.
115. K. Tashiro, J. Yoshino, *Macromolecules*, Vol.31, p. 5430, 1998.
116. S.L. Kwolek, U.S. Patent 30,352 (Du Pont), 1980.
117. S.L. Kwolek, Liquid Crystalline Polyamides; Am. Inst. Chem. *The Chemist*: Washington DC, 1980, Vol. 57, pp. 9–12.
118. S.L. Kwolek, Wholly aromatic carbocyclic polycarbonamide fiber having orientation angle of less than about 45°, US Patent 3,819,587, assigned to Dupont, June, 25, 1974.
119. S.L. Kwolek, P.W. Morgan, J.R. Schaefgen, L.W. Gulrich, *Macromolecules*, Vol. 10, p. 1390, 1977.
120. S.L. Kwolek, Optically anisotropic aromatic polyamide dopes, US Patent 3,671,542, assigned to Dupont, June, 20, 1972.
121. H. Blades, Dry jet wet spinning process, US Patent 3,767,756, Oct. 23, 1973.

122. H. Blades, High strength polyamide fibers and films, US Patent 3,869,429, assigned to Dupont, Mar. 4, 1975.
123. D. Tanner, J.A. Fitzgerald, P.G. Riewald, High Technology Fibers Part B; Lewin, M., Preston, J., Eds.; Marcel Dekker: New York, 1989.
124. D. Tanner, J.A. Fitzgerald, W.F. Knoff, J.J. Pigliacampi, P.G. Riewald, Proc. Int. Symp. *Fiber Sci. Tech.*; Hakone: Japan, 1985.
125. D. Tanner, A.K. Dhingra, J.J. Pigliacampi, *Journal of Metals*, Vol. 38, p. 21, 1986.
126. D. Tanner, V. Gabara, J.R. Schaefgen, J. R. *Polymers for Advanced Technologies*; Lewin, M., Ed.; V C R Publishers: Israel, 1987.
127. H.H. Yang, *Aromatic High-Strength Fibers*; Wiley & Sons: New York, 1989.
128. H.H. Yang, *Kevlar Aramid Fiber;* Wiley & Sons: New York, 1993.
129. W.B. Black, J. Preston, *High Modulus Wholly Aromatic Fibers*; Marcel Dekker: New York, 1973.
130. J.R. Schaefgen, Strength and Stiffness of Polymers; Zachariades, A. E., Porter, R. S., Eds.; Marcel Dekker: New York, 1983.
131. R.S. Jones, M. Jaffe, High Performance Aramid Fibers; Lewin, M., Preston, J., Eds.; Marcel Dekker: New York, 1985.
132. F.W. Billmeyer, *Textbook of Polymer Science*; Wiley: New York, 1984.
133. P.J. Flory, *Advances in Polymer Science*, Vol. 59, p. 1, 1984.
134. R.B. Seymour, R.S. Porter, *Manmade Fibers: Their Origin and Development;* Elsevier Science Publishers: England, 1993.
135. B. Mark, M. Overherger, *Encyclopedia of Polymer Science and Engineering;* John Wiley and Sons: New York, 1985.
136. M.G. Northolt, *European Polymer Journa*l, Vol. 10, p. 799, 1974.
137. Y. Rao, A.J. Waddon, R.J. Farris, *Polymer*, Vol. 42, p. 5937, 2000.
138. T.I. Blair, P.W. Morgan, Optically anisotropic spinning dopes of polycarbonamides, US Patent 3,673,143, assigned to Dupont, June, 27, 1972.
139. T.I. Blair, P.W. Morgan, Wholly aromatic carbocyclic polycarbonamide fiber having initial modulus in excess of 170 GPD and orientation angle of up to 40°, US Patent 3,817,941, assigned to Dupont, June 18, 1974.
140. H. Herlinger, H.P. Hoerner, F. Druschke, W. Denneler, F. Haiber, Applied Polymer Symposia, p. 201, 1973.
141. F. Higashi, Y. Nakano, M. Goto, H. Kakinoki, *Journal of Polymer Science, Polymer Chemistry Edition*, Vol. 18, p. 1099, 1980.
142. F. Higashi, M. Goto, Y. Nakano, H. Kakinoki, *Journal of Polymer Science, Polymer Chemistry Edition*, Vol. 18, p. 851, 1980.
143. F. Higashi, S. Ogata, Y. Aoki, *Journal of Polymer Science, Polymer Chemistry Edition*, Vol. 20, p. 2081, 1982.
144. F. Higashi, N. Akiyama, S. Ogata, *Journal of Polymer Science, Polymer Chemistry Edition*, Vol. 21, p. 913, 1983.
145. M. G. Northolt, *European Polymer Journal*, Vol. 10, p. 799, 1974.
146. K. Haraguchi, T. Kajiyama, M. Takayanagi, *J. Appl. Polym. Sci.*, Vol. 23, p. 915, 1979.
147. K. Yabuki, H. Ito, T. Ota, *Sen'i Gakkaishi*, Vol. 31, p. 524, 1975.
148. M.G. Northolt, L.L. Chapoy, Elsevier Applied Science Publishers: London, 1985; pp. 299–310.
149. S.J. DeTeresa, R.S. Porter, R.J. Farris, *Journal of Materials Science*, Vol. 23, p. 1886, 1988.

150. L.P. Myasnikova, V.A. Marikhin, E.M. Ivan'kova, P.N. Yakushev, *Journal of Macromolecular Science*, Physics, Vol. B40, p. 473, 2001.
151. M.G. Dobb, C.R. Park, R.M. Robson, *Journal of Materials Science*, Vol. 27, p. 3876, 1992.
152. S.R. Allen, *Journal of Materials Science*, Vol. 22, p. 853, 1987.
153. S. Rebouillat, J.B. Donnet, T.K. Wang, *Polymer*, Vol. 38, p. 2245, 1997.
154. S. Rebouillat, J.C.M. Peng, J.B. Donnet, *Polymer*, Vol. 40, p. 7341, 1999.
155. A. Tonelli, M. Sirinivasarao, *Polymers from the Inside Out: An Introduction to Macromolecules;* John Wiley and Sons: New York, 2001.
156. H.F. Mark, *Encyclopedia of Polymer Science and Technology*, 3rd Edn.; John Wiley and Sons: New York, 2003.
157. C.Y. Yue, K. Padmanabhan, *Composites, Part B: Engineering*, Vol. 30B, p. 205, 1999.
158. A. Ohnishi, E. Fujioka, K. Kosuge, N. Ikuta, *Composite Interfaces*, Vol. 11, p. 263, 2004.
159. K.E. Perepelkin, I.V. Andreeva, E.A. Pakshver, I. Morgoeva, Fibre Chemistry (Translation of Khimicheskie Volokna), Vol. 35, p. 265, 2003.
160. S. Bourbigot, X. Flambard, M. Ferreira, E. Devaux, F. Poutch, *Journal of Materials Science*, Vol. 38, p. 2187, 2003.
161. P.J. Lemstra, R. Kirschbaum, T. Ohta, T. H. Yasuda, Developments in Oriented Polymers-2 Ward, I. M. Ed.; Elsevier Applied Science: London, 1987; pp. 39–79.
162. A.J. Pennings, K.E. Meihuizen, *Ultra-High Modulus Polymers*, Cifferi, A., Ward, M., Eds.; Applied Science Publishers: London, 1979, p. 117.
163. P. Smith, P.J. Lemstra, Process for making polymer filaments which have a high tensile strength and a high modulus, U.S. Patents 4,344,908; assigned to Stamicarbon, Aug. 17, 1982.
164. S. Kavesh, D.C. Prevorsek, High tenacity, high modulus polyethylene and polypropylene fibers intermediates therefore, U.S. Patents 4,413,110; assigned to Allied Corp., Nov. 1, 1983.
165. K. Tashiro, M. Kobayashi, H. Tadokoro, *Macromolecules*, Vol. 11, p. 914, 1978.
166. A. Odajima, T. Maeda, *Journal of Polymer Science, Polymer Symposia*, Vol. 15, p. 55, 1966.
167. P.J. Lemstra, C.W.M. Bastiaansen, S. Rastogi, Basic aspects of solution (Gel)-spinning and ultra-drawing of ultra-high molecular weight polyethylene, Structure Formation in Polymeric Fibers; Salem, D. R., Ed.; Hanser: Munich, 2000, pp. 186–223.
168. Y. Termonia, P. Smith, *Macromolecules*, Vol. 20, p. 835, 1987.
169. Y. Termonia, P. Smith, *Polymer*, Vol. 27, p. 1845, 1986.
170. P. Smith, Y.Termonia, *Polymer Communications*, Vol. 30, p. 66, 1989.
171. G. Odian, *Principles of Polymerization*; 4th Edn.; Wiley-Interscience: Hoboken, 2004.
172. "Ferrocene"; http://en.wikipedia.org/wiki/Ferrocene (2005).
173. W. Kaminsky, *Advances in Catalysis*, Vol. 46, p. 89, 2001.
174. H.W. Birnkraut, Synthesis of UHMWPE. In Ultra High Molecular Weight Polyethylene as Biomaterial in Ortho-paedic Surgery; Willert, H. G., Buchhorn, G. H., Eyere, P., Eds.; Hogrefe & Huber Publishers: New York, 1991, pp. 3–5.
175. P. Smith, P.J. Lemstra, *Journal of Materials Science*, Vol. 15, p. 505, 1980.

176. A.E. Zachariades, M.P.C. Watts, T. Kanamoto, R.S. Porter, *Journal of Polymer Science, Polymer Letters Edition*, Vol. 17, p. 485, 1979.
177. G.T. Pawlikowiski, D.J. Mitchell, R.S. Porter, *J. Polym Sci., Part B: Polym. Phys.*, Vol. 26, p. 1865, 1988.
178. P. Smith, H.D. Chanzy, B.P. Rotzinger, *Polymer Communications*, Vol .26, p. 258, 1985.
179. P. Smith, H.D. Chanzy, B.P. Rotzinger, *Journal of Materials Science*, Vol. 22, P.523, 1987.
180. T. Kanamoto, T. Ohama, K. Tanaka, M. Takeda, R.S. Porter, *Polymer*, Vol. 28, p. 1517, 1987.
181. T. Kanamoto, A. Tsuruta, K. Tanaka, M. Takeda, R.S. Porter, *Macromolecules*, Vol. 21, p. 470, 1988.
182. J.L.J. Van Dingenen, *Materials and Design*, Vol. 10, p. 101, 1989.
183. D.C. Prevorsek, Ultra-Strong Polyethylene Fibers. Polymeric Materials Encyclopedia; Salamore, Joseph C. Ed.; CRC Press Inc.: New York, 1996, pp. 8411–8417.
184. P.M. Pakhomov, S.D. Khizhnyak, A. Golikova, V.P. Galitsyn, *Physics of the Solid State*, Vol. 47, p. 1028, 2005.
185. Y. Ohta, H. Murase, T. Hashimoto, *Journal of Polymer Science, Part B: Polymer Physics*, Vol. 43, p. 2639, 2005.
186. P. Smith, P.J. Lemstra, J.P.L. Pijpers, *Journal of Polymer Science, Polymer Physics Edition*, Vol. 20, p. 2229, 1982.
187. A. Schaper, D. Zenke, E. Schulz, R. Hirte, M. Taege, *Physica Status Solidi A: Applied Research*, Vol. 116, p. 179, 1989.
188. D.C. Prevorsek, H.B. Chin, Y.D. Kwon, J.E. Field, *Journal of Applied Polymer Science: Applied Polymer Symposium*, Vol. 47, p. 45, 1991.
189. S. Kavesh, D.C. Prevorsek, *International Journal of Polymeric Materials*, Vol. 30, p. 15, 1995.
190. L. Xiaoyan, W. Yu *Journal of Applied Polymer Science*, Vol. 97, p. 310, 2005.
191. B. Dessain, O. Moulaert, R. Keunings, A.R. Bunsell *Journal of Materials Science*, Vol.27, p. 4515, 1992.
192. D.J. Dijkstra, PhD thesis, University of Groningen: Groningen, The Netherlands, University of Groningen, 1988.
193. F.X. Kromm, T. Lorriot, B. Coutand, R. Harry, J.M. Quenisset, *Polymer Testing*, Vol. 22, p. 463, 2003.
194. S.H. Sung, W.S. Yoon, J.H. Choi, S.Y. Kim, B.C. Ji, W.S. Lyoo, *Journal of Applied Polymer Science*, Vol. 66, p. 1583, 1997.
195. Y.L. Hsieh, X.P.J. Hu, *Polym. Sci., Part B: Polym. Phys.*, Vol. 35, p. 623, 1997.
196. A.J. Pennings, A.Zwijnenburg, *Journal of Polymer Science, Polymer Physics Edition*, Vol. 17,p. 1011, 1979.
197. A. Kaji, Y. Ohta, H. Yasuda, M. Murano, *Polymer Journal*, Vol. 22,p. 455, 1990.
198. Y. Fu, W. Chen, M. Pyda, *Journal of Macromolecular Science, Physics*, Vol. B35,p. 37, 1996.
199. W.R. Busing, *Macromolecules*, Vol. 23, p. 4608, 1990.
200. Y.L. Hsieh, J.Ju, *J. Appl. Polym. Sci.*, Vol. 53, p. 347, 1994.
201. J.G. Lavin, Carbon fibers in "High performance fibers" Ed. Hearle, J. W. S.; Woodhead Publishing Ltd., Cambridge 2001, 156–190.
202. E.T. Thostenson, R. Zhifeng, T.W. Chou *Composites Science and Technology*, Vol. 61, p. 1899, 2001.

203. S. Iijima, *Nature*, Vol. 354, p. 56, 1991.
204. C. Journet, W.K. Mase, P. Bernier, A. Loiseau, M.L. de la Chapelle, S. Lefrant, *Nature*, Vol. 388, p. 756, 1997.
205. A.G. Rinzler, J. Liu, H. Dai, P. Nikolaev, C.B. Huffman, F.J. Rodriguez-Macias, *Applied Physics A*, Vol. 67, p. 29, 1998.
206. P. Nikolaev, M.J. Bronikowski, R.K. Bradley, F. Fohmund, D.T. Colbert, K.A. Smith, *Chemical Physics Letters*, Vol. 313, p. 91, 1999.
207. Z.F. Ren, Z.P. Huang, J.W. Xu, D.Z. Wang, J.G. Wen, J.H. Wang, *Applied Physics Letters*, Vol. 75, p. 1086, 1999.
208. Z.F. Ren, Z.P. Huang, J.W. Xu, J.H. Wang, P. Bush, M.P. Siegal, *Science*, Vol. 282, p. 1105, 1998.
209. Z.P. Huang, J.W. Xu, Z.F. Ren, J.H. Wang, M.P. Siegal, P.N. Provencio, *Applied Physics Letters*, Vol. 73, p. 3845, 1998.
210. J.A. Cuculo, J.F. Q. Zhou, in *Structure Formation in Polymeric Fibers*, Salem D. R., ed., Hanser: Munich, 2000, 94–117.
211. A. Ziabicki, in *Fundamentals of Fibre Formation*, Ziabicki, A., ed., Wiley: New York, 1976.
212. D.J. Blundell, D. H. MacKerron, W. Fuller, *Polymer*, Vol. 37, p. 3303, 1996.
213. A. Mahendrasingam, C. Martin, W. Fuller, D.J. Blundell, R.J. Oldman, J.L. Harvie, D.H. MacKerron, C. Riekel, P. Engstrom, *Polymer*, Vol. 40, p. 5553, 1999.
214. D.J. Blundell, A. Mahendrasingam, C. Martin, W. Fuller, D.H. MacKerron, J.L. Harvie, R.J. Oldman, C. Riekel, *Polymer*, Vol. 41, p. 7793, 2000.
215. A. Mahendrasingam, D.J. Blundell, C. Martin, W. Fuller, D.H. MacKerron, J.L. Harvie, R.J. Oldman, C. Riekel, *Polymer*, Vol. 41, p. 7803, 2000.
216. G.E. Welsh, DD.J. Blundell, A.H. Windle, *Macromolecules*, Vol. 31, p. 7562, 1998.
217. G.E. Welsh, D.J. Blundell, A.H. Windle, *Journal of Materials Science*, Vol. 35, p. 5225, 2000.
218. A. Mahendrasingam, C. Martin, W. Fuller, D.J. Blundell, R.J. Oldman, D.H. MacKerron, J.L. Harvie, C. Riekel, *Polymer*, Vol. 41, p. 1217, 2000.
219. J.E. Spruiell, J.L. White, *Polymer Engineering and Science*, Vol. 15, p. 660, 1975.
220. J.A. Cuculo, P.A. Tucker, G.Y. Chen, F. Lundberg,"Melt spinning of ultra-oriented crystalline polyester filaments, U.S. Patent, 5,149,480, assigned to North Carolina State University, Sep. 22, 1992.
221. J.A. Cuculo, P.A. Tucker, C.Y. Lin, F. Lundberg, Process for producing high strength, high modulus thermoplastic fibers, U. S. Patent 5,171,504, assigned to North Carolina State University, Dec. 15, 1992.
222. J.A. Cuculo, P.A. Tucker, F. Lundberg, J.Y. Chen, G. Wu, G.Y., Ultra-oriented crystalline filaments and method of making same, U. S. Patent 5,733,653, assigned to North Carolina State University, Mar. 31, 1998.
223. J.A. Cuculo, P.A. Tucker, G.Y. Chen, F. Lundberg, Ultra-oriented crystalline filaments, U. S. Patent 5,405,696, assigned to North Carolina State University, Apr. 11, 1995.
224. C.Y. Lin, P.A. Tucker, J.A. Cuculo, *Journal of Applied Polymer Science*, Vol. 46, p. 531, 1992.
225. B. Huang, P.A. Tucker, J.A. Cuculo, *Polymer*, Vol. 38, p. 1101, 1997.
226. F.J. Hotter, J.A. Cuculo, P.A. Tucker, B.K. Annis, *Journal of Applied Polymer Science*, Vol. 69, p. 2051, 1998.

227. J.Y. Chen, P.A. Tucker, J.A. Cuculo, *Journal of Applied Polymer Science*, Vol. 66, p. 2441, 1997.
228. Q. Zhou, G. Wu, P.A. Tucker, J.A. Cuculo, *Journal of Polymer Science: Part B: Polymer Physics*, Vol. 33, p. 909, 1995.
229. G. Wu, J.D. Jiang, P.A. Tucker, J.A. Cuculo, *Journal of Polymer Science: Part B: Polymer Physics*, Vol. 34, p. 2035, 1996.
230. G.Wu, P.A. Tucker, J.A. Cuculo, *Polymer*, Vol. 38, p. 1091, 1997.
231. G. Wu, Q. Zhou, J.Y. Chen, J.F. Hotter, P.A. Tucker, J.A. Cuculo, *Journal of Applied Polymer Science*, Vol. 55, p. 1275, 1995.
232. G. Wu, T. Yoshida, J.A. Cuculo, *Polymer*, Vol. 39, p. 6473, 1998.
233. P. Chen, M. Afshari, J.A. Cuculo, R. Kotek, *Macromolecules*, Vol. 42, p. 5437, 2009.
234. A. Pawlak, A. Galeski, *Macromolecules*, Vol. 38, p. 9688, 2005.
235. A. Pawlak, A. Galeski, *Macromolecules*, Vol. 41, p. 2839, 2008.

10

Synthesis and Characterization of Poly (aryl ether ketone) Copolymers

G Wang

College of Chemistry, Jilin University, Changchun, China

Abstract

In this chapter, two general synthetic methods of poly (aryl ether ketone) copolymers were introduced, that is, (1) nucleophilic substitution step copolycondensation of at least two different monomers of bisphenol and at least one dihalobenzoid compound or at least one monomer of bisphenol and at least two different dihalobenzoid compounds; (2) electrophilic Friedel–Crafts copolycondensation of at least two different monomer of diphenyl ether and terephthaloyl chloride or at least one monomer of diphenyl ether and terephthaloyl chloride as well as isophthaloyl chloride. Some representative monomers were included. By the method (1), the synthesis and characterization of structural poly (aryl ether ketone) copolymers—poly (ether ether ketone)-poly (ether ether ketone ketone) (PEEK-PEEKK), poly (ether ether ketone)-poly (ether biphenyl ether ketone) (PEEK-PEDEK), poly (ether ether ketone ketone)-poly (ether biphenyl ether ketone ketone) (PEEKK-PEDEKK), poly (ether ether ketone)-poly (ether ether ketone biphenyl ketone) (PEEK-PEEKDK) and poly (ether biphenyl ether ketone)-poly (ether biphenyl ether ketone biphenyl ketone) (PEDEK-PEDEKDK) were discussed. The synthesis and characterization of the functional PAEK copolymers, such as liquid crystal poly (aryl ether ketone) copolymers, poly (aryl ether ketone) copolymers with pendent group of low dielectric constant and poly (aryl ether ketone) copolymers with crosslinking moieties were also discussed in details. These PAEK copolymers showed a lot of special performance and can maybe be applied in optical waveguides, microelectronics, display devices, membrane materials and so on.

Keywords: High performance polymer, poly (aryl ether ketone), copolymers, synthesis, characterization

Vikas Mittal (ed.) High Performance Polymers and Engineering Plastics, (341–386)
© Scrivener Publishing LLC

10.1 Introduction

High performance polymers have received considerable attention over the past decade owing to their increased demands as replacements for metals or ceramics. Poly (aryl ether ketone)s (PAEKs) are a class of important high-performance aromatic polymers with excellent mechanical properties, good solvent resistance, size-accuracy, electrical characteristics, and superior thermal stability [1–3]. This class of advanced materials is currently receiving considerable attention for potential applications in aerospace, automobile, electronics, and other high technology fields [4–8]. However, in spite of having excellent combination of properties, PAEKs have some serious drawbacks, e.g., insolubility in common organic solvents, intractability in processing, infusibility and strong color that often limit their utility in various advanced technological applications. For example, low refractive index, low dielectric constant, high optical transparency along with good mechanical properties and high thermal stability are the important properties required for applications in optical waveguides, microelectronics and display devices. Moreover, for membrane applications, the polymers need to have good film forming ability, high chemical resistance, thermal stability, low moisture uptake and a good balance of permeability and selectivity [9–14]. To obtain the desired solubility, processability and other essential properties, the PAEKs with pendant groups and copolymers have been developed [15–22].

10.2 General Synthetic Methods of PAEK Copolymers

In general, PAEK copolymers have been synthesized by two methods: (1) nucleophilic substitution step copolycondensation of at least two different monomers of bisphenol and at least one dihalobenzoid compound or at least one monomer of bisphenol and at least two different dihalobenzoid compounds; (2) electrophilic Friedel–Crafts copolycondensation of at least two different monomer of diphenyl ether and terephthaloyl chloride or at least one monomer of diphenyl ether and terephthaloyl chloride as well as isophthaloyl chloride. Some of bisfluoro, bisphenol monomers, aromatic bisbenzoyl chloride and diphenyl ether used for the synthesis of poly (aryl ether ketone) copolymers have been included in Table 10.1.

Table 10.1 List of bisfluoro and bisphenol monomers reported in literature (ref. added below each figure).

Bisfluoro and Diphenyl Ether Monomers	Bispbenol and Aromatic Bisbenzoyl Chloride Monomers
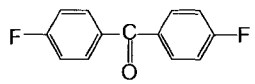 [23–25]	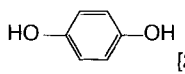 [23–25]
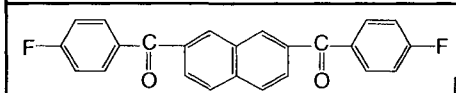 [13, 23, 26]	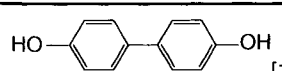 [13, 26–27]
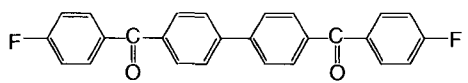 [27]	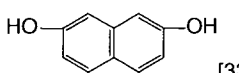 [33–34]
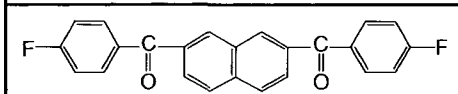 [28]	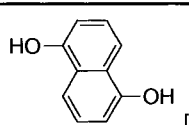 [35–36]
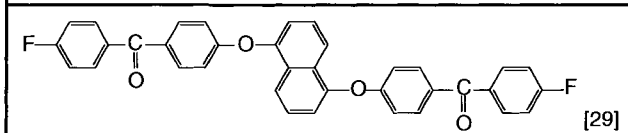 [29]	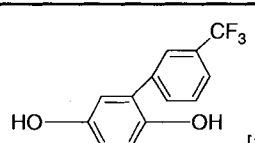 [13, 37]

(Continued)

Table 10.1 List of bisfluoro and bisphenol monomers reported in literature (ref. added below each figure). (Continued)

Bisfluoro and Diphenyl Ether Monomers	**Bispbenol and Aromatic Bisbenzoyl Chloride Monomers**
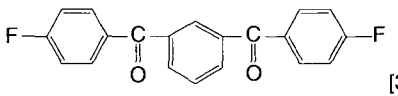 [30]	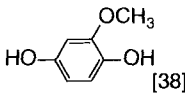 [38]
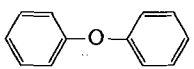 [31]	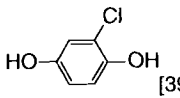 [39]
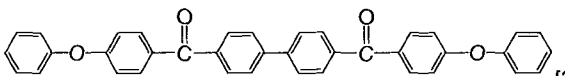 [32]	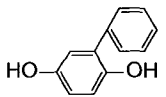 [39]
Aromatic Bisbenzoyl Chloride Monomers	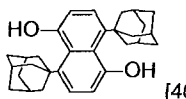 [40]
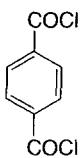 [32] 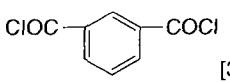 [32]	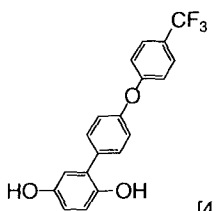 [41]

10.3 Synthesis and Characterization of Structural Poly (aryl ether ketone) Copolymers

In order to obtain PAEK copolymers with different properties, such as thermal properties, mechanical properties, etc., a lot of novel monomers and corresponding PAEK copolymers are synthesized.

1. Poly (ether ether ketone)-poly (ether ether ketone ketone) (PEEK-PEEKK) copolymer

The thermal properties and mechanical properties of PAEKs will be modified by changing number of phenyl, ether bond or ketone bond in constitutional unit of PAEKs. PEEK-PEEKK copolymer could be synthesized by copolymerizing with 4,4′-difluorobenzophenone (DFB), 1,4-bis(*p*-fluorobenzoyl)benzene (BFB) and hydroquinone (HQ) according to Scheme 10.1 [23].

A typical synthetic procedure is as follows: The four-neck flask of 1000 ml was fitted with a mechanical stirrer, thermometer, nitrogen inlet, and a Dean Stark trap fitted with a condenser and a nitrogen outlet. After the reaction vessel was purged with dry nitrogen, DFB/BFB/HQ/Na_2CO_3/K_2CO_3 (molar ratio: 0.4/0.1/0.5/0.44/0.1) and 360g diphenyl sulfone (DPS) in a solid content of 30 wt% were

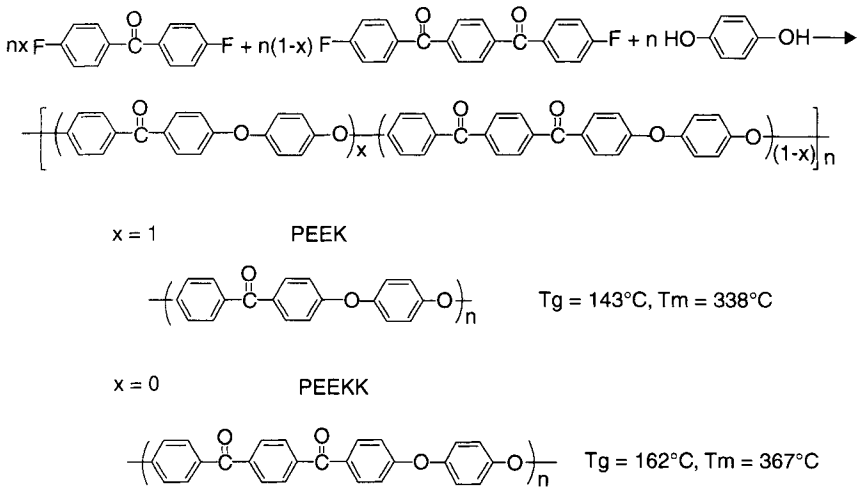

Scheme 10.1 Synthesis routes of PEEK-PEEKK copolymers [23].

added. The mixture was slowly heated to 180°C and held at that temperature for 2 h in a nitrogen atmosphere, and then reaction temperature was gradually raised to 240–250°C and kept for 1 h. After the polymerization reaction temperature was raised to 290°C and held for 1 h, the reaction temperature was raised to 320°C to polymerize 4 h. The resulted mixture was slowly poured into cool distilled water by strip form. The solid obtained was pulverized and after filtration, washed with ethanol under reflux to remove DPS completely, then washed with hot distilled water to remove by-products, and dried at 140°C in oven for 12 h to give PEEK-PEEKK (DFB/BFB = 0.4/0.1) as an off-white powder in 96% yield.

The other PEEK-PEEKK copolymers with different ratio of DFB/BFB were prepared by the same method. The relation of melting point of PEEK-PEEKK copolymers vs the mole fraction of BFB was shown in Figure 10.1.

The results exhibited that the melting point of PEEK-PEEKK copolymers increased with the mole fraction of BFB because of increase of PEEK-PEEKK copolymers' rigidity, in other words, the heat-resistance of copolymers increased by introducing more ketone bonds into copolymers. So the properties of PEEK-PEEKK copolymers could be optimized by adjusting the ratio of copolymerization monomers.

Based on the Scheme 10.1, PEEK could be synthesized when x = 1 and PEEKK could be prepared when x = 0. The basic properties of PEEK (x = 1) and PEEKK (x = 0) were listed in Table 10.2.

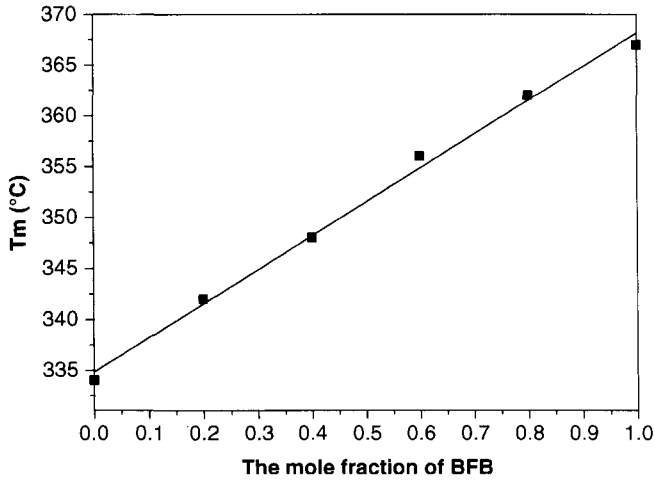

Figure 10.1 The relation of melting point of PEEK-PEEKK copolymers vs the mole fraction of BFB.

Table 10.2 The basic properties of PEEK and PEEKK.

Properties	Unit	PEEK	PEEKK
T_g	°C	143	162
T_m	°C	338	367
Tensile strength	MPa	94	110
Elongation at break	%	60	40
Flexural strength	MPa	160	180
Flexural modulus	GPa	3.8	4.0

From the data of Table 10.2, it could be found that heat-resistant, mechanical properties of PEEKK were more excellent than those of PEEK.

2. Poly (ether ether ketone)-poly (ether biphenyl ether ketone) (PEEK-PEDEK) copolymer

PEEK-PEDEK copolymer could be synthesized by copolymerizing with 4,4′-difluorobenzophenone (DFB), 4,4′-diphenol(DP) and hydroquinone (HQ) according to Scheme 10.2.

Figure 10.2a and Figure 10.2b showed that the thermal properties of PEEK-PEDEK copolymers.

One could find from Figure 10.2a and Figure 10.2b that the T_g of PEEK-PEDEK copolymers increased with increase of biphenyl content of copolymers, but the T_m of PEEK-PEDEK copolymers firstly decreased with increase of biphenyl content until the biphenyl content increased 30% and then T_m of PEEK-PEDEK copolymers gradually increased with increase of biphenyl content. The T_m change of PEEK-PEDEK copolymers was different from that of PEEK-PEEKK copolymers. This phenomenon maybe resulted from different link mode of phenyl, ether bond or ketone bond in polymer chain.

3. Poly (ether ether ketone ketone)-poly (ether biphenyl ether ketone ketone) (PEEKK-PEDEKK) copolymer

PEEKK-PEDEKK copolymer could be synthesized by copolymerizing with 1,4-bis(*p*-fluorobenzoyl)benzene (BFB), 4,4′-diphenol(DP) and hydroquinone (HQ) according to Scheme 10.3.

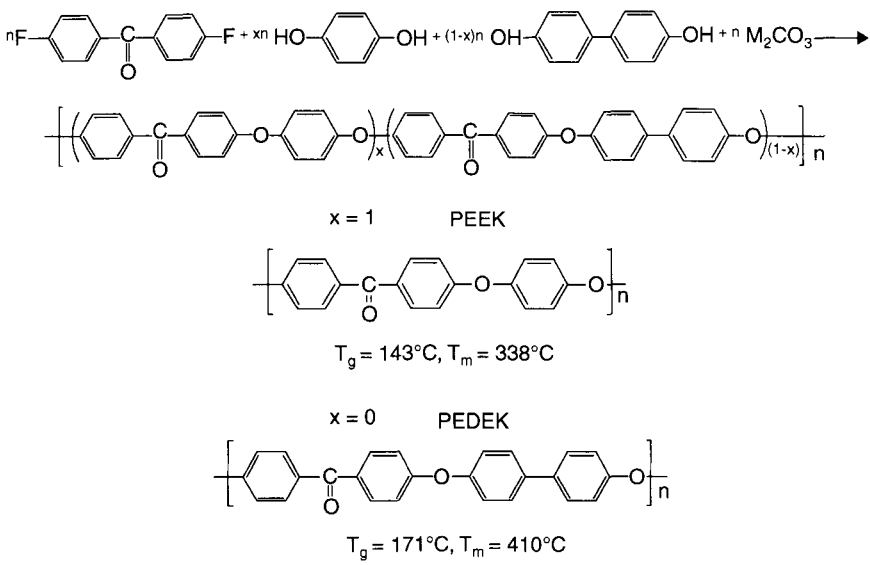

Scheme 10.2 Synthesis routes of PEEK-PEDEK copolymers.

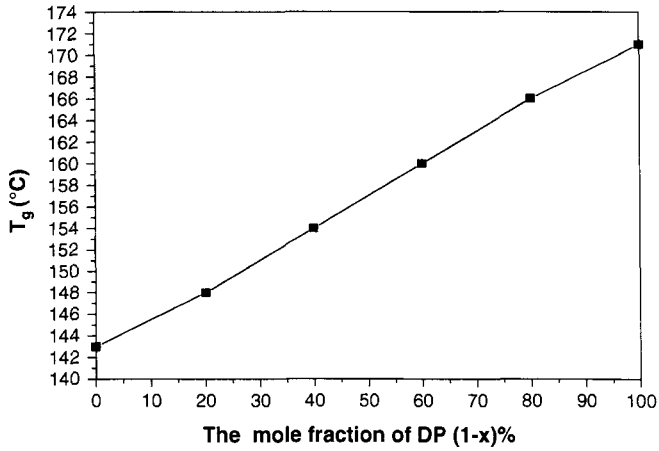

Figure 10.2a The T_g of PEEK-PEDEK copolymers with different mole fraction of DP.

The T_g and T_m change trend of PEEKK-PEDEKK copolymers was the same as those of PEEK-PEDEK copolymers, as shown in Figure 10.3a and Figure 10.3b.

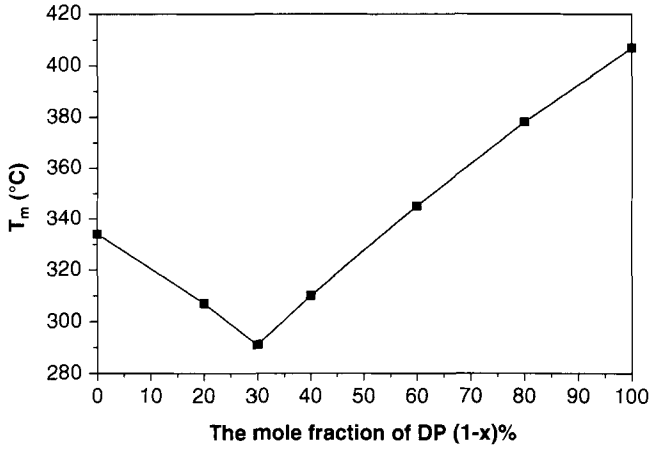

Figure 10.2b The T_m of PEEK-PEDEK copolymers with different mole fraction of DP.

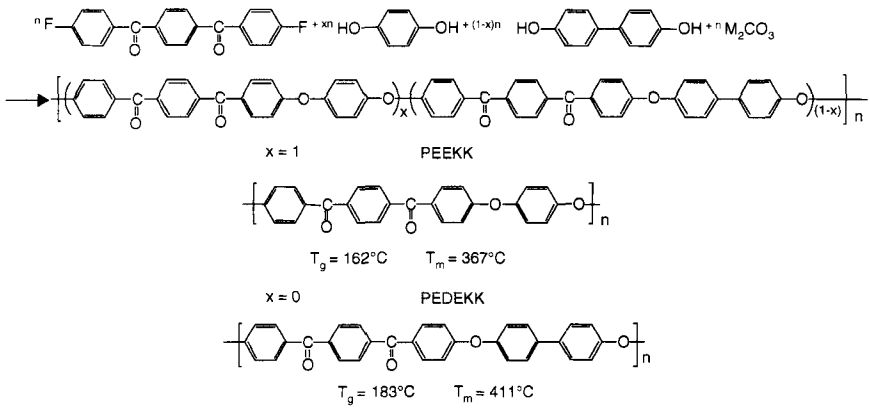

Scheme 10.3 Synthesis routes of PEEKK-PEDEKK copolymers.

4. Poly (ether ether ketone)-poly (ether ether ketone biphenyl ketone) (PEEK-PEEKDK) copolymer

PEEK-PEEKDK copolymer could be synthesized by copolymerizing with 4,4'-bis(4-fluorobenzoyl)biphenyl (BFBB), 4,4'-difluorobenzophenone (DFB) and hydroquinone (HQ) according to Scheme 10.4.

The T_g and T_m change trend of PEEK-PEEKDK copolymers was the same as those of PEEK-PEDEK copolymers, as shown in Figure 10.4a and Figure 10.4b.

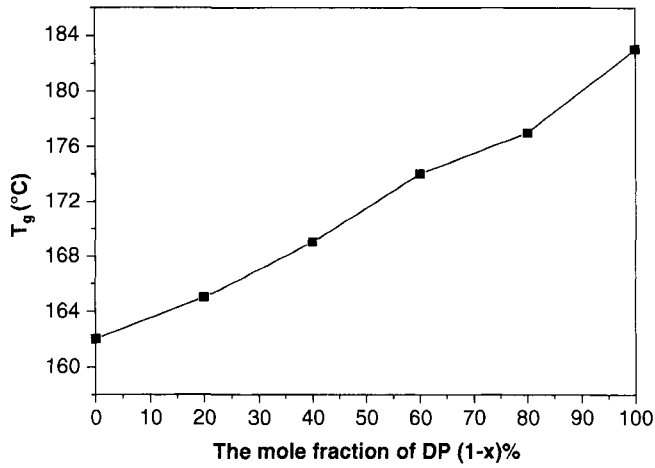

Figure 10.3a The T_g of PEEKK-PEDEKK copolymers with different mole fraction of DP.

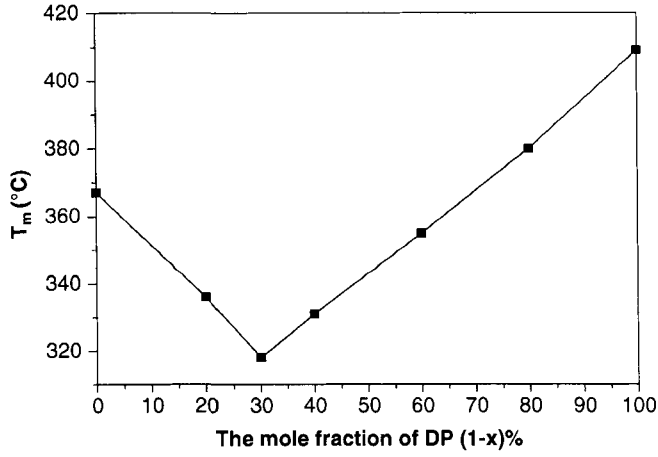

Figure 10.3b The T_m of PEEKK-PEDEKK copolymers with different mole fraction of DP.

5. Poly (ether biphenyl ether ketone)-poly (ether biphenyl ether ketone biphenyl ketone) (PEDEK-PEDEKDK) copolymer

PEDEK-PEDEKDK copolymer could be synthesized by copolymerizing with 4,4′-bis(4-fluorobenzoyl)biphenyl (BFBB), 4,4′-difluorobenzophenone (DFB) and 4,4′-diphenol(DP) according to Scheme 10.5.

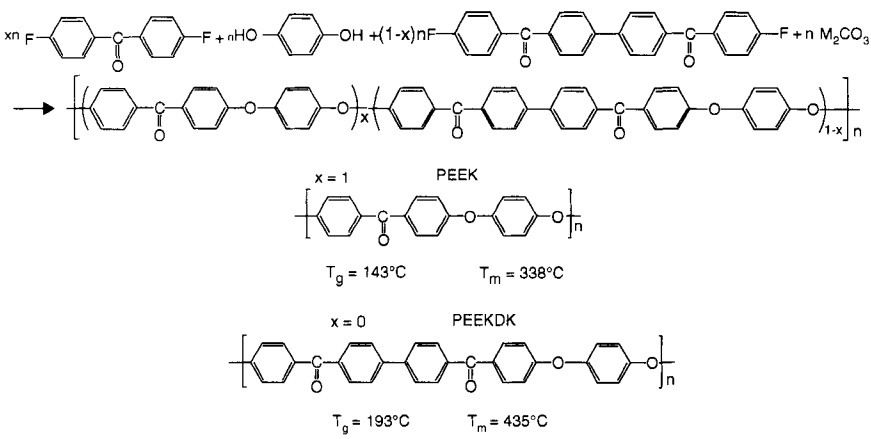

Scheme 10.4 Synthesis routes of PEEK-PEEKDK copolymers.

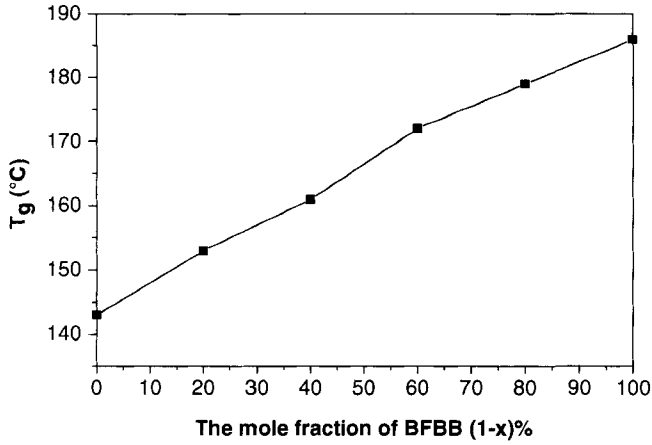

Figure 10.4a The T_g of PEEK-PEEKDK copolymers with different mole fraction of BFBB.

The T_g and T_m change trend of PEDEK-PEDEKDK copolymers was the same as those of PEEK-PEDEK copolymers, as shown in Figure 10.5a and Figure 10.5b.

10.4 Synthesis and Characterization of Liquid Crystalline Poly (aryl ether ketone) Copolymers

High melting temperature and high melt viscosity are characteristics of PAEKs, which are also the primary drawbacks associated with

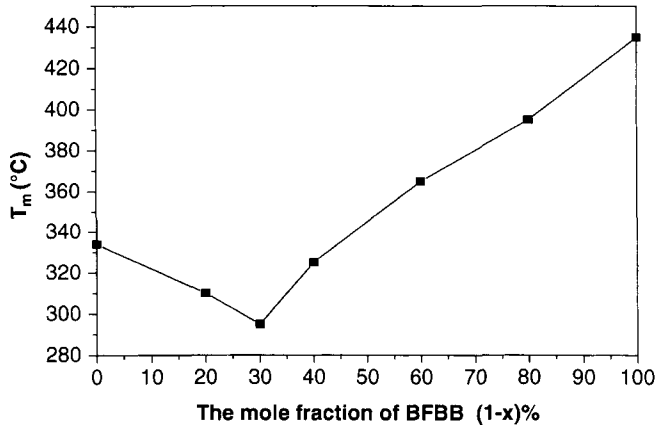

Figure 10.4b The T_m of PEEK-PEEKDK copolymers with different mole fraction of BFBB.

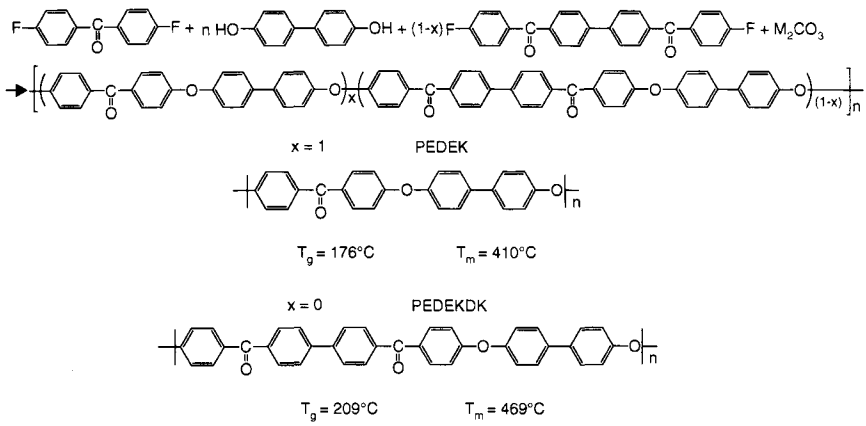

Scheme 10.5 Synthesis routes of PEDEK-PEDEKDK copolymers.

their processing. Thermotropic liquid crystalline polymers (LCPs) are known to have lower melt viscosities compared with structurally similar polymers due to the existence of an isotropic melt state. In addition, it is common knowledge that LCPs show a high modulus and a very low thermal expansion in the direction of the macroscopic orientation. Some novel thermotropic liquid crystalline PAEK copolymers were synthesized by the reaction of a monomer containing liquid crystalline mesogen, 4,4-biphenol (BP), and crystal disrupting substituted monomer with 4,4-difluorobenzophenone or 1,4-bis(*p*-fluorobenzoyl)benzene (BFB) [42–44].

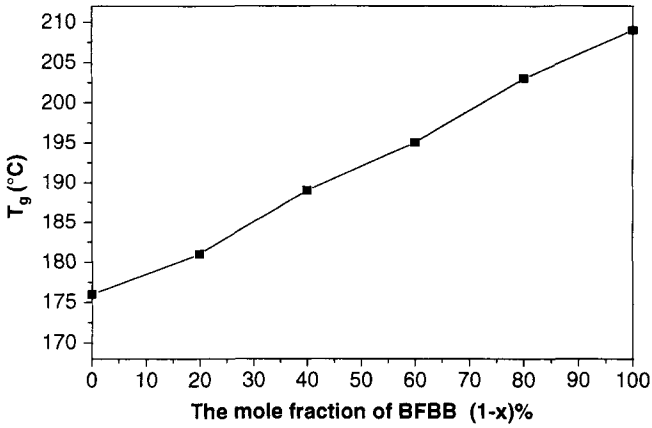

Figure 10.5a The T_g of PEDEK-PEDEKDK copolymers with different mole fraction of BFBB.

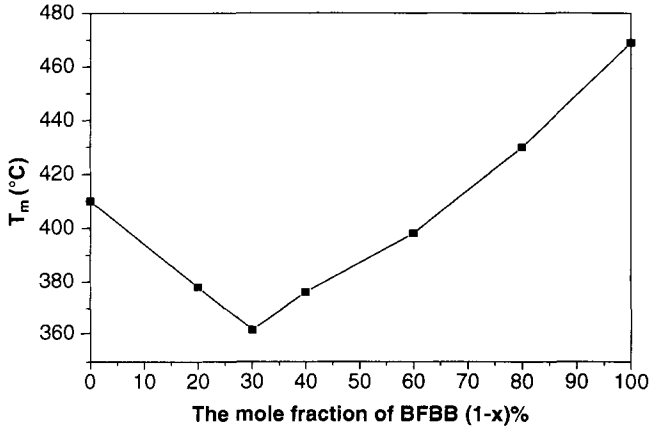

Figure 10.5b The T_m of PEDEK-PEDEKDK copolymers with different mole fraction of BFBB.

1. The synthesis and characterization of a full aromatic thermotropic liquid crystalline poly (aryl ether ketone) with pendant chlorine group (ClPAEK)

A full aromatic thermotropic liquid crystalline poly (aryl ether ketone) was synthesized by the reaction of 4,4′-biphenol (BP) and 2-chlorohydroquinone with 4,4′-difluorobenzophenone according

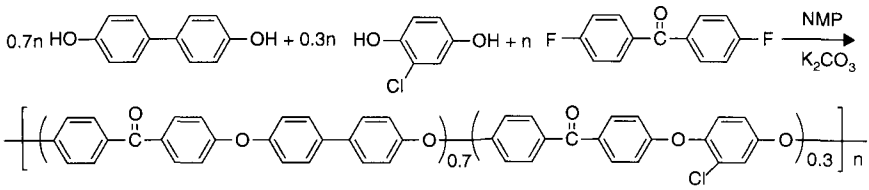

Scheme 10.6 The synthesis reaction of liquid crystalline ClPAEK [43].

to Scheme 10.6 [43]. In a typical procedure, 2.3 g (0.0159 mol) of 2-chlorohydroquinone, 3.0 g (0.0161 mol) of 4,4'-biphenol and 7.0 g (0.032 mol) of 4,4'-difluorobenzophenone were placed in a 250 ml three-necked flask equipped with a thermometer, nitrogen inlet, magnetic stirrer and a Dean-Stark trap. 6.2 g (0.0449 mol) of potassium carbonate, 50 ml of xylene and 100 ml of *N,N'*-dimethyl pyrrolidone were added into the flask. Over a period of 3 h the temperature was slowly raised to 160°C to allow phenolate formation and water/xylene azeotrope distillation which was collected in the trap. Subsequently the reaction temperature was gradually raised to 180°C. For the polymerization this temperature was kept over a period of 6–8 h. The resulting polymer was separated by precipitation of the reaction mixture in methanol. The crude product was purified by hot methanol and water, and dried for 24 h under vacuum to obtain a white polymer powder.

The characterization of ClPAEK was carried on using DSC, PLM and X-ray. In Figure 10.6, the DSC heating scan consists of two first order transitions which were associated with crystal-to-liquid crystal transition (T_m = 338°C with ΔH_m = 115.4 J/g) and liquid crystal-to-isotropic transition (T_i = 368°C with ΔH_i = 6.2 J/g). The reversibility of the phase transitions was evidenced by the presence of the corresponding peaks (crystallization temperature = 283°C and liquid crystallization temperature = 354°C) in the cooling curve. The T_g of ClPAEK measured by second heating scan of sample was 168°C and the thermal degradation temperature of ClPAEK was 430°C by TGA. ClPAEK couldn't be dissolved in organic solvent, inorganic strong alkalies and strong acids except for strong sulfuric acid. The PLM result showed a typical nematic texture in Figure 10.7. The WAXD curves of crystalline, quenched and amorphous sample were showed in Figure 10.8.

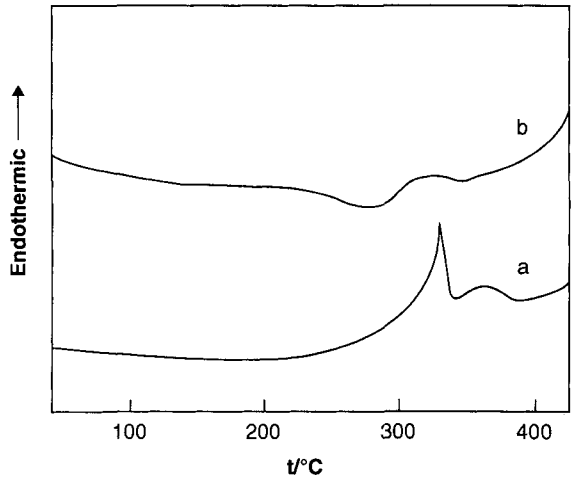

Figure 10.6 DSC scan of the ClPAEK sample in the first heating (a) and cooling cycle (b) [43].

Figure 10.7 Schlieren texture of the sample quenched from the LC state to room temperature [43].

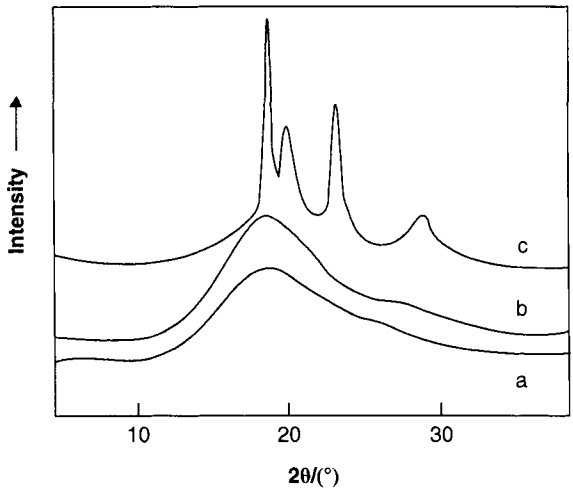

Figure 10.8 WAXD curves of the amorphous sample (a), quenched from the LC state sample (b) and no quenched sample (c) [43].

2. The synthesis and characterization of the novel poly (aryl ether ketone) copolymers with liquid crystallinity

A series of novel thermotropic liquid crystalline poly (aryl ether ketone) copolymers were synthesized by the reaction of 4,4'-biphenol (BP) and substituted hydroquinone with 4,4'-difluorobenzophenone according to Scheme 10.7 [39]. The synthesis procedure of copolymers is like that of reference [43].

The characterization of copolymers (named 70BP/30CH/100DF, 50BP/50CH/100DF, 70BP/30PH/100DF and 50BP/50PH/100DF, respectively) was carried on using DSC, TGA, PLM and X-ray.

1) Thermal properties

The thermal properties of four samples were listed in Table 10.3. All of samples showed better thermal stability below 703K. The melting point, enthalpy change of the same series samples were downtrend with the increase of the substituted hydroquinone content because of copolymerization [45]. The DSC results indicated that there are multi-first order phase transition temperatures in heating process of samples. The samples became viscous, and could be sheared and occur strong birefraction above the low phase transition temperature. The samples became the isotropic liquid when the temperature was over high phase transition temperature.

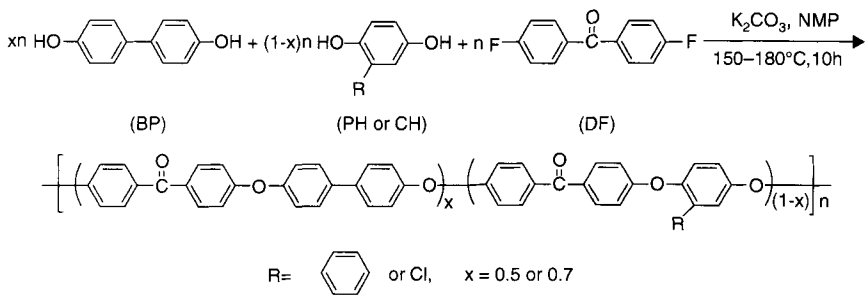

Scheme 10.7 The synthesis reaction of liquid crystalline R-PAEK [39].

Table 10.3 The thermal properties of the novel copolymers of poly (aryl ether ketone) [39].

Copolymer	x	T_m/ K	T_i/ K	ΔH_m/ ($J \cdot g^{-1}$)	ΔH_i/ ($J \cdot g^{-1}$)	T_d/K
70BP/30CH/100DF	0.7	611	641	115	6	703
50BP/50CH/100DF	0.5	609	623	19	19	731
70BP/30PH/100DF	0.7	593	646	50	5	737
50BP/50PH/100DF	0.5	553	608, 617	1	66	750

The heating and cooling curves of four samples were shown in Figure 10.9 (A) and (B) respectively. Except for 50BP/50PH/100DF, all of other samples presented two endothermic peaks in the heating curves and two exothermic peaks in the cooling curves. Two endothermic peaks in the heating curves were associated with crystal-to-liquid crystal transition and liquid crystal-to-isotropic transition. Two exothermic peaks in the cooling curves were associated with liquid crystallization and crystallization temperature. DSC curve of 50BP/50PH/100DF sample presented three endothermic peaks; the weak endothermic peak near 280°C was corresponded with crystalline phase to high ordered smectic phase transition, the strong endothermic peak near 335°C was corresponded with smectic phase to nematic phase transition and the shoulder peak near 345°C was corresponded with nemaric phase to isotropic phase transition. There is only one wide exothermic peak in the cooling curve, which was reported in other main chain liquid crystal polymers [46].

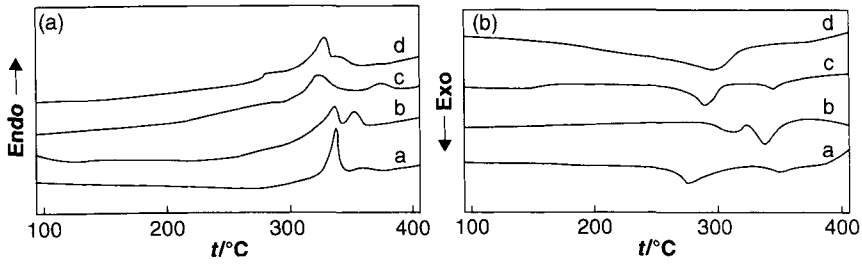

Figure 10.9 Sets of DSC heating (A) and cooling (B) curves for 70BP/30CH/100DF(*a*), 50BP/50CH/100DF(*b*),70BP/30PH/100DF(*c*) and 50BP/50PH/100DF(*d*) [39].

2) Morphological texture

The polarized light picture of 70BP/30CH/100DF was shown in Figure 10.10. Figure 10.10 A indicated that the sample of 70BP/30CH/100DF displayed a typical nematic silky texture. The director of the sample approximately presented uniform orientation and the perpendicular banded texture to shearing direction was observed under orthogonal polarized microscope because of the relexation of molecular chain by a very little shearing force (Figure 10.10 B), which resulted from the periodical bending optical effect of the nematic liquid crystalline polymer microfiber [47]. The sample of 50BP/50CH/100DF exhibited a typical fan-shaped texture after the heat treatment (Figure 10.10 C).

The sample of 70BP/30PH/100DF displayed a nematic silky texture that resembles that of Figure 10.10 A. The sample of 50BP/50PH/100DF presented many kinds of liquid crystalline textures. The sample of 50BP/50PH/100DF showed a typical nematic silky texture after it was annealed at 320°C and cooled at once (Figure 10.11 A). It showed a red and yellow colorized banded texture after it was sheared (Figure 10.11 B). It displayed a mosaic texture that resembles the small molecular liquid crystal after the sample was cooled from the isotropic state to 300°C (Figure 10.11 C). This indicated that this phase was high ordered smectic texture [48–49].

3) The structure of liquid crystalline phase

The WAXD patterns of four samples were shown in Figure 10.12. The main crystalline phase diffraction peaks of four copolymers were similar to that of PEEK and crystalline phase belonged to

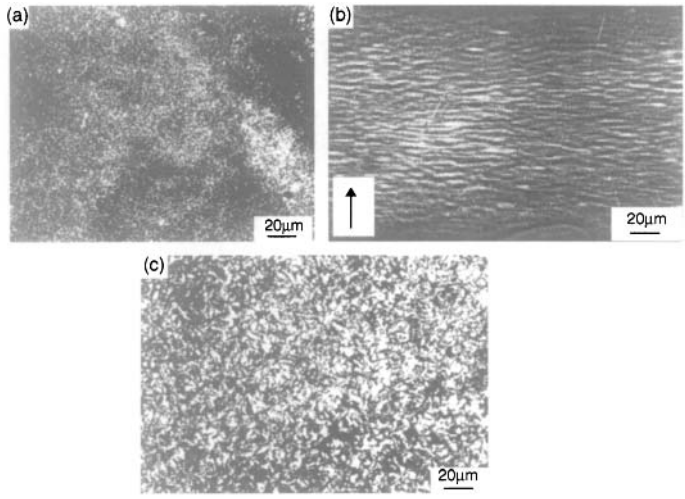

Figure 10.10 PLM morphological observations of 70BP/30CH/100DF (A,B) and of 50BP/50CH/100DF(C) (A) Without mechanical shearing; (B) With mechanical shearing. The arrow shows the shearing Direction [39].

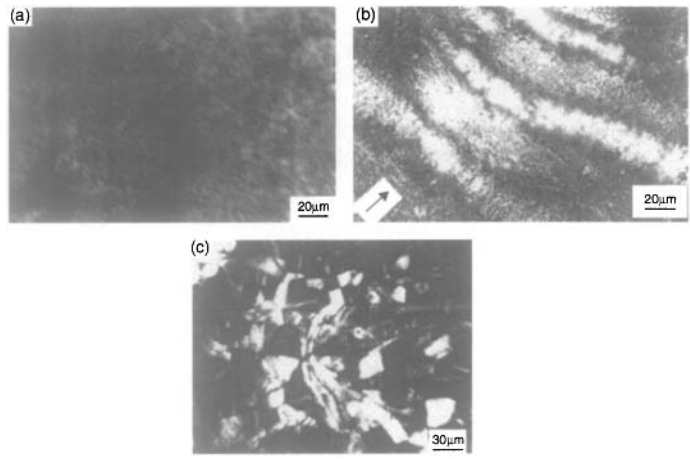

Figure 10.11 PLM morphological observations of 50BP/50PH/100DF at 320°C without shearing (A),with shearing (B), and at 300°C (C) The arrow shows the shearing direction [39].

orthorhombic, space group Pbcn. The patterns of amorphous samples were dispersion peak with $2\theta = 19°$.

The 70BP/30CH/100DF WAXD patterns of three phases were shown in Figure 10.12 A. The pattern of liquid crystalline phase was typical nematic diffraction distribution with a dispersion peak

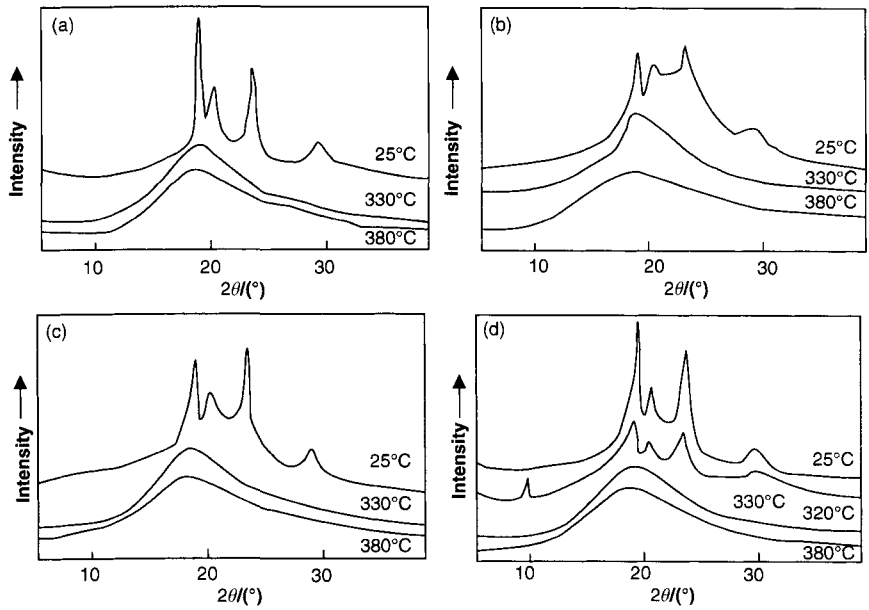

Figure 10.12 Sets of WAXD powder patterns of 70BP/30CH/100DF (A), 50BP/50CH/100DF (B), 70BP/30PH/100DF (C) and 50BP/50PH/100DF (D) [39].

at $2\theta = 19.2°$ corresponding with molecular chain spacing. The correlation length of diffraction was 1.5 nm from the Scherrer equation, which indicated that the molecular structure was short-range order and this liquid crystalline phase was nematic phase [50].

Figure 10.12 B was the diffraction curves of 50BP/50CH/100DF. The pattern of liquid crystalline phase was a sharp single peak with $2\theta = 19.1°$. The correlation length of diffraction was 2.0 nm and was long range order [50]. This indicated that the liquid crystalline phase was semectic A phase.

The 70BP/30PH/100DF WAXD patterns resembled the 70BP/30CH/100DF WAXD patterns and the liquid crystalline phase exhibited nematic phase. Figure 10.12 D was the diffraction curves of 50BP/50PH/100DF. The diffraction of sample at 320°C was a dispersion peak of typical nematic phase with correlation length of 1.7 nm. A sharp diffraction peak appeared at low-angle of $2\theta = 9°$ and its correlation length was 26.6 nm (long range order) [50] at 300°C besides the diffraction peaks similar to crystalline phase. The correlation length of $2\theta = 19.0°$ and 23.3° in wide angle section was 20.2 nm and 27.0 nm, respectively and all of them were long range order. The results of x-ray diffraction

indicated that dispersion of this phase was evidently strengthened than that of crystalline phase. At the same time, the sharp diffraction peak appeared in low-angle section and the diffraction peak of resembling the hexagonal packing appeared in wide-angle section, which showed this phase was high ordered smectic phase [42] and it was smectic G phase based on the definition of small molecular smectic phase [48–49].

3. Synthesis and characterization of thermotropic liquid crystalline poly(aryl ether ketone) copolymers with pendant 3-(trifluoromethyl) phenyl groups

Novel poly(aryl ether ketone) copolymers with pendant 3-(trifluoromethyl)phenyl groups (FPAEKs) were synthesized by the reaction of a crystal-disrupting monomer, 3-(trifluoromethyl)phenylhydroquinone (FH) and a mesogenic monomer, 4,4-biphenol (BP) with 1,4-bis(*p*-fluorobenzoyl)benzene (BF). The synthetic routes of FPAEKs are shown in Scheme 10.8.

A typical synthetic procedure is as follows. The four-neck flask was fitted with a mechanical stirrer, thermometer, nitrogen inlet, and a Dean Stark trap fitted with a condenser and a nitrogen outlet. After the reaction vessel was purged with dry nitrogen, FH/BP/BF/K_2CO_3 (molar ratio: 0.0–1.0/1.0–0.0/1.0/1.1) and tetramethylene sulfone/xylene (weight ratio: 75/25) in a solid content of 15 wt% were added. The mixture was slowly heated to 160°C and held at that temperature for 2 h in a nitrogen atmosphere. During that time, the water produced was removed by azeotropic distillation, and then reaction temperature was gradually raised to 220–240°C as xylene was distilled. After the polymerization reaction at 240°C

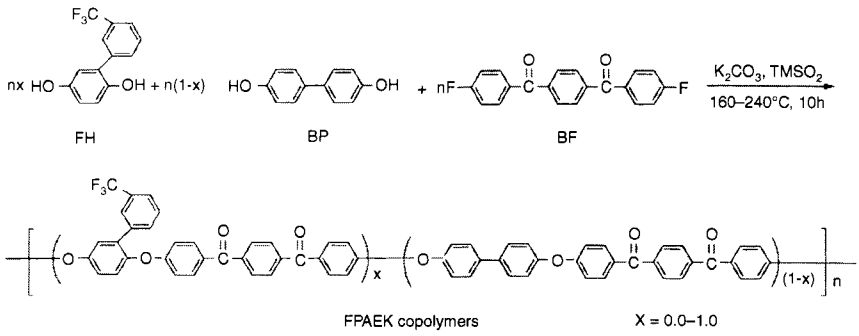

Scheme 10.8 The synthetic routes of FPAEKs.

for 8 h, the reaction mixture was slowly poured into distilled water. The solid obtained was pulverized after filtration, washed with hot distilled water, and dried at 120°C under vacuum for 24 h to give FPAEK (FH 0.0–1.0) as an off-white powder in 90–95% yield.

Thermotropic liquid crystalline behavior of the copolymers was investigated by means of differential scanning calorimetry, polarized optical microscope and wide-angle X-ray diffraction. The results were as follows:

1) DSC and TGA analysis

The results of DSC measurements of the copolymers are summarized in Table 10.4. Three FPAEK copolymers with high FH molar ratio (FH 1.0, 0.9, 0.8) showed only one glass transition temperature (T_g) in the DSC thermograms and no melting endotherm was observed. Other FPAEK copolymers with lower FH molar ratio (FH 0.7–0.0) showed both T_g (128–185°C) and melting temperature Tm (277–411°C), indicating that these FPAEK copolymers are semicrystalline. T_g and T_m decreased with increasing molar ratio of FH, namely increasing the molar ratio of the crystal disrupting bulky group. Among these copolymers, FPAEK (FH 0.7–0.2) showed two endothermic peaks related to crystal-to-liquid crystal (T_m) and liquid crystal-to-isotropic transitions (T_i). Both the T_m and T_i decreased with increasing molar ratio of FH. Figure 10.13 shows the first cooling and second heating DSC thermograms of FPAEK (FH 0.5) as a typical DSC thermogram of the liquid crystalline FPAEK. Two main first-order transitions on the second heating scan are attributed to crystal-to-liquid crystal transition (T_m = 285°C) and isotropization of liquid crystal phase (T_i = 354°C) respectively. In general, the stability of liquid crystal can be evaluated by the temperature range of liquid crystal ($\Delta T = T_i - T_m$) [51]. The wider the temperature range of the liquid crystalline state is, the more stable is the liquid crystalline phase. The main factors affecting the stability of liquid crystal are the space-obstructing effect and the polarity effect. The view of Flory–Onsager is that the space obstructing effect is greater than the polarity effect, whereas Maier–Saupe hold the opposite view, that the key factor affecting stability of liquid crystal is molecular polarity [52]. The ΔT value of the copolymers decreases with increasing molar ratio of FH. There is no doubt that the bulky trifluoromethylphenyl group destabilizes the liquid crystalline phase based on the space-obstructing 4,4_-biphenylene moieties. The ΔT

Table 10.4 Thermal properties of FPAEK copolymers [13]. Reproduced with permission from Wiley.

Sample	FH/BP/BF molar ratio	T_g (°C)	T_m (°C)	T_i (°C)	ΔT^a (°C)	$_H_m$ (Jg^{-1})	ΔH_i (Jg^{-1})	$T_d{}^b$ (°C)
FPAEK (FH0.0)	0/100/100	185	411	–	–	90	–	520
FPAEK (FH0.1)	10/90/100	173	376	–	–	60	–	Non[c]
FPAEK (FH0.2)	20/80/100	139	301	376	75	24	62	480
FPAEK (FH0.3)	30/70/100	135	297	365	68	20	46	500
FPAEK (FH0.4)	40/60/100	133	294	362	68	17	42	498
FPAEK (FH0.5)	50/50/100	132	285	354	69	15	22	Non[c]
FPAEK (FH0.6)	60/40/100	131	281	345	64	12	20	484
FPAEK (FH0.7)	70/30/100	128	277	334	57	8	11	510
FPAEK (FH0.8)	80/20/100	135	–	–	–	–	–	Non[c]
FPAEK (FH0.9)	90/10/100	142	–	–	–	–	–	Non[c]
FPAEK (FH1.0)	100/0/100	147	–	–	–	–	–	505

[a]$\Delta T = T_i - T_m$.
[b]The temperature at which a 5% weight loss occurred.
[c]Not tested by TGA.

values (57–75°C) of FPAEK copolymers is higher that those of general liquid crystalline polyesters (20–50°C). It is thought that the polar trifluoromethyl group may contribute to the stabilization of the liquid crystalline state to some extent. The heat of melting (ΔH_m) was smaller than the heat of isotropization (ΔH_i), indicating that the difference in order between the semi-crystalline state and mesophase is smaller than the difference between the mesophase and the isotropic melt. This result suggests that the mesophase is

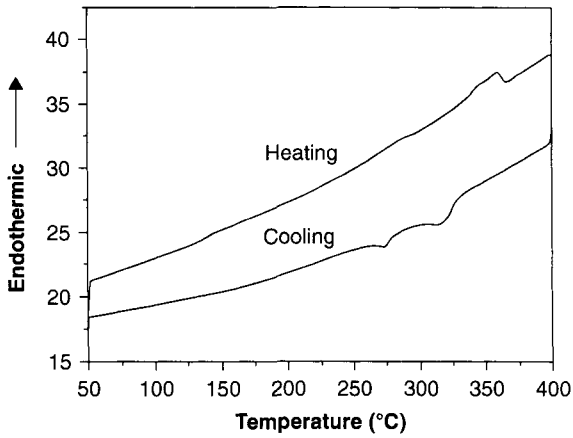

Figure 10.13 DSC thermograms of FPAEK (FH0.5) during the first cooling and second heating scans at a rate of 10°C min^{-1} [13]. Reproduced with permission from Wiley.

highly ordered [53]. Regarding the thermal stability, all the copolymers had very high 5% weight loss temperatures (T_d) ranging from 480 to 520°C.

2) Polarized optical microscope and WAXD analyses

Liquid crystalline textures are observed by the optical polarized microscopy. FPAEK (FH 0.3–0.4) copolymers showed liquid crystalline textures such as mosaic and fan-shaped textures related to smectic phase, when the samples were melted at above T_i, cooled to the liquid crystalline temperature, and annealed at the temperature for 10 min (Figure 10.14 and 10.15). For example, FPAEK (FH 0.3) showed unspecified texture, like mosaic texture and fan-shaped texture, when annealed at 345°C (seen in Figure 14). FPAEK (FH 0.4) also showed mosaic texture and fan-shaped texture when annealed at 335°C (seen in Figure 10.15). The observation of these textures suggests that the copolymers form a highly ordered smectic phase similar to small molecular weight small molecular liquid crystals [49]. Namely the FPAEK (FH 0.2–0.5) copolymers showed mosaic texture and fan-shaped texture. However, the FPAEK (FH 0.6–0.7) copolymers only showed thread-like texture at the liquid crystal temperature, indicative of a nematic phase (seen in Figure 10.16).

Figure 10.17 shows the temperature-dependent WAXD patterns of FPAEK (FH 0.3–0.4) at the heating rate of 5°C min^{-1}. The

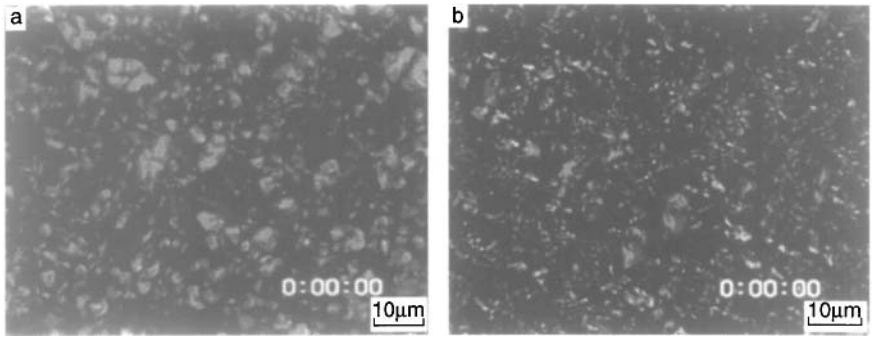

Figure 10.14 Optical texture of FPAEK(FH0.3) sample, melted at 420°C for 2 min, then cooled to 345°C at 10°C min^{-1}, and maintained at 345°C for 10 min [13]. Reproduced with permission from Wiley.

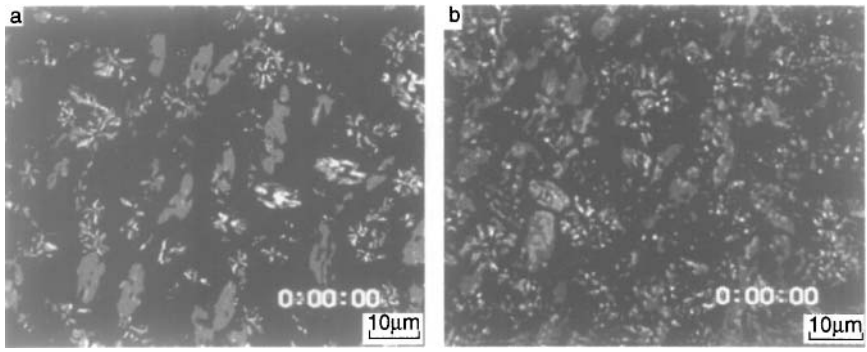

Figure 10.15 Optical texture of FPAEK(FH0.4) sample, melted at 410°C, then cooled to 335°C at 10°C min^{-1}, and maintained at 335°C for 10 min [13]. Reproduced with permission from Wiley.

X-ray diffraction patterns of FPAEK (FH 0.3–0.4) below the crystal melting temperature (297°C) show strong reflections with four peaks $2\theta = 18.4°, 19.6°, 22.7°$ and 28.5°, which are assigned as (110), (111), (200) and (211), respectively, based on orthorhombic packing [54]. This implies that the copolymers have a typical crystal structure, which is similar to other regular members of poly(aryl ether ketone) family. When the sample is heated to liquid crystalline temperature range of 300–368°C, the peak intensity in the high-angle region decreased remarkably, which suggests that the crystal structure is being destroyed. However, the diffraction peak in the low-angle region does not appear synchronously, which may

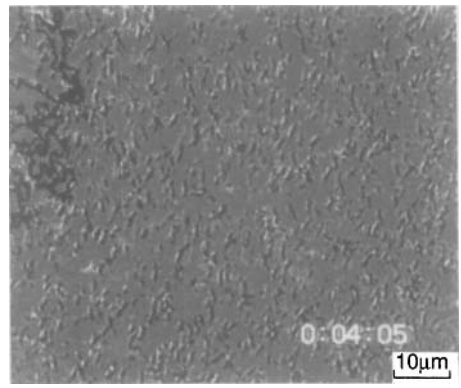

Figure 10.16 Optical texture of FPAEK(FH0.6) sample, melted at 390°C, then cooled to 315°C at 10°C min^{-1}, and maintained at 315°C for 10 min [13]. Reproduced with permission from Wiley.

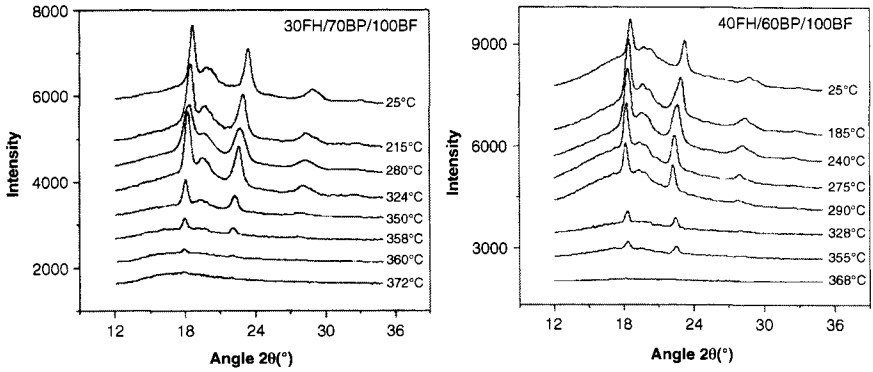

Figure 10.17 Temperature dependence of WAXD patterns for FPAEK(FH0.3) and FPAEK(FH0.4) at a heating rate of 5°C min^{-1} [13]. Reproduced with permission from Wiley.

be attributable to the limit of instrument of characterization. In the case of the condition of our current instrument, because the mode of the clamping sample is vertical we cannot achieve isotropy on T_i and anneal between T_m and T_i so as to form the highly ordered smectic phase either. If we let the sample achieve isotropy on T_i and achieve anneal between T_m and T_i, the sample shows liquid state and pollutes the instrument, so we adopt a process of gradually increasing temperature for the obtained polymer in order to decrease the probability of polluting the instrument. However, forming the highly ordered smectic phase of the obtained polymer

becomes difficult under gradually increasing temperature, namely it is very difficult to get a diffraction peak of obtained polymers in the low angle region by WAXD characterization. Therefore we cannot yet provide data about the layer thickness of the X-ray characterization. We hope that the work can be perfected in the future. Upon further heating to the isotropic phase (372°C), all the peaks in high angle regions disappeared, which suggests the crystal structure is completely destroyed.

10.5 Synthesis and Characterization of Poly (aryl ether ketone) Copolymers with Pendent Group

1. Synthesis and characterization of poly(aryl ether ketone) with trifluoromethyl-substituted benzene in the side chain

In recent years, considerable attention has been devoted to the preparation of fluorine-containing polymers due to their unique properties and high-temperature performance. The incorporation of fluorine atoms (or groups containing fluorine atoms) into polymer chains changes solubility of polymers, glass transition temperature (T_g) and thermal stability, while also led to decreased moisture absorption and dielectric constant. The aromatic fluoropolymers have currently been used as films, coatings microelectronics devices [37, 55–60].

A new monomer (4-(4′-trifluoromethyl)phenoxyphenyl)hydroquinone (TFPOPH) was synthesized in a three-step synthesis. A series of poly (aryl ether ketone) copolymers were prepared by the reaction of (4-(4′-trifluoromethyl)phenoxyphenyl) hydroquinone and hydroquinone (HQ) with 4,4′-difluorobenzophenone (DFB) in the presence of potassium carbonate. A typical polymerization was carried out as follows: To a three-neck round bottom flask were added hydroquinone and (4-(4′-trifluoromethyl)-phenoxyphenyl) hydroquinone (TFPOPH) (total 0.10mol) in molar ratios of 100:0, 80:20, 60:40, 40:60, 20:80 and 0:100, 4,4′-difluorobenzophenone (DFB), toluene and 3.04 g (0.022 mol) of potassium carbonate and tetramethylene sulfone (TMS) (a prescribed amount shown in Table 10.5) and heated to 140°C to remove produced water by azeotropic distillation with toluene and then rose up to 210°C for 4–6 h. The copolymer was precipitated by pouring the hot reaction mixture into a large amount of distilled water, filtered, and washed

Table 10.5 Experimental data and properties of PAEK copolymers containing trifluoromethyl-substituted benzene in the side chain [41]. Reproduced with permission from Taylor and Francis.

No.	DFB (mol)	HQ (mol)	TFPOPH (mol)	Molar fraction of TFPOPH[a]	T_g (°C)	T_m (°C)	T_d[b] (°C)	η_{inh}[c] (dL/g)
1	0.10	0.10	0.00	0.00	143	334	561	0.79
2	0.10	0.08	0.02	0.20	145	284	531	0.56
3	0.10	0.06	0.04	0.40	149	–	575	0.95
4	0.10	0.04	0.06	0.60	146	–	555	0.68
5	0.10	0.02	0.08	0.80	142	–	573	0.52
6	0.10	0.00	0.10	1.00	140	–	553	0.54

[a]Molar ratio of TFPOPH/(TFPOPH + HQ).
[b]T_d is the temperature at which the weight loss of the polymer is 5.0%.
[c]Measured at the concentration of 0.1 g/dL solution in 98% sulfuric acid at 258°C.

with acetone and distilled water several times. Drying at 120°C for 12 h afforded an off-white polymer in 90–95% yield.

The copolymers were characterized by DSC, TGA, X-ray and impedance gain-phase analyzer. The results and discussion was specified as follows:

1) Synthesis of monomer

The synthesis of the three fluorine-containing diphenol is shown in Scheme 10.9. TFPOPH was synthesized by reducing the diquinone compound (**2**) that were derived from 1,4-benzoquinone with compound (**1**). The chemical structure of TFPOPH was confirmed by elemental analysis, FTIR, NMR and MS.

2) Synthesis of the Copolymers Containing 4-(4′-trifluoromethyl) phenoxyphenyl Side Chain

Scheme 10.10 outlines the synthesis of poly(aryl ether ketone) s copolymers derived from different molar ratio of TFPOPH and hydroquinone with 4,4′-difluorobenzophenone by the nucleophilic substitution reaction method.

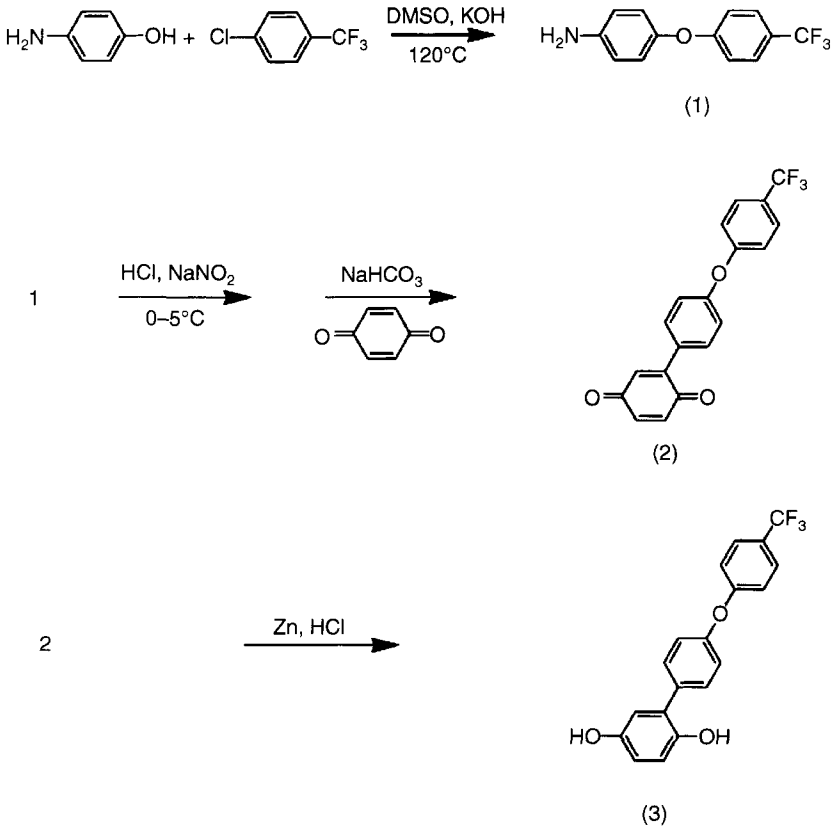

Scheme 10.9 Synthesis of monomer, (4-(4′-trifluoromethyl)phenoxyphenyl) hydroquinone.

The polymerizations were completed at a solid content of about 20%, and toluene was used for the azeotropic removal of water. After the completion of bisphenolate formation in about 2 h, the reaction temperature was increased to 220°C. High molecular weight polymers were readily obtained in 4–6 h. The resulting copolymers had high inherent viscosities of 0.52–0.95 dL/g (Table 10.5).

3) Copolymer Solubility

The solubility of the PAEK copolymers is listed in Table 10.6 that was qualitatively determined by mixing 1.5 g of solid with 8.5 g of organic solvents, followed by stirring in nitrogen for 24 h to determine if the solid was completely or partly dissolved in organic

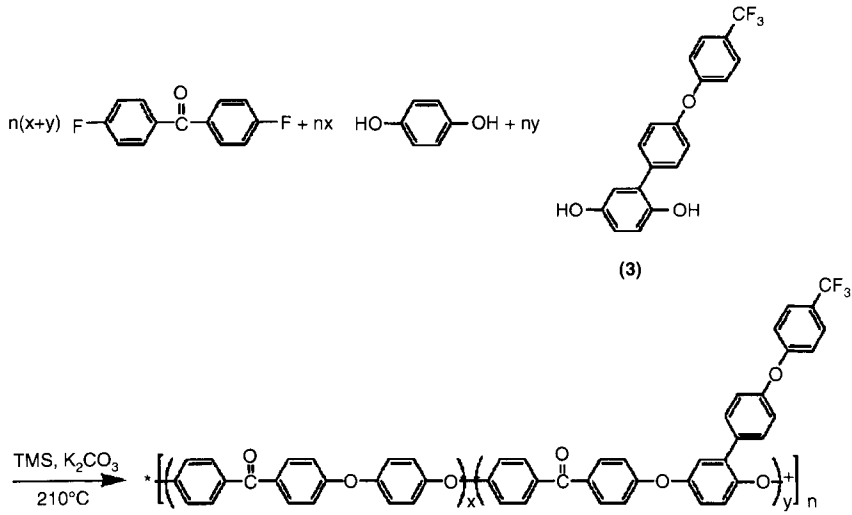

Scheme 10.10 Synthesis of the copolymers containing 4-(4′-trifluoromethyl) phenoxyphenyl moieties.

Table 10.6 Solubility of PAEK copolymers containing trifluoromethyl-substituted benzene in the side chain [41]. Reproduced with permission from Taylor and Francis.

No.	Molar fraction of TFPOPH	Solvent					
		DMF	DMAc	NMP	THF	CH_2Cl_2	Acetone
1	0.00	–	–	–	–	–	–
2	0.20	–	–	–	–	–	–
3	0.40	+	+	+	–	–	–
4	0.60	+	+	+	±	±	–
5	0.80	++	++	++	+	+	–
6	1.00	++	++	++	++	++	–

++, soluble at room temperature; +, soluble on heating; ±, swelling on heating; –, insoluble.

solvents. The solubility of poly(aryl ether ketone)s copolymers increased with increasing content of 4-(4′-trifluoromethyl)phenoxyphenyl side chain. The excellent solubility of these CoPAEKs could be attributed to the presence of bulky pendant groups, which led to increased free volume and broken crystallinty of polymers.

4) Thermal Behaviors

Figure 10.18 shows the DSC traces of the quenched samples of the copolymers in the heating run. When the molar fraction of TFPOPH is over 0.2, the clear cold-crystallization temperature (T_c) and Tm cannot be detected. For the copolymer samples with a TFPOPH molar fraction of not more than 0.2, the T_m decreased with increasing the content of TFPOPH, while T_c showed the reverse tendency. These results are thought to be attributed to the disturbance of the segmental movement and the destruction of the symmetry and regularity of the molecular chains due to the introduction of 4-(4'-trifluoromethyl)phenoxyphenyl pendant group. The glass transition temperature (T_g) increased and then decreased with increasing the content of TFPOPH moieties. One possible explanation for the change is the affection of molecule weight [16, 61], the other is that the introduction of bulky pendant group would block the mobility of segments and the atom of fluorine would lead to an internal plasticization in addition to the geometry and free-volume factors [62].

The 5.0% weight loss temperatures (T_d) of the copolymers were determined by thermogravimetric analysis given in Table 10.5. The copolymers with a TFPOPH molar fraction of 0.20 showed the T_d (531°C), which is little lower than that of PEEK (561°C). However, the copolymers sustained the T_d over 530°C.

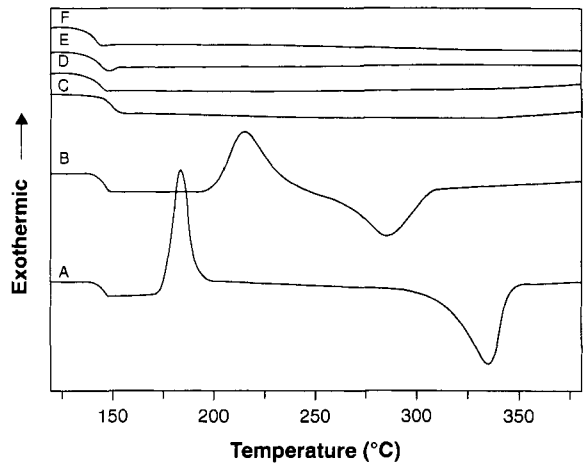

Figure 10.18 DSC traces of PAEK copolymers containing trifluoromethyl-substituted benzene (A) 0.00, (B) 0.20, (C) 0.40, (D) 0.60, (E) 0.80, (F) 1.00 [41]. Reproduced with permission from Taylor and Francis.

5) Wide-angle X-ray Diffraction Analysis

The results of WAXD measurement of PEEK and the copolymers are shown in Figure 10.19. The pattern of diffraction peaks and the values of 2θ for each diffraction peak are the same as each other, suggesting that the crystal structure of the copolymer is a rhombic system in the same manner as is PEEK [63].

The intensity of diffraction peaks decreased with increasing content of TFPOPH moieties. It can therefore be presumed that the segments containing TFPOPH moieties in the copolymer are not in the crystal unit cell of the copolymer but in the amorphous phase between the crystalline lamellae.

6) Dielectric Constants and Water Sorption

The dielectric constants of the copolymers, as listed in Table 10.7, were measured on the thin films. At 1MHz, the dielectric constant of conventional PEEK without pendant groups was 3.3. The dielectric constants of the copolymers decreased when the bulky 4-(4′-trifluoromethyl) phenoxyphenyl increased.

There is a related factor that the pendant groups may affect the dielectric properties of the polymers. The bulky side groups attached to the polymer main chains might have pushed the neighboring chains apart, and this resulted in loosely packed polymers

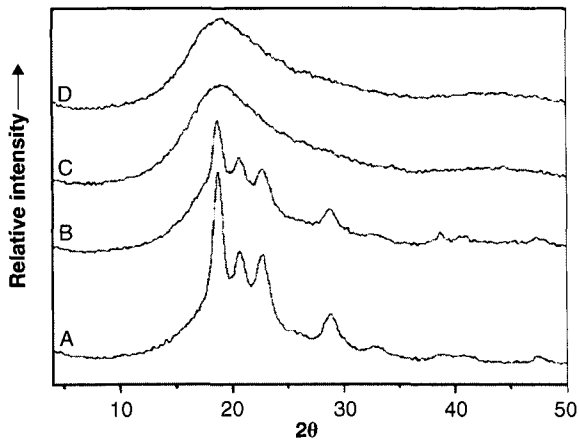

Figure 10.19 WAXD patterns of the copolymers with the molar fraction of TFPOPH (A) 0.00, (B) 0.20, (C) 0.40, (D) 0.60 [41]. Reproduced with permission from Taylor and Francis.

Table 10.7 Dielectric constant of PAEK copolymers containing trifluoromethylsubstituted benzene in the side chain [41]. Reproduced with permission from Taylor and Francis.

No.	DFB (mol)	HQ (mol)	TFPOPH (mol)	Molar Fraction of TFPOPH	Dielectric Constant (at 1 MHz)
1	0.10	0.10	0.00	0.00	3.30
2	0.10	0.08	0.02	0.20	3.22
3	0.10	0.06	0.04	0.40	3.00
4	0.10	0.04	0.06	0.60	2.87
5	0.10	0.02	0.08	0.80	2.72
6	0.10	0.00	0.10	1.00	2.67

and a low dielectric constant. By the same token, the incorporation of bulky pendant groups disrupted the crystallinity, leading to a less dense amorphous structure and a decreased dielectric constant.

2. Synthesis of Poly(aryl ether ketone) Copolymers Containing Adamantyl-substituted Naphthalene Rings

Adamantane has attracted a great interest in the fields of medicine, polymer industry, and fine chemical industry, and so on because of its unique physical and chemical characters. The incorporation of adamantine as a pendant group on the polymer backbone leads to several property modification results, which include decreasing crystallinity, improving solubility, enhancing glass transition temperature, and modifying dielectric properties of polymer [64–67]. At the same time, owing to the excellent thermal stability of adamantly groups, the thermal stability of the polymer will not be decreased by its incorporation [64, 65].

A new double adamantyl-substituted aromatic bisphenol monomer, 4,8-bis (1-adamantly)-1,5-dihydroxynaphthalene (AdNp) was successfully synthesized *via* the Friedel-Crafts reaction as depicted Scheme 10.11, and two new PAEKs containing adamantly groups (Ad-PAENKs) were synthesized based on the new monomer of AdNp, (3-trifluoromethyl)phenyl hydroquinone (3FHQ) and 4,4′-difluorobenzophenone (DFB) via the nucleophilic aromatic substitution polymerization as depicted Scheme 10.12.

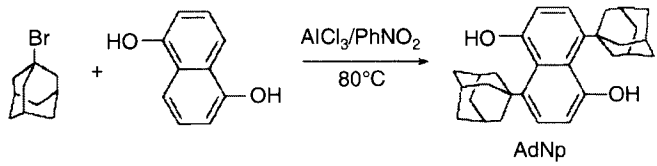

Scheme 10.11 Synthesis of 4,8-bis(1-adamantly)-1,5-dihydroxynaphthalene(AdNp).

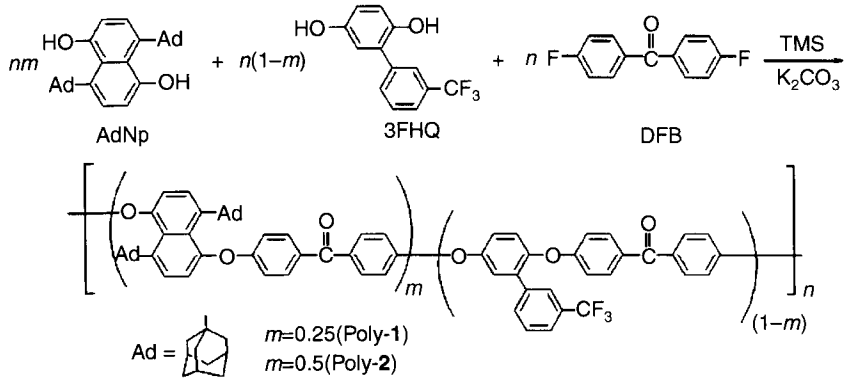

Scheme 10.12 Synthesis of PAENKs containing adamantyl pendant group.

Typically, AdNp (4.28 g, 0.01 mol), 3FHQ (2.54 g, 0.01 mol), DFB (4.36 g, 0.02 mol), and potassium carbonate (2.90 g, 0.021 mol) were dissolved in TMS (30 mL) and toluene (10 mL) in a reaction flask fitted with a nitrogen inlet, a mechanical stirrer, and a Dean-Stark trap. The mixture was heated to reflux with stirring under nitrogen gas flow for 2 h to remove produced water by azeotropic distillation with toluene, followed by the gradual removal of toluene from the reaction flask by increasing the flask temperature up to 220°C. The reaction mixture was maintained at 220°C with vigorous stirring for 10 h and then poured into distilled water. The crude precipitated polymer was pulverized, washed thoroughly with hot distilled water and ethanol several times, and dried at 120°C for 24 h to yield an off-white powder. The structure and basic properties of Ad-PAENKs were characterized by several analysis methods.

The results and discussion were described as follows:

1) Synthesis of Polymers

New PAEKs containing adamantyl-substituted naphthalene were derived from AdNp and 3FHQ with DFB by a nucleophilic

polycondensation reaction as shown in Scheme 10.12. The polycondensation reaction was completed in 10 h and resulted in copolymers with reasonable molecular weight and polymerized index as summarized in Table 10.8, which indicates that in spite of the presence of the bulky adamantyl in the polymerization process, high molecular weight polymers could be obtained by the co-polymerization of AdNp with other aromatic bisphenol.

FTIR was used to characterize the structure of Ad-PAENKs. The characteristic absorption bands of aryl carbonyl groups appeared near 1660 cm^{-1}, and that of aryl ether linkages at 1220 cm^{-1}; the characteristic absorption bands of adamantyl groups appeared at about 2920 cm^{-1} (—CH_2—) and 2850 cm^{-1} (—CH_2—), and proved that the adamantyl groups were successfully incorporated into the polymers, which confirmed that the nucleophilic polycondensations proceeded, leading to the formation of Ad-PAENKs.

2) Characterization of Ad-PAENKs

The solubilities of Ad-PAENKs were tested in various solvents (see Table 10.9). All Ad-PAENKs were soluble at room temperature in polar solvents such as DMAc, NMP, $CHCl_3$, and THF. The good solubilities of the polymers were attributed to the incorporation of bulky (3-trifluoromethyl) phenyl and adamantly groups, which led to increasing the free volume and destroying the crystallinity of the polymers. Also, they were easy to form films by solution casting technique owing to their good solubilities.

The T_gs of the adamantyl substituted polymers were determined by DSC. The results are given in Table 10.8. The glass transition temperature (T_g) dramatically increased with increasing the content of adamantly moiety. When the AdNp molar fraction was up to 50% (Poly-**2**), a T_g of 205°C was displayed, which is a marked increase of 70°C compared to that of the homopolymer (135°C [68]) derived from 3FHQ and DFB and is considerably higher than the value reported for commercial PEEK (VitrexTM, 143°C). This large increase in T_g may be attributed to the bulky adamantane group inhibiting chain mobility [64]. The DSC traces of the copolymers indicate that they had no melting transitions, which are considered to be attributed to the destruction of the regularity of the molecular chains and the crystallinity of polymers owing to the introduction of trifluoromethyl and adamantyl-substituted naphthalene groups. According to the TGA test as summarized in Table 10.8, the Ad-PAENKs exhibit good thermal stability and have 5% weight

Table 10.8 Experimental data and thermal properties of PAENKs containing adamantyl pendent group[40].

Polymer	*n*(AdNp) mol	*n*(3FHQ) mol	*n*(DFB) mol	Molar fraction of AdNp[a] (%)	$10^3 M_w$	$10^3 M_n$	M_w/M_n	T_g °C	T_{d5}[b] °C
Poly-1	0.025	0.075	0.10	25	241	562	2.32	171	493
Poly-2	0.050	0.050	0.10	50	87	48	1.83	205	494

[a]Molar ratio of AdNp/(AdNp+3FHQ);
[b]decomposition characterized by 5.0% weight loss in N_2.

Table 10.9 Solubility behavior of PAENKs containing adamantyl pendent group [40].

Polymer	Solvent				
	Acetone	DMAc	$CHCl_3$	THF	NMP
Poly-**1**	–	+	+	+	+
Poly-**2**	–	+	+	+	+

+, Soluble at room temperature; –, insoluble.

loss (DT_5) at temperatures around 490°C in nitrogen, which showed that the introduction of the bulky aliphatic adamantyl groups had not significantly reduced the thermal stability of the polymers. This result can be attributed to the unique multi-cage structure of the adamantyl groups, which leads to the high thermal stability of adamantly groups [64]. The mechanical properties of the polymer thin films cast from $CHCl_3$ are summarized in Table 10.10.

All the films are transparent, tan, and rigid. Their Young's moduli are similar to that of commercial PEEK (Vitrex™, 2.21 GPa); however, their tensile strength and elongation at break rapidly decrease with the increased molar fraction of AdNp.

10.6 Synthesis and Characterization of poly (aryl ether ketone) copolymers with Containing 2 ,7 -Naphthalene Moieties

In order to develop materials with properties and structural modifications, such as introducing crosslinking lateral groups and functional groups onto the main chain of a polymer or synthesizing copolymers have been attempted [69–72]. Naphthalene rings have been introduced into polymer structures by some authors since a naphthalene ring has a larger volume than a benzene ring, which can enlarge the proportion of rigid groups in a main chain, reduce the mobility of segments and therefore increase the T_gs of polymers [73–82]. A series of poly (aryl ether ketone) copolymers containing naphthalene moieties (PANEKs) were synthesized *via* a nucleophilic substitution reaction. It was made up of hydroquinone (HQ), 2,7-dihydroxynaphthalene (DHN) and 4,4′ -difluorobenzophenone

Table 10.10 Mechanical properties of PAENKs containing adamantyl pendent group [40].

Polymer	Tensile Strength (MPa)	Young's Modulus (GPa)	Elongation at Break (%)
Poly-**1**	89.4	1.95	7
Poly-**2**	55.0	2.15	3

(DFB). The paper's attention is focused on the relationship between the polymer compositions and the balance between their T_g and T_m.

A typical procedure, DFB (0.20 mol) and diphenyl sulfone (DPS) (a prescribed amount shown in Table 10.11) were added into a three-necked round bottom flask and heated to 160°C to give a homogenous solution. With stirring and under nitrogen protection, HQ and DHN (with a total amount of 0.2000 mol) with molar ratios of 95:5, 90:10, 85:15, 80:20, 70:30, 60:40, 50:50, 40:60, 30:70, 20:80, 10:90, and 0:100 were added into the solution, respectively. In a typical process, after reacting at 200°C for 1 h, the mixture was gradually heated to 280–330°C, and kept at the temperature for 3–6 h. The copolymer was precipitated by pouring the hot mixture into a large amount of distilled water, ground, and washed with acetone and distilled water several times. Poly (aryl ether ketone) copolymers containing 2,7-naphthalene moieties were obtained after drying at 120°C for 12 h.

Poly (aryl ether ketone) copolymers having various compositions of 2.7-dihydroxynaphthalene and HQ were synthesized by the nucleophilic substitution reaction of 4,4'-difluorobenzophenone (DFB) with HQ and DHN in the presence of sodium carbonate and potassium carbonate (Scheme 10.13).

The copolymers were characterized by DSC, TGA and WAXD, etc. The results were discussed as follows:

1) FTIR Spectral Analysis

The FTIR spectra of the synthesized polymers are shown in Figure 10.20. It is obvious that there are four types of ether stretching corresponding to four types of ether linkages in the copolymers containing naphthalene moieties, which are denoted as A, B, C and D in Scheme 10.14. The ether stretching (corresponding to A) will

Table 10.11 Experimental data and the properties of PAEK copolymers containing 2,7-naphthalene moieties [33].

n(DFB)/mol	*n*(HQ)/mol	*n*(2,7-DHN)/mol	Molar fraction of 2,7-DHN[a] (%)	η_{iv}[b](dL . g^{-1})	T_g/K	T_m/K	T_d[c]/K
0.2000	0. 19	0.01	5	0. 86	418	601	829
0. 2000	0. 18	0. 02	10	0. 80	419	595	82 1
0.2000	0. 17	0. 03	15	0. 65	421	589	783
0.2000	0. 16	0. 04	20	0. 84	425	572	814
0.2000	0. 14	0.06	30	1.20	429	–	783
0.2000	0.12	0.08	40	1.01	430	–	774
0.2000	0.10	0.10	50	0. 59	433	–	770
0.2000	0.08	0.12	60	1.00	433	–	763
0.2000	0.06	0.14	70	0. 60	435	–	769
0.2000	0.04	0.16	80	0.54	435	–	755
0.2000	0.02	0.18	90	0. 99	437	–	768
0.2000	0.00	0.20	100	0.67	438	–	769

a. Molar frartion of 2,7-DHN in the mixture of HQ and 2,7-DHN; *b*. measured at the concentration of 0.1 g/dL solution in 98% sulfuric acid at 25°C ; *c*. T_d is the temperature at which the mass loss of the polymer is 5.0%.

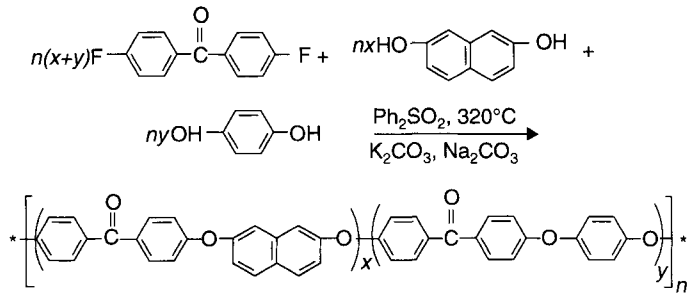

Scheme 10.13 Polymerization reaction of DBF with HQ and DHN.

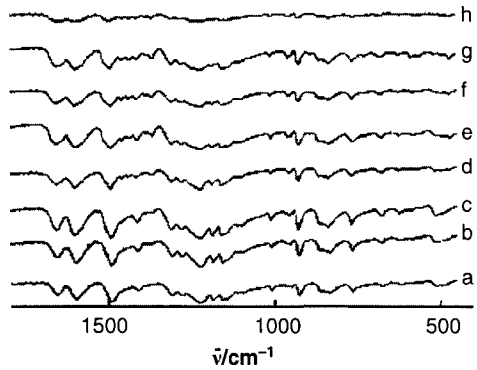

Figure 10.20 IR spectra of the PANEK copolymers with different molar fractions of DHN. a. 0.05; b. 0.10; c. 0.15; d. 0.20; e. 0.30; f. 0.40; g. 0.60; h. 0.90 [33].

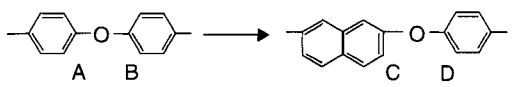

Scheme 10.14 Four types of ether linkages in copolymer PANEK.

decrease with increasing the naphthalene moieties in the copolymers. On the contrary, the ether stretching (corresponding to C) will increase. The ether stretching (corresponding to B) and the ether stretching (corresponding to D) will result in the absorbance peaks with similar positions in the infrared spectra with the assumption that the long-range interaction could be ignored. Figure 10.20 shows the infrared spectra in the ether stretching region (1100 to 1300 cm^{-1}) of the copolymers containing naphthalene moieties,

in which three absorbance peaks are observed. The absorption at 1220 cm^{-1}, the absorbance of which decreases with increasing the naphthalene moieties in the copolymers, is assigned to the ether stretching (corresponding to A in Scheme 10.14).

The absorption at 1180 cm^{-1} is enhanced with increasing the naphthalene moieties and is assigned to the ether stretching (corresponding to C). The absorption at 1200 cm^{-1} is attributed to the synergetic effect of the ether stretching (corresponding to B) and the ether stretching (corresponding to D), which is constant when the naphthalene content of the copolymer is varying.

2) Thermal Behavior

Figure 10.21 shows the DSC thermograms of the quenched samples of the copolymers. The composition dependencies of T_g and T_m for the copolymers are shown in Table 10.11. The T_g values increase with increasing the content of the naphthalene moieties. When the molar fraction of DHN is over 0.3, the peaks corresponding to the clear cold-crystallization temperature (T'_c) and T_m cannot be detected. For the synthesized copolymers with a DHN molar fraction being less than 0.3, the T_m decreases with increasing the content of the naphthalene moieties, while T'_c shows a reverse

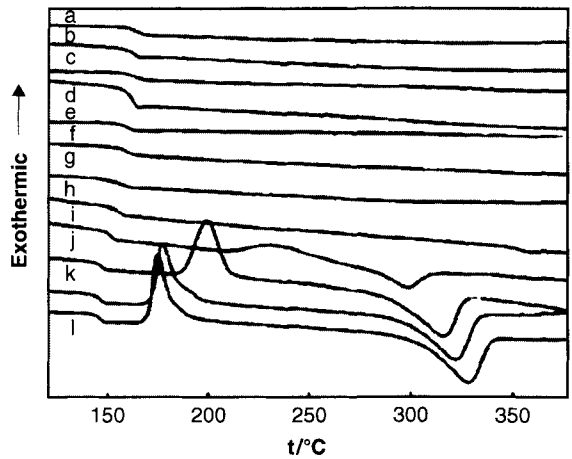

Figure 10.21 DSC thermograms recorded during the first runs at 20°C/min for the quenched samples of PAEK copolymers. Molar fraction of DHN: a. 1.00; b. 0.90; c. 0.80; d. 0.70; e. 0.60; J. 0.50; g. 0.40; h. 0.30; i. 0.20; j. 0.15; k. 0.10; l. 0.05 [33].

tendency. These results are attributed to the disturbance of the segmental movement and the destruction of the symmetry and regularity of the molecular chains due to the introduction of the naphthalene moieties.

3) TGA analysis

The 5% weight loss temperatures (T_d) of the copolymers were determined by thermogravimetric analysis. T_d decreases with increasing the content of the naphthalene moieties (Table 10.11). However, the polymer containing a DHN molar fraction of 100% with the poorest heat resistance shows a T_d over 450°C (Table 10.11 and Figure 10.22).

4) Wide-angle X-ray Diffraction Analysis

The results of WAXD measurements of the semi-crystalline copolymers are shown in Figure 10.23. The patterns of the diffraction peaks, the values of 2θ for each diffraction peak and crystal cell parameters are the same for all the samples, suggesting that the crystal structures of the copolymers belong to a rhombic system in the same manner as that of PEEK [81]. The intensities of the diffraction peaks decrease with the increase of the content of the

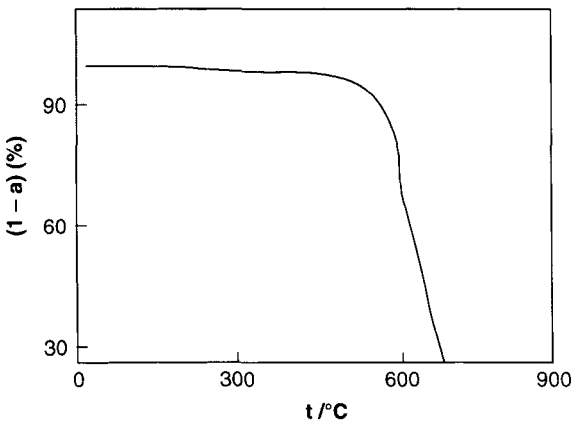

Figure 10.22 The TGA curve of the PAEK copolymer with the molar fraction of DHA to be 1.00% [33].

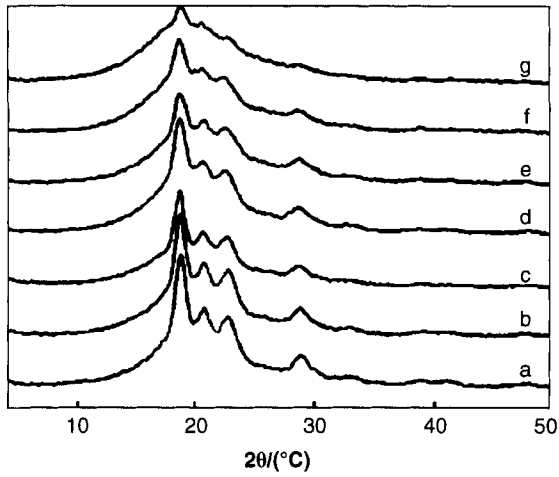

Figure 10.23 WAXD patterns of the PAEK copolymers with various molar fractions of DHN. a. 0.05; b. 0.10; c. 0.15; d. 0.20; e. 0.30; f. 0.40; g. 0.50 [33].

naphthalene moieties. It can therefore be presumed that the segments containing naphthalene moieties in the copolymers are not in the crystal unit cell of the copolymers, but in the amorphous phase between the crystalline lamellae.

10.7 References

1. T.E. Attwood, P.C. Dawson, and J.L. Freeman, *Polymer*, Vol. 22, p. 1096, 1981.
2. R.V. Lakshmana, *Journal of Macromolecular Science Reviews*, Vol. 35, p. 661, 1995.
3. P.M. Hergenrother, B.J. Jensen, and S.J. Havens, *Polymer*, Vol. 29, p. 358, 1988.
4. X.L. Ji, W.J. Zhang, and Z.W. Wu, *Polymer*, Vol. 37, p. 4205, 1996.
5. J.K. Cao, W.C. Su, Z.W. Wu, T. Kitayama, and K. Hatada, *Polymer*, Vol. 35, p. 3549, 1994.
6. X.L. Ji, D.H. Yu, W.J. Zhang, and Z.W. Wu, *Polymer*, Vol. 38, p. 3501, 1997.
7. J.B. Rose, *Polymer*, Vol. 15, p. 456, 1974.
8. V.L. Rao, *Journal of Macromolecular Science Reviews*, Vol. C35, p. 661, 1995.
9. M. Dhara, and S. Banerjee, *Progress in Polymer Science*, Vol. 35, p. 1022, 2010.
10. G. Maier, *Progress in Polymer Science*, Vol. 26, p. 3, 2001.
11. Y. Zhao, F. Wang, A. Li, B. Liu, Z. Wu, and D. Zhang, *et al.*, *Materials Letters*, Vol. 58, p. 2365, 2004.
12. G.B. Wang, Z.H. Jiang, H.W. Zhou, Z.W. Wu, *et al.*, *Polymer Preprints*, Vol. 40, p. 803, 1999.
13. G.B. Wang, Z.H. Jiang, S.L. Zhang, C.H. Chen, and Z.W. Wu, *Polymer International*, Vol. 55, p. 657, 2006.

14. X.L. Zhu, S.L. Zhang, D.F. Ren, S.W.Guan, G.B.Wang, and Z.H. Jiang, *Chem. Res. Chinese. U.*, Vol. 25, p. 261, 2009.
15. G.S. Bennett, R.J. Farris, and S.A. Thompson, *Polymer*, Vol. 32, p. 1633, 1991.
16. F. Wang, J. Roovers, and P.M. Toporowski, *Macromolecules*, Vol. 26, p. 3826, 1993.
17. F. Wang, and J. Roovers, *Journal of Polymer Science, Polymer Chemistry*, Vol. 32, p. 2413, 1994.
18. R. Singh, and A.S. Hay, *Macromolecules*, Vol. 24, p. 2637, 1991.
19. W. Risse, and D.Y. Sogah, *Macromolecules*, Vol. 23, p. 4029, 1990.
20. Y.M. Niu, X.L. Zhu, and L.Z. Liu, *Reactive and Functional Polymers*, Vol. 66, p. 559, 2006.
21. B.J. Liu, C.H. Chen, and W. Hu, *Chem. J. Chinese U.*, Vol. 23, p. 321, 2002.
22. W. Risse, and D.Y. Sogah, *Macromolecules*, Vol. 23, p. 4029, 1990.
23. Z.W. Wu, C.H. Chen, and Z.H. Jiang, *et al., Patent*, 2004, CN 1158319C (in Chinese).
24. M.M. Guo, B.J. Liu, Z.H. Jiang, *et al., Journal of Membrane Science*, Vol. 362, p. 38, 2010.
25. G.B. Wang, Z.H. Jiang, Z.W. Wu, *et al., Patent*, 2008, CN 101104684A (in Chinese).
26. Z.W. Wu, W.J. Zhang, Y.B. Zheng, *et al., Patent*, 2000, CN 1050616C (in Chinese).
27. H.W. Zhou, *Doctoral Thesis, Jilin University*, 1999.
28. Y.M. Niu, X.B. Chen, Y.H. Zhang, X.L. Zhu, and Z.H. Jiang, *Journal of Macromolecular Science, Pure and Applied Chemistry*, Vol. A41, p. 1095, 2004.
29. Y.M. Niu, S.X. Zhang, G.B. Wang, Z.H. Jiang, *et al., Journal of Macromolecular Science, Pure and Applied Chemistry*, Vol. A42, p. 641, 2005.
30. P.X. Xing, G.P. Robertson, M.D. Guiver, *et al., Polymer*, Vol. 46, p. 3257, 2005.
31. M.Z. Cai, F. Xiao, C. S. Song, *et al., Polymers for Advanced Technologies*, Vol. 20, p. 981, 2009.
32. M.Z. Cai, Q. Xi, C.S. Song, *et al., Journal of Applied Polymer Science*, Vol. 114, p. 1543, 2009.
33. S.J. Liu, Y.M. Niu, X.L. Zhu, G.B.Wang, *et al., Chem. Res. Chinese U.*, Vol. 22, p. 114, 2006.
34. S.J. Liu, X.B. Sun, G.B.Wang, Z.H. Jiang, *et al, Journal of Applied Polymer Science*, Vol. 102, p. 2527, 2006.
35. Y.M. Niu, *Doctoral Thesis, Jilin University*, 2005.
36. Y.M. Niu, G.B. Wang, Z.H. Jiang, *et al., Polymer International*, Vol. 54, p. 180, 2005.
37. G.B. Wang, D. Wang, Z.H. Jiang, *et al., Chem. J. Chinese U.*, Vol. 22, p. 1053, 2001.
38. S.J. Zhang, L.X. Fu, D.C. Yang, Z.W. Wu, *et al., Macromolecular Chemistry and Physics*, Vol. 201, p. 649, 2000.
39. S.J. Zhang, Y.B. Zheng, Z.W. Wu, D.C. Yang, *et al., Chem. J. Chinese U.*, Vol. 19, p. 984, 1998.
40. X.L. Zhu, S.L. Zhang, G.B. Wang, *et al., Chem. Res. Chinese U.*, Vol. 25, p. 261, 2009.
41. Y.M. Niu, X.L. Zhu, L.Z. Liu, G.B. Wang, *et al., Journal of Macromolecular Science, Pure and Applied Chemistry*, Vol. A43, p. 1459, 2005.
42. G.S. Bennett, and R.J. Farris, *Polymer Engineering and Science*, Vol. 34, p. 781, 1994.
43. S.J. Zhang, Y.B. Zheng, Z.W. Wu, D.C. Yang, *et al., Chem. J. Chinese U.*, Vol. 18, p. 484, 1997.

44. S.J. Zhang, L.X. Fu, D.C. Yang, G.B. Wang, Z.W. Wu, *et al.*, *Chem. J. Chinese U.*, Vol. 22, p. 334, 2001.
45. S.J. Zhang, Y.B. Zheng, Z.W. Wu, *et al.*, *Polymer Bulletin*, Vol. 38, p. 621, 1997.
46. L.M. Milson, *Liquid Crystals*, Vol. 17, p. 277, 1994.
47. S. Chen, W. Song, Y. Jin, *et al.*, *Liquid Crystals*, Vol. 15, p. 247, 1993.
48. D. Demus, and L. Richter, *Texture of Liquid Crystals*, 2nd Edition, New York, Weinheim, 1978.
49. G.W. Gray, and J.W.G. Goodby, *Smectic Liquid Crystals: Textures and Structures*, Philadelphia, Leonard Hill, 1984.
50. Y. Yoon, A. Zhang, S.Z.D. Cheng, *et al.*, *Macromolecules*, Vol. 29, p. 294, 1996.
51. A. Coassolo, M. Foa, and D. Dainelli, *Macromolecules*, Vol. 24, p. 1701, 1991.
52. H. Toriumi, and E.T. Samulski, *Mol Cryst Liq Cryst*, Vol. 101, p. 163, 1983.
53. H. Jonson, and P.E. Werner, *Macromolecules*, Vol. 22, p. 1683, 1989.
54. S. Wang, J. Wang, T. Liu, Z. Mo, H. Zhang, D. Yang, *et al.*, *Macromolecular Chemistry and Physics*, Vol. 198, p. 969, 1997.
55. G. Maier, *Progress in Polymer Science*, Vol. 126, p. 3, 2000.
56. P.E. Cassidy, T.M. Aminabhavi, and J.M. Farley, *Journal of Macromolecular Science Reviews*, Vol. C29, p. 365, 1989.
57. P.E.Cassidy, *Journal of Macromolecular Science Reviews*, Vol. C34, p. 1, 1994.
58. C. Hamciuc, M. Bruma, and M. Klapper, *Journal of Macromolecular Science*, Vol. A38, p. 659, 2001.
59. R.D. Miller, *Science*, Vol. 286, p. 421, 1999.
60. T.M. Long, and T.M. Swager, *Journal of the American Chemical Society*, Vol. 125, p. 14113, 2003.
61. J. Roovers, J.D. Cooney, and P.M. Toporowski, *Macromolecules*, Vol. 23, p. 1611, 1990.
62. G. Hougham, G. Tesoro, A. Viehbeck, and J.D. Chapple-Sokol, *Macromolecules*, Vol. 27, p. 5964, 1994.
63. P.C. Dawson, and D.J. Blundell, *Polymer*, Vol. 21, p. 577, 1980.
64. L.J. Mathias, C.M. Lewis, and K.N. Wiegel, *Macromolecules*, Vol. 30, p. 5970, 1997.
65. J.J. Jensen, M. Grimsley, L.J. Mathias, *Journal of Polymer Science, Part A*, Vol. 34, p. 397, 1996.
66. Y.T. Chern, and H.C. Shiue, *Macromolecular Chemistry and Physics*, Vol. 199, p. 963, 1998.
67. S.H. Hsiao, C.T. Lee, Y.T. Chern, *Journal of Polymer Science, Part A*, Vol. 37, p. 1619, 1999.
68. G.B. Wang, C.H. Chen, H.W. Zhou, *et al.*, *Chem. J. Chinese Universities*, Vol. 21, p. 1325, 2000.
69. Y. Gao, G.P. Robertson, M.D. Guiver, *et al.*, *Macromolecules*, Vol. 37, p. 6748, 2004.
70. F.A. Bottino, G.D. Pasquale, and A. Pollicino, *Polymer*, Vol. 14, p. 3199, 1998.
71. Z.H. Gao, X.H. Fan, X.F. Chen, *et al.*, *Chem. J. Chinese Universities*, Vol. 26, p. 1579, 2005.
72. H. Li, H.W. Zhou, C.H. Chen, *et al.*, *Chem. J. Chinese Universities*, Vol. 24, p. 1691, 2003.
73. Z.Y. Wang, and A.L. Guen, *Macromolecules*, Vol. 28, p. 3728, 1995.
74. M. Ohno, T. Takata, and T. Endo, *Journal of Polymer Science, Part A*, Vol. 33, p. 2647, 1995.

75. S. Matsumura, N. Kihara, and T. Yakata, *Macromolecules*, Vol. 34, p. 2848, 2001.
76. F.A. Bottino, G.D. Pasquale, N. Leonardi, *et al., Journal of Macromolecular Science, Pure and Applied Chemistry*, Vol. A32, p. 1947, 1997.
77. S. Yoshida, A.S. Hay, *Journal of Macromolecular Science, Pure and Applied Chemistry*, Vol. A34, p. 1299, 1997.
78. Y.M. Niu, X.B. Chen, Y.H. Zhang, *et al., Journal of Macromolecular Science, Pure and Applied Chemistry*, Vol. A41, p. 1095, 2004.
79. R.X. Ruan, Z.H. Jiang, W.L. Xu, *et al., Die Angewandte Makromolekulare Chemie*, Vol. 1999, p. 270, 33.
80. J. Devaux, D. Delimoy, D. Daoust, *et al., Polymer*, Vol. 26, p. 1994, 1985.
81. P.C. Dawson, and D.J. Blundell, *Polymer*, Vol. 21, p. 577, 1980.
82. H.G. KennCorwin, S.H. Benjamin, and L.F. Katherine, *Polymer*, Vol. 35, p. 2290, 1994.

11

Liquid Crystalline Thermoset Epoxy Resins

P. Kannan and P. Sudhakara

Department of Chemistry, Anna University, Chennai, India

Abstract

The increasing demand of new materials for aircraft industry has pushed resin suppliers to identify on new systems to meet the requirement for high performance composite applications. Many efforts were directed towards the increase of toughness by means of admitting functionalized rubbers in glassy thermosets. However, higher fracture energies are negatively balanced by T_g reduction and consequently decrease of mechanical properties. Hence, as far as composite applications are concerned, the goal is to design resin with high Tg, high modulus and superior fracture toughness. With demand for new high performance polymers, the scientific community devoted many efforts to synthesis of liquid crystalline polymers. The synthesis of the some of the important Liquid Crystalline Epoxy Resins is disclosed. The cure reaction of LCERs can have a large influence on the liquid crystalline phase as physical properties of the final cured material. The mechanical and thermal properties of the LCT are discussed in this chapter.

Keywords: Liquid crystalline thermosets, liquid crystalline epoxy resins, curing reactions, mechanical properties, thermal properties

11.1 Liquid Crystals

The name liquid crystals suggests that it is a state of a matter in between the liquid and crystal that mixes the properties of both liquid and solid states and intermediate between the two in many of its property. In other words, liquid crystals are partially ordered, anisotropic fluids, thermodynamically located between the three

Vikas Mittal (ed.) High Performance Polymers and Engineering Plastics, (387–422)
© Scrivener Publishing LLC

dimensionally ordered solid state crystal and isotropic liquid as shown in Figure 11.1 and this is the origin of the term mesogenic state, used synonymously with liquid crystal state. Material that exhibit such unusual properties are often called mesogens and the various phases in which they could exist are termed mesophases. The anisotropic nature of liquid crystals is responsible for the unique optical properties exploited by scientists and engineers in a variety of applications. The molecules in liquid crystal phases diffuse much like molecules in a liquid, but they maintain some degree of orientational order and sometimes some positional order too. The amount of order in a liquid is quite small as compared to a crystal. Liquid crystalline materials are generally divided into two categories the *thermotropic* and the *lyotropic* mesophases. Thermotropic liquid crystal phases are observed by a change of temperature, while lyotropic phases form in the presence of a suitable (isotropic) solvent.

Liquid crystalline materials in general may have various types of molecular structure. What they all have in common is that they are anisotropic. Either their shape is such that one axis is very different from the other. Thermotropic liquid crystals are generally further distinguished with respect to the molecular shape of the constituent molecules, being called *calamitic* for rod-like, *discotic* for disk-like, and *sanidic* for brick- or lath-like molecules as shown in Figure 11.2. A common structural feature of calamitic mesogens is that the mesogenic molecule be fairly rigid for at least some portion of its length, often incorporating phenyl and biphenyl groups, and two flexible end groups, often alkyl or alkoxy chains, since it must maintain an elongated shape to produce interactions that favor alignment. In discotic mesogens six flexible end groups are commonly attached to a rigid, disk-like core. Obviously, numerous

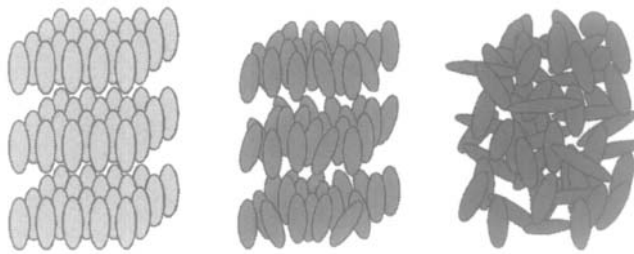

Figure 11.1 Schematic representation of the order of solid, liquid crystal and liquid.

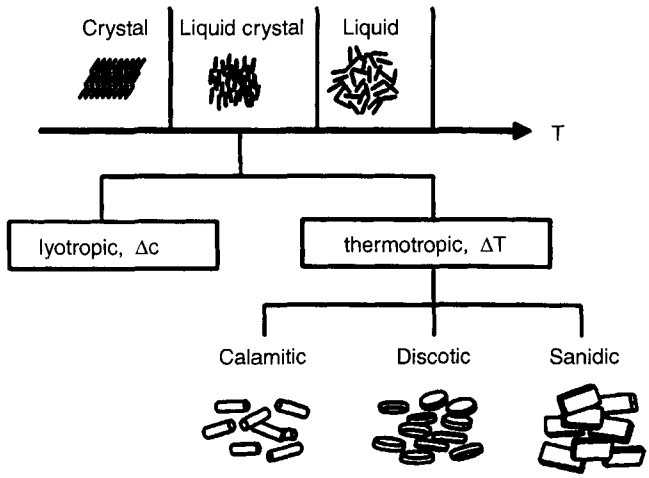

Figure 11.2 Classification of liquid crystals. Reproduced from reference 6.

variations to these general molecular structures may be implemented, leading to the large variety of mesogenic compounds.

Based on the arrangement of molecules (in terms of their orientational and translational degrees of freedom), the liquid crystalline phases are classified broadly in to two main types: nematic and smectic mesophases. The nematic mesophase frequently adopts a characteristics "threaded" texture, clearly visible between crossed Polaroid, and the word nematic stems from the Greek, nematos-thread-like. The word "smectic" is derived from the Greek word for soap. This is explained by the fact that the thick, slippery substance often found at the bottom of a soap dish is actually a type of smectic liquid crystal. The nematic phase is the simplest liquid crystal phase. In this phase the molecules maintain a preferred orientational direction as they diffuse throughout the sample with no positional order but tend to point in the same direction along the director. When the crystalline order is lost in two dimensions, one obtains stacks of two-dimensional liquids: such systems are called smectics. In smectic phases molecules show a degree of translational order, tend to align themselves in layers or planes with a well-defined interlayer spacing. There exist several types of smectic phase with layer structures in which the molecules inside the layer possess effective rotational symmetry around their long axes and are arranged in a hexagonal (S_B) or pseudo hexagonal (S_F, S_G, S_I, S_J) manner. Some of the smectic phases are showed in Figure 11.3.

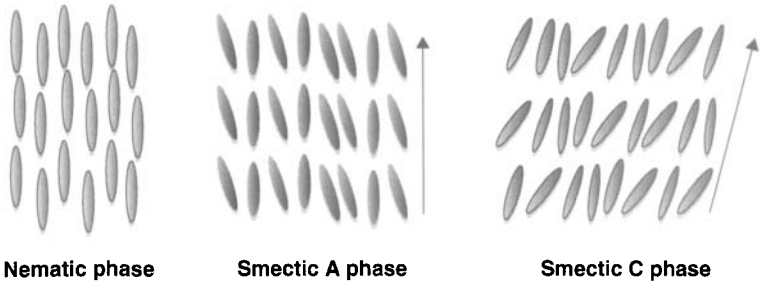

Figure 11.3 Schematic representation of Nematic, Smectic-A and Smectic-C phases.

To quantify just how much order is present in a material, an order parameter (S) is defined. Traditionally, the order parameter is given as follows:

$$S = (1/2)\,(3\cos^2\theta - 1)$$

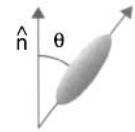

Where, θ is the angle between the director and the long axis of each molecule. In an isotropic liquid, the average of the cosine terms is zero, and therefore the order parameter is equal to zero. For a perfect crystal, the order parameter evaluates to one. Typical values for order parameter of a liquid crystal range between 0.3 and 0.9, with exact value a function of temperature, as a result of kinetic molecular motion [1–10].

11.1.1 Characterization of Liquid Crystals

Different experimental techniques have been used to characterize structural and phase behavior of liquid crystalline materials. Polarizing optical microscopy is one of the essential tools for the characterization of newly synthesized mesogenic materials, together with differential scanning calorimetry (DSC) and x-ray investigations, while DSC provides information on phase transition temperatures and order of transitions. X-ray investigations for actual structural evaluation, i. e. determination of phase type, have to be performed on macroscopically well oriented samples, which is often time consuming and sometimes hard to realize. Therefore

X-ray studies are often carried out on unoriented samples, while the results only allow limited characterization of the structural features. X-ray studies are very much useful especially to identify the ordered smectic phases. Polarizing microscopy on the other hand can provide a determination of both phase transition temperatures and phase type [5–7].

11.1.2 Electric and Magnetic Field Effects

The response of liquid crystal molecules to an electric field is the major characteristic utilized in industrial applications. The ability of the director to align along an external field is caused by electric nature of the molecules. When an external electric field is applied to liquid crystal, the dipole molecules tend to orient themselves along the direction of the field [10].

In the diagram below (Figure 11.4), the black arrows represent the electric field vector and the gray arrows show the electric force on the molecule. Even if a molecule does not form a permanent dipole, it can still be influenced by an electric field. In some cases, the field produces slight re-arrangement of electrons and protons in molecules such that an induced electric dipole results. While not as strong as permanent dipoles, orientation with external field still occurs.

The effects of magnetic fields on liquid crystal molecules are analogous to electric fields. Because magnetic fields are generated by moving electric charges, permanent magnetic dipoles are produced by electrons moving about atoms. When a magnetic field is applied, the molecules will tend to align with or against the field [6–9].

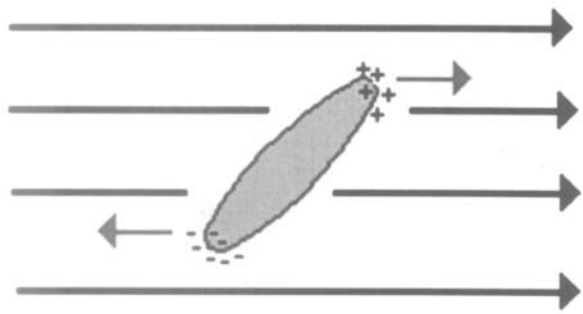

Figure 11.4 Representation of the alignment of a liquid crystal molecule in an electric field.

11.1.3 Liquid Crystalline Polymers (LCPs)

The liquid crystalline polymers are generally comprises of low molecular weight mesogenic moieties. This means that the same mesophases can be obtained for liquid crystalline polymers as to that of low molecular weight counterparts. At the same time, they combine the properties of polymers with those of liquid crystals. Generally, liquid crystalline polymers are classified into two types. The placement of the mesogens play a major role in determining the type of LCPs, such as Main-Chain Liquid Crystalline Polymers (MC-LCPs) are formed when the mesogens are themselves part of the main chain of a polymer. Conversely, Side-Chain Liquid Crystalline Polymers (SC-LCPs) are formed when the mesogens are connected as side chains to the polymer by a flexible "bridge" (called the spacer normally methylene units).

A number of liquid crystal polymers (LCPs) were produced in the 1970s which displayed order in the melt (liquid) phase analogous to that exhibited by non-polymeric liquid crystals. However, the commercial introduction of liquid crystal polymer resins did not occur until 1984, at that time liquid crystal polymers could not be injection molded. Today, liquid crystal polymers can be melt processed on conventional equipment at fast speeds with excellent replication of mold details and efficient use of regrind [11].

11.2 Liquid Crystalline Thermosets Based on Epoxy Resins

As one of the most widely used thermoset materials, epoxy resins have special chemical characteristics compared with other thermosetting resins: no byproducts or volatiles are formed during curing reactions, thus shrinkage is low; epoxy resins are cured over a wide range of temperatures; and the degree of cross-linking can be controlled. Depending on the chemical structure of curing agents and on curing conditions, the properties of cured epoxy resins are versatile, including excellent chemical and heat resistance, high adhesive strength, low shrinkage, good impact resistance, high strength and hardness, and high electrical insulation. Curing can result in a tridimensional network with properties depending on the extent and density of crosslinking. Aromatic amines generally lead to thermosets with higher T_gs, superior thermal resistance and mechanical

performances. If aliphatic acids are used as curing agents a more flexible material will result with lower T_g [12–15].

The increasing demand of new materials for aircraft industry has pushed resin suppliers to identify on new systems to meet the requirement for high performance composite applications. Many efforts were directed towards the increase of toughness by means of admitting functionalized rubbers in glassy thermosets. However, higher fracture energies are negatively balanced by T_g reduction and consequently decrease of mechanical properties. Hence, as far as composite applications are concerned, the goal is to design resin with high Tg, high modulus and superior fracture toughness. With demand for new high performance polymers, the scientific community devoted many efforts to synthesis of liquid crystalline polymers [16, 17].

In the early stage, in 1975, De Gennes [18] suggested that nematic polymers might be cross linked to produce networks of quite remarkable properties such as high strength, low creep, excellent corrosion and weather resistance. These characteristics arise by the incorporation of mesogenic structures in the cured networks and the resultant materials are called as liquid crystalline thermosets (LCTs). The low viscosity of LCTs in the initial stage of processing make it possible to fill complicated molds easily or thoroughly penetrating the fiber weaves or mats for the formation of composites [19–21]. The microstructure of LCTs, having overall isotropic properties, consists of anisotropic domains with properties, such as strength, different along and across their molecular orientations. This leads to the deviation of crack propagation from a straight line and suggests that in-homogeneities and localized anisotropy of nematic structure are the main reasons for gain of mechanical properties in liquid crystalline materials.

Liquid crystalline epoxy resins (LCERs) may be obtained by end-capping mesogenic or rigid-rod molecules with reactive epoxy groups (crosslinking end-groups) (Figure 11.5) in the presence of suitable curing agent, typically diamines. While this general concept implies that the monomer and cured thermoset have the same liquid crystalline order, in fact the liquid crystalline order can be affected by the cure reaction. The selection of both glycidyl terminated compound and curing agent are important to achieve an ordered thermoset and that it is not essential the epoxy monomer and curing agent form a liquid crystalline phase by themselves [22]. The structural difference between some of conventional

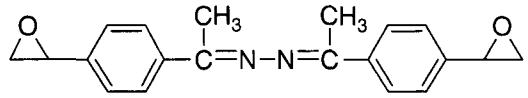

EF3

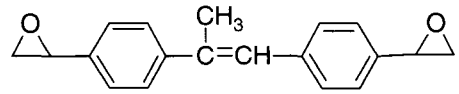

DOMS

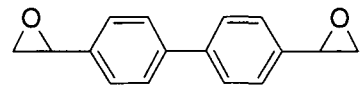

DIF

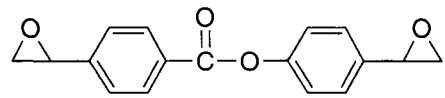

PHBHQ

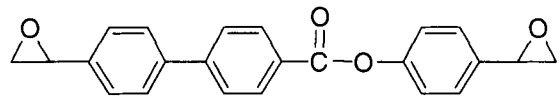

DIFHB

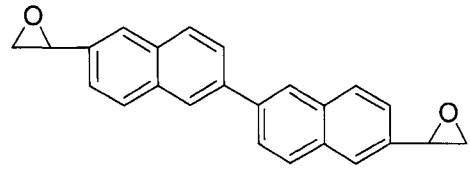

EPBN

Figure 11.5 Rigid monomers for the preparation of LCERs.

epoxy resins and LCERs can be found from Figure 11.5 and Figure 11.6 respectively. If geometry of bisphenol A (Figure 11.6) is taken into account, it can be easily demonstrated that this molecule is kinked: therefore, in order to get a liquid crystalline structure for cured epoxy resin, new glycidyl terminated monomers, having a rigid skeleton, needed to be synthesized (Figure 11.5.)

Epoxy LC networks were first claimed in a Japanese Patent issued in 1984 [23]. Followed by, Bayer AG and the Dow Chemical Company were issued a number of patents on thermosets based on glycidyl

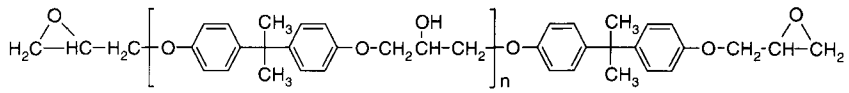

DGEBA

(a) Diglycidyl ether of bisphenol-A (DGEBA)

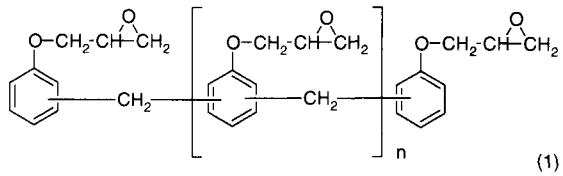

(1)

(b) Novolac epoxy resin

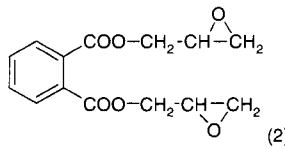

(2)

(c) Diglycidyl phthalate

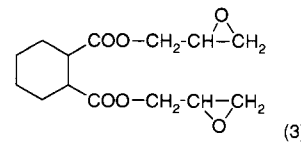

(3)

(d) Diglycidyl hexahydrophthalate

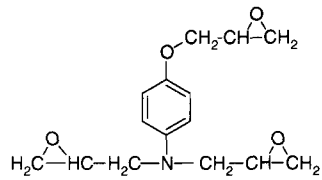

(d) Triglycidyl ether of *p*-aminophenol

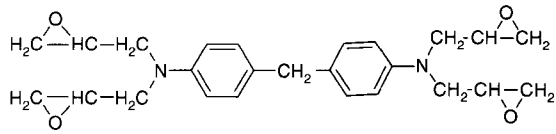

Tetraglycidyl methylenedianiline (MDA)

Figure 11.6 Some of the conventional epoxy resins.

end-capped mesogenic structures [24–26]. These LC epoxy systems consisted of rigid-rod monomers such as the diglycidyl ethers of 4-hydroxyphenyl 4-hydroxybenzoate, 4,4′-dihydroxybiphenol and 4,4′-dihydroxy-a-methylstilbene (shown in Figure 11.5) cross-linked with a variety of reagents; for example, with anhydrides, amines and

sulfanilamide. Retention of the mesomorphic character of the monomers in the resulting networks was described despite the introduction of non-LC crosslinking reagents during the curing reaction.

11.3 Synthesis and Physical Properties of LCERs

11.3.1 Synthesis of LCERs

Various types LCERs are available in the literature, however the synthesis of the some of the important LCERs are discussed in this section. To find the effect of mesogenic structure on the properties of LCER, the mesogenic length of the LCER was changed by changing the length of the rigid rod unit of LCER and it was correlated with the curing behavior and thermomechanical properties of LCE resins. The structure of the LCERs is depicted in Figure 11.7 followed by synthetic procedure [27].

LCER 1 [1,4-Di(2,3-epoxypropenyloxy)benzene)]. Diallyl monomer 1,4-Di(2-propenyloxy)benzene (19 g, 0.2 mol) was added to 300 ml CH_2Cl_2 solution containing 3-chloroperoxybenzoic acid (78 g 0.45 mol) and the mixture was boiled for 48 h, cooled and

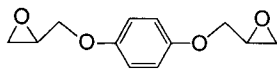

LCER1

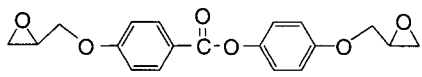

LCER2

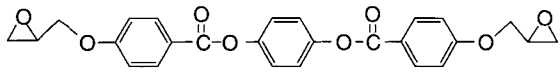

LCER3

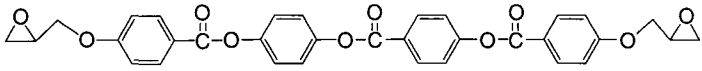

LCER4

Figure 11.7 Chemical structures of liquid crystalline epoxy resins with deferent mesogenic length. Reproduced from reference 27.

filtered. The filtrate is washed with 5% aqueous solution of Na_2SO_3 (200 ml), 5% aqueous solution of $NaHSO_3$ (200 ml) and saturated aqueous solution of NaCl (200 ml). The CH_2Cl_2 layer was dried over $MgSO_4$ and CH_2Cl_2 was evaporated. Yield: 68% (30 g) Tm: 113°C.

The similar procedure was adopted for the synthesis of LCER 2, LCER 3 and LCER 4 as described for the synthesis of LCER 1 with small variations. LCER 2 [4,4'-Di(2,3-epoxypropenyloxy)phenyl benzoate] was prepared by oxidizing the diallyl monomer 4,4'-Di(2-propenyloxy)phenyl benzoate (31 g, 0.1 mol) with 3-chloroperoxybenzoic acid and recrystallizing the product in acetonitrile/isopropanol (1:1). Yield: 75% (25 g) T_m: 116°C. LCER 3 [p-Phenylene-di[4-(2,3-epoxypropenyloxy)benzoate] was synthesized by oxidizing diallyl monomer p-phenylene-di[4-(2-propenyloxy)benzoate] (13 g, 0.030 mol), obtained pure product after recrystallization from ethylacetate/isopropanol. Yield: 68% (8.9 g). The pure product of LCER 4 [4,4'-di[4''-(2,3-epoxypropenyloxy)benzoyloxy]phenyl benzoate] was obtained by oxidizing the diallyl monomer 4,4'-di[4''-(2,3-epoxypropenyloxy)benzoyloxy]phenyl benzoate. Yield: 66% (7.7 g).

Two series of liquid-crystalline epoxy resins were prepared by varying spacer length (methylene groups) as well as central aromatic imine mesogen (naphthalene and biphenylene) linked to glycidylic groups as presented in Figure 11.8a and b [28, 29] respectively and the procedure for synthesis of naphthalene containing epoxy resins is given as follows [28].

Synthesis of *N,N'*-bis[(4-(2,3-epoxypropoxy)-benzyliden) naphthalene-1,5-diamine] (A): A mixture of epichlorohydrin (6 mol) and the bisphenol *N,N'*-bis[(4-hydroxybenzylidene)-naphthalene-1,5-diamine] (0.1 mol) was heated to 110°C, and solid benzyltrimethylammonium chloride (BTMA), (0.01 mol) was added in one batch and the mixture was heated at reflux temperature for 30 min. A homogeneous solution was formed cooled to room temperature, and the solid that crystallized upon cooling was filtered off, washed with ether, and dried *in vacuo*. The product was recrystallized from benzene. Yield: 80%; mp: 212–215°C.

Synthesis of diglycidylic compounds A2, A4, A6, A8, and A10: A mixture of bisphenol {*N,N'*-bis[(4-hydroxybenzylidene)- naphthalene-1,5-diamine]} (5 mmol), (w -bromo-1-alkyl) glycidylether (10 mmol), K_2CO_3 (25 mmol), and 18-*crown*-6 (0.5 mmol) in 50 mL of acetone was heated at reflux temperature for 24 h. The solvent was evaporated, and the solid was dissolved in CH_2Cl_2 and

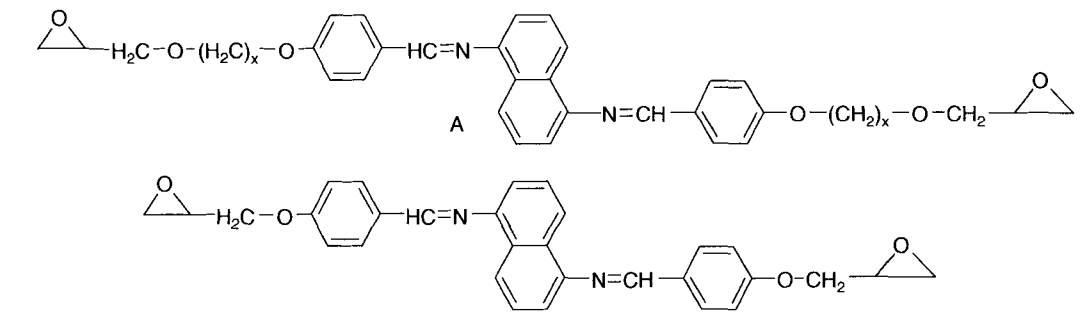

Figure 11.8 Chemical structures of naphthalene (a) and biphenyl (b) containing liquid crystalline epoxy resins. Reproduced from reference 28, 29.

washed with water. The organic phase was evaporated under vacuum to obtain a solid that was recrystallized from benzene and dried *in vacuo*. The structure of all five diepoxides is conformed by, FTIR, ^{1}H NMR and ^{13}C NMR spectroscopy. The biphenyl containing LCERs can also prepared in the similar manner with slight modifications.

11.3.2 Cure Behavior LCERs

The cure reaction of LCERs can have a large influence on the liquid crystalline phase as physical properties of the final cured material. Depending on the nature of the LC monomer and the type of reactive group, the liquid crystalline order may either decrease or increase as a result of the cure. Thus, examples exist in the literature of LCT's that undergo transitions from isotropic to nematic or smectic phases from nematic to smectics from nematic or smectic to isotropic and from smectic to nematic [30–37].

To clearly illustrate the phase changes that occur during cure and their relationship to physical and chemical changes, Cho and Douglas proposed a liquid crystalline phase-time-temperature-transformation (LCPTTT) diagram, as shown in Figure 11.9. To construct these diagrams, DOMS (Figure 11.10) was melted at 150°C, and a stoichiometric amount of sulfanilamide (SAA) was dissolved in the melt. The mixture was poured into an aluminum boat and kept in a freezer to prevent further reaction. The DOMS formulation was placed between two 12 mm round, glass microscope coverslips and isothermally cured at various temperature between 120 and 170°C. Gelation and vitrification are determined using oscillatory parallel plate rheology, and the liquid crystalline phases are observed with optical microscopy between crossed polarizers by heating the monomer isothermally [38].

For this material the order increases during cure, changing from isotropic to smectic A. The DOMS monomer itself is actually a monotropic nematic. The formation of the smectic phase during cure is directly attributable to the use of sulfonilamide (SAA) as the curing agent. The two amine groups of SAA have unequal reactivities. Thus, during cure the aromatic amine preferentially reacts with the epoxide groups of DOMS first, allowing primarily chain extension to occur. Entropic considerations suggest that as the length of the rod increases, it will undergo a transition from a disordered to an ordered phase. This ordering is likely enhanced by electronic

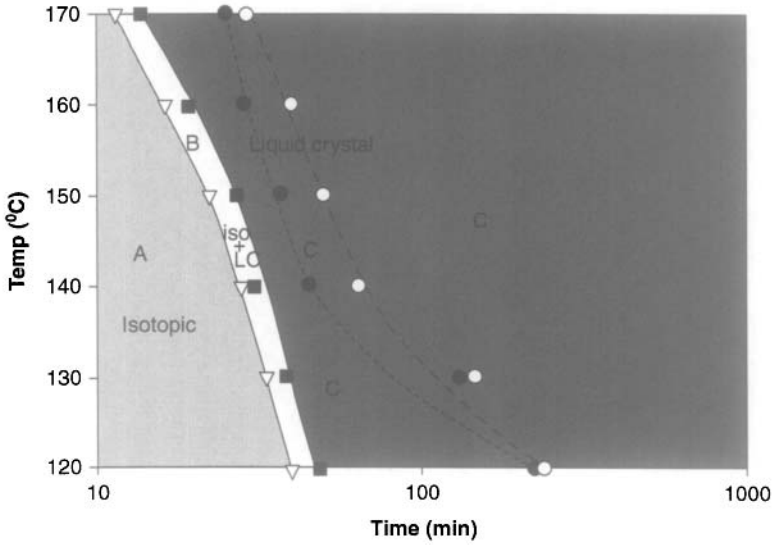

Figure 11.9 LCPTTT diagram for DOMS/SAA stoichiometric mixtures. All phase changes and physical changes are observed during isothermal cure. Light grey indicates the region where the material is isotropic, dark grey indicates smectic, and white indicates a biphasic structure. Filled circles are the gel times at each temperature and open circles are the vitrification times. Reproduced from reference 38.

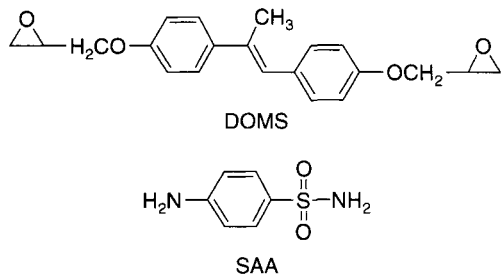

Figure 11.10 Structure of 4,4′-diglycidyloxy-α-methylstilbene (DOMS) and sulfanilamide (SAA)

interactions between stilbene units on neighboring chains. In the later stages of cure sulfonamide groups react with remaining epoxide groups, causing crosslinking.

Figures 11.11 and 11.12 explains gelation and liquid crystalline phase development in a liquid crystalline epoxy curing system.

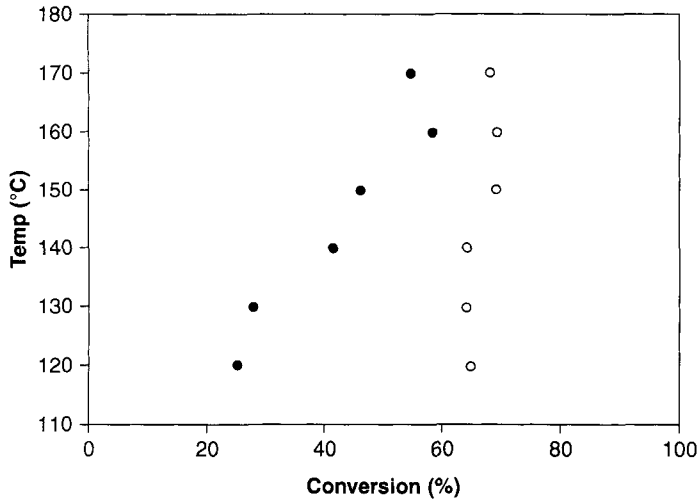

Figure 11.11 Temperature vs conversion for phase transition (•) and gelation (o). Reproduced from reference 38.

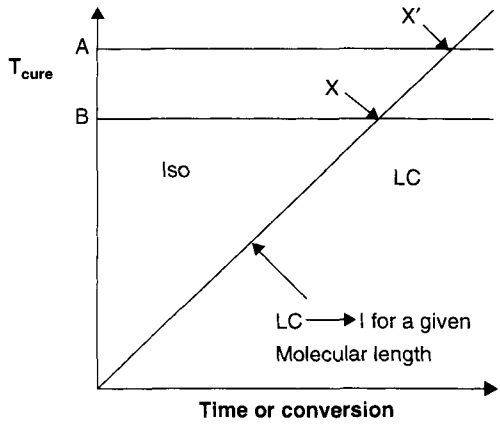

Figure 11.12 Idealized plot for cure temperature vs time or conversion. Reproduced from reference 38.

Figure 11.11 shows the conversion at the gel point as a function of cure temperature.

Even though DOMS/SAA experiences different amounts of cure in liquid crystalline phases at different cure temperature, the system seems to hold isoconversion theory of gelation. For example, at the cure temperature of 120°C, cure in the isotropic phase occurs up

to a conversion of 25%, while at 160°C cure in the isotropic phase occurs up to a conversion of 59% (Table 11.1). At both temperatures gelation occurs at 70% conversion, so at 120°C considerably more of the reaction prior to gelation occurs in the liquid crystalline phase. Even though the amount of reaction that occurs in the liquid crystalline phase is different at these different cure temperatures, the isoconversion theory of gelation fits quite well. Thus, gelation is independent of liquid crystalline phase as well as cure temperature.

Figure 11.11 also shows the plot of phase transition temperature vs conversion. In contrast to gelation, the phase transitions do not show isoconversion behavior. Instead, the conversion at the point where the isotropic phase changes to a liquid crystalline phase tends to increase with temperature. This is due to the fact that critical length of the molecules needed for liquid crystallinity increases with temperature.

Figure 11.12 is an idealized plot that explains this phenomenon. The straight line shows the increase of isotropization temperature with increasing cure time or molecular length (i.e., conversion). If DOMS is cured at temperature A, it will start to show liquid crystallinity at point X, where the straight line and cure temperature line cross. If the cure temperature increases to B, DOMS needs more time to show liquid crystallinity (X'). Therefore, molecular length needs to be longer; i.e., the conversion needs to be higher. This result indicates the increase in transformation time as cure temperature increases for DOMS-SAA system (isotropic-to-smectic transition) suggesting that this is a general phenomenon related to mechanism of epoxy cure and is not dependent on type of liquid crystalline phase that forms.

Table 11.1 Times of liquid crystalline phase appearance (t_{lc}), gel point (t_{gel}), and conversion at phase transition (α_{lc}) and at gel point (α_{gel}). Reproduced from reference 38.

T (°C)	t_{lc} (min)	t_{gel} (min)	α_{lc}(%)	α_{gel}(%)
120	48.03	222.50	25.17	70.16
130	37.52	131.50	28.10	64.56
140	30.05	44.50	41.49	64.14
150	26.70	37.00	46.27	69.44
160	19.00	28.50	58.63	69.71
170	14.93	22.00	54.73	68.15

Finally, it is summarized that by curing the liquid crystalline epoxy, 4,4′-diglycidyloxy-a-methylstilbene, with the curing agent, sulfanilamide, the isoconversion theory of gelation was confirmed; i.e., the conversion at gelation was uniform regardless of the liquid crystalline phase as well as cure temperature. This result indicates that the actual network formed by these molecules is unaffected by any long-range order that may be present and is only controlled by the functionality of the individual molecules. It is to be noted that this study does not address the issue of whether the reaction actually occurs at a faster rate in liquid crystalline phase, but rather that gelation occurs in the same manner as non-liquid crystalline epoxies with respect to conversion dependence and structure of the resulting network.

11.3.3 Properties of Liquid Crystal Epoxy Thermosets Cured in a Magnetic Field

The use of a magnetic field to prepare macroscopically oriented polymers has an important advantage over mechanical stretching or electrical alignment since samples with different geometries (rods, sheets, and blocks) can be readily prepared [39–48].

Influence of the field on molecular alignment

By comparing X-ray diffraction images obtained for the same sample cured in an external magnetic field and out of field, it is possible to estimate the influence of the field on direction and quality of molecular alignment in the investigated sample. Examples of diffraction patterns for MU (Figure 11.13) material are shown in Figure 11.14.

Samples without externally enforced orientation exhibit some spontaneous alignment of the molecules in the direction roughly parallel to the capillary axis, due to interactions with boundary surfaces. After applying a magnetic field in the direction perpendicular to the capillary axis orientation of the molecules changes and the crescent-shaped reflections become shorter and less diffuse. This means that the applied magnetic field of 1.8T was quite effective in enforcing requested orientation of the sample [49].

Mechanical properties

Compared to samples cured outside the field under the same conditions, the oriented LCTs show an improvement in their mechanical properties for the diepoxides and diamines combinations

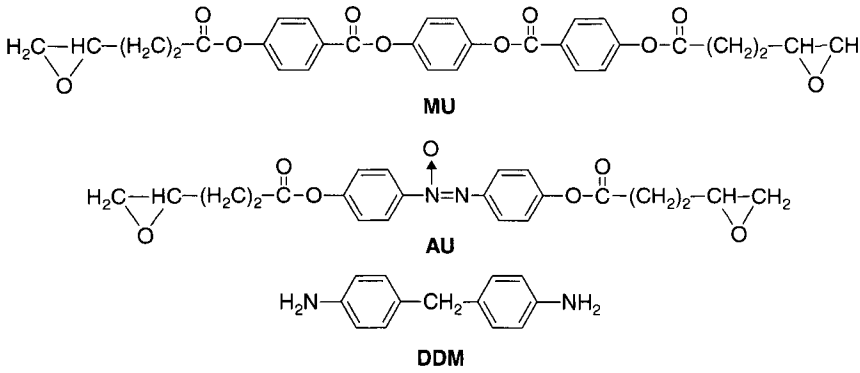

Figure 11.13 Chemical structure of bis[4-(4,5-epoxypentanoyloxy)benzoate] p-phenylene (MU), 4,4'-bis(4,5- epoxypentanate) azoxydiphenyl (AU) and 4,4'-diaminodiphenylmethane

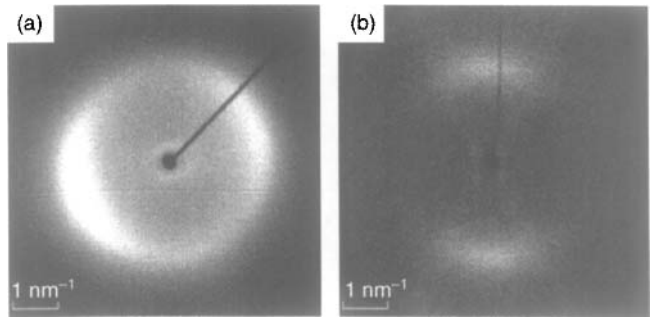

Figure 11.14 Examples of diffraction patterns for MU compound, registered at $T = 180°C$ (a) without magnetic field, (b) with external magnetic field of $B = 1.8T$. Reproduced from reference 49.

(Figure 11.15, Table 11.2). Diepoxide **A** exhibits a nematic phase from 175 to 250°C. Diepoxide **B** melts directly to form a liquid at 155°C, but a monotropic smectic phase was observed upon cooling of the isotropic phase to 147°C. Mixtures of **A** and **B** exhibit an enantiomeric nematic phase when the weight percentage of **B** ranges from 0 to 50%. The diamine **C** melts at 124°C and does not exhibit any mesomorphism but can form nematic mixtures with compound **A** or **B** [50]. To study the effect of macroscopic molecular orientation on the mechanical properties of the LCTs, two samples with a diepoxide/diamine mole ratio of 4:1 were cured in a

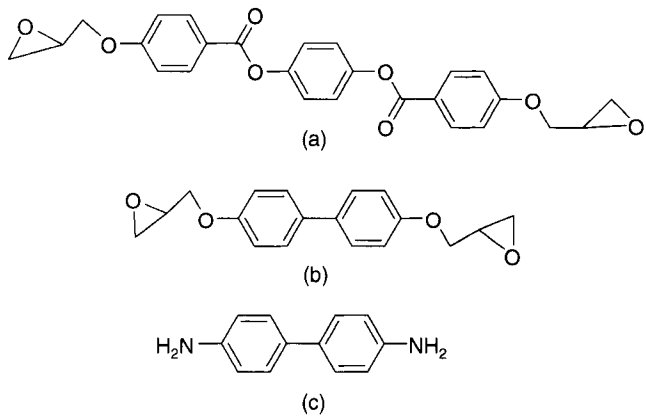

Figure 11.15 Chemical structures of diepoxide monomers and cross-linking agent. Reproduced from reference 51.

Table 11.2 Tensile properties of selected samples. Reproduced from reference 51.

Sample No.	Tensile Modulus (GPa)	Elongation at Break (%)	Break Strength (MPa)
A/C, unoriented	1.44	6.15	15.5
A/C, oriented	2.48	10.65	33.4
[A+B]/C, unoriented	1.85	6.08	20.2
[A+B]/C, oriented	2.98	11.24	42.5

magnetic field for 6 h. For one sample, only diepoxides **A** is used; for the other, the mole ratio of **A**/**B** was 4:1. The measured mechanical properties of the unoriented and oriented polymers are listed in Table 11.2. The data show that the modulus, break strength, and elongation for both oriented samples were about 2 times as large as the corresponding parameters for unoriented polymer samples. The tensile modulus and elongation at break are comparable to those of most commercial epoxy resins, but the break strength is 40–50% smaller. The likely reason for this behavior is the rigidity of the mesogenic core of the monomers, which is nevertheless a basic requirement for the formation of liquid crystals. The storage modulus also increased by a factor of about 1.8. Interestingly, the

glass transition temperature and the cross-linking density of the oriented sample are smaller than those of the sample cured outside the magnetic field. A possible explanation for this behavior is that the magnetic field aligns the monomer molecules, and the extent of cross-linking is reduced in the curing process [51].

11.3.4 Curing of LCERs at Different Temperatures

Depending on the temperature, the reaction may require different amounts of time to reach its completion. By varying the curing temperature it is possible to obtain a cross-linked resin in a nematic, or isotropic structure. It is also well known that temperature of curing affects the properties of final product. High temperatures may cause thermal degradation of material. Temperatures too low may prevent full cure, leaving many of the reactive groups still not converted. One of potentially important factors in the case of liquid crystalline materials is the relation between temperature of curing and temperature range of the mesophases [52, 53].

The curing of a diepoxide (AU) with DDM (Figure 11.13) carried out at different temperatures can be compared from the dynamic DSC curves (Figure 11.16) recorded for products cured in 120°C, 140°C and 160°C. The data demonstrate that stable materials with no phase transitions were formed (despite the small peak visible at about 50°C in all the cases), however the shapes of individual curves are somewhat different. Therefore it can be concluded that - as expected - different

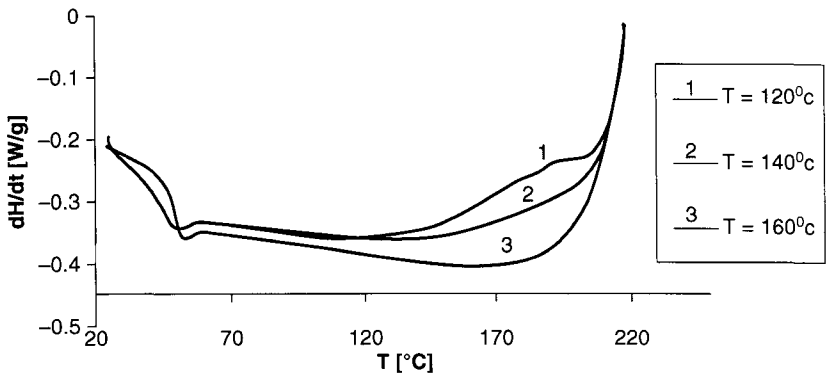

Figure 11.16 Dynamic DSC thermograms for the products of AU/DDM system cured at various temperatures. Data recorded in the course of heating. Reproduced from reference 49.

conditions of cure and varying dynamics of the reaction lead to slightly different final products, which is a common observation for epoxy resins. However the structural order of the finally cured products can be conformed by WAXS and DSC techniques.

11.3.5 Curing of LCERs with Deferent Curing Agents

Curing of LCERs with different curing agent like primary aromatic diamines and tertiary amines etc may affect the formation of liquid-crystalline phases as well as the properties of the cured thermosets. For example crosslinking of biphenyl epoxy monomers (Figure 11.8b) with primary aromatic diamine 2,4-diaminotoluene (DAT) led to nematic networks, some of which contained crystal inclusions, however, through curing with tertiary amine 4-(*N,N*-dimethylamino)pyridine (DMAP) as catalytic agents smectic C organized thermosets were obtained. Tables 11.3 and 11.4 shows the curing conditions, the final order achieved, and the thermal stability data obtained for DAT and DMAP cured LCTs. We can also note that the LCTs obtained with tertiary amines are slightly less thermally stable than the LCTs obtained when DAT was used as the curing. The similar properties can be observed in the case of naphthalene containing epoxy monomers (Figure 11.8a) when cured with same diamines.

11.3.6 Fracture Mechanism of LCTs

The fracture of amorphous, isotropic thermosets based on non-LC epoxy monomers has been studied extensively. The fracture mechanism is explained here by comparing the conventional DGEBA and Liquid crystalline DOMS cured with DMA as explained in Figures 11.17 and 11.18 [54]. The load (N) versus displacement (μm) curves for the three-point bend, chevron-notched fracture toughness experiments are given in Figure 11.17a–d and the data is presented in Table 11.5. The isotropic DGEBA/MDA thermoset exhibits a linear load versus displacement curve (Figure 11.17a) up to a maximum load, at which time a crack is initiated and propagates catastrophically in a brittle manner across the sample. The fracture surface appears smooth and featureless under the SEM (Figure 11.18a), a typical characteristic of brittle fracture.

The DOMS/MDA isotropic, rigid-rod and nematic thermosets exhibit stable crack propagation, which takes place in two steps

Table 11.3 Data from the isothermal curing of monomers A to A10 with DAT and thermal stability data of the networks measured by TGA in a dynamic scan at 10°C/min. Reproduced from reference 29.

Monomer	*X*	Curing Temperature (°C)	Time (min)	Intial State	Final State	Onset Temperature (°C)[a]	Maximum Temperature (°C)[a]	Char yield (%)[a]
A	–	200	15	N	K-N[b]	338	394	54
A2	2	160	15	N	K-N[b]	357	410	47
A4	4	170	30	N	K-N[b]	336	395	42
A6	6	150	30	N	K-N[b]	318	457	25
A8	8	190	10	S_A	N	308	420	30
A10	10	190	10	S_A	N	300	412	26

[a]Determined by TGA in an N_2 atmosphere.
[b]Crystalline microphase dispersed in the nematic matrix.

Table 11.4 Data from the isothermal curing of monomers A to A10 with 1 phr DMAP and thermal stability data of the networks measured by TGA in a dynamic scan at 10°C/min. Reproduced from reference 29.

Monomer	X	Curing Temperature (°C)	Time (h)	Final State	Onset Temperature (°C)[a]	Maximum Temperature (°C)[a]	Char Yield (%)[a]
A	–	250	1	N	283	238	62
A2	2	200	1	N	270	410	48
A4	4	200	10	S_c	263	446	31
A6	6	200	10	S_c	292	452	33
A8	8	200	10	S_c	267	457	38
A10	10	200	10	S_c	271	450	26

[a]Determined by TGA in an N2 atmosphere.

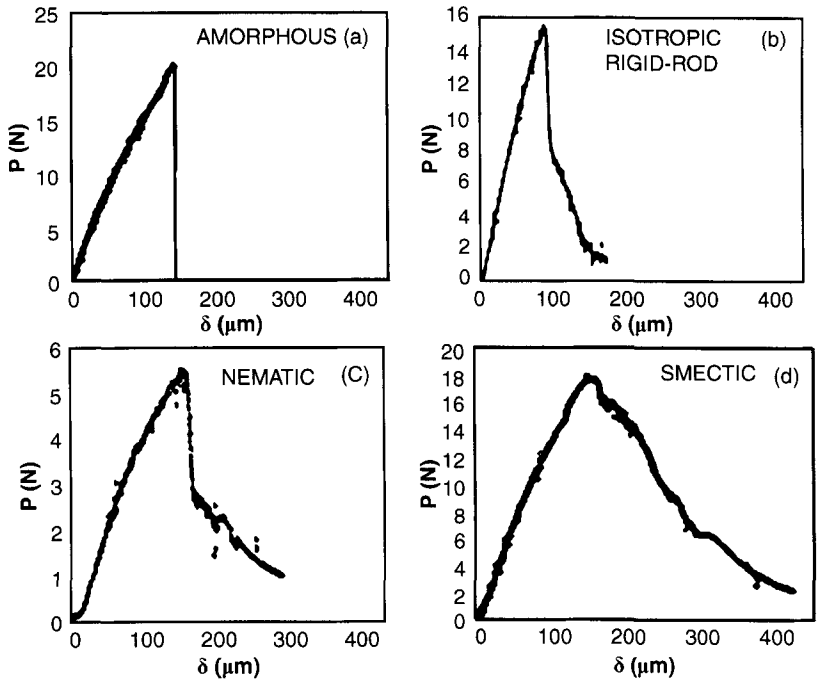

Figure 11.17 Typical load, *P*, versus displacement, d, curves for thermosets in the chevron-notched three-point bend fracture toughness tests: (a) DGEBA/ MDA isotropic thermoset, (b) DOMS/MDA isotropic, rigid-rod thermoset, (c) DOMS/ MDA nematic LCT, and (d) DOMS/MDA smectic LCT. Reproduced from reference 54.

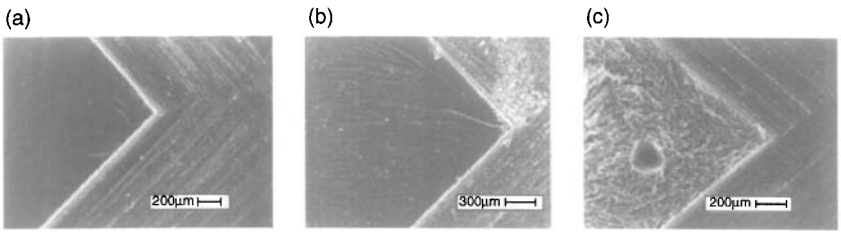

Figure 11.18 Scanning electron micrographs (SEM) of cross sectional surfaces of thermosets fractured in the chevron notched three-point bend technique: (a) DGEBA/MDA isotropic thermoset, (b) DOMS/MDA nematic LCT, and (c) DOMS/MDA smectic LCT. Reproduced from reference 54.

Table 11.5 Estimates of the plane strain fracture toughness for the Thermosets measured by the Chevron-Notched three-point bend fracture toughness test. Reproduced from reference 54.

Thermoset	G_{Ic} (kJ/m^2)	K_{Ic} (MPa·m$^{1/2}$)
DOMS/MDA, smectic	1.62	1.59
DOMS/MDA, nematic	0.75	1.46
DOMS/MDA, isotropic, rigid-rod	0.68	1.27
DGEBA/MDA, isotropic	0.40	1.21

G_{Ic} (kJ/m2) The critical strain energy release rate K_{Ic} (MPa·m$^{1/2}$) critical stress intensity factor.

(Figure 11.17b, c). First, they exhibit a regime of relatively fast crack propagation followed by more non-uniform crack propagation at slower speeds (as indicated by the reduced slope and nonlinearity of the P versus $\ddot{a}$ curve at high displacements). A cross-sectional SEM (Figure 11.18b) of the fracture surfaces shows that the isotropic, rigid-rod and nematic DOMS/MDA samples exhibited parabolic, elongated deformation markings, indicative of some limited plastic deformation. The DOMS/MDA smectic LCT exhibits only slow, stable crack propagation for the duration of the experiment, (Figure 11.17d) indicative of complex, ductile fracture. A cross-sectional SEM (Figure 11.18c) of the fracture surface shows that the smectic DOMS/MDA thermosets exhibited voiding and an extremely rough and highly deformed fracture surface, suggesting that bulk plastic deformation had occurred. Overall, there is a general increase in fracture toughness with decreasing $T_{base\ cure}$, i.e., when the local order is increased from isotropic and nematic to smectic. The smectic phase exhibited the highest fracture toughness with values of G_{Ic} = 1.62 kJ/m^2 and K_{Ic} = 1.59 MPa·m$^{1/2}$.

Proposed Toughening Mechanism of Smectic LCT's

Figure 11.19 shows the proposed fracture mechanism responsible for high fracture toughness of the smectic LCT's. As the network is deformed, it is difficult to maintain the continuity of the poly domain microstructure (especially with such a high cross-link density) and, instead, it is likely that the LC domains prefer to fail in an individual and isolated manner. The network strands of unfavorably oriented domains (perpendicular or nearly perpendicular to the stress direction) should be "softer" and fail first, thus

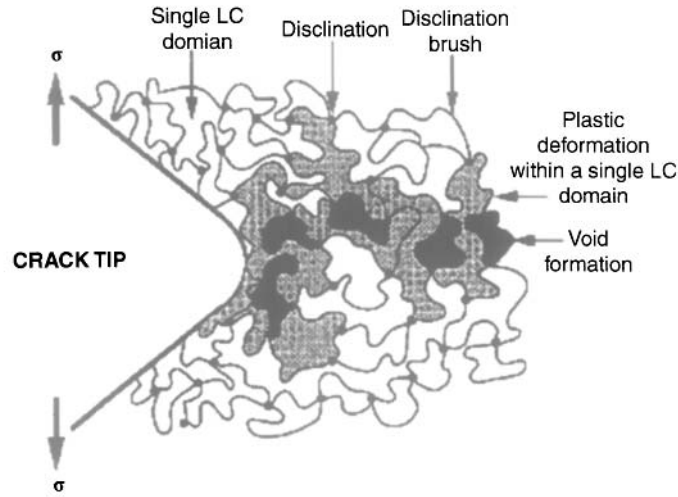

Figure 11.19 Schematic of proposed fracture mechanism in a polydomain smectic liquid crystalline thermoset. (σ = Deformation). Reproduced from reference 54.

producing microscopic voids and defects ahead of the crack tip. Neighboring domains can then deform under uniaxial rather than triaxial stress and undergo significant plastic deformation, similar to rubber-modified thermosets. This type of fracture is similar to non-catastrophic micro-crack formation in polycrystalline metals, which also results in extensive plastic deformation. The stable crack propagation observed in the smectic LCT's most likely takes place through the slow growth and interconnecting of these voids, leading to the macroscopically fibrillar fracture surfaces observed under the SEM. Most likely, we do not observe as much plastic deformation in the nematic LCT's because the domain size is too small to generate voids of a large enough size.

The similar fracture behavior can be observed by comparing the fracture surfaces (Figure 11.20) of commercial DGEBA and a LCER 2,5-bis(4-diglycidyloxyphenyl)-1,3,4-oxadiazole (DGEOD) cured with DDM as observed for DOMS/DDM system. The fracture surface appears smooth and featureless under the SEM (Figure 11.18a), a typical characteristic of brittle fracture [55].

11.3.7 Water Absorption

The presence of absorbed water generally has a devastating effect on the integrated properties including dielectric, thermal and mechanical

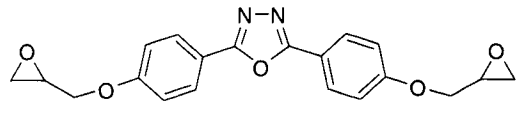

DGEOD

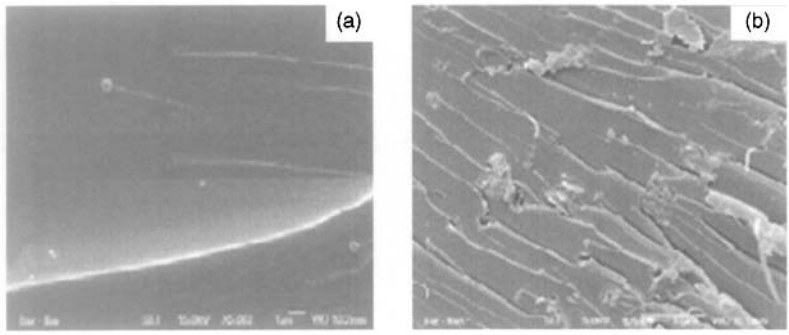

Figure 11.20 Fracture surface of (a) DGEBA/DDM thermoset, (b) DGEOD/ DDM cured at 120°C and post cured at 185°C. Reproduced from reference 55.

properties of a resin, due to plasticization, creation of internal stresses, and crack initiation, so outstanding water resistance is an important property for high performance resins. Liquid crystalline polymers are well known to have reduced permeability to gases and liquids due to the molecular packing in the liquid crystalline phase. It would therefore be expected that LCT's would also have reduced permeability. In the case of epoxies, enhanced barriers to moisture diffusion would be of benefit for composite applications. Diffusion coefficients for water transport were determined for DOMS/SAA and DGEBA/SAA with varying amine/epoxide ratios by measuring the moisture permeability [56]. It was found that for all stoichiometry the diffusion coefficients of the non-liquid crystalline DGEBA/SAA were approximately twice that of the smectic DOMS/SAA. In addition, the diffusion coefficient for both materials decreases monotonically with increasing amine content. The difference between the two materials can be considered as a direct consequence of the packing of the epoxy molecules in the liquid crystalline phase, which limits the amount of free volume available for the water molecules and restricts their ability to diffuse through both the hard and soft phases.

The combinations LCE and non liquid crystalline CE resins (Figure 11.21) possess significantly smaller water absorption than cure CE resin, and the resin with larger content of LCE has smaller

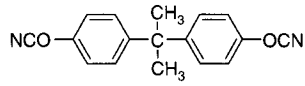

2, 2'-Bis(4-cyanatophenyl) isopropylidene (CE)

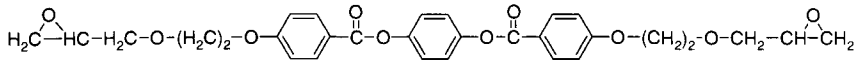

(LCE)

Figure 11.21 2,2'-Bis(4-cyanatophenyl) isopropylidene (CE) and Liquid crystalline epoxy resin (LCE).

water absorption. For example, the water absorptions of LCE10/CE and LCE20/CE are about 81.2%, and 46.7% of that of CE resin, respectively, indicating that LCE/CE resins have better water resistance than CE resin [57].

It is thus theorised that the mesogen-induced reduction in chain motion leads to a concomitant reduction in the polymer free volume, and that there is thus much less available space within the network matrix to accommodate solvent guest molecules. However, water does not wet most epoxy resins significantly, and the variance in solvent absorption is greatly magnified when organic species are used [58].

11.3.8 Thermal Properties

Thermal properties include many aspects, of which glass transition temperature (T_g) thermal coefficients of expansion (TCE) and thermal stability are most important parameters to decide the utility of the resins for high performance applications. The degree of order at the microdomain level can be related to the network physical properties, and thus increasing mesogen content (or long rigid rod mesogen) leads to increased intermolecular interactions between the polymer chains and hence reduced micro-Brownian motion and reduced free volume. These properties are manifested as increased elastic moduli at high temperatures, reduced thermal coefficients of expansion, increased decomposition onset temperatures and reduced solvent.

Glass transition temperature

Figure 11.22 illustrates the correlation among the mesogenic length, glass transition temperature and modulus of liquid crystalline thermosets obtained for the LCERs in Figure 11.7 cured with DDS.

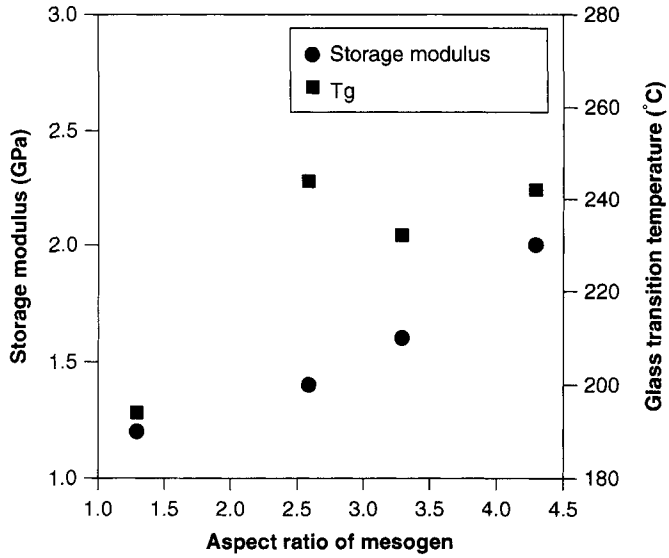

Figure 11.22 Plot of storage modulus and T_g against mesogen aspect ratio. Reproduced from reference 27.

This result indicates that modulus of LCE resins is closely related with the aspect ratio of the mesogen. This also implies that activation energy for local motion of cured thermoset is higher for the LCE resins with long mesogen than for short mesogen. The relationship between modulus and aspect ratio was maintained up to 200°C. Glass transition temperature of LCER resin showed the same tendency as storage modulus. In common, epoxy resins crosslinking density is the major factor in determining the glass transition temperature of cured thermoset resin. The adverse tendency was observed for the glass transition temperature of LCE resins synthesized in this experiment, indicates that mesogenic length plays a major role in determining the glass transition temperature of LCE resin [27].

A common bifunctional epoxy resin has a T_g around 200°C and a tetrafunctional epoxy resin has a T_g of about 250°C. It was even close to the T_g of polyimide (300°C), widely used as a heat-resistant material. This suggests that the T_g of the LCE networks can be elevated drastically by controlling the chemical structure of mesogen. DDS is a typical amine curing agent for high performance conventional epoxy resins. In spite of its kinked geometry, Curing of 6,6′-bis(2,3-epoxypropoxy)-2,2′-binaphthyl (EPBN) with 4,4′-diaminodiphenyl

sulphone, promote the alignment of the prepolymeric chains, leading therefore to networks with liquid crystalline order reveals the Tg at 254°C. In the case of conventional epoxy resins cured with DDS, lower T_gs was resulted [59].

Thermal stability

Most typical epoxy resins undergo thermal decomposition at relatively low temperatures, usually losing up to 10% of their mass between 250 and 300°C in air, and the scant TGA data for liquid crystalline systems seem to corroborate this generalization. Indeed, the maximum recommended use temperature for most epoxy resins is between 80 and 110°C, and thus it would be advantageous if the temperature at which onset of decomposition occurs could be increased in line with the other physical properties for liquid crystalline polymers [58, 59].

Thermal stability of DDS cured LCER (Figure 11.7) networks shows maximum decomposition temperature and char yield were high for LCE networks with long mesogenic group. This is due to the fact that long rigid rod mesogen is resistant to the thermal decomposition. The initial decomposition temperature was above 350°C for LCER 3 and LCER 4. Therefore, we can conclude that thermal stability of LCE resins is enhanced with increasing the mesogenic length. The combination of 2,5-bis(4-diglycidyloxyphenyl)-1,3,4-oxadiazole (DGEOD) (Figure 11.20) with DDM and DDS epoxy resin also provide high thermal stability 355°C and 404°C respectively [55, 60].

The poor flammability of organic epoxy resins a major drawback in many applications, e.g., structural materials for aircraft, motor vehicle construction, and electronics. Among the various flame retardant systems, organophosphorus compounds were identified as better fire retardant materials in terms of environmental and health safety, which generate less toxic plume than halogen-containing counterpart [61–65]. By combining the liquid crystallinity and flame retardant properties, organophosphorus epoxy liquid crystalline were prepared from the monomers [(diepoxide; diglycidylphenylphosphate (DGPP) and diglycidylbiphenylphosphate (DGBP), aromatic diamines: 2,5-bis (p-aminophenyl)1,3,4-oxadiazole(BPOD), diaminodiphenyl sulphone (DDS) and 4,4-diaminobiphenyl (BPD)] established in Figure 11.23 [66, 67]. Though the resins and diamines are inherently non LC compounds, during the curing reaction of epoxy/amine system, oligomers are formed at initial stages and attain sufficient high molecular weight species, thus phase separation (nematic) took place (representative LC photographs are shown in Figure 11.24).

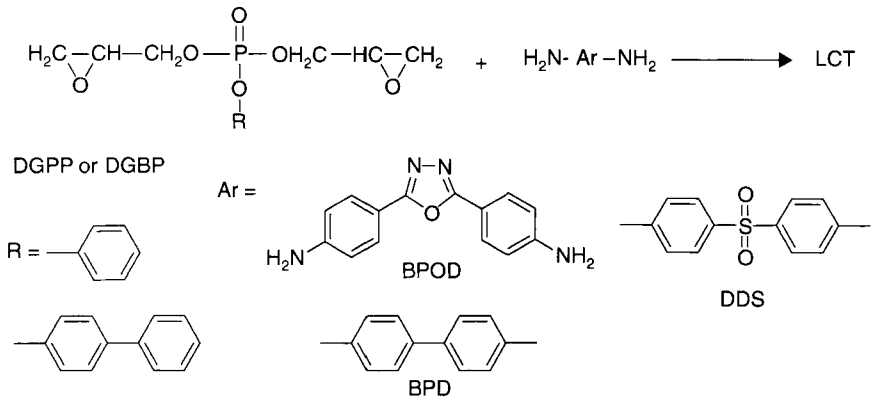

Figure 11.23 Chemical structures of organophosphorus epoxy resins and diamines.

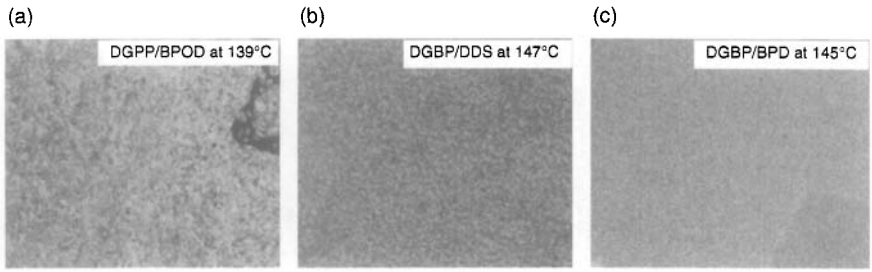

Figure 11.24 LC photographs of DGPP/BPOD (a), DGBP/DDS and DGBP/BPD taken at various temperatures. Reproduced from reference 66, 67.

Continuation of post-cure in the nematic state results in the development of permanent linkages between the secondary reactive groups that stabilize the nematic phase.

Flame retardant properties and thermal stability data are presented in Table 11.6, and the TGA thermograms are shown in Figure 11.25. Unlike the one-stage weight loss behaviour of a conventional epoxy system, the DGPP/diamine LCTs showed two-stage weight loss. A similar trend has been observed in some other phosphorylated-epoxy systems [68–71]. This phenomenon indicates an important role in improving the flame retardancy of the resins. When the resin is burning, the phosphorus segments decompose in the first-stage degradation and then form a phosphorus-rich residue that prevent further decomposition of the thermosets by raising the second decomposition

Table 11.6 TGA and LOI data cured LCTs.

Epoxy Resin/ Curing Agent	Temperature of Weight Loss (°C)			Temperature of Rapid Weight Loss in (°C)		Char Yield (%)	Phosphorus Content (%)	LOI (%)
	5%	10%	50%	Step I	Step II			
DGPP/BPOD	265	274	556	291	432	48	7.5	47
DGPP/DDS	292	313	419	309	402	37	8.1	35
DGPP/BPD	261	294	418	306	394	36	7.4	37
DGBP/BPOD	278	286	570	298	455	45	6.3	46
DGBP/DDS	297	325	443	320	430	41	6.8	43
DGBP/BPD	289	305	425	306	410	39	6.3	43

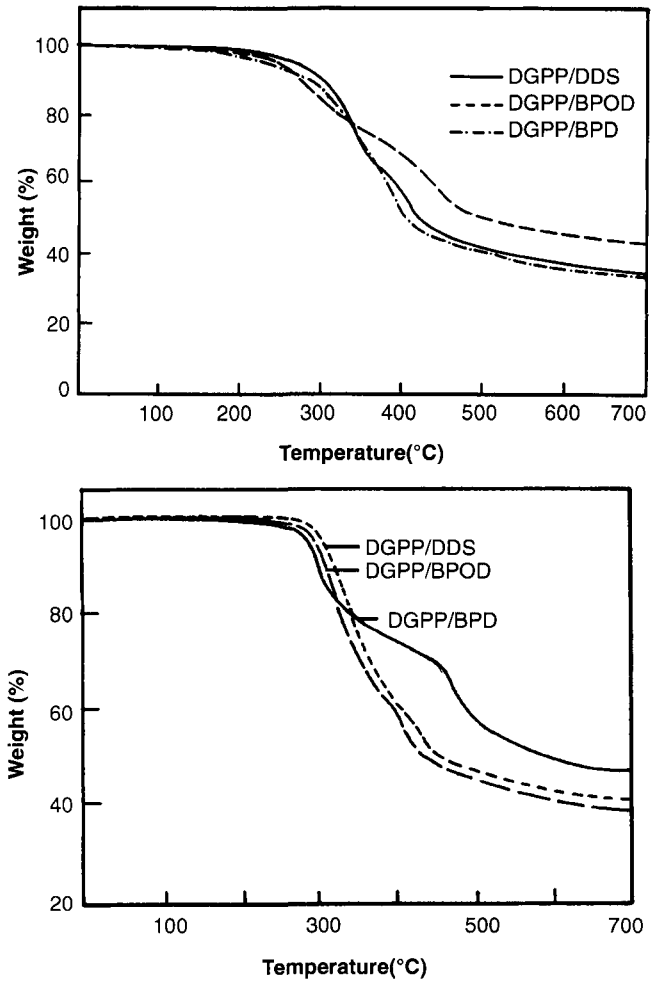

Figure 11.25 TGA thermograms of cured DGPP/(DDS,BPOD and BPD) and DGBP/(DDS, BPOD and BPD) LCT's. Reproduced from reference 66, 67.

to higher temperature and resulting in high char yield. The formation of high char yield during combustion of materials can usually limits the production of combustible carbon-containing gases, which decreases the exothermicity due to pyrolysis reactions, and decrease the thermal conductivity of the burning materials, thus the flammability gets reduced. The flame retardant properties of the cured LCTs were examined by measuring the limiting oxygen index (LOI) values and the results (Table 11.6) showed higher LOI values 35–47. The char

residue 36–48% obtained in the TGA is fairly linearly proportional to the oxygen index for these thermosets. Generally the LOI values for the polymers should be >26 to meet the requirements of flame retardant applications [71]. It is ascertained from the TGA and LOI data that high char residue is indicative of high LOI value [72–73].

11.4 References

1. F. Reinitzer, *Monatshefte für Chemie* Vol . 9, P. 421, 1888.
2. O. Lehmann, *Zeitschrift für Physikalische Chemie* Vol. 4, P. 462, 1889.
3. P.G. De Gennes, *The Physics of Liquid Crystals*, Clarendon Press, Oxford, 1974.
4. P.G. De Gennes, J. Prost, *The Physics of Liquid Crystals*, Clarendon Press, Oxford, 1993.
5. S. Singh, *Physics Reports*, Vol. 324, P.107, 2000.
6 I. Dierking, *Textures of Liquid Crystals*, Wiley-Vch Verlag GmbH & Co. KGaA, Weinheim, 2003.
7. S. Chandrasekhar, *Liquid Crystals*, Cambridge Univ. Press, Cambridge, 1992.
8. P.J. Collings, and M. Hird, *Introduction to liquid crystals: chemistry and physics*, Taylor and Francis, London, 1997.
9. I. C. Koo, *Liquid crystals*, Wiely-Interscience A John Wiley & Sons, Inc, publication, 2007.
10. External Influences on Liquid Crystals. http://plc.cwru.edu/tutorial/enhanced/files/lc/external/external.htm
11. A.M. Donald, A.H. Windle, and S. Hanna, *Liquid Crystalline Polymers*, Cambridge Univ. Press, Cambridge, 2006.
12. W.G. Potter, *Epoxide Resins*, Springer-Verlag, New York, 1970.
13. H. Lee, and K. Nevills, *Handbook of Epoxy Resins*, McGraw-Hill Book Company, New York, 1967.
14. C.A. May and Y. Tanaka, *Epoxy Resin Chemistry and Technology*, Marcel Dekker, New York, 1973.
15. T.F. Mika and R.S. Bauer, "Curing Agents and Modifiers in Epoxy Resins", in C.A. May ed., Epoxe Resin Chemistry and Technology, Dekker, New York, PP. 465–550, 1988.
16. A. Roviello, and A. Sirigu, *Journal of Polymer Science Polymer Letters* Vol.13, P. 455, 1975.
17. W.J. Jackson and H.F. Kuhfuss, *Journal of Polymer Science Part A: Polymer Chemistry*, Vol. 14, P. 2043, 1976.
18. P.G. De Gennes, 'The physics of liquid crystals', Clarendon Press, Oxford, London, 1975.
19. E.P. Douglas, D.A. Langlois, and B.C. Benicewicz , *Chemistry of Materials*, Vol. 6, P. 1925, 1994.
20. A. Shiota, H. Korner, and C.K Ober, *Macromolecular Chemistry and Physics*, Vol. 198, P. 2957, 1997.
21. M. Giamberini, E. Amendola, and C. Carfagna, *Polymer Engineering and Science*, Vol. 39, P. 534, 1999.
22. C. Carfagna, E. Amendola, M. Giamberini, A.G. Filippov, and R.S. Bauer, *Liquid Crystals*, 19, 571–584, 1993.

23. Japanese Kokai Tokkyo Koho Jp 58.206.579 [83,206, 579], Agency of Industrial Science and Technology; Chem. Abstr. 100, 138934x (1984).
24. R. Dhein, H.P. Moller, H.M. Meier, and R. Gipp, US Patent 4762901, 1988.
25. H.P Muller, R. Gipp, and H. Heine, US Patent 4764581, 1988.
26. J.D. Earls, and R.E. Heener, European Patent EP 379057, 1990.
27. J.Y. Lee, J. Jang, *Polymer*, Vol. 47, P. 3036, 2006.
28. P. Castell, A. Serra, M. Galia, *Journal of Polymer Science Part A: Polymer Chemistry*, Vol. 41, P.1536, 2003.
29. P. Castel, M. Galia, and A. Serra, *Journal of Polymer Science Part A: Polymer Chemistry*, Vol. 42, P. 3631, 2004.
30. A. Shiota, and C.K. Ober, *Polymer*, Vol. 38, P. 5857, 1997.
31. A. Shiota, and C.K., Ober, *Journal of Polymer Science Part A: Polymer Chemistry*, Vol. 34, P. 1291, 1996.
32. Q. Lin, A.F. Yee, H.J. Sue, J.D. Earls, and R.E. Hefner Jr, *Journal of Polymer Science Part B: Polymer Physics*, Vol. 35, P. 2363, 1997.
33. G.G. Barclay, and C. K Ober, K.I Papathomas, and D.W. Wang, *Journal of Polymer Science Part A: Polymer Chemistry*, Vol. 30, P. 1831, 1992.
34. Q. Lin, A.F. Yee, J.D. Earls, R.E. Hefner Jr, and H.J. Sue, *Polymer*, Vol. 35, P. 2679, 1994.
35. J.J. Mallon, and P.M Adams, *Journal of Polymer Science Part A: Polymer Chemistry*, Vol. 31, P. 2249, 1993.
36. M. Giamberini, E. Amendola, and C. Carfagna, *Polymer Engineering and Sciience*, Vol. 39, P. 534, 1999.
37. W. Mormann, and M. Brocher, *Macromolecular Chemistry and Physics*, Vol. 197, P. 1841, 1996.
38. S. Cho, and E.P. Douglas, *Macromolecules*, Vol. 35, P. 4550, 2002.
39. S. Jahromi, W.A.G. Kuipers, B. Norder, and W.J. Mijs, *Macromolecules* Vol. 28, P. 2201, 1995.
40. C.M. Paleos, and M.M. Labes, *Molecular Crystals and Liquid Crystls*, Vol. 11, P. 385, 1970.
41. E. Perplies, H. Ringsdorf, and J.H. Wendorff, *Journal of Polymer Science - Polymer Letters Edition*, Vol. 13, P. 243, 1975.
42. G.G. Barclay, and C.K. Ober, K.I. Papathomas, and D.W. Wang, *Macromolecules*, Vol. 25, P. 2947, 1992.
43. S. Jahromi, *Macromolecules*, Vol. 27, P. 2804, 1994.
44. C.E. Hoyle, T. Watanabe, and J.B. Whitehead, *Macromolecules*, Vol. 27, P. 6581, 1994.
45. E. Amendola, C. Carfagna, M. Giamberini, and G. Pisanniello, *Macromolecular Chemistry and Physics*, Vol. 196, P. 1577, 1995.
46. K.C. Lim, J.D. Margerum, A.M. Lackner, E. Sherman, M.S Ho, B.M. Fung, W.B. Genetti, and B.P. Grady, *Molecular Crystals and Liquid Crystls*, Vol. 302, P. 187, 1997.
47. J.W. Schultz, and R.P. Chartoff, *Polymer*, Vol. 39, P. 319, 1997.
48. B.C. Benicewicz, M.E. Smith, J.D. Earls, R.D. Priester, Jr., S.M. Setz, R.S. Duran, and E.P. Douglas, *Macromolecules*, Vol. 31, P. 4730, 1998.
49. M. Włodarska, B. Grzegorz, B. Mossety-Leszczakb , and H.J. Galinab, *Journal of Materials Processing Technology*, Vol. 209, P. 1662, 2009.
50. W. Mormann, and M. Broecher, *Macromolecular Chemistry and Physics*, Vol. 199, P. 853, 1998.

51. C. Tan, H. Sun, B.M. Fung, and B.P. Grady, *Macromolecules*, Vol. 33, P. 6249, 2000.
52. S.L. Simon, and J.K. Gillham, *Journal of Applied Polymer Science*, Vol. 46, P. 1245, 1992.
53. G. Wisanrakkit, and J.K. Gillham, *Journal of Applied Polymer Science*, Vol. 41, P. 2885, 1990.
54. C. Ortiz, R. Kim, E. Rodighiero, C.K. Ober, and E.J. Kramer, *Macromolecules*, Vol. 31, P. 4074, 1998.
55. R. Balamurugan, and P. Kannan, *High Performance Polymers*, Vol. 21, P. 251, Vol. 2009.
56. J. Feng, K.R. Burger, and E.P Douglas, *Journal of Materials Science*, Vol. 39, P. 3413, 2004.
57. X. Zhang, A. Gu, G. Liang, D. Zhuo, and L. Yuan, *Journal of Polymer Research*, DOI 10.1007/s10965-010-9549-3.
58. C. Farren, M. Akatsuka, Y. Takezawa, and Y. Itoh, *Polymer* 2001, 42, 421507–1514.
59. C. Carfagna , E. Amendola , Giamberini, M. *Progress in Polymer Science*, Vol. 22, P. 1607, 1997.
60. R. Balamurugan, and P. Kannan, *Journal of Materials Science*, Vol. 45, P. 1321, 2010.
61. X. Wang , and Q. Zhang, *European Polymer Journal*, Vol. 40, P. 385, 2004.
62. P. Sudhakara, P. Kannan, K. Obireddy, and A. Varada Rajulu, *Journal of Materials Science*, Vol. 46, P. 2778, 2011.
63. S. Levchik, A. Piotrowski, E. Weil, and Q. Yao, *Polymer Degradation and Stability*, Vol. 88, P. 57, 2005.
64. S.V. Levchik, and E.D. Weil, *Polymer International*, Vol. 53, P. 1901, 2004.
65. S.Y. Lu, and I. Hamerton. *Progress in Polymer Science*, Vol. 27, P. 1661, 2002.
66. P. Sudhakara, and P. Kannan. *Polymer Degradation and Stability*, Vol. 94, P. 610, 2009.
67. P. Sudhakara, and P. Kannan. *Soft Materials*, Vol. 7, P.198, 2009.
68. Y.L. Liu, G.H. Hsiue, Y.S. Chiu, *Journal of Polymer Science Part A: Polymer Chemistry*, Vol. 35, P. 565, 1997.
69. Y.W.C. Yang, H.F. Lee, and C.Y. Yuan, *Journal of Polymer Science Part A: Polymer Chemistry*, Vol. 38, P. 972, 2000.
70. C.S. Wang, and J.Y. Shieh, *Journal of Applied Polymer Science*, Vol. 73, P. 3533, 1999.
71. D. W. Van Krevelen, *Properties of polymers*, Elsevier, NewYork, 1990.
72. C.S Wang, and J.Y Shieh, *Journal of Applied Polymer Science*, Vol. 73, P. 3533, 1999.
73. Y.L. Liu, G.H. Hsiue, Y.S. Chiu, R.J. Jeng, C. Ma, *Journal of Applied Polymer Science*, Vol. 59, P. 1619, 1996.

Index

"Ideal" polymer, 64, 65
2,2',3,3'-Oydiphthalic anhydride, 217
2,2',3,3'-Biphenyltetracarboxylic dianhydride, 212
2,3,3',4'-Oxydiphthalic anhydride, 217
2,3,3',4'-Biphenyltetracarboxylic dianhydride, 212
3,3',4,4'-Oxydiphthalic anhydride, 217
3,3',4,4'-Biphenyltetracarboxylic dianhydride, 212
3,3',4,4'-p-Terphenyl tetracarboxylic dianhydride, 223
3,3',4,4'-p-Quaterphenyl-tetracalboxylic dianhydride, 222
3,3',4,4'-p-Quinquephenyl-tetracalboxylic dianhydride, 222
3,3',4,4'-p-Sexiphenyltetracal-boxylic dianhydri, 223
9,9-Bis[(3,4-dicarboxyphenoxy) phenyl]fluorene, 236
9,9-Bis[(4-(amino-phenoxy)phenyl) fluorine, 236

Adamantane, 373
Adamantine, 238
Advances in improving performance of conventional fibers, 323
  Conventional spinning methods, 324
  Crystallization, 331
  Focus Ion Beam, 330
  Lamellae, 331
  Liquid Isothermal Bath(LIB), 325
  Morphology LIB fibers, 330–331
  Orientation, 331
  Precursor, 331
  Properties of LIB fibers, 327–330
  WAXD, 330
APICAL, 222
Applications
  Flamme protection, 26–28
  Membrane materials, 20–26
  Phosphorylcholine, 23, 24
Aromatic, 341, 342, 373, 375
Aromatic bisbenzoyl chloride, 342–344
Aromatic ionomers, 82
Aromatic polyamide, 296
  Fiber properties, 302–306
  Fiber spinning, 301–302
  General properties, 296–299
  Polymerization, 299–301
  Structure, 302–306
Aromatic polyamides, 111–112, 121–122, 134, 149, 151, 153–154
Aromatic polyesters, 2

BDT copolymers
  benzo[c][1,2,5]selenadiazole (BSe), 66

benzo[c][1,2,5]thiadiazole (BT), 66
bithiazole (BTz), 70
di-2-thienyl thiadiazolo[3,4-c] pyridine (DTPyT), 72–73
di-2-thienyl-2,1,3-benzothiadiazole (DTBT), 71
di-2-thienyl-2,1,3-triazole (TAZ), 73–74
diketopyrrolopyrrole (DPP), 67
ethylene, 66
ethylenedioxythiophene (EDOT), 66
fluorinated benzothiadiazole (ffBT), 73
perfluorination, 75
pyrido[3,4-b]pyrazine (PP), 69
quinoid, 74
thiazolothiazole (TzTz), 70
thieno[3,4-b]thiophene (TT), 74, 75
thieno[3,4-c]pyrrole-4,6-dione (TPD), 67–69
thiophene, 66
BDT monomer synthesis
benzo[1,2-b:4,5-b'] dichalcogenophenes, 52
halogen-lithium exchange, 52
intramolecular cyclization, 52
selenophene, 52
sulfur anion, 52
tellurophene, 52
thiophene derivatives, 51
BDT side chains
alkoxy chain, 52, 60, 72, 75
alkyl chain, 53, 59, 60, 71, 75
Biphenyl, 347
Biphenyl-type polyimide, 206, 212
Bis(trimellitic acid anhydride) phenyl ester, 231
Bisfuoro monomer
1,4-bis(p-fluorobenzoyl)benzene (BFB), 345–347, 352, 361
4,4'-bis(4-fluorobenzoyl) biphenyl (BFBB), 348–349, 351–353
4,4'-difluorobenzophenone(DFB), 345–349, 352–353, 356, 367, 373, 378
Bisphenol monomer
(4-(4'-trifluoromethyl) phenoxyphenyl) hydroquinone(TFPOPH), 367–368, 371
2-chlorohydroquinone, 353
3-(trifluoromethyl) phenylhydroquinone(FH), 361, 373
4,4'-diphenol(DP), 347, 349, 352, 353, 356, 361
4,8-bis (1-adamantly)-1,5-dihydroxynaphthalene (AdNp), 373
Hydroquinone (HQ), 345, 347–348, 367, 378
Blend membrane, 13
Block copolymers, 85, 107
Block length, 103, 104
Bulk-heterojunction (BHJ) configuration, 63

Carbon fiber, 318
Application, 322
Electrical conductivity, 323
Mechanical properties, 322
PAN-based carbon fiber, 319
Pitch-base carbon fiber, 319–321
Thermal conductivity, 323
Vapor-grown carbon fiber, 321
Carbon nanotube, 321–322
Multi-walled, MWCNT, 321
Single-waaled, SWCNT, 321
Cardo moieties, 113, 115, 122, 131, 146
Cardo structure, 236
Chemical imidation, 218
Chemical treatment, 207

Cis-trans isomer, 221
Click chemistry
  1,3-dipolar cycloaddition, 244
  azide and alkyne reaction, 244
Coefficient of thermal expansion, 206
Conductivity, 15
Continuous cooling transformation (CCT), 324
Cooling curve, 324
Copolymers, 342, 345–346, 356, 362–363, 367, 373, 377, 383
Crosslinking, 87, 90–91, 101
Crystal structure, 2
Crystallization, 222, 229
CTE, 206, 211–212, 216–217, 225–229, 231–235

Decomposition temperature, 261–264, 2
Decrease in E′ at the Tg, 217, 221, 223
Degradation pattern, 11
Degradation temperature Td, 90, 93, 97–98
Degree of phosphonation (DP), 87–88, 90, 96, 98
Degree of polymerization, 3
Degree of sulfonation, 6, 11
Degree of sulfonation (DS), 86, 90–91
Derivatives of polyamic acids, 208
Dielectric constant, 206, 208, 212, 235, 237
Dielectric properties, 260–263
Diphenyl ether, 342–344
Diphenyl sulfone (DPS), 345, 378
Direct Methanol Fuel Cell (DMFC), 88, 101, 107
DMA, 255–256
Doping, 15
DSC, 251, 254, 257, 354–358, 362, 364, 368, 371, 375, 378, 381
Dynamic mechanical analysis, 215

Electrochromic polyamides, 135, 156–161
Electrophilic substitution, 85–86
Ether bond, 345, 347

Fan-shaped, 364
Flame retardant epoxy resins, 417–419
Flexibilizing spacers, 113, 122
Fluorene, 236
Fluorinated diamines, 117–118, 134, 135
Fluorinated polyamides, 133
Fluoro-poly(ether amide)s, 3
Fluoropoly(ether amide-imide)s, 3
Fracture mechanism of LCTs, 407
Free volume, 236, 239

Gas diffusion, 81
Gas permeability, 152–153
Glass transition temperature, 5, 251, 253–259
Glass transition temperature (Tg), 414–415
Grazing-incidence X-ray diffraction (GIXRD), 60, 69, 75

Heat-resistance, 346
High Performance Fibers, 269
High Tenacity-high Modulus Fibers, 269
High-pressure synthesis, 209
Hydrolytic desulfonation, 88–89
Hygrothermal stability, 5
Hyperbranched polyamides, 111, 134–136, 138–139

Ideal properties of OFET materials, 57–58
IKAROS, 222
Imidation-induced in-plane orientation, 233

Internal charge transfer (ICT), 66–67
Ion exchange, 149
Ion Exchange Capacity (IEC), 82, 86, 88, 90–91, 93, 94, 96, 98–101, 105
Ionic clusters/clustering, 91, 93–94, 105
Ionic function/groups, 82, 83, 85
Ionic liquid, 120, 129
Ionomer, 82, 88, 91, 99–101, 107

Kapton, 206, 211
Ketone bond, 345–347
Kevlar
  Applications, 306–307
  Body armor, 303
  Bullet proof vest, 306
  Helmet, 306
Kevlar 149, 302
Kevlar 29, 290
  Physical properties, 298
Kevlar 49, 302, 304
Kevlar, polyparaphenylne terphthalamide, 296, 285, 297
Kevlar®, 112

LCPs, 351–352
Liotropic liquid crystals, 388
Liquid crystal polymers, 2
Liquid crystalline epoxy resins (LCERs), 393
  physical properties of LCERs, 399–419
  synthesis of LCERs, 396
Liquid crystalline phase-time-temperature transformation (LCPTTT), 399, 401
Liquid crystalline polymers, 392
Liquid crystalline thermosets (LCT), 392
Liquid crystals, 387, 390
Long range order, 360
Luminescent, 156

M5, 269, 270, 276, 280, 306
  Monomer, 271
  Polymer synthesis, 271
  Polymerization, 273
M5 applications, 278–279
  UV resistance, 279, 281
M5 fiber
  Compressive strength, 278, 294
  Fiber properties, 274–278
  Fiber spinning, 274–278
  Flame properties, 279
  Mechanical properties, 280
  WAXS, 278
Mechanical properties, 259–260, 111–112, 115, 121, 123, 133, 143–144, 157
Melting point, 346, 351, 356
Membrane disintegration, 94, 98
Methanol Crossover, 81, 101
Methanol permeability, 94, 98
Methanol selectivity, 88, 101, 102, 105
Microfibrils, 315
Microwave, 119, 129–130
Monomers
  alkynes, 246–249
  azides, 246–249
Mosaic, 358, 364
Multi-block copolymers, 101–105

Nafion®, 81, 88, 90–91, 94, 103, 105
Nanofiltration, 153–154
Nano-scale separation, 91
Naphthalene, 373, 377, 381, 383
Nematic, 354, 358–360, 364, 389
Nomex, 279, 296
Nomex®, 112, 153, 157

Norbornene, 238
Nucleophilic (Aromatic) substitution, 85–86, 90, 100, 103

OFET materials
  curvature, 61
  geometrical arrangement, 60–61
  monomer angle, 61
  octyltrichlorosilane (OTS-8), 60
  P3HT, 58
  post-deposition thermal annealing, 59
Oligomers
  alkyne-capped triazole oligomers, 245, 250
One-step procedure, 208
Optically active polyamides, 155
Ordered structure, 223, 229
Organic field effect transistors (OFET)
  device architectures, 56
  OFET electrodes, 57
Ortho-to-ether position, 83, 86–87, 89
Ortho-to-sulfone position, 83, 86, 89, 96

Partially imidized polyamic acid, 228
PBZT, 288
PEDEK-PEDEKDK copolymer, 349–350, 352, 353
PEEKK-PEDEKK copolymer, 347–348
PEEK-PEDEK copolymer, 347–349
PEEK-PEEKDK copolymer, 348–352
PEEK-PEEKK copolymer, 345–347
PEN, 269, 327
  properties, 329–330
Perfluorosulfonic acid based polymers (PFSA), 81, 107
Permeation rate, 150
Permselectivity, 150
Pervaporation, 133, 149–151
Pervaporation separation index, 150
PET, 324, 326–327
  properties, 328, 330
Phase separation, 83, 93, 95, 97, 104, 13
Phenyl, 345, 347
Phenylphthalide, 238
Phosphonated polysulfones, 87, 90, 97, 107
Phosphonation, 86–87
Phosphonic acid, 85–86, 88, 90, 96–98
PIPD, 270, 275–276, 280
PLM, 354, 356, 359
Poly (aryl ether ketone) (PAEK)
  ClPAEK, 353–355
  FPAEK, 361–365
  PEEK, 372, 377, 382
Poly(amide imide)s, 124
Poly(amide-sulfonamide)s, 149
Polyamic acid, 207–208
Polyamic acids derived from aliphatic diamines, 208
Polyamide-hydrazides, 123, 154
Polybenzoxazine, 10
Polycondensation, 83, 99
Polyether sulfone (UDEL), 83, 85, 99
Polyimides containing ester linkages, -$COOC_6H_4OCO$-, between phthalimides, 211, 230
Polyimides containing ether linkages, -O-Ar-O- (Ar: Bulky moiety), 211, 235

Polyimides containing
p-phenylene units, -(C_6H_4)
m- (m=2,3,4), between
phthalimides, 211, 221
Polyimides from isomeric
biphenyltetracarboxylic
dianhydrides, 211, 222
Polyimides from isomeric
oxydiphthalic anhydride,
211, 217
Polyimides with a connecting
group (-X-) between
phthalimides, 212
Polyisoimide, 210
Polymer Electrolyte Membrane
(PEM), 81–84, 107
Polymer solar cells
fill factor (FF), 62, 64
open circuit voltage (Voc), 62–63
power conversion efficiency, 62
short circuit current (Jsc)), 62, 64
Polymerization methods
Microwave assisted coupling
reactions, 56
Oxidative coupling, 54
Stille coupling
polycondensations, 54, 59
Suzuki coupling, 55
Transition metal catalyzed
coupling polymerization, 54
Yamamoto-type
polycondensation, 55
Polyoxadiazoles
coating materials, 33–38
conductivity, 39, 41–42
fuel cells, 38–41
mechanical and thermal
properties, 26–32, 43–44
nanocomposites, 42–45
oxadiazole-hydrazide
copolymer, 23–24, 34–37
synthesis, 21–25
Polysulfone based ionomers,
83, 96, 107
Polytriazole
crosslinkable polytriazole,
244–245, 254–263
linear polytriazole, 244–245, 253,
259, 263
preparation, 245
Processability, 111–113, 115, 121,
124, 152, 162
Properties
FTIR and NMR spectra,
12–13
Mechanical properties, 17–18,
341–342, 345–346, 377–378
Thermal and thermooxidative
properties, 13, 18–19
Thermal properties, 342, 345,
347, 356, 363, 376
Properties of OFET devices
current on/off ratio, 57
field-effect mobility, 57–58
threshold voltage, 57
Proton conductivity, 81–82, 88,
90–91, 94–95, 98, 101, 103–104
Proton Exchange Membrane
Fuel Cell (PEMFC), 81, 83,
90–91, 107

Quantum yields, 19

Random copolymers, 104–105
Reaction kinetics
apparent curing activation
energy, 252
Redox-active, 19
Restriction of internal rotation,
216, 220, 223
Reticulation, 85
Reverse osmosis, 149, 153
Rigidity, 346
Ring opening polymerization, 11

Semi-crystalline polymers, 331
Service-temperature, 2
Shish-Kebab, 314

Short-range order, 360
Smectic, 358, 360–361, 364, 389
Solar cell applications, 20
Solidification, 325
Solubility, 209, 214, 218, 238
Solution blending, 6
Spectra 1000, 290
Sperctra, Dyneema
  Application, 318
  Bullet proof vest, 318
  Glove, 318
  Helmet, 318
  Hybrid composite, 318
Sperctra, Dyneema, UHMWPE, 269, 307–309
  Fiber properties, 312–318
  Fiber spinning, 312–318
  Polymerization, 309–312
Spiro, 115, 131, 132
Step-growth polymerization, 83, 85, 99
Stress-induced crystallization (SIC), 324
Stress-induced orientation (SIO), 324
Structural advantages of BDT, 65
Structure-property relationship
  chain rigidity, 253, 256, 260
  crossinked network, 254–259, 260–263
  curing temperature, 245, 251
  degradation temperature, 261–264
  glass tranisition temperature, 251, 253–259
Sulfonated Aromatic Polymers, 82
Sulfonated Polysulfones, 86, 90–91, 100, 107
Sulfonation, 85–86, 89
Sulfonic acid, 85–86, 88, 90–91, 94, 96, 105, 107
Sulphonated polyetherimide, 5
Sweep volume, 211, 217, 223, 239
Synthesis
  Electrophilic and nucleophilic reactions, 2, 4, 6, 8
  Polycondensation reactions, 10–11
  Post-polymerisation reactions, 2, 3, 4–9
Synthesized, 342, 345, 347–349, 352, 356, 361, 373, 377
Synthetesis of polyimides, 207

Tanδ, 220
Technora, 297, 301
Temperature dependence of E', 228
Temperature dependence of storage modulus, 215, 217, 222, 225–227, 230
Texture, 354–355, 358, 364–365
Tg, 347–351, 354, 362, 368, 371, 375, 381
TGA, 262–264, 354, 356, 362–363, 368, 375, 378, 382
Thermal conversion, 207
Thermal curing, 4
Thermal imidation, 214, 218, 223, 231, 236
Thermal properties
  glass tranisition temperature, 253–259
  thermal curing behavior, 251
  thermal stability, 261–264
Thermal stability, 83, 88, 96, 98, 104, 111, 114–115, 120, 126–128, 130, 135, 138, 142, 144, 157–158, 160, 162, 341, 356, 373, 377
Thermoplasticity, 222
Thermotropic liquid crystals, 388
Three-step procedure, 210
Ti, 354, 356, 362–363, 366

Tm, 347–351, 354, 362, 366, 368, 371, 381
Toray, 319
Transition, 354, 356–357, 362, 373
Trifluoromethyl, 113, 115, 122, 125, 132–133
Twaron, 297
Two-step procedure, 207
Viscosity, 3

WA, 206, 211, 225, 232, 234–236
Water absorption, 206, 225–226, 231–235
WAXD, 354–355, 358, 360, 364, 366, 367, 372, 378, 382–383
Wittig-Horner polymerization, 16
X-ray, 354, 356, 360, 365, 367–368
XRD spectroscopy, 3

Zylon, 290
  Applications, 295
Zylon AS, 290
Zylon, PBO, 269, 279, 285–286, 290
  Fiber properties, 290
  Fiber spinning, 285–287
  Monomer synthesis, 281–283
  Morphology, 287–290
  Polymerization, 283–285
  Solution properties, 285
  Structure, 287–290
Zylon,HM, 290

Also of Interest

Check out these published and forthcoming related titles from Scrivener Publishing

Handbook of Bioplastics and Biocomposites Engineering Applications
Edited by Srikanth Pilla
Published 2011. ISBN 978-0-470-62607-8

Biopolymers: Biomedical and Environmental Applications
Edited by Susheel Kalia and Luc Avérous
Published 2011. ISBN 978-0-470-63923-8

Renewable Polymers: Synthesis, Processing, and Technology
Edited by Vikas Mittal
Forthcoming September 2011. ISBN 978-0-470-93877-5

Plastics Sustainability
Towards a Peaceful Coexistence between Bio-based and Fossil Fuel-based Plastics
Michael Tolinski
Forthcoming October 2011. ISBN 978-0-470-93878-2

Polymers from Renewable Resources
Ram Nagarajan
Forthcoming Spring 2012. ISBN 978-0-470-62609-2

Green Chemistry for Environmental Remediation
Edited by Rashmi Sanghi and Vandana Singh
Forthcoming September 2011 ISBN 978-0-470-94308-3

Polymer Nanotube Nanocomposites: Synthesis, Properties, and Applications
Edited by Vikas Mittal.
Published 2010. ISBN 978-0-470-62592-7

Handbook of Engineering and Specialty Thermoplastics
Part 1: Polyolefins and Styrenics by Johannes Karl Fink
Published 2010. ISBN 978-0-470-62483-5
Part 2: Water Soluble Polymers by Johannes Karl Fink
Published 2011. ISBN 978-1-118-06275-3
Part 3: Polyethers and Polyesters edited by Sabu Thomas and Visakh P.M.
Published 2011. ISBN 978-0-470-63926-9
Part 4: Nylons edited by Sabu Thomas and Visakh P.M.
Forthcoming October 2011. ISBN 978-0-470-63925-2

A Concise Introduction to Additives for Thermoplastic Polymers
By Johannes Karl Fink.
Published 2010. ISBN 978-0-470-60955-2

Introduction to Industrial Polyethylene: Properties, Catalysts, Processes
By Dennis P. Malpass.
Published 2010. ISBN 978-0-470-62598-9

The Basics of Troubleshooting in Plastics Processing
By Muralisrinivasan Subramanian
Published 2011. ISBN 978-0-470-62606-1

Miniemulsion Polymerization Technology
Edited by Vikas Mittal
Published 2010. ISBN 978-0-470-62596-5